INDC(NEA)-2/Sp.

COMITATO NAZIONALE ENERGIA NUCLEARE
DIPARTIMENTO RICERCA TECNOLOGICA DI BASE ED AVANZATA

# PROCEEDINGS OF THE SPECIALISTS' MEETING ON NEUTRON CROSS SECTIONS OF FISSION PRODUCT NUCLEI

HELD AT

"E. CLEMENTEL" CNEN CENTRE

BOLOGNA, ITALY

DECEMBER 12-14, 1979

C. COCEVA, G. C. PANINI, EDITORS

RELAZIONE TECNICA INTERNA

RIT/FIS-LDN(80) 1

NEANDC(E) 209 "L"

# FOREWORD

At its 20th meeting (Oak Ridge, April 3-7, 1978) the Nuclear Energy Agency Nuclear Data Committee (NEANDC) deemed it advisable to hold a "specialists' meeting" on the neutron cross-sections of fission product nuclei, at the end of the year 1979. This in view of the time elapsed since the Petten meeting (Fission product nuclear data, September 5-9, 1977) and of recent progress in measurements and evaluations, and in consideration of the more stringent requirements set on the cross-sections of this class of nuclei.

The meeting was then organized under the auspices of the NEANDC and hosted, by the Laboratorio Dati Nucleari at the "E. Clementel" CNEN Centre in Bologna (Italy), December 12-14, 1979. Main scope was to review and assess experimental results and evaluations, taking the Petten meeting as a starting point, in the more restricted field of neutron cross-sections.

The presentation of invited and contributed papers was organized into three sessions, devoted to:

1) Measurements of differential and integral data and experimental techniques.

2) Resonance parameters: average values and systematics.

3) Neutron cross sections: theory and evaluations,

and into two Working Groups with the task of assessing:

1) Status of the capture cross-section for the most important fission product nuclei.

2) Status of evaluation and theory on $\langle D \rangle$, $\Gamma_\gamma$ and the neutron and gamma strength functions.

The restricted attendance and the competence of the participants favoured frank and animated discussions on the various subjects.

The conclusions of the meeting are summarized in the reports of the three session chairmen and of the two working groups.

The editors thank all participants and wish to acknowledge the cooperation of the chairmen of the sessions and of the working groups. The assistance of the members of the organizing committee, and the kind help of the secretary Mrs. P. Cenni is also gratefully acknowledged.

C. Coceva

G.C. Panini

TABLE OF CONTENTS

SESSION 1: Measurements of differential and integral data and experimental techniques.

Chairman: M.S. Moore

Chairman Report ..... 1

Integral cross section measurements on fission-product nuclides in fast neutron fields ..... 5

Y.D. Harker, R.A. Anderl

Measurements of capture cross sections in the FP mass region ..... 19

N. Yamamuro, A. Asami

Techniques for the determination of capture cross sections of radioactive fission product nuclides ..... 41

M.S. Moore, G.F. Auchampaugh

Neutron resonance parameters for Pd isotopes ..... 53

E. Cornelis, L. Mewissen, F. Poortmans, G. Rohr, R. Shelley, P. Staveloz, T. Van der Veen

Neutron capture cross sections of Rubidium, Yttrium, Niobium, Cesium, Cerium and Gadolinium between 0.5 and 3.0 MeV ..... 63

J. Voignier, S. Joly, G. Grenier

Capture cross section measurements on natural Xenon, natural Krypton and on various Krypton isotopes between 3 and 250 keV neutron energy ..... 69

B. Leugers, F. Käppeler

Low energy neutron cross section measurements of radioactive FP nuclides ..... 77

H.G. Priesmeyer

Fast neutron capture cross section measurements, evaluation and model calculation of fission product nuclei ..... 85

W.P. Poenitz

Measurements of the total and partial neutron cross sections of Cerium and Thulium in the energy range from 1.8 meV to 1.8 eV using TOF and Neutron Diffraction techniques ..... 95

M. Adib, A. Abdel-Kawy, R.M.A. Maayouf, I. Hamouda (not orally presented)

Recent capture cross section data from ORELA above 2.6 keV ..... 103

R.L. Macklin, R.R. Winters, J. Halperin (not orally presented)

SESSION 2: Resonance parameters: average values and systematics.

Chairman: F.H. Fröhner

Chairman Report ..... 113

Review of the different methods to derive average spacing from resolved resonance parameter sets ..... 121

E. Fort, H. Derrien, D. Lafond

Efficient estimation of strength functions and average level spacings from resonance parameters ..... 145

F.H. Fröhner

Statistical analysis of neutron resonance parameters ..... 161

M. Stefanon

Maximum likelihood analysis of resolved resonance parameters for some fission product nuclides ..... 169

G. Delfini, H. Gruppelaar

Status of radiative widths, neutron strength functions and improved evaluations using Lane-Lynn theory ..... 179

S. Mughabghab

Phenomenological and theoretical basis for the parameterization of nuclear models used in reactor data evaluation ..... 195

G. Reffo (oral presentation only)

Evaluation of average level spacings and S-wave strength functions performed for more than 240 nuclei ..... 197

G. Rohr, L. Maisano

The level density systematics applied to fission product nuclei ..... 207

G. Rohr, L. Maisano, R. Shelley

BCS level density calculations and consistent estimate of radiative widths by means of a thermodynamic model ..... 215

V. Benzi, G. Maino, E. Menapace, A. Ventura

SESSION 3: Neutron cross sections: theory and evaluations.

Chairman: G. Reffo

Chairman Report ..... 231

On optical model calculations in the mass region A=80 to A=170 ..... 233

Ch. L. Lagrange

ENDF/B-5 fission product cross section evaluations ..... 253

R.E. Schenter, T.R. England

The contribution of (n,p) and (n,$\alpha$) reactions to fission-product capture cross sections ..... 285

H. Gruppelaar, B.P.J. Van den Bos

Intercomparison of adjusted data sets for capture cross sections of fission products ..... 299

H. Gruppelaar, P. Hammer, L. Martin-Deidier

Fission product neutron cross section evaluations for JENDL and the integral tests ..... 317

S. Iijima, T. Watanabe, T. Yoshida, Y. Kikuchi

Fission product nuclear data at the NEA data bank ..... 347

P.D. Johnston, W.W. Osterhage

Neodymium, Samarium and Europium capture cross section adjustments based on EBR-II integral measurements ..... 363

R.A. Anderl, Y.D. Harker, F. Schmittroth

Status of pseudo fission-product cross sections for fast reactors; sensitivity studies for sodium void effects ..... 375

R.J. Heijboer, A.J. Janssen, F. Lekkerkerk

Neutron cross section calculations for fission product nuclei ..... 391

E.D. Arthur, D.G. Foster, jr. (not orally presented)

Working Group 1 - Status of the capture cross section for the most important FP nuclei ..... 403

Working Group 2 - Status of evaluation and theory on $\langle D \rangle$ , $\Gamma_\gamma$ and the neutron and gamma strength functions .... 419

LIST OF PARTICIPANTS ..... 423

Chairman's Summary of the Highlights of Session I :

Measurements of differential and integral data and experimental techniques

at the NEANDC Specialists' Meeting on Neutron Cross Sections of Fission Product Nuclei, Bologna (1979)

The current status of integral cross-section measurements on fission-product nuclides in fast neutron fields was reviewed by Y.D. Harker and R.A. Anderl. In the presentation, Harker noted that there are three complementary techniques that have been used : activation, reactivity and transmutation. The last is relatively new, and involves long term irradiation and subsequent mass-spectroscopic analysis of the irradiated material to infer the average capture cross sections. Most of the integral data on fission product nuclides that have been obtained were done by the activation technique; Harker reported that a complete re-analysis of all the data taken with the Coupled Fast Reactivity Measurement Facility (CFRMF) was carried out for this meeting, using more recent decay schemes and a consistent flux normalisation. The primary result of the re-analysis was a lowering of the uncertainty estimates previously reported; the measured integral cross sections are, on the average, still ~ 25% lower than calculations based on ENDF/B - IV evaluations, or ~ 17% lower than calculations based on the reevaluations done for ENDF/B - V. Harker noted that comparisons of CFRMF activation measurements with calculations based on ENDF/B dosimetry evaluations were found to give much better agreement, ~ 5%, and that good agreement is generally found between integral measurements made with the CFRMF and with those done at the STFK facility at ECN. Harker suggested that some of the discrepancy between calculation and experiment might be attributed to resonance self shielding, corrections for which had not been made in the comparison of calculated and experimental integrals. It may be noted that evidence to support this conjecture is found in Table III of this paper : the largest discrepancies listed by Harker are for the three even isotopes of Nd, 148, 150 and 152 which have large s-wave neutron strength functions (~ $3 \times 10^{-4}$) and which (because they are even-even targets) would be expected to show relatively the largest corrections for resonance self shielding. If these three results are excluded from the comparison, one finds that the ratio of calculated to experimental integrals goes from 1.25 to 1.12 for the ENDF/B IV comparison, and from 1.17 to 1.05 for ENDF/B V. Harker also suggested that new measurements on $^{99}$Tc, $^{100}$Mo, $^{107}$Ag, $^{109}$Ag, $^{127}$I, and the Nd isotopes should be considered and that CFRMF reactivity data might be used to infer average scattering cross sections. He noted that measurements using the transmutation method with EBR - II or FFTF for Zr, Ru, Pd and Mo isotopes were being proposed.

In the second invited paper of this session, N. Yamamuro of the Research Laboratory for Nuclear Reactors, Tokyo Institute of Technology (KURRI) and A. Asami of the Japan Atomic Energy Research Institute (JAERI) reported capture cross section measurements on certain of the most important fission products. At the KURRI 46 MeV Linac, average capture measurements are determined between 3 and 80 keV by a two-step technique : 1) an absolute determination at 24 keV, using an iron-filtered beam, and 2) a shape measurement between the black resonances at 2.85 keV in sodium and at 103 keV in sulphur. Capture yields were determined with $C_6F_6$ or $C_6D_5$ detectors at an 11.7 m flight path; a carbon scatterer was used to monitor the scattered neutron background, which was found to vary roughly as 1/v and permitted the background to be analytically described as having a linear dependence in time of flight. The relative measurements were then normalized at 24 keV, the flux shape having been determined with $^{10}$B(n, $\alpha\gamma$) reaction. Data were reported for Nb-93, I-127 and Cs-133 with an overall accuracy of 5% (estimated in Ref. 1, the preliminary report of this work presented at the Harwell conference in September 1978).

The capture measurements at the 120 MeV JAERI Linac are made with a large-volume (3500-l) liquid scintillator tank; and particular attention is paid to a careful determination of the background. The time dependent capture background can be assumed to arise primarily from neutrons scattered by the sample, moderated in the capture tank, and subsequently captured in the tank or its vicinity. The shape of the background was assumed to follow that observed with a pure scatterer (Pb), which was then normalized to results obtained with various notch (black-resonance) filters inserted in the beam. Similar considerations are used to normalize the flux monitor backgrounds, although here it appears not to be necessary to take into account the shape of the time-dependent background between notches. Average data were presented for natural Eu, Eu-151, 153, Nd-143,145,146, 148 and Sm-147, 149 and compared with the work of others. In the resonance region data were obtained for Tb-159, Br-79, 81 and Sm-147, 149. Evidence for intermediate structure on steps in the cumulative plot of the s-wave neutron strength function as a function of neutron energy was found for Br-81 and Sm-149.

In the last invited paper of this session, H.G. Priesmeyer of the University of Kiel summarised low energy ( < 1 keV) neutron cross section measurements on radioactive fission product nuclides performed since the 1977 Petten meeting. There are three experimental programs that have been active over the past few years, two fast-chopper groups, at Kiel and Dimitrovgrad, and the electron linac at RPI, used in collaborative measurements by groups at RPI and KAPL. New measurements on Cs-134, Cs-135, Cs-137, Tc-99, I-129, Sm-151, Pd-107, Pm-147, Eu-154, Eu-155 and gross fission product samples were described. Priesmeyer summarised the current situation in his concluding remarks :

a) For the measurer, E. Forts's review paper at the Petten meeting (IAEA-213, p.139) is still a source for measurement needs. Radioactive candidates could be Ru-103, Ru-106, Kr-85 and Sr-90.

b) Difficulties in getting the sample material are often prohibitive to measurements. (This was one of the strong points made by Priesmeyer in the text. The interest and active participation by radiochemists in the measurement program is crucial. An example is the KAPL - RPI collaboration.)

c) In order to deduce the capture cross sections, one needs more than total cross section measurements. Priesmeyer mentioned total plus scattering, or direct capture measurements. For those nuclides that are gamma active, direct capture requires very high neutron fluxes to surmount the decay-gamma background.

d) Gas production by radioactive nuclides is still an open problem.

e) Techniques should be improved and experience gathered for radioactive material. (It may be noted that much of the expertise that had been developed over the past twenty years in this field is essentially lost, having been dissipated as reprogramming of funding reflects changing goals and priorities.)

Priesmeyer noted that future needs include the extension of measurements to higher energies, and investigation of nuclides with shorter half lives. He emphasised the importance of irradiating the samples, performing the necessary chemistry and/or packaging, assaying to assure quality control, and rapid transportation to the spectrometer to carry out the measurement.

In a contributed paper, M.S. Moore and G.F. Auchampaugh of LASL described techniques for the determination of capture cross sections of radioactive nuclides. The techniques are the same as those for stable isotopes : calculation based on systematics, modifying the calculation by comparing to microscopic measurements, and adjusting the resulting evaluation by using integral measurements. The emphasis changes when little or no data exist. It was suggested that one might provide total cross sections for highly radioactive species by extrapolating experimental data on neighbouring stable isotopes; however, this idea has yet to be proven. It was felt that the occurrence of intermediate structure in the low-energy neutron

strength functions of fission product nuclides was a general problem, and important enough that one should consider low-resolution microscopic measurements. The relative capability of currently existing and projected high intensity neutron sources was reviewed. It was projected that the necessary data could be obtained if the data requirements were sufficiently urgent to [illegible] the extra-ordinary effort that will be required.

Recent total, capture, elastic scattering and resonance parity assignments for resonances in Palladium isotopes were described in a contributed paper by P. Staveloz, E. Cornelis, L. Mewissen, F. Poortmans, G. Rohr, R. Shelley and T. van der Veen. The data on Pd-104, 105, 106, 108 and 110 have been taken at GELINA, the electron linac facility at the CBNM in Geel, Belgium. Most of the experiments are finished, and an important part of the data have been analysed. The parity, or s- and p- wave neutron assignments, are made by the high-/low-bias technique : most of the low-lying states in the odd Pd nuclides have positive parity, and strong (E1) transistions to these states from a resonance level can be taken as evidence that the level has negative parity and arises from p-wave neutron capture in the even-even target. Strong evidence for intermediate structure in the energy dependence of the neutron strength function is reported for $^{106}$Pd and $^{110}$Pd. The resonance parity assignments are being done to show whether this structure is due to s- or p-wave neutrons or both.

Neutron capture at selected energies between 0.5 and 3.0 MeV for Rb, Y, Nb, Gd, and for isotopes Gd-155, 156, 157, 158 and 160 were reported in a contributed paper by J. Voignier, S. Joly and G. Grenier. The data were obtained by recording pulse-height capture spectra in a NaI spectrometer with a NaI annulus, operated in the anti-compton and single-photon-escape modes. The pulse-height spectra are unfolded and corrected for spectrometer efficiency to obtain absolute cross sections $\sigma(E,E\gamma)$, at each neutron energy point E. The data were obtained with neutrons from the $^{7}$Li(p,n) and T(p,n) reaction with a 4 MV Van de Graaff accelerator. The data are compared to existing measurements and evaluations; the agreement with recent measurements is generally acceptable, for the cases for which such a comparison can be made. Additional measurements have been made for Cs and Ce samples, and data reduction is still in progress.

A contributed paper by B. Leugers and F. Käppeler reported measurements of the total and capture cross sections of natural Kr and Xe and of Kr-80, 82 and 83 from 3 to 250 keV taken with the Karlsruhe 3 MV Van de Graaff. The capture detectors were $C_6D_6$ scintillators with pulse-height weighting; the estimated accuracy of the data is 5 -10%. Käppeler noted that a major problem in measuring the fission product noble gas is the insufficiency of sample material. Attempts to use liquid targets were unsuccessful because of the large amount of material necessary for the cooling cell; the measurements were eventually carried out with high pressure gas samples ( ~ 300 bar) giving 25-30% of the liquid density. Comparison of the data on natural Kr with the isotopic samples showed that essentially all the observable structure in natural Kr in this energy range is attributable to Kr-84 (57% abundant). The data obtained for natural Xe show the magnitude typical of even targets in this mass range: the capture cross section is similar to that of natural Te or Ba, and significantly lower than that of I or Cs.

In the last contributed paper of this session, W.P. Poenitz described the integrated program of fast neutron capture cross section measurements, evaluation, and model calculation for fission-product nuclei at ANL. Poenitz noted particularly large discrepancies (of a factor of 5) between evaluated capture cross sections of fission product nuclides and even larger discrepancies if no data existed. Poenitz described the radiative capture measurement program at ANL, for which a 1300 l scintillator tank and grey neutron flux monitor are used. Capture measurements of Rh-103, Pd, Nd and Sm relative to the capture cross section of Au were reported in this paper. These were compared to data reported by others and with several nuclear

model calculations in which the parameter sensitivity was studied. Poenitz concluded that nuclear model calculations can represent the capture cross section of a typical fission product nucleus like Rh-103 fairly well, but that large uncertainties due to the large number of parameters can be expected, especially at higher energies, if experimental data do not exist. He noted particularly that calculations cannot give satisfactory results until optical model parameters in this range of nuclei is well established, i.e. until there is a better and more complete data base than is presently available.

# INTEGRAL CROSS-SECTION MEASUREMENTS ON FISSION-PRODUCTS IN FAST NEUTRON FIELDS

Y. D. Harker, R. A. Anderl
EG&G Idaho, Inc.
P. O. Box 1625
Idaho Falls, Idaho 83415
USA

## ABSTRACT

An integral measurement program is in progress at the Idaho National Engineering Laboratory (INEL). The major emphasis in this program is on neutron capture cross-section measurements in the Coupled Fast Reactivity Measurement Facility (CFRMF) and in the Experimental Breeder Reactor II (EBR-II). The CFRMF measurements utilize activation techniques to arrive at integral capture cross-section data and similarly the EBR-II measurements utilize isotope dilution mass spectrometry. This paper will review the status of the INEL measurement program and compare measured data with the ENDF/B derived integrals. Briefly, the results of those comparisons show that the ENDF/B IV data are the order of 25% greater than the CFRMF.

## I. INTRODUCTION

In recent years, integral data (capture reaction rates and reactivity worth measurements in fast-reactor fields) have played an important role in the evaluation of fission-product capture cross sections of importance to reactor systems. In the simplest evaluation application for isotopes with sparse or no measured differential data, integral measurements have been used to normalize the capture cross sections based exclusively from nuclear model calculations. For isotopes with a more extensive base of measured differential data, integral measurements have been used to make integral tests of cross-section curves based on the differential measurements and nuclear model calculations. Such integral tests have been helpful to the evaluator in sorting out normalization problems between differential measurements. In a more sophisticated application, integral data obtained from measurements in different spectra have been used to adjust both multigroup and/or point-wise cross sections. This latter application requires a realistic treatment of the uncertainties and correlations in the integral data and in the a-priori flux spectra and fission-product cross sections.

At two previous meetings, comprehensive review papers were given by Bustraan/1/ and Gruppelaar/2/ on the status of integral measurements in fast neutron fields and on the application of integral data in cross-section evaluation efforts. A significant fraction of the measurements covered in

those reviews dealt with the activities undertaken at the STEK facility (ECN Laboratory, The Netherlands), and, to a lesser extent at the CFRMF (Idaho National Engineering Laboratory, USA). At the time of the 1977 Fission-Product Meeting, the STEK facility had been shut down and work at the Netherlands' Laboratory was limited to data analysis and cross-section evaluation. The experimental effort at the INEL has continued, however, and this paper is based principally on the activity in our laboratory.

At the Idaho National Engineering Laboratory (USA) two facilities are available for use in fast neutron integral cross-section measurements. The first is the well-known Experimental Breeder Reactor II (EBR II), a high power test reactor used primarily for reactor fuels and materials development in the U.S. fast reactor development effort. The second is the Coupled Fast Reactivity Measurement Facility (CFRMF), a low power reactor used primarily for fast integral cross-section measurements. This paper will discuss in sufficient detail the measurements performed in the CFRMF. Because the EBR-II measurements are new and different they will be covered separately in a contributed paper at this meeting./3/

## II. MEASUREMENT TECHNIQUES

The primary interest in fission-product cross-section data is currently the capture effect, however there is some concern that the scattering effect may also be significant in high burnup fuels. Nevertheless, the major efforts both in measurements and evaluations have focused on improving capture cross-section data. Integral capture cross sections are derived primarily from three measurement techniques categorized as activation, reactivity and transmutation. In the activation technique the capture effect is based on a measurement of the specific activity of the radioactive capture product produced from an irradiation of a sample in a well-characterized neutron field. In this technique the post-irradiation analysis is done by gamma-ray spectrometry using either NaI(Tl) or Ge(Li) spectrometers. The advantages of this technique are:

1. The specific capture reaction is easily separated from other effects.

2. Small samples are usually required and need not require extensive isotope enrichment, however sample composition must be accurately known.

3. Measurements can be performed in both low and high power irradiation facilities.

The disadvantages of the technique are:

1. It is limited to those capture effects where a radioactive product is produced.

2. The accuracy of the method is limited by the quality of the decay data available for the capture product.

The first disadvantage places a constraint on the number of nuclides that can be measured by this technique and emphasizes the need for complementary techniques for other nuclides. With the advent of improved decay data, the second disadvantage is of less concern.

In measurements utilizing the reactivity techniques the sample is placed in a critical assembly and the reactivity effect due to the introduction of the sample is measured. By careful analysis, this effect can be

evaluated in terms of the capture and scattering contributions. The advantages of this technique are:

1. Method applies to almost any material so long as sufficient quantities (∿ grams) are available.

2. Depending on the core makeup the data may have direct application in reactor design and analysis.

The disadvantages of the technique are:

1. Separation of capture and scattering effects is difficult and relies extensively on reactor physics calculations.

2. Availability of gram quantities of certain materials places a constraint on the nuclides that can be studied.

3. High isotope enrichment in the sample is generally required.

The third technique known as "transmutation" is similar to activation, however in this case the capture product need not be radioactive. In a transmutation measurement the amount of the capture product produced is measured by mass spectrometry. The advantages of the activation technique also apply to transmutation, however the sensitivity of current state-of-the-art mass spectrometry dictates that high-power irradiation facilities be used and that the samples be of ultra-high isotopic enrichment.

All three techniques are applied in the INEL integral measurement program for fission products. The results over the course of the program using the activation technique will be reviewed in this paper. The use of transmutation has been applied recently in the EBR-II irradiation experiment. Reactivity measurements in the CFRMF have been performed using enriched samples from the isotope pool at Oak Ridge National Laboratory, however the high scattering sensitivity of CFRMF tends to make this effect dominent. Consequently, the reactivity measurements have not been applied to capture cross section determinations, but may play a significant role in evaluating scattering cross-section data for fission products.

## III. THE COUPLED FAST REACTIVITY MEASUREMENTS FACILITY (CFRMF)

The CFRMF is a zoned-core critical assembly with a fast-neutron spectrum zone in the center of an enriched $^{235}U$, water-moderated thermal "driver." The core is located in a large pool about 4.5 m beneath the surface. The concept, preliminary considerations, and most details of the CFRMF have been documented./4-9/ Originally designed as a high-precision static-reactivity measurements facility operating at a flux level of approximately $10^8$ n/cm$^2$-sec, the CFRMF has more recently found much use in the fast breeder reactor program as a fast-neutron field for the irradiation of materials of interest at flux levels up to approximately $10^{12}$ n/cm$^2$-sec.

Figure 1 is a cutaway pictorial diagram of the CFRMF. The core has quadrantal symmetry with respect to structural assembly and fuel loading. The thermal driver zone fuel elements are conventional plate elements of aluminum-clad, fully enriched (approximately 93%) $^{235}U$. The fueled portion of the core is 60.96 cm long, and each element is 8.183 cm square.

The fast zone at the center of the reactor is produced by means of a water-tight assembly which "filters" or "tailors" the neutron energy spectrum from the thermal driver. In the filter assembly the boron in the boral plates attenuates the neutrons below approximately 1 keV by absorption. The $^{235}U$

annulus has no significant effect on the real flux spectrum other than supplying some fast-fission neutrons, but this annulus does affect the importance function (adjoint flux) which is of concern in reactivity measurements.

When the CFRMF functions as a high-precision irradiation facility, the power-level control system must reproducibly establish the desired neutron level and energy spectrum without changing the flux distribution at the location of the experiment. Control device locations are shown in Figure 1. The safety rods are not used for normal operation control purposes and are completely out-of-core during irradiations. The shim rod, a 1-mm-thick, 15.24-cm X 60.96-cm cadmium plate on a flat surface parallel to the core, is

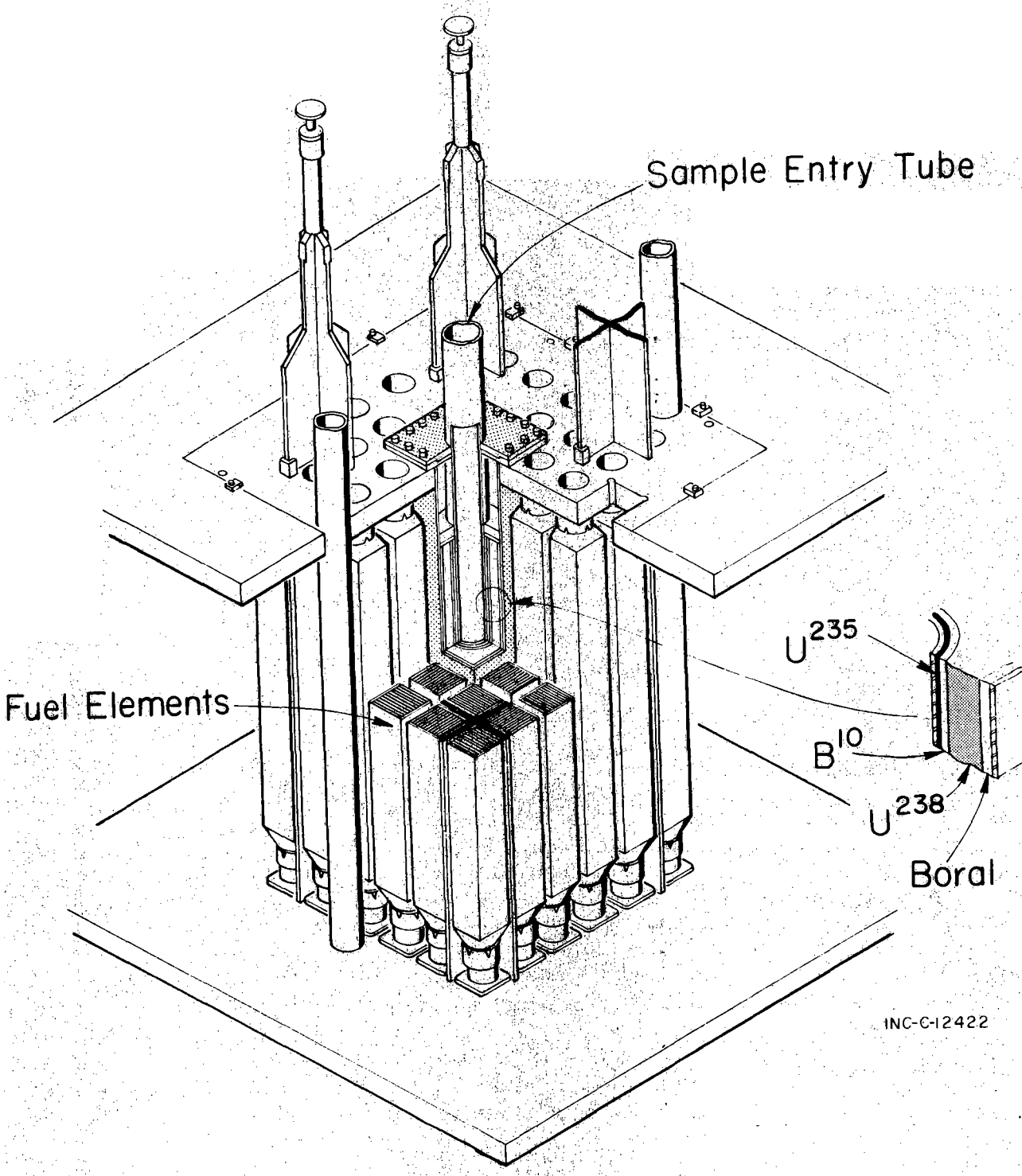


Figure 1 Pictorial View of CFRMF

always set at the same position for related irradiations and can be repositioned to within $\pm 5 \times 10^{-4}$ of a degree of rotation (equivalent to $1.5 \times 10^{-7}$ $\Delta k/k$), which causes no detectable changes in the flux distribution in the experiment region.

The power of the CFRMF is maintained at a constant and preset level by means of a conventional dc servo system. This servo system is composed of a boron-lined compensated ion chamber (CIC), appropriate amplifiers, a reference voltage source, and a torque motor-driven regulating rod. The regulating rod, under servo control, is capable of holding the power level steady to better than $10^{-6}$% at low power levels, at which reactivity measurements are done. At the power levels normally used for irradiations, the flux level deviations are approximately $\pm$.01%. Day to day reproducibility of the power level is $\pm$.5% when no changes are made in the instrumentation configuration.

A considerable effort has been directed to characterize the neutron environment in the experiment region of the fast zone. Neutron spectrometry using proton-recoil proportional chambers and $^{6}$Li coated semi-conductor diodes have been applied/6-9/ as well as multiple-foil and conventional neutron dosimetry. Reactor physics calculations utilizing transport, Monte Carlo and resonance computer codes have been used to generate the neutron spectrum and investigate its dependency on neutron cross section variations and modeling approximations. Comparisons of the spectrum measurements with calculations are given in references 6-8. The current recommended spectrum for the midplane position in the experiment region is that derived from a 1D, P1, S6 transport calculation using ENDF/B IV data (Figure 2). A new series of calculations using ENDF/B V is about to commence and a new spectrum will undoubtedly be recommended. It is expected, however, the nature of the changes from the current to the new spectrum will not alter significantly the calculated spectral averaged cross sections for fission product capture effects.

The degree to which calculated spectral-average cross sections, derived using the current spectrum agree with corresponding measured values is demonstrated in a comparison made with 21 threshold, resonance, and broad response reactions on the ENDF/B IV dosimetry file./9/ In this case the overall agreement is in the neighborhood of 5%. However, for many standard reactions the agreement is much better.

## IV. CAPTURE CROSS-SECTION MEASUREMENTS

Integral capture cross sections have been measured in the CFRMF for 39 reactions involving 33 intermediate-mass nuclides. These measurements were made by the activation technique and utilized either NaI(Tl) or Ge(Li) gamma spectrometers. An earlier report summarizes the results of our original analyses and details the sample descriptions./9/ The integral data presented in reference 9 were based on somewhat outdated decay-data information and were referenced to either the $^{197}$Au(n,$\gamma$) or $^{235}$U(n,f) spectral-averaged cross sections. As part of the preparation of this paper all of the earlier measurements were re-evaluated and re-analyzed. The results of the re-analyses which included the use of current decay data and a more consistent flux normalization scheme are detailed in this paper.

The source of the decay data used to update the original analyses is the INEL Decay Data Master File /10/ from which the ENDF/B-V decay data are taken. These data are tabulated in Table I for the reactions of interest in this paper.

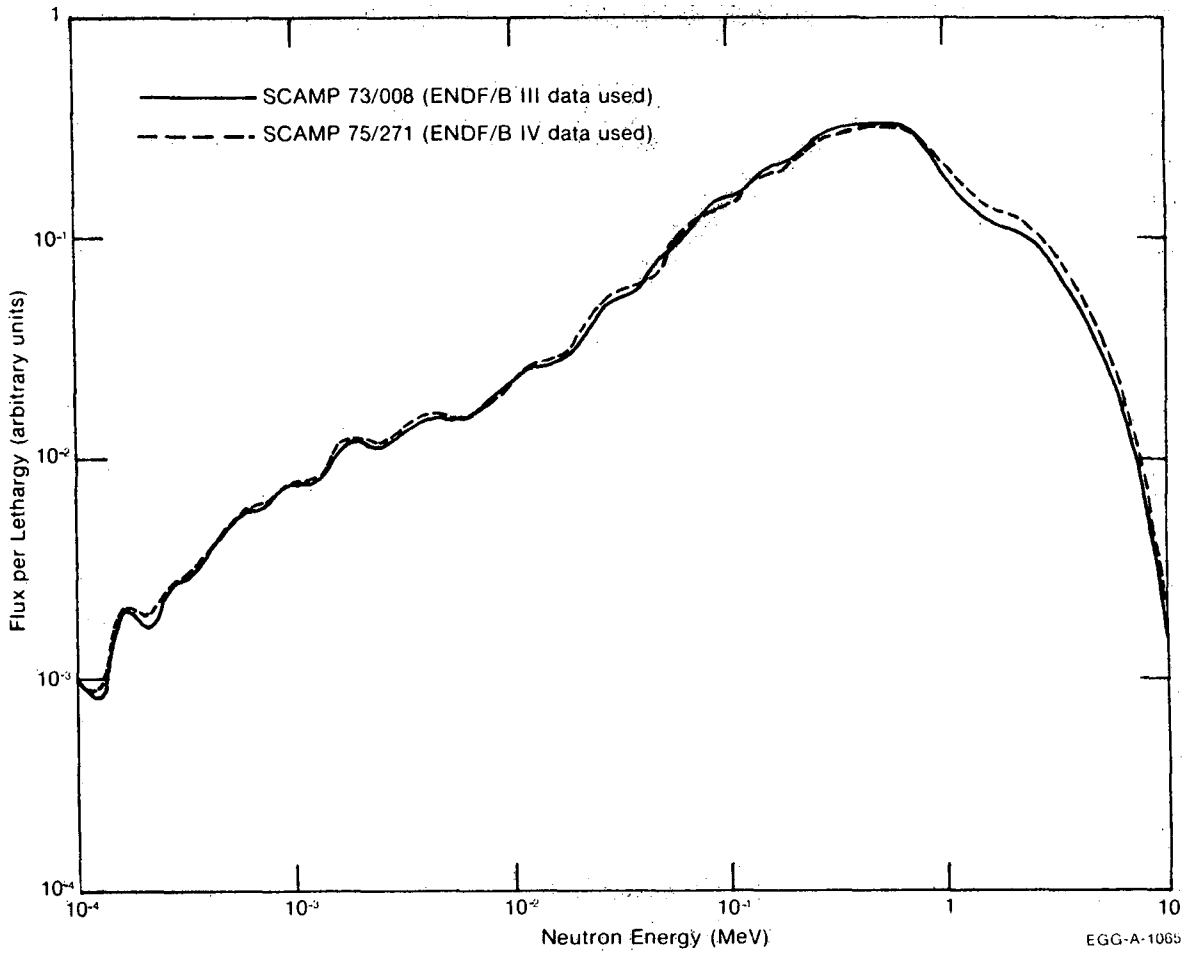


Figure 2 CFRMF Neutron Spectrum

As part of our reanalyses, absolute integral cross sections were derived from the reevaluated fission-product reaction rates and a more consistent flux normalization scheme.

The flux normalization procedure is based on the correlation of measured reaction rates for the gold monitors which accompanied each FP experiment with neutron flux measurements made as part of the Interlaboratory LMFBR Reaction Rate (ILRR) program./11, 12/ Listed in Table II are the data which are used to trace each measurement in the program to an absolute flux level and therefore to a determination of absolute cross sections. From the data presented in Table II the absolute flux was determined from each fission product monitor reaction rate. The uncertainty for each flux determination using this technique is ±3.3%.

TABLE I

Decay Data Used in Analysis of Activation Measurements

| Nuclide | $t_{1/2}$ | $E_\gamma$(keV) | $I_\gamma$(abs.)[a] |
|---|---|---|---|
| $^{88}Rb$ | 17.8m | 898.03 | .145(6.4%) |
| | | 1836.00 | .221(6.4%) |
| $^{90m}Y$ | 3.19h | 202.51 | .9658(.19%) |
| | | 479.53 | .9071(.077%) |
| $^{94m}Nb$ | 6.26m | 871.10 | .0048(21%) |
| $^{100}Tc$ | 15.8s | 539.59 | .070(10%) |
| | | 590.83 | .057(12%) |
| $^{99}Mo$ | 66.0h | 739.48 | .1215(66%) |
| | | 140.51 | .4909(.082%) |
| $^{101}Mo$ | 14.6m | 191.93 | .173(6.9%) |
| $^{103}Ru$ | 39.28d | 497.08 | .8640(2.8%) |
| $^{105}Ru$ | 4.44h | 724.21 | .4740(1.3%) |
| $^{108}Ag$ | 2.37m | 433.93 | .0054(17%) |
| | | 632.98 | .0175(17%) |
| $^{110}Ag$ | 24.6s | 657.75 | .0450(4.4%) |
| $^{110m}Ag$ | 249.9d | 657.75 | .9474(1.0%) |
| | | 763.93 | .2236(1%) |
| | | 884.67 | .7286(1%) |
| | | 937.48 | .3431(1%) |
| | | 1384.27 | .2435(1%) |
| $^{109}Pd$ | 13.46h | | .0372(3.0%) |
| $^{109m}Pd$ | 4.69m | 188.90 | .5640(1.1%) |
| $^{111}Pd$ | 22.00m | 580.10 | .0087(11%) |
| $^{111m}Pd$ | 5.50h | 172.20 | .3111(3.3%) |
| $^{116m}In$ | 54.15m | 1097.30 | .5621(2.0%) |
| | | 1293.54 | .8440(2.0%) |
| | | 2112.10 | .1553(2.8%) |
| $^{122}Sb$ | 2.70d | 564.00 | .7100(5.6%) |
| | | 696.60 | .0392(5.6%) |
| | | 1188.00 | .00004 |
| | | 1257.00 | .0078(5.1%) |

Table I (cont'd)

Decay Data Used in Analysis of Activation Measurements

| Nuclide | $t_{1/2}$ | $E_\gamma$(keV) | $I_\gamma$(abs.)[a] |
|---|---|---|---|
| $^{124}Sb$ | 60.20d | 602.72 | .9792(.051%) |
| | | 722.78 | .1126(1.4%) |
| | | 1691.00 | .4880(1.6%) |
| $^{128}I$ | 24.99m | 422.91 | .1598 |
| $^{130}I$ | 12.36h | 418.01 | .3416(2.0%) |
| | | 536.09 | .9900(2.0%) |
| | | 668.54 | .9613(2.1%) |
| | | 739.48 | .8227(2.2%) |
| $^{133m}Xe$ | 2.188d | 233.18 | .1030(2.9%) |
| $^{133}Xe$ | 5.245d | 81.00 | .3718(1.9%) |
| $^{135}Xe$ | 9.09h | 249.79 | .9021(.23%) |
| $^{134m}Cs$ | 2.90h | 127.42 | .129(6.2%) |
| $^{134}Cs$ | 2.062y | 795.76 | .854(.47%) |
| | | 801.84 | .0873(.46%) |
| $^{140}La$ | 40.26h | 1596.18 | .9540(.084%) |
| $^{141}Ce$ | 32.50d | 145.44 | .4900(4.1%) |
| $^{143}Ce$ | 33.0h | 293.26 | .434(5.1%) |
| $^{142}Pr$ | 19.13h | 1575.75 | .03699(14%) |
| $^{148m}Pm$ | 41.3d | 550.10 | .9817(2.5%) |
| | | 629.9 | .9350(1.6%) |
| | | 725.60 | .3441(2.5%) |
| | | 915.30 | .1992(4.1%) |
| $^{148}Pm$ | 5.37 | 550.10 | .233(3.4%) |
| | | 914.90 | .1251(4.3%) |
| | | 1465.10 | .2218(4.5%) |
| $^{147}Nd$ | 11.06d | 91.11 | .2794(.75%) |
| | | 531.02 | .131(5.6%) |
| | | 319.41 | .01956(5.8%) |

Table I (cont'd)

Decay Data Used in Analysis of Activation Measurements

| Nuclide | $t_{1/2}$ | $E_\gamma$ (keV) | $I_\gamma$ (abs.)[a] |
|---|---|---|---|
| $^{149}Nd$ | 1.73h | 114.32 | .1878(10%) |
| | | 155.88 | .06061(9.9%) |
| | | 208.15 | .02921(12%) |
| | | 443.55 | .01504(10%) |
| | | 540.51 | .07699(10%) |
| | | 654.83 | .07344(10%) |
| | | 211.31 | .2730(6.4%) |
| $^{151}Nd$ | 12.4m | 116.76 | .4468 |
| | | 138.95 | .08246 |
| | | 170.77 | .02399 |
| | | 255.70 | .1979 |
| | | 1180.88 | .124 |
| $^{153}Sm$ | 46.7h | 103.18 | .283(2.1%) |
| $^{155}Sm$ | 22.4m | 104.26 | .679 |
| $^{152m1}Eu$ | 9.32h | 841.63 | .1460(11%) |
| | | 963.34 | .1202(11%) |
| $^{152m2}Eu$ | 96 m | 89.85 | .72(1.4%) |
| $^{152}Eu$ | 13.33y | 778.91 | .1296(.53%) |
| | | 1085.91 | .1016(.45%) |
| | | 1112.12 | .1356(.42%) |
| | | 1408.01 | .2085(.40%) |
| | | 244.28 | .2658(.71%) |
| $^{154}Eu$ | 8.6y | 723.30 | .1970(3.1%) |
| | | 1004.76 | .1740(3.3%) |
| | | 1274.45 | .355(3.1%) |

[a] I (abs.) is the absolute gamma-ray intensity in gammas per disintegration.

TABLE II

Flux Normalization

| Nominal Power | FP Au Mon. (rps/a) | ILRR Au Mon. (rps/a) | $^{235}U(n,f)$ $\phi\sigma$ (fps/a) | $\phi$ (n/cm$^2$-sec) |
|---|---|---|---|---|
| 10 KW | $4.859 \times 10^{-14}$ ($\pm$.31%) | $4.785 \times 10^{-14}$ ($\pm$.06%) | | |
| 6 KW | | $3.008 \times 10^{-14}$ ($\pm$1%) | $1.221 \times 10^{-13}$ ($\pm$1.4%) | |
| 10 KW | | | $1.9977 \times 10^{-13}$ ($\pm$1.4%) | $1.286 \times 10^{11}$[a] ($\pm$1.9%) |

[a] Referenced to NBS $^{252}Cf$ (see references 11 and 12).

The major impact of the re-analysis effort has been to reduce the uncertainties associated with the integral data. In the previous report of the integral cross-section data /9/, the quoted errors were 10% with the major contribution from the decay data. Based on the re-analysis, data summarized in the next section have errors of 5% to 7% for most reactions. The major contributiors to the errors in the new integral data are ∿5% for gamma detection efficiency and ∿3% for neutron flux determination.

## V. RESULTS

The measured integral cross-section data as well as calculated values from ENDF/B IV and/or the HEDL evaluation/13/ are given in Table III. The HEDL evaluation will eventually be part of ENDF/B V fission product file. The calculated cross sections for both evaluations are biased high compared to the measurements. This average bias for the ENDF/B IV derived integrals is 25% where as the bias for the HEDL evaluation derived results is 17%. The spread is the C/E ratios is about the same for both evaluations. The bias could be due in part to not correcting for neutron self shielding.

## VI. DISCUSSION

In this paper the status of integral cross-section measurements for fission products using the CFRMF have been reviewed. The data presented in this paper are the results of a comprehensive reanalysis of all measurements performed in the CFRMF using the activation technique. Two areas were considered in depth, the first was the updating of the radioactive decay data used in analyses of measurements and the second was a careful consideration of the treatment of errors. As a result, the quality of the measured integral data are improved overall and the uncertainties are now in the range of 5%-7%. This is an improvement over earlier reports on the data/9/ where the overall uncertainties were quoted as ∿10%. It is felt that for most reactions any additional improvement in the accuracy of the data would require new measurements using better calibrated equipment than that used in the past. At this time, better calibrated systems are used routinely in the measurement programs at INEL and with this equipment the ultimate accuracy for integral cross section measurement is ∿3%-4%.

TABLE III

Integral Capture Cross Sections (CFRMF)

| Reaction | Measured[a] σ(barns) | Calculated (ENDF/B IV) σ(barns) | ENDF/B IV C/E | Calculated (HEDL) (barns) | HEDL C/E |
|---|---|---|---|---|---|
| $^{87}Rb(n,\gamma)^{88}Rb$ | .0120(±10%) | .0119 | .98 | | |
| $^{89}Y(n,\gamma)^{90m}Y$ | $3.38\times10^{-4}$(±4.8%) | | | | |
| $^{93}Nb(n,\gamma)^{94m}Nb$ | .074(±21%) | | | | |
| $^{99}Tc(n,\gamma)^{100}Tc$ | .267(±15%) | .278 | 1.04 | .337 | 1.26 |
| $^{98}Mo(n,\gamma)^{99}Mo$ | .0564(±6.4%) | .0695 | 1.23 | .0617 | 1.09 |
| $^{100}Mo(n,\gamma)^{101}Mo$ | .055(±17%) | .0496 | .90 | .0493 | .90 |
| $^{102}Ru(n,\gamma)^{103}Ru$ | .0889(±6.6%) | .125 | 1.41 | .112 | 1.26 |
| $^{104}Ru(n,\gamma)^{105}Ru$ | .0826(±6.3%) | .0877 | 1.06 | .0829 | 1.00 |
| $^{107}Ag(n,\gamma)^{108}Ag$ | .38(±19%) | .423 | 1.11 | .404 | 1.06 |
| $^{109}Ag(n,\gamma)^{110}Ag$ | .507(±9.7%) | .306 | .60 | .436 | .86 |
| $^{108}Pd(n,\gamma)^{109}Pd$ | .144(±6.7%) | | | .154 | 1.07 |
| $^{110}Pd(n,\gamma)^{111m}Pd$ | $5.08\times10^{-3}$(±6.9%) | | | | |
| $^{115}In(n,\gamma)^{116m}In$ | .279(±4.3%) | .306 | 1.10 | | |
| $^{121}Sb(n,\gamma)^{122}Sb$ | .251(±8.3%) | .308 | 1.23 | .180 | .72 |
| $^{123}Sb(n,\gamma)^{124}Sb$ | .154(±7%) | .168 | 1.09 | .175 | 1.14 |
| $^{127}I(n,\gamma)^{128}I$ | .298(±10%) | .341 | 1.14 | .369 | 1.24 |
| $^{129}I(n,\gamma)^{130}I$ | .184(±6.6%) | .233 | 1.27 | .218 | 1.19 |
| $^{132}Xe(n,\gamma)^{133}Xe$ | .0439(±7.7%) | | | | |
| $^{134}Xe(n,\gamma)^{135}Xe$ | .0146(±6.9%) | .0241 | 1.65 | | |
| $^{133}Cs(n,\gamma)^{134}Cs$ | .276(±6.6%) | .302 | 1.09 | .301 | 1.09 |
| $^{137}Cs(n,\gamma)^{138}Cs$ | .09(±25%) | | | | |
| $^{139}La(n,\gamma)^{140}La$ | .0176(±5.2%) | | | .0220 | 1.25 |
| $^{140}Ce(n,\gamma)^{141}Ce$ | $8.4\times10^{-4}$(±6.7%) | .0139 | 16.5 | | |
| $^{142}Ce(n,\gamma)^{143}Ce$ | .0184(±7.4%) | .0249 | 1.35 | | |
| $^{141}Pr(n,\gamma)^{142}Pr$ | .073(±15%) | .102 | 1.40 | .075 | 1.03 |

Table III (cont'd)

Integral Capture Cross Sections (CFRMF)

| Reaction | Measured[a] σ(barns) | Calculated (ENDF/B IV) σ(barns) | ENDF/B IV C/E | Calculated (HEDL) (barns) | HEDL C/E |
|---|---|---|---|---|---|
| $^{147}Pm(n,\gamma)^{148}Pm$ | .641(±13%) | .777 | 1.21 | .790 | 1.23 |
| $^{146}Nd(n,\gamma)^{147}Nd$ | .058(±6.5%) | .0912 | 1.57 | .0867 | 1.49 |
| $^{148}Nd(n,\gamma)^{149}Nd$ | .089(±14%) | .163 | 1.83 | .123 | 1.39 |
| $^{150}Nd(n,\gamma)^{151}Nd$ | .0666(±12%) | .146 | 2.19 | .169 | 2.54 |
| $^{152}Sm(n,\gamma)^{153}Sm$ | .277(±6.4%) | .300 | 1.08 | .174 | .63 |
| $^{151}Eu(n,\gamma)^{152}Eu$ | 2.39(±5.8%) | 2.28 | .95 | | |
| $^{153}Eu(n,\gamma)^{154}Eu$ | 1.45(±7.04%) | 1.42 | .98 | | |

[a] These values do not include corrections for neutron resonance self-shielding.

The measured integral cross sections presented in this paper were also compared with calculated values using differential cross section from the ENDF/B IV fission product file and from the HEDL evaluation which will be part of the ENDF/B V fission product file. The calculated data are on the average 25% greater than the measured data for ENDF/B IV source data and 17% greater for the HEDL source data. The spread in C/E's is approximately 30% for both cases. Biases of this magnitude are not observed in similar comparisons involving measurements and calculations for reactor dosimetry materials and the spread in C/E's for the latter is considerably less ( 5%). The larger differences are, however, expected for fission product comparisons. Comparisons using dosimetry reactions serve to eliminate any doubt about an inherent bias in our application of the activation technique. One effect which could count significantly toward explaining the bias is neutron self-shielding in the sample. This can be accounted for in the calculations and there has been some attempt to do this in the HEDL generated integrals. Experimentally, self-shielding can be eliminated by using progressively smaller (thinner) samples and with the current power level (≃100 KW) of the CFRMF this is certainly a possibility in future measurements.

In reviewing the existing integral cross section data from CFRMF measurements it would appear that new measurements for $^{98}Tc$, $^{100}Mo$, $^{107}Ag$, $^{109}Ag$, $^{127}I$ and Nd isotopes should be considered. Recommendations from this meeting concerning these and possibly other nuclides would certainly carry much weight in the direction the INEL program will take.

Scattering effects from fission products in high burnup fuels is considered by some to be significant in such considerations as the changes in the sodium void coefficient versus burnup. This meeting should address the

reality of these effects and determine requirements for fission product scattering data. The role that measurements can play should be discussed. As an example, the reactivity data from the CFRMF is dominated by scattering effects and consideration should be given as to what extent these data may be of benefit in the evaluation of scattering data.

Transmutation measurements using EBR-II or FFTF as an irradiation source is a new method available to the INEL program. Currently measurements have successfully been applied to Nd, Sm and Eu isotopes and future measurements for Zr, Ru, Pd and Mo isotopes are being proposed. The capabilities in ultra-high enrichment isotope separation, high sensitivity mass spectrometry and advanced neutron dosimetry are combined to produce integral data of sufficient quality to use in the evaluation effort. This is demonstrated in a contributed paper to be presented at this meeting.

CFRMF and STEK integral data have been used by Schenter/13/ and Gruppelaar/2/ in data evaluations. It has been stated that for most reactions where measurements have been performed in both facilities good consistency has been observed between CFRMF and STEK data. The combination of CFRMF and STEK data along with the results from the EBR II irradiations and other integral measurements measured differential data where available form the basis for performing data adjustments in the evaluation process. This aspect of data evaluation is coming of age and maturing in its degree of sophistication. As such it is placing more stringent requirements on the measurements in that supporting covariance information must be provided and generally better accuracy is being sought. The CFRMF in its role as a benchmark for fission product, actinide and dosimetry data in the U.S. evaluation effort is slated for sensitivity analysis on the derived neutron spectrum. As such supporting covariance information will be available. Combined with the improved accuracies currently obtainable, the CFRMF is expected to continue to play a significant role in the evaluation effort.

## REFERENCES


1a. M. Bustraan, "Integral Determination of Neutron Absorption by Fission Products," RP 14 IAEA Panel On Fission-Product Nuclear Data, Bologna, Italy, (26-30, November, 1973).

1b. M. Bustraan, "Integral Determination of FP Neutron Cross-Sections," RP 14, Second IAEA Advisory Group Meeting on Fission-Product Nuclear Data, ECN Petten, Netherlands (5-9 September 1977).

2. H. Gruppelaar, "Impact of Integral Measurements on the Capture Cross-Section Evaluations of Individual Fission Product Isotopes," RP8, Second IAEA Advisory Group Meeting on Fission Product Nuclear Data, ECN Petten, Netherlands (5-9 September 1977).

3. R. A. Anderl, Y. D. Harker, F. Schmittroth, "Neodymium, Samarium and Europium Capture Cross-Section Adjustments Based on EBR-II Integral Measurements," NEANDC Specialists' Meeting on Neutron Cross Sections of Fission Product Nuclei, CNEN, Bologna, Italy (2-14 December 1979).

4. E. Fast, C. L. Beck, D. A. Millsap, R. G. Nisle, JW Rogers and J. J. Scoville, Use of ARMF for a Fast Reactor Support Program. I-N1143 (November 1967).

5. E. E. Burdick, E. Fast, and D. W. Knight, The Advanced Reactivity Measurements Facilities, IDO-17005 (October 1964).

6. JW Rogers, D. A. Millsap, and Y. D. Harker, CFRMF Neutron Field Flux Spectral Characterization, Nuclear Technology 25, 330 (February 1975).

7. JW Rogers, Y. D. Harker, and D. A. Millsap, "Fast Neutron Spectrum and Dosimetry Studies in the CFRMF," First ASTM-EURATOM Symposium on Reactor Dosimetry (September 1975). EUR 5667e/f, Part II pp 277-298.

8. G. DeLeeuw-Gierts, S. DeLeeuw, H. H. Helmick and JW Rogers, "Neutron Spectrometry Data in LMFBR Benchmark and Standard Neutron Fields" First ASTM-EURATOM Symposium on Reactor Dosimetry, (September 1975). EUR 5667e/f, Part I pp 99-118.

9. Y. D. Harker, JW Rogers, D. A. Millsap, Fission Product and Reactor Dosimetry Studies at Coupled Fast Reactivity Measurements Facility, TREE-1259/ENDF-266, (March 1978).

10. R. L. Bunting, C. W. Reich private communication.

11. R. C. Greenwood, R. G. Helmer, JW Rogers, R. J. Popek, R. R. Heinrich, N. D. Dudey, L. S. Kellog and W. H. Zimmer, "Radiometric Reaction-Rate Measurements in CFRMF and Big-10," NUREG/CP-0004, Vol 3, 1207 (1978).

12. JW Rogers, Y. D. Harker, D. A. Millsap, I. E. Stepan, "Reactor Dosimetry Studies of the Coupled Fast Reactivity Measurements Facility (CFRMF)," NUREG/CP-0004, l/o 13, 1237 (1978).

13. R. E. Schenter, private communication.

# MEASUREMENTS OF CAPTURE CROSS SECTIONS IN THE FP MASS REGION

N. Yamamuro
Research Laboratory for Nuclear Reactors, Tokyo Institute of Technology
O-okayama, Meguro-ku, Tokyo, Japan
and
A. Asami
Japan Atomic Energy Research Institute
Tokai-mura, Ibaraki-ken, Japan

Neutron capture cross sections of the following FP nuclides have been measured. For $^{93}$Nb, $^{127}$I and $^{133}$Cs, $C_6F_6$ and $C_6D_6$ scintillation detectors at the 12-m flight path of the KURRI linac TOF spectrometer were used. For $^{143}$, $^{145}$, $^{146}$, $^{148}$Nd, $^{147}$, $^{149}$Sm, Eu, and $^{151}$, $^{153}$Eu, a large liquid scintillator tank at the 52-m path of the JAERI spectrometer was used. The energy range covered in the measurements is above 3 keV until 100 keV or 300 keV. Transmission and capture measurements were made of 79, $^{81}$Br, $^{147}$, $^{149}$Sm and $^{159}$Tb in the resonance energy region. The resonance parameters of more than 150 levels were obtained for each nuclide except $^{81}$Br, for which those of 100 levels were determined.

## 1. Introduction

The significance of nuclear data on fission product nuclides is well recognized, and for these years a considerable effort has been put forth to measure neutron cross sections of some of the most important fission product nuclides. Although there are many kinds of fission product, about 40 nuclides, which are of higher fission yields, account for 95% of all neutron absorbing rate in a core of fast reactor. The good accuracy for capture cross section of these important nuclides is requested, buy some data show the appreciable discrepancies between the experimental results.

Our experiments have separately been performed by two research groups, using the different gamma-ray detectors and the different method of absolute normalization of cross sections. Including the $^{133}$Cs and $^{149}$Sm, those are ranked in the class of highest contribution to capture rate, the capture cross sections of $^{93}$Nb, $^{127}$I, and $^{133}$Cs /1/ were measured in the keV region with non-hydrogeneous liquid scintillation detectors at the Kyoto University Research Reactor Institute and the capture cross sections of $^{143}$, $^{145}$, $^{146}$, $^{148}$Nd /2/, natural Eu /3/, $^{151}$, $^{153}$Eu /4/, and $^{147}$, $^{149}$Sm /5/ were measured in the keV-region with a large liquid scintillator tank at the Japan Atomic Energy Research Institute. In addition to the keV capture cross

sections, the transmission and capture measurements for $^{79,81}Br$ /6/, $^{147,149}Sm$ /5/, and $^{159}Tb$ /7/ were carried out in the resonance region with a $^{6}Li$-glass scintillator and a Moxon-Rae detector and the resonance parameters of many levels were obtained.

Because of its importance for an accurate cross section measurement in the keV region, attention was particularly paid to determination of the background, and techniques were devised by each group and successfuly applied. The methods of experimental and data analysis for both groups are discribed in Sections 2 and 3, and the results and discussions in Section 4.

## 2. Experiment and Data Analysis at KURRI

The KURRI 46-MeV linac was used as the neutron generator for the measurements of capture cross sections in the keV region with time-of-flight method. At the 11.7 m from the neutron source, samples were placed and capture gamma-rays were detected with $C_6F_6$ or $C_6D_6$ liquid scintillation detectors. The absolute value of the capture cross sections can be determined by the two types of measurements. One is the absolute measurement at one-energy point by the use of an iron-filtered beam, and the other is the measurement of cross section shape as a function of neutron energy between the resonance energies of notch filters, sodium (2.85 keV) and sulfur (103 keV).

The measurement of absolute capture cross sections near 24 keV has been described in some detail in earlier paper /8/, so that the principle of the method is briefly explained here. A sample was irradiated with an Fe-filtered neutron beam and the emitted gamma-ray spectrum was measured. Multiplying the observed spectrum C(E) by the weighting function W(E), previously prepared for the detector used, the weighted spectrum can be obtained which satisfies the formula

$$\Sigma\ C(E)\cdot W(E) \approx \Phi\cdot Y\cdot (BE), \qquad (1)$$

where $\Phi$, Y and (BE) are the neutron flux incident on a sample, the capture yield and the neutron binding energy of the compound nucleus. If we measure the incident flux, the capture yield of a sample can be calculated by using the well known constant (BE). The error of the pulse height weighting technique is shown to be within the 2% /9/.

The neutron flux was derived from the measurement of a $^{10}B$ sample. The gamma-ray emission probability of the $^{10}B$ sample $Y_B$ was estimated from $^{10}B(n,\alpha)$ cross section and the branching ratio of $^{10}B(n,\alpha\gamma)$ reaction using Monte-Carlo calculation for multiple scattering correction. To determine the detection efficiency of the detector for the 480-keV gamma-ray, the counts for the gamma-rays from $^{10}B$ was compared with those from a silver plate at the neutron energy of 5.2 eV, where a "black" capture resonance of $^{109}Ag$ exists. Table I shows the exprimental results of 24-keV capture cross section measurements for the nuclides in the FP mass region.

The relative measurements have been performed by replacing the iron-filter with a sodium and a sulfur notch filter in the neutron beam. In the biginning of the experiment, the neutron sensitivities of $C_6F_6$ detector mounted on an EMI-9818 photomultiplier and $C_6D_6$ detector viewed by a RCA-4525 photomultiplier were compared by counting the background gamma-rays emitted from surrounding materials, which were due to capture the scattered neutrons with carbon scatterer. As the result of the measurement, it was seen that the $C_6D_6$ detector system had about three times lower sensitivity than that of $C_6F_6$, as shown in Fig. 4. The over-all 1/v dependence of neutron sensitivity can be seen, except near the resonance of sulfur notch filter.

The time dependent background was assumed to be $aI^{-b}$, where a and b are constants determined from the counts corresponding to sodium and sulfur resonances and I is the channel number of the time analyzer. The background due to neutrons scattered by the sample, which is determined in proportion to the neutron sensitivity of the detector, was also subtracted.

For samples of $^{127}I$ and $^{133}Cs$, lead-iodide ($PbI_2$) and cesium-oxide ($Cs_2O$), encapsulated in an aluminum can, were used respectively. The experimental conditions and thicknesses for each sample are summarized in Table I.

In order to obtain the absolute cross sections from the relative capture yields, we calculate the normalization factor R with

$$R = \frac{\overline{Y}_{24}}{\overline{Y}_R} ,$$

where

$$\overline{Y}_R = \frac{\Sigma\, Y_R(I)\Phi(I)}{\Sigma\Phi(I)} , \qquad (2)$$

and $\overline{Y}_{24}$ is the absolute yield near 24 keV determined with the Fe-filtered neutron beam, $Y_R(I)$ shows the relative capture yield in the channel I, and $\Phi(I)$ the profile of the Fe-filtered beam. The summations in the eq. (2) were performed over the range in which the absolute yield $\overline{Y}_{24}$ was calculated. The absolute yields from 3.2 keV to 80 keV could be obtained by multiplying the relative capture yield by the normalizing factor R and these yields were summed up over channels covering the required energy intervals. For $^{133}Cs$, the experiment without sulfur filter was carried out, so that the data to 270 keV were given.

The resonance self-shielding and multiple scattering corrections for the neutrons in the sample were made by the method of Dresner /10/ and Macklin /11/ with the appropriate cross sections and parameters of s- and p-wave resonances. The uncertainty in the correction factors is estimated to be about 2% /11/, but for $^{93}Nb$, the uncertainty becomes larger in the energy range below 20 keV, because the sample thickness approachs to 0.2 of a mean free path which is the range of applicability of the correction.

## 3. Experiment and Data Analysis at JAERI

### 3.1 Method

Neutrons are produced with the 120-MeV JAERI linac, which has been gradually improved from the original 1A peak current with the energy of 100 MeV /12/ to the present 3A peak current with the energy of 140 MeV for a 30 nanosecond pulse width.

A block diagram of the detector and associated electronic circuits used for the keV capture cross section measurements is shown in Fig. 1. The length of neutron flight path is 52 m. A capture event is detected with a 3500-l liquid scintillator tank viewed by four EMI-9545B photomultipliers. Two sample changers are used, one at the center of the tank with a sample and a scattering sample (lead) mounted on it, and the other about 10 m from the neutron producing target. The neutron flux is measured with a $^6Li$-glass or a $^{10}B$-NaI(Tl) detector placed about 4-m downstream from the sample in the neutron beam. In our detector system the $^6Li$-glass detector has a higher detection efficiency than the $^{10}B$-NaI detector, and is used in the low energy region; the $^{10}B$-NaI detector has detection efficiency varying more smoothly in

the higher energies than the $^6$Li-glass detector whose efficiency depends on the large resonance at 250 keV in $^6$Li.

In average capture cross section measurement in the keV region, it is essential to determine the background exactly in order to obtain the accurate cross section values, because its determination is ambiguous and the signal to background ratio is much lower in the keV region than in the resonance region. The black resonance technique used for this determination is not sufficiently accurate, and therefore a new technique was developed which is similar to that described in ref /13/; the background is estimated by analyzing five neutron TOF spectra. Neutron and capture TOF spectra were measured for all combinations of the two sample changers; each combination amounts to eight spectra, six for capture cross sections and the other two for the transmission values as shown in Fig. 3. The details are described in Ref. /2/.

In the resonance energy region measurements were mainly made at flight path lenght 47 m with the detectors positioned as in Fig. 2 /7/. In these measurements no sample changer was used, because the signal to background ratio is higher than in the keV region measurements at flight path 52 m, and the neutron flux was always accurately measured with a transmission type monitor set about 2-m upstream of the sample as shown in Fig. 2. In the case of $^{81}$Br, an intermideate structure in the resonance level was observed as described in Section 4, so that higher-resolution transmission measurements were made to examine the structure clearly with a neutron detector /12/ at flight path 190 m.

A little more detailed experimental conditions for respective samples are shown in Table II. The isotope samples are enriched ones, loand from ORNL.

3.2 Data analysis of capture cross sections

Neutron capture yield is calculated from the relation

$$Nc = \Phi \cdot Y \cdot \eta, \qquad (3)$$

where Nc is capture count, $\Phi$ the neutron flux, Y the capture yield, and $\eta$ the efficiency of capture detector. Y is a function of neutron capture cross section and given by

$$Y = (1-e^{-n\sigma}t) \cdot \sigma_c/\sigma_t \cdot (1+f), \qquad (4)$$

where n is the thickness of the sample, $\sigma_t$ and $\sigma_c$ are the total and capture cross sections, and f is a correction factor for the multiple scattering effect in the sample. In obtaining $\Phi$, the neutron detector efficiency is calculated with a multiple scattering correction, which was made by Schmitt's method /14/ or a Monte Carlo method /15/. The calculation of eq. (4) for the effects of multiple scattering and self-shielding of the sample was made similarly to the above and with the appropriately evaluated cross section values or by the method of Dresner /10/ and Macklin /11/.

In order to obtain the absolute capture cross section values, the relative cross sections were normalized at suitable saturated resonances at low energies, where Monte Carlo calculations /16/ were made to give exact capture yields for Y in eq. (3). The efficiency $\eta$ was assumed to remain constant over the region of measurement including the saturated resonances.

### 3.3 Resonance analysis

Transmission and capture data were analyzed for all samples except the samarium isotopes, with a modified Atta-Harvey program /17/ and a CAFIT program /18/ respectively. In the CAFIT program Monte Carlo method is used to calculate the multiple scattering effect on the capture yield. For samarium isotopes, the transmission data were analyzed with a SIOB program /19/, based on the multi-level Breit-Wigner formula, and the capture data with TACASI program /20/.

Combining the transmission data of different sample thicknesses with the capture data yielded $\Gamma_\gamma$ values of resonances in favourable cases, and also spin values in more favourable cases.

## 4. Results and Discussions

In the keV region, the average capture cross sections of $^{93}$Nb, $^{127}$I, and $^{133}$Cs were obtained at KURRI and those of natural Eu, $^{151}$, $^{153}$Eu, $^{143}$, $^{145}$, $^{146}$, $^{148}$Nd, and $^{147}$, $^{149}$Sm were determined at JAERI. In the resonance region, the resonance parameters of many levels, average level spacings, and s-wave strength functions were obtained for $^{159}$Tb, $^{79}$, $^{81}$Br, and $^{147}$, $^{149}$Sm at JAERI. In the following, the experimental results are discussed and compared with other data.

The discrepancies between $^{93}$Nb(n,$\gamma$) data, shown in Fig. 5, are relatively large. Gibbons et al. /21/ used 760 ± 50 mb for the In(n,$\gamma$) cross section at 30 keV for the absolute normalization. Kompe /22/ obtained the capture cross section relative to that of $^{197}$Au determined by himself. It seems that these differences of the reference cross sections cause the discrepancies in both the absolute values and the gradient with neutron energy. The present data agree with the Macklin's data /23/ except at lower energy region.

Fig. 6 shows the $^{127}$I(n,$\gamma$) cross sections, which are fairly in agreement /24/~/25/, except for Stavisskii's data /26/. The systematically higher values of this data seems to come from the values of his reference cross section, $^{235}$U(n,f).

Cesium is one of the most important fission product nuclide and the agreement between the data of capture cross sections is poor. Our previous 24-keV capture cross section was 580 ± 35 mb /27/. After that, we remeasure the capture cross section using thicker iron-filter, thicker sample and lower neutron sensitive $C_6D_6$ detector system, resulting in 24-keV capture cross section of 630 ± 35 mb. Normalizing the cross section to this new absolute value, the $^{133}$Cs(n,$\gamma$) cross sections above 3.2 keV until 270 keV have been determined, as shown in Fig. 7. The result shows the agreement with Popov and Shapiro's data /24/ in the region overlap one another. The evaluated values of JENDL-1 almost follow these cross sections, but Booth's /28/, and Kompe's experimental data /22/, and ENDF/B-IV show higher values. Fujita et al. /29/ have measured 55-keV and 147-keV capture cross sections by the use of a silicon-filtered beam resulting in agreement with our data at 147 keV and disagreement at 55 keV.

Figs. 8(a) and 8(b) show the capture cross sections of $^{151}$Eu and $^{153}$Eu, respectively, in the neutron energy region of 3 to 100 keV together with those by Hockenbury et al. /30/, Moxon et al. /31/, and Kononov et al. /32/. Except the data of Kononov et al., agreements are reasonably good in most part of the region. The capture cross sections of natural europium are shown in Fig. 8(c) /3/, /33/. A purpose of this experiment was to obtain a normalization factor for the $^{151}$, $^{153}$Eu data shown in Figs. 8(a) and 8(b).

The results of the capture cross section measurements of neodymium isotopes are shown together with other data /34/ in Figs. 9(a) to (d). The preliminary values reported /2/ were obtained only from the experimental data with a $^{6}$Li-glass flux detector. Since that time considerable improvement has been made in efficiency calculation of this flux detector; with this refined efficiency these capture data were analyzed again and also the data taken with the $^{10}$B-NaI detector. Although the results shown in Figs. 9(a) to (d) are appreciably different from those in ref. /2/ at higher energies, the discussion made in ref. /2/ still holds in the comparison with other data /34/ previously reported.

Figs. 10(a) and 10(b) show the cross sections of $^{147}$Sm and $^{149}$Sm, respectively. As shown in the figures, there is on the whole a reasonably good agreement between the two recent data /32/,/35/ and the present one for $^{149}$Sm, but for $^{147}$Sm the data of Kononov et al. /32/ appear to be too large in both the absolute values and the slope with energy.

Concerning the resonance levels in $^{159}$Tb, the energy range covered by the previous measurements /36/ are from 3 eV to 753 eV. The present experiment extended the upper limit up to 1192 eV /7/, and in the extended region 51 levels were newly observed and analysed. In the region of overlap the parameters of 157 levels were obtained, which agreed with those previously reported /36/. In the extended region, statistical properties of the resonances are nearly the same as in the overlapped region, and a cumulative plots of $g\Gamma_n$ vs. neutron energy is well approximated by a straight line, as shown in Fig. 11. The similar plot for number of resonances continues smoothly to the extended region, showing a gradual increase in the number of missed levels.

The following average resonance parameters are obtained; the average spacing D = 4.4 eV, s-wave strength function $s_0 = (1.55 \pm 0.5) \times 10^{-4}$, and $\langle\Gamma\gamma\rangle = 107 \pm 7$ meV. The value of $s_0$ is determined in the region up to 1.2 keV and $\langle\Gamma\gamma\rangle$ is calculated from 25 levels below 238 eV.

Before the present experiment on $^{79}$Br and $^{81}$Br, resonance parameters were obtained of 157 levels in natural bromine in the region below 4 keV /37/, and isotopic identification was made for only 10 levels at low energies /37/. In the present experiment /6/ the parameters of 156 levels were obtained for $^{79}$Br in the region below 10 keV, and those of 100 levels for $^{81}$Br in the region below 15 keV; from these parameters, statistical properties of these nuclides were studied.

Average level distances are D = 45 ± 6 eV, and D = 70 ± 16 eV for $^{79}$Br and $^{81}$Br, respectively. A cumulative plot of $g\Gamma_n$ value vs. neutron energy is approximately linear for $^{79}$Br, however, for $^{81}$Br the plot shows steep rises at certain energies as shown in Figs. 12(a) and 12(b). From the figures $s_0 = (1.27 \pm 0.14) \times 10^{-4}$ for $^{79}$Br, and $s_0$ for $^{81}$Br appears to have two values, $0.54 \times 10^{-4}$ and $3 \times 10^{-4}$. However, if these intermediate structures are ignored, $s_0 = (0.86 \pm 0.14) \times 10^{-4}$ for $^{81}$Br.

For $^{147}$Sm and $^{149}$Sm resonances, parameters were previously available in the regions up to 1200 eV and to 240 eV respectively /38/. These regions were extended in the present experiment /5/ up to 2000 eV and to 520 eV, and 212 and 157 levels were analyzed, respectively. Statistical properties of these levels are similar to those in the lower regions. That is, the cumulative plot of $g\Gamma_n$ varies with energy as a smooth extention of the lower region, as shown in Figs. 13(a) and 13(b). In Fig. 13(b) the plot rises steeply at low energies, this agrees with that previously reported /38/. Average parameters are D = 5.7 ± 0.5 eV, $s_0 = (4.8 \pm 0.5) \times 10^{-4}$ for $^{147}$Sm, and they are D = 2.2 ± 0.2 eV and $s_0 = (4.6 \pm 0.6) \times 10^{-4}$ for 149Sm if simple averaging is made in the whole region in Fig. 13(b).

The authors are very grateful to Y. Fujita, K. Kobayashi of KURRI, M. Igashira of TIT, and Y. Nakajima, M. Mizumoto, Y. Kawarasaki, Y. Furuta, M. Sugimoto of JAERI for their cooperation in preparing this report. One of the authors wishes to thank K. Sugiyama of Tohoku Univ., Y. Kanda of Kyusyu Univ. for useful discussions. He also wishes to thank K. Tsukada for supporting this research and C. L. Rogosa for his considerations in procuring the enriched isotope samples.

References

/1/ N. Yamamuro et al., Proc. Int. Conf. Neutron Phys. Nuclear Data, Harwell p.432 (1979).
N. Yamamuro et al., to be published.

/2/ Y. Nakajima et al., Proc. Int. Conf. Neutron Phys. Nuclear Data, Harwell p.438 (1979).

/3/ A. Asami et al., Topical Conf. Tech. of Neutron Capture Cross Section Measurements at NEANDC Meeting, Oak Ridge, Apr. 1978.
A. Asami et al., to be published.

/4/ M. Mizumoto et al., J. Nucl. Sci. Technol., 16, 711 (1979).

/5/ M. Mizumoto et al., Neutron Radiative Capture and Transmission Measurements of $^{147}$Sm and $^{149}$Sm, Proc. Conf. Nucl. Cross Sections Tech., Knoxville (1979).

/6/ M. Ohkubo, Y. Kawarasaki, M. Mizumoto, Neutron Resonance Parameters of $^{79}$Br and $^{81}$Br up to 15 keV, Proc. Conf. Nucl. Cross Sections Tech., Knoxville (1979).

/7/ M. Ohkubo, Y. Kawarasaki, J. Nucl. Sci. Technol., 16, 701 (1979), JAERI-M 7545 (1978).

/8/ N. Yamamuro et al., J. Nucl. Sci. Technol., 15, 663 (1978).

/9/ N. Yamamuro et al., Nucl. Instrm. Methods, 133, 531 (1976).

/10/ L. Dresner, ibid., 16, 176 (1962).

/11/ R.L. Maclin, ibid., 26, 213 (1964).

/12/ H. Takekoshi et al., JAERI-1238, 1975 (in Japanese).
Y. Nakajima et al., Proc. Conf. Nucl. Cross Sections Tech., Washington, p.738 (1975).

/13/ A. Asami, Y. Nakajima, Nucl. Instrm. Methods, 147, 577 (1977).

/14/ H.W. Schmitt, ORNL-2883.

/15/ M. Sugimoto, M. Mizumoto, A. Asami, to be published.

/16/ M. Ohkubo, JAERI-M 7988 (1978).

/17/ A. Tachibana et al., JAERI-memo 3728 (1969).
A. Atta, J.A. Harvey, ORNL-3205 (1961).

/18/ M. Ohkubo, to be published.

/19/ G. de Saussure, D.K. Olsen, R.B. Perez, ORNL TM-6286 (1978).

/20/ F.H. Frohner, GA-6906 (1966).

/21/ J.H. Gibbons et al., Phys. Rev., 122, 182 (1961).

/22/ D. Kompe, Nucl. Phys., A 133, 513 (1969).

/23/ R.L. Macklin, Nucl. Sci. Eng., 59, 12 (1976).

/24/ Yu.P. Popov, F.L. Shapiro, Soviet Phys., JETP, 15, 683 (1962).

/25/ L.W. Westen et al., Annals Phys. 10, 477 (1960).

/26/ Yu.Ya. Stavisskii, Atom. Energ., 10, 158 (1961).

/27/ N. Yamamuro et al., NEANDC (J) 44L, p.65 (1976).

/28/ R. Booth et al., Phys. Rev., 112, 226 (1958).

/29/ Y. Fujita et al., Private communication (1979).

/30/ R.W. Hockenbury, H.R. Knox, N.N. Kaushal, Proc. Conf. Nucl. Cross Sections Tech., Washington, p.905 (1975).

/31/ M.C. Moxon, D.A.J. Endacott, J.E. Jolly, Ann. Nucl. Energy, 3, 399 (1976).

/32/ V.N. Kononov et al., Proc. 4th All Union Conf. Neutron Phys., Kiev, Apr. 1977.

/33/ M.C. Moxon et al., Ann. Nucl. Energy, 3, 399 (1976),
R.L. Macklin et al., Phys. Rev. 129, 2695 (1963),
J.B. Czirr, Lawrence Radiation Lab. Report UCRL 50804 (1970),
V.A. Konks, Yu. I. Fennin, Conf. Interaction of Neutrons with Nuclei, Report No 1845, Dubna p.100 (1964).

/34/ A.R. deL. Musgrove et al., AAEC/E401 (1977).
V.N. Kononov et al., Yad. Fiz. 27, 10 (1978).

/35/ R.W. Hockenbury et al., ERDA/NDC-3/U (1976).
R.L. Macklin, J.H. Gibbons, T. Inada, Nature 197, 370 (1963).

/36/ H. Derrien, M. Alix, CEA-N-1867 (1976).
A.B. Popov, H. Faikov, H. Cher Gov, Yad. Fiz. 26, 14 (1977), Sov. J. Nucl. Phys. 26, 6 (1977).
B.P. Alfimenkov et al., Yad. Fiz., 25, 930 (1977), Sov. J. Nucl. Phys. 25, 495 (1977).

/37/ J.B. Garg, W.W. Javens, J. Rainwater, Phys. Rev. 136, B177 (1964).
J. Julien et al., Nucl. Phys. 66, 433 (1965).

/38/ H.M. Eiland, S. Weinstein, K.W. Seeman, Nucl.Sci. Eng. 54, 286 (1974).
E.N. Karzhavina, A.B. Popov, Sov. J. Nucl. Phys. 15, 225 (1972).

Table I. Experimental conditions at KURRI and 24-keV capture cross sections

| Target nucleus | Energy range (keV) | Notch filters | Sample thickness ($10^{-3}$atoms/b) | $\sigma_c(24)$ (mb) |
|---|---|---|---|---|
| $^{93}$Nb | 3.2 - 80 | Na, S | 5.26(abso. meas.)<br>21.10(rela. meas.) | 340 ± 17 |
| $^{115}$In | 23.7 | | 3.64 | 770 ± 50 |
| $^{127}$I | 3.2 - 80 | Na, S | 4.96 | 780 ± 40 |
| $^{133}$Cs | 3.2 - 270 | Na, S<br>Na | 9.92 | 630 ± 35 |
| $^{165}$Ho* | 3.2 - 80 | Na, S | 6.63 | 1280 ± 60 |

* The experimental result of $^{165}$Ho from 3.2 to 80 keV is not shown in the present paper.

Table II. Experimental conditions at JAERI
(a) keV capture cross section measurements

| Sample | $^{151,153}$Eu | Eu, $^{143,145,146,148}$Nd | $^{147,149}$Sm |
|---|---|---|---|
| Neutron energy range (keV) | 3 - 100 | 5 - 300 | 3 - 300 |
| Linac energy (MeV) | 100 | 120 | 140 |
| Linac current (A) | 1 | 1.8 | 2.7 |
| Pulse repetition (Hz) | 150 | 150 | 150, 300 |
| Pulse width (nsec) | 100 | 30, 80 | 30, 80 |
| Channel width (nsec) | 100 | 25 | 25 |
| Background samples | Al, Na | $Al_2O_3$, Al<br>Na, Mn, Co | $Al_2O_3$, Al<br>Na, Mn, Co |
| Flux detector | $^6$Li-glass | $^6$Li-glass<br>$^{10}$B-NaI | $^6$Li-glass<br>$^{10}$B-NaI |

(b) Resonance region measurements

| Sample | Tb | $^{79,81}$Br | $^{147,149}$Sm |
|---|---|---|---|
| Neutron energy range (eV) | 3 - 1200 | 30 - 10.000($^{79}$Br)<br>15.000($^{81}$Br) | 1.5 - 2.000($^{147}$Sm)<br>520($^{149}$Sm) |
| Linac energy (MeV) | 100 | 140 | 140 |
| Linac current (A) | 1.8 | 2.7 | 2.7 |
| Pulse repetition (Hz) | 150 | 150, 300 | 150, 300 |
| Pulse width (nsec) | 80 | 30, 80 | 30, 80 |
| Channel width (nsec) | 125 | 31.25, 25 | 25 |
| Path length (m) | 47.08 | 47.08, 190 | 51.95 |
| Flux monitor | $^6$Li-glass* | $^6$Li-glass* | $^6$Li-glass |

* Transmission type

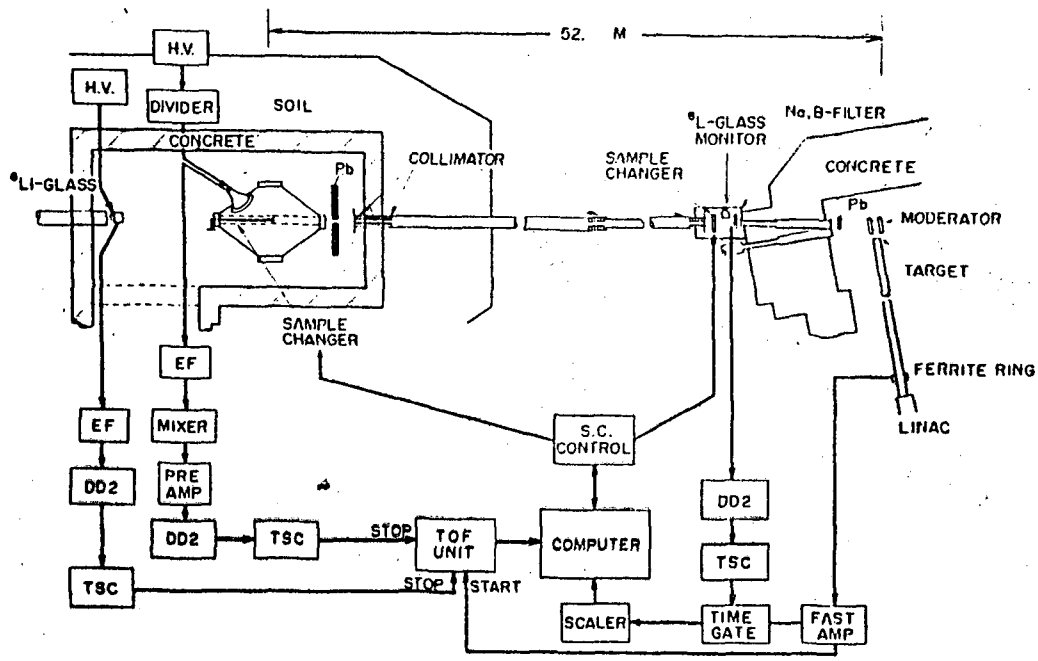


Fig. 1 Experimental arrangement at JAERI
DD2: Double delay line amp.,
TSC: Timing single channel discri.,
EF: Emitter follower

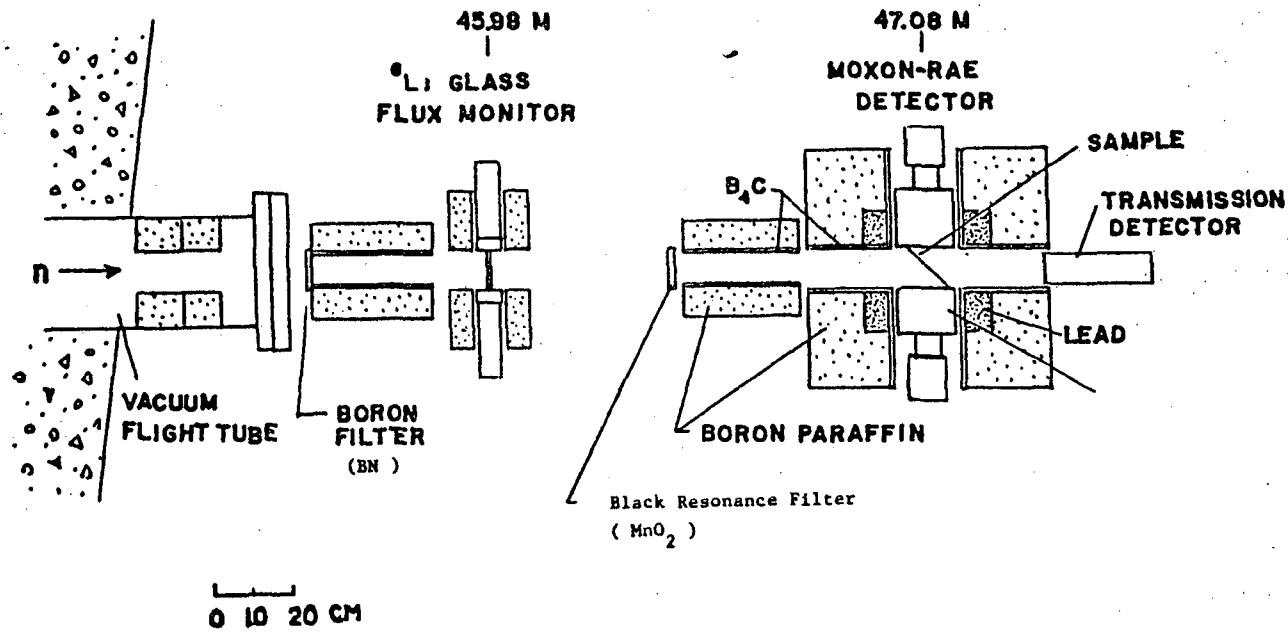


Fig. 2 Arrangement in the 47-m station

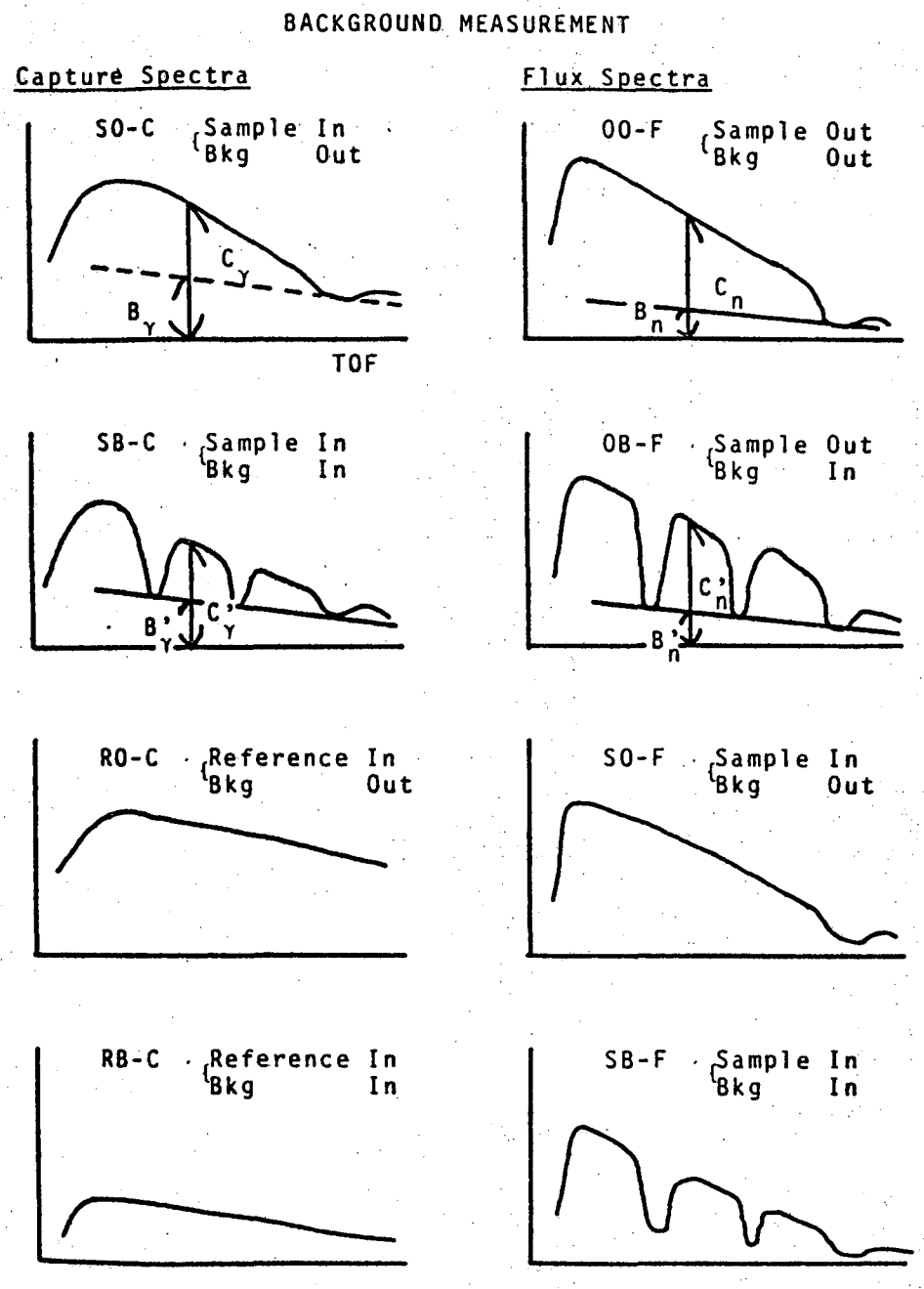


Fig. 3 Schematic figures of background measurement

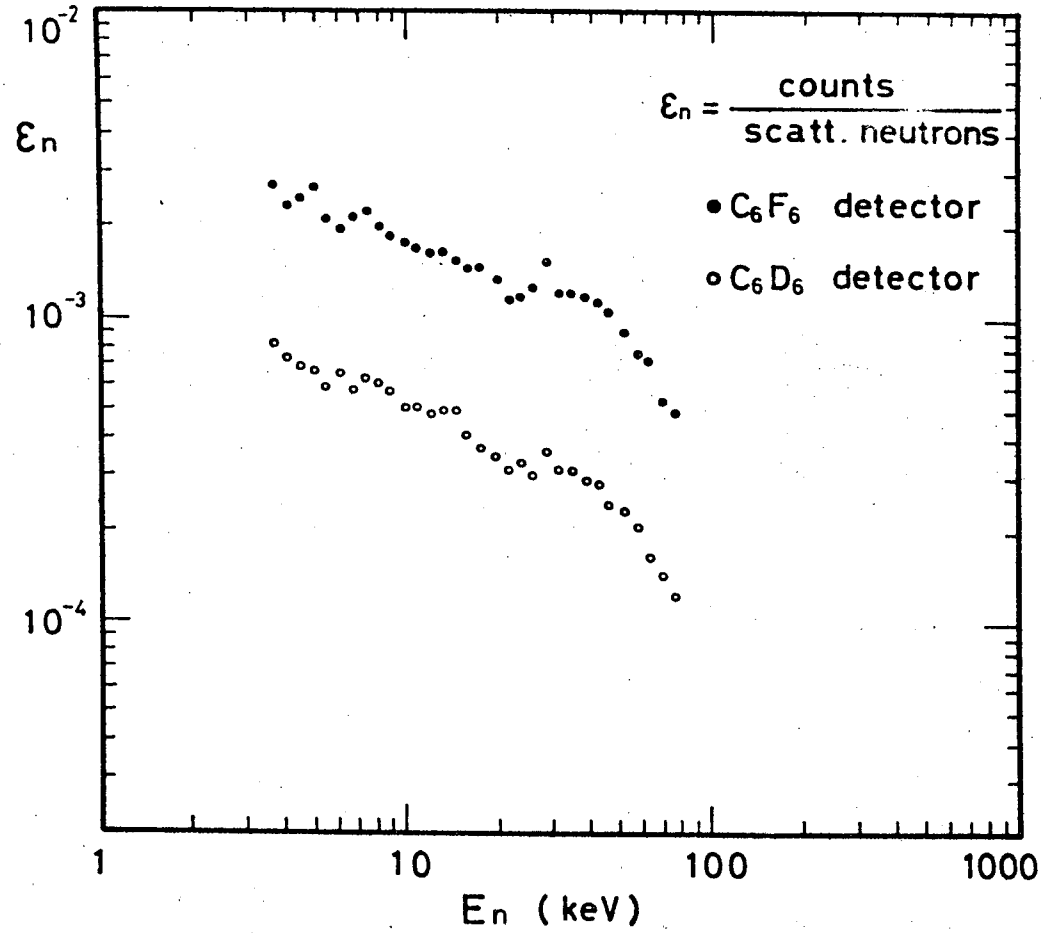


Fig. 4 Neutron sensitivities of $C_6F_6$ and $C_6D_6$ detectors

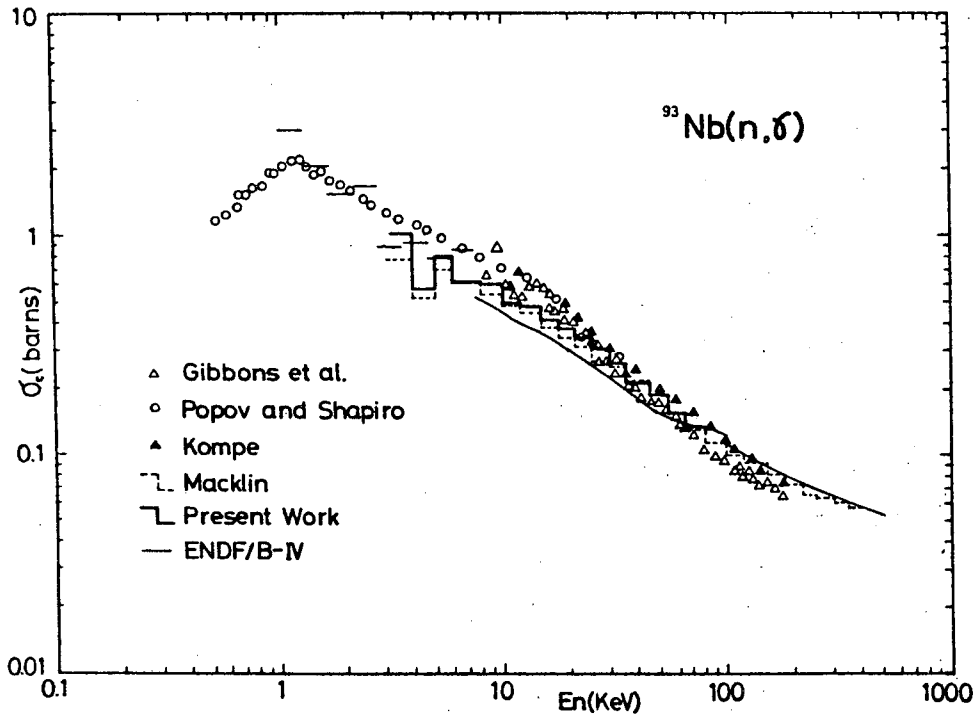


Fig. 5 Neutron capture cross sections of Nb-93

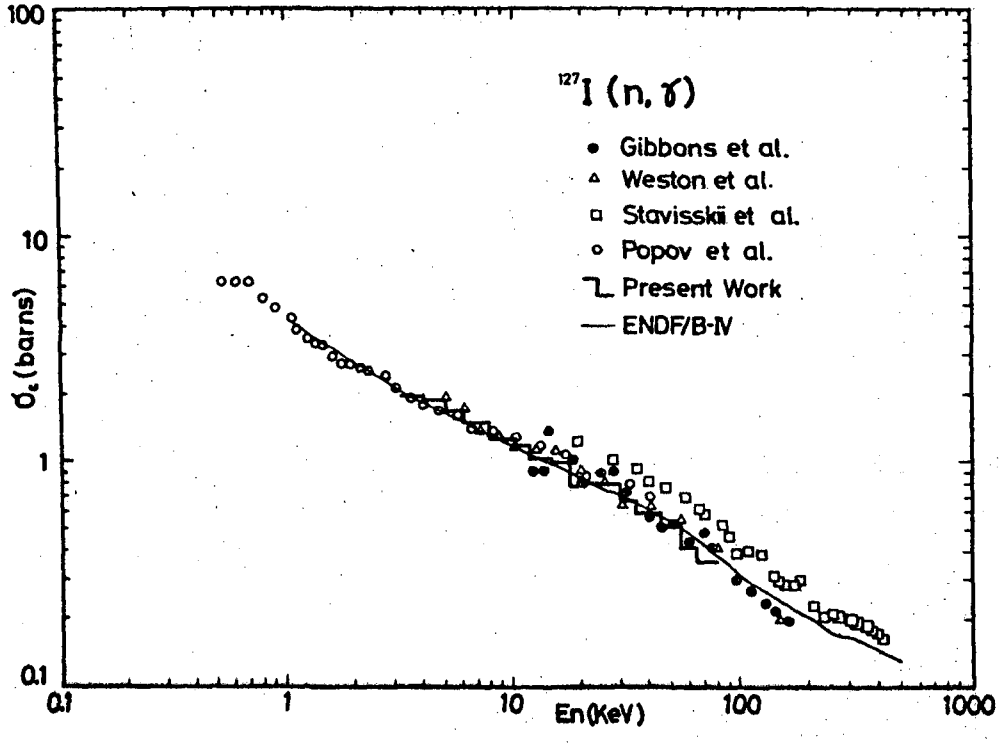


Fig. 6 Neutron capture cross sections of I-127

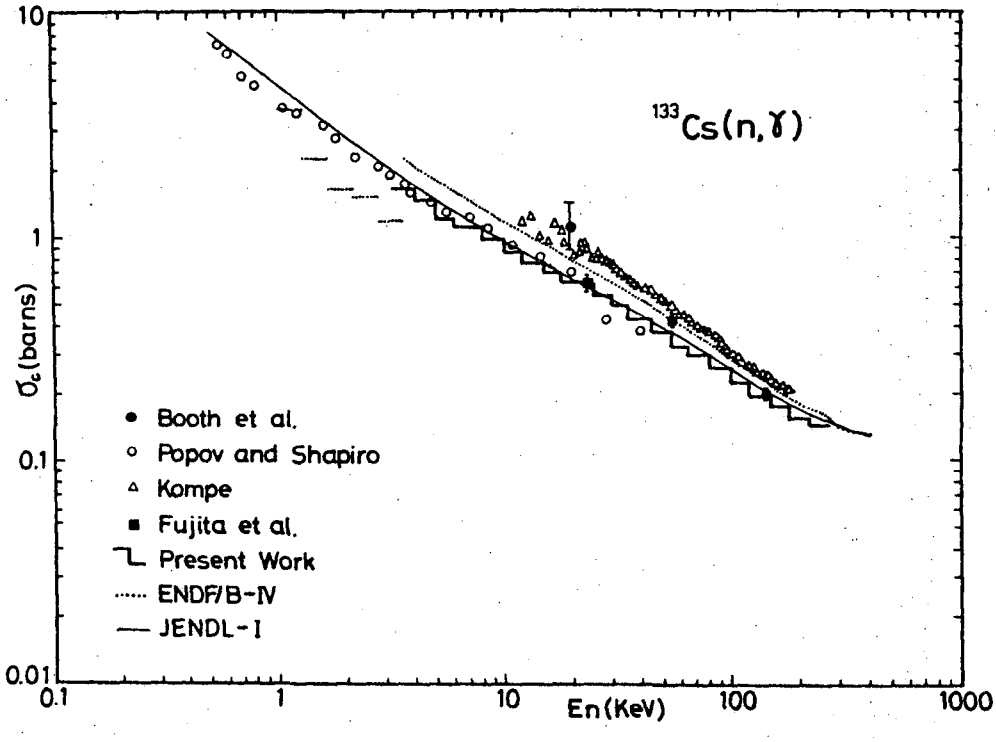


Fig. 7 Neutron capture cross sections of Cs-133

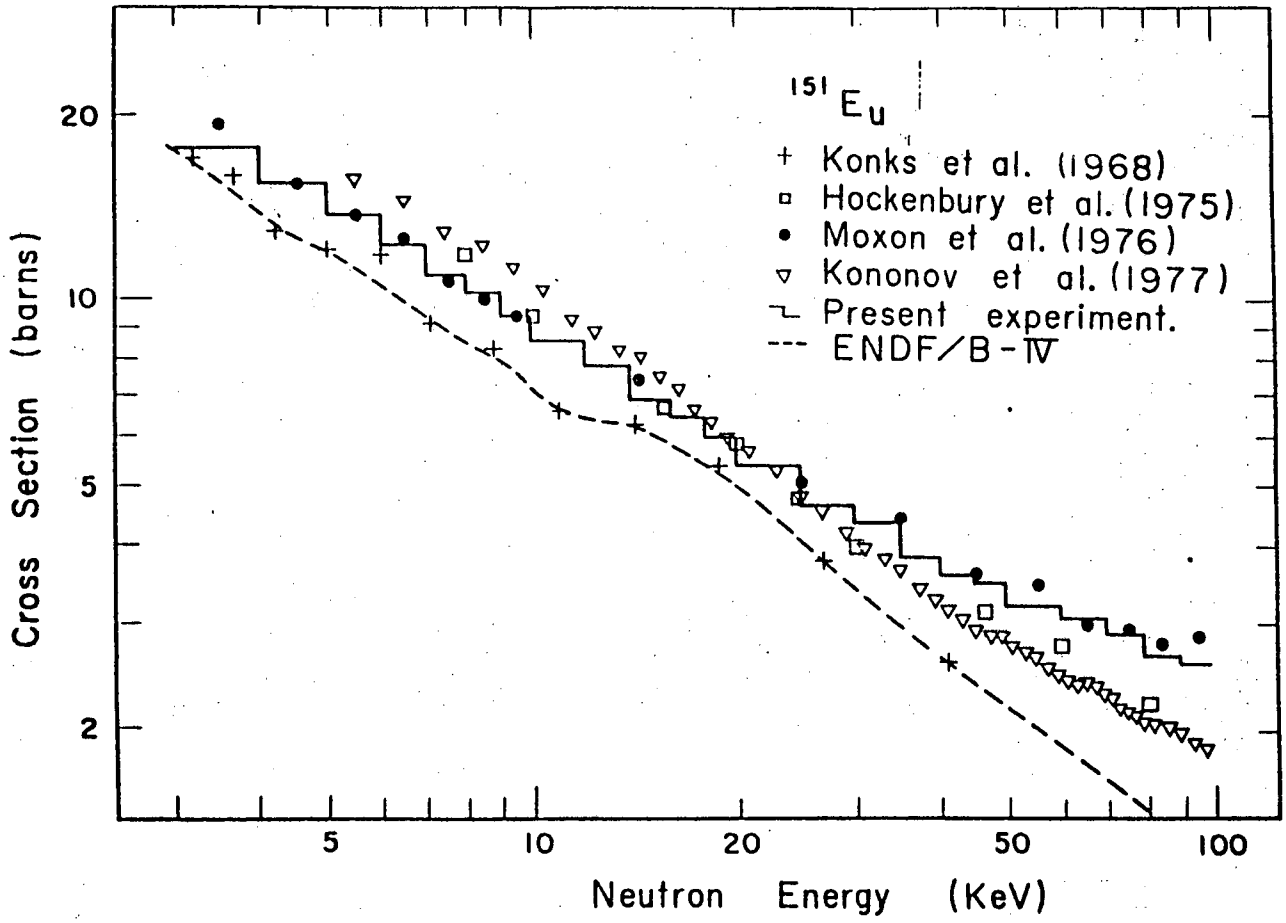


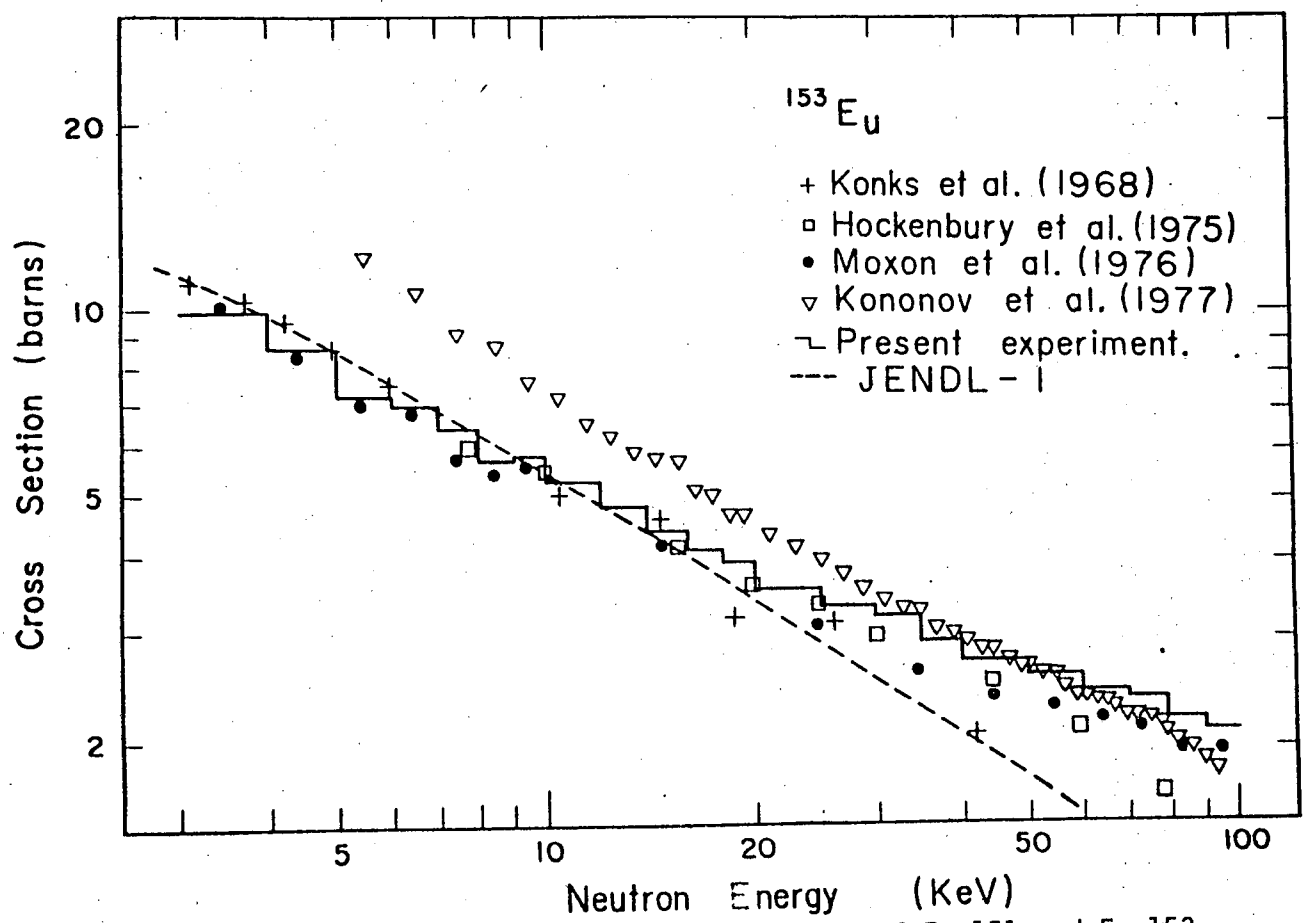


Fig. 8 (a),(b) Neutron capture cross sections of Eu-151 and Eu-153

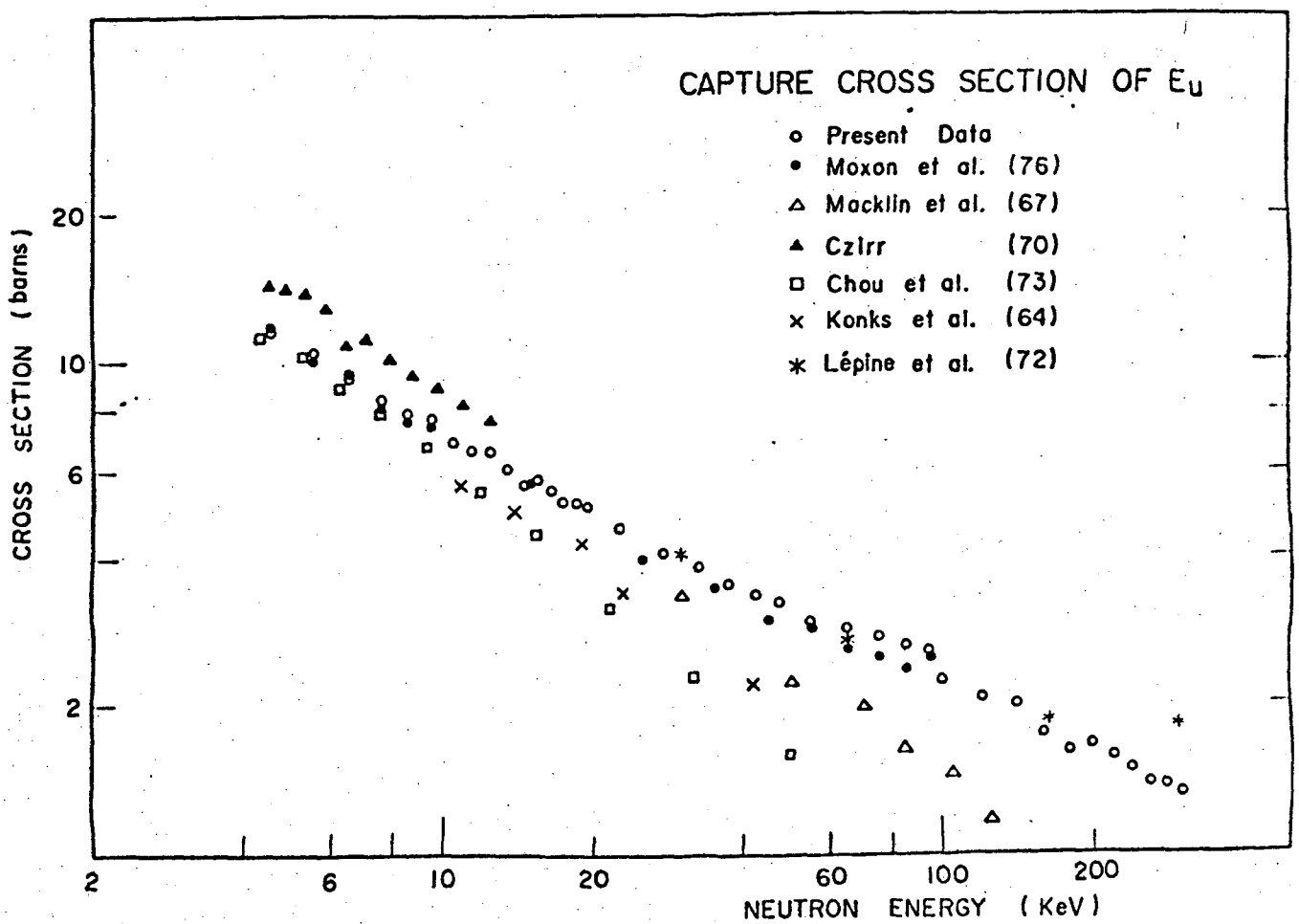


Fig. 8 (c) Neutron capture cross sections of nat.-Eu

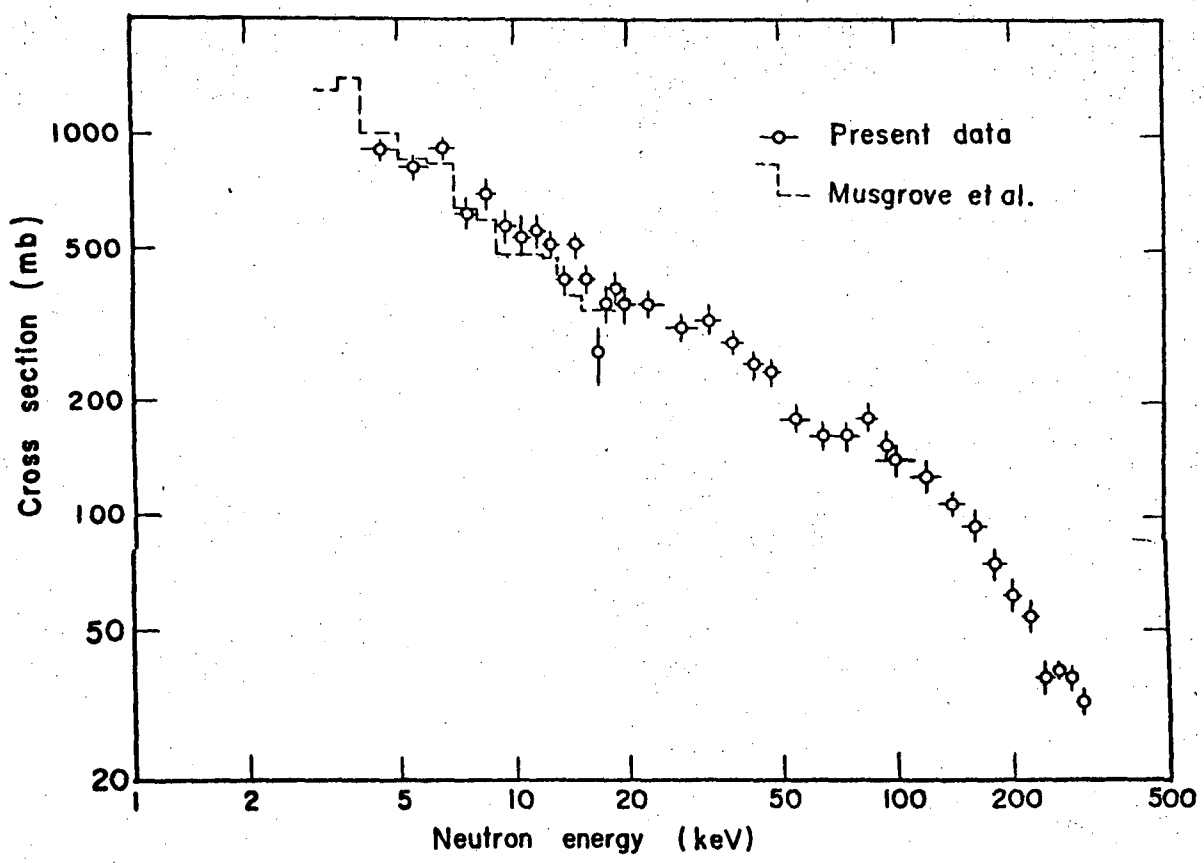


Fig. 9 (a) Neutron capture cross section of Nd-143

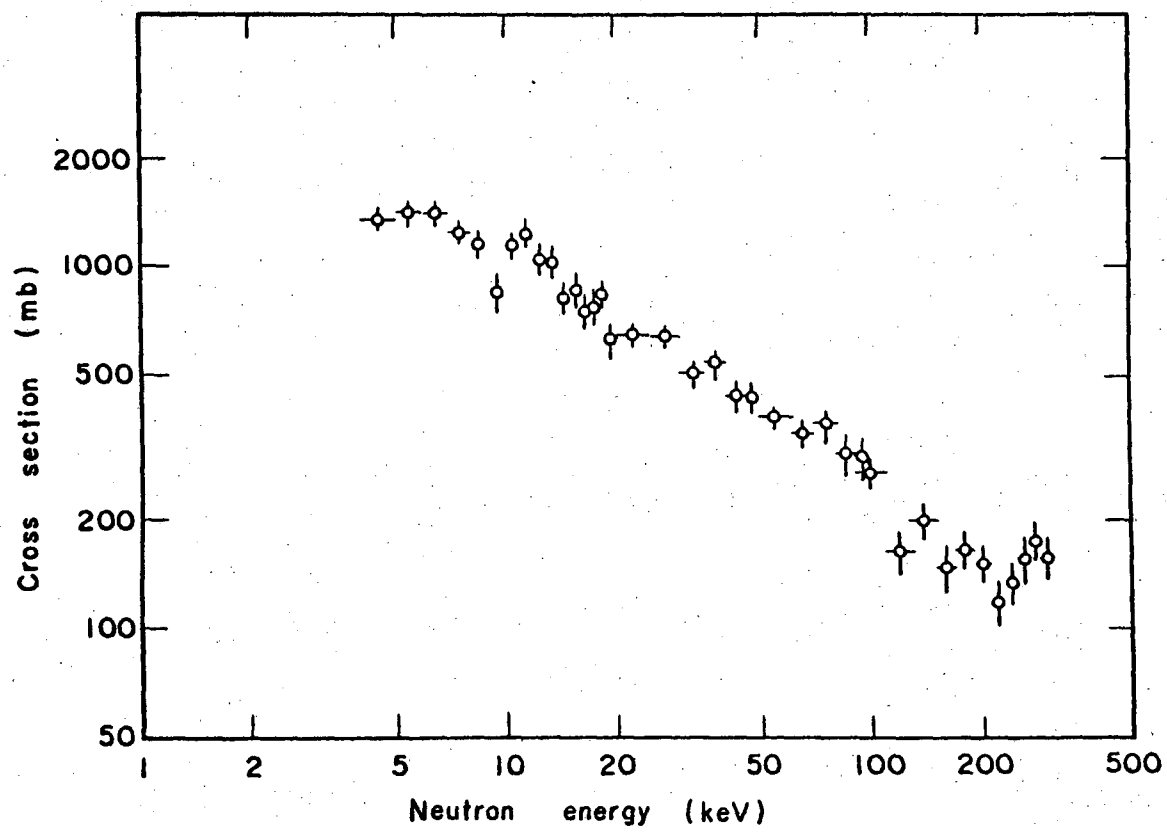


Fig. 9 (b) Neutron capture cross section of Nd-145

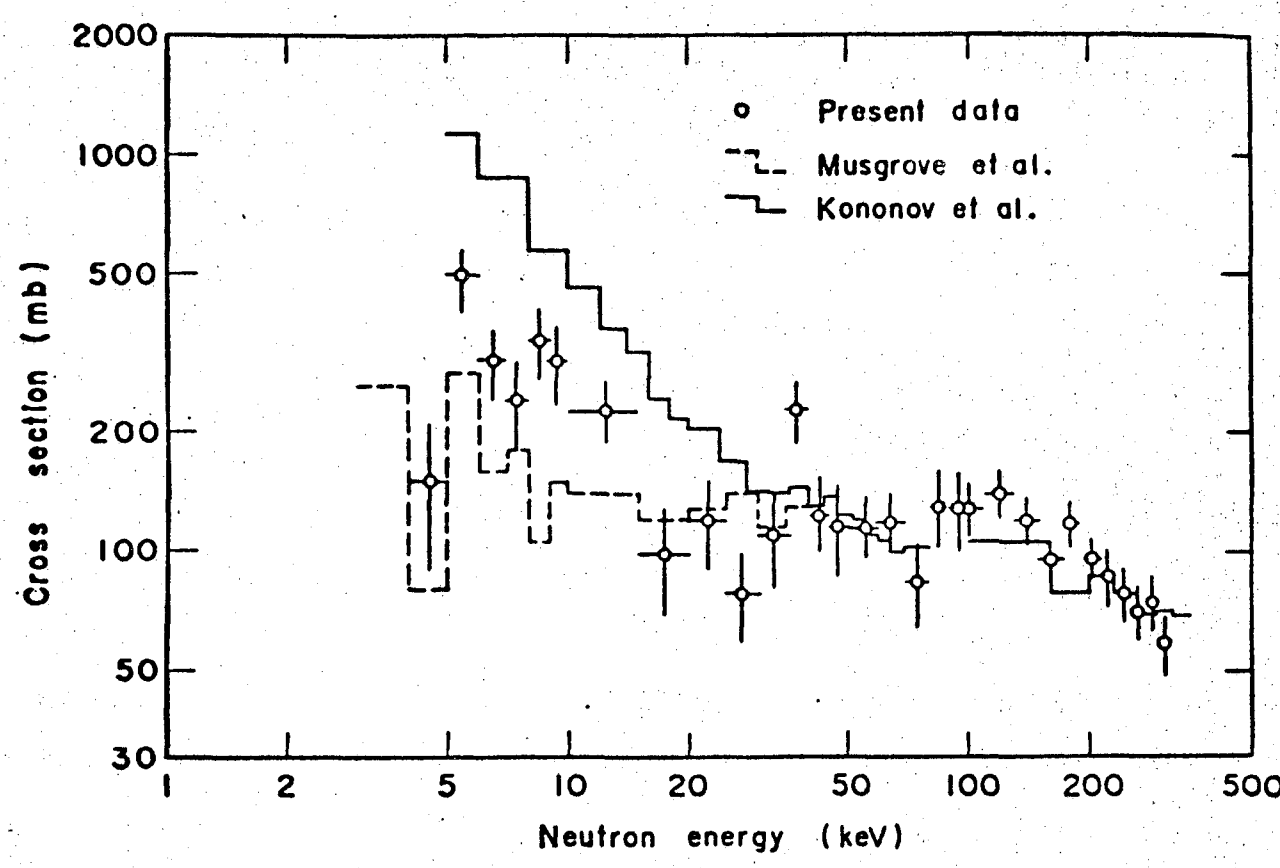


Fig. 9 (c) Neutron capture cross section of Nd-146

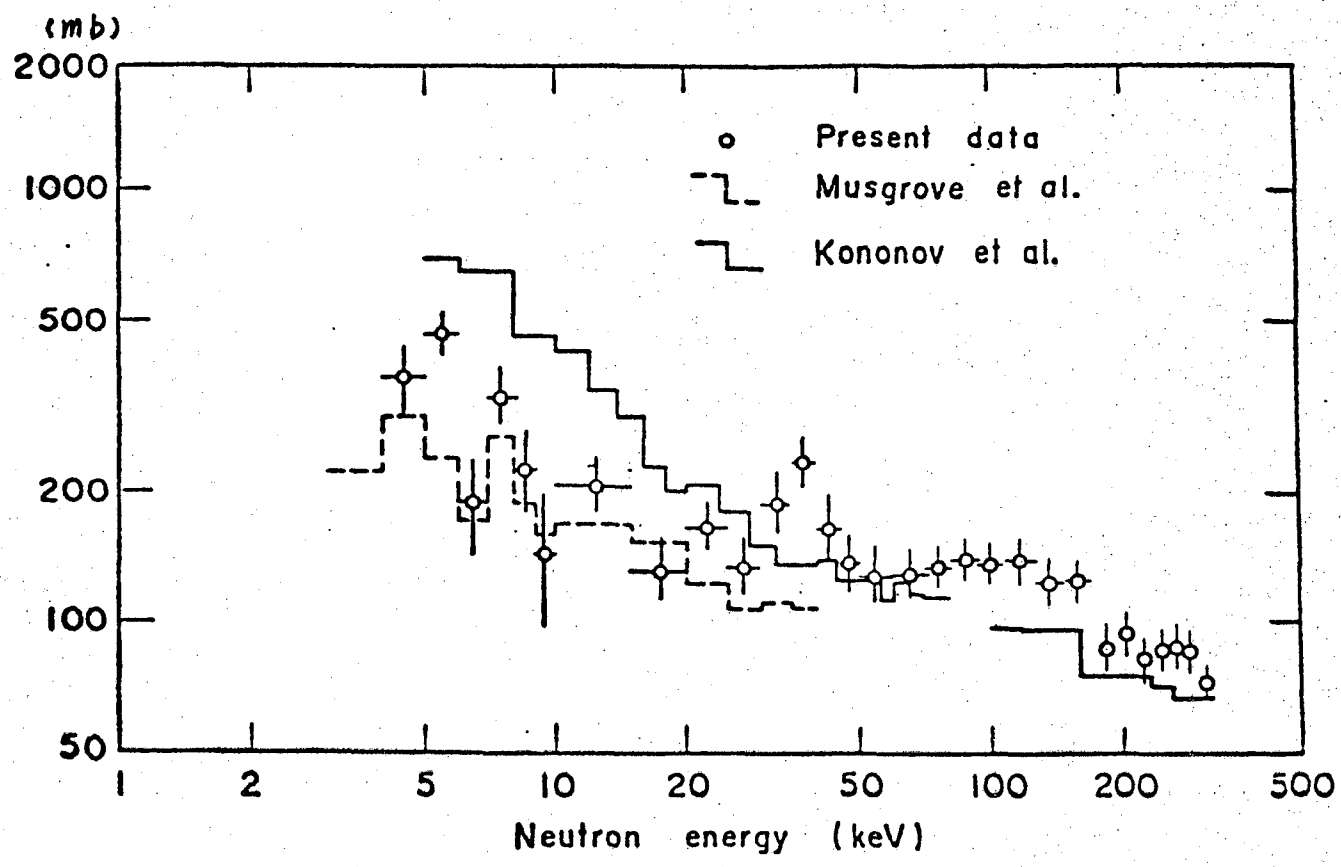


Fig. 9 (d) Neutron capture cross section of Nd-148

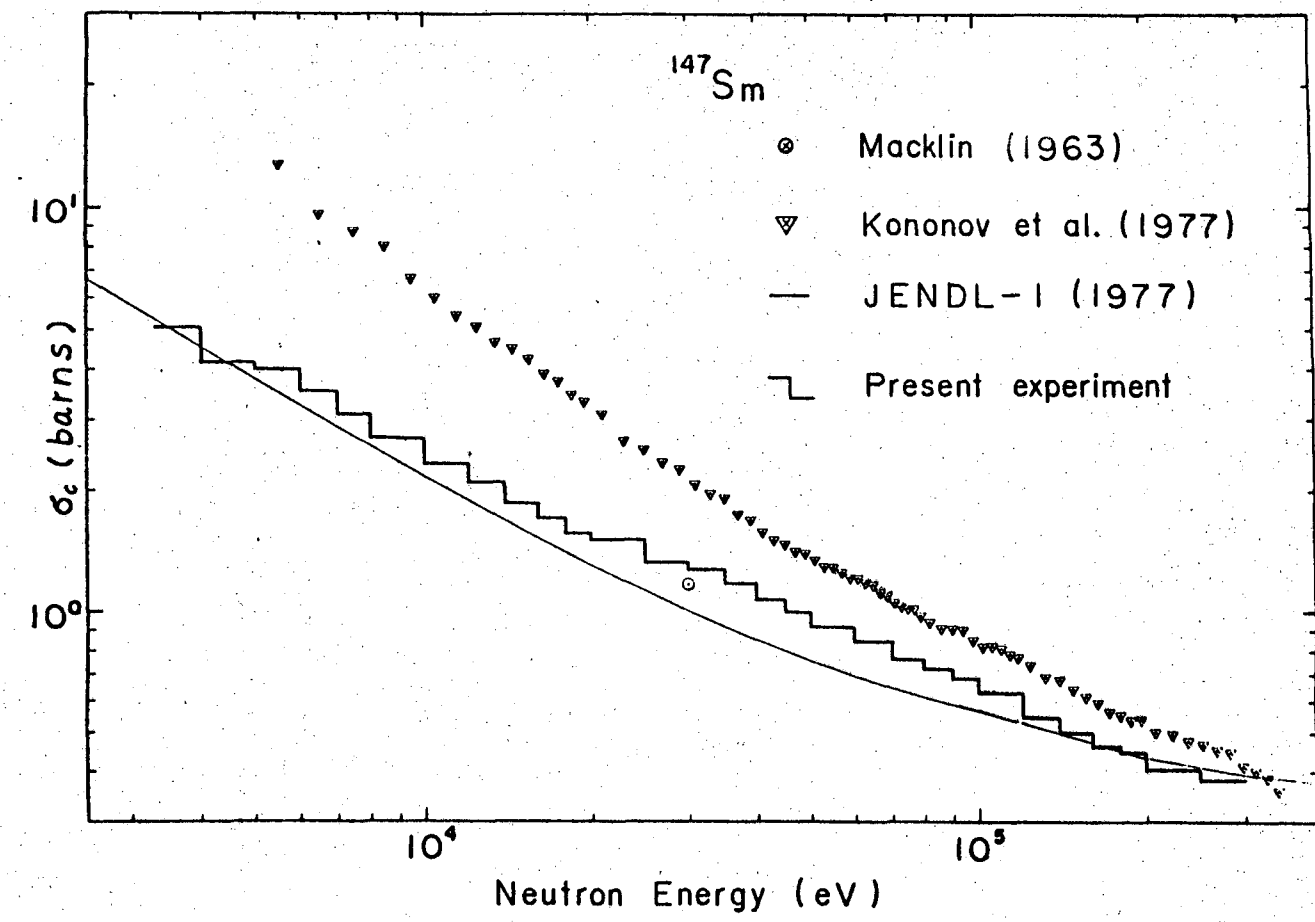


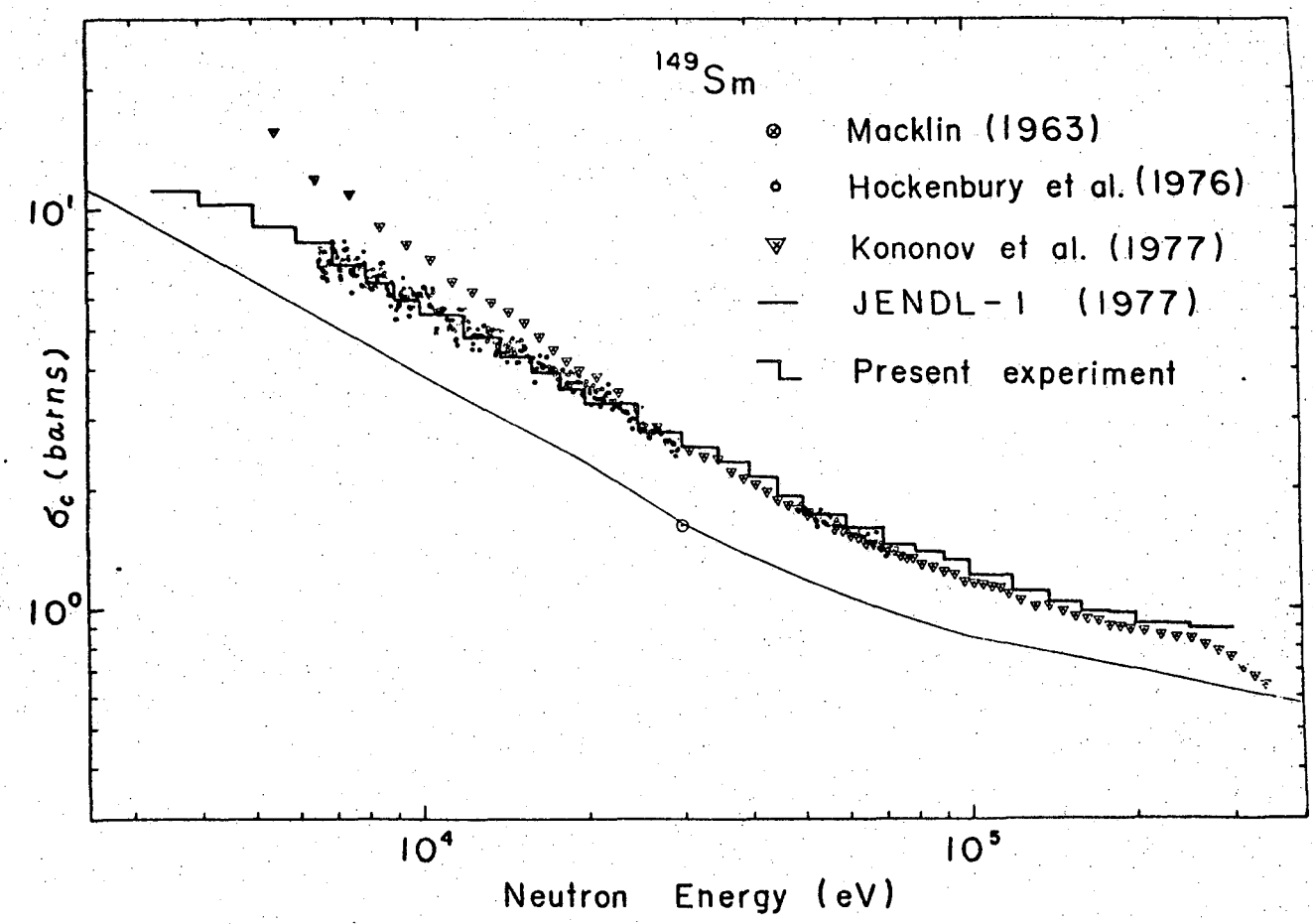


Fig. 10 (a),(b) Neutron capture cross sections of Sm-147 and Sm-149

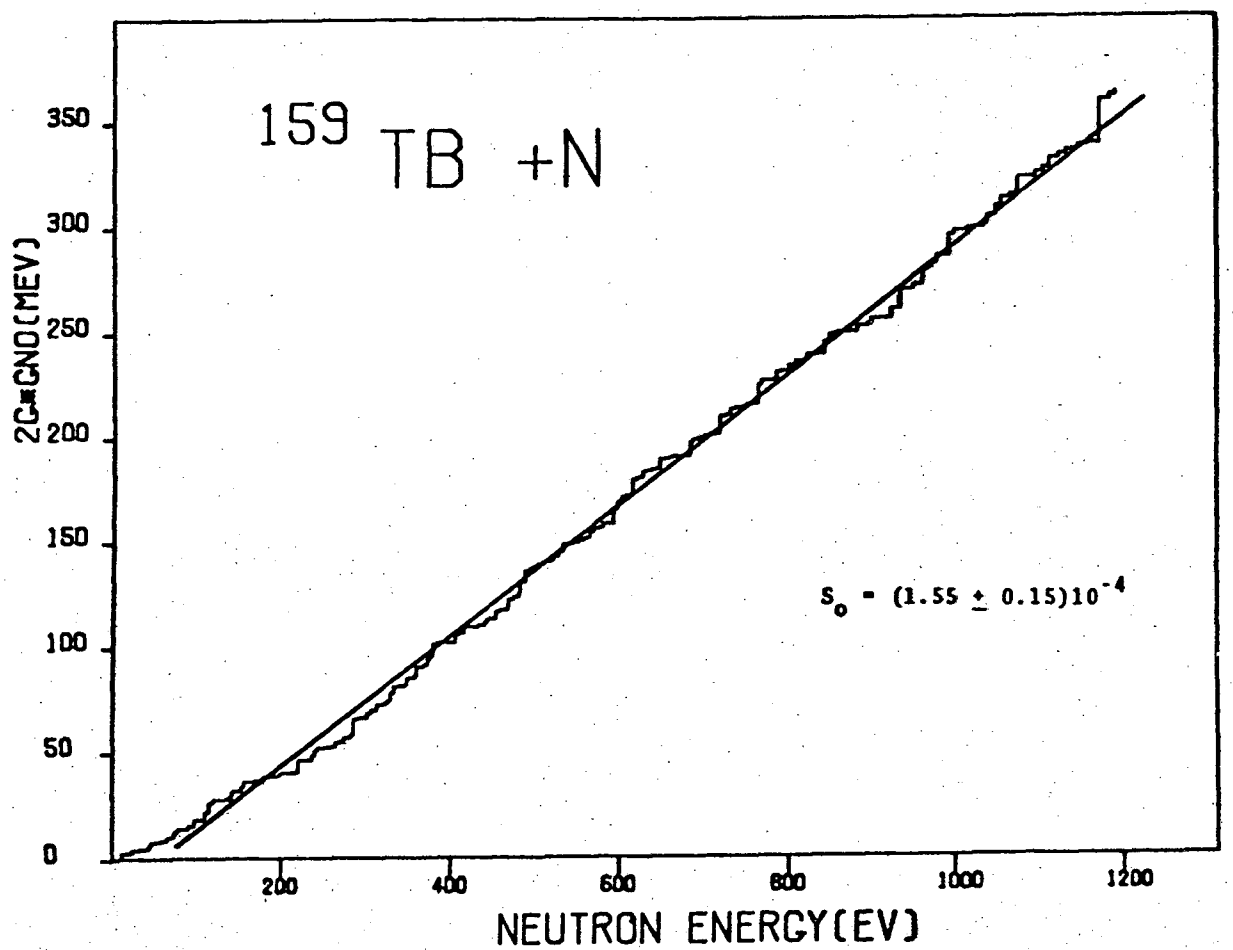


Fig. 11 Cumulative values of $2g\Gamma_n^o$ vs. neutron energy for Tb-159

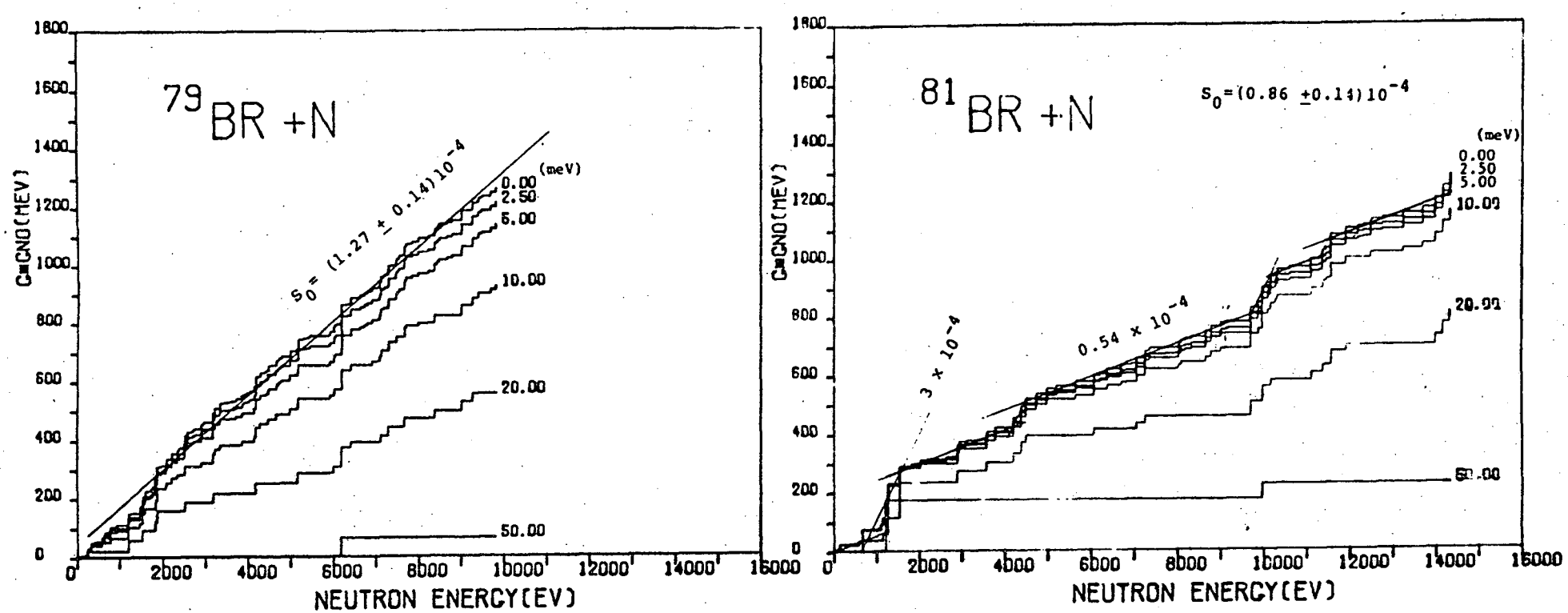


(a) (b)

Fig. 12 Cumulative values of $g\Gamma_n^0$ vs. neutron energy for Br-79 and Br-81

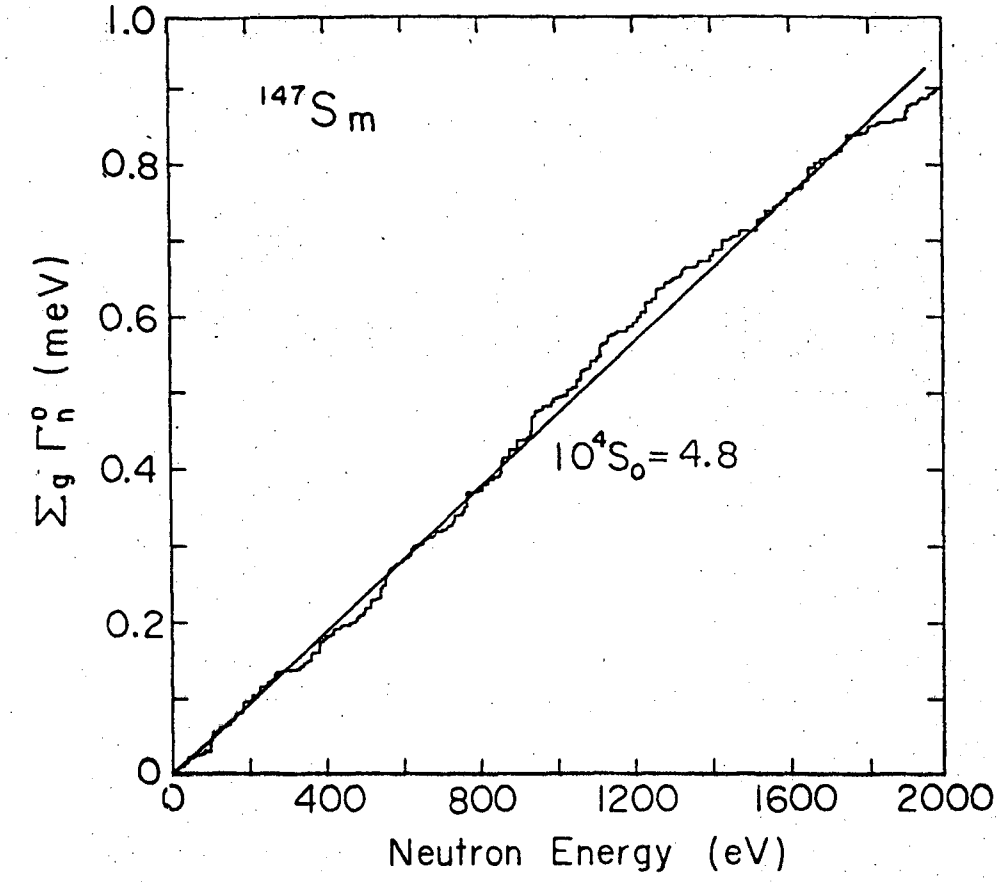


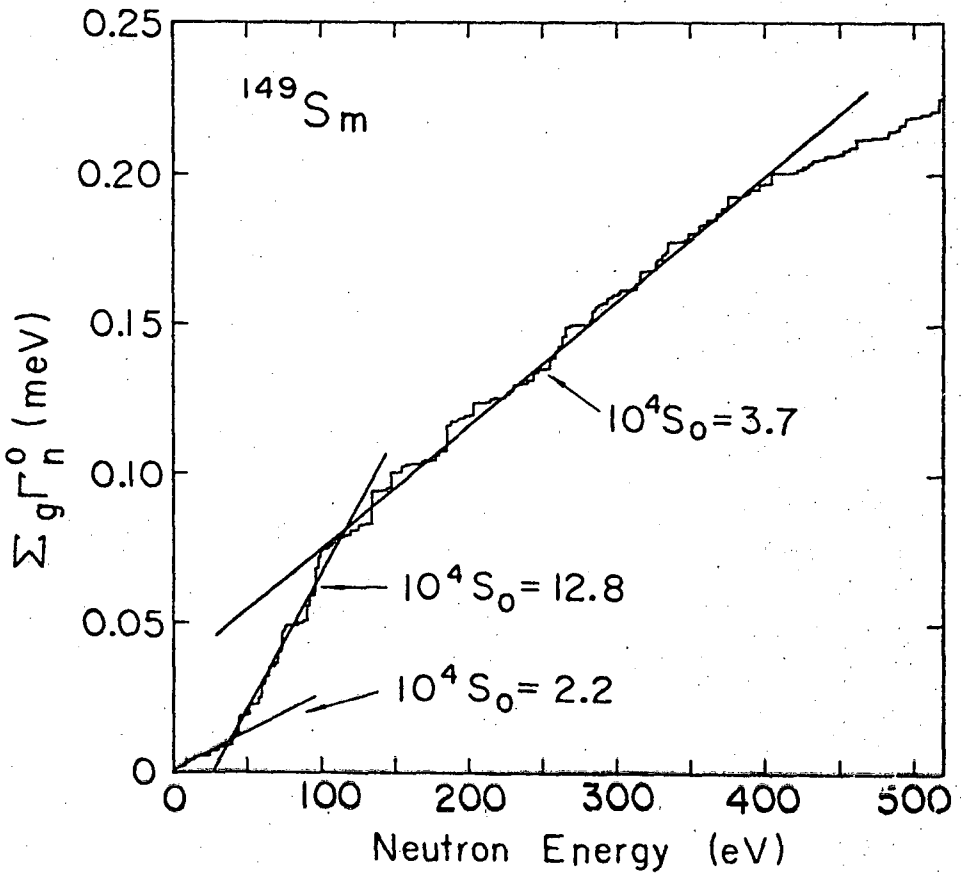


Fig. 13 (a),(b) Cumulative values of $g\Gamma_n^0$ vs. neutron energy for Sm-147 and Sm-149

# TECHNIQUES FOR THE DETERMINATION OF CAPTURE CROSS SECTIONS OF RADIOACTIVE FISSION PRODUCT NUCLIDES ☆

M.S. Moore★ and G.F. Auchampaugh
University of California, Los Alamos Scientific Laboratory
Los Alamos, New Mexico 87545

The determination of capture cross sections of radioactive fission products relies heavily on model calculations and systematics to provide a data base, particularly where experimental measurements are sparse or non-existent. Under ideal conditions, such calculations may be reliable to an estimated accuracy of 25%. Much of the experimental data base that exists was obtained several years ago by total cross section measurements on fast choppers, by capture cross section measurements with lead slowing-down spectrometers, and, in a very few cases, with nuclear explosion sources.

In this paper, we assess the capability of modern laboratory neutron sources, the electron linac and proton spallation neutron sources, to provide the data required to refine the calculations.

## I. Introduction

A survey of the status of cross sections of radioactive fission product nuclides with half-lives longer than a few hours, as shown in Table I, reveals several points which may be of interest. Two deserve special notice. First, there are only a few nuclides that are considered to be of importance. There are 182 fission product nuclides for which cross section data were provided in ENDF/B-IV, but only 57 of these are radioactive. The ratio is roughly the same for the isotopes that most affect neutron economy in reactor design. Of the 43 most important fission products, rated in order of the global capture rate at the Specialists' Meeting on Fission Product Nuclides at Petten in 1977[1]), there are 14 that are not stable. There are 34 radioactive nuclides for which requests have been made for additional measurements in the WRENDA compilation[2]); however, the conclusion reached by the specialists at the Petten meeting were that required accuracy of 10-30% in the capture cross sections could be considered to have been met for all but 15 of these.

Secondly, one may note that while there has been a great deal of activity devoted to evaluation of radioactive fission product cross sections, the evaluations are based, in many cases, on no experimental data at all. Even for the best studied nuclides, i.e. for $^{99}$Tc and $^{147}$Pm, the data are sparse and of low accuracy compared to those for stable isotopes in the vicinity. It has been argued that even when no data exist, the accuracy of an evaluation can be judged

---

☆Work performed under the auspices of the U.S. Dept. of Energy

★Address during academic year 1979-1980 : CEC, JRC, Central Bureau for Nuclear Measurements, Steenweg op Retie, 2440 GEEL, Belgium

as adequate if the results of calculations based on that evaluation differ from results based on other, presumably independent, evaluations by less than the user's accuracy requirement. This is most probably an unwarranted assumption, yet even for the 15 most wanted isotopes for which the data are considered inadequate, evaluation based upon integral results may presently be the only feasible way: five of them have lifetimes shorter than 40 days, and the techniques and expertise used in the past to make measurements on such materials[3,4] are no longer available. Lynn[5] has concluded that, in ideal cases, a calculation of the radiative capture cross section of a nuclide for which no data exist can be expected to be accurate to ± 25%. If the evaluated data are required to higher accuracy, then the evaluation must be constrained, either directly, by integral and/or differential measurements, or by a higher degree of understanding of the systematics involved than has been used before. The existence of intermediate structure in the neutron and partial radiation widths of important stable fission products emphasizes the need for measurements to verify and improve the evaluations.

In this paper, we outline a threefold approach for providing cross-section data for the fifteen radioactive fission products for which the current accuracy is considered to be inadequate. The approach involves 1) using systematics of total cross sections to provide an evaluation constraint, 2) measuring the microscopic cross sections of the longer lived species, and 3) using integral measurements for adjustment.

## II. Total cross section measurements on separated isotope samples as an evaluation constraint.

The evaluation process invariably begins with a set of transmission coefficients obtained from optical model fits to experimental data. Perhaps the approach outlined by Lagrange[6] is typical : the optical model parameterization is obtained by fitting the total cross sections, the s- and p-wave strength functions at the neutron binding energy, and the elastic scattering angular distributions. If the experimental data do not exist, the evaluator uses global optical-model parameter sets, or interpolates and extrapolates the optical model parameters as best he can to obtain transmission coefficients to use in subsequent statistical model calculations. For fission product nuclides, this procedure must be used with caution, because of the close proximity of the N and $Z = 50$ and $N = 82$ closed shells in the region. One might expect that the procedure would be better suited for actinide nuclides than for fission product nuclides, because the actinides are all rigidly deformed and lie far from the nearest closed shell at $^{208}Pb$. However, one finds that for $^{242}Pu$, discrepancies among several evaluations led to differences of factors of 2 or so in calculated bulk neutronics properties such as the critical mass. A recent measurement of the total cross section of $^{242}Pu$ [7] showed that none of these evaluations could be considered to be completely adequate, yet there was a prescription that did describe the $^{242}Pu$ data to the level of accuracy of ~ 1%: the simple ansatz of using the well-known total cross section of $^{238}U$, and correcting for the extra four nucleons by adding to the $^{238}U$ values the difference between the total cross sections of $^{239}Pu$ and $^{235}U$[8]. The point to be made is that an adequate description of the total cross section of $^{242}Pu$ existed before the measurement was made. If the evaluators had used these data to constrain their optical-model description, one could assume that the large discrepancies in these evaluations would have been substantially reduced. The procedure may also well be valid for describing the elastic angular distribution, because these too vary only slightly from nucleus to nucleus.

The question of interest at this specialists' meeting is whether the same procedure would be useful in providing a constraint to the optical model parameterization of radioactive fission-product cross sections. Here, the extrapolation of optical model parameters may be far less reliable than for actinide nuclides. Schmittroth and Schenter[9] have compared fission-product-data evaluations, noting that large differences exist if there are no experimental data.

Thus, we feel that the total cross section extrapolation procedure should be explored.

To illustrate the approach, let us consider certain of the nuclides from Table I, e.g. those ranging from Zr to Cd. Among these there are six of the 14 most important radioactive fission products, and also six of the 15 for which the existing data are thought to be inadequate. Let us assume that a systematic study of the total neutron cross sections and elastic angular distributions can be done for the 26 stable isotopes in this range for which the amount of isotopic sample material is adequate, i.e. for the isotopes whose natural abundance is ~ 10% or higher. The isotopes to be studied are $^{90,91,92,94}$Zr, $^{93}$Nb, $^{92,94,95,96,97,98,100}$Mo, $^{99,100,101,102,104}$Ru, $^{103}$Rh, $^{104,105,106,108,110}$Pd, and $^{107,109}$Ag. With these data in hand, one first needs to determine over what range the technique may be adequate. For example, knowing the cross sections of $^{96,97,98}$Mo and $^{100,102}$Ru, it should be possible to calculate that of $^{101}$Ru under the assumption that it bears the same relation to $^{100,102}$Ru as does $^{97}$Mo to $^{96,98}$Mo. The isotope $^{101}$Ru, is, of course, also one of the stable isotopes. If the approach turns out to be useful, it is then a simple matter to provide an estimate of the cross section for any of the important radioactive isotopes in this region which could then be used in optical model fitting. It may be noted that any of the important radioactive isotopes listed in Table I in this range can be bracketed for interpolation from a stable isotope no further than four mass units away, with the exception of 3.5h $^{92}$Y.

If, however, one attempts to assess the validity of the approach, he concludes that the required data base is too fragmentary. The systematic study of total cross sections by Foster and Glasgow[10] gave important qualitative understanding of deformation effects, but this study was done with elemental samples. The systematic total, differential elastic and inelastic scattering measurements by Smith's group at the Argonne National Laboratory have been completed for $^{93}$Nb [11] and for the even isotopes of Zr [12] and Mo [13], but not for the odd ones. For the isotopes of Ru and Pd, data do not exist, nor do appropriate samples. While there is separated material available (a modest fraction of one gram-atom is enough to permit such measurements), the material should be fabricated into right circular cylinders a few cm long, instead of the plates needed for most other cross section studies.

Finally, we should emphasize that a reliable set of optical model transmission coefficients is only the first step in determining fast capture cross sections of isotopes for which measurements are lacking. Perhaps the most important additional piece of information needed is the energy dependent level density. Systematics can then be used to provide a reasonably accurate ( ~ 20-30% ) estimate of the average radiative capture width[14] and in principle the calculation of the average capture cross section should provide an evaluation satisfying the data needs. In practice, one notes that there is still another phenomenon that is not understood and which can lead to much larger uncertainties : intermediate structure as manifested by large local fluctuations in the neutron strength for isotopes in this important fission-product region [15-17]. At present, there appears to be no way to provide data with the required accuracy without making microscopic measurements.

## III. Measurement capability for fast capture cross sections of radioactive fission products.

The problem of making direct measurements of the capture cross sections of radioactive fission products is one of overriding the background signal arising from the sample activity. In 1972, Theobald[18] recognised that the nuclear explosion neutron source is ideally suited to solving this problem, and he proposed a collaborative measurement of fast capture cross sections of fission products with groups at the Los Alamos Scientific Laboratory who had been concentrating on fission cross section measurements. The collaboration was not implemented; the physics measurements with nuclear explosions have been essentially discontinued and in the last few years the expertise has been lost. This option

of providing the required data should no longer be seriously considered.

The technique that seems to be the most promising is that developed by Block at Rensselaer Polytechnic Institute[19] and discussed at this specialists' meeting[20]: the lead slowing-down-spectrometer used in conjunction with one of the modern laboratory pulsed neutron sources such as an electron linac or proton spallation source. An assessment of the properties of the lead slowing-down-spectrometer is conveniently done by using neutron slowing-down theory, as suggested by Harris[21]. The slowing-down-spectrometer is useable in the energy range below about 50 keV, and gives a resolution of about 30% in energy. Calculations based on slowing-down theory for an infinite spectrometer suggest that the spectrometer behaviour is comparable to a conventional time-of-flight measurement done at a flight path of 6.1 m, and with an effective gain in neutron fluence on target of a factor of ~6000, depending on energy and relative positioning of source and sample. These parameters are very nearly the same as those quoted by Block[22] for the 75-ton Rensselaer Intense Neutron Source (RINS): a gain in fluence of ~ $10^4$ at a flight path equivalent of 5 m. A 30% resolution in energy corresponds to 15% in time of flight. A 50 keV neutron takes 2 $\mu$s to travel 6.1 m, so the width of the driving pulse needs to be short compared to the 300 ns that describes the effective slowing-down-time resolution in the spectrometer.

Table II summarizes the feasibility of making capture cross section measurements on radioactive sample materials with a lead slowing-down-spectrometer, using one of the currently existing high intensity pulsed neutron sources recently reviewed by Auchampaugh[23]. We conclude that many of the measurements of interest can be done; others require development of future sources comparable to the Proton Storage Ring currently under construction at LASL. Whether the 30% resolution intrinsic to the lead slowing-down-spectrometer is sufficient to reveal the structure of interest in these cross sections is a question that needs careful consideration by both users and measurers.

Finally, we should like to address the question of measuring these data by conventional techniques. The neutron fluence on the sample increases inversely as the square of the decrease in distance. There is also a compression of the data collection time, such that if overriding background is the primary consideration, the effective signal-to-noise ratio varies inversely as the cube of the distance. One could thus expect to reproduce the data quality obtainable with the lead slowing-down spectrometer by making conventional measurements at a flight distance of $5/(10^4)^{1/3}$ m, or 23 cm, provided he could attain an overall time resolution shorter than 11 ns at 50 keV. Monte-Carlo calculations carried out for the target-moderator geometry of the WNR facility at LASL give ~ 12 ns as the typical timing uncertainty introduced by the moderation time; this is the dominant contribution to the timing uncertainty. We then can conclude that the entries of Table II are also valid for a measurement carried out by conventional techniques.

Figures 1 and 2 show the comparative performance of several of the new, planned or upgraded neutron facilities in the resonance- and fast-neutron energy regions. The LASL Proton Storage Ring will not be useful for data production for several more years. One can conclude that in the near future, any of the white-source facilities will show roughly comparable performance. It should be noted that one of the primary criteria for the present application is the signal to noise ratio, which should be compared to facility performance on a "per-pulse" basis. There will be unanticipated problems associated with making data measurements at very short flight paths. Browne et al[24], with the Lawrence Livermore Laboratory electron linear accelerator, have shown that such measurements are feasible. We conclude that if the need for measurements is sufficiently great, the data can be provided.

## References


1. Fission Product Nuclear Data (FPND) 1977, IAEA-213 (1978), Vol.II, p.743 The ranking of the 43 most important fission products was part of a contributed paper by G. Langlet and Martin Deidier, published in INDC(NDS)-87 (1978)
2. World Request List for Nuclear Data Measurements, INDC(SEC)-46/U (1975)
3. J.R. Berreth, Nuc. Appl. 1, 230 (1965) discusses preparation of samples for nuclear data measurements on highly radioactive isotopes. See also a report by J.W. Codding WASH-1124, p.99 (1968), of sample preparation of 2g of 27d $^{233}$Pa for a capture measurement with a nuclear explosion source.
4. G.J. Kirouac, H.M. Eiland, C.A. Conrad, R.E. Slovacek and K.W. Seemann, Nuc. Sci. Eng. 52, 310 (1973), measured $\sigma_T$ for 41d $^{148}$Pm, using 9.6 mg of material, which gave a dose rate of ~ 6x10$^5$ R/hr at 2 inches 19 days after the irradiation to produce the sample.
5. J.E. Lynn, UKAEA Report AERE-R 7468 (1974). It should be noted that this study was carried out for the ideal case of actinide nuclei, not for fission products.
6. Ch. Lagrange in 'Critique of Nuclear Models and their Validity in the Evaluation of Nuclear Data", JAERI-M 5984, NEANDC(J)38L, INDC(JAP)25L, p.58(1974)
7. M.S. Moore, P.W. Lisowski, G.L. Morgan, G.F. Auchampaugh and R.E. Shamu in 'Nuclear Cross Sections for Technology', Knoxville, (1979)
8. R.B. Schwartz, R.A. Schrach and H.T. Heaton II, Nuc. Sci. Eng. 54, 322 (1974). It is perhaps significant that all three measurements were made by this group at this time, such that any small systematic errors are expected to be common ones and not to appear in the correction term.
9. F. Schmittroth and R.E. Schenter, HEDL TMI 73-63, ENDF-194 (1973)
10. D.G. Foster and D.W. Glasgow, Phys. Rev. C3, 576 (1971)
11. A.B. Smith, P.T. Guenther and J.F. Whalen, Z. Phys. 64 379 (1973)
12. P.T. Guenther, A.B. Smith and J.F. Whalen, Phys. Rev. C 12 1797 (1975)
13. A.B. Smith, P.T. Guenther and J.F. Whalen, Nuc. Phys. A244 213 (1975)
14. J.E. Lynn, Theory of Neutron Resonance Reactions, Clarendon Press, Oxford 1968 p. 325. The use of the formalism was illustrated by M.S. Moore in 'Neutron Physics and Nuclear Data', Harwell (1978) p.331, again for the ideal case of actinide nuclides.
15. G. Rohr, H. Weigmann and J. Winter, Nuc. Phys. A150, 97 (1970)
16. H. Weigmann, S. Raman, J.A. Harvey R.L. Macklin and G.G. Slaughter, Phys. Rev. C20 115 (1979)
17. P. Staveloz, E. Cornelis, L. Mewissen, F.Poortmans, G. Rohr, R. Shelley and T. van der Veen in 'Nuclear Cross Sections for Technology', Knoxville (1979)
18. J.P. Theobald in INDC(SEC) 26 (1972)
19. R.C. Block, R.W. Hockenbury, D.S. Cramer, E. Bean and R.E. Slovacek, in 'Neutron Cross Sections and Technology', Washington (1975)
20. R.C. Block et al. in 'Fission Product Nuclear Data', Bologna (1979)
21. D.R. Harris, private communication, (1970)
22. R.C. Block, private communication to R.W. Benjamin, Savannah River Lab.(1975)
23. G.F. Auchampaugh in 'Nuclear Cross Sections for Technology' Knoxville (1979)
24. J.C. Brown, R.W. Benjamin and D.G. Karraker, Nuc. Sci Eng. 65 166 (1978)

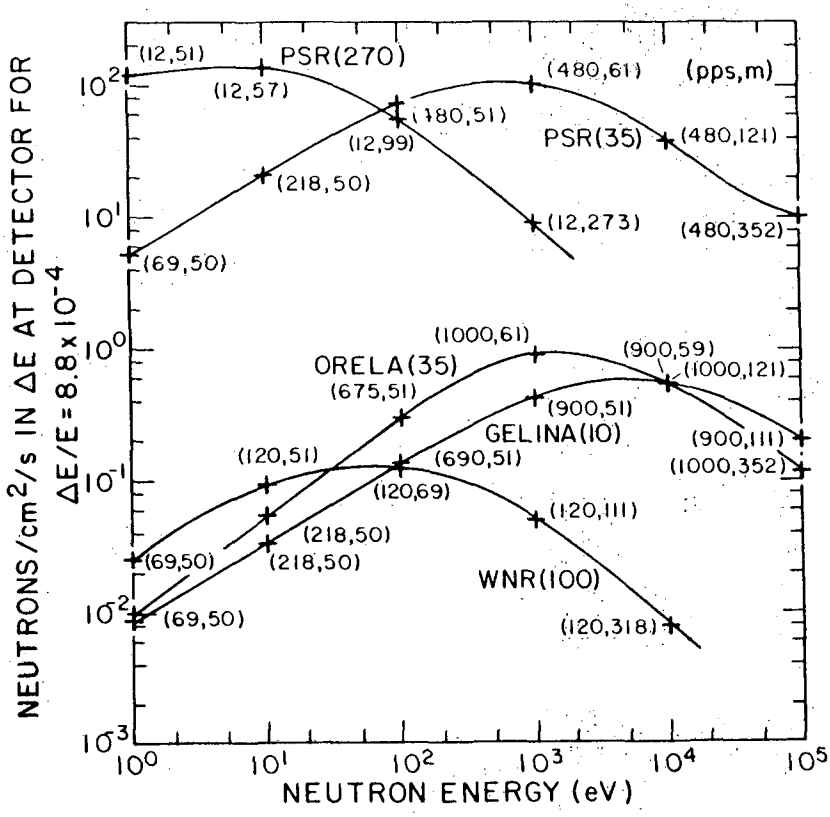


Fig. 1 : Comparative performance of several new, planned and upgraded 'white' neutron sources in the resonance energy range.

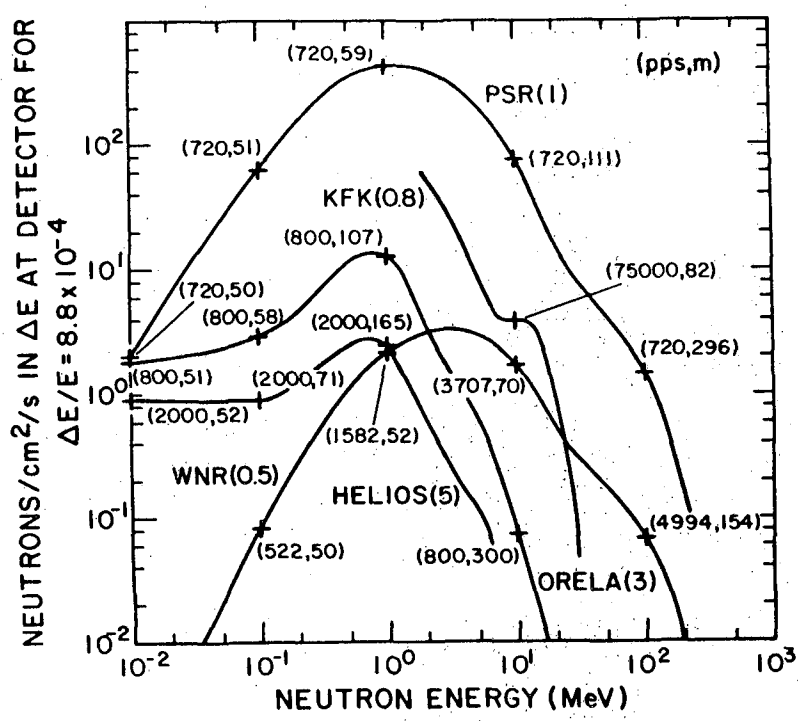


Fig. 2 : Comparative performance of several new, planned and upgraded fast 'white' neutron sources.

Table I. Radioactive fission-product nuclides

| $\tau$ 1/2 | Isotope | $^{235}U$ Thermal Yield(%) | Evaluations | Integral Expt. | Diff. Expt. | Comments |
|---|---|---|---|---|---|---|
| 26.3h | As-76 | 0.0012+n $\gamma$ | 1 | | | |
| 8.8h | As-77 | 0.0082 | 1 | | | |
| $<6.5\cdot10^4$y | Se-79 | 0.056 | 1 | | 11 | |
| 35.3h | Br-82 | 0.21 + n $\gamma$ | 1 | | | |
| 10.7y | Kr-85 | 1.32 | 1,2 | 8,9 | 11 | |
| 18.8d | Rb-86 | 1.32 + n $\gamma$ | 1,2 | | | |
| 50.5d | Sr-89 | 4.80 | 1,2 | | | |
| 28.8y | Sr-90 | 5.89 | 1,2,3 | 8 | | |
| 9.5h | Sr-91 | 5.93 | 1 | | | |
| 64.1h | Y-90 | 4.8 + n $\gamma$ | 1,2,5 | 8 | | |
| 58.5d | Y-91 | 5.93 | 1,2,4,5 | 8 | | |
| 3.54h | Y-92 | 5.97 | 5 | | | |
| 10.2h | Y-93 | 6.40 | 1 | | | |
| $1.5\cdot10^6$y | Zr-93 | 6.40 | 1,2,3,4 | 9,10 | 11 | a,b(2),c(2),d(22) |
| 64.0d | Zr-95 | 6.50 | 1,2,3 | | | b(2),c(2) |
| 16.9h | Zr-97 | 6.03 | 1 | | | b(2),c(2) |
| $2\cdot10^4$y | Nb-94 | Ind. | 6 | 8,9 | 11 | |
| 35.0d<br>87h | Nb-95<br>Nb-95m) | 6.50 | 1,2,4,6 | (9) | | c(2) |
| 66.0h | Mo-99 | 6.13 | 1,2 | | | a,b(2),c(3) |
| $2.1\cdot10^5$y | Tc-99 | 6.13 | 1,2,3,4,7 | 8,9,10 | 11,12,13,14 | a,b(1),c(2),d(4) |
| 39.4d | Ru-103 | 3.12 | 1,2 | | | a,b(2),c(2),d(14) |
| 4.44h | Ru-105 | 0.93 | 1,2 | | | |
| 367d | Ru-106 | 0.39 | 1,2,3,4 | 8,9 | | d(33) |

Table I continued

| $\tau$ 1/2 | Isotope | $^{235}$U Thermal Yield(%) | Evaluations | Integral Expt. | Diff. Expt. | Comments |
|---|---|---|---|---|---|---|
| 4.34m | Rh-104m | 3.12 + n $\gamma$ | | 8 | | c(1),e |
| 35.4h | Rh-105 | 0.93 | 1,2 | 8,9 | | a,b(2),c(2) |
| 2.17h | Rh-106 | 0.93 + n $\gamma$ | | | | c(1),e |
| $6.5 \cdot 10^6$y | Pd-107 | 0.17 | 1,2,3,4,7 | 8,9,10 | 11 | a,b(1),c(1),d(5) |
| 13.4h | Pd-109 | 0.03 | 1,2 | | | |
| 21.1h | Pd-112 | 0.012 | 1 | | | |
| 7.45d | Ag-111 | 0.017 | 1,2 | 8,9 | | |
| 44.8d | Cd-115m | 0.011 | 1,2 | | | |
| 27h | Sn-121 | 0.014 | 1 | | | |
| 55g | Sn-121m | | 1 | | | |
| 129d | Sn-123 | 0.016 | 1,2 | | | |
| 9.62d | Sn-125 | 0.03 | 1,2 | | | |
| ~$10^5$y | Sn-126 | 0.055 | 1,2 | | | b(1) |
| 2.7d | Sb-122 | 0.014 + n $\gamma$ | 1 | | | |
| 60.2d | Sb-124 | 0.016 + n $\gamma$ | 1,2 | 8,9 | | |
| 2.7y | Sb-125 | 0.030 | 1,2 | | | b(3) |
| 12.4d | Sb-126 | 0.030 + n $\gamma$ | 1 | | | |
| 3.9d | Sb-127 | 0.125 | 1 | | | b(3) |
| 9.1h | Sb-128 | 0.35 | 1 | | | |
| 109d | Te-127m | 0.125 | 1,2 | | | b(3),c(2) |
| 33.5d | Te-129m | 0.65 | 1,2 | | | b(3) |
| 30h | Te-131m | 2.82 | 1 | | | |
| 78h | Te-132 | 4.20 | 1 | | | |
| $1.6 \cdot 10^7$y | I-129 | 0.65 | 1,2,3,4,7 | 8,9 | 11 | a,c(2) |
| 12.4h | I-130 | 0.65 + n $\gamma$ | 1,2 | 8 | | |
| 8.04d | I-131 | 2.82 | 1,2 | 8,9 | | |
| 20.9h | I-133 | 6.75 | 1 | | | c(2) |
| 6.61h | I-135 | 6.60 | 1,2 | | | |

Table I continued

| $\tau$ 1/2 | Isotope | $^{235}U$ Thermal Yield(%) | Evaluations | Integral Expt. | Diff. Expt. | Comments |
|---|---|---|---|---|---|---|
| 5.25d | Xe-133 | 6.75 | 1,2 | | | b(3),c(2) |
| 9.10h | Xe-135 | 6.60 | 1,2 | 8,9 | 11 | b(2),c(1) |
| 2.06y | Cs-134 | 6.75 + n $\gamma$ | 1,2 | 8,9 | | |
| $3 \cdot 10^6$y | Cs-135 | 6.60 | 1,2,3,4 | | 11 | a,b(1),c(1),d(11) |
| 13d | Cs-136 | 6.60 + n $\gamma$ | 1 | | | |
| 30.2y | Cs-137 | 6.26 | 1,2,3,4 | 8 | 11 | a,d(36) |
| 12.79d | Ba-140 | 6.36 | 1,2 | 8,9 | | |
| 40.3h | La-140 | 6.50 + n $\gamma$ | 1,2 | 8,9 | | |
| 32.5d | Ce-141 | 5.82 + n $\gamma$ | 1,2,4 | 8 | | |
| 33.0h | Ce-143 | 5.95 | 1,2 | 8 | | |
| 284d | Ce-144 | 5.39 | 1,2,3,4 | 8,9 | | c(1),d(39) |
| 19.2h | Pr-142 | 5.87 + n $\gamma$ | 1,2 | 8 | | |
| 13.58d | Pr-143 | 5.95 | 1,2,4 | 8 | | d(42) |
| 11.0d | Nd-147 | 2.25 | 1,2,4,7 | 8 | | a,b(1),c(1) |
| 2.62y | Pm-147 | 2.25 | 1,2,3,4 | 8,9,10 | 11,12,13 | a,b(1),d(8) |
| 5.37d | Pm-148 | 2.25 + n $\gamma$ | 1 | 8,9 | | b(3),c(2) |
| 41.3d | Pm-148m) | | 1,2 | 8,9 | 11 | c(2) |
| 53.1h | Pm-149 | 1.07 | 1,2 | 8 | | a,c(2) |
| 28h | Pm-151 | 0.42 | 1,2 | 8 | | c(2) |
| 90y | Sm-151 | 0.42 | 1,2,3,4,7 | 8,9,10 | 11 | a,b(2),c(1),d(7) |
| 46.8h | Sm-153 | 0.16 | 1,2 | 8 | | b(3),c(2) |
| 13y | Eu-152 | 0.42 + n $\gamma$ | 2 | 8 | 12 | a,c(1) |
| 8.5y | Eu-154 | 0.164 + n $\gamma$ | 1,2,4 | 8 | | a,c(1),d(32) |
| 4.9y | Eu-155 | 0.0325 | 1,2,3,4 | 8 | | a,b(3),c(1),d(20) |
| 15d | Eu-156 | 0.0133 | 1,2 | | | b(3) |
| 15.1h | Eu-157 | 0.0084 | 1,2 | | | |

Table I continued

| $\tau$ 1/2 | Isotope | $^{235}$U Thermal Yield(%) | Evaluations | Integral Expt. | Diff. Expt. | Comments |
|---|---|---|---|---|---|---|
| 18.6d | Gd-159 | 0.001 | 1 | | | |
| 72.1d | Tb-160 | 0.001 + n $\gamma$ | 1,2 | | | |
| 6.9d | Tb-161 | 0.001 | 1 | | | |

a) FPND Specialists' Meeting at Petten (1976) concluded that data requirements not met.

b) Highest priority of request for data in WRENDA - 75/6

c) Highest priority of request for data in DOE/NDC -16U (1979)

d) Ranking among 43 most important F.P. isotopes according to fraction of global captures (see Ref. 1)

e) Isotopes listed as Ru, but with half-life information corresponding to Rh in DOE/NDC -16U

1) Australian AEC Library, see AAEC / TM -587
2) ENDF/B-IV, see T.R. England and R.E. Schenter, LA-6116-MS, ENDF-223 (1975)
3) Japan Atomic Energy Library, JENDL-1 (1977), JAERI - M - 5752 (1974)
4) Bologna evaluation, CEC(71)-2(1971), NEANDC (E) 182 (1977)
5) Los Alamos evaluation, LA 6971 (1977)
6) Lawrence Livermore evaluation, see Gardner, Harwell (1978)
7) Reactor Centrum Nederland evaluation ECN-33 (1977)

8) Thermal (maxwellian averaged) capture measured.
9) Capture resonance integral measured.
10) Absorption cross section in fast reactor spectrum measured.
11) Total cross section measured in resonance range.
12) Capture cross section measured in resonance range.
13) Total cross section measured in MeV range.
14) Partial cross section measured at 14 MeV.

Table II. Assessment of differential measurement capability for some important radioactive fission products.

| $\tau$ 1/2 | Isotope | Radiation level a) (Rhm/g) | PSR relative signal b) (Rhm/g) | Signal-to-noise ratio |
|---|---|---|---|---|
| $1.5\cdot10^6$y | Zr-93c) | <.001 | $5.8\cdot10^4$ | > $10^6$ |
| 64d | Zr-95 | $1.4\cdot10^4$ | $5.5\cdot10^4$ | 3.9 |
| 16.9h | Zr-97 | $1.4\cdot10^6$ | $4.4\cdot10^4$ | 0.03 |
| 35.0d | Nb-95 | $1.7\cdot10^4$ | $4.8\cdot10^4$ | 2.8 |
| 66.0h | Mo-99c) | $3.6\cdot10^4$ | $5.5\cdot10^4$ | 1.5 |
| $2.1\cdot10^5$y | Tc-99c) | <.001 | $4.5\cdot10^4$ | > $10^6$ |
| 39.4d | Ru-103c) | $8.7\cdot10^3$ | $5.7\cdot10^4$ | 6.6 |
| 35.4h | Rh-105c) | $3.5\cdot10^4$ | $4.1\cdot10^4$ | 1.2 |
| $6.5\cdot10^6$y | Pd-107c) | <.001 | $5.7\cdot10^4$ | > $10^6$ |
| ~ $10^5$y | Sn-126 | 0.058 | $3.1\cdot10^4$ | $5\cdot10^5$ |
| 2.7y | Sb-125 | 254. | $3.3\cdot10^4$ | 130. |
| 3.9d | Sb-127 | $9.6\cdot10^4$ | $3.2\cdot10^4$ | 0.33 |
| 109d | Te-127m | 9.4 | $4.6\cdot10^4$ | 4900. |
| 33.5d | Te-129m | 690 | $4.4\cdot10^4$ | 630. |
| $1.6\cdot10^7$y | I-129c) | <.001 | $3.3\cdot10^4$ | > $10^6$ |
| 20.9h | I-133 | $3.1\cdot10^5$ | $3.1\cdot10^4$ | 0.10 |
| 5.25d | Xe-133 | $2.4\cdot10^3$ | $4.2\cdot10^4$ | 18 |
| 9.10h | Xe-135 | $3.3\cdot10^5$ | $3.9\cdot10^4$ | 0.12 |
| $3.10^6$y | Cs-135c) | <.001 | $3.3\cdot10^4$ | > $10^6$ |
| 30.2y | Cs-137c) | 27.8 | $2.2\cdot10^4$ | 780. |
| 284d | Ce-144 | 25.5 | $2.2\cdot10^4$ | 860. |
| 11.0d | Nd-147c) | $5.1\cdot10^3$ | $3.3\cdot10^4$ | 6.5 |
| 2.62y | Pm-147c) | <.001 | $2.7\cdot10^4$ | > $10^6$ |
| 5.37d | Pm-148 | $6.0\cdot10^4$ | $3.2\cdot10^4$ | 0.54 |
| 41.3d | Pm-148m | $2.5\cdot10^4$ | $3.3\cdot10^4$ | 1.3 |
| 53.1h | Pm-149c) | $1.6\cdot10^3$ | $2.5\cdot10^4$ | 15. |
| 28h | Pm-151 | $9.9\cdot10^4$ | $2.6\cdot10^4$ | 0.25 |
| 90y | Sm-151 | 1.6 | $3.6\cdot10^4$ | $2.3\cdot10^4$ |
| 46.8h | Sm-153 | $3.3\cdot10^4$ | $3.4\cdot10^4$ | 1.0 |
| 13y | Eu-152c) | 98. | $3.7\cdot10^4$ | 380. |
| 8.5y | Eu-154c) | 91. | $3.5\cdot10^4$ | 385. |
| 4.9y | Eu-155c) | 26.7 | $2.7\cdot10^4$ | 1000. |
| 15d | Eu-156 | $4.0\cdot10^4$ | $3.2\cdot10^4$ | 0.79 |

a) Approximate values of Roentgens/h at 1 m per g of material, taken from LA-4400(1970), adjusted for daughter activities. Approximately, Rhm=Ci·0.55·E$\gamma$, where Ci is the activity in curies, E$\gamma$ is the average gamma energy in MeV.

b) The PSR relative signal is the signal level produced by a 1g sample with the capture cross section Mo-97 in a Pb spectrometer, driven by the LASL proton storage ring. Currently existing neutron sources are estimated to give a factor of 100 lower signal.

c) Data requirements are not met for these isotopes (Petten 1976).

# NEUTRON RESONANCE PARAMETERS FOR PALLADIUM ISOTOPES

P. Staveloz*, E. Cornelis†, L. Mewissen*, F. Poortmans*,
G. Rohr☆, R. Shelley☆ and T. van der Veen☆
*S.C.K./C.E.N., B-2400 Mol, Belgium
†University of Antwerp, R.U.C.A., B-2020 Antwerp, Belgium
☆CEC - JRC, Central Bureau for Nuclear Measurements, B-2440 Geel, Belgium

We have undertaken a systematic study of neutron resonance parameters for the isotopes Pd-104,105,106,108 and 110 (enriched isotopes on loan from ORNL) in response to requests for such data on important fission products. Various neutron time-of-flight experiments have been performed at GELINA - capture, elastic scattering and total cross section measurements. Parity assignments are made on the basis of low-bias to high-bias ratios deduced from capture gamma ray spectra. The resonance parameter analysis is completed for Pd-105 and partial results are available for Pd-106, 108 and 110.

## Introduction

We are performing at GELINA a series of neutron time-of-flight experiments on the stable Palladium isotopes in the resolved resonance range. Our aim is to deduce for each isotope a set of resonance parameters Eo, $g\Gamma_n$ and $\Gamma_\gamma$ and to determine strength functions, mean level spacings and average capture widths. Most of the experiments are finished and an important part of the data has been analysed. Preliminary results were already communicated at the Harwell/1/ and Knoxville/2/ conferences.

Transmission experiments were performed for $^{105}$Pd up to 2 keV and for the even isotopes up to approximately 40 keV. Elastic scattering experiments have been done for $^{105}$Pd and $^{108}$Pd up to 2 keV. Capture cross section experiments were done for $^{105,106,108,110}$Pd and are in preparation for $^{104}$Pd. Parity assignments of resonances are made on the basis of low bias to high bias ratios deduced from capture gamma ray spectra.

Most of our work is complementary to what has been done previously in other laboratories for the Pd isotopes. Spin assignments/3/ and neutron widths deduced from transmission data/4,5/ were published for $^{105}$Pd resonances. Capture and transmission experiments were performed at RPI/6/ for $^{107}$Pd up to 660 eV. Capture cross section measurements were done recently at ORELA/7/ from 2.6 keV up to the inelastic $2^+$ level threshold for the even isotopes and up to 750 keV for $^{105}$Pd. The capture cross section for $^{105}$Pd was also measured at RPI/8/ up to 200 keV but no resonance parameters were published.

## Experimental Details

The experiments were performed on the neutron time-of-flight spectrometer of the 150 MeV Linac of CBNM. Operating conditions were 4 nsec beam burst and minimum channel width of 4 nsec for the capture experiments and 10 nsec for

the transmission and scattering experiments. The samples were prepared from metallic, highly enriched isotopes which we have on loan from Oak Ridge

Capture Experiments

Capture data were taken at a 60 metre flight path. The sample thicknesses were respectively 8.94 $10^{-4}$ atoms/barns (97.38%) for $^{105}Pd$, 2.25 $10^{-3}$ atoms/barns (98.48%) for $^{106}Pd$, 2.50 $10^{-3}$ atoms/barns (98.88%) for $^{108}Pd$ and 1.47 $10^{-3}$ atoms/barns (97.73%) for $^{110}Pd$.

The capture detection system consisted of a pair of cylindrical deuterated liquid scintillators ($C_6D_6$) each with a diameter of 4 inches and a length of 3 inches, the faces of which were in optical contact with EMI photomultipliers (2823 QKB). Using a bias of 0.1 MeV in amplitude, the data have been taken in two parameters, 14 time-of-flight and 8 amplitude bits, using a data acquisition system developed at CBNM/9/. A weighting over 256 amplitude channels was applied to achieve a detector response proportional to the total energy released in the capture process. The weighting factors used have been calculated by means of a Monte Carlo based computer code originally developed at Cadarache/10/ and later modified for our detector system in collaboration with Karlsruhe/11/. The neutron flux was measured using the same $C_6D_6$ detector system by replacing the Pd sample with a $^{10}B$ slab. Absolute calibration was obtained by the black resonance technique using resonances in Ag below 72 eV. The thickness of the Ag sample was 5.87 $10^{-3}$ atoms/barn.

Elastic Scattering Experiments

The scattering experiments were performed at a 30 metre flight path station only for the isotopes $^{105}Pd$ and $^{108}Pd$ using the same samples as in the capture experiments. The scattering detector system consisted of six $^{3}He$ gaseous scintillators mounted around an evacuated cylindrical tube with sample holder. The angle between the scattered and the incoming neutron beams was 140 degrees. The scattering cross sections were measured using lead and carbon as standard scattering samples. The background was determined using black resonances in Na (2850 eV), Mn (337 eV), Co (132 eV) and W (18.8 eV).

Transmission Experiments

Four $^{3}He$ high pressure gaseous scintillators were installed as transmission detector at 30 metres for $^{105}Pd$ and at 60 metres for the even isotopes. The samples were cooled at liquid nitrogen. The sample thicknesses were : 8.32 $10^{-3}$ atoms/barn (95.25%) for $^{104}Pd$, 1.096 $10^{-2}$ atoms/barn (97.38%) for $^{105}Pd$, 1.048 $10^{-2}$ atoms/barn (98.48%) for $^{106}Pd$, 2.50 $10^{-3}$ atoms/barn (98.88%) for $^{108}Pd$ and 6.06 $10^{-3}$ atoms/barn (97.73%) for $^{110}Pd$.

The background was measured with the black resonance technique using the same black resonance filters as in the scattering experiment plus Al (34.7 keV).

p-wave Assignment of Neutron Resonances

Excited states at low energy of the uneven compound nuclei $^{105,107,109}Pd$ are predominately of positive parity permissable for E1 transitions from p-wave resonances. So it is to be expected that the capture gamma ray spectra for p-wave resonances show more high energy transistions to low lying states than for the s-wave resonances. Not much information is known on the energies and spin and parity of low-lying states in the compound nucleus $^{111}Pd$, but we suppose that the overall picture will be the same as for the other Pd isotopes.

To make a parity assignment of neutron resonances, we compare, in the capture data, the resonance areas of the time-of-flight data taken with a high bias for the gamma rays (binding energy minus 1 MeV) to the resonance data taken with a low bias. The high bias to low bias ratios are taken from the capture cross section data, measured with the $C_6D_6$ detector system, in the two parameter mode but are also deduced from a separate experiment with a

7"x 6" NaI(Tl) scintillator as capture detector on a 30 metre station.

## Analysis

The transmission data are analysed with the multi-level Breit-Wigner fitting routine SIOB/12/.

The scattering data are corrected for multiple interaction effects using a Monte-Carlo computer code. An area analysis of the corrected data yields $\Gamma_n$ as a function of $\Gamma_\gamma$.

The capture data have been analysed using a modified Tacasi area analysis program /13/ which includes corrections for Doppler and resolution effects. The influence of multiple scattering on the capture area is taken into account by means of a Monte-Carlo routine.

## Results

For the analysis of the data, we have given highest priority for the isotope $^{105}$Pd and this work is completed. Concerning the even isotopes, the analysis of the transmission data is finished for $^{106,108,110}$Pd and nearly completed for $^{104}$Pd. However, an additional transmission experiment is planned for $^{108}$Pd, using a thicker sample. The present data for $^{108}$Pd could only be analysed up to 5 keV.

The transmission data were analysed up to 20 keV for $^{106}$Pd and up to 40 keV for $^{110}$Pd. However, above 10 keV, the data begin to suffer from important time-of-flight resolution broadening. So the analysis above 10 keV is mainly performed in order to look at the behaviour of the strength functions but not for obtaining accurate (better than 10%) values for the individual resonance widths.

The capture cross section data and high to low bias ratio capture experiments are analysed for $^{108}$Pd up to 5 keV. The anlysis for the other even isotopes is in progress.

The results for the various isotopes are summarised below. As stated before, the $^{105}$Pd case is completed but the results for the even isotopes are of a preliminary nature.

### $^{105}$Pd

Resonance parameter analysis was performed up to 2051 eV. The results reported in Table I are from the complete analysis of capture, elastic scattering and transmission data. Neutron widths were determined for 200 resonances and the capture widths for 71 of them.

The average capture width was determined as :

$$\langle \Gamma_\gamma \rangle = 150 \text{ meV} \pm 1 \text{ meV (stat. error)} \pm 8 \text{ meV (syst. error)}$$

The 5% systematic error is introduced to take into account possible systematic uncertainties in the normalization of the capture cross section data. Because of the good agreement between the results from transmission, scattering and capture data, we are confident that the systematic error is not larger than 5%.

The contribution from p-wave resonances to the strength function can be neglected in this energy range so that the s-wave strength function can be determined from the data :

$$So = \frac{\Sigma\, g\, \Gamma_n{}^{o}}{\Delta E} = 0.63 \pm 0.07 \times 10^{-4} \text{ (200 resonances below 2051 eV)}$$

The level spacing has been determined using a method/14/ which separates large s-wave resonances from smaller ones and from resonances with higher angular momentum ($\ell \geqslant 1$) by means of the Bayes' theorem. The number of s-wave resonances lost in this procedure has been estimated assuming a Porter Thomas distribution of the reduced neutron widths. For $^{105}$Pd this yields a value of :

$$D = (10.0 \pm 0.5)\ \text{eV}.$$

The capture cross section measurements in the unresolved resonance range performed at RPI[8] were normalized to the resonance capture area of the 55.2 eV resonance taking a neutron width of $2g\,\Gamma_n = 6.9$. We find $2g\,\Gamma_n = 6.70 \pm 0.04$ meV (st. error) for that resonance, in good agreement with the RPI value but larger than the value $6.36 \pm 0.12$ meV of ref. 2 and smaller than the value $2g\,\Gamma_n = 8.4 \pm 0.4$ meV stated in BNL 325.

Our results for the parameters So, D and $\langle \Gamma_\gamma \rangle$ are consistent with the analysis of the average capture cross section data above 10 keV[7,8].

$^{106}$Pd

The neutron widths were determined from the transmission data for 172 resonances up to 20 keV. In fig. 1 is shown the cumulative sum of reduced neutron widths ( $\Gamma_n / \sqrt{E_o}$) versus neutron energy. As can be seen on that figure, the strength function is roughly two times larger below 4 keV than above that limit.

We did not perform, up to now, a parity-assignment of the neutron resonances. However, below 4 keV, more than 80% of the strength is due to strong s-wave resonances which can be identified by their strong resonance-potential interference term in the total cross section. So we conclude that the structure is probably in the s-wave strength function.

$^{108}$Pd

All the cross section data have been analysed up to 5 keV. Parity assignment of resonances has been performed in the same energy range by comparing the resonance areas of the time-of-flight spectrum taken with a high (5 MeV) and a low (.550 MeV) amplitude bias. These ratios and their errors ($R \pm \Delta R$) are plotted versus reduced neutron widths ( $\Gamma_n / \sqrt{E_o}$ ) in fig. 2. As can be seen in this figure, for the strong resonances (large $\Gamma_n^o$) which in this energy range may be supposed to be s-wave resonances, the values $R + \Delta R$ are all smaller than $R_{\ell m} = 7.25\ 10^{-2}$. If we suppose that all resonances for which $R - \Delta R > R_{\ell m}$ are p-wave resonances, a total number of 22 resonances can be assigned as being p-wave below 5 keV. For 16 of these p-wave resonances, the neutron width was measured. The results plotted in fig. 2 are from data taken with the NaI(Tl) experiments and are in good agreement with the results from the capture cross section experiments taken with the $C_6D_6$ detector system. However the NaI(Tl) data have much better statistical precision especially in the high bias amplitude time-of-flight spectrum.

At the present stata of the analysis we have obtained the following results for $^{108}$Pd :

$$\langle \Gamma_\gamma \rangle = 76.8\ \text{meV} \pm 2.8\ \text{meV (stat. error)} \pm 4\ \text{meV (syst. error)}$$

$$S_o = 0.76 \begin{matrix} +\,0.19 \\ -\,0.15 \end{matrix} \times 10^{-4}$$

$^{110}$Pd

Neutron widths were deduced from the shape-analysis of the transmission experiments for 121 resonances up to 40 keV. However because of resolution and Doppler effect, the analysis above 25 keV was only possible for 16 broad resonances. The data show a very pronounced structure in the strength functions as can be seen from figures 3 and 4.

In fig. 4 we show the strength function over intervals of 4 keV. There are fluctuations of as large as a factor of 7. Although the strength function has a minimum below 4 keV, we have detected 26 resonances in that energy range which means that the error on the strength function is approximately 30% for that energy interval. At higher energies, and especially above 25 keV, the data are poor. However, we are quite confident that we have analysed a large fraction

of the resonances contributing significantly to the strength function and that we may state that the error on the strength function for each interval of 4 keV is much smaller than the magnitude of the structure. We have not yet completed our low bias to high bias ratio capture experiments, but for the same reason as in the $^{106}$Pd case, we believe that the structure is in the s-wave strength function.

## Conclusions

Resonance parameters and their average properties were obtained for the important fission product $^{105}$Pd from capture, scattering and transmission data. The work for the even isotopes is not completed yet but preliminary results show very pronounced intermediate structure effects in the strength function.

## Acknowledgement

Thanks are due to the sample preparation group of CBNM for preparing the metallic Pd samples, to the electronic and mechanical workshops of CBNM and S.C.K. for technical support, and to the linac operation group.

## References

1. P. Staveloz, E. Cornelis, L. Mewissen, F. Poortmans, G. Rohr, R. Shelley and T. van der Veen, in Proceedings of the Conference on Neutron Physics and Nuclear Data, Harwell 1978 (OECD Publication, 1978) p. 701
2. P. Staveloz, E. Cornelis, L. Mewissen, F. Poortmans, G. Rohr, R. Shelley and T. van der Veen, communication at the International Conference on Nuclear Cross Sections for Technology, Knoxville, October 22-26 1979, to be published.
3. C. Coceva, F. Corvi, P. Giacobbe and G. Carraro, Nucl. Phys. A117 (1968)586
4. A.V. Popov, K.Trzeciak, Khvan Cher Gu, Report SINR, 83-11013, 1977
5. Hvan Cher Gu, A.B. Popov, K. Trzeciak, in Proceedings of the Conference on Neutron Physics and Nuclear Data, Harwell, 1978 (OECD Publication, 1978) p. 327
6. V.N. Singh, R.C. Block and Y. Nakagama, Nucl. Sci. Eng. 67 (1978) 54
7. R.L. Macklin, J. Halperin and R.R. Winters, Nucl. Sci. Eng. 71 (1979) 182
8. R.W. Hockenbury, H.R. Knox and N.N. Kanshal, in Proceedings of the Conference on Nuclear Cross Sections and Technology, Washington, D.C. USA, 1975, ed. by R.A. Schrack and C.D. Bowman (NBS Special Publication 425, Vol.II, 1979) p.905
9. T. Babeliowsky, C. Cervini and A. De Keyser, "A data acquisition system for weighted multiparameter measurements", in preparation.
10. C. Le Rigoleur and A. Armand, Proceedings of NEACRP/NEANDC Specialists' Meeting at Karlsruhe, published in report KFK 2046 (1975)
11. F. Hensley, private communication
12. G. de Saussure, D.K. Olsen and R.B. Perez, Report ORNL/TM-6286, 1978
13. F.H. Fröhner, Report GA-6906 (1966)
14. G. Rohr, L. Maisano and R. Shelley, contributed paper at this meeting

Table I. Resonance parameters of $^{105}Pd$

| $E_0$ (eV) | $2g\Gamma_n$ (meV) | $\Gamma_\gamma$ (meV) | $E_0$ (eV) | $2g\Gamma_n$ (meV) | $\Gamma_\gamma$ (meV) |
|---|---|---|---|---|---|
| 11.79 ± 0.01 | 0.21 ± 0.01 | 151.1 ± 2.1 | 482.54 ± 0.16 | 5.2 ± 0.3 | |
| 13.23 ± 0.01 | 2.29 ± 0.03 | 174.5 ± 3.4 | 492.05 ± 0.16 | 0.18 ± 0.04 | |
| 25.15 ± 0.01 | 3.92 ± 0.05 | 135.1 ± 2.5 | 499.11 ± 0.17 | 0.32 ± 0.04 | |
| 30.12 ± 0.01 | 0.36 ± 0.01 | 151.7 ± 4.1 | 511.58 ± 0.17 | 2.50 ± 0.05 | |
| 38.44 ± 0.02 | 0.35 ± 0.01 | 154.1 ± 6.7 | 512.99 ± 0.18 | 3.31 ± 0.06 | |
| 42.58 ± 0.02 | 0.07 ± 0.02 | | 532.30 ± 0.18 | 28.5 ± 0.6 | 167. ± 25. |
| 55.21 ± 0.03 | 6.70 ± 0.04 | | 543.32 ± 0.19 | 1.96 ± 0.05 | |
| 68.32 ± 0.04 | 1.68 ± 0.02 | 137. ± 15. | 547.21 ± 0.20 | 89.4 ± 1.3 | 152. ± 15. |
| 77.73 ± 0.05 | 14.0 ± 0.2 | 138. ± 18. | 568.08 ± 0.20 | 27.7 ± 0.7 | 114. ± 15. |
| 86.72 ± 0.05 | 16.1 ± 0.3 | 125. ± 15. | 578.97 ± 0.21 | 22.6 ± 0.6 | |
| 101.09 ± 0.06 | 0.06 ± 0.01 | | 591.05 ± 0.22 | 95.2 ± 1.6 | 130. ± 15. |
| 101.71 ± 0.07 | 0.03 ± 0.01 | | 593.24 ± 0.22 | 34.3 ± 0.8 | |
| 104.00 ± 0.07 | 1.32 ± 0.03 | | 605.32 ± 0.23 | 84.3 ± 1.4 | 155. ± 10. |
| 117.01 ± 0.08 | 0.14 ± 0.01 | | 611.27 ± 0.23 | 1.69 ± 0.06 | |
| 126.33 ± 0.09 | 3.5 ± 0.04 | | 617.08 ± 0.23 | 4.9 ± 0.6 | |
| 130.59 ± 0.09 | 0.11 ± 0.01 | | 621.31 ± 0.24 | 29.4 ± 0.8 | 171. ± 40. |
| 134.12 ± 0.09 | 0.30 ± 0.01 | | 628.93 ± 0.24 | 1.65 ± 0.06 | |
| 136.42 ± 0.10 | 0.12 ± 0.01 | | 659.33 ± 0.26 | 2.01 ± 0.06 | |
| 141.21 ± 0.10 | 11.5 ± 0.1 | 145. ± 25. | 663.22 ± 0.26 | 67.9 ± 1.9 | 140. ± 20. |
| 150.21 ± 0.11 | 58.8 ± 1.5 | 130. ± 20. | 671.36 ± 0.27 | 1.40 ± 0.06 | |
| 155.04 ± 0.12 | 4. ± 0.06 | | 682.64 ± 0.27 | 8.7 ± 0.9 | |
| 158.87 ± 0.12 | 7.2 ± 0.07 | | 697.00 ± 0.28 | 39.4 ± 1.4 | 137. ± 20. |
| 168.38 ± 0.13 | 1.5 ± 0.1 | | 700.66 ± 0.28 | 25.8 ± 1.2 | |
| 170.73 ± 0.14 | 0.20 ± 0.01 | | 712.11 ± 0.29 | 94. ± 3.8 | |
| 183.97 ± 0.15 | 16.8 ± 0.1 | 171. ± 13. | 717.36 ± 0.29 | 2.53 ± 0.08 | |
| 202.63 ± 0.18 | 11.8 ± 0.1 | | 724.44 ± 0.30 | 63.9 ± 1.8 | 217. ± 25. |
| 208.38 ± 0.19 | 0.07 ± 0.01 | | 733.74 ± 0.30 | 2.37 ± 0.08 | |
| 215.91 ± 0.20 | 0.19 ± 0.02 | | 738.31 ± 0.31 | 1.76 ± 0.07 | |
| 226.75 ± 0.21 | 8.6 ± 0.1 | | 750.70 ± 0.31 | 6.45 ± 0.09 | |
| 251.40 ± 0.24 | 6.4 ± 0.4 | | 757.64 ± 0.32 | 68.9 ± 2.1 | 163. ± 10. |
| 252.49 ± 0.25 | 38.4 ± 0.5 | | 780.73 ± 0.33 | 130.1 ± 2.7 | 155. ± 5. |
| 259.99 ± 0.26 | 43.8 ± 0.5 | 140. ± 15. | 789.45 ± 0.34 | 70.8 ± 1.9 | 108. ± 7. |
| 286.98 ± 0.30 | 6.1 ± 0.2 | | 794.54 ± 0.34 | 95.6 ± 2.3 | 145. ± 6. |
| 305.63 ± 0.08 | 106.9 ± 0.9 | 150. ± 15. | 808.03 ± 0.35 | 29. ± 1.4 | 120. ± 30. |
| 313.94 ± 0.09 | 4.3 ± 0.2 | | 819.71 ± 0.36 | 15.7 ± 1.6 | |
| 328.14 ± 0.09 | 3.4 ± 0.2 | | 824.74 ± 0.36 | 37.3 ± 1.9 | 102. ± 25. |
| 339.86 ± 0.10 | 0.74 ± 0.03 | | 833.11 ± 0.36 | 5.6 ± 1.4 | |
| 347.24 ± 0.10 | 60.6 ± 0.9 | 175. ± 7. | 839.38 ± 0.37 | 36.4 ± 1.9 | 128. ± 30. |
| 354.66 ± 0.11 | 76.4 ± 1.4 | 185. ± 8. | 857.74 ± 0.37 | 12.7 ± 1.6 | |
| 370.66 ± 0.11 | 24. ± 0.34 | 116. ± 17. | 861.30 ± 0.38 | 25.5 ± 1.8 | |
| 377.49 ± 0.12 | 5.6 ± 0.3 | | ☆ 872.98 ± 0.38 | 31.7 ± 2.0 | |
| 389.40 ± 0.12 | 27.1 ± 0.4 | 159. ± 20. | 875.74 ± 0.39 | 1.5 ± 0.1 | |
| 392.94 ± 0.12 | 0.86 ± 0.03 | | 890.13 ± 0.40 | 21.8 ± 1.9 | |
| 395.08 ± 0.12 | 1.07 ± 0.03 | | 897.47 ± 0.41 | 4.2 ± 1.6 | |
| 401.87 ± 0.13 | 7.5 ± 0.2 | | 904.06 ± 0.42 | 8.1 ± 1.7 | |
| 411.88 ± 0.13 | 0.94 ± 0.04 | | 925.57 ± 0.43 | 208.0 ± 5.7 | 165. ± 5. |
| 418.59 ± 0.13 | 2.7 ± 0.2 | | 940.96 ± 0.44 | 77.1 ± 3.2 | 129. ± 10. |
| 431.41 ± 0.14 | 64.2 ± 0.9 | 115. ± 5. | 958.63 ± 0.45 | 163. ± 3.9 | 198. ± 7. |
| 449.73 ± 0.15 | 53.5 ± 0.7 | 189. ± 8. | 977.73 ± 0.46 | 102.9 ± 2.8 | 159. ± 7. |
| 466.77 ± 0.15 | 112. ± 2. | | 986.84 ± 0.48 | 14. ± 1.6 | |

☆ Mixture with even isotope resonance

Table I continued

| $E_0$ (eV) | 2g $\Gamma_n$(meV) | $\Gamma_\gamma$ (meV) |
|---|---|---|
| 1015.08 ± 0.13 | 8.9 ± 1.6 | |
| 1020.52 ± 0.13 | 34.5 ± 2. | 93. ± 25. |
| 1035.34 ± 0.13 | 6.7 ± 1.7 | |
| 1038.14 ± 0.13 | 4.4 ± 0.1 | |
| 1057.53 ± 0.13 | 99. ± 4. | 153. ± 8. |
| 1070.23 ± 0.13 | 34.9 ± 3.0 | |
| 1081.25 ± 0.14 | 30.7 ± 2.7 | |
| 1085.60 ± 0.14 | 17.7 ± 2.7 | |
| 1101.87 ± 0.14 | 8.7 ± 3.0 | |
| 1106.62 ± 0.14 | 132.3 ± 5.3 | 146. ± 8. |
| 1113.10 ± 0.14 | 3.0 ± 0.2 | |
| 1117.08 ± 0.14 | 4.5 ± 1.7 | |
| 1124.51 ± 0.14 | 43.9 ± 2.3 | 123. ± 25. |
| 1131.15 ± 0.15 | 3.0 ± 0.2 | |
| 1138.29 ± 0.15 | 4.0 ± 2.0 | |
| 1151.90 ± 0.15 | 3.3 ± 1.9 | |
| 1157.71 ± 0.15 | 14.7 ± 2.1 | |
| 1161.02 ± 0.15 | 23.5 ± 2.2 | |
| 1165.26 ± 0.15 | 5.6 ± 0.2 | |
| 1178.40 ± 0.15 | 3.5 ± 0.2 | |
| ☆1192.09 ± 0.16 | 21.5 ± 2.2 | |
| 1204.74 ± 0.16 | 2.8 ± 0.2 | |
| 1210.59 ± 0.16 | 18.4 ± 2.4 | |
| 1223.11 ± 0.16 | 106. ± 3.9 | |
| 1227.36 ± 0.17 | 95. ± 3.8 | 159. ± 10. |
| 1241.41 ± 0.17 | 206.4 ± 5.3 | 166. ± 5. |
| 1261.66 ± 0.17 | 129.7 ± 4.0 | 164. ± 5. |
| 1286.44 ± 0.17 | 182.2 ± 5.0 | 150. ± 5. |
| 1296.70 ± 0.18 | 51.6 ± 3.0 | 115. ± 10. |
| 1312.87 ± 0.18 | 59.6 ± 3.3 | 143. ± 20. |
| 1320.15 ± 0.18 | 3.3 ± 0.2 | |
| 1337.88 ± 0.19 | 49.6 ± 2.7 | 95. ± 15. |
| 1342.74 ± 0.19 | 43.1 ± 2.6 | 137. ± 30. |
| 1360.93 ± 0.19 | 24.3 ± 2.4 | |
| 1375.78 ± 0.19 | 113.1 ± 3.6 | 246. ± 15. |
| 1384.18 ± 0.20 | 15.1 ± 2.4 | |
| 1400.02 ± 0.20 | 49.7 ± 2.9 | 87. ± 17. |
| 1413.08 ± 0.20 | 47.9 ± 3.0 | 111. ± 25. |
| 1423.88 ± 0.20 | 1.5 ± 0.2 | |
| 1436.24 ± 0.21 | 7.2 ± 0.2 | |
| 1443.32 ± 0.21 | 36.3 ± 3.9 | |
| 1448.77 ± 0.21 | 131.5 ± 5.5 | 125. ± 7. |
| 1457.00 ± 0.21 | 41.8 ± 3.8 | |
| 1466.37 ± 0.21 | 67.2 ± 4.3 | 119. ± 17. |
| 1480.82 ± 0.22 | 238.5 ± 7.3 | 248. ± 12. |
| 1515.29 ± 0.22 | 30.6 ± 4. | |
| 1525.23 ± 0.23 | 36. ± 4.2 | |
| 1537.56 ± 0.23 | 12.5 ± 3.9 | |
| 1548.38 ± 0.23 | 242.1 ± 8.6 | 194. ± 5. |
| 1557.05 ± 0.23 | 6.3 ± 3.9 | |
| 1565.27 ± 0.24 | 168. ± 7. | 113. ± 5. |
| 1585.53 ± 0.24 | 6.1 ± 0.2 | |
| 1601.29 ± 0.24 | 140.1 ± 7.2 | 108. ± 7. |
| 1604.81 ± 0.25 | 129.3 ± 7. | 126. ± 8. |
| 1608.15 ± 0.25 | 47.4 ± 0.7 | |
| 1632.00 ± 0.25 | 79. ± 5.5 | 151. ± 23. |
| 1640.33 ± 0.25 | 91.3 ± 5.8 | 147. ± 23. |
| 1651.76 ± 0.26 | 134. ± 6.8 | 210. ± 25. |
| 1664.39 ± 0.26 | 6.8 ± 0.2 | |
| 1671.14 ± 0.26 | 1.4 ± 0.2 | |
| 1691.10 ± 0.26 | 3.4 ± 0.2 | |
| 1710.35 ± 0.27 | 2.1 ± 0.2 | |
| 1719.01 ± 0.27 | 9.0 ± 0.3 | |
| 1723.91 ± 0.27 | 3.6 ± 0.2 | |
| 1731.02 ± 0.27 | 5.8 ± 0.3 | |
| 1737.63 ± 0.28 | 11.0 ± 0.3 | |
| 1743.16 ± 0.28 | 2.9 ± 0.2 | |
| 1750.40 ± 0.28 | 18.7 ± 4.8 | |
| 1763.03 ± 0.28 | 8.5 ± 0.3 | |
| 1782.37 ± 0.28 | 30. ± 5.1 | |
| 1796.80 ± 0.29 | 6.7 ± 0.3 | |
| 1805.24 ± 0.29 | 18.1 ± 0.4 | |
| 1813.04 ± 0.29 | 171.4 ± 8.1 | 152. ± 6. |
| 1816.99 ± 0.30 | 32.3 ± 0.7 | |
| 1824.40 ± 0.30 | 7.8 ± 0.3 | |
| 1830.65 ± 0.30 | 7.7 ± 0.3 | |
| ☆1844.46 ± 0.30 | 63.5 ± 6.3 | |
| 1849.30 ± 0.30 | 49.7 ± 6.0 | |
| 1869.47 ± 0.31 | 102.1 ± 7.3 | 115. ± 7. |
| 1873.79 ± 0.31 | 12.6 ± 0.4 | |
| 1880.92 ± 0.31 | 297.3 ± 11. | 178. ± 5. |
| 1900.03 ± 0.32 | 33.1 ± 0.3 | |
| 1902.55 ± 0.32 | 5.9 ± 0.3 | |
| 1909.85 ± 0.32 | 5.0 ± 0.3 | |
| 1932.31 ± 0.32 | 181. ± 10. | 199. ± 15. |
| 1938.15 ± 0.33 | 166.1 ± 9.8 | 156. ± 8. |
| 1942.39 ± 0.33 | 24.5 ± 0.6 | |
| 1953.20 ± 0.33 | 49.3 ± 7.1 | |
| 1960.46 ± 0.33 | 69.5 ± 7.5 | |
| 1970.09 ± 0.33 | 61.1 ± 7.5 | |
| 1976.77 ± 0.34 | 18.1 ± 0.4 | |
| 1984.16 ± 0.34 | 2.3 ± 0.3 | |
| 1998.38 ± 0.34 | 9.4 ± 0.4 | |
| 2003.50 ± 0.34 | 220.3 ± 12. | 141. ± 6. |
| 2009.66 ± 0.35 | 76.4 ± 8.5 | |
| 2030.77 ± 0.35 | 76.9 ± 0.3 | |
| 2043.74 ± 0.35 | 122.6 ± 10. | 154. ± 15. |
| 2053.28 ± 0.36 | 80. ± 9.22 | |

☆Mixture with even isotope resonance

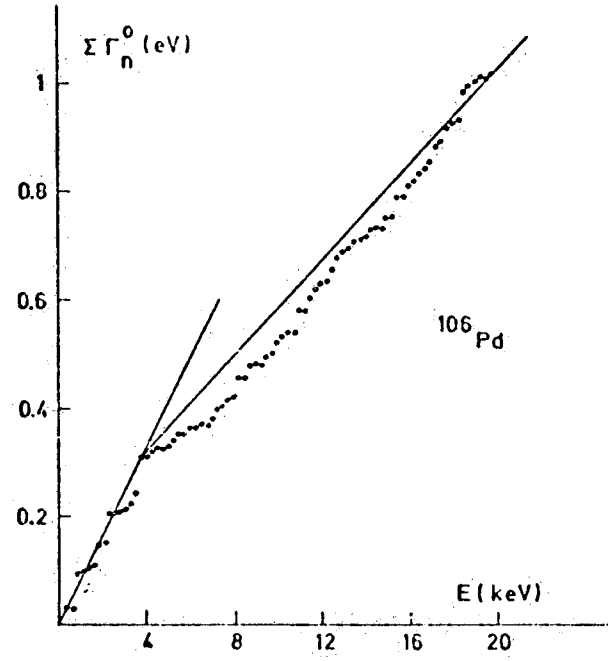


Fig. 1 : $^{106}$Pd cumulative sum of reduced neutron widths versus neutron energy

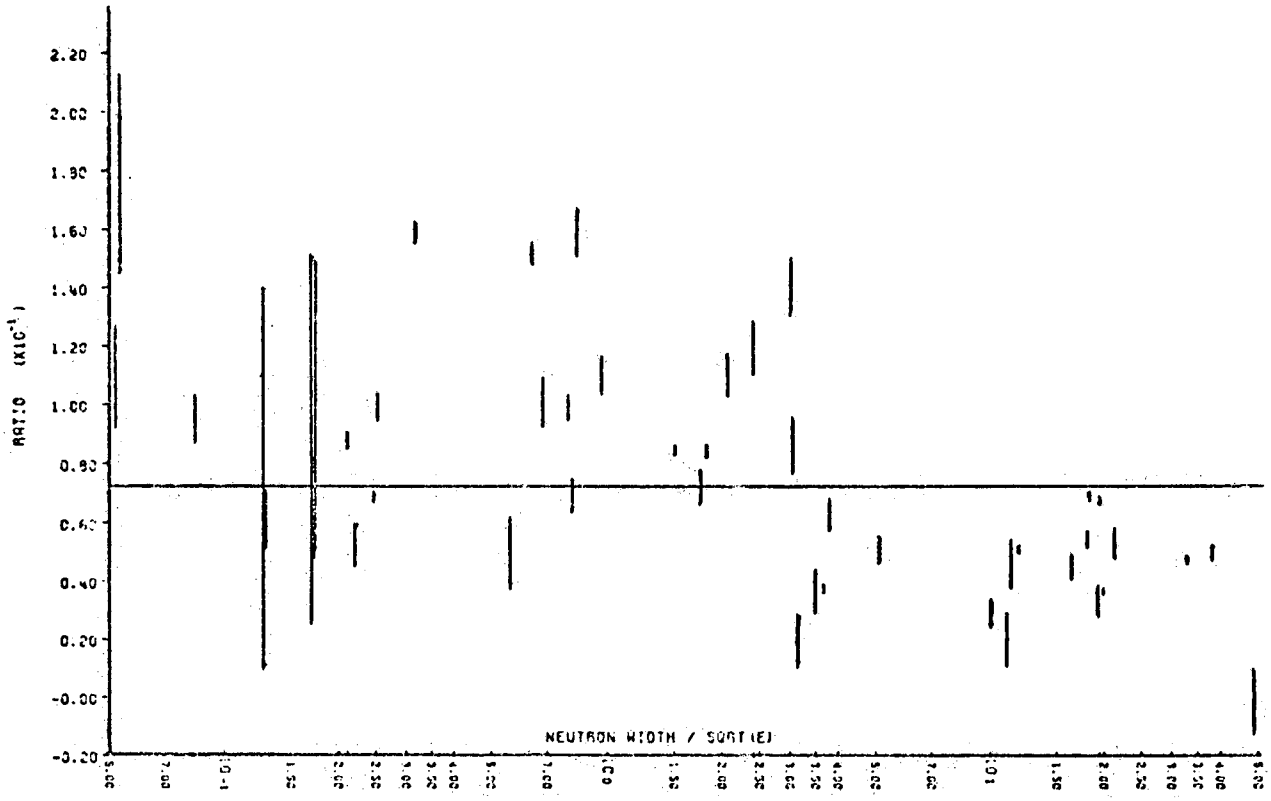


Fig. 2 : $^{108}$Pd - Ratio R of resonance areas with a high (5MeV) and with a low (0.55MeV) bias versus reduced neutron width.

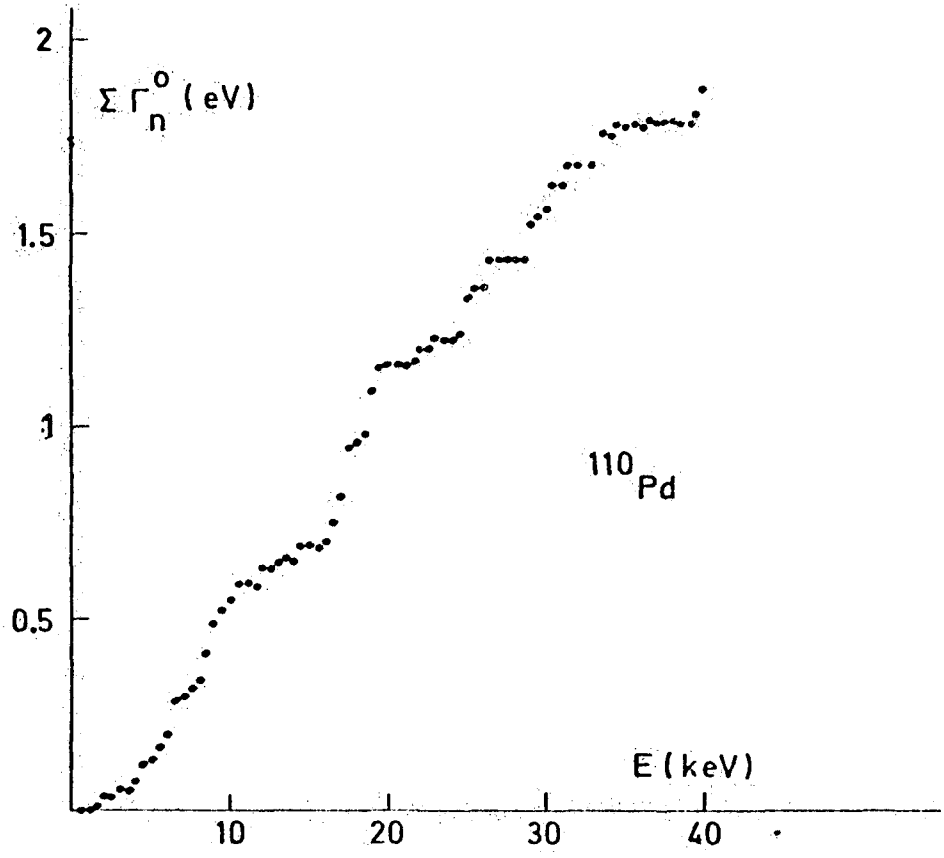


Fig. 3 : $^{110}$Pd - cumulative sum of reduced neutron widths versus neutron energy

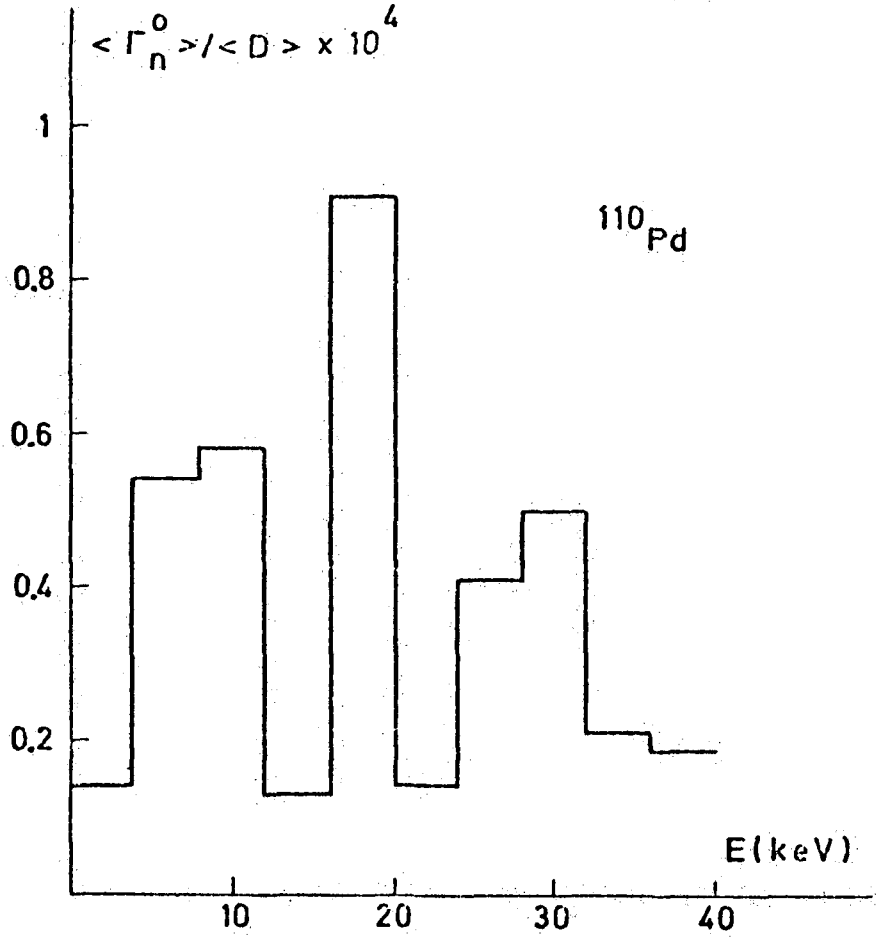


Fig. 4 : $^{110}$Pd - 'Strength function' averaged over energy intervals of 4 keV, s- and p-wave resonances

# NEUTRON CAPTURE CROSS SECTIONS OF RUBIDIUM, YTTRIUM, NIOBIUM, CESIUM, CERIUM AND GADOLINIUM BETWEEN 0.5 AND 3.0 MeV

J.Voignier, S.Joly and G.Grenier

*Service de Physique Neutronique et Nucléaire*
*Centre d'Etudes de Bruyères-le-Châtel*
*B.P. n° 561*
*92542 MONTROUGE CEDEX, France*

ABSTRACT

Neutron capture cross sections have been measured for the nuclides Rb, Y, Nb, Cs, Ce, Gd and for the isotopes $^{155}$Gd, $^{156}$Gd, $^{157}$Gd, $^{158}$Gd and $^{160}$Gd in the 0.5 MeV to 3.0 MeV neutron energy range. Absolute capture cross sections are determined by combining the technique used to study gamma-ray strength functions and the spectrum method of measuring partial neutron capture cross sections. The gamma rays are detected by a NaI scintillator surrounded by an annular NaI detector. Time-of-flight techniques are used to improve the signal-to-background ratio. Present results are compared with ENDF evaluations and with recent results obtained from statistical model calculations.

## 1. INTRODUCTION

Fast neutron capture spectra and cross sections measurements are important in nuclear technology specially on fission product nuclei. Except for some isotopes for which activation methods can be used, capture cross section measurements are generally limited to neutron energies below 600 keV.

In the present method, neutron capture cross sections are determined through the direct γ-ray spectrum emitted by the sample. The γ-rays are detected by a NaI scintillator surrounded by an annular NaI detector. Because the solid angle is small, the probability of detection of more than one γ-ray of the cascade is small and the energy distribution of the capture γ-rays can be recorded.

## 2. EXPERIMENTAL CONDITIONS

Monoenergetic neutrons are produced by the $^{7}$Li(p,n)$^{7}$Be and T(p,n)$^{3}$He reactions. The 4 MV Van de Graaff accelerator of the Centre d'Etudes de Bruyères-le-Châtel is used to produce proton pulses of 1 ns width. The targets consist of metallic lithium or tritium adsorbed in titanium on tantalum and are from 40 to 80 keV thick for incident protons.

The samples are disks 60 mm in diameter and from 1.5 to 6.0 mm thick. Glass containers are used for rubidium and cesium. The spectrometer is working both in the anti-Compton (AC) and first escape (PE) modes at the same time. The

γ-ray detector efficiency is determined by calibrated radioactive sources and by nuclear reactions. The same sources and reactions are used to build response functions (AC and PE modes) of the spectrometer.

The γ-ray detector and the annulus are surrounded by a heavy shield of lead, lithium carbonate and boric acid. The collimator is filled by a 20 cm long $^{6}$LiH cylinder for attenuation of neutrons scattered by the sample. A tungsten shadow bar is added to shield the γ-ray detector from direct target radiation. The time dependent background is very sensitive to the shadow bar position. The neutron flux is monitored by a directional long counter.

## 3. DATA PROCESSING

Pulse-height spectra are recorded with time spectrum for both modes (AC and PE). The time-independent window is chosen to be six times wider than the capture γ-peak window in order to reduce the time-independent contribution to the pulse-height variance.

The net pulse-height spectra (background subtracted) are unfolded and corrected for the spectrometer efficiency. Several corrections are required to obtain absolute cross sections. Except for neutron transmission through the sample obtained experimentally and the γ-ray attenuation in the sample, all other corrections are calculated by a modified version of the Monte Carlo programme of D.L. SMITH [1] (multiple scattering, neutron source anisotropy and neutron attenuation in the sample).

## 4. RESULTS AND DISCUSSION

The integrated spectrum method used to determine capture cross sections from the γ-ray distribution has been described elsewhere [2]. Present results are compared with other data and with statistical model calculations obtained at Bruyères-le-Châtel.

- Rubidium capture cross sections versus neutron energy are shown in fig. 1. The solid curve represents a calculation made by SIMON [3] in 1979. The calculated values are in agreement, except at $E_n$ = 2.5 MeV which appears to be 30% too high.

- Yttrium capture cross sections are presented in fig. 2. All cross sections above 0.5 MeV are obtained by the activation method. We agree very well with STUPEGIA [4] data and, above 1 MeV, with values of KOROLEVA [5] . The discrepancy in this energy region is 5%. The solid curve represents a calculation made by THOMET in 1975 [6]. The ENDF/B IV evaluation is systematically too high.

- Results concerning the capture cross section of niobium are given in fig. 3. Most results for niobium were obtained with prompt γ-ray methods (large liquid scintillators, Maier-Leibnitz detectors). Our results up to 1.2 MeV are in good agreement with recent data of MACKLIN [7] and POENITZ [8] and with previous values of STAVIISKY [9] and DIVEN [10].

Above 2 MeV, our value is 20% higher than those of POENITZ. Calculations of LAGRANGE and DELAROCHE [11] fit very well most recent data.

- Cesium and cerium data reduction is in progress.

- Capture cross sections of the isotopes $^{155}$Gd, $^{156}$Gd, $^{157}$Gd, $^{158}$Gd and $^{160}$Gd as well as the natural gadolinium are shown in figs.4 through 9 . Except for $^{158}$Gd, there are no data in the energy range 0.5-3.0 MeV for the other gadolinium isotopes. FRIESENHAHN [12] data on natural gadolinium with a large liquid scintillator are in agreement with our measurements. Above 700 keV, no experimental data are available. The solid curve is the ENDF/B IV evaluation. The dashed line represents the BENZI evaluation [13].

Capture cross sections of $^{158}Gd$ can be obtained by the activation method. The available experimental data are in agreement except our value at 0.5 MeV which is too high. Our experimental data relating to $^{160}Gd$ are again in good agreement with calculations made at BRC [14]·KOMONOV [15] and FAWCETT [16] data seem systematically lower. Our data concerning the five separated gadolinium isotopes have been combined according to their natural isotopic abundances to obtain the natural gadolinium capture cross section. The values obtained are very close to our direct measurement on the natural sample.

## REFERENCES


[1] - D.L. SMITH, ANL/NDM-17 (1975), Argonne National Laboratory, Argonne.

[2] - S. JOLY et al., Nucl. Instr. Methods 153, 493 (1978).

[3] - G. SIMON (BRC), private communication.

[4] - D.C. STUPEGIA et al., J. of Nucl. Energy, 22, 267 (1968).

[5] - V.P. KOROLEVA et al., Conf. Intern. sur les données nucléaires, Paris (1966) p. 473.

[6] - P. THOMET, Conf. KieV (1975) Vol. 1, p. 252.

[7] - R.L. MACKLIN, Nucl. Sci. and Eng., 59, 12 (1976).

[8] - W.P. POENITZ, Report ANL/NDM-8 (1974).

[9] - Y.Y. STAVIISKI et al., J. Nucl. Energy A316 496 (1962) and Atom. Energy 10 255 (1962).

[10] - B.C. DIVEN et al., Phys. Rev. 120, 556 (1960).

[11] - J.P. DELAROCHE, Interactions of neutrons with nuclei, Conf. Lowell, Juillet 1976, CONF-760715-P2, p. 1291.

[12] - S.J. FRIESENHAHN et al., Nucl. Phys. A146, 337 (1970).

[13] - V. BENZI et al., Report DOC CEC (71) 9 (1971).

[14] - J.P. DELAROCHE (BRC), private communication.

[15] - V.N. KOMONOV et al., Conf. KieV (1977) Vol. 2, p. 206.

[16] - R.L. FAWCETT et al., Nucl. Sci. and Eng. 49,317 (1972).

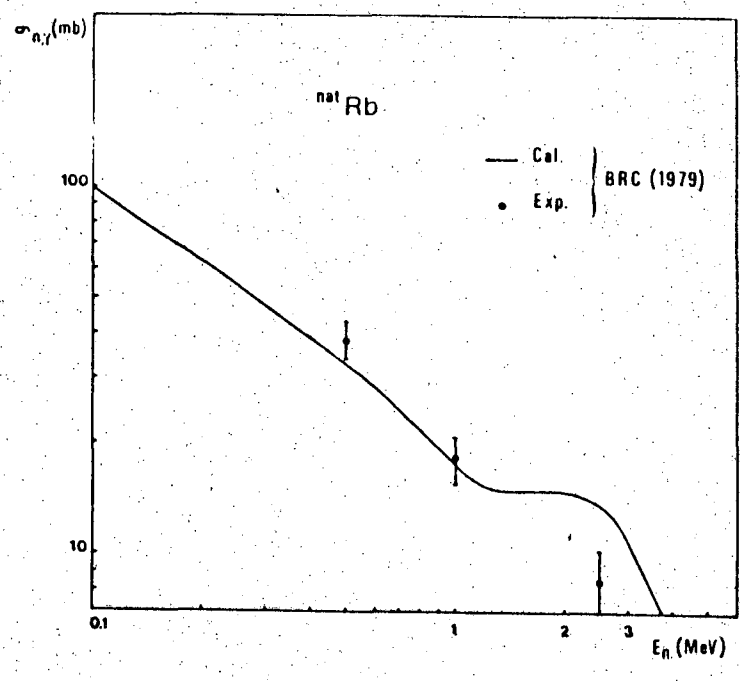


*Fig.1. Neutron capture cross section for $^{nat}Rb(n,\gamma)$.*

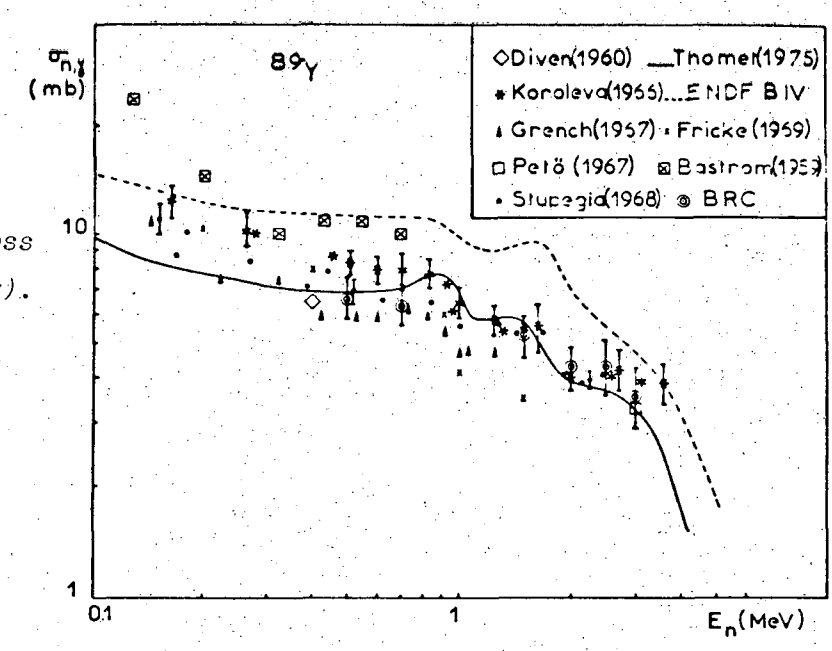


*Fig.2. Neutron capture cross section for $^{89}Y(n,\gamma)$.*

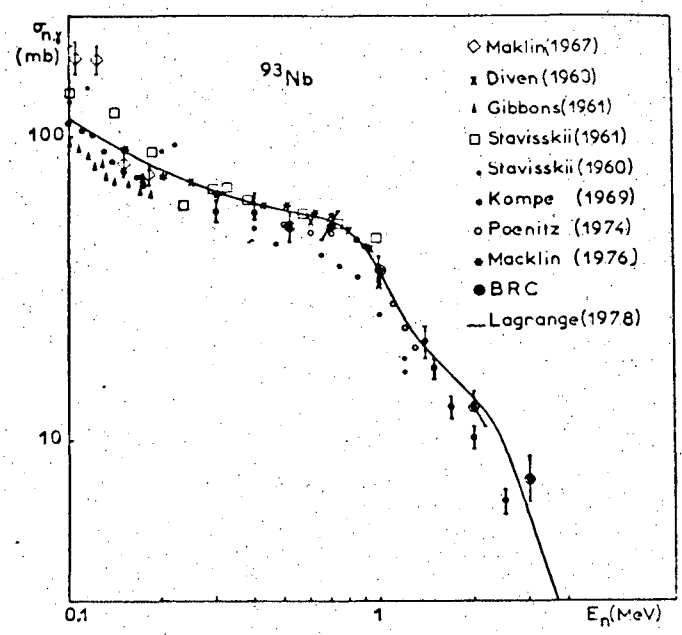


*Fig.3. Neutron capture cross section for $^{93}Nb(n,\gamma)$.*

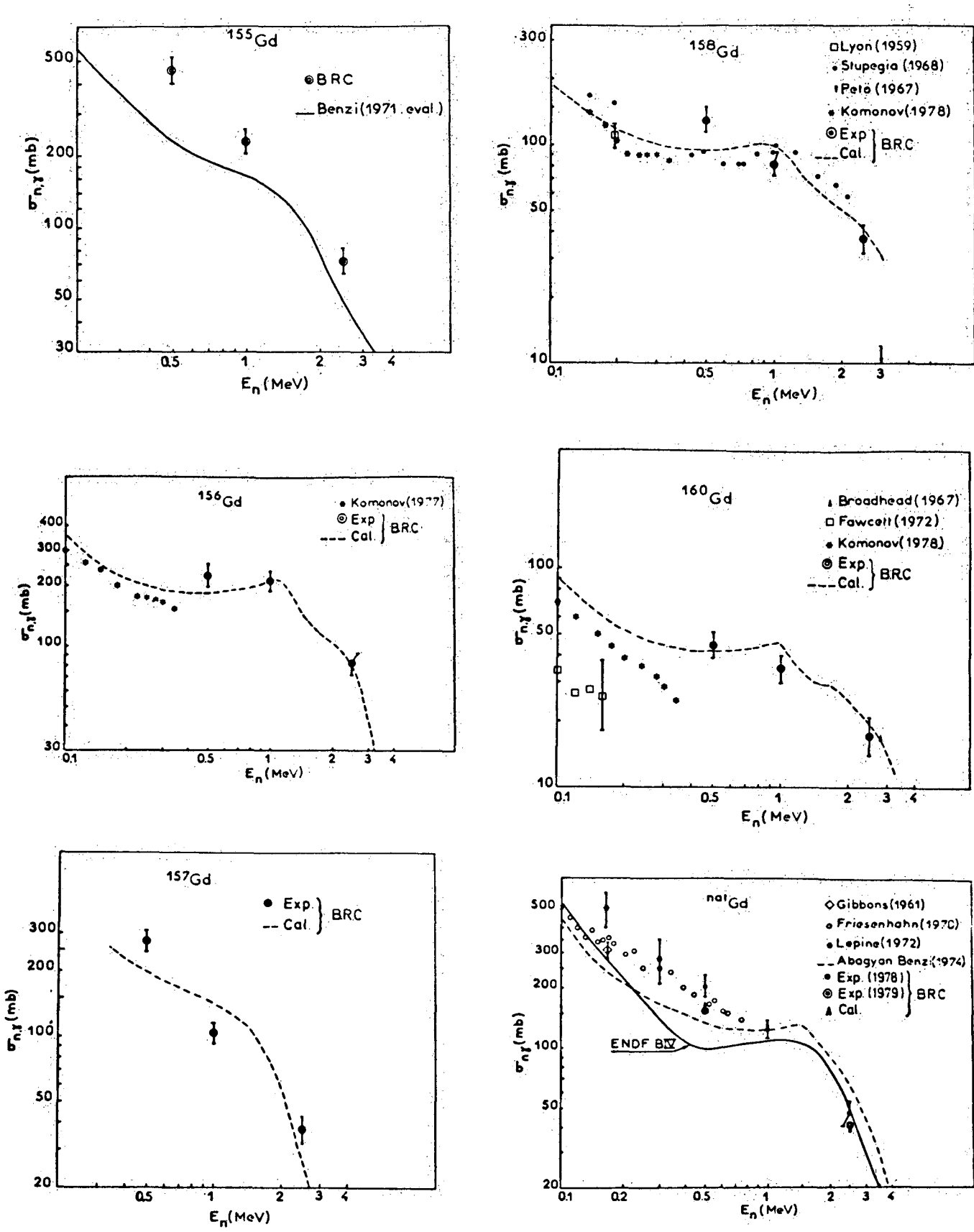


*Figs.4-9 : Neutron capture cross sections of $^{155}Gd$, $^{156}Gd$, $^{157}Gd$, $^{158}Gd$, $^{160}Gd$ and $^{nat}Gd$.*

# CAPTURE CROSS SECTION MEASUREMENTS ON NATURAL XENON, NATURAL KRYPTON AND ON VARIOUS KRYPTON ISOTOPES BETWEEN 3 AND 250 keV NEUTRON ENERGY

F. Käppeler and B. Leugers
Kernforschungszentrum Karlsruhe GmbH
Institut für Angewandte Kernphysik
D-7500 Karlsruhe, P.O.B. 3640
Federal Republic of Germany

The neutron capture cross sections of natural Xe, natural Kr, $^{84}$Kr and three samples enriched in $^{80}$Kr, $^{82}$Kr and $^{83}$Kr were measured at the Karlsruhe 3 MV Van de Graaff accelerator in the energy range from 3 to 250 keV. Neutron energies were determined by the time-of-flight technique with a resolution of 1.5 ns/m. Two $C_6D_6$-detectors with off-line pulse height weighting served for the detection of capture gamma-rays. For the capture cross sections an accuracy between 5 and 10 % was achieved. Furtheron, information on the overall gamma-ray multiplicity was derived from the probability for coincident observation of a single capture event in both detectors. In addition, the total neutron cross sections were measured simultaneously in the same experiment.

## 1. INTRODUCTION

For fast reactor applications the keV capture cross sections of krypton and xenon isotopes are of twofold interest. Most of these isotopes are fission products which determine the gas pressure in fuel elements. The residual isotopes which are shielded by neutron rich isobars and therefore do not occur in fission, can be used as tag materials to detect and locate fuel failure. For that purpose the capture cross sections are important to trace the isotopic composition of these tag materials during burn-up.

Measurements of capture cross sections on noble gases for neutron energies above 10 keV are not published in the literature so far. There is only one experiment by Maguire et al. /1/ on natural krypton and a mixture enriched in $^{78}$Kr and $^{80}$Kr which covered the energy range up to ∿10 keV. This situation was improved by the present measurement of the capture cross sections for the natural elements krypton and xenon as well as for the stable isotopes of krypton. In this report some aspects of this work are described. For more details see Ref. /2/.

## 2. MEASUREMENTS

The measurements were carried out at the Karlsruhe pulsed 3 MV Van de Graaff accelerator. As the neutron flight path had to be as short as possible, the main experimental problem was the design of a sufficiently dense sample.

Our first approach was to liquify the noble gases /3/ but it turned out that sample handling was difficult and that there were enhanced background problems from the required cryostat. Therefore we decided to use high pressure gas samples which worked reasonably well.

The experimental set-up is outlined in Fig. 1. Neutrons are produced by a fast pulsed proton beam via the $^7Li(p,n)$-reaction using metallic Li-targets. The beam repetition rate was 1 MHz, the pulse width 500 ps and the average current 5 μA. Neutron energies were determined by time-of-flight (TOF) between the neutron target and the samples which were located at a flight path of 60 cm. The neutron beam was collimated by a system of $^6LiCo_3$, boron resin and boron loaded paraffin.

The sample cannings were spheres of 2 cm diameter and 0.5 mm wall thickness and could withstand gas pressures up to 500 bar. For safety reasons the pressure used in the measurements was always below 300 bar. Capture events were registered by two 1ℓ $C_6D_6$-detectors at 5 cm distance from the samples with an overall time resolution of 0.8 ns. Therefore, the resolution in neutron energy was dominated by the sample thickness rather than by the timing. For example, at 50 keV neutron energy the resolution was 900 eV. The TOF and pulse height information from the two $C_6D_6$-detectors was stored in two 1024x16 channel matrices for off line pulse height weighting. In addition to the spectra of the individual detectors also a TOF spectrum from coincident events was recorded, to obtain information on the average multiplicity of the capture gamma-ray cascade.

At a flight path of about 1 m a $^6Li$ glass detector was used to measure the transmission through the samples with an energy resolution comparable to that of the capture measurement. Although this geometry is not ideal for a transmission measurement it allowed to determine the total cross sections with an accuracy of 10-20 %. This was sufficient for the correction of the capture data with respect to the neutron sensitivity of the $C_6D_6$ detectors.

In the experiment 6 samples were mounted on a sample changer perpendicular to the plane of Fig. 1 and cycled into the measuring position in intervals corresponding to equal neutron fluence. These intervals were defined by a neutron monitor at an angle of 90 deg to the beam axis. At a time, we used 3 gas samples, a gold reference sample as a cross section standard as well as an empty canning and a canning filled with a graphite sphere for background determination. The compositions of the gas samples are given in Table I.

The measurements were carried out in 3 runs. Two runs served for the determination of the spectra for all gas samples relative to gold. For data analysis the evaluated gold cross section of ENDF/B-IV was adopted. The uncertainty associated with this standard is not included in the estimates given in Table II. The third run was performed to investigate a possible background due to the massive high pressure valves. This was found to be negligible.

## 3. RESULTS

In the following some typical results are given. More complete information on data analysis and the evaluation of uncertainties is available in Ref. /2/.

a) Average multiplicity - The ratio of the coincident and the non-coincident count rates of the two $C_6D_6$-detectors yields immediately the quantity $(\bar{M}-1)\cdot C$ for the average multiplicity $\bar{M}$ of the capture gamma ray cascade. The constant $C = \Omega/4\pi\ \varepsilon(\bar{E}_\gamma)$ contains the solid angle $\Omega$ between sample and detectors and the efficiency for the average cascade energy $\bar{E}_\gamma$. Fig. 2 shows

this ratio as a function of neutron energy for three gas samples and for the gold reference sample. It is found that the natural krypton and xenon samples exhibit a considerably higher multiplicity than gold or $^{84}$Kr. The difference between natural krypton and $^{84}$Kr may be explained partly because the excitation energy of the compound system ($^{84}$Kr+n) is rather low (due to the comparably low neutron separation energy of $^{85}$Kr) and partly because the number of accessible compound levels is limited by the ground state spin of $^{84}$Kr. The large fluctuations with neutron energy in this case reflect the pronounced resonance structure of the $^{84}$Kr cross section in the keV region.

b) Total cross sections - Fig. 3 displays the total cross sections of $^{84}$Kr and natural krypton. The error bars on the data points indicate the statistical uncertainties. These are much smaller than the systematic uncertainties, which vary from about 20 % at 7 keV neutron energy to 7 % at 200 keV. Obviously, the resonance structure in the cross section for natural krypton is predominantly due to $^{84}$Kr. The dashed line above 100 keV represents a recent optical model calculation by Prince /3/ which describes existing measurements above 100 keV rather well.

c) Capture Cross Sections - The capture cross section of natural xenon is shown in Fig. 4. Again the error bars indicate only the statistical uncertainties. At present a systematic uncertainty of 15 % has to be quoted which is dominated by the uncertainty of the effective neutron binding energy for the isotopic mixture as it is required in the calculation of the cross section by the pulse height weighting technique.

In Fig. 5 the respective results for natural krypton and $^{84}$Kr are given. Compared to natural xenon the cross sections are much smaller leading to rather large statistical uncertainties below 10-20 keV. Similar to the total cross sections the $^{84}$Kr resonances clearly show up in the capture cross section of natural krypton, too. For $^{84}$Kr a systematic uncertainty of less than 4 % was estimated. The cross section of natural krypton was calculated with an effective binding energy

$$B_n = \frac{\sum \sigma_i H_i B_i}{\sum \sigma_i H_i} \qquad (1)$$

where the index i denotes the various isotopes and $H_i$ are the relative isotopic abundances. As averaged capture cross sections $\sigma_i$ were used in equ. (1), the estimated systematic uncertainty of about 5 % is also only valid for the average capture cross section of natural krypton. Therefore, the cross section is overestimated by up to 15 % in those energy intervals which correspond to strong $^{84}$Kr resonances. In Table II the capture cross sections of natural xenon and natural krypton are listed for energy bins of 10 and 20 keV.

Similar results were obtained for the mixtures enriched in $^{83}$Kr, $^{82}$Kr and $^{80}$Kr. These data together with the relative abundances and the isotopic cross sections define a system of linear equations. The solution of this system for the isotopic cross sections is complicated by the unexpected large values for $^{78}$Kr, so that the systematic uncertainties for the cross sections of $^{80}$Kr and $^{82}$Kr are of the order of 15-20 %.

## 4. CONCLUSIONS

The use of thin walled high pressure gas samples allowed the experimental determination of capture cross sections of noble gases in the keV neutron energy range. Measurements were performed on samples of natural krypton, $^{84}$Kr and on three mixtures enriched in $^{83}$Kr, $^{82}$Kr and $^{80}$Kr, from which the isotopic cross sections can be deduced. In addition, the capture cross

sections of natural xenon was measured in the same experiment. Simultaneously, information was obtained on the average multiplicity of the capture gamma-ray cascade and on the total neutron cross sections as well.

For completion of the data set for the krypton isotopes additional measurements are planned on pure $^{86}$Kr and on a mixture enriched in $^{78}$Kr.

## 5. REFERENCES

/1/ H.T. Maguire, jr., H.M. Fisher, R.C. Block, Proc. Int. Conf. on Neutron Physics and Nuclear Data for Reactors and Other Applied Purposes, Harwell (1978), p. 472.

/2/ B. Leugers, "Die Neutroneneinfangquerschnitte der Kryptonisotope und ihre Bedeutung für die Astrophysik", KfK-Report 2895, Kernforschungszentrum Karlsruhe, December 1979.

/3/ F. Hensley, "Annual Report Teilinstitut Kernphysik", KfK-Report 2504, Kernforschungszentrum Karlsruhe, October 1977.

/4/ A. Prince, "ENDF/B-IV Neutron Cross Section Evaluation for the Krypton Isotopes", BNL-Report NCS-51028, Brookhaven National Laboratory, January 1979.

Table I Isotopic compositions of the krypton samples

| Sample | Isotopic Enrichment (%) | | | | | |
|---|---|---|---|---|---|---|
| | $^{78}Kr$ | $^{80}Kr$ | $^{82}Kr$ | $^{83}Kr$ | $^{84}Kr$ | $^{86}Kr$ |
| $^{84}Kr$ | - | - | - | - | 100 | - |
| "$^{83}Kr$" | - | - | 16.1 | 71.0 | 12.9 | - |
| "$^{82}Kr$" | 0.18 | 20.3 | 75.6 | 3.8 | 0.2 | - |
| "$^{80}Kr$" | 9.0 | 35.0 | 34.7 | 9.5 | 11.6 | 0.3 |

Table II Average capture cross sections of natural xenon and natural krypton including the statistical uncertainties. The systematic uncertainties are 5 % for natural krypton and 15 % for natural xenon.

| Neutron Energy Interval (keV) | Capture Cross Section(mb), Statistical Uncertainty(%) | | | |
|---|---|---|---|---|
| | natural Krypton | | natural Xenon | |
| 10-20 | 119.0 | 2.4 | 491 | 1.2 |
| 20-30 | 77.5 | 2.0 | 416 | 0.7 |
| 30-40 | 63.7 | 1.6 | 370 | 0.6 |
| 40-50 | 52.3 | 1.6 | 302 | 0.6 |
| 50-60 | 46.4 | 1.7 | 259 | 0.6 |
| 60-80 | 41.1 | 1.3 | 207 | 0.5 |
| 80-100 | 34.4 | 1.5 | 173 | 0.5 |
| 100-120 | 30.0 | 1.6 | 150 | 0.6 |
| 120-140 | 27.7 | 1.7 | 137 | 0.7 |
| 140-160 | 26.4 | 1.7 | 128 | 0.7 |
| 160-180 | 24.3 | 1.9 | 122 | 0.7 |
| 180-200 | 23.2 | 2.3 | 116 | 0.9 |

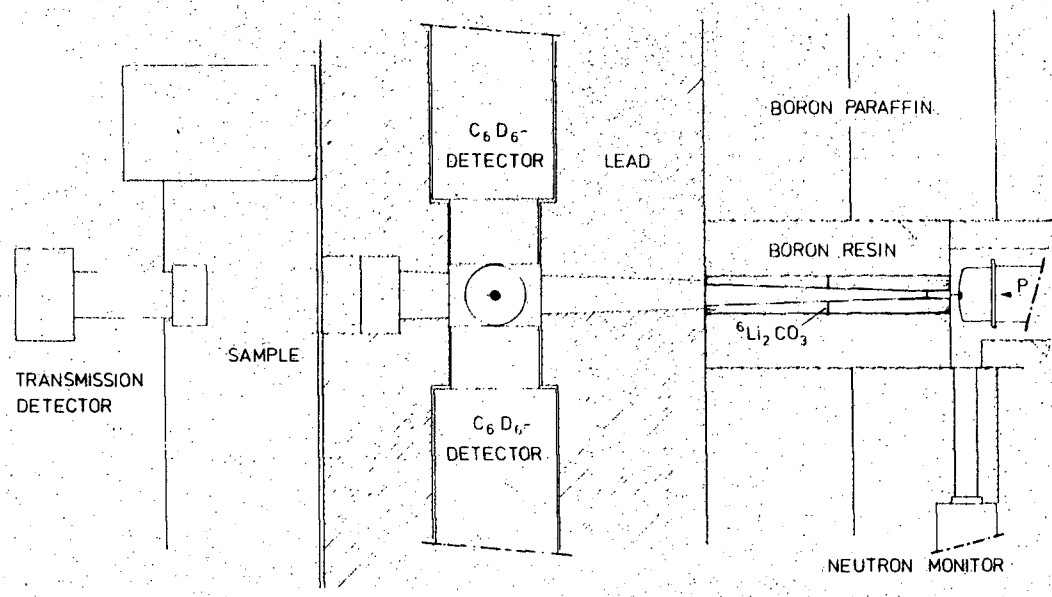


Fig. 1 Schematic view of the experimental setup.

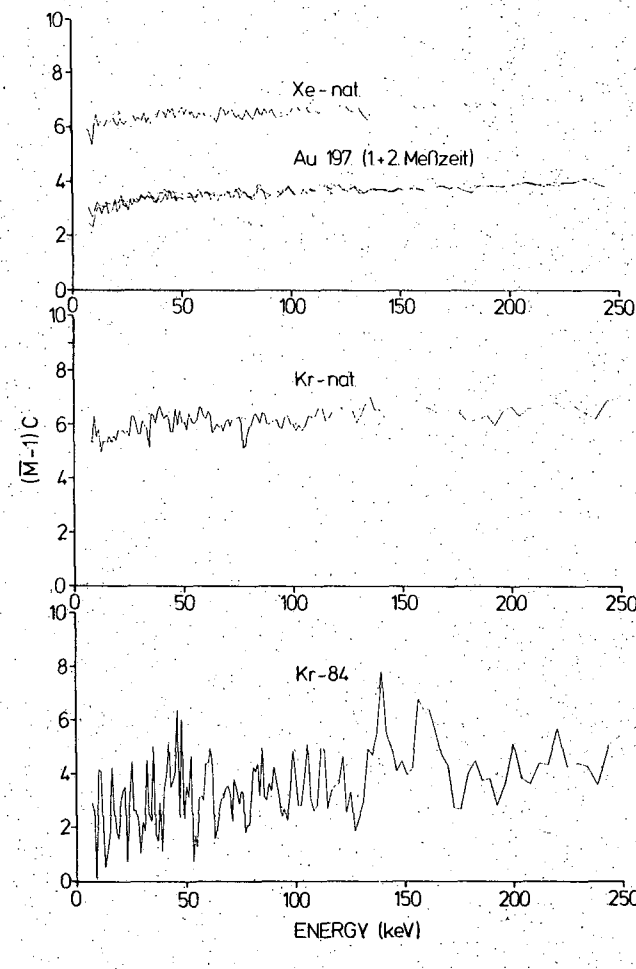


Fig. 2 The energy dependence of the expression $(\bar{M}-1)C$ in relative units. $\bar{M}$ is the average capture gamma ray multiplicity.

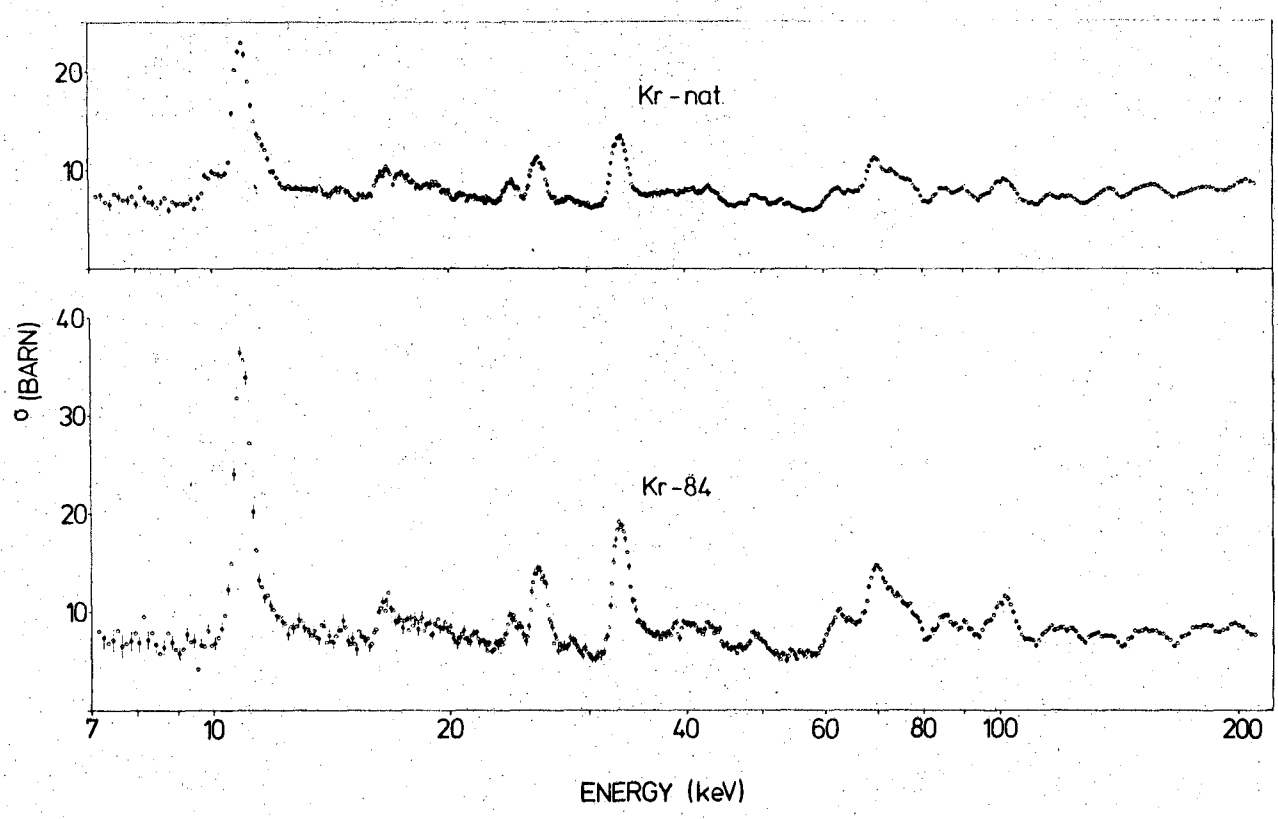


Fig. 3 The total neutron cross sections of natural krypton and $^{84}Kr$ between 7 and 200 keV. The errors bars indicate the statistical uncertainty.

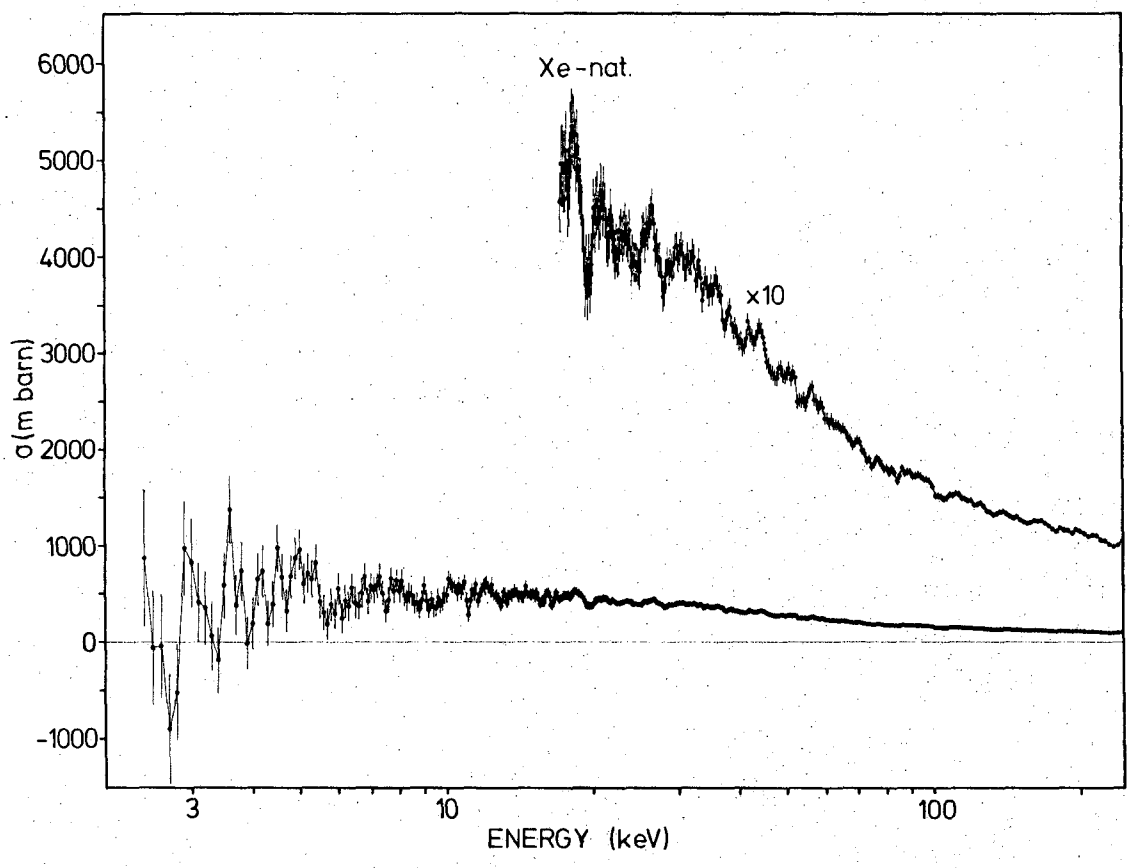


Fig. 4 The neutron capture cross section of natural xenon between 2.5 and 200 keV. The error bars indicate the statistical uncertainty only.

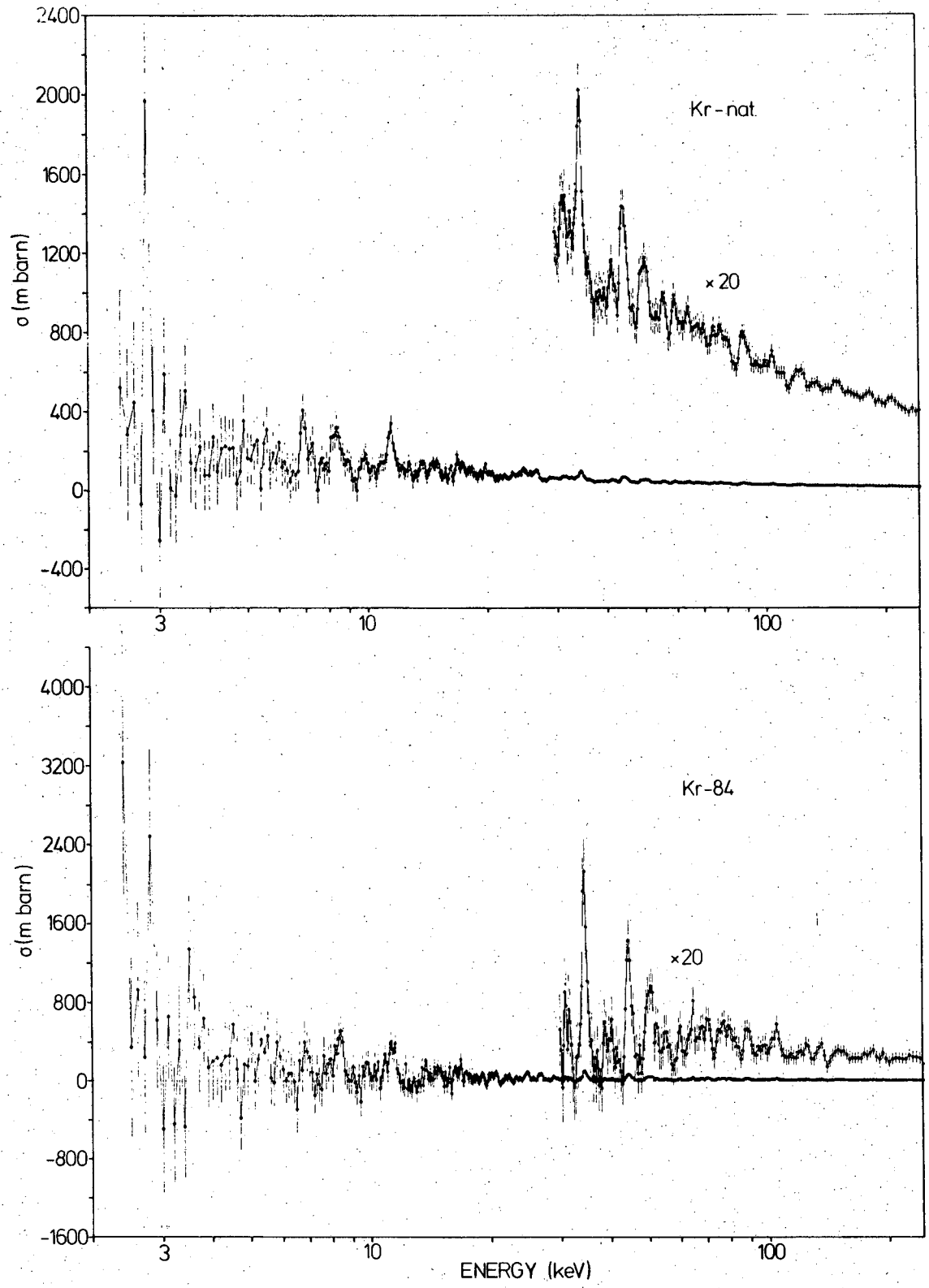


Fig. 5 The neutron capture cross sections of natural krypton and $^{84}Kr$ between 2.5 and 250 keV. The error bars indicate the statistical uncertainty only.

# LOW ENERGY NEUTRON CROSS SECTION MEASUREMENTS OF RADIOACTIVE FP NUCLIDES

H.G.Priesmeyer
Institut für Reine und Angewandte Kernphysik, Universität Kiel
IKK, Reaktorstation
D- 2054 Geesthacht, Germany

## Abstract

This paper summarizes cross section measurements and resonance parameter determinations on radioactive nuclides, which have been performed after the second FPND meeting at Petten in 1977. By "low energy" the range below about 1 keV is defined. Results are compared to requirements given in Review Paper 7 of the Petten meeting.
Future needs include the extension of measurements to higher energies, in order to improve resonance statistics, investigation of FP nuclides with shorter halflives, and measurements of radioactive nuclides produced by irradiation.
Systematics and completeness of cross-section data should be an important impetus for measurements, when data needs for reactors seem to be largely satisfied.

## Introduction

Since the second FPND Advisory Group Meeting and the publication of the recommendations of E.FORT in Review Paper 7 /1/, a number of measurements have been performed. In these measurements, fast-chopper time-of-flight spectrometers still play an important role /2/, but LINAC experiments /3/ seem to be necessary to extend the energy range.

The major difficulties of such experiments arise from the radioactive sample material. But not all measurements imply the same degree of difficulty, since there are qualitative differences between "radioactive" samples, not only as handling and health physics are concerned, but also as regards to the kind of experiment intended: several thousands of curies of 99 Tc are easier to handle and shield than a few curies of 90 Sr; for a pure ß - emitter it is much easier to perform a capture experiment than for a nucleus, that produces a high $\gamma$- ray background by its radioactive decay; long-lived nuclides have

usually smaller specific activities (Ci/g), depending on their decay constant and molecular weight; often a compromise has to be found between the amount of sample material necessary for the measurement and tolerable from the handling point of view and the amount of material available.

Techniques and experimental methods

Sample preparation and handling has almost always been a crucial point in the measurements on radioactive material. The easiest way to start with is a stable isotope, pure or highly enriched, to manufacture a suitable sample geometry, and to produce the nucleus desired by irradiation in a high neutron flux. This method does of course depend on the appropiate capture cross section for the original isotope. But it has been used in early measurements like those on 198 Au and 233 Pa performed at Idaho /4/ as well as recent measurements of the Russian group at Dimitrovgrad /5/ on 134 Cs and 60 Co /6/. At Kiel university, we have tried a different approach, by investigating gross fission product samples, produced by fission of 235 U /7/.
It seems to become practise that sample geometries are such that three measurements with different sample thicknesses can be performed on the same sample, according to the three space axes. Different sample thicknesses are necessary if one uses the area method for resonance parameter analysis.

Gram amounts of material are usually necessary for the measurements, but the tendency goes to less weight. Even if the preparation of samples of isotopes taken from nuclear waste could become easier in the future - which is not selfevident, since a higher degree of automation in the course of reprocessing leaves less possibilities for such special demands - one has to live with the isotopic mixture as it is produced by fission. Two "necessities" emerge from this fact: a.) the isotopic composition depends on the burnup history, therefore the fractional abundances have to be determined by mass spectrometry ( isotopically enriched material is not available), b.) besides the radioactive FP isotopes there are always the stable ones of the nuclide present in the sample; therefore it is useful to measure also a sample of the stable element, with the natural abundances or certain enrichments of the isotopes.

In cases, where the sample has been prepared by irradiation, one should have a second identical, but unirradiated sample for open beam compensation in the case of transmission experiments.

A quality control for a radioactive sample can be done by several methods, in oder to assure homogeneity and geometric size of the material. We have used $\gamma$-scan with our Cs fission product mixture, autoradiography for unirradiated U samples, neutron and X-ray radiography for other samples like 99 Tc or Ru. Radiographic methods yield a rapid survey over the whole sample area and are superiour to pointwise scanning when isotopic homogeneity can be assumed. At our institution neutron radiography with Gd or Dy foil detectors has also proven to be very useful with highly $\gamma$-radioactive material. Accuracies can be down to 0.1 mm spatial resolution.

Small samples require precise positioning in the neutron beam. To achieve this we also use neutron radiography with Dy foil and Polaroid film.

Among the time-of-flight spectrometers used for fission product experiments, choppers have certain "inherent" advantages , as far as total and scattering cross section experiments are concerned, because of their close relation to reactors:

a.) The sample is placed between neutron source and chopper rotor. Therefore the radiation from the sample is shielded by the rotor and the background contribution from $\gamma$ rays is reduced. This is especially important when Li-6 glass scintillators or B-10/NaI detectors are used as neutron

detectors.

b.) Most reactors are equipped with irradiation facilities implying the possibilities of handling highly radioactive material (hot cells, radiography, chemistry etc.). This allows irradiation of samples and rapid transportation to the spectrometer.

Choppers can work on very small samples, provided they are operated at a reactor with high neutron flux. Their main disadvantage is the limited energy range and resolution, but for energies from thermal up to about 20 eV they are more economic than other pulsed sources becauseof their high duty cycle.

Background-to-signal ratios for single rotor choppers (like the Kiel chopper, with Li-6 glassdetectors) are in the vicinity of 15%, depending on the energy range, but can be considerably reduced ( max. 4%, Dimitrovgrad) when three phased rotors and He-3 counters are used. The use of the latter detectors implies a reduction in resolution. Therefore the choice of high-pressure He-3 gas-scintillators with an efficiency of 30% at 1 keV and low $\gamma$ ray sensitivity would be an advantage. On the other hand B-10/NaI detectors can only be used, when the $\gamma$ ray background is very low.

## Summary of recent experiments on radioactive samples

Laboratories involved:

D = Dimitrovgrad fast chopper
K = Kiel fast chopper
RPI = Rensselaer Linac

### 133 Cs, 134 Cs (D) /5/

The 134 Cs ($T_{1/2}$ = 2.06 y) was produced by irradiating stable 133 CsCl in the reactor SM 2 at a neutron flux of $\approx$ 4. $10^{14}$ n/cm$^2$ s. The energy range investigated was from 1 eV to 400 eV with 70 ns/m resolution and less than 4% background. Of the 20 resonances found in 133 Cs, those up to 240 eV yield statistical data, which differ slightly from BNL 325/III. ( $\bar{D}$ = 16.3±2.3 eV, $S_0$= (1.02±0.43).$10^{-4}$, $I_\gamma$ = 404±90 b ). In 134 Cs six new resonances were found. They lead to an estimate for the statistical properties: $\bar{D}$ = 27.0 ± 7.5 eV, $2g\bar{\Gamma}_n^0$ = 0.49 ± 0.28 meV, $S_0$= ( 0.09 ± 0.06 ).$10^{-4}$ , $I_\gamma$ 22±12 b.
(A seventh resonance at 42.13 eV must be assigned to 135 Cs!)

### 133 Cs, 135 Cs, 137 Cs FP mixture (K)

The sample was investigated for the first time in 1969. Two resonances were seen, but no isotopic identification could be given. The isotopic abundances at that time were 133:135:137 = 0.488:0.171:0.341. After 10 years 21% of the original 137 Cs have decayed; this is adequate to allow for an isotopic identification of the resonances. The spectrometer resolution was 16 ns/m and the background ratio 15%. Resonance analysis is in progress. A first result (cf. Fig.1) is that the resonance at 42.08 eV can be assigned to 135 Cs. ( $T_{1/2}$ = 2.3 .$10^6$ y). The resonance was SHAPE - analysed and has a $\Gamma$ = 214 meV and $2g\Gamma_n$ = 33.4 meV. It contributes to the capture resonance integral with $\approx$33 b. This result is consistant with our earlier measurement as well as with the data of /5/, who found a neutron width of the order of

30 meV. (Our value 7 ± 2 meV , quoted in /5/, is not for $\Gamma_n$, but for $2fg\Gamma_n$. This has led the Russian group to assign the resonance to 134 Cs.)
Our final results will be published in ATOMKERNENERGIE( ATKE ).

99 Tc (K) /20/

The transmission experiment on this isotope is completed and the results are being published. The first two resonances at 5.62 eV and 20.39 eV have been reinvestigated because of the exceptionally high values ( $\Gamma_\gamma$ = 260 meV) of the capture width found by /8/ in a slowing -down - time spectrometer experiment. The same material as in /8/ has been used. The resonance parameters found are: $\Gamma$ = 171 meV, $2g\Gamma_n^0$ = 1.42 ± 0.05 meV at 5.62 eV and $\Gamma$ = 176 meV, $2g\Gamma_n^0$ = 1.489 ± 0.002 at 20.39 eV. They were derived from SHAPE analysis. The $\Gamma_\gamma$ values are now consistant with those given by ADAMCHUK /9 / for resonances above 20 eV as well as those communicated by LITTLE /10/. The two resonances contribute to the resonance capture integral with 253 b. The reason for the high values for $\Gamma_\gamma$ given by /8/ may be twofold: a.) Neutronradiography of their samples has shown, that the holders were sealed by a hydrogen-containing adhesive. b.) The inner cannings of the double-canned samples were stainless steel, instead of aluminum, which they had assumed to analyse the data.

129 I (K)

129 I has a halflife of 1.6 . $10^7$ y and is a $\beta^-$ and low-energy $\gamma$ emitter. The transmissions of two samples of $PbI_2$ with a total amount of 1.42 g I, enriched in 129 I to 86.1% (127 I : 13.9%) are presently investigated at Kiel. The energy range is from 20 eV to 1 keV with a resolution of 16 ns/m. Results will be published in ATKE.

151 Sm ( RPI , D)

Ref. /1/ states that an experimental effort should be made on this isotope. But the results of KIROUAC /12/ were possibly not taken into consideration ( $\bar{D}$ = 1.72 ± 0.07 eV, resolved resonances between 0.46 eV and 300 eV, $\sigma_{th}$ = 15200 b ). Meanwhile the results of another experiment have been published /13/. 11 levels have been discovered up to 18 eV.

107 Pd (RPI)

An extensive neutron capture and transmission measurement has been made at RPI /3/, giving the resonance parameters of 34 levels below 700 eV. The fission product Pd mixture ( 9.254 g powdered metal ) was used, which had a fractional abundance in 107 Pd of 15.7%. The average level spacing is 10.7 ± 1.5 eV, s-wave strength function 0.56 .$10^{-4}$. From the resonance at 6.834 eV a capture width of 125 ± 15 meV was deduced. Assuming the same value for all the other resonances, the resonance capture integral is found to be 87 b.

147 Pm (D)

A total cross section measurement was made by the Russian group /14/ from 0.02 to 250 eV with 70 ns/m resolution. 28 resonances were observed below 180 eV, among them three new ones. A total thermal cross section of 190±15 b was measured and a bound level at - 1.58 eV deduced. The total resonance integral is calculated to be 1840± 280 b.
From the resonances below 55 eV, an average level spacing $\bar{D}$ = 3.58 ± 0.50 eV and a strength function (2.9 ± 1.1) .$10^{-4}$ are found. For 11 resonances the $\Gamma_\gamma$ values have been deduced. The authors find that the $\Gamma_\gamma$ values group around two averages: 72 ± 6 meV ( 5 resonances) and 125 ± 9 meV ( 6 resonances ), but they use the average of 100 meV for the area analysis of other resonances.(cf. Fig. 2 )

153 Eu, 154 Eu, 155 Eu (D)

Very recently the results of fast chopper experiments on radioactive 154 Eu and 155 Eu were published /15/. For 154 Eu 20 levels between 0.188 eV and 27.30 eV were found and a $\bar{\Gamma}_\gamma$ = 130 meV, a $\bar{D}$ = 1.1±0.1 eV and a strength function $S_o$= 2.5 .$10^{-4}$ was calculated. The resonance capture integral is 1620 ± 240 b. The situation for 155 Eu is as follows: 7 levels in the 0.602 to 33.10 eV range, $\bar{D}$ = 4.8 ± 0.4 eV, $S_o$= 2.35 .$10^{-4}$, $I_\gamma$ = 17600 ± 4000 b

Gross Fission Products (K, KAPL)

At Kiel, we have produced several gross fission product samples by irradiating 235 U in different enrichments with different burnup histories ( diff. neutron fluxes and irradiation times). /16/, /17/, /18/. Below about 50 eV resolved resonance structure can be seen. These samples have cooled since several years and will be remeasured in the near future. The new transmissions will be compared to the old data, to look for buildup or decay in the resonance structure. Up to about 20 eV, this structure is already well understood. The results are comparable to those found at KAPL /19/.

Concluding remarks

a.) For the measurer, Ref. /1/ is still a source for measurement needs ( including stable FP nuclides at higher energies ). Radioactive candidates could be 103 Ru, 106 Ru , 85 Kr and 90 Sr.

b.) Difficulties in getting the sample material are often prohibitive to measurements, especially on radioactive targets. Isotope production by reactor irradiation of stable nuclides may be an advantage.

c.) In order to deduce the very important capture properties of $\gamma$ - radioactive FP nuclides, total plus scattering measurements or measurements in neutron fluxes that produce very high capture rates to surmount the decay - $\gamma$ - rates can be thought of.

d.) Gas production is a question of technological importance. Radioactive nuclei decay, because they are more or less apart from the

line of stability. On the other hand the binding energy of $\alpha$ - particles goes negative in the middle of the periodic table. Positive Q values make the (n, $\alpha$) - process probable in some cases. (Examples: 59Ni(n,$\alpha$)56 Fe 5.09 MeV, 147 Pm(n,$\alpha$) 144 Pr +7.38 MeV). Therefore the investigation of $\Gamma_\alpha$ can be taken into consideration.

e.) Techniques must be improved and experiences gathered for radioactive material. Future needs may imply the data for gas production (n , p ; n, $\alpha$ ) or for nuclear transmutation on isotopes produced by neutron irradiation (e.g. in structure materials ). Low-energy measurement techniques can be useful precursors to such experiments at higher energies.

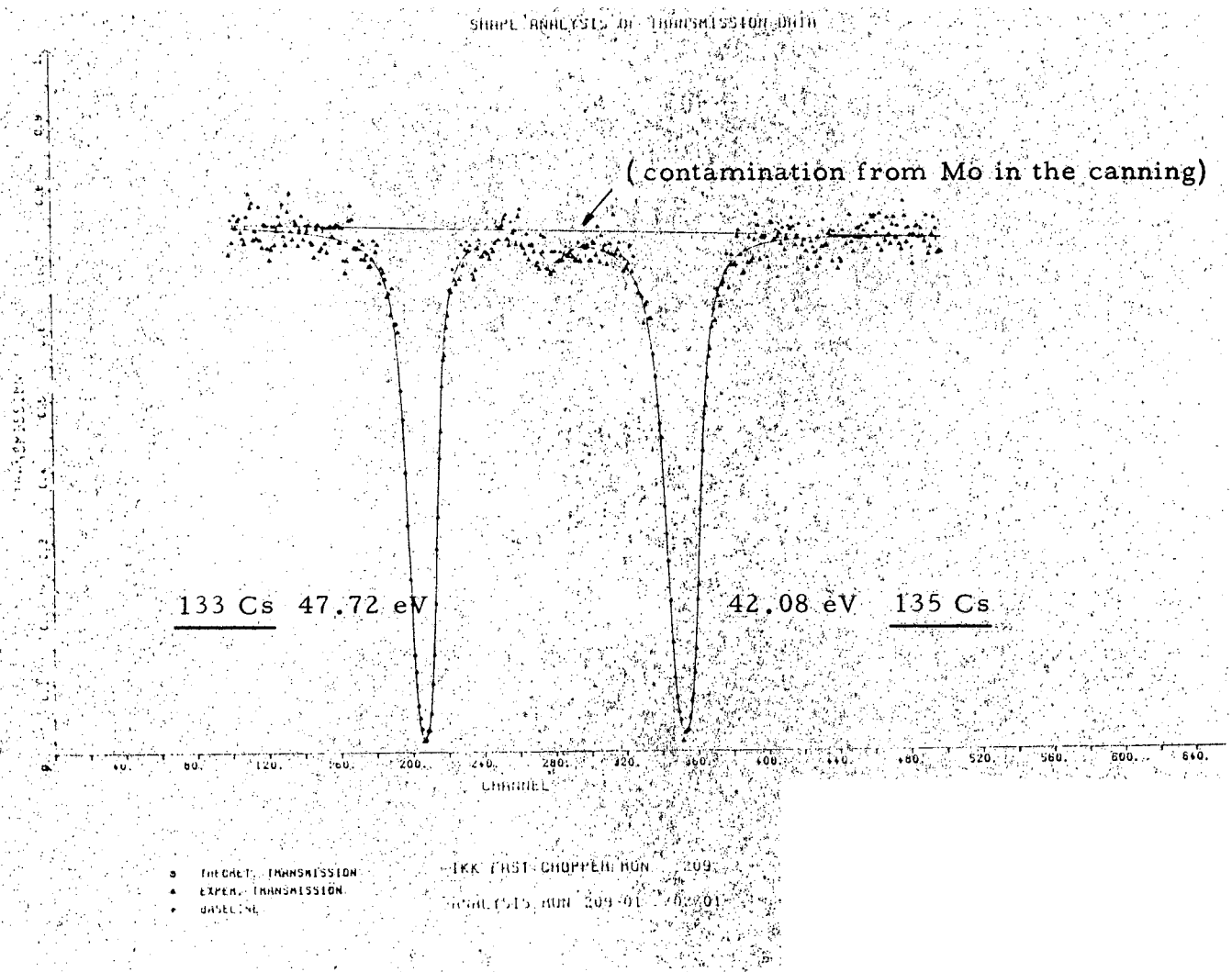


Figure 1 : SHAPE fit in the energy range 40 to 50 eV for the transmission of the Cs-FP-mixture

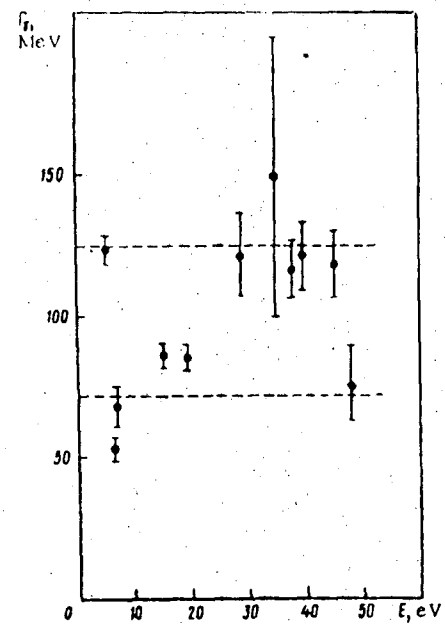


Figure 2: Grouped $\Gamma_\gamma$ - values for 11 levels in 147 Pm
( adopted from /14/ )

## References


/1/ E.FORT Review Paper No.7, FPND-1977, IAEA-213 , p.139

/2/ BELANOVA et al. Report NIIAR-P-6(272)

/3/ SINGH, BLOCK, NAKAGOME Nucl.Sc.Eng. 67 (1978), 54

/4/ SIMPSON, SCHUMAN EANDC Meeting ,Saclay 1961, p.85

/5/ BELANOVA et al. Sov.At.Energy 43(1978), 828

/6/ BELANOVA et al. Sov.At.Energy 46(1979), 57

/7/ JUNG, PRIESMEYER ATKE 17(1971), 144

/8/ CHOU, WERLE J.Nucl.Energy 27(1973), 811

/9/ ADAMCHUK et al. 73Kiev 2 172

/10/ LITTLE priv. communication RPI

/11/ PATTENDEN Nucl.Sc.Eng. 17(1963), 371

/12/ KIROUAC Phys, Rev. C, 11(1975), 895

/13/ ANUFRIEV et al. 77Kiev 2 263

/14/ ANUFRIEV et al. Sov. At.Energy 45(1978) , 453

/15/ ANUFRIEV et al. Sov.At.Energy 46(1979), 158

/16/ PRIESMEYER, HARZ ATKE 25 (1975), 109

/17/ PRIESMEYER, HARZ NBS SP 425, vol.2, p.744

/18/ PRIESMEYER, HARZ IAEA Symp. Safeguard.Nucl.Mat. (1976), II, 625

/19/ KIROUAC priv. communication KAPL

/20/ FISCHER, HARZ, PRIESMEYER 78Harwell conf. , p.718

# FAST NEUTRON CAPTURE CROSS SECTION MEASUREMENTS, EVALUATIONS AND MODEL CALCULATIONS OF FISSION PRODUCT NUCLEI*

W. P. Poenitz
Argonne National Laboratory
Argonne, Illinois 60439, USA

## ABSTRACT

The fast neutron capture cross sections of elemental rhodium, palladium, neodymium, and samarium were measured in the energy range 0.5 - 4.0 MeV relative to the standard capture cross section of gold. A large liquid scintillator and the time-of-flight technique were used in these measurements. Experimental data are rare or non-existent in this energy range and evaluations differ substantially, with a factor of 5 being common. The present data were used together with other experimental data and nuclear model calculations in order to provide a consistent set of isotopic and elemental capture cross sections.

## INTRODUCTION

The fast neutron capture cross sections of the more frequently occuring fission product nuclei play a significant role in the calculation of fast reactor reactivity, after-heat and sodium void effects, and are important for spent fuel-handling considerations. A 1% uncertainty of the calculated reactivity would result from a 30% uncertainty of these cross sections./1/ This led to uncertainty requests of ±10% for fast neutron capture cross sections of fission product nuclei between 1 keV and 10 MeV./2,3/ Whereas such requests may be modified to allow for larger uncertainties in the higher keV and MeV range, it is obvious from the consideration of existing (or nonexisting) data and evaluations that uncertainties are largest at higher energies. A recent comparison of evaluated neutron capture cross sections of 27 fission product nuclei at 2 MeV shows differences of a factor of 5 to be common while factors of 10 or more are encountered./4/

The fast neutron capture cross sections of fission product nuclei are a prime example for the proposition that nuclear model parameters can be determined with experimental data of some nuclei and cross sections for other nuclei can be calculated subsequently with these parameters. It has been observed that substantial differences exist between such calculated cross sections for nuclei where experimental data do not exist./5/ A similar

* This work was supported by the U.S. Department of Energy.

observation can be derived from a table containing 30 - keV capture cross sections for 27 fission product nuclei./4/ This table compares five different evaluations with experimental values where such are available.

Some remarkable improvements of the evaluated capture cross sections have been obtained by using integral measurements as a constraint./6,7/ However, such integral data are more likely to help in the normalization of cross sections in the lower-keV range where evaluation differences are less pronounced than for the MeV range.

Present measurements were carried out in the 0.5 - 4.0 MeV range for Zr, Mo, Sb, Nb, Y, In, Rh, Pd, Ag, Cd, Ho, La, Yb, Sm, Nd, Gd, Dy, Eu, Tb, Er, Hf, W, Re, Ta, Au, Th, and U. Data for Ho, Nb, Ta, Au, Th and U were reported previously and the data for Rh, Pd, Nd, and Sm are presented here. Isotopes of the latter elements are among the 20 most important fission product nuclei./1,8/ The present data should provide a useful constraint for the evaluation of these cross sections.

## MEASUREMENTS

The $^{7}Li(p,n)^{7}Be$ reaction was used as a neutron source with the primary proton beam accelerated with the Argonne National Laboratory Fast Neutron Generator (FNG). The proton beam was pulsed with a repetition rate of 2 MHz and bunched to ~1 nsec. Metallic lithium was evaporated onto a 0.025 cm thick tantalum backing with a thickness appropriate to provide neutrons with energy spreads betwen 50 keV and 100 keV in the energy range from 0.5 to 4.0 MeV. The neutron energy was determined from the known kinematic relations, the primary proton energy (calibrated with $^{7}Li(p,n)$- and $^{10}B(p,n)$-thresholds), the stopping cross sections and the target thickness as measured near the $^{7}Li(p,n)$-threshold.

The neutron source was surrounded with a $4\pi$-lithium-baron-polyethylene shield in order to reduce $\gamma$-ray and neutron background for the capture and neutron detectors. A conical opening in the $4\pi$-shield provided a well collimated neutron beam which penetrated the capture sample after a flight-path of 250 cm. The neutron beam was totally captured in a neutron monitor at a flight-path of 380 cm.

The capture samples were metallic discs with a diameter of 8.0 cm and they ranged in thickness from ~0.012 at/b (Rh, Pd) through ~0.006 at/b (Au) to ~0.005 at/b (Nd, Sm) and were at least 99.9% chemically pure. They were placed in the center of a 1300 liter large liquid scintillator tank which approximated a sphere in shape and was well shielded by low-activity iron, 5 - 15 cm of lead and 60 cm of concrete. The scintillator was a mixture of pseudo-cumene, p-terphenyl, POPOV, and baron-methyl. The scintillation light was detected with 12 8"-photo multipliers which were uniformly spaced over the surface of the tank. The timing of all multipliers was carefully matched and a rise-time correction was applied with an on-line computer resulting in a time-resolution of ~3 nsec. The gamma-ray energy resolution was 26% for the $^{60}Co$ decay gamma rays. The time-resolution and flight-path of the present experiment permitted the separation, by time-of-flight, of capture events produced by the second neutron group of the $^{7}Li(p,n)$-reaction up to ~3 MeV. The electronic threshold for the detection of capture events was usually set at ~2 MeV and $(n,n'\gamma)$ events were rejected for higher primary neutron energies with digital selection in the on-line computer system.

A grey neutron detector/9/ was used as a neutron monitor. Specific features of this detector are not of great importance for the present experiment, because the measurements were made relative to the capture cross section of gold.

Measurements were carried out between 500 keV and 4 keV with irradiation times in the range of 1 to 2 hours. With exception of palladium two sets of measurements were made. These yielded consistency which was usually better than 5%.

The time-of-flight spectrum and the energy pulse height spectra for the capture events corresponding to the neutron capture peak in the time-of-flight spectrum and for an equally spaced adjacent time interval were stored with the on-line computer./10/ Background was subtracted from the time-of-flight spectrum and additional measurements were made with carbon-samples, without a sample, and with a plugged collimator hole. These measurements showed that below 2 MeV all background was ambient, and non-ambient background above 2 MeV lead to only a small correction. The measured energy spectra were extrapolated to zero pulse-height. The neutron energy dependence of this extrapolation could be described very well by a simple analytical representation of the spectra with a weighted neutron binding energy for the elemental samples (within 1-2%). Inelastic scattering events were eliminated by setting appropriately higher integration limits in the energy pulse-height spectra. The capture detection efficiency was in the range of 65 - 85%. This is the major limiting factor of measurements with a large liquid scintillator because the exact shape of the energy spectra below 2 MeV cannot be determined due to high background.

The major correction besides the detection efficiency is attributed to capture events produced by neutrons which scatter once or more within the sample. Such corrections may be large due to the small size of the capture cross section relative to scattering cross sections, to the energy loss due to inelastic scattering which increases the capture probability due to the substantially higher capture cross sections at lower energies, and to the increase of the average path through the sample due to both elastic and inelastic scattering. This correction was calculated with a Monte Carlo Code which is exact at lower energies but uses approximate solutions at higher energies where details of inelastic level structure are not known or the scattering data is unavailable, and the complexity due to the many isotopes involved is enormous. Other corrections were applied for the flux attenuation in the samples and the secondary components of the neutron beam.

The general experimental procedure and the corrections have been discussed in more detail at previous occasions./11-14/ The results from the present measurements are shown in Fig. 1. The ENDF/B-V standard capture cross section of gold was used as reference. The present data for palladium, neodymium and samarium provide the sole source of experimental cross section information for these nuclei since no previous data exist in this energy range. Previous data are available for rhodium and the more recent data are compared with the present results in Fig. 2. All data shown in Fig. 2 were obtained with the prompt detection technique. The data by LeRigoleur et al. /18/, Macklin/15/, and by Drake et al./16/ were obtained with the spectra weighting technique, the data by Knox et al./17/ were, as were the present data, obtained with a large liquid scintillator. The present data agree reasonably with the recent results by Macklin but indicate, as do all other data shown in Fig. 2, lower cross sections (~10 - 15%).

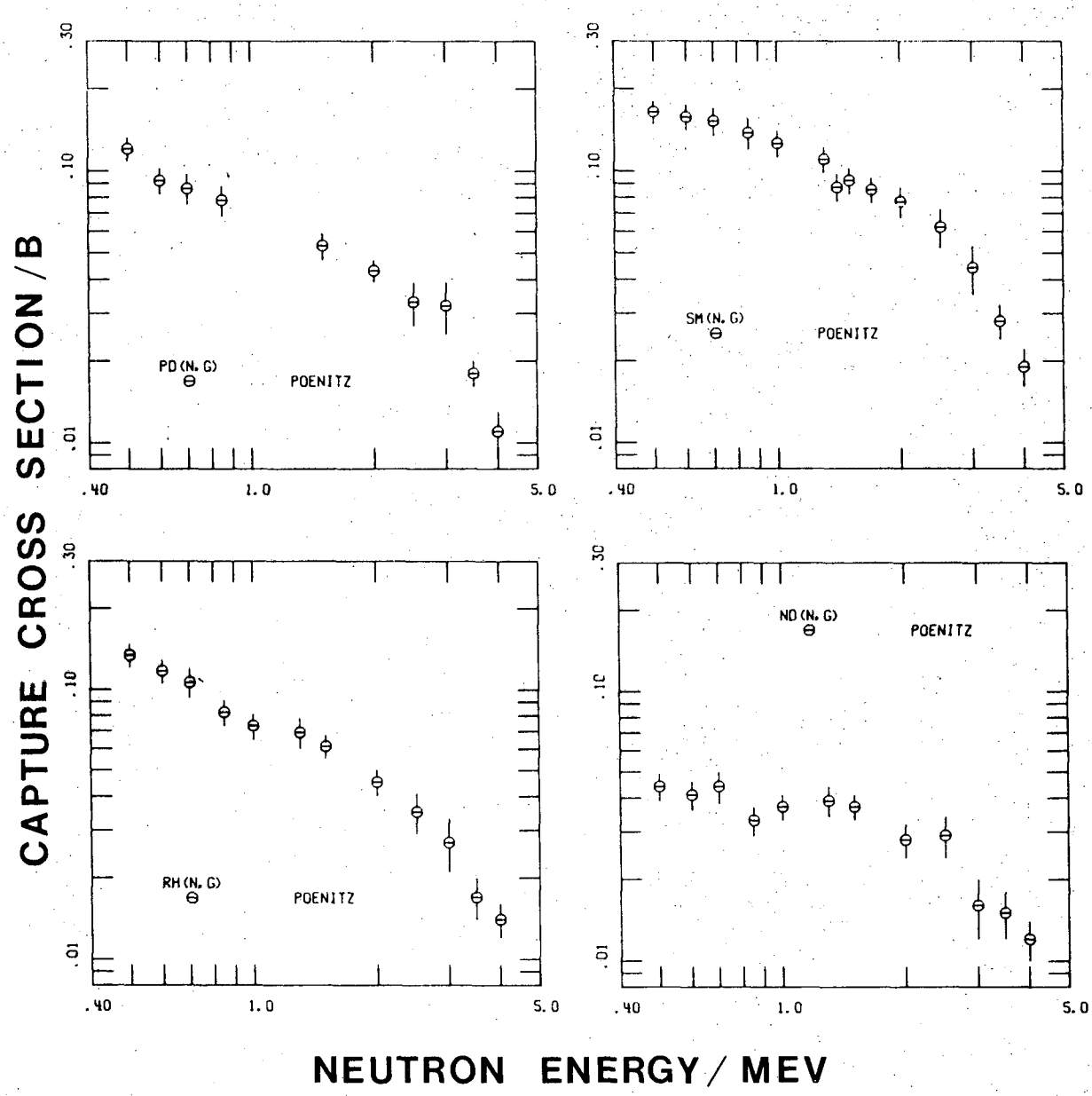


Fig. 1. Experimental Results from the Present Measurements.

## DATA INTERPRETATION

The average capture cross sections of medium and heavy nuclei can be calculated in terms of the statistical model and the optical model. Since the bulk reactivity effects of fission product nuclei are of major interest, one might expect that satisfactory results from such calculations can be obtained if experimental elemental capture cross sections are used as a constraint in such calculations. Recent model calculations of capture cross sections for heavy actinides have yielded good results and a similar approach was used in the present calculations. The statistical and optical model code ABAREX/19/ was used in the present calculations. A major concern is the large number of parameters available to adjust the calculated cross section used to represent the experimental data. It cannot be expected that a parameter set derived only from fitting some experimental capture cross sections will reasonably describe capture cross sections of other nuclei for which experimental data are unavailable. Additional experi-

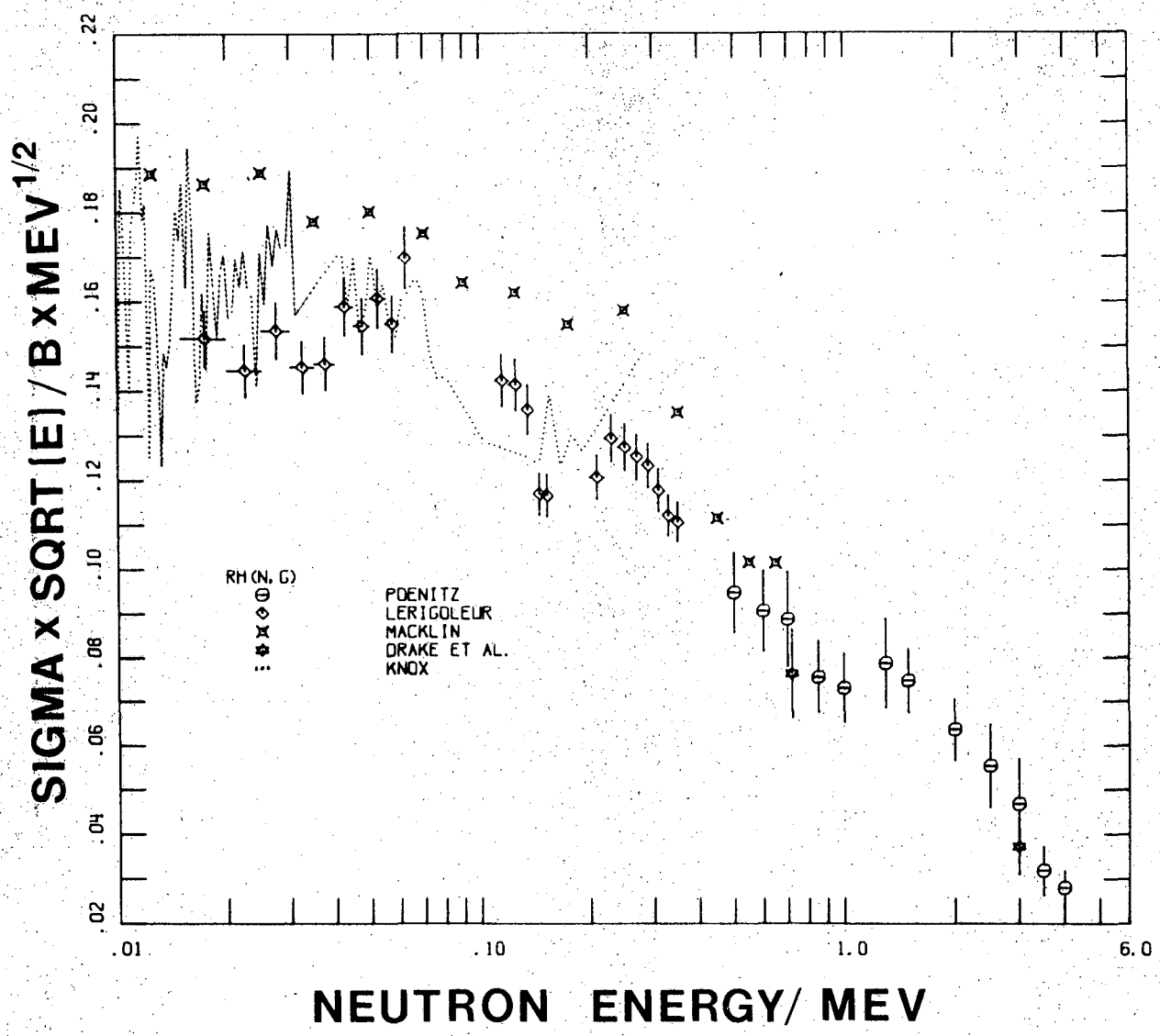


Fig. 2. Comparison of the Present Results with Other Recent Data of Rh(n,$\gamma$).

mental information will have to be used to establish some of the parameters. Total, and elastic and inelastic scattering cross sections were used in the previous calculations to establish the optical model parameters./5/ The major parameter sets to be determined are:

*Optical Model Parameters*

These can be determined by fitting total cross sections and angular distributions of elastically and inelastically scattered neutrons, polarization data etc. ABAREX uses a spherical optical model which was shown to represent well also deformed nuclei if the deformation of these nuclei is similar. However, parameter sets cannot be derived which would have global validity and ultimately a deformed nuclear model should be used. There is a substantial lack of neutron scattering and total cross section data in the range of the fission product nuclei (e.g. Pd, Nd, considered here) which hampers the determination of optical model parameter sets.

*Low Energy Levels of the Target Nucleus*

Inelastic scattering has the most pronounced effect on the calculated capture cross section. In the range of major importance of these cross sections (< 1 MeV), the levels structure is now fairly well known and the information given in Ref. 20 was used in the present calculations.

*Target Level Density*

Most level density formulas, for example the one derived from the Fermi-gas model, assume high excitation energies of the nucleus and cannot be expected to represent very well the true level density at low excitation energies./25/ Thus, the level density of the target nucleus is one of the more uncertain quantities of such calculations and can be adjusted to represent the measured data well. ABAREX used the Gilbert and Cameron/21/ formalism and the level density of the target nucleus is represented by $\rho \sim \exp((E-E_0)/T)/T$.

*Compound Nucleus Level Density*

The level density of the compound nucleus is represented in ABAREX, following Gilbert and Cameron, by a Fermi-gas model. The parameters, a and $\sigma$, may be adjusted to yield the experimental average level spacing measured for s-wave resonances at low neutron energies. However, the available data needed for this purpose are sparse and uncertain.

*Average Radiation Width*

The average radiation width can be calculated with an appropriate level density formula and a giant-dipole resonance for the - transition probability. The parameters for the $\gamma$-transition probability can be determined from $(\gamma,n)$-cross section measurements, however, it is common to utilize $\Gamma_\gamma/D$ values determined in the low eV energy range for resolved resonances. Such data are sparse and substantial uncertainty exists. $\Gamma_\gamma/D$ values are, for example, only available for one of the palladium isotopes (105). The high resolution data from RPI/17/ for Rh (Fig. 2) show substantial fluctuation of the cross section. Such fluctuations are now well known and were discussed for $^{238}U$ and $^{232}Th$ in a recent review./5/ The implications of these fluctuations are the existence of local values of $\Gamma_\gamma/D$ and the neutron strength function and they cast doubt at the use of resolved resonance parameters for the calculation of cross sections at higher energies./22/

The parameter sensitivity of the capture cross section of $^{103}Rh$ is investigated in Figs. 3 and 4. Only the experimental data by LeRigoleur et al. and by Macklin are shown at lower energies. The calculated cross section labeled H results in a reasonable description of the data. This curve was calculated with optical model parameters obtained in a fit of the total cross section (unpublished data by Whalen/23/ below 700 keV and data given in BNL 325 at higher energies). The curve C was obtained with the global optical model parameters by Moldauer/24/ and the black-nucleus approximation was used to calculate neutron transmission coefficients to the continuum of the target nucleus. Curve A used the same optical model parameters as H, but also the black-nucleus approximation for the continuum. For curve B the width fluctuation correction was omitted. All other parameters were identical for the calculated cross sections shown in Fig. 3.

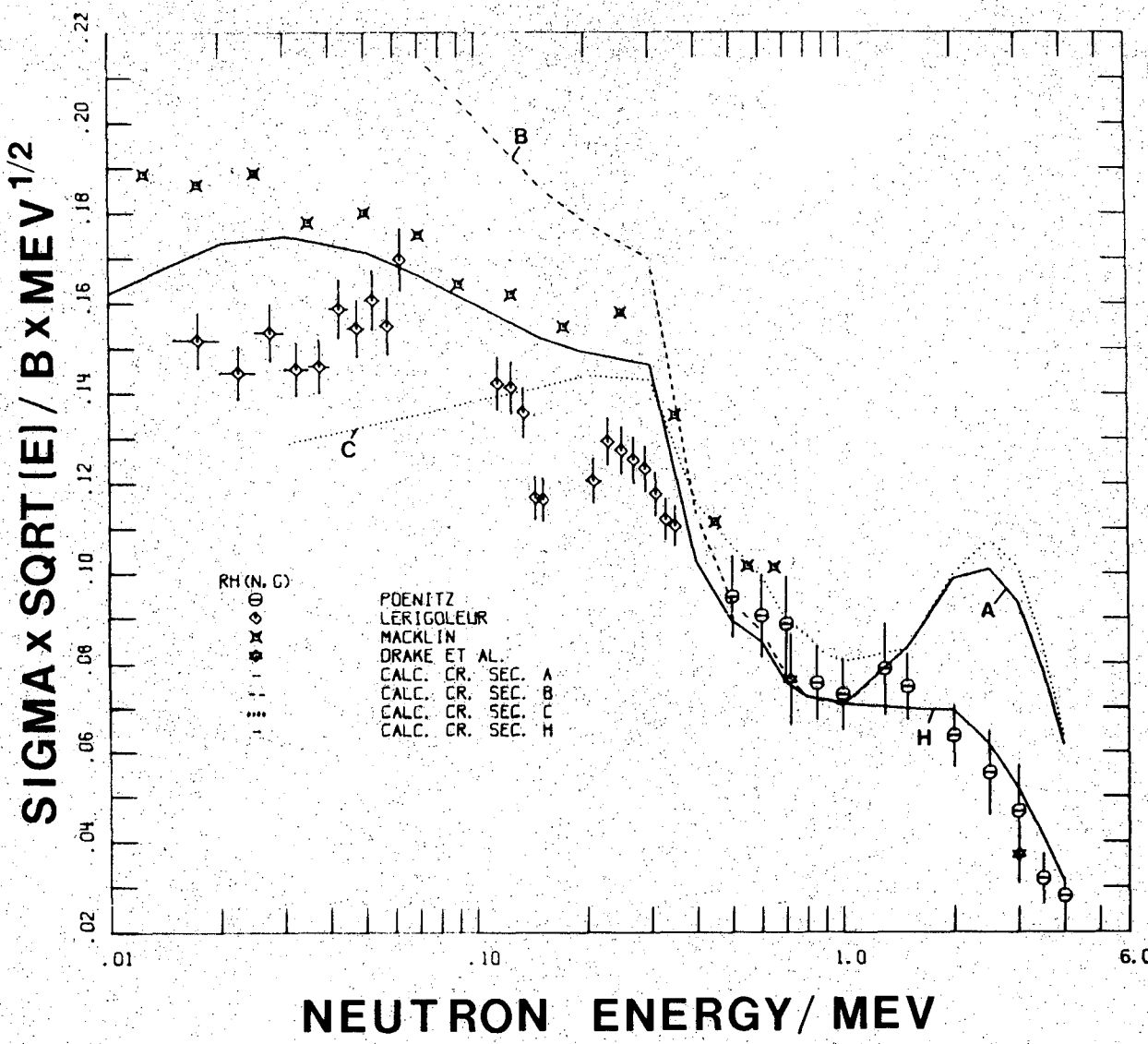


Fig. 3. Comparison of Nuclear Model Calculations with Experimental Data of Rh(n,$\gamma$). (See Text.)

All calculated cross sections shown in Fig. 4 used the optical model parameters obtained in the fit of the total cross section but the $\Gamma_\gamma$/D normalization was changed by 10% for curve I, the compound nucleus level density parameter a was lowered for curve D, and $\sigma$ was increased for curve E. The target nuclear level density was increased for curve F. In all calculations for Fig. 4 the black-nucleus approximation was used for the transmission coefficients to the target nuclear continuum.

It is obvious that optical model calculations more realistically describe nuclear behavior and Figs. 3 and 4 demonstrate that the black nucleus approximation should not be used for the calculation of capture cross sections. With a well established normalization ($\Gamma_\gamma$/D) the cross section is insensitive to level density formula parameters at low energies and only sensitive to optical model parameters and the fluctuation correction. The range between ~500 keV and the beginning of the target nucleus continuum (~1 - 2 MeV) can be used to adjust the compound nucleus level density parameters. Agreement with experimental data at higher energies can then be achieved by adjusting target nucleus level density parameters.

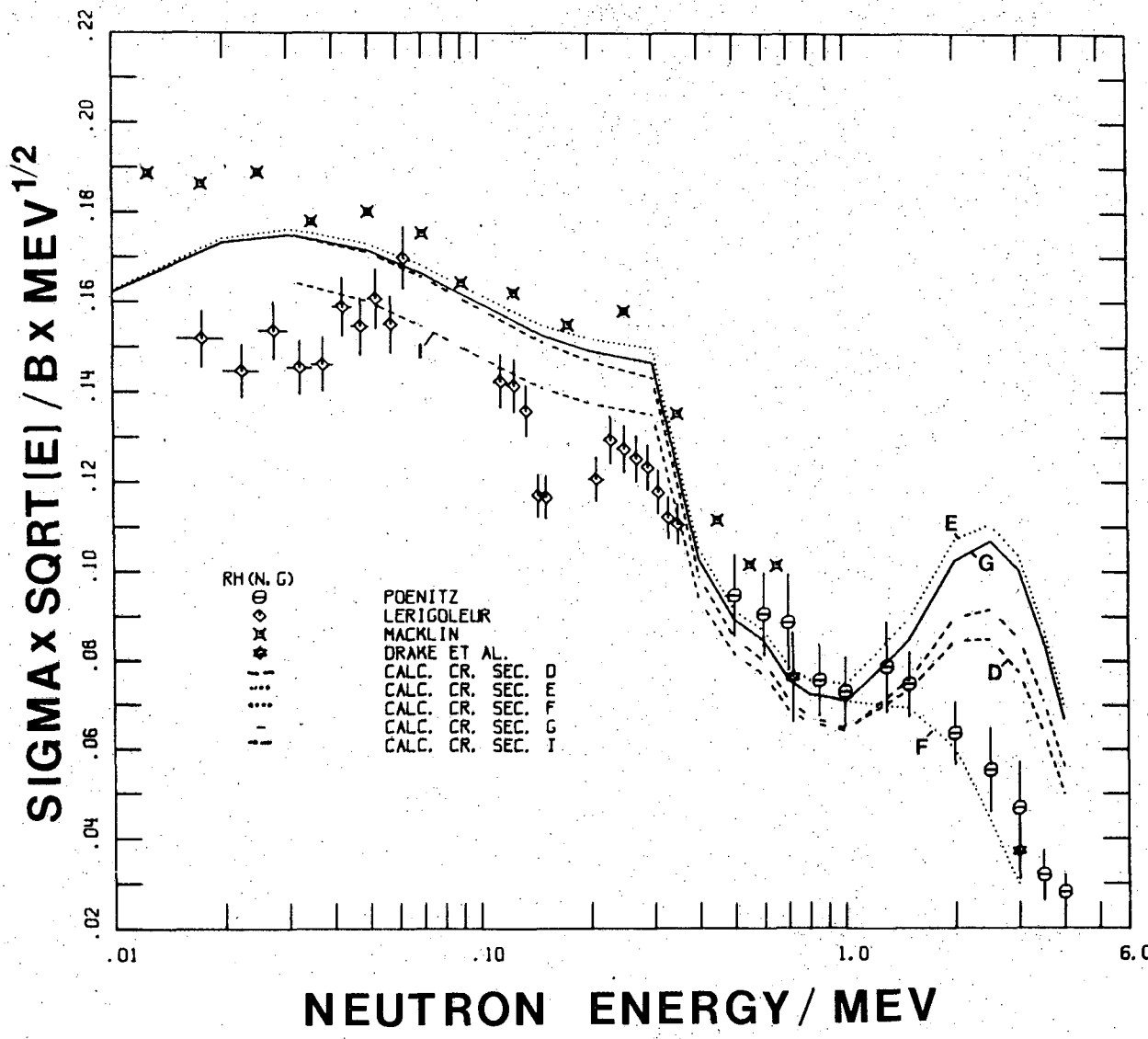


Fig. 4. Comparison of Nuclear Model Calculations with Experimental Data of Rh(n,$\gamma$). (See Text.)

Calculations were also carried out for the six stable isotopes of Pd. The optical model parameters obtained for Rh were slightly adjusted to give a good representation of the total cross section of Pd. The result for the elemental cross section is compared in Fig. 5 with the present experimental values and the recent data by Macklin.

## CONCLUSIONS

Nuclear model calculations can represent the capture cross sections of fission product nuclei reasonably well, however, the uncertainties due to a large number of parameters is large if experimental data do not exist. This specifically applys to the higher energy range where different calculations resulted in large differences with a factor of 5 being common. The present measurements of the elemental cross sections above 500 keV provide a valuable constraint for such calculations, and should considerably reduce the uncertainties, specifically for bulk reactivity effects. Calculations of capture cross sections for which experimental data do not

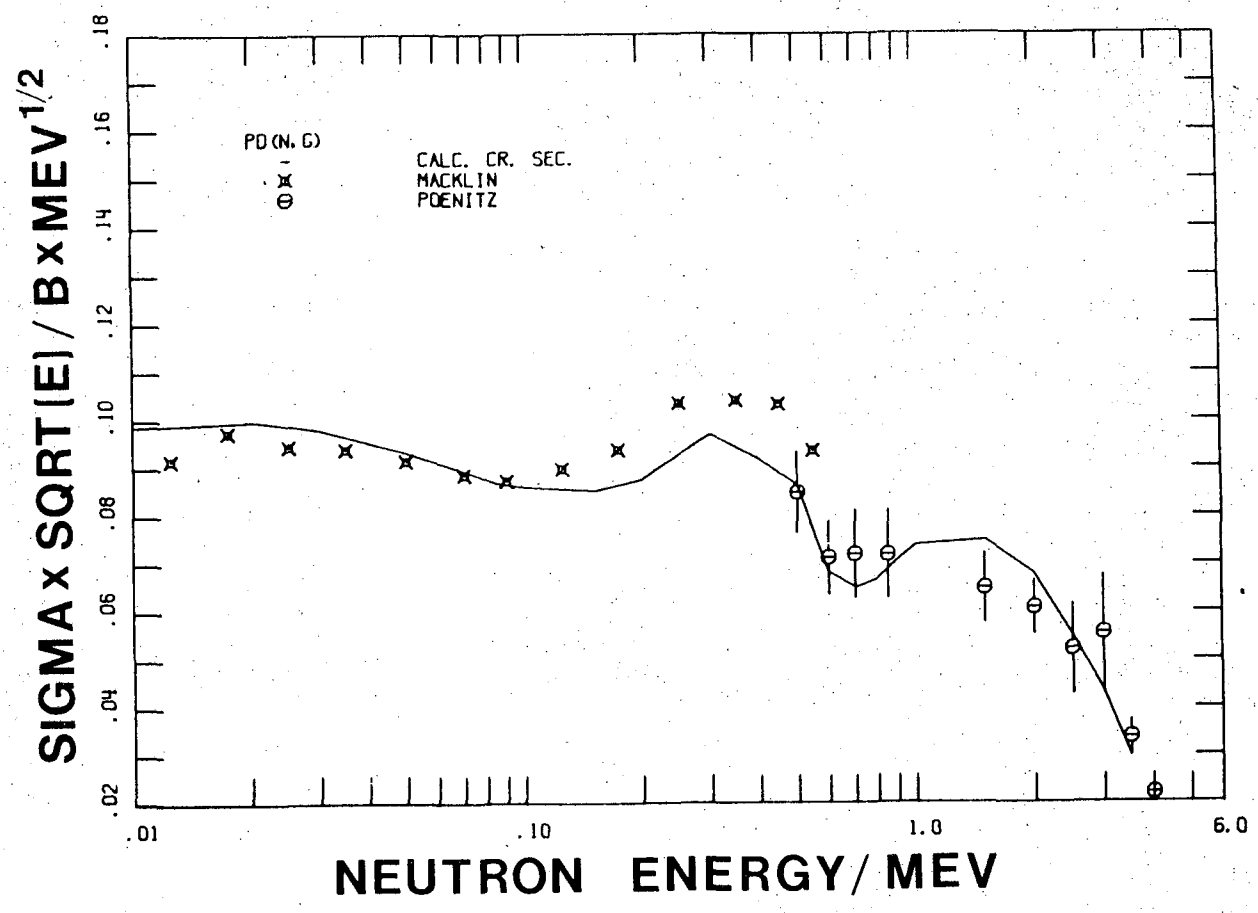


Fig. 5. Comparison of Nuclear Model Calculations with Experimental Data of Pd(n,$\gamma$).

exist cannot be expected to yield satisfactory values until optical model parameters in the range of the fission product nuclei are well established. This seems to require a better and more complete data base than presently available.

REFERENCES

1. J. L. Rowlands, Proc. Conf. Neutr. Physics, Harwell 7 (1978), D. Ilberg et al., Nucl. Technol. 24, 111 (1974), Y. Kikudi et al., Proc. Int. Conf. Fast Reactor Physics, Tokyo (1973), T. Tone, JAERI-M 5449 (1973).

2. WRENDA, World Request List for Nuclear Data, INDC (SEC)-55/URSF, R. M. Lessler, Editor.

3. Compilation of Requests for Nuclear Data, BNL-NCS-51005 (1979).

4. S. Iijima et al., J. Nucl. Sci. and Tech. 14, 161 (1977).

5. W. P. Poenitz, "Fast-Neutron Cross Sections of Importance in Technological Applications," Conf. on Neutron Cross Sections and Technology, Knoxville (1979).

6. R. Schenter et al., "Evaluations of Fission Product Nuclei for ENDF/B-V," private communication, (1979).

7. G. Langlet and L. Martin-Deidier, INDC (NDS)-87/GO + Sp (1978).

8. Proc. 2nd Advisory Group Meeting on Fission Product Nuclear Data, Petten (1977), IAEA-213, Conclusions.

9. W. P. Poenitz, Nucl. Instr. Methods 58, 39 (1968).

10. W. P. Poenitz and J. F. Whalen, ANL-8026 (1973).

11. W. P. Poenitz, ANL-NDM-8, (1974).

12. W. P. Poenitz, ANL-NDM-15, (1975).

13. W. P. Poenitz, Nucl. Sci. Eng. 57, 300 (1975).

14. W. P. Poenitz, Proc. Conf. Nucl.Cross Sect. and Tech., 902 (1975).

15. R. L. Macklin, private communication, also see this Conf. (1979).

16. D. Drake et al., Conf. Neutron Physics, Kiev (1977).

17. H. D. Knox et al., Proc. Conf. Nucl. Cross Sections and Technology, 905 (1975).

18. C. LeRigoleur et al., Conf. Nucl. Cross Sect. and Tech., 953 (1975).

19. P. A. Moldauer, unpublished (1979).

20. C. M. Ledener and V. S. Shirley, Editors, Table of Isotopes, 7th Edition, J. Wiley α Sons, Inc., (1979).

21. A. Gilbert and A.G.W. Cameron, Can. J. Physics 43, 1446 (1965).

22. W. P. Poenitz, Proc. Conf. Nucl. Data, Helsinki, Vol. I, 209 (1970).

23. J. F. Whalen, private communication (1979).

24. P. A. Moldauer, Nucl. Phys. 47, 65 (1963).

25. G. Reffo, INDC (NDS)-87, 165 (1978).

# MEASUREMENTS OF THE TOTAL AND PARTIAL NEUTRON CROSS-SECTIONS OF CERIUM AND THULIUM IN THE ENERGY RANGE FROM 1.8 meV to 1.8 eV USING TOF AND NEUTRON DIFFRACTION TECHNIQUES

M.Adib, R.M.A.Maayouf, A.Abdel-Kawy, and I.Hamouda
Reactor and Neutron Physics Department
Atomic Energy Establishment, Cairo, Egypt.

ABSTRACT

Total neutron cross-section measurements have been carried out for cerium and thulium in the energy range from 1.8 meV to 1.8 eV. The measurements were performed using the time-of-flight and neutron diffraction spectrometers installed infront of the horizontal channels of the ET-RR-1 reactor. The obtained total neutron cross-sections were analyzed using the single level Breit-Wigner formula and the magnetic form factors. The potential scattering cross-section of Ce was found to be 3.14 ± 0.3 barns. Its coherent scattering amplitude was determined from the Bragg reflections observed in the total cross-section of $CeO_2$ and found to be 4.8 ± 0.2 barns. The potential scattering and absorption cross-sections of Tm, at E = 0.025 eV, were found to be 7.45 ± 0.75 barns and 89.3 ± 4.5 barns respectively.

## 1. INTRODUCTION

The only available experimental measurement of Ce cross-section /1/, is a value of the total scattering cross-section $\sigma_s$ = (4.7 ± 0.3) b at V = 2200 m/sec, obtained using the time of flight technique and the $4\pi$ -geometry. Concerning the total neutron cross-section of Ce, Vertebnii et al /1/ did not present their values as they reported, because of difficulties, connected with neutron optical effects and small angle scattering.

It seems useful to study the total neutron cross-section of Ce, since its total cross-section at neutron energies below 0.01 eV can provide a valuable information about the coherent scattering amplitude of Ce.

The only measurements of the total neutron cross-section of Tm in the energy range from 0.001-10 eV was reported by Zimmerman et al. /2/. Zimmerman et al. /2/ determined the absorption cross-section of Tm at very low energy (~0.001 eV) by subtracting the asymptotic value of the paramagnetic cross-section from the measured value of the total neutron cross-

section ; they extrapolated the determined value of the absorption cross-section to higher neutron energies taking into account the deviation from 1/v which, as they reported /2/, is almost entirely due to the first resonance at 3.92 eV. They reported the values (134 ± 2) b and (106 ± 3) b respectively for the total and absorption cross-sections at 0.025 eV thermal neutron energy.

In the present work are reported the results of total neutron cross-section measurements, carried out for Ce and Tm in the energy range from 1.8 meV to 1.8 eV, along with the resulting partial cross-sections.

## 2. EXPERIMENTAL DETAILS

### 2.1 Samples Preparation

The samples used were prepared from spec. pure fine oxide powders, packed in perspex containers. The emission spectrographic method was used for the spectroscopic analysis of the samples. The spectrographic analysis of the used oxides assured that they are free from Cd and Sm, as well as other elements with high absorption cross-section, in the energy range under consideration.

Cerium : The spectroscopic analysis was : Fe : 5 ppm, Na: 1ppm, Cu: < 1ppm, Mg: 1ppm and Ag: < 1ppm; one sample of thickness 5.11gm/cm$^2$ was prepared.

Thulium: The spectroscopic analysis was : Ca : 1ppm, Si: 2ppm, Fe: 5ppm, Na: 1ppm and Mg: < 1ppm. One sample of thickness 1.23 gm/cm$^2$ was prepared.

### 2.2 Crystal Structure of $CeO_2$

$CeO_2$ crystallyzes in a cubic system related to the space group $F_m 3_m - O_H^5$. A determination of such structure was made using the neutron diffraction technique. A neutron diffraction pattern was obtained with the $CeO_2$ powder packed into a thin walled cylindrical aluminum can. The measurements were performed on a crystal spectrometer placed at one of the horizontal beams of the ET-RR-1 reactor operating at a power of 2 MW. Monochromatic neutrons with $\lambda$ = (1.03±0.01) A° were selected from the reactor spectrum by diffraction from a Zn single crystal cut along the (111) plane, The collimation was determined by two Soller type collimators with an angular resolution of 20'. The spectrometer is described in details elsewhere /3/.

The neutron diffraction pattern obtained between $2\theta$ = 12° and 60° at room temperature is shown in Fig. (1). Nine well-separated peaks are obtained confirming the structure of $CeO_2$, where no lines other than for the pure $CeO_2$ were observed.

## 2.3 Cross-Section Measurements

The total cross-section of $CeO_2$ and $Tm_2O_3$ were measured for neutron energies from 1.8 meV to 1.8 eV using a time-of-flight spectrometer. The spectrometer was described thoroughly in details elsewhere /4,5/. The neutrons were obtained from one of the horizontal channels of the ET-RR-1 reactor, operating at a power of 2 MW. The time-of-flight was analyzed by a 400 channel time analyzer; the analyzer channel width could be varied from 12 μsec to 96 μ sec. The spectrometer resolution at a flight path of 5.66 m and rotor speeds of 1415 rpm and 2880 rpm is 23 μsec/m and 11 μsec/m, respectively. The methods used for the check-up of the spectrometer's linearity and its calibration are described in details elsewhere /6,7/.

## 3. RESULTS AND DISCUSSION

### 3.1 Cerium

Fig. (2) shows the total neutron cross-section of $CeO_2$ as a function of the neutron wave length and energy (closed circles). The total neutron cross-section of Ce obtained, by subtraction of the oxygen cross-section incoherently, in the energy range from 1.8 eV to 0.02 eV (the first observed Bragg cut-off) is also represented in the same figure (open circles). The total neutron cross-section obtained at 0.025 eV was found to be :

$$\sigma_t\ (0.025\ \text{eV}) = (5.28 \pm 0.30)\ \text{b}.$$

The value of $\sigma_t$ obtained in the present work is in reasonable agreement with the value (4.7 ± 0.3) b for the total scattering cross-section of Ce reported by Vertebnii et al. /1/.

The paramagnetic scattering cross-section of Ce was calculated using the tabulated form factors reported by Blume et al. /8,9/ and incoherently subtracted from the obtained value of the total neutron cross-section. The residual cross-section (Figure 2, closed triangles) was found to fluctuate near a constant value (3.1 ± 0.3) b which corresponds to the potential scattering cross-section of Ce. This value is in good agreement with the value of (2.92 ± 0.05) b reported in BNL-325 /10/.

The total contribution of the Ce neutron resonances to the thermal absorption cross-section was calculated using the single level Breit-Wigner formulae /11/. It was found that this contribution at 0.025 eV does not exceed the value of 0.3 b which is comparable with the statistical error in the total cross-section measurements. This behaviour is in consistence with the energy independence of the scattering cross-section at thermal neutron energies (Fig. 2 closed triangles).

The observed behaviour of the total neutron cross-section of $CeO_2$ shows sharp cut-offs at neutron wavelengths corresponding to the double interplanar distance d of the $CeO_2$ cubic structure. A value of 5.8 F for the scattering

amplitude of oxygen was taken for the determination of the coherent scattering amplitude $b_{coh}$ of Ce.

The coherent scattering amplitude of Ce is calculated for each hkl plane. The average value of $b_{coh}$ have been determined and found to be $b_{coh} = (4.8 \pm 0.2)$ F which is in a good agreement, within the statistical accuracy, with the value of $(4.8 \pm 0.06)$ F reported in BNL-325 /10/.

3.2 Thulium

Fig. (3) shows the total neutron cross-section dependence on wavelength and energy for Tm. The cross-section behaviour obtained in the present work is compared, in the same figure, with that obtained by Zimmerman et al. /2/; (closed squares). It is noticeable that both sets of data are in reasonable agreement. The value obtained for the total cross-section at 0.025 eV is :

$$\sigma_t \ (0.025 \text{ eV}) = (126 \pm 6) \text{ b}$$

in agreement with the value of $(134 \pm 2)$ b reported by Zimmerman et al. /2/.

The paramagnetic scattering cross-section $\sigma_{pm}$ for Tm has been also calculated and subtracted incoherently from the total cross-section at all energies. The residual cross-section is also shown in Fig. (3) as open circles. The contribution of the known close and faraway resonances upon the cross section have been calculated using the single level Breit-Wigner formulae reported by Seth et al. /11/, where the required resonance parameters were taken from BNL-325 /10/ Fig. (3) shows also the difference between the total cross-section and the total resonance contribution versus neutron energy. It was found, as is shown in Fig. (3), that the difference $(\sigma_t - \sigma_{pm} - \sigma_r)$, which corresponds to the potential scattering cross section $\sigma_s$ , is energy dependent which indicates the contribution of a bound energy level.

A negative energy level with the parameters, $E_o = 6$ eV, $2g\Gamma_n = 2.8$ meV and $\Gamma_\gamma = 88$ meV was introduced to account for the obtained energy dependence of $(\sigma_t - \sigma_{pm} - \sigma_r)$. A value of $(7.5 \pm 0.7)$ b was obtained for Tm potential scattering cross-section.

REFERENCES

/1/ Vertebnii V.P. et al.; IAEA Second Int. Conf. on Nucl. Data for Reactors, Helsinky, 1970.

/2/ Zimmerman R.L. et al. Nucl. Phys. A 95 (1967) 683.

/3/ Hamouda, I. et al. Proc. of the Fifth Arab Scientific Conference, Bagdad, March 27-31 (1966).

/4/ Hamouda I., R. Maayouf, M.Salama, M.Abu-El-Ela, V.Nesterenko and A.Stupak, Nucl. Inst & Meth. 40(1966)153.

/5/ Hamouda I., M.Salama, V.Nesterenko, A.Stupak,R.Maayouf and M.Abu-El-Ela: U.A.R.A.E.E. Rep.-15 (1966).

/6/ Adib, M., M.Salama, A.Abdel-Kawy and I.Hamouda, Nucl. Inst & Meth. 116 (1974) 509

/7/ Adib M., A. Abdel-Kawy S.Faragalla, S.Sadek, M.Salama and I.Hamouda: Atomkernenergie (ATKE) Bd. 27 (1976)117

/8/ Blume, M. et al., J. Chem. Phys., 37 (1962) 1245.

/9/ Blume M., et al., J. Chem. Phys. 41 (1964) 1878.

/10/ Hughes, D.J. and R.Schwartz, Neutron Cross-Sections, BNL-325, Supplement No 2 (1966) and Supplement (1975).

/11/ Seth, K.K. et al., Phys. Rev. 110 (1958) 692.

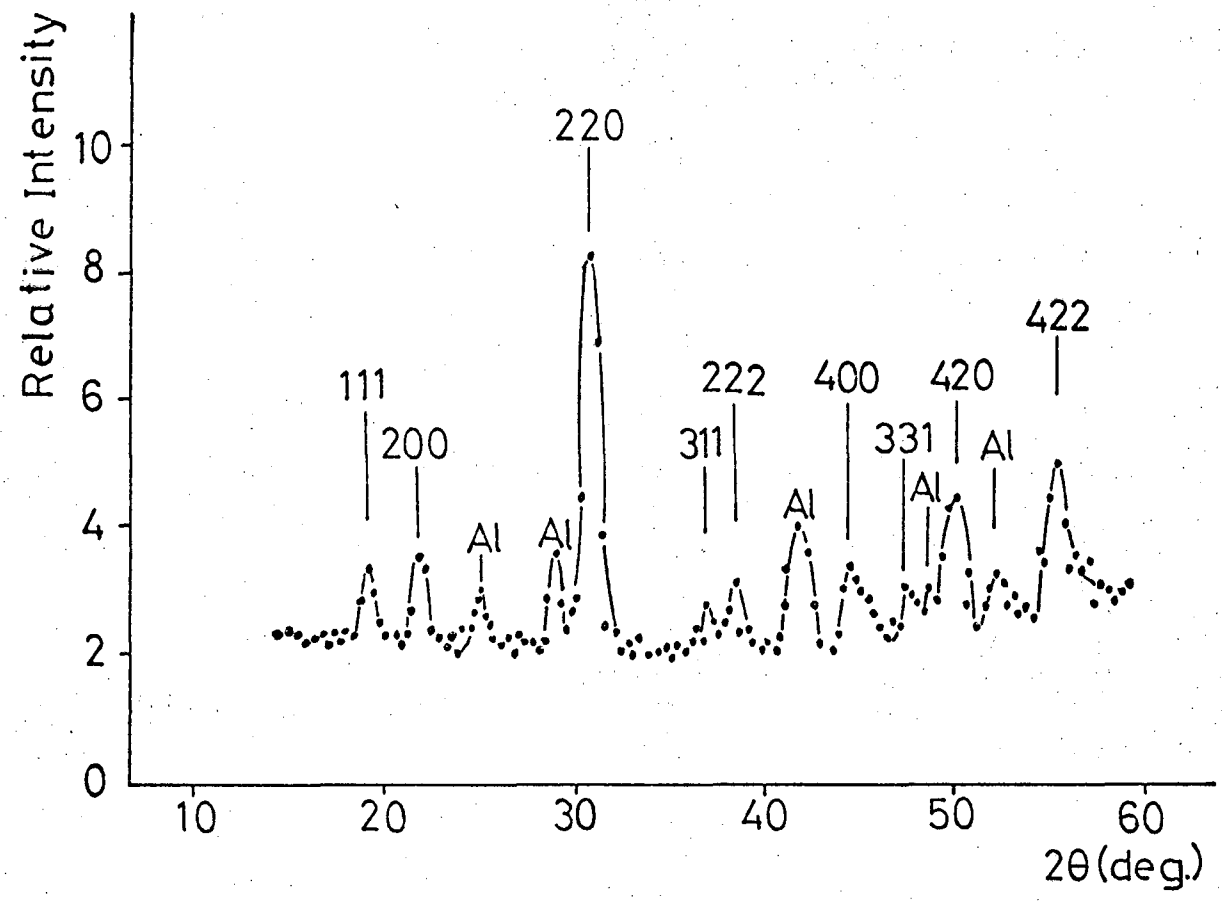


Fig.1: Neutron diffraction pattern of $CeO_2$

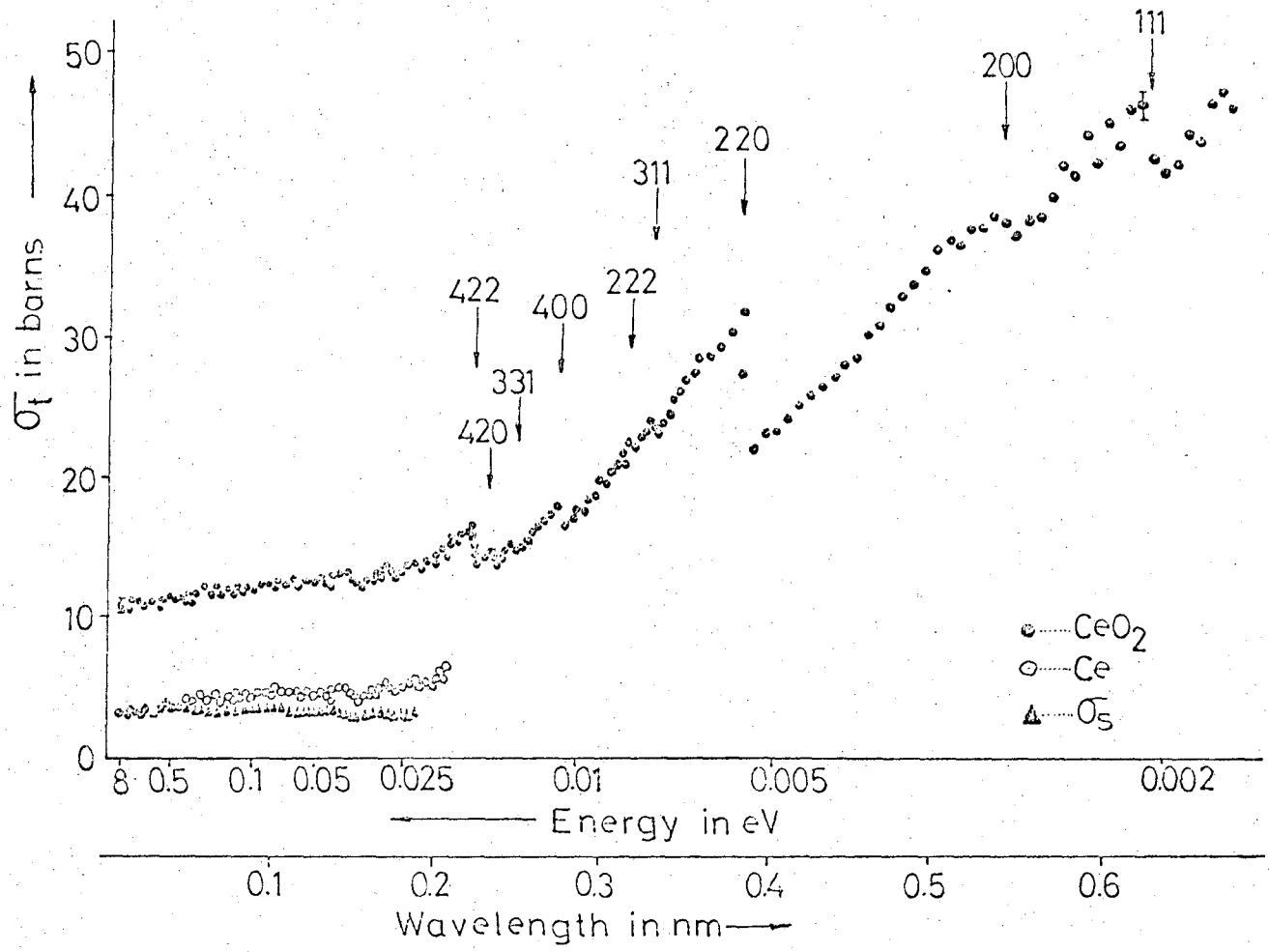


Fig. 2 : The total cross-section of cerium vs. neutron wavelength and energy

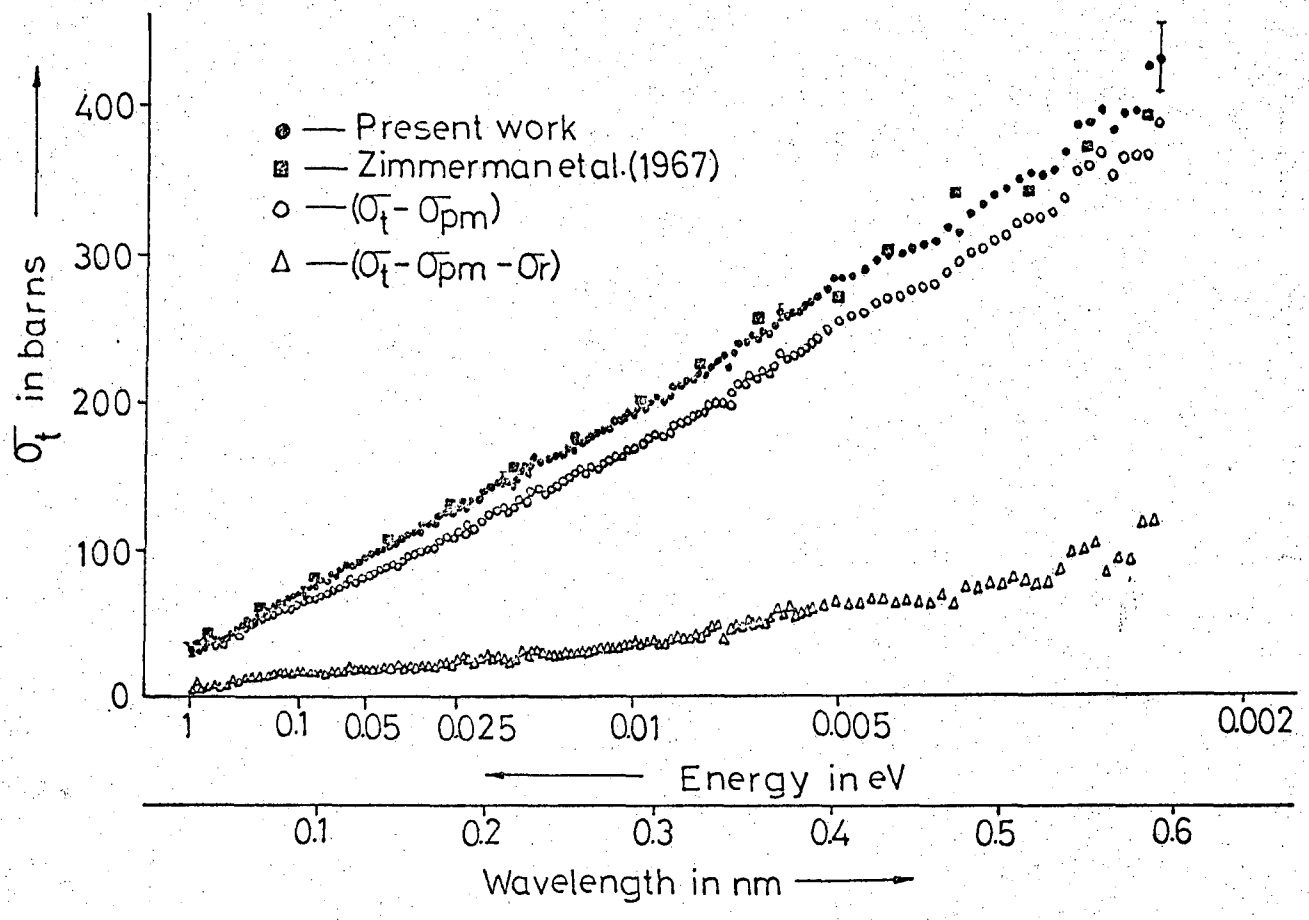


Fig. 3: The total cross-section of thulium vs. neutron wavelength and energy

# RECENT CAPTURE CROSS SECTION DATA FROM ORELA ABOVE 2.6 keV

R. L. Macklin, R. R. Winters[+] and J. Halperin
Oak Ridge National Laboratory
Oak Ridge, Tennessee 37830
[+]Denison University, Granville, Ohio 43023

## Abstract

Neutron capture by natural rhodium ($^{103}$Rh) and enriched stable isotopes of ruthenium (100-104) and palladium (104-110) were measured at the Oak Ridge Electron Linear Accelerator pulsed neutron facility. Average pure isotope cross sections from three to several hundred keV were derived. The neutron flux shape was determined relative to ENDF/B V standard $^{6}$Li(n,$\alpha$) and $^{235}$U(n,f) cross sections below and above 70 keV respectively. Strength functions were adjusted to fit the data by least squares. The $^{101}$Ru fission product would appear to cause less poisoning than $^{105}$Pd or $^{103}$Rh in plutonium fueled fast reactors.

## Introduction

$^{101}$Ru, $^{103}$Rh and $^{105}$Pd through a combination of strong neutron capture and high fission yield are among the most important stable isotopes in regard to the poisoning effect in fast reactors. The even stable isotopes in this mass range are also significant neutron absorbers. Evaluations of the microscopic cross sections /1,2/ have had to rely on fragmentary experimental results (except for $^{103}$Rh) or average statistical properties of nuclei in the general mass range.

## Experimental Technique

Enriched samples of $^{100}$Ru, $^{101}$Ru, $^{102}$Ru, $^{104}$Ru, $^{104}$Pd, $^{105}$Pd, $^{106}$Pd, $^{108}$Pd and $^{110}$Pd were measured at 40 meters from the Oak Ridge Electron Linear Accelerator pulsed neutron source. A natural $^{103}$Rh metal sample was included in the study. Prompt capture gamma rays were observed with $C_6F_6$ based liquid scintillators which have a low sensitivity ($10^{-3}$-$10^{-4}$) for scattered neutrons and give negligible neutron moderation. Both time-of-flight and pulse height were recorded for the first pulse (if any) recorded after a neutron burst. By weighting each event as a function of the pulse height, an unbiased estimate of the total gamma energy is obtained. As the excitation energy of the compound nucleus after neutron capture is well known, this leads directly to the number of neutrons captured during a measurement. The time-of-flight resolution is adequate to resolve a hundred or so resonances per isotope in the few keV neutron energy range. The analysis of individual resonance peaks is reported separately. /3,4/

The neutron flux was monitored by a thin (0.5 mm) $^{6}Li$ glass scintillator half a meter upstream from the sample. While the absolute cross section was determined at 4.9 eV using the saturated resonance technique, we must rely on an efficiency vs energy curve for the flux monitor at high energy. This has been recently redetermined relative to the $^{235}U(n,f)$ ENDF/B V standard cross section. /5/

## Cross Sections

The enriched isotope sample yields (corrected for measured backgrounds, dead time losses, gamma energy loss in each sample, etc. /3,4/) were linearly combined to derive pure isotope yields. /3/ These were then corrected for average resonance self-protection and multiple scattering of neutrons within each sample to give average isotopic cross sections. Table I summarizes the cross sections averaged over various energy regions, and the figures show them as histograms. Uncertainties in cross section are estimated at 4-5% up to 100 keV or so, increasing to perhaps 10% at the highest energies reported for each isotope.

## Analysis

Average cross sections up to about 110 keV in quarter keV steps were well represented by strength functions $S^0$, $S^1$, $S^2$ and $\overline{\Gamma}_\gamma/D_0$ through least squares adjustment. For the even isotope capture data it was found necessary to adopt a fixed value of the s-wave strength function $S^0$ (see Table II). At higher energies competition from inelastic scattering is seen as a reduction in capture above most inelastic thresholds. Hauser-Feshbach codes may be able to fit the higher energy data also, but this has not been done.

## Discussion

Cross section agreement with prior evaluation and data adjustments /1,2/ is good except for $^{102}Ru$ which we find 5% to 40% lower at various energies. Two more recent values for $^{103}Ru(n,\gamma)$ at 520 ± 80 keV and 720 ± 80 keV /6/ are about 20% below ours. Below about 10 keV for the even isotopes studied the cross section is best represented by single resonance parameters. /3,4/ In the higher energy region around 100-200 keV where fast reactor spectra peak, the highest cross section appears to be for $^{105}Pd$, followed by $^{103}Rh$ and $^{101}Ru$. The lower $^{101}Ru$ capture is attributable both to radiative strength (28% below $^{105}Pd$) and the lower threshold for competition by inelastic scattering (∿130 keV vs ∿300 keV for $^{103}Rh$ or $^{105}Pd$). For a plutonium fuelled fast reactor this would predict $^{105}Pd$ as the leading fission product poison. For a fast reactor with much $^{233}U$ or $^{235}U$ fission, the lower mass $^{101}Ru$ might become most significant.

The research was sponsored by the Division of Nuclear Sciences, U.S. Department of Energy, under contract No. W-7405-eng-26 with the Union Carbide Corporation.

## References

/1/ S. Iijima et al., Nucl. Sci. Technol. 14, 161 (1977).
/2/ R. E. Schenter, private communications (1979).
/3/ R. L. Macklin, J. Halperin, and R. R. Winters, "$^{104,105,106,108,110}Pd(n,\gamma)$ Cross Sections above 2.6 keV", Nucl. Sci. Eng. 71, 182 (1979).
/4/ R. L. Macklin and J. Halperin, "$^{100,101,102,104}Rh(n,\gamma)$ and $^{103}Rh(n,\gamma)$ Cross Sections above 2.6 keV", unpublished (1979).
/5/ R. L. Macklin, R. W. Ingle, and J. Halperin, "$^{6}Li(n,\alpha)T$ Cross Section

from 70 to 3000 keV from the $^{235}U(n,f)$ Calibration of a Thin Glass Scintillator", Nucl. Sci. Eng. 71, 205 (1979).
/6/ S. Joly et al., Nucl. Sci. Eng. 70, 53 (1979).

Figure Caption

Average neutron capture cross sections as histograms and fitted curves from least squares adjusted strength functions for samples of a) $^{100,101}Ru$, b) $^{102}Ru$ and $^{103}Rh$, c) $^{104}Ru$ and $^{104}Pd$, d) $^{105,106}Pd$, and e) $^{108,110}Pd$. The vertical arrows indicate thresholds for inelastic neutron scattering which often shows significant competition with neutron capture.

Table I. Histogram of the Average Neutron Capture Cross Sections

| $E_n$ keV | $^{100}Ru$ mb | $^{101}Ru$ mb | $^{102}Ru$ mb | $^{103}Rh$ mb | $^{104}Ru$ mb | $^{104}Pd$ mb | $^{105}Pd$ mb | $^{106}Pd$ mb | $^{108}Pd$ mb | $^{110}Pd$ mb |
|---|---|---|---|---|---|---|---|---|---|---|
| 3 | 748.6 | 2652.6 | 703.5 | 2639.5 | 411.2 | 747.0 | 2452.1 | 1124.5 | 1029.6 | 869.5 |
| 4 | 575.5 | 2074.1 | 510.0 | 2524.9 | 533.4 | 1172.8 | 2380.0 | 900.5 | 869.1 | 817.7 |
| 6 | 586.5 | 1880.6 | 476.2 | 1902.4 | 529.9 | 958.6 | 2014.7 | 891.9 | 699.6 | 707.9 |
| 8 | 460.1 | 1746.2 | 443.3 | 1793.2 | 350.7 | 978.2 | 1816.7 | 709.7 | 751.8 | 726.8 |
| 10 | 339.9 | 1512.3 | 355.2 | 1687.4 | 292.5 | 712.5 | 1695.2 | 564.0 | 569.4 | 446.0 |
| 15 | 342.4 | 1299.2 | 269.9 | 1408.3 | 239.2 | 604.8 | 1504.4 | 568.8 | 482.9 | 385.3 |
| 20 | 220.3 | 1127.6 | 222.1 | 1193.7 | 186.4 | 499.6 | 1279.4 | 435.1 | 385.7 | 271.7 |
| 30 | 191.6 | 933.4 | 164.0 | 950.9 | 143.4 | 411.8 | 1093.8 | 362.3 | 304.9 | 246.9 |
| 40 | 147.3 | 762.6 | 128.9 | 805.6 | 113.6 | 330.2 | 930.1 | 270.0 | 248.7 | 196.6 |
| 60 | 127.0 | 610.4 | 107.5 | 662.4 | 92.8 | 259.2 | 771.5 | 221.6 | 205.7 | 146.9 |
| 80 | 103.4 | 526.2 | 95.5 | 547.2 | 83.1 | 221.9 | 668.5 | 192.8 | 178.2 | 135.3 |
| 100 | 91.5 | 441.2 | 86.6 | 457.9 | 74.8 | 194.6 | 575.0 | 172.9 | 153.9 | 123.8 |
| 150 | 88.2 | 342.4 | 83.1 | 370.0 | 73.6 | 176.6 | 485.1 | 156.9 | 146.8 | 115.0 |
| 200 | 81.4 | 277.7 | 79.3 | 315.9 | 70.7 | 169.9 | 422.9 | 153.5 | 142.4 | 110.9 |
| 300 | 81.3 | 196.5 | 79.3 | 228.4 | 61.9 | 159.1 | 299.5 | 149.0 | 141.2 | 100.9 |
| 400 | 86.9 | 149.1 | 78.1 | 166.3 | 41.8 | 166.5 | 219.4 | 161.3 | 122.1 | 70.4 |
| 500 | 78.2 | 123.3 | 60.1 | 137.1 | 38.9 | 159.8 | 174.6 | 132.1 | 95.6 | |
| 600 | 64.0 | 101.6 | | 125.7 | 37.6 | 126.0 | 152.1 | 117.7 | | |
| 700 | | | | | | | | | | |

Table II. Least-Squares-Adjusted Strength Functions and Average Neutron Capture

| Strength Function | $^{100}Ru$ | $^{101}Ru$ | $^{102}Ru$ | $^{103}Rh$ | $^{104}Ru$ | $^{104}Pd$ | $^{105}Pd$ | $^{106}Pd$ | $^{108}Pd$ | $^{110}Pd$ |
|---|---|---|---|---|---|---|---|---|---|---|
| $10^4 S^0$ | (0.58)[a] | 0.59 ± 0.04[b] | (0.55) | 1.04 ± 0.13 | (0.52) | (0.50) | 0.50 ± 0.02 | (0.50) | (0.50) | (0.50) |
| $10^4 S^1$ | 6.5 ± 0.9 | 6.1 ± 0.4 | 5.0 ± 0.7 | 7.9 ± 0.7 | 5.7 ± 0.9 | 6.65 ± 0.59 | 5.80 ± 0.29 | 6.70 ± 0.62 | 5.91 ± 0.62 | 8.05 ± 0.91 |
| $10^4 S^2$ | 1.2 ± 0.3 | 2.1 ± 0.5 | 0.94 ± 0.25 | 2.3 ± 0.7 | 0.97 ± 0.20 | 1.77 ± 0.44 | 2.90 ± 0.52 | 1.65 ± 0.36 | 1.51 ± 0.35 | 1.47 ± 0.24 |
| $10^4 \overline{\Gamma}_\gamma/D_0$ | 3.47 ± 0.15 | 101.3 ± 2.7 | 3.24 ± 0.15 | 59.5 ± 2.3 | 2.63 ± 0.11 | 9.11 ± 0.37 | 140.5 ± 3.8 | 7.35 ± 0.28 | 6.60 ± 0.28 | 4.40 ± 0.15 |
| $\overline{\sigma}$(mb)[c] (30 keV) | 209 | 1011 | 189 | 1072 | 163 | 447 | 1189 | 382 | 345 | 264 |
| | | 1097[d] | 314[d] | 984[d] | 177[d] | | 1178[d] | | | |

a. Values in parentheses were assumed and not adjusted to the data by least squares.
b. Standard deviations derived from the fluctuations in the data by the fitting code are shown. The effect of overall uncertainties in cross section is not included. Correlation coefficients among the three adjusted parameters for the three even targets were less than 0.80 in absolute magnitude. For the four parameter sets of the odd targets values ranged up to 0.92.
c. The 30 keV average capture cross sections are those predicted from our fitted strength functions. Systematic uncertainties are estimated at 4% (Ru and Rh), and 5% (Pd).
d. Calculated value from Reference 1.

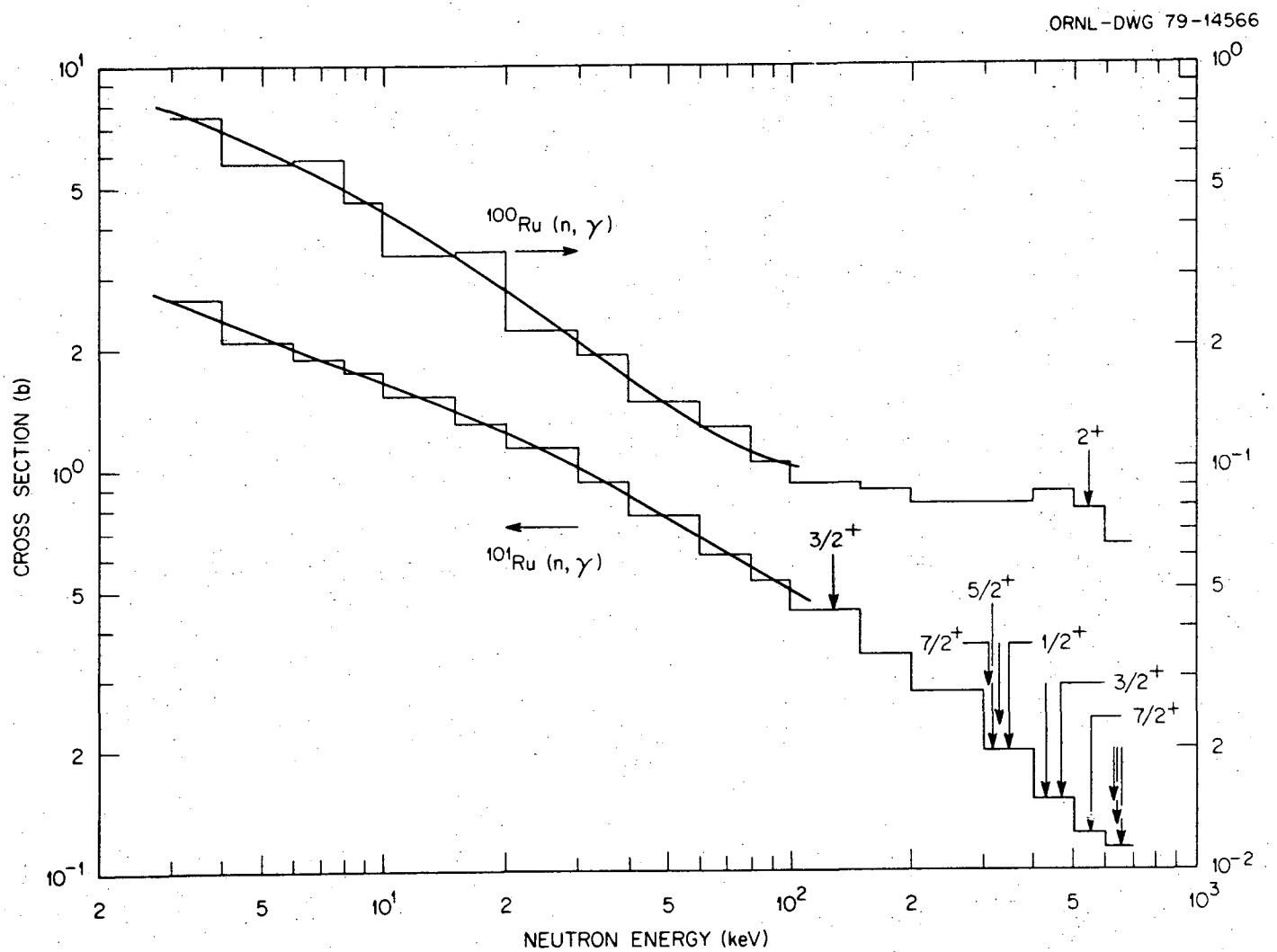
ORNL-DWG 79-14566
CROSS SECTION (b)
NEUTRON ENERGY (keV)
$^{100}$Ru (n, γ)
$^{101}$Ru (n, γ)
2+
3/2+
5/2+
7/2+
1/2+
3/2+
7/2+

ORNL-DWG 79-14567

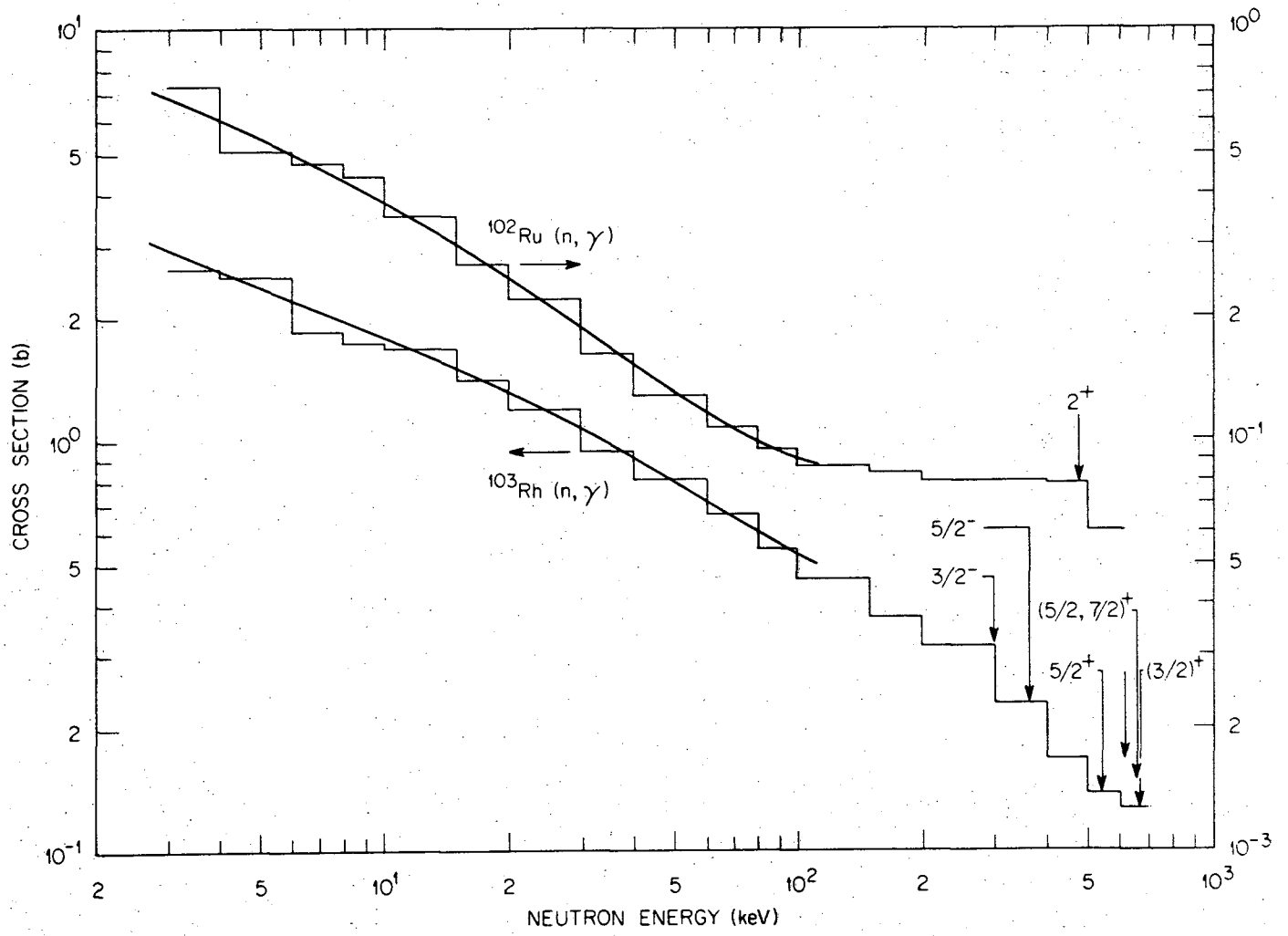

ORNL-DWG 79-14565

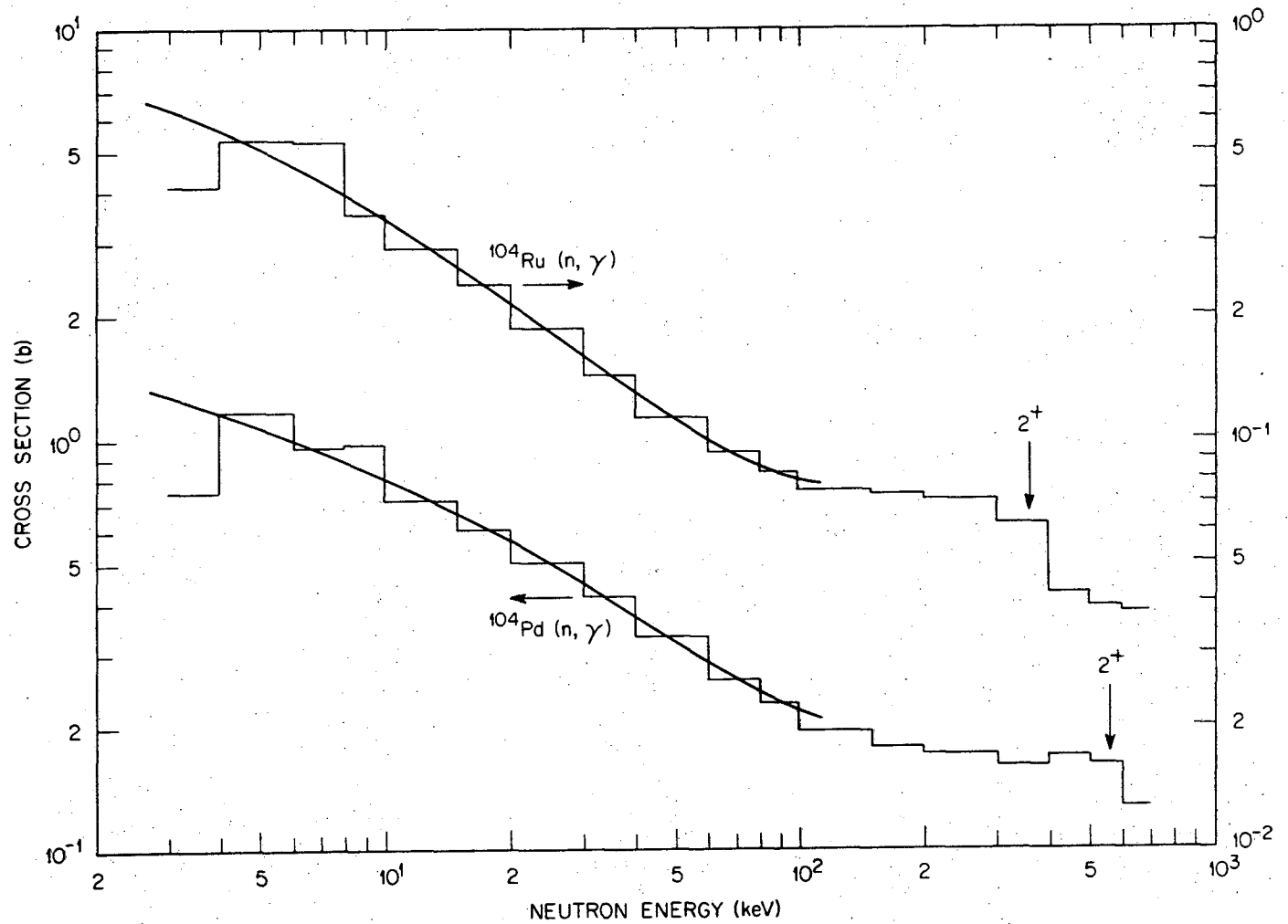

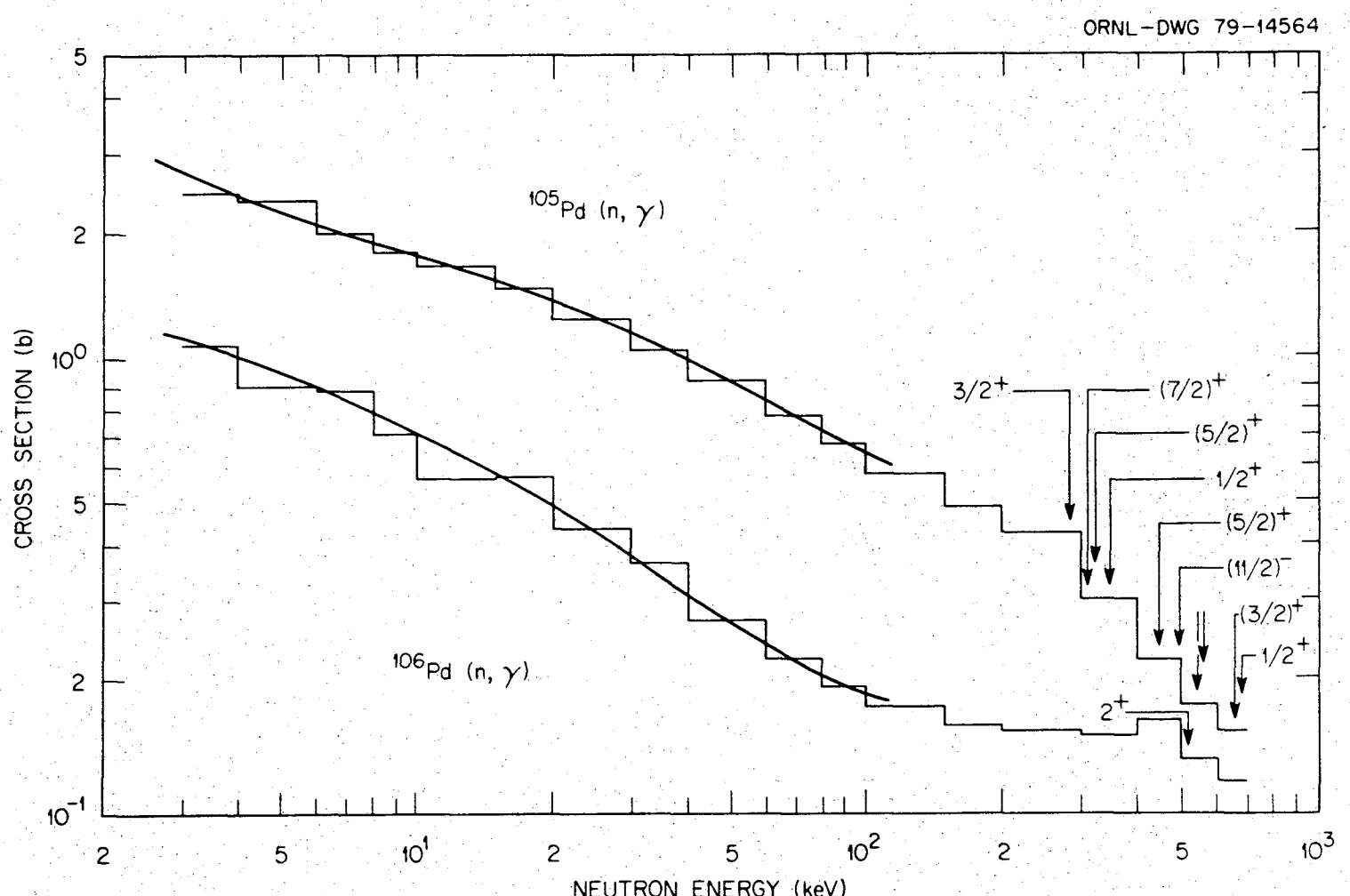
ORNL-DWG 79-14564
CROSS SECTION (b)
NEUTRON ENERGY (keV)
$^{105}$Pd (n, γ)
$^{106}$Pd (n, γ)
3/2+
(7/2)+
(5/2)+
1/2+
(5/2)+
(11/2)−
(3/2)+
1/2+
2+
5
2
$10^0$
5
2
$10^{-1}$
2
5
$10^1$
2
5
$10^2$
2
5
$10^3$

ORNL-DWG 79-14563

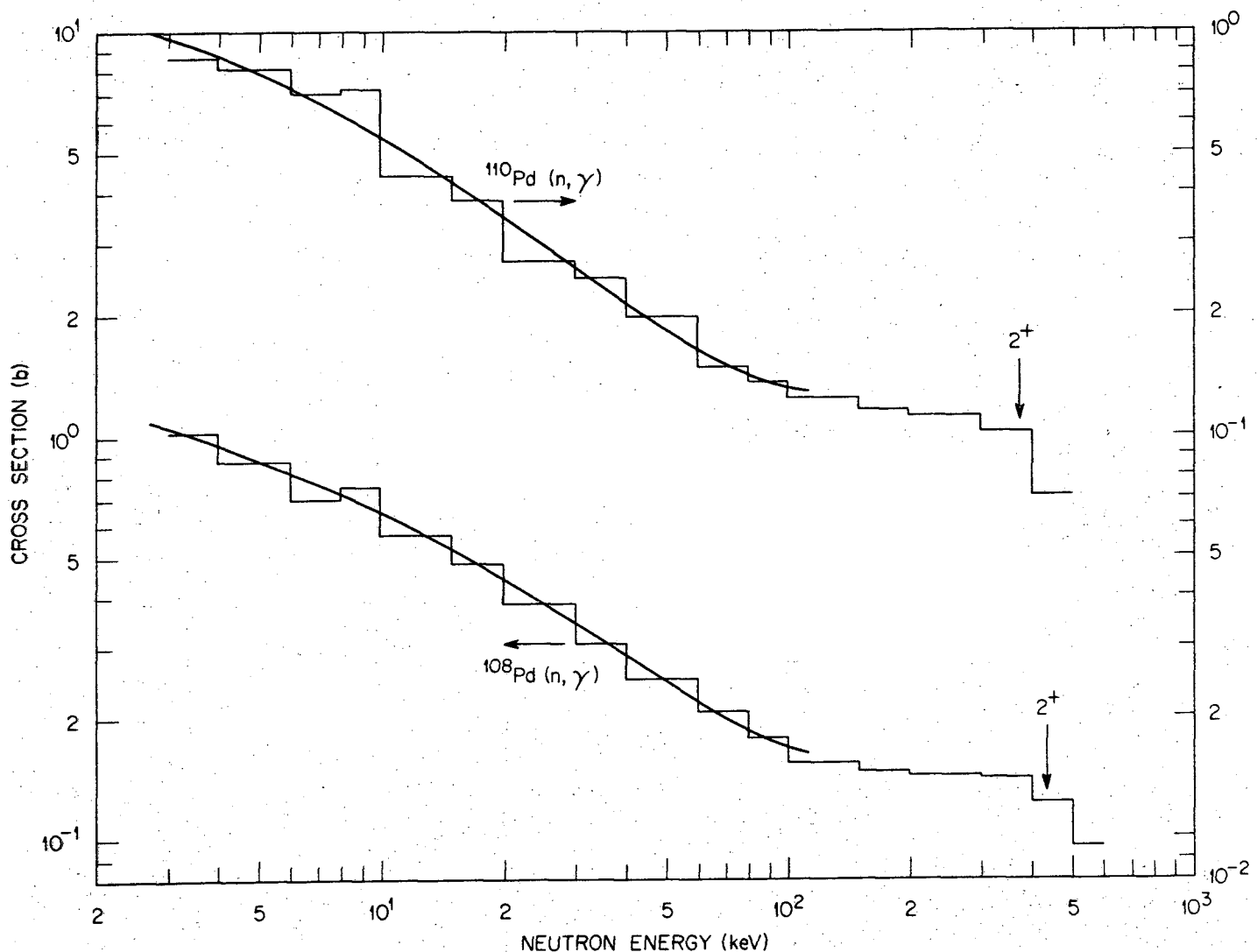

Summary of Session 2
(Resonance parameters: average values and systematics)

F. H. Fröhner (chairman)

The papers presented fall into two categories: (1) papers on statistical estimation of level densities and strength functions from resonance parameters and other experimental data, (2) papers on theoretical interpretation and prediction of average parameters by means of nuclear models and systematics.

## 1. Estimation of level-statistical parameters from experimental data

Techniques for level density extraction from resonance parameters were reviewed in the paper by Fort, Derrien and Lafond, who distinguish mainly three types of methods, viz.

I Monte Carlo simulation,

II methods based on the theory of nuclear spectra (random matrix theory) and observed level positions,

III methods based on estimation of the number of missing levels with the Porter-Thomas distribution.

Examples ($^{151}$Sm+n, $^{148}$Nd+n) showed large discrepancies between results obtained with I and II on one hand and III on the other.

The authors emphasised that the quality of an estimated mean level spacing may depend more on the quality of the resonance data than on the mere number of levels utilised. Usually the frequency of unresolved doublets increases with energy. Only Monte Carlo simulation can deal with this problem whereas for the more convenient methods of type III it may be better to ignore affected data and utilise only the low-energy part of the resolved region.

The following papers described various methods of type III. There was consensus that methods of type II are quite unreliable. In particular Dyson's $\Delta_3$ statistic (linear fit to the level number staircase curve) is found inadequate to check purity and completeness of resonance samples. The maximum-likelihood codes ESTIMA (described by Fort in a working group session), STARA (Fröhner), CAVE (Stefanon, see also the paper by Delfini

and Gruppelaar) and the code described by Rohr, Maisano and Shelley use besically the same statistical assumptions. They differ mainly in their degree of generality and in the use of thresholds.

Cave is the most general of these codes, applicable to mixed s- and p-wave levels with unassigned parities,whereas the other three require samples of definite parity. To ensure pure s-wave samples ESTIMA and Rohr's code impose a lower limit $\eta$ on $g\Gamma_n$. This (energy dependent) limit is chosen high enough to make the fraction of p-wave levels with $g\Gamma_n > \eta$ negligible. In CAVE a similar threshold is used such that all levels with $g\Gamma_n > \eta$ can be safely assumed to be observed. In all three codes the threshold is varied to check stability of the results against variations of the threshold. STARA employs only the actual observability threshold, estimating its energy dependence automatically from the curvature of the level number staircase plot. Apart from being very convenient this avoids a certain arbitrariness and loss of information and leads to very simple likelihood expressions especially for pure, but also for mixed samples. Both Stefanon and Rohr used Monte-Carlo generated resonance samples to establish confidence limits while Fröhner used general statistical arguments to arrive at practically the same prescription as Coceva and Stefanon.

Reported results obtained with different codes for the same nuclei are gathered in Table 1. Level spacings agree within few percent and also strength functions where the energy range is the same. An exception is $^{143}$Nd+n where the different strength functions obtained with CAVE and STARA are not explicable by different energy ranges but are due to different resonance parameter sets. The $^{151}$Sm results for the very narrow interval 0-14 eV suffer from bad resonance statistics and perhaps also from spurious p-wave levels.

A number of noteworthy points emerged from the discussions.

1. From a linear increase of the cumulative number of observed levels with energy one can only conclude that the fraction of missing levels does not depend on energy. <u>It is a mistake to conclude that no levels are missing.</u>

2. This resulted in a clear trend to abolish level density estimators based on level number staircase plots in favour of missing-level estimators based on the Porter-Thomas distribution, both in the US (Keyworth et al.) and Europe (ESTIMA, CAVE, STARA codes, Rohr et al.).

3. Strength functions obtained from resonance parameters in relatively narrow energy intervals may have only local significance. Even strength functions estimated from several hundred levels have uncertainties around 10% due to Porter-Thomas fluctuations. In the fission product range there is the additional problem of intermediate structure and valency effects which are averaged out only if the energy interval is much wider than the spacing between intermediate-structure peaks. Strength functions should therefore be determinated from energy intervals as large as possible.

4. A meaningful estimation of p-wave strength functions from resonance parameters is only possible for the light group of fission products. It is more reliable for even-even nuclei than for others because less level sequences are involved which means less unresolved multiplets and also because of the theoretical questions mentioned under (7) below affecting target nuclei with non-zero spin. In any case it is advisable to include fits to average total cross sections in the analysis.

5. In contrast to strength functions the level densities are believed to be unaffected by intermediate structure. Unresolved doublets, triplets etc. are more problematic, however, especially at higher energies. Level densities should therefore be determined only from high-quality resonance data even if this means narrower energy intervals.

6. As a final step in statistical resonance analysis it is recommended to check the consistency between the two-dimensional distribution of levels (with respect to $g\Gamma_n$ and energy) and the statistical model (Porter-Thomas hypothesis, constant level density, thresholds). This check is part of the ESTIMA and, in a particularly convenient representation, of the STARA procedure.

7. It is usually assumed that reduced neutron widths for given I and $\ell$ are distributed according to a $\chi^2$ distribution with $\nu$ (= 1 or 2) degrees of freedom, where $\nu$ is the number of possible entrance channels. Thus for target spin $I \geq 1/2$ there are sequences of p-wave resonances with $J = I + 1/2$ for $I = 1/2$, with $J = I + 1/2$ and $J = I - 1/2$ for $I \geq 1$) which can be excited via 2 entrance channels and whose reduced neutron widths should then obey an exponential distribution ($\nu$=2). This assumption is consistent with the extreme weakness of spin-spin interaction in the optical model.
Stefanon and others pointed out, however, that a direct verification appears to be lacking. If for instance the relevant transition matrix elements differed only by a spin-geometrical factor the Porter-Thomas distribution ($\nu$=1) apply also in these cases, but with twice the average width as compared to the other p-wave level sequences.

## 2. Theoretical interpretation and prediction of level-statistical parameters

Mughabghab reported on methods employed to establish strength functions and radiation widths for the 4th edition of the "barn book" BNL 325.
Questioned about level spacings he said that these are derived from the linear portion of level number staircase plots in much the same way as those for the last edition. He drew attention to the simple formula

$$\bar{\Gamma}_\gamma = 3 \cdot 10^{-2} \, (A^{2/3} \, U/a)^{7/2}$$

(U, $a^{-1}$ in MeV, $\bar{\Gamma}_\gamma$ in meV) recently published by Zaretskij and Sirotkin, which seems to be useful for fission products. An especially elegant use of nuclear theory and systematics is the prediction of thermal capture cross sections $\sigma_\gamma$ for nuclei where potential capture is expected to dominate.

*)

both the authors' and Mughabghab's form of the equation contain typographical errors

The Lane-Lynn theory of potential capture, with R' taken from optical-model calculations and (d,p) spectroscopic strengths from neighbour nuclei, was used to predict thermal capture cross sections for 78 h $^{132}$Te and 12.4 d $^{126}$Sn.

Reffo treated the very important question of the estimation of input parameters for nuclear-model calculations (Fermi gas, superfluidity, Nilsson model, radiation width formulae).
He made the point that the most sophisticated models and codes are not worth much if the input parameters are not adequately known and he showed what guidance nuclear theory and systematics can provide on the proper choice of unknown parameters. He advocates the use of local systematics wherever possible, instead of global systematics.

Kohr, Maisano and Shelley are in progress of estimating level densities from resonance parameters for more than 240 nuclei. Then they used the Fermi gas formula with pairing energies and spin cut-off values as recommended by Gilbert and Cameron to establish a consistent data base of level density parameters a. Apart from shell effects they observe a stepwise linear increase of a with A and relate the steps to a stepwise increase of the number of quasi-particles excited at neutron binding energy. Taking this stepwise linear behaviour seriously as a working hypothesis they deduce modified pairing energies and even contemplate the possibility to modify Nilsson single-particle levels so as to be consistent with the postulated behaviour of a.

Benzi, Maino, Menapace and Ventura calculate level densities from Nilsson levels and treat pairing with BCS theory, adjusting the gap parameter to get the empirical level densities. The systematics of the gap parameters is then used to predict unknown level densities. Even in its present state the method gives encouraging results (about 30% accuracy).
Benzi's surprisingly simple idea to estimate radiations widths by treating the excited nucleus as a radiating black body, its temperature being related to the excitation energy by the BCS equations, works well. The result,

$$\overline{\Gamma}_\gamma = \frac{T^3}{(22A)^{1/3}} ,$$

($\overline{\Gamma}_\gamma$ in meV, T in MeV) gives again an accuracy of about 30%. It looks quite different from the formula of Zaretskij and Sirotkin, derived for a Fermi gas without pairing and with giant dipole resonance behaviour of the radiative

strength, even after substitution of $U/a = T^2$. Contrary to wide-spread bel. f superfluidity was found to persist to rather high exci. on energies. In fact, most of the nuclei studied were still superfluid at the neutron binding energy.

The following comments appear appropriate:

1. The prescription $\sigma^2 = 0.0888(aU)^{1/2}A^{2/3}$ used by Gilbert and Cameron for the spin cut-off should be replaced by $\sigma^2 = 0.146(aU)^{1/2}\ A^{2/3}$ in applications of the Gilbert-Cameron formula. This correponds to replacement of $\langle m^2 \rangle = 0.146\ A^{2/3}$, derived by Jensen and Luttinger from all occupied shell-model states, by the recommendation of Facchini and Saetta-Manichella, $\langle m^2 \rangle = 0.24\ A^{2/3}$, derived only from the states near the Fermi energy as is appropriate for level density calculations. Furthermore, the behaviour of $\sigma^2$ at low energies is problematic (see Reffo's paper).

2. The widely used composite level density formula of Gilbert and Cameron begins to show its limitations. BCS theory tells that a fermion system with pairing interaction is superfluid below a critical excitation energy where the level density is discontinuous as a function of energy. Thus there is no real basis for the smooth behaviour postulated by Gilbert and Cameron. The fact that many nuclei are still superfluid at the neutron binding energy demands special caution in the interpretation of a and $\Delta$ values derived from neutron resonances with the Gilbert-Cameron formula.

3. More recent semi-empirical level density formulae are due to Kataria, Ramamurthy and Kapoor (Phys. Rev. C18 (1978)549) and Ignatyuk, Istekov and Smirenkin (Sov. J. Nucl. Phys. 29 (1979) 450). Their use and critical comparison with the Gilbert-Cameron formula ought to be encouraged.

4. The issue of enhancement factors accounting for collective excitations in level-density formulae is still far from clear, especially as far as vibrations are concerned. More theoretical work and high-quality level-spacing data, obtained with the best statistical methods available, are needed.

5. Another related problem are the different single-particle potentials (Nilsson, Woods-Saxon, self-consistent) that are used in level-density studies. Some of the conclusions concerning enhancement factors seem to depend on the type of potential used as starting point. This needs clarification.

6. It should be a challenge for theorists to see whether the stepwise linearity of a vs. A postulated by Rohr et al. can be more rigorously derived from BCS theory. The quasi-particle number representation developped by Ignatyuk and Sokolov (Sov. J. Nucl. Phys. 28 (1978) 469) may be an appropriate tool.

Table 1 Level-statistical parameters estimated from resonance parameters by Delfini and Gruppelaar with the code CAVE, by Fröhner with STARA and by Fort, Derrien and Lafond with ESTIMA.

| Compound System | Code | Energy Range (eV) | Levels above Threshold | $10^4 S_o$ | $D_o$ (eV) |
|---|---|---|---|---|---|
| $^{143}$Nd+n | CAVE | 0-2500 | 49 | $2.7 \pm 0.8$ | $36.5 \pm 4.0$ |
| | STARA | 0-2500 | 58 | $3.9 {}^{+1.0}_{-0.7}$ | $36.0 \pm 1.9$ |
| $^{145}$Nd+n | CAVE | 0-2250 | 113 | $3.3 \pm 0.6$ | $17.0 \pm 1.6$ |
| | STARA | 0-4650 | 191 | $4.1 {}^{+0.5}_{-0.4}$ | $17.1 \pm 0.6$ |
| $^{149}$Sm+n | CAVE | 0-160 | 63 | $7.5 \pm 2.2$ | $1.9 \pm 0.3$ |
| | STARA | 0-250 | 87 | $4.8 {}^{+1.3}_{-0.9}$ | $2.0 \pm 0.1$ |
| $^{151}$Sm+n | STARA | 0-14 | 10 | $4.3 {}^{+3.2}_{-1.3}$ | $0.56 \pm 0.14$ |
| | STARA[a)] | 0-106 | 64 | $3.3 {}^{+0.6}_{-0.4}$ | $1.14 \pm 0.13$ |
| | ESTIMA[b)] | 0-105.85 | 64 | 3.2 | $1.08 \pm 0.11$ |

a) recalculated after the Bologna meeting with the same resonance parameters as in the ESTIMA calculation

b) according to Fig.9 and 10 and the last table in the contribution of Fort, Derrien and Lafond.

# REVIEW OF THE DIFFERENT METHODS TO DERIVE AVERAGE SPACING FROM RESOLVED RESONANCE PARAMETERS SETS

E. Fort, H. Derrien, D. Lafond
Commissariat à l'Energie Atomique
DRNR/SEDC/SPNR/BEDN
Centre d'Etudes Nucléaires de Cadarache
Boîte Postale N°1
F.13115 - SAINT-PAUL-LEZ-DURANCE - (France)

## ABSTRACT

The average spacing of resonances is an important parameter for statistical model calculations, especially concerning non fissile nuclei.

The different methods to derive this average value from resonance parameters sets have been reviewed and analyzed in order to tentatively detect their respective weaknesses and propose recommendations. Possible improvements are suggested.

## I - INTRODUCTION -

For statistical model calculations the required parameters are neutron strengh functions, average radiative widths and the average spacing <D> of "S" resonances. These parameters are generally obtained from the analysis of the resonance parameters sets. The fact that the experimental resolution and sensitivity are limited in quality will result in an incomplete (missing levels) or distorded (error on partial width determination) information on the resonance parameters.

Generally, this fact has no practical consequence on strength functions or Gamma width determination. On the contrary, in most cases average spacing cannot be directly deduced from resonance sequency and it is difficult to correct exactly for missing resonances.

As a fact, a look in the litterature shows that, concerning this parameter, discrepancies by a factor 2 are common and even in some cases they can reach a factor 10.

However the importance of average spacing is basic since the average capture cross-section for non fissile nuclei : $\sigma_c = 2\pi^2 \lambda\!\!\!^{-2}\, g_j\, 1/\langle D\rangle \quad \langle\Gamma n\rangle\langle\Gamma\gamma\rangle/(\langle\Gamma n\rangle+\langle\Gamma\gamma\rangle)$ strongly depends on <D> either on the whole statistical energy range (large values of <D>), or in the high energy part (small values of <D>). In these cases $\Gamma\gamma \ll \Gamma n$ and the above expression reduces to : $\sigma_c = 2\pi^2 \lambda\!\!\!^{-2}\, g_j \langle\Gamma\gamma\rangle/\langle D\rangle$.

On the other hand and more generally, the average spacing is a normalization constant for compound nucleus level density which governes the behaviour with the energy of the partial widths (except for fission width).

The need for an average spacing determination of good quality is justified by the progresses made recently in the theoretical knowledge of level densities.

## II - THEORETICAL LAWS FOR RESONANCE PARAMETER DISTRIBUTIONS - GENESIS -

### II-1/ Level spacings :

Considering a compound nucleus at a finite excitation energy, the following assumptions were first made :
1) the distribution of resonance energies Er is not different from the distribution of the eigenvalues $E_\lambda$ of the Hamiltonian H of the compound nucleus ;
2) the distribution of a limited size sample is not different from the complete set.

In absence of very precise informations on the nuclear forces, the only thing which can be done is to assume a statistical distribution for eigenvalue spacings that directly result from a guess about the statistical nature of H matrix elements. In the frame of this hypothesis, WIGNER [1] first showed that the probability f(D) to find a spacing between D and D+dD is proportional to the spacing itself. $f(D) \simeq D$ , with consequently for spacing distribution law a form :

$$p(D) \simeq D \exp\left\{-\int_0^D f(D)dD\right\} \simeq De^{-D^2/2}$$

More precisely he guessed that the exact law should be :

$$p\left(\frac{D}{\langle D\rangle}\right) = \frac{\pi}{2}\ \frac{D}{\langle D\rangle} \exp - \frac{\pi}{4}\left(\frac{D}{\langle D\rangle}\right)^2 \qquad (1)$$

This law shows that nul spacings are excluded ("Level repulsion" property) and large spacings are poorly probable.

All the theoritical work developped afterwards considered different statistical distributions for H matrix elements.

By numerical computations of matrices of relatively high order ($\simeq$ 40) whose elements were independently distributed according to Gaussian Law with 0 mean, many authors did calculate spacings, collected in histograms well represented by the law (1).

The extension of such calculations to matrices of very high order is really hard , but MEHTA [3] determined the upper and lower bounds for the theoritical integral distribution law :

$$F_{low} = 1-\exp\left\{-\left(\frac{\pi}{4}\ \frac{D}{\langle D\rangle}\right)^2\right\} \qquad (2)$$

$$F_{upper} = 1-\exp\left\{-\left(\frac{\pi}{4}\ \frac{D}{\langle D\rangle}\right)^2\right\}\left\{1-\frac{1}{3}\left(\frac{\pi}{4}\ \frac{D}{\langle D\rangle}\right)^2\right\} \qquad (3)$$

These bounds are verified by WIGNER's surmise.

Proceeding from MEHTA's work, GAUDIN obtained the distribution function of spacings as an infinite product rapidly converging, differing from WIGNER's surmise only by less than 5% up to $D/\langle D\rangle < 2.5$ (See Fig. 1). For $D/\langle D\rangle < 2$, MEHTA proposes :

$$F_M(D/\langle D\rangle) = 1-\left[1+0.078\left(\frac{\pi}{2}\frac{D}{\langle D\rangle}\right)^2\right]^{-1.003} \times \exp\left[-\frac{1}{4}\left(\frac{\pi}{2}\frac{D}{\langle D\rangle}\right)^2\right] \qquad (4)$$

which is a better approximation of the exact integral distribution given by GAUDIN [14] than what can be extrapolated from (1).

DYSON [4] proposed a new ensemble E in which a compound nucleus system is represented by a N x N unitary matrix S, instead of an Hamiltonian H, the relationship between S and H being unspecified. The energy levels are related to the eigenvalues of the matrix S which are N complex numbers exp. $i\Theta j$ distributed on the unit circle. According to Dyson the basic hypothesis is that "the behaviour of n consecutive levels of an actual system, where n is small compared to the total number of levels, is statistically equivalent to the behaviour in the ensemble E of n consecutive angles $\Theta$ on the unit circle, where n is small compared to N". Dyson imagined different systems. In particular, if the S matrices are symetric unitary matrices, the ensemble E is the $E_1$ orthogonal ensemble such as the system is unvariant under time inversion or space rotation, which are obvious physical requirements. For large values of spacings, Dyson gave the relationship :

$$p\left(\frac{D}{\langle D\rangle}\right) = A\frac{D^{17/8}}{\langle D\rangle} \exp\left\{-\left(\frac{\pi}{4}\frac{D}{\langle D\rangle}\right)^2 - \frac{\pi}{4}\frac{D}{\langle D\rangle}\right\} \qquad (5)$$

From it, we see that Wigner's law underestimates the frequency of large spacings. That has no practical consequences since the probability of large values of D is very small.

Now, it is worth mentionning the correlations.

The correlations (short range, long range) which have been foreseen by theory and put in evidence by experiment cannot be extracted from Wigner's formula.

PORTER [5] using matrices of order 3 from the Gaussian Ensemble and KAHN [6] with matrices of high order from orthogonal ensemble obtained very close results for the first order spacing distribution.

Using matrices of order 10 from Gaussian Orthogonal Ensemble, PORTER [7] calculated $n^{th}$ order spacing distribution ($n = 1,\ldots 9$). His results were confirmed by GARRISON [8] on experimental distributions.

As concluding remark, Wigner's conjecture can be considered as an excellent approximation of what we think to be the "truth" as far as the spacing distributions of a single class level population are concerned and for $D/\langle D\rangle$ less than 2.5.

In the case of superposition of two uncorrelated classes of level the spacing distribution given by LYNN [2] is :

$$p_{1+2}(x) = \frac{1}{\bar{x}_1+\bar{x}_2}\left[\frac{\pi x\bar{x}_1}{2\bar{x}_2^2}\exp\left(-\frac{\pi x^2}{4x_2^2}\right)\left\{1-\mathrm{erf}\left(\frac{x\sqrt{\pi}}{2\bar{x}_1}\right)\right\}\right.$$

$$+\ 2\exp\left\{-\frac{\pi x^2}{4}\left(\frac{1}{x_1^2}+\frac{1}{x_2^2}\right)\right\}$$

$$\left.+\ \frac{\pi x\bar{x}_2}{2\bar{x}_1^2}\exp\left(-\frac{\pi\bar{x}^2}{4\bar{x}_1^2}\right)\left\{1-\mathrm{erf}\left(\frac{x\sqrt{\pi}}{2\bar{x}_2}\right)\right\}\right] \qquad (6)$$

where $x = \frac{D}{\langle D\rangle}$ .

II-2/ Neutron widths distribution :

The neutron widths of same spin and parity fluctuate strongly from resonance to resonance. The general expression of neutron width being $\Gamma_n = 2P_L\gamma_n^2$ , these fluctuations are due to reduced neutron width $\gamma_n^2$ since the penetration factor varies smoothly with energy.

In the frame of R matrix theory :

$$\gamma_{\lambda(c)} = \left(\frac{\hbar^2}{2Ma_c}\right)^{1/2}\int_{r_c=a_c}\varphi_c^*\,\chi_\lambda\,dS_c$$

where $\chi_\lambda$ is the eigenfunction in the internal region and $\varphi_c^*$ the joint surface function. According to PORTER-THOMAS [11] the integral can be approximated by sum over many cells in the configuration space. If the linear dimensions of cells are correctly chosen ($\pi/K$), the number of cells is large $(KR/\pi)^{3A}$ and the contributions from cells of positive and negative signs are equally probable. The application of the central limit theorem results in Gaussian form with 0 mean for $\gamma_{\lambda(c)}$ distribution.

The frequency function for the reduced widths follows from this fact :

$$p(\gamma_n^2)d\gamma_n^2 = \frac{1}{\sqrt{2\gamma_n^2\ \pi\langle\gamma_n^2\rangle}}\exp\left(-\frac{\gamma_n^2}{\langle\gamma_n^2\rangle}\right)d\gamma_n^2 \qquad (7)$$

It has to be noted that Porter-Thomas frequency function is a particular case of the "chi squared" frequency function with $\nu$ degrees of freedom :

$$p_\nu(x)dx = \Gamma(\nu/2)^{-1}(\nu/2\langle x\rangle)^{\nu/2}\,x^{(\nu-2)/2}e^{-\nu x/2\langle x\rangle}\,dx \qquad (8)$$

## III - EXAMINATION OF POSSIBLE ERRORS ON RESONANCE PARAMETERS COMING FROM EXPERIMENTAL TECHNICS AND ANALYSIS METHODS -

The resonances are revealed when transmission or reaction cross-sections are measured with low energy incident neutrons. In this chapter, we investigate the possible causes of errors on the knowledge on resonance parameters due to the imperfections of the experimental technics and the analysis methods of the raw data.

## III-1/ Experimental effects :

### . Effects due to sample thickness :

The area of a weak resonance is : $A_T = \pi/2\ n\ \sigma_0\ \Gamma$ for total cross-section, and $A_r = \pi/2\ \sigma_0\ \Gamma_r$ for reaction cross-section ($\sigma_0 = 4\pi\lambda^2 g\ \Gamma_n/\Gamma$, $\Gamma$ resonance total width).

So, a compromise is to be found in transmission experiment between the sample thickness and sensitivity threshold taking into account the statistical fluctuation and the fact that the potential transmission introduces an important background compared to small resonances. Reaction cross-sections measurements are certainly more efficient to reveal weak resonances.

Connected with sample thickness are the neutron multiple scattering and self screening effects. They affect only reaction cross-sections data and are calculated by MONTE-CARLO and analytical methods respectively. They deforme the shape of the cross-section with poor consequences on level energy determination, but with substantial modification of partial widths.

### . Doppler and energy resolution effects :

These effects have consequences on both level spacings and resonance widths. The Doppler effect is assumed to be Gaussian in shape with a width defined as :

$$\Delta = 2\sqrt{k\frac{E}{A}\ T_{eff}}$$

$T_{eff}$ is the effective temperature of the sample as defined by LAMB [10]. It is an experimental parameter of importance. By reducing $T_{eff}$ by a factor 4 (T going from 300°K to 77°K) resulting in a reduction of $\Delta$ by a factor 2, it was possible to detect three new resonances in 235U [9].

The energy resolution is expressed as $\Delta(E) = k\ \frac{E^{3/2}}{36.15L}\Delta t$ in time of flight experiment.

The Doppler effect is preponderant at low energy and up to some KeV.

These effects have consequences on both level spacings and resonance widths due to the fact that the doublets may not be separated.

### . Neutron background determination :

An error on neutron background determination reacts directly on partial width values. But, according to many authors [12], [13], this error can be revealed by the shape analysis method.

## III-2/ Effects of analysis methods :

There are two methods to analyze raw data : Area Analysis method, and Shape Analysis Method :

. Area analysis method :

The total resonance area is expressed in terms of the partial widths of the resonance and sample thickness e. For different values of this latter parameter a system of curves $F(\Gamma_n, \Gamma_\gamma, e)$ is obtained whose convergence zone determines $\Gamma_n$ and $\Gamma_\gamma$ with more or less accurate results.

The advantage of this method is that the resonance area is not sensitive to Doppler and Resolution effects.

The disadvantages are that this method can hardly be applied to non-isolated resonances and to detect errors on background determination.

. Shape analysis method :

If obtained by a sample of small thickness, the raw data are written in the following way :

$\sigma_{eff}(E) = \sigma(E) \times D(E) \times R(E)$ for reaction cross-section data

For transmission data we have $T_r = (e^{-n\,\sigma(E) \times D(E)}) \times R(E)$ .

D(E) and R(E) are Doppler broadening and Resolution functions respectively. $\sigma(E)$ which is the "True" cross-section is calculated by a formalism which can be very sophisticated (multichannel, multilevel), but which has to be adequately chosen in function of the type of cross-section. On the other hand, Doppler and Resolution widths must be small compared to natural resonance widths. This method uses the whole of experimental informations. It is fast and can detect errors in normalization or background determination.

It is basically the more efficient method if used with least squares procedure.

## IV - REVIEW OF THE DIFFERENT METHODS USED TO DERIVE AVERAGE SPACINGS -

There are three classes of methods :
- the method of MONTE-CARLO simulation ;
- the methods which use the statistics concerning the position of the levels ;
- the methods based on the fit of the reduced neutron width distribution by a PORTER-THOMAS Law.

### IV-1/ Method of MONTE-CARLO simulation (M1) :

A set of resonance parameters is generated using WIGNER's and PORTER-THOMAS laws with estimated values for <D> and <gΓn>. It is used to simulate a total cross-section in the energy interval of interest taking into account the experimental effects (Resolution, Doppler). This simulated cross-section is analyzed in the same way as the experimental cross-section. The percentage of missing resonances found in the simulated cross-section is supposed to be the same for the experimental one. This method is valid if the percentage of loss of resonances is not sensitive to the starting value of <D>. This method was used, for example, by DERRIEN [15], for 241 Am.

IV-2/ Methods using statistics concerning the position of the levels :

There is a method, often used even nowadays, which consists of the plot of the cumulative number N(E) of levels as a function of energy ("Staircase" method) This method is based on the assumption, very questionable, that in the energy interval $\Delta E$ where the behaviour of N(E) is linear with the energy there are no missing resonances, and <D> is given by $\langle D\rangle = \Delta E/N(E)^{\Delta E}$

One method, directly derived from the previous one, is based on the $\Delta_3$ statistics given by Dyson and MEHTA [16] The best fit of N(E) is given by least squares procedure and a parameter $\Delta$ is defined as :

$$\Delta = \min \left\{ \frac{1}{\Delta E} \int_{\Delta E} \left\{ N(E) - (AE+B) \right\}^2 dE \right.$$

The $\Delta_3$ parameter for the theoretical distribution is $1/\pi^2$ (Log. N-0.0687) with a variance independent of N $\sigma(\Delta_3) = 1.17/\pi^2 = 0.11$ for a multiplicity egual to 1) If $\Delta$ is such as : $\Delta_3 - \sigma(\Delta_3) < \Delta < \Delta_3 + \sigma(\Delta_3)$, the experimental set of resonances is supposed complete and <D> is given by $\langle D\rangle = \Delta E/\int_{\Delta E}(AE+B)dE$

This method has theoretical basis of high quality, but does not seem to be adequate for mean spacing determination because

- not very accurate : for a sample of 100 resonances, the accuracy allowed for $\Delta$ is $\sigma(\Delta_3)/\Delta_3 = 0.24$ ;
- it is not true that the omission of a few levels or the presence of spurious resonance will cause a large discrepancy between the theoretical value and the experimental value of $\Delta_3$ (see 148Nd and 151Sm treated as examples)

IV-3/ Methods based on PORTER-THOMAS law :

In addition to <D> these methods give access to $\langle g\Gamma n\rangle$ and then to neutron strength function

The missing level estimator (M3) [17] uses properties of PORTER-THOMAS law resulting from partial integrations According to KEYWORTH and al, the method consists in "calculating the quantity $n\Sigma g\Gamma n/(\Sigma\sqrt{g\Gamma n})^2$ starting with the largest value of $g\Gamma n$ in the interval and adding additional levels, one at a time, going from larger to smaller in the ordered array of observed values of $g\Gamma n$. When this quantity equals 1.206 , the total number of levels in the interval is n/0.617" This method which is quick and does not require any judgement is sensitive to the quality of the determination of the largest widths.

Least squares fitting procedure (M4) :

In this method initiated at SACLAY [9], the fit concerns the part of the integral distribution above a given threshold of $g\Gamma n^0$, which is relatively small compared to the mean value. The assumption is made that only the small values of $g\Gamma n^0$ are missed with no consequence for the shape of the distribution above this threshold In the case of the presence of "p" wave resonances the method is also applied if it is still possible to choose a threshold which eliminates the quasi totality of the "p" wave resonances Several authors use the method by varying the threshold and keeping the value which gives the best fit to the remaining distribution

Maximum likelihood method : "ESTIMA" method (M5) :

For a distribution of reduced neutron width of a single class, the likelihood function is defined as the product of the frequences of each datum $x_i$ having a frequency function $P\nu(x)$ :

$$L(\nu,\bar{x}) = \prod_i P\nu(x_i)$$

The values of parameters which maximise the function L or its logarithm are the most likely values.

In ESTIMA code [19], [20], [21], the parameter $\nu$ is kept equal to 1 with the justification that a departure from unity can be caused by instrumental bias or by surimposition of two populations. Consequently, the conditions of application of this code are the following :

- in the energy interval $\Delta E$ of interest, the unresolved doublets are judged very improbable on the basis of the experimental conditions ;
- the analyzed set of resonances contains only "sure" "s" wave resonance defined as such either by the author of the experiment, or by using a criterion based on the comparison with the possible largest magnitude for the "p" wave neutron widths for the considered nucleus. (In a recent code [22] the probability for a resonance to be "p" wave is explicitly included in the likelihood function).

A maximum of informations (detection of systematic errors) is obtained if the method is applied to truncated distributions. At each position of the threshold corresponds a theoretical distribution fitting the data, characterized by a value for $\langle g\Gamma n\rangle$ and resulting in an estimated total number $N_t$ of resonances in the energy interval under analysis. So, a set of most likely values is obtained for $\langle g\Gamma n\rangle$ and $N_t$. These values fluctuate with the threshold positions. Those which correspond to a "stabilization" are judged as "most physical" (see figure 4 ).

The average spacing is obtained by $\langle D\rangle = \Delta E/N_t^{st}$.

The oscillations in the stabilization region give the error on the estimation of $N_t^{st}$. The "sampling" error is given by Dyson and Mehta as :

$$\frac{\Delta D}{D} = \frac{0.45}{N}\sqrt{\mathrm{Log}(2\pi N)+0.343}\ ,$$

where N is the number of the "observed" resonances. A check of the final results is obtained by loocking at the distributions of $g\Gamma n$ around $\langle g\Gamma n\rangle$ as function of energy (partial integration, see fig. 7 and 10).

## V - INTERCOMPARISON OF THE VARIOUS METHODS -

It is interesting to know for the reviewed methods the degree of sensitivity to the experimental effects. These ones have the following consequences on the spacing and the reduced neutron width distributions.

Spacing distribution :

The loss of resonances results in a deformation of the distribution in its whole and there is no possibility to correct it. On the other hand, due to its principle itself the $\Delta_3$ statistics is unable to correct for a constant percentage of missing resonances.

Reduced neutron width distribution :

The loss of resonances (weak resonances) has no consequence on the shape of the distribution above a given threshold. The contamination by "p" wave resonances is easily detectable :

- either the "p" wave resonances have small $\langle g\Gamma n \rangle$. In that case only a small part of the distribution is perturbed which has to be analyzed above a given threshold ;
- or the "p" wave resonances have average width comparable in magnitude to those of "s" wave resonances (sample of resonances extending up to high energy or nuclei of 3p region with A ≈ 90). In that case, two solutions : take into account the probability of existence of "p" wave resonances or work on sample populated only with sure "s" wave resonances.

The detection of contamination by doublets requires in many cases a further analysis which can be a critical study of experimental conditions (Doppler effect, energy resolution) or a study of the variation of the largest widths as a function of energy (see figure 10bis). It has to be noted that even-even nuclei have a small probability to exhibit doublets ("repulsion effect").

The presence of very large (or small) neutron widths has as no influence on the results given by the maximum likelihood methods or $\chi^2$ procedure provided that the threshold is positionned at low energy. The results obtained by Missing Level Estimator can be affected by such defaults.

In Annex one finds a partial illustration of the considerations mentionned above.

148Nd and 151Sm treated as sample cases show how discrepant can be the results on <D> obtained by the different methods from the same set of resonances :

$\langle D \rangle_{ev}$

| Nucleus \ Method | M1 | M2 | M3 | M4 | M5 |
|---|---|---|---|---|---|
| 151 Sm | 1.62 | 1.73 | 1.58 | 1.11 | 1.05 |
| 148 Nd | 91. | 113. | 158. | 171. | 191. |

- CONCLUSION -

The parameters obtained for 151Sm and 148Nd show clearly that there is a large discrepancy in the indications given by the methods based on spacing distribution (M1, M2) and those given by the methods based on neutron width distribution (M3, M4, M5). So, it is obvious that the choice of the method to derive average spacing can be at the origin of large errors. But it is also obvious, and that is probably the essential point, that the choice of the resonance sampling plays a major role. In this choice the following considerations should be taken into account :

1/ The analysis of set of resonance parameters should be performed jointly with a critical analysis of the experimen-

tal conditions (sample thickness, resolution, background) and of the method used to obtain the resonance parameters (shape or area analysis, formalism , ...) ;

2/ The priority should be given to the quality of the sampling rather than to the number of resonances.

- REFERENCES -

[1] E.P. WIGNER Conf. on Neutron Physics by time of fligth, Gatlinburg 1956, ORNL Report 2309 (1957).

[2] J.E. LYNN, The theory of neutron resonance reactions. The international series of monographs on physics. Clarendon Press-Oxford 1968).

[3] M.L. MEHTA, Nucl. Physics 18, 395 ( 1960).

[4] F.J. DYSON, Journal of Math. Phys., vol 3, N°1, 140 (1962).

[5] C.E. PORTER, Nucl. Phys. 40, 167 (1963).

[6] P.B. KAHN, Nucl. Phys. 41, 159 (1963).

[7] C.E. PORTER, BNL Report 6763 (1963).

[8] J.D. GARRISON, Ann.Phys. 30, 269 (1964), BNL Report 7402.

[9] H. DERRIEN, Private communication.

[10] W.E. LAMB, Phys. Rev. 55 (1939) 190.

[11] C.E. PORTER, R.G. THOMAS (1956), Phys. Rev. 104, 483 (1956).

[12] H. DERRIEN, Report BNL 50451, p. 45 (1975).

[13] J.P. L'HERITEAU, P. RIBON, Proc. of Conference - Neutron cross section and technology. Conf-710301, vol. 3, p. 438.

[14] M. GAUDIN, Nucl. Phys. 25, 447 (1961).

[15] H. DERRIEN, Proc. of Conference-Nuclear cross sections and technology, Washington D.C. March 3-7, 1975.

[16] F. DYSON, M.L. MEHTA, Journal of Mathematical Physics, Vol. IV, N5, 489.

[17] K. KEYWORTH, M.S. MOORE, J.O. MOSES, ANL 7690 - Argonne Conference (1976).

[18] F. FROHNER, Contribution to this meeting.

[19] P. RIBON, E. FORT, KREBS, TRAN QUOC THUONG, CEA Report - CEA-N-1832 (1975).

[20] TRAN QUOC THUONG, EANDC(E)- 160 AL.

[21] E. FORT, Review paper 7 presented at the advisory group mee-

ting on F.P nuclear data, Petten (1977)

[22] C COCEVA, M STEPHANON, Nucl Phys A 315 (1979).

# ANNEX

## 151Sm

## SOME COMMENTS ON THE CONDITIONS OF THE EXPERIMENT OF KIROUAC AND EILAND (Physical Review C, 11, 3, 895, 1975)

- ANNEX -

The experiment was performed by time of fligth method with a Linac and a 31.6 m fligth path. The nominal resolution was 4.4 ns/m at 20 ev and seems to be good enough to separate most important resonances up to about 100 ev. The sample thicknesses were $0.2858 \times 10^{-3}$ and $0.0728 \times 10^{-3}$ at/b giving a potential transmission of about 1, which is not adequate for the detection of weak resonances. We can infer from this fact that there is probably an important loss of weak resonances - even at low energy where the resolution is good - which are hided by the statistical fluctuations in the experimental transmission curves. On figure 10 bis, we see that there are no resonances below a threshold $S_{\Delta}(E) = 8.10^{-4}\ E^{1/2}$ (ev) in the energy range 0 ev to 100 ev. Above this energy, a mathematical expression of the sensitivity threshold is rather difficult to be justified on the basis of technical arguments. The only comments which can be made are of qualitative nature :

- the missed resonances have increasing value of $g\Gamma_n^0$
- the observed resonances have an increasing average value (existence of doublets, neutron background determination ?)
- the number of non separated doublets is increasing (between 100 ev and 150 ev the number of resonances having $g\Gamma n$ such as $0.2\langle g\Gamma n\rangle < g\Gamma n < \langle g\Gamma n\rangle$ is reduced by a factor 2, the sensitivity threshold being unchanged).

It seems from this examination of KIROUAC and EILAND experiment that the resonance sampling to be treated should stop at 100 ev neutron energy, with the very simple question : how many resonances are missed below the threshold $S_{\Delta}(E) = 8.10^{-4}\ E^{1/2}$(ev) ?

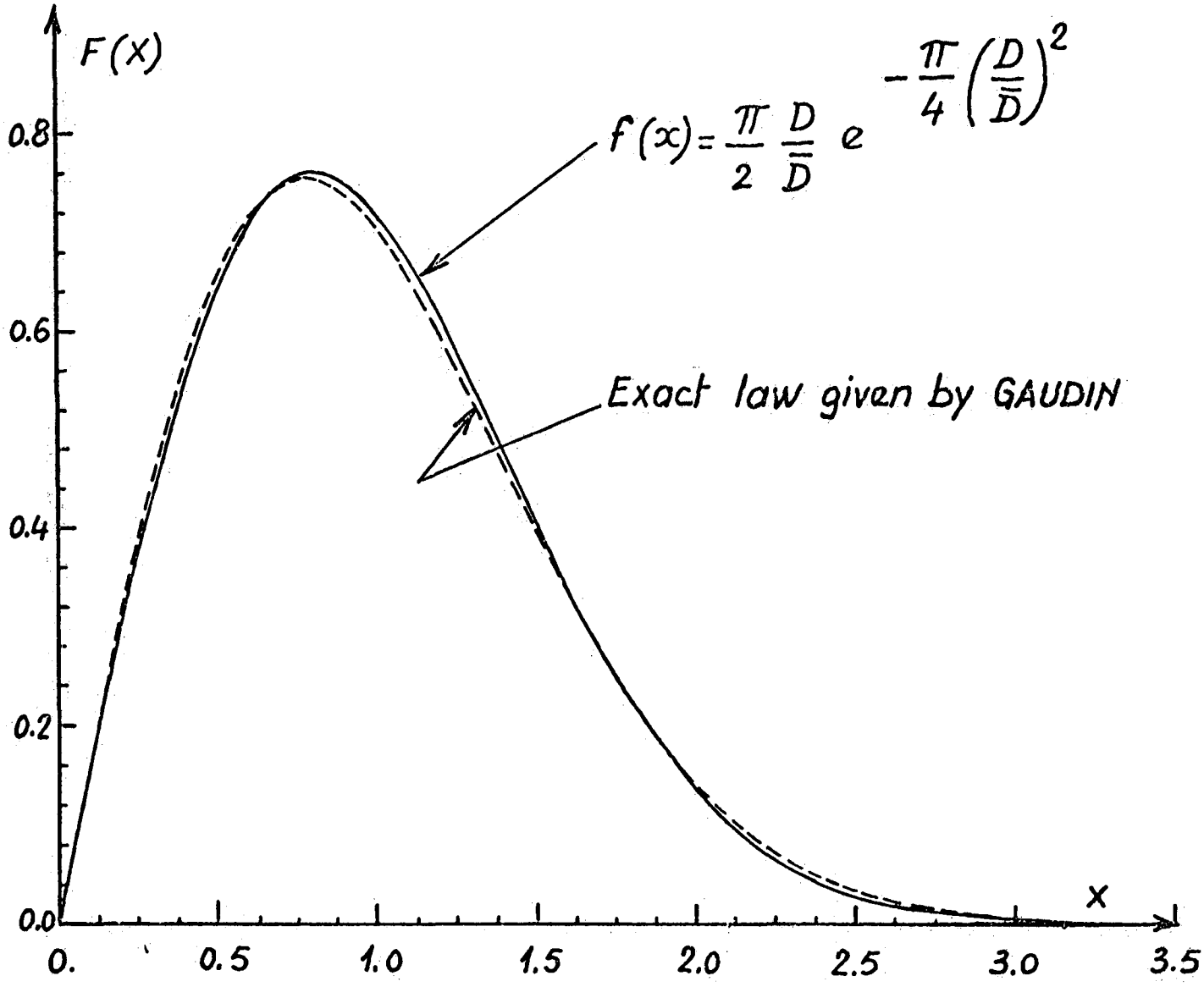
F(X)
0.8
0.6
0.4
0.2
0.0
0.
0.5
1.0
1.5
2.0
2.5
3.0
3.5
X
$f(x) = \frac{\pi}{2} \frac{D}{\bar{D}} e^{-\frac{\pi}{4}\left(\frac{D}{\bar{D}}\right)^2}$
Exact law given by GAUDIN

Fig. 1

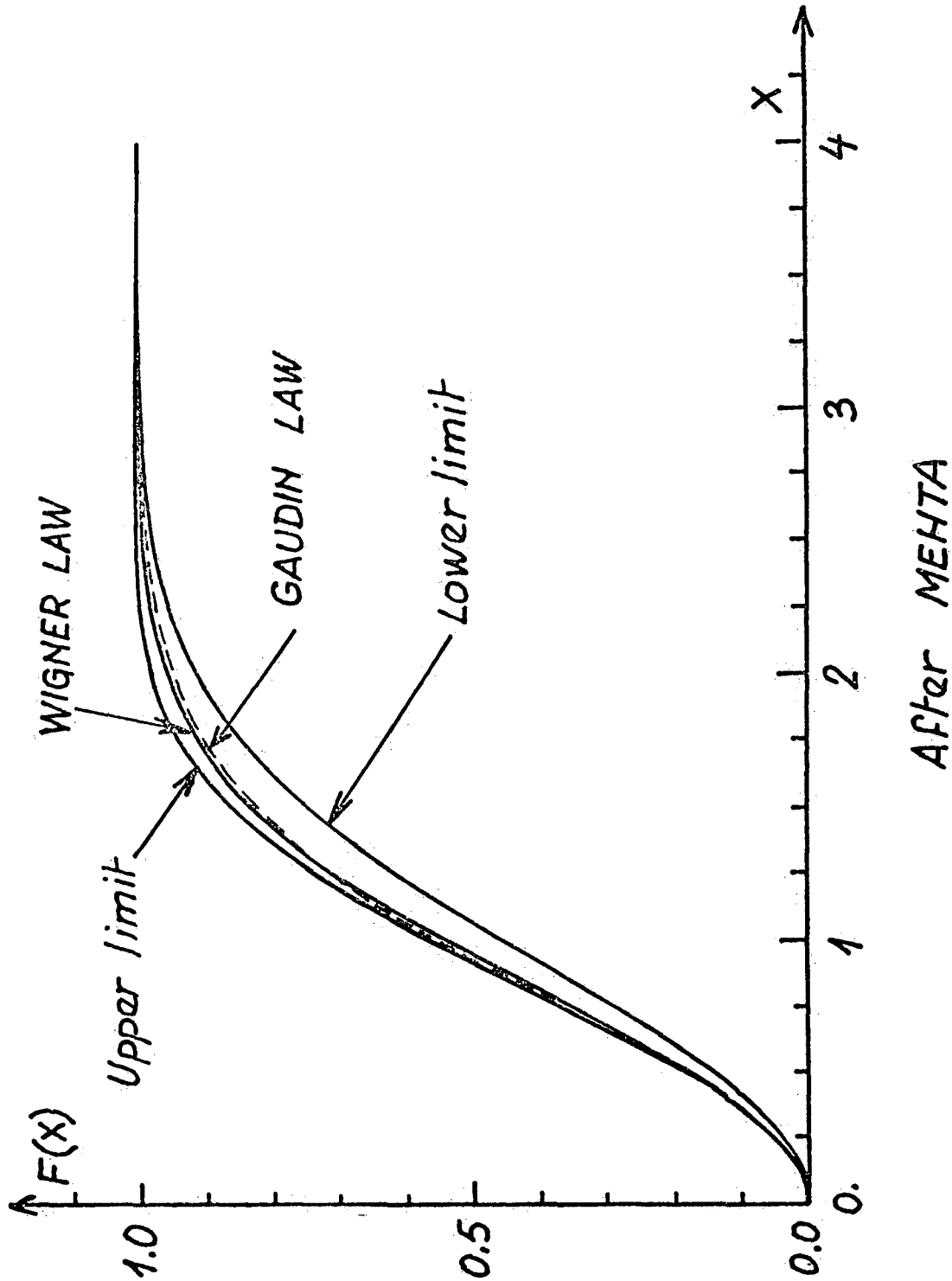
F(x)
1.0
0.5
0.0
0.
1
2
3
4
X
WIGNER LAW
GAUDIN LAW
Lower limit
Upper limit
After MEHTA

Fig. 2

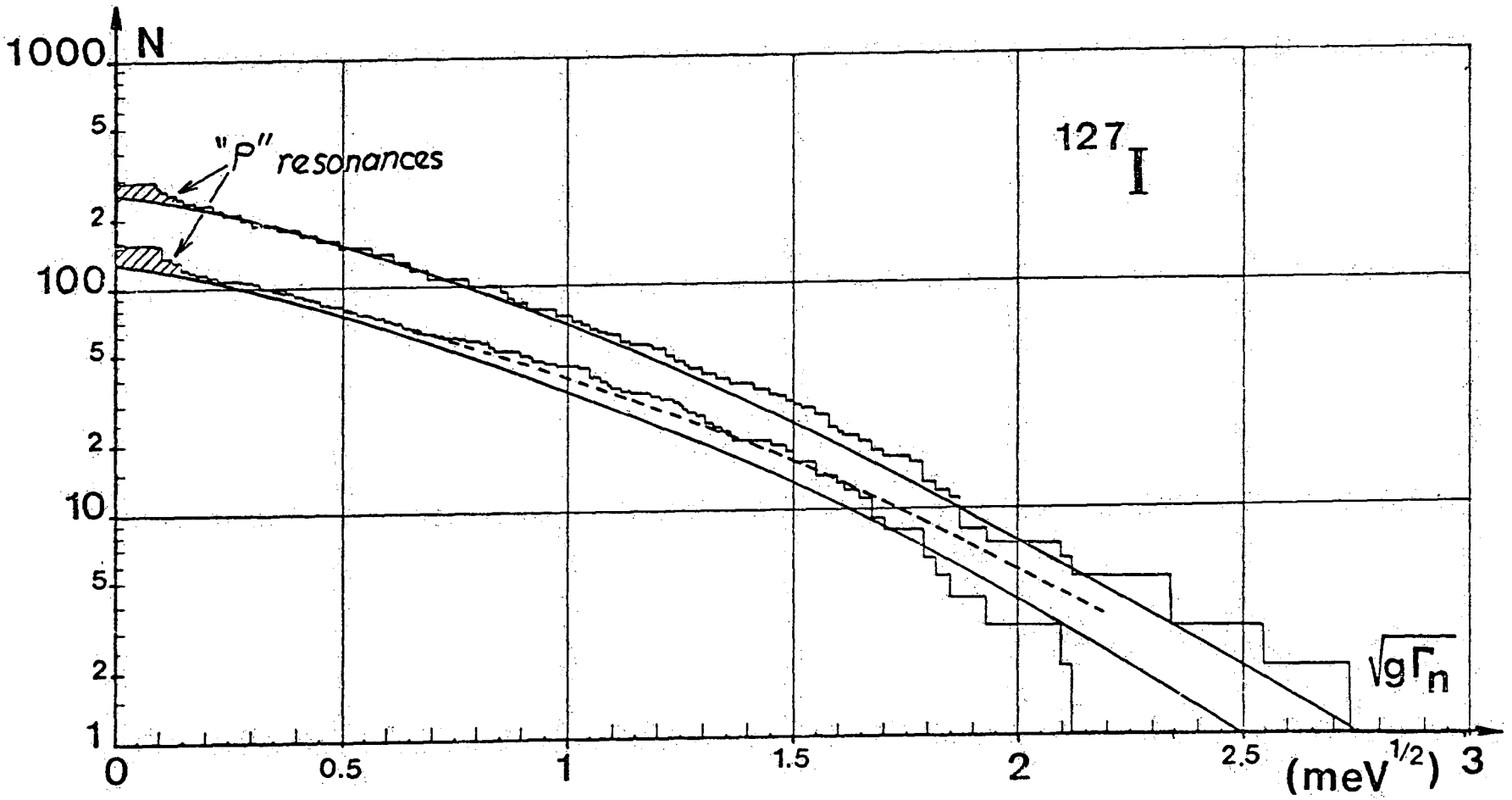


AFTER REFERENCE [19]

Fig.3

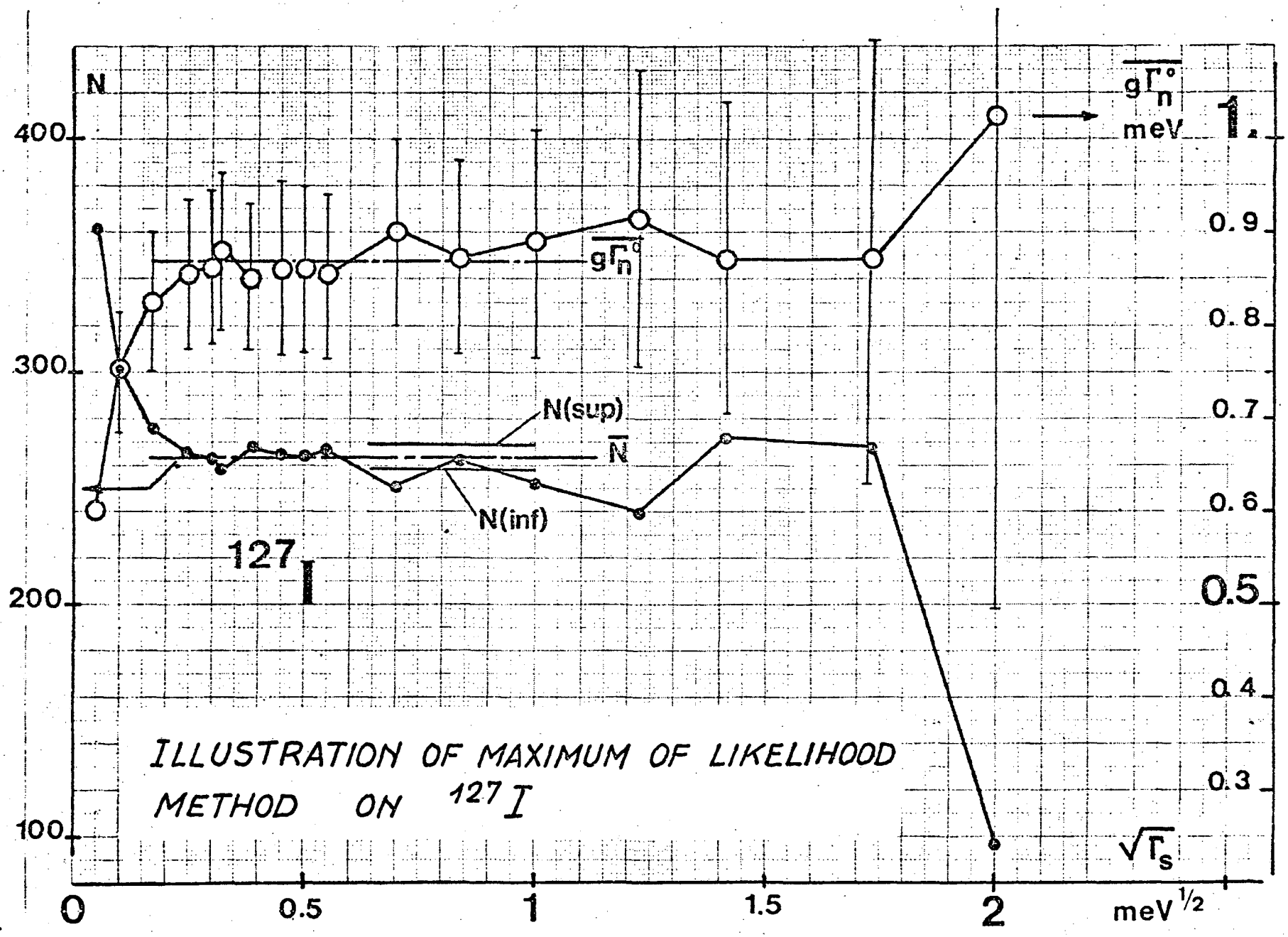


Fig. 4

AFTER REFERENCE [19]

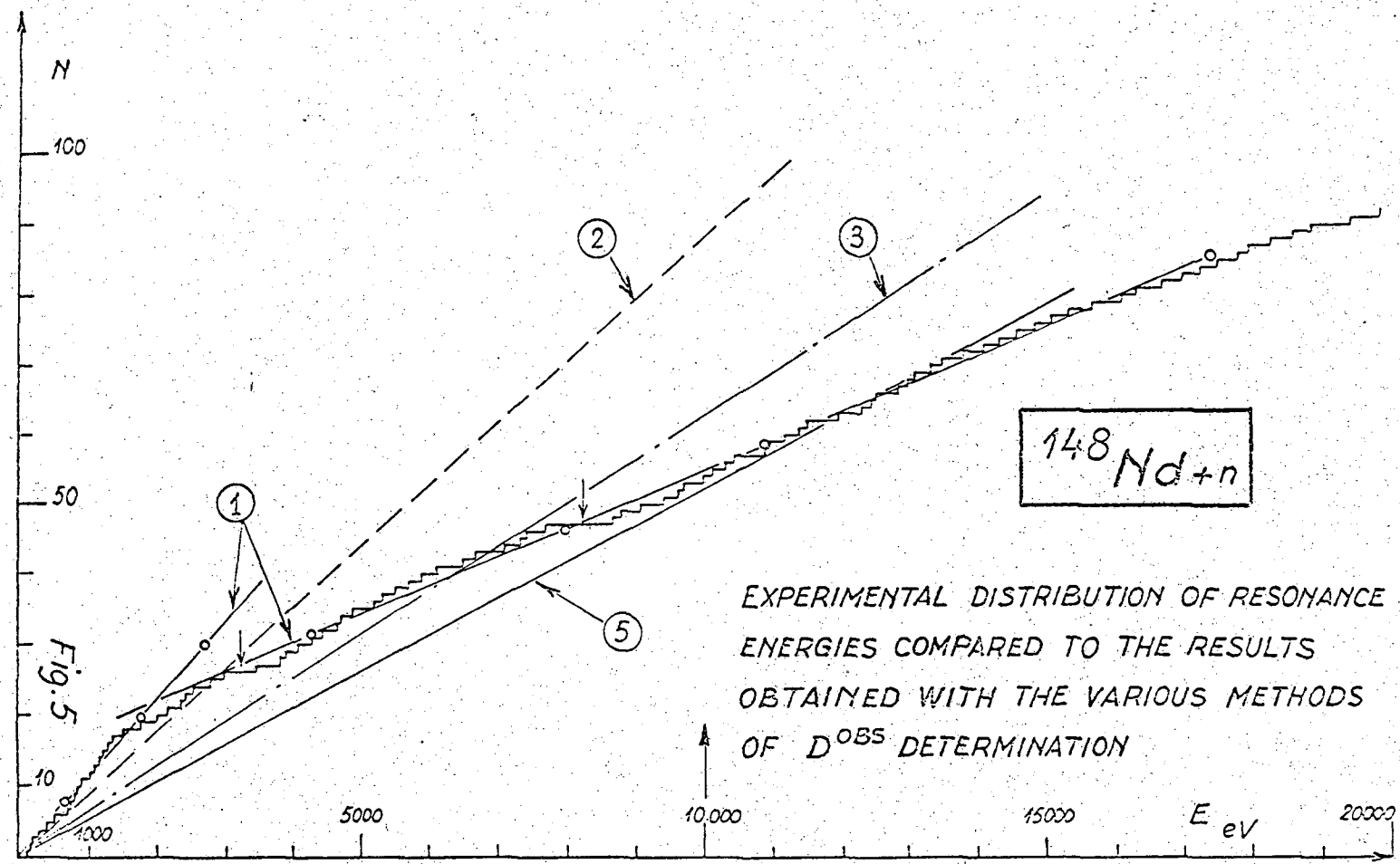


Fig. 5

EXPERIMENTAL DISTRIBUTION OF RESONANCE ENERGIES COMPARED TO THE RESULTS OBTAINED WITH THE VARIOUS METHODS OF $D^{OBS}$ DETERMINATION

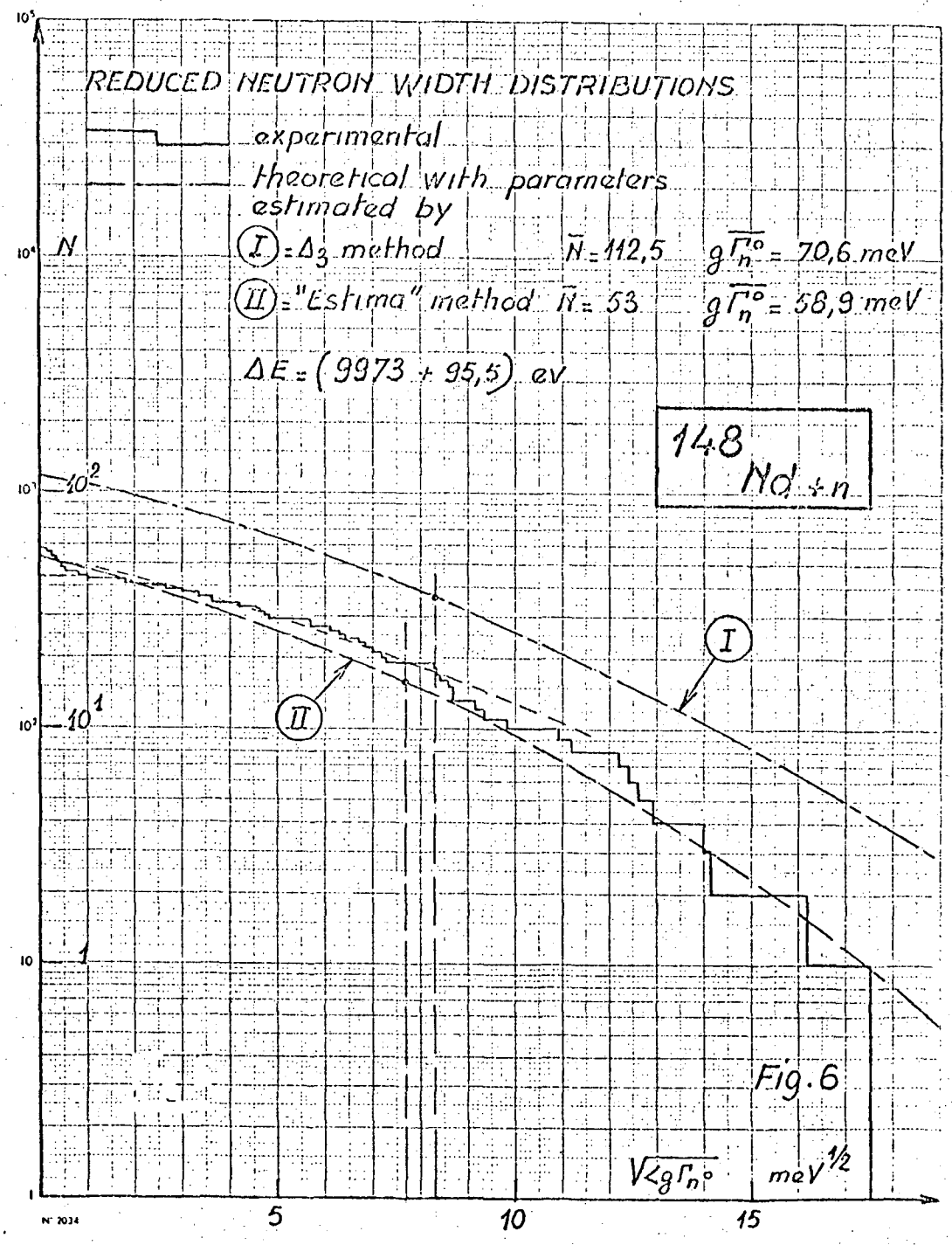
REDUCED NEUTRON WIDTH DISTRIBUTIONS
experimental
theoretical with parameters estimated by
(I) = Δ3 method
N̄ = 112,5
gΓn° = 70,6 meV
(II) = "Estima" method
N̄ = 53
gΓn° = 58,9 meV
ΔE = (9973 ± 95,5) ev
148 Nd + n
N
10²
10¹
1
(I)
(II)
√gΓn°
meV^1/2
5
10
15
N° 2034

Fig. 6

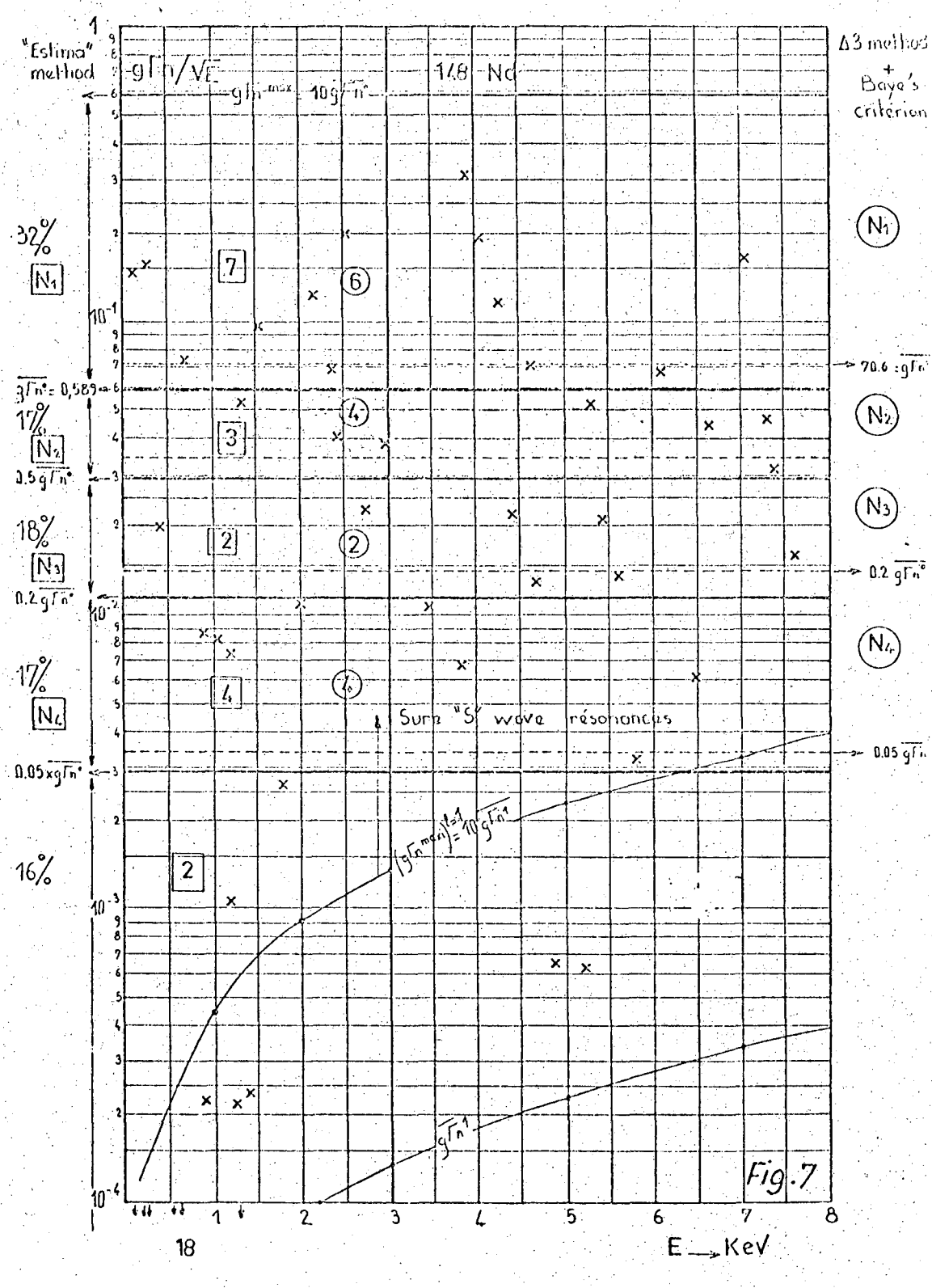
"Estima" method
$g\Gamma_n/\sqrt{E}$
$g\Gamma_n^{max} = 10\,g\Gamma_n^0$
148 Nd
Δ3 methods + Baye's criterion
32%
17%
18%
17%
16%
$N_1$
$N_2$
$N_3$
$N_4$
$\overline{g\Gamma_n^0} = 0,589$
$0.5\,\overline{g\Gamma_n^0}$
$0.2\,\overline{g\Gamma_n^0}$
$0.05\times\overline{g\Gamma_n^0}$
$70.6\,\overline{g\Gamma_n^0}$
$0.2\,\overline{g\Gamma_n^0}$
$0.05\,\overline{g\Gamma_n}$
Some "S" wave résonances
$(g\Gamma_n^{max})^{1/2} = 10\,\overline{g\Gamma_n^0}$
$\overline{g\Gamma_n^0}$
Fig.7
E → KeV

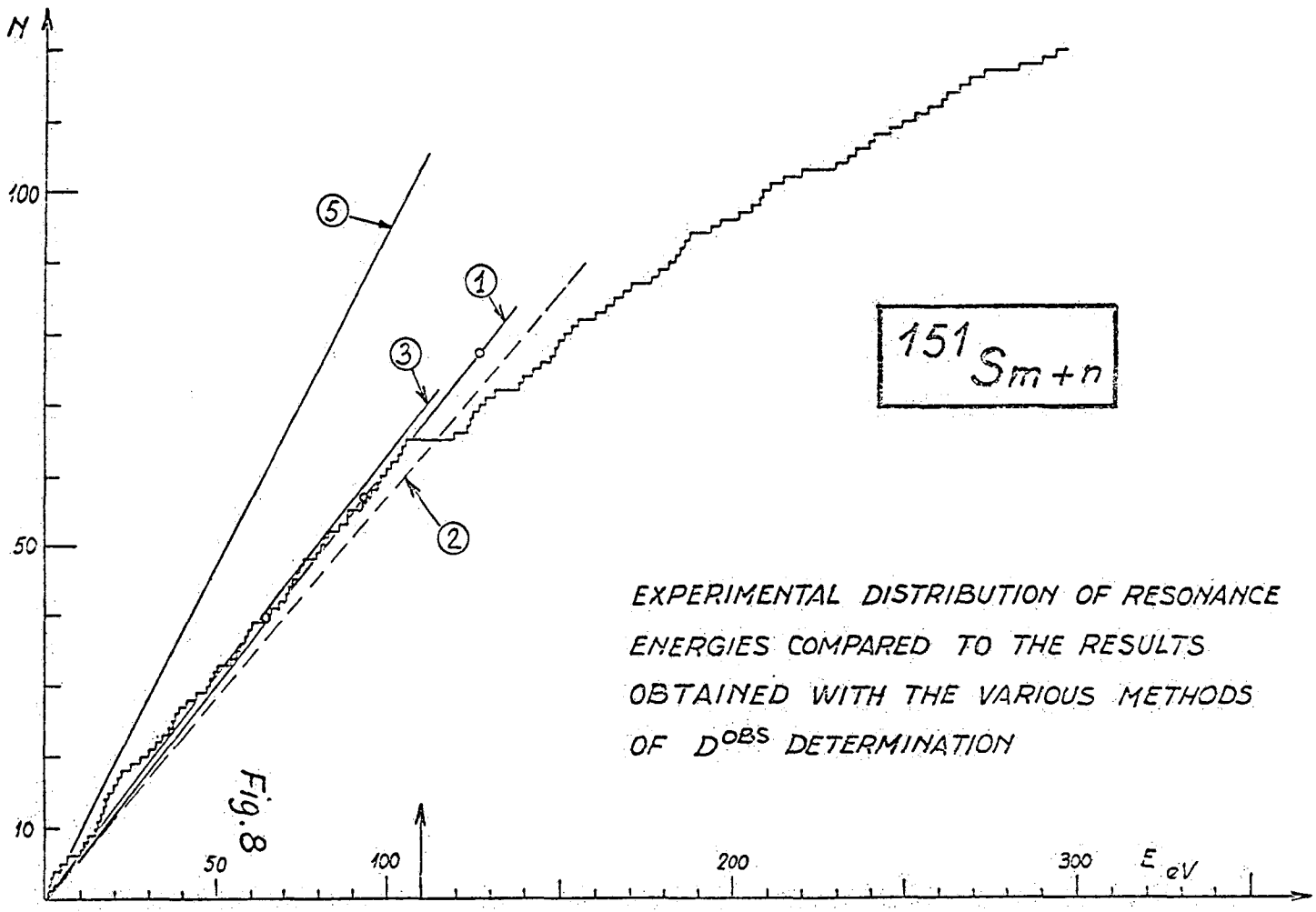


EXPERIMENTAL DISTRIBUTION OF RESONANCE ENERGIES COMPARED TO THE RESULTS OBTAINED WITH THE VARIOUS METHODS OF $D^{OBS}$ DETERMINATION

Fig. 8

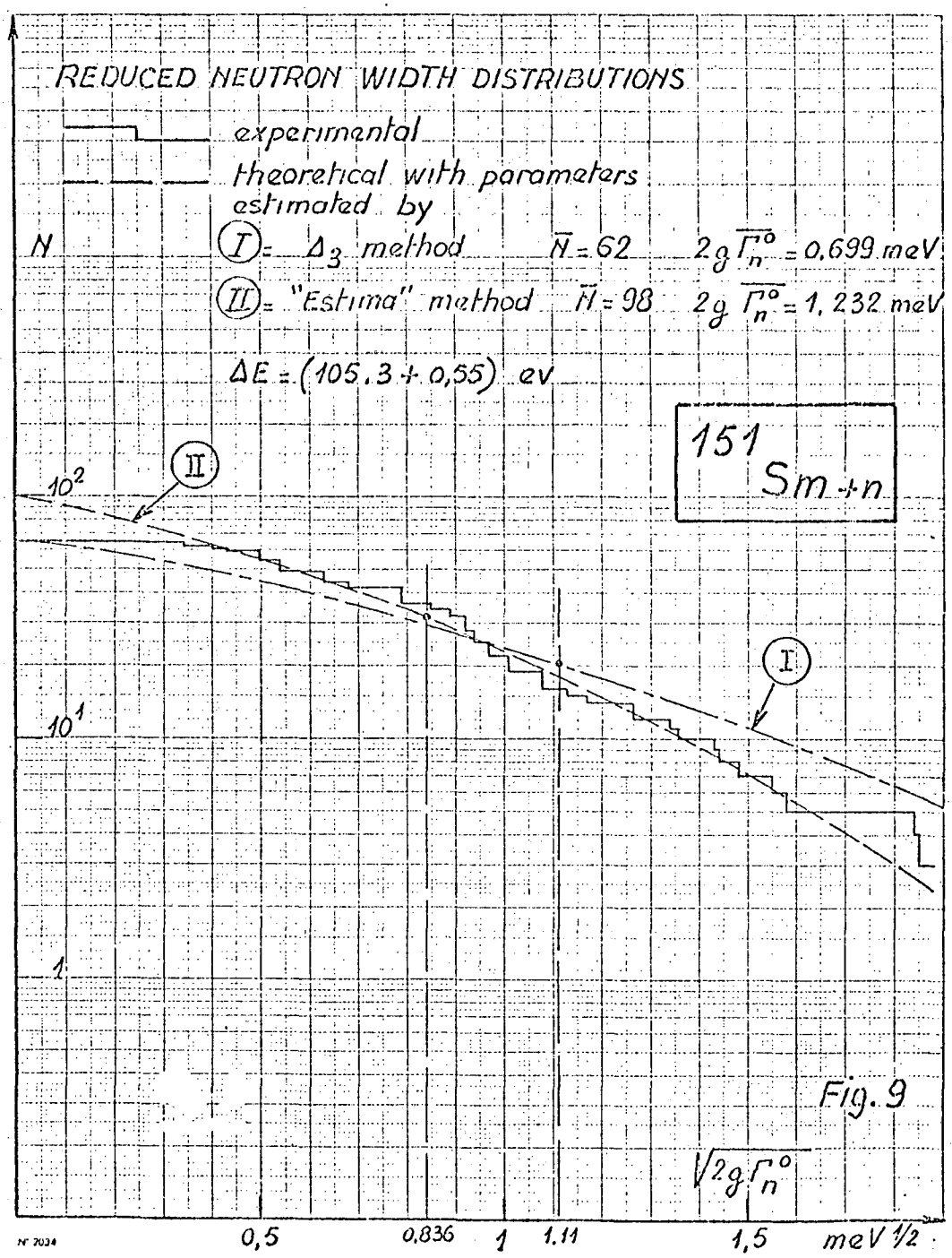
REDUCED NEUTRON WIDTH DISTRIBUTIONS
experimental
theoretical with parameters estimated by
I = Δ3 method N̄ = 62 2g Γn° = 0,699 meV
II = "Estima" method N̄ = 98 2g Γn° = 1,232 meV
ΔE = (105,3 ± 0,55) eV
151 Sm + n
N
10²
10¹
1
II
I
0,5
0,836
1
1,11
1,5
meV 1/2
√2gΓn°
Nº 7034

Fig. 9

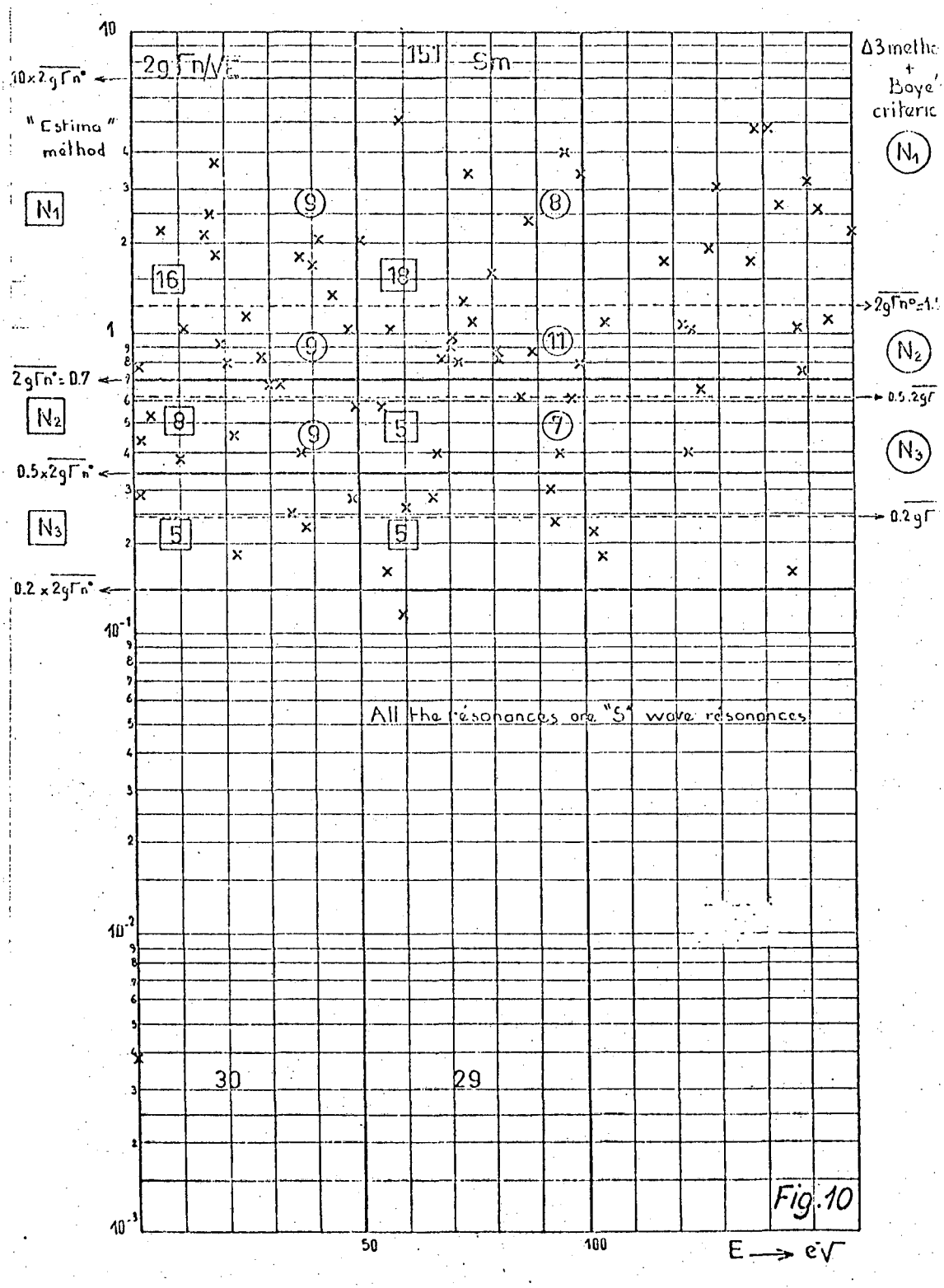
2gΓn/√E
151 Sm
10×2gΓn°
"Estima" méthod
N1
N2
N3
2gΓn° = 0.7
0.5×2gΓn°
0.2×2gΓn°
Δ3 methe + Boye' criteric
N1
N2
N3
2gΓn° = 1.
0.5.2gΓ
0.2gΓ
All the résonances are "S" wave résonances
30
29
E → eV

Fig.10

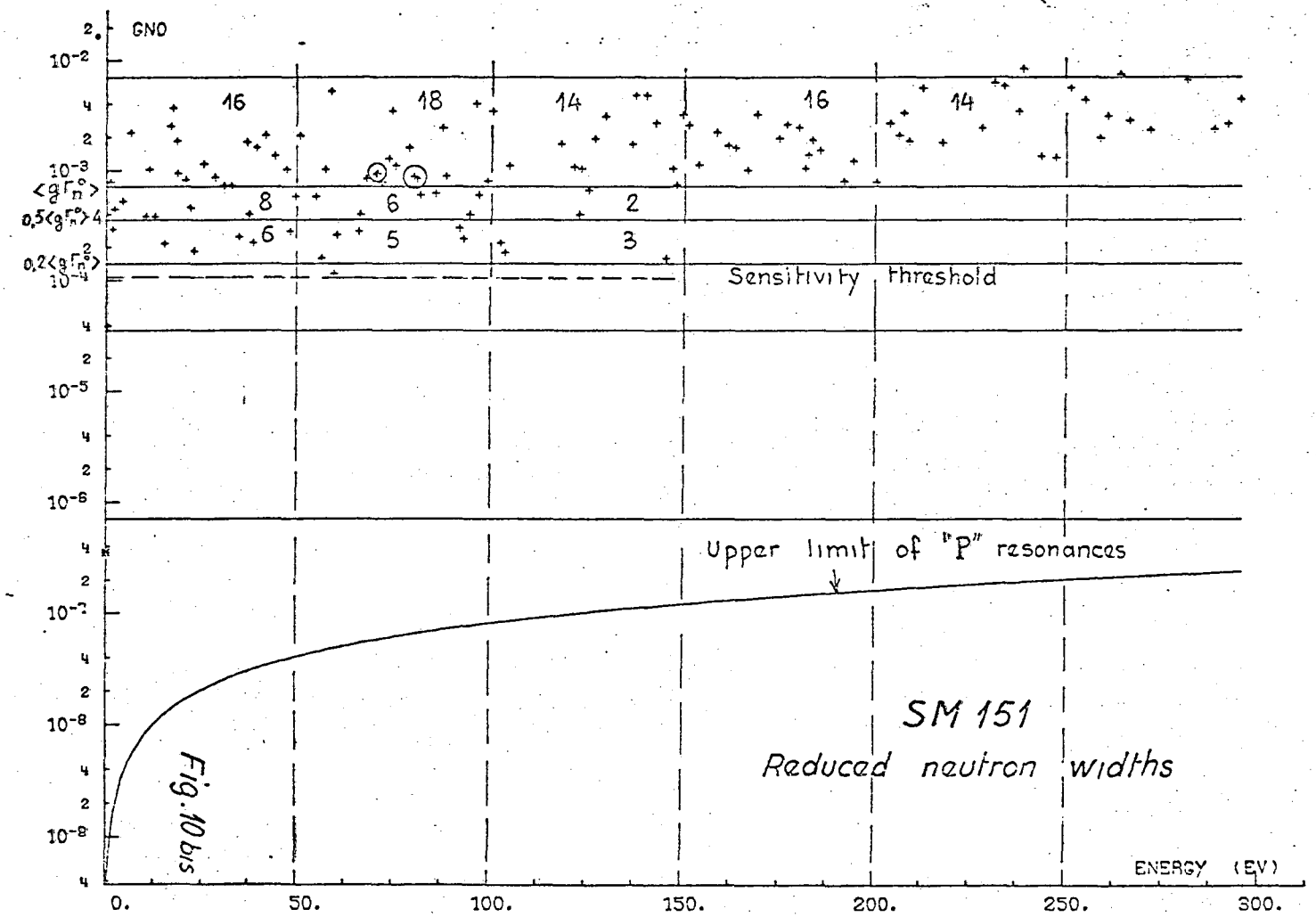
GNO
16
18
14
16
14
8
6
2
6
5
3
Sensitivity threshold
Upper limit of "P" resonances
SM 151
Reduced neutron widths
ENERGY (EV)
0.
50.
100.
150.
200.
250.
300.

Fig. 10 bis

$D^{obs}_{ev}$

| TARGET NUCLIDE | I | SCHMITROM 73 | JAERI 77 | ENDF/ BIV | RCN 76 | CNEN/ CEA 76 | RECOM-MENDED | ACCURACY % (1σ) |
|---|---|---|---|---|---|---|---|---|
| 94 Mo | | | | | 1740. | | | |
| 95 Mo | | 114. | 69.3 | 127 | 82. | 85 | 86 | 10 |
| 96 Mo | | 1387. | | | 1300 | | | |
| 97 Mo | | 77.5 | 72.3 | 66.5 | 68. | 65 | 47. | 15 |
| 98 Mo | | 1014 | | 1275. | 1000. | 730 | 910. | 15 |
| 100 Mo | | 1339 | | 1200. | 700. | 520. | 700. | 25 |
| 99 Tc | | | 16.2 | 14.2 | 18.6 | 18.6 | 17.6 | 6 |
| 101 Ru | | 18.3 | 13.8 | 14. | 16.7 | 16.7 | 16.7 | 15 |
| 102 Ru | | | 290.5 | 264. | 573 | 550. | 550. | 30 |
| 103 Ru | | | | 23. | | 7.5 | 7.5 | 50 |
| 104 Ru | | 285 | 588 | 784 | 265 | 270. | 300. | 25 |
| 103 Rh | | 27.4 | 26.1 | 20.3 | 26.1 | 26.4 | 26.4 | 5 |
| 102 Pd | | | | | 1130. | 880 | | |
| 104 Pd | | | | | 530. | 460 | | |
| 105 Pd | | 10.1 | 11.1 | 8.8 | 10. | 10.2 | 10.2 | 15 |
| 106 Pd | | | | 463 | 330. | 270 | | |
| 107 Pd | | | 10.0 | 10.4 | 4.2 | 5.5 | 5 | 50 |
| 108 Pd | | | | 290. | 200. | 200. | 200. | 40 |
| 110 Pd | | | | 900. | 146. | | | |
| 107 Ag | | 32.2 | | | 19. | | | |
| 109 Ag | | 19.5 | 12.7 | | 17.5 | 18. | 17.7 | 42.5 |
| 127 I | | 14.7 | | 14.7 | 12.2 | 15. | 13.7 | 3 |
| 129 I | | 26.1 | 21. | 26. | 30. | 30. | 30. | 25. |
| 131 Xe | | 39.2 | 33.2 | | | | | |
| 133 Cs | | 20.2 | 23.2 | | 20. | 23.4 | 23.4 | 4 |
| 135 Cs | | | 60.0 | 328. | | 82. | 70. | 50 |
| 137 Cs | | | 1100. | 1930. | | | | |
| 141 Pr | | | | | 120 | 132. | 132 | |
| 143 Nd | | 32.0 | 46.4 | | | 39. | 39 | 10 |
| 145 Nd | | 18.9 | 24.2 | | | 19. | 19. | 10 |
| 147 Sm | | 8.18 | 4.26 | | 6.3 | 7.4 | 7.2 | |
| 148 Sm | | | | | 107 | 114. | 110. | 20 |
| 149 Sm | | 2.88 | 1.63 | 1.7 | 2.0 | 1.97 | 1.9 | 10 |
| 150 Sm | | | | | 56.5 | 66 | 64 | |
| 151 Sm | | | 1.50 | | 1.72 | 1.05 | 1.05 | 10 |
| 152 Sm | | | | | 53.8 | | | |
| 153 Eu | | | 1.46 | 1.3 | | 1.05 | | |
| 155 Eu | | | 2.50 | .86 | | 0.92 | | |
| 139 La | | | | 262. | 286. | 270. | 270. | 10 |
| 147 Pm | | | 4.7 | 6.8 | | 4.7 | 5. | 15 |
| | | | | | | | | |
| | | | | | | | | |
| | | | | | | | | |

# Efficient Estimation of Strength Functions and Average Level Spacings from Resonance Parameters

F.H. Froehner

Kernforschungszentrum Karlsruhe
Institut für Neutronenphysik und Reaktortechnik
Postfach 3640, D-7500 Karlsruhe

Strength functions and mean level spacings for s-wave resonances are conventionally extracted from resonance parameters by comparison of the neutron width distribution above an artificial cut-off with the Porter-Thomas distribution, the cut-off ensuring that p-, d-, ... levels are excluded. It is more efficient and convenient, however, to estimate the natural cut-off, viz. the observability threshold and its energy dependence directly from the observed level density. This eliminates all arbitrariness connected with artificial thresholds and leads to general expressions for the likelihood function which contain the strength functions $S_0$, $S_1$,... and the mean spacing as parameters and otherwise depend only on the level energies and $g\Gamma_n$ values. Especially simple expressions are obtained for pure s-wave or p-wave samples. Estimation of confidence limits is difficult but the expressions for complete s-wave samples can serve as guideline. Results obtained with the code STARA illustrate the method.

## 1. Introduction

Level densities, average reduced widths and strength functions are usually extracted from resonance parameters with the maximum-likelihood method. It is easy to show |1| that, given a sample $\Gamma_1, \Gamma_2, \ldots \Gamma_N$ of reduced neutron widths from a Porter-Thomas distribution |2|

$$p(\Gamma)\, d\Gamma = \frac{e^{-x}}{\sqrt{\pi x}}\, dx \,, \qquad 0 < x \equiv \frac{\Gamma}{2\langle\Gamma\rangle} < \infty \,, \tag{1}$$

with unknown true average $\langle\Gamma\rangle$, the maximum likelihood estimator for $\langle\Gamma\rangle$ is simply the sample average,

$$\overline{\Gamma} = \frac{1}{N} \sum_{\lambda=1}^{N} \Gamma_\lambda \,. \tag{2}$$

In other words the choice $\langle\Gamma\rangle = \overline{\Gamma}$ maximises the likelihood that N observed widths have just the values $\Gamma_1, \Gamma_2, \ldots \Gamma_N$ (in small intervals $d\Gamma$). In the language of mathematical statistics $\overline{\Gamma}$ is a minimal sufficient statistic, i. e. a quantity that can be calculated from the sample, contains all information about $\langle\Gamma\rangle$ that the sample contains, and has the smallest variance of all possible estimators. It is an unbiased estimator because $\overline{\Gamma} \to \langle\Gamma\rangle$ for $N \to \infty$. Its frequency distribution is a $\chi^2$ distribution with N degrees of freedom,

$$p(\bar{\Gamma})\, d\bar{\Gamma} = \Gamma(N/2)^{-1} e^{-y} y^{N/2-1} dy\ , \quad 0 < y \equiv \frac{N\bar{\Gamma}}{2\langle\Gamma\rangle} < \infty\ , \tag{3}$$

where $\Gamma(N/2)$ is the gamma function. The 68% confidence interval following from Eq. 3 is (see |3|)

$$\frac{N/2}{y_+}\,\bar{\Gamma} < \langle\Gamma\rangle < \frac{N/2}{y_-}\,\bar{\Gamma} \tag{4}$$

with $y_+$ and $y_-$ defined |3| by

$$\Gamma(N/2)^{-1} \int_0^{y_-} e^{-y} y^{N/2-1} dy = \Gamma(N/2)^{-1} \int_{y_+}^{\infty} e^{-y} y^{N/2-1} dy$$

$$= \frac{1}{2}\,\mathrm{erfc}\,\frac{1}{\sqrt{2}}\ . \tag{5}$$

In practice things are not so simple. The smallest, but according to (1) most frequent, widths are invariably missing from experimental resonance data because of limited resolution, counting statistics etc. As a consequence the apparent level spacing distribution is usually distorted badly. The width distribution, on the other hand, is only affected at its lower end. It is therefore common practice to determine level densities $\rho$ not from the spacings but from the reduced-width distribution whose undistorted part yields $\langle\Gamma\rangle$ which in turn permits estimation of the number of missing levels and thus of $\rho$.

This approach works satisfactorily if the entire sample belongs to a single level sequence (same nuclide, same level spin J and parity $\Pi$). To the extent that the approximations (6) and (7) below are adequate it works also for mixed sequences as long as all of them belong to the same I=0 nuclide and orbital angular momentum (only s- or only p-wave levels), because then the Porter-Thomas distribution applies again to the $g\Gamma_n^{\ell}$ values (g: spin factor, $\Gamma_n^{\ell}$: reduced neutron width, $\ell$: orbital angular momentum quantum number). An example are the even-even fission products with nucleon numbers A around 140. Due to their low p- to s-wave strength function ratio and the small centrifugal-barrier penetrability $v_{\ell}$ for $\ell$=1 the width distribution is dominated by s-wave levels.

For light fission products with A $\sim$ 90 the ratio $S_1/S_0$ is nearly two orders of magnitude larger and observed samples are mixtures of s- and p-wave levels. The determination of $\ell$ is quite difficult especially for resonances with small neutron widths. Therefore methods were developped to estimate strength functions and level densities from mixed samples without $\ell$ assignment, e.g. by Weigmann et al. |4|, Rohr et al. |5| and, very carefully, by Coceva and Stefanon |6|. One uses artificial cut-offs to suppress small levels, e.g. p-wave levels or unobservable levels generated by Monte Carlo sampling. As will be seen below a considerable simplification results if not an artificial but the natural cut-off effected by the experimental observability threshold is used. The latter can be estimated directly from the observed (apparent) level density as a function of energy. This eliminates all arbitrariness in, and improves the efficiency of, the estimation procedure since no information is discarded.

## 2. Treatment of neutron width and level energy samples with unassigned spins and parities

The following derivations are based on the assumptions (a) that strength functions are the same for all reaction channels with a given $\ell$ regardless of J, i.e.

$$S_{\ell J} = S_\ell \,, \tag{6}$$

(b) that the level densities for given parity $\Pi$ but different J are related by

$$\rho_{J\Pi} = (2J+1)\rho_{0\Pi} \,. \tag{7}$$

For resonances with unassigned spin and parity one knows only $g\Gamma_n = g\Gamma_n^\ell v_\ell \sqrt{E/1\ \mathrm{eV}}$ but not $g\Gamma_n^\ell$ to which the Porter-Thomas distribution applies. With the abbreviations

$$G \equiv g\Gamma_n \sqrt{(1\ \mathrm{eV}/E)} \,, \qquad G_\ell \equiv \langle g\Gamma_n^\ell \rangle \tag{8) (9}$$

one can write the frequency distribution of G-values for a given $\ell$ which follows from the Porter-Thomas distribution with the approximations (6) and (7) for even-even nuclei in the form

$$p_\ell(G)\, dG = \frac{1}{\sqrt{2\pi G G_\ell v_\ell}} \exp\left(-\frac{G}{2G_\ell v_\ell}\right) , \quad 0 < G < \infty \,. \tag{10}$$

For $\ell=0$ this is just the Porter-Thomas distribution with $G = g\Gamma_n^0$ and with constant average $G_0 v_0 = \langle g\Gamma_n^0 \rangle$. For $\ell \geq 1$, however, the averages $G_\ell v_\ell$, proportional to the penetrabilities $v_\ell$, increase with growing energy. Therefore one must distinguish the G-distributions in the various infinitesimal energy ranges dE. The probability of a resonance with arbitrary $\ell$ to be found in dE at E, with a $g\Gamma_n$-value in dG at G, is given by the bivariate frequency distribution

$$p(G,E)\, dG\, dE = \frac{dE\, dG \sum_\ell \rho_\ell p_\ell}{\int dE \int dG \sum_\ell \rho_\ell p_\ell} \,, \tag{11}$$

where $p_\ell$ is the true density of all levels for a given $\ell$.

The normalising double integral covers the domain of observation. We consider resonances observed in the energy range $E_a < E < E_b$ and G-values above a given observability threshold $\eta(E)$, as indicated in Fig. 1. Performing the integration over G in the nominator one finds

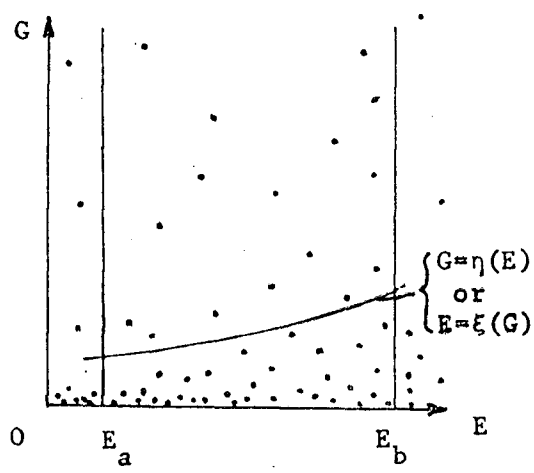


Fig. 1

$$\int_{E_a}^{E_b} dE \int_{\eta(E)}^{\infty} dG \sum_\ell \rho_\ell p_\ell$$

$$= \int_{E_a}^{E_b} dE \sum_\ell \rho_\ell \,\mathrm{erfc}\sqrt{\frac{\eta(E)}{2G_\ell v_\ell(E)}}$$

$$\equiv \int_{E_a}^{E_b} dE \sum_\ell \bar{\rho}_\ell(E) = \int_{E_a}^{E_b} dE\, \bar{\rho}(E) \equiv \bar{N} \,, \tag{12}$$

where $\bar{\rho}(E)$ is the apparent level density and $\bar{N}$ the expected number of levels observed. The complementary error function is the fraction of observable levels in dE.

One can reduce the number of parameters of the G-distribution (11) by exploiting the fact that the $\rho_{J\Pi}$ are interrelated by Eq. 7 or, more rigorously, by Bethe's prescription |7|

$$\rho_{J\Pi} \propto \exp\left(-\frac{J^2}{2\sigma^2}\right) - \exp\left(-\frac{(J+1)^2}{2\sigma^2}\right) , \tag{16}$$

so that the level density ratios $\zeta_\ell \equiv \rho_\ell/\rho_0$ can be calculated with good accuracy for any reasonable guess of the spin cut-off $\sigma$. Furthermore, the observability threshold $\eta(E)$ is implicitly given in terms of the expected observed level density $\bar{\rho}(E)$ and the unknown parameters $\rho_0$, $G_0$, $G_1$,... by the equation

$$\bar{\rho}(E) = \rho_0 \sum_\ell \zeta_\ell \operatorname{erfc}\sqrt{\frac{\eta(E)}{2G_\ell v_\ell(E)}} . \tag{17}$$

Equating $\bar{\rho}$ to the actually observed level density (as a function of energy) one is left with $\rho_0$, $\langle g\Gamma_n^0\rangle$, $\langle g\Gamma_n^1\rangle$,... as the only unknown parameters. Writing, for instance,

$$\bar{\rho}(E) = a_1 + a_2E + \ldots + a_mE^{m-1}, \tag{18}$$

and integrating over E one gets

$$\bar{n}(E) = \int_{E_a}^{E} dE'\bar{\rho}(E') = a_0 + a_1(E-E_a) + \ldots + \frac{a_m}{m}(E-E_a)^m . \tag{19}$$

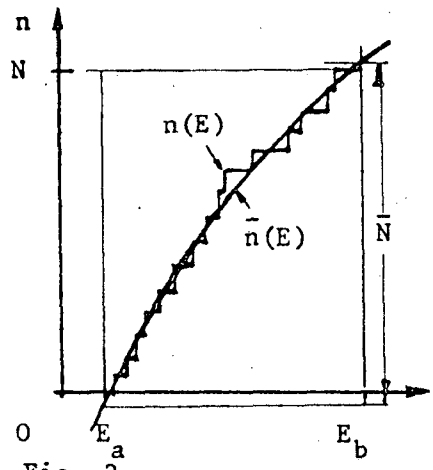

Fig. 2

The coefficients can be determined by a least-squares fit of this smooth function to the familiar staircase curve n(E), the number of observed levels vs. energy, as shown schematically in Fig. 2. Usually a parabolic fit is quite adequate as the examples given below will demonstrate.

The usual maximum-likelihood procedure demands a sampling domain that does not depend on the estimated parameters. The lower limit $\eta(E)$ of G-values, however, depends on these as Eq.17 shows. Therefore we integrate Eq. 11 over energies in order to obtain, using Eqs.12, the marginal distribution

$$p(G)\,dG = dG\,\frac{\rho_0}{\bar{N}} \sum_\ell \zeta_\ell \int_{E_a}^{E_L} dE\; p_\ell , \quad \eta(E_a) < G < \infty , \tag{20}$$

where

$$E_L \equiv \begin{cases} \xi(G) & \text{if } \eta(E_a) < G < \eta(E_b), \\ E_b & \text{otherwise.} \end{cases} \tag{21}$$

Here $\xi$ is the inverse function to $\eta$, i.e. the solution of the equation

$$\bar{\rho}(\xi) = \rho_0 \sum_\ell \zeta_\ell \operatorname{erfc}\sqrt{\frac{G}{2G_\ell v_\ell(\xi)}} \tag{22}$$

(see also Fig. 1). Furthermore it follows from Eq. 17 that

$$\bar{\rho}(E_a) > \rho_0 \sum_\ell \zeta_\ell \operatorname{erfc}\sqrt{\frac{G}{2G_\ell v_\ell(E_a)}} \quad \text{implies} \quad G > \eta(E_a) \ , \tag{23}$$

$$\bar{\rho}(E_b) \lesseqgtr \rho_0 \sum_\ell \zeta_\ell \operatorname{erfc}\sqrt{\frac{G}{2G_\ell v_\ell(E_b)}} \quad \text{implies} \quad G \lesseqgtr \eta(E_b) \tag{24}$$

and vice versa. With the last three relations we can eliminate $\eta$ and write the distribution of G-values in the final form

$$p(G)dG = dG \frac{\rho_0}{\bar{N}} \sum_\ell \zeta_\ell \int_{E_a}^{E_L} dE \ p_\ell \tag{25}$$

with

$$E_L = \begin{cases} \xi(G) & \text{if} \quad \rho_0 \sum_\ell \zeta_\ell \operatorname{erfc}\sqrt{\frac{G}{2G_\ell v_\ell(E_b)}} > \bar{\rho}(E_b) \ , \\ E_b & \text{otherwise} \ , \end{cases} \tag{26}$$

$\xi$ being the solution of Eq. 22 and $\bar{N}$ the expected number of levels observed in the interval $E_a \ldots E_b$ as defined in Eqs. 12. Now everything is expressed in terms of G, the known quantities $\bar{\rho}$, $\zeta_0$, $\zeta_1, \ldots$ and the unknown level-statistical parameters $\rho_0$, $G_0 = \langle g\Gamma_n^0 \rangle$, $G_1 = \langle g\Gamma_n^1 \rangle, \ldots$ It should be noted that $\eta(E)$ was assumed to increase monotonically with E which is the usual behaviour. Furthermore we neglected all properties of level sequences other than the existence of a more or less well defined level density which was assumed to be practically constant in the energy range $E_a \ldots E_b$. In particular we neglected level repulsion, spacing correlations and similar features which depend on the exact relative position of levels. In view of the statistical treatment itself and the "crystalline" regularity of nuclear level sequences |8| this appears reasonable. Finally it should be mentioned that we also neglected the possibility that levels are missing although their G-value exceeds the observability threshold, for instance due to unresolved doublets. This latter limitation cannot be overcome with such a fairly simple analytical approach but requires Monte Carlo cross section generation as employed e.g. by Derrien and Lucas |9|.

One can now find the most likely set of level-statistical parameters by maximisation of the likelihood function

$$L = \prod_{i=1}^{N} p(G_i) \ . \tag{27}$$

Inserting Eq. 25 along with Eqs. 26 and 22 and forming the derivatives

$$\frac{\partial L}{\partial \rho_0} = 0 \ , \quad \frac{\partial L}{\partial G_0} = 0 \ , \quad \frac{\partial L}{\partial G_1} = 0 \ , \ \ldots \tag{28}$$

one gets, however, very complicated expressions so that it seems best to use a numerical algorithm with stepwise parameter variation to find the maximum of L. Only in the case of pure s- or p-wave samples are the derivatives simple enough to be useful.

## 3. Specialisation to pure s- or p-wave samples

Retaining only the s-wave term in Eq. 25 one gets from Eqs. 27 and 28 with the abbreviations

$$x_i \equiv \frac{G_i}{2G_0} = \frac{(g\Gamma_n^0)_i}{2\langle g\Gamma_n^0\rangle}, \qquad \xi_i \equiv \xi(G_i) \qquad (29) \quad (30)$$

the two equations

$$\frac{1}{\rho_0} = -\frac{1}{N}\sum_i{}' \frac{\operatorname{erfc}\sqrt{x_i}}{(\xi_i - E_a)\bar{\rho}'(\xi_i)}, \qquad (31)$$

$$\bar{G} = G_0\left[1 - \frac{2\rho_0}{\sqrt{\pi}N}\sum_i{}' \frac{e^{-x_i}\sqrt{x_i}}{(\xi_i - E_a)\bar{\rho}'(\xi_i)}\right], \qquad (32)$$

where $\bar{G}$ denotes the sample average and the primed sums include only terms from the distorted part of the Porter-Thomas distribution where $G_i < n(E_b)$ or $\bar{\rho}(E_b) < \rho_0 \operatorname{erfc}\sqrt{(G_i/(2G_0))}$. With a parabolic fit to the level number staircase curve, i.e. with $\bar{\rho}(E) = a_1 + a_2E$, $\bar{\rho}'(E) = a_2$, one finds (cf. Eqs. 17 and 18)

$$1 = \frac{1}{N}\sum_i{}' \frac{\operatorname{erfc}\sqrt{x_i}}{\bar{\rho}(E_a)/\rho_0 - \operatorname{erfc}\sqrt{x_i}} \qquad (33)$$

$$\overline{g\Gamma_n^0} = \langle g\Gamma_n^0\rangle\left[1 + \frac{1}{N}\sum_i{}' \frac{2}{\sqrt{\pi}} \frac{e^{-x_i}\sqrt{x_i}}{\bar{\rho}(E_a)/\rho_0 - \operatorname{erfc}\sqrt{x_i}}\right] \qquad (34)$$

a result already given in |3|. It can also be used for pure p-, d-,...wave samples from even-even target nuclei if the super- and subscripts 0 are replaced by 1, 2,... These two equations are employed in the statistical resonance analysis code STARA.

## 4. The STARA code - results and limitations

The FORTRAN code STARA solves Eqs. 33, 34 by iteration, starting from the initial values $\rho_\ell = N/(E_b - E_a)$ and $\langle g\Gamma_n^\ell\rangle = \overline{g\Gamma_n^\ell}$ after determining $\bar{\rho}(E)$ by a parabolic fit to the level number staircase curve. The strength function is then calculated as $S_\ell = \langle g\Gamma_n^\ell\rangle\rho_\ell/(2\ell+1)$.

Confidence intervals are estimated as follows: Statistical fluctuations of $\overline{g\Gamma_n^\ell}$ are mainly due to the strongest levels which are practically unaffected by the observability threshold. Hence the effects of their final number can be estimated in close analogy to the case of no missing levels. The prescription adopted is essentially that of Eqs. 4 and 5 with N being interpreted as the number of observed levels rather than the true number. The effect of experimental uncertainties of the individual $G_i$ is taken into account by an extension of the lower and upper confidence limits by factors of $1-\delta G/G$ and $1 + \delta G/G$, respectively, where $\delta G$ is the uncertainty of the sample average caused by the individual errors $\delta G_i$ of the $G_i$. The uncertainty of $\rho_0$ is estimated by adding the squared error contributions from (i) the uncertainty of the number of missing levels, taken essentially as the square root of this number, (ii) orthogonal-ensemble statistics |8|, (iii) uncertainties from the parabolic fit to the level number staircase curve. Apart from (iii) this is the prescription of Ref. 6.

Graphical output consists of five plots which are shown in Figs. 3 and 4 for the s-wave resonances of $^{238}$U+n below 4 keV as evaluated by Keyworth and Moore |10|. The first plot shows the distorted integral distribution

as observed and as calculated in each step of the iteration process.(Since for the almost complete sample of $^{238}U$ resonances already the first iteration is quite close to the final result we show in Fig. 5 the curves for $^{131}Xe+n$ where the convergence to the final curve is clearly visible). A second plot shows the observed distribution together with the undistorted integral Porter-Thomas distributions corresponding to the final result and the lower and upper confidence limits. The third plot is the observed level strength staircase diagram with the straight lines corresponding to the estimated strength function and its confidence limits. A fourth plot shows the observed level number staircase curve together with the parabolic fit and with the three straight lines corresponding to the final estimate of the level density (or level spacing) and its confidence limits. The last plot shows the distribution of reduced widths and level energies in the E-u plane where $u \equiv \mathrm{erfc}\sqrt{\Gamma_n^0/\langle 2\Gamma^0\rangle}$ . In terms of u the Porter-Thomas distribution assumes the form $p(\Gamma_n^0)d\Gamma_n^0 = -du$ which shows that the u-values should be uniformly distributed between 0 and 1 for complete samples, and between 0 and $\mathrm{erfc}\sqrt{n/\langle 2\Gamma_n^0\rangle} = \bar{\rho}/\rho_0$ for a finite observability threshold causing levels to be missed. In the parabolic approximation for $\bar{n}(E)$ the function $\bar{\rho}(E)/\rho_0$ appears as a straight line in this kind of plot, below which the points representing the observed resonances should be uniformly distributed. The fifth plot thus provides a check on the correct estimation of the observability threshold and the fraction of missed levels per energy increment and also on the consistency of the average reduced width with the Porter-Thomas hypothesis. The results obtained for $^{238}U$ with the STARA code are given in Table 1 together with those found by Keyworth and Moore with a simpler estimation procedure described in |10|.

Table 1 - Level-statistical parameters for $^{238}U+n$

| | $D_0 = 1/\rho_0$ (eV) | $S_0$ ($10^{-4}$) | $D_1 = 1/\rho_1$ (eV) | $S_1$ ($10^{-4}$) |
|---|---|---|---|---|
| | Range: 0 - 4 keV | | Range: 0 - 1.5 keV | |
| STARA results | 20.4 ± 0.3 | $1.16^{+0.14}_{-0.11}$ | 7.8 ± 0.4 | $1.86^{+0.26}_{-0.20}$ |
| Keyworth + Moore | 20.9 ± 1.5 | 1.134±0.10 | 7.25± 0.52 | 1.70±0.51 |

Further examples for fission products, calculated with "barn book" parameters |11|, are shown in Figs. 6-8. The light fission product $^{97}Mo$ provides an example for the limitations of the STARA code. Since the sample is a mixture of s- and p-wave levels the G-distribution cannot be represented by a single (distorted) Porter-Thomas distribution (Fig. 6a) and the points in the E-u diagram are not uniformly distributed but show an excess of weak (p-wave) levels near the observability threshold (Fig. 7). The other fission products belong to the heavy group where the observed levels are practically all s-wave resonances. Correspondingly the plots look quite satisfactory. The level-statistical parameters estimated for these and a few more heavy fission products are listed in Table 2. Further STARA results - on structural materials - were presented in |12|.

Table 2 - Statistical s-wave parameters obtained with the STARA code for some heavy fission products. Resonance parameters were taken from BNL 325 |11| .

| Target Nucleus | Energy Range (eV) | No. of observed levels | $D_0 = 1/\rho_0$ (eV) STARA | $S_0$ ($10^{-4}$) STARA | BNL 325 |
|---|---|---|---|---|---|
| $^{131}Xe$ | 0 - 2600 | 37 | 48 ± 4 | $0.90^{+0.29}_{-0.18}$ | - |
| $^{143}Nd$ | 0 - 2500 | 58 | 36 ± 2 | $3.9^{+1.0}_{-0.7}$ | 3.1 ± 0.5 |
| $^{145}Nd$ | 0 - 4650 | 191 | 17.1 ± 0.6 | $4.1^{+0.5}_{-0.4}$ | 4.2 ± 0.5 |
| $^{147}Pm$ | 0 - 325 | 38 | 5.8 ± 0.5 | $3.3^{+1.2}_{-0.7}$ | 3.1 ± 0.5 |
| $^{149}Sm$ | 0 - 250 | 87 | 2.0 ± 0.1 | $4.8^{+1.3}_{-0.9}$ | 5.1 ± 0.9 |
| $^{151}Sm$ | 0 - 14 | 10 | 0.56 ± 0.14 | $4.3^{+3.2}_{-1.3}$ | 4.0 ± 1.8 |
| $^{153}Eu$ | 0 - 98 | 76 | 1.16 ± 0.05 | $2.4^{+0.5}_{-0.4}$ | 2.5 ± 0.2 |

## 5. Conclusions

Concise expressions for the observable distribution of $g\Gamma_n$-values for spin- and parity-mixed resonance samples are presented (Eqs. 25, 26) which can be used for numerical maximum-likelihood estimation of the level-statistical parameters $\rho_0 = 1/D_0$, $\langle g\Gamma_n^0\rangle$, $\langle g\Gamma_n^1\rangle$,... The input consists only of $g\Gamma_n$-values and level energies. The observability threshold is automatically estimated from the latter. Apart from being very convenient this procedure avoids a certain arbitrariness and loss of efficiency encountered with artificial thresholds. A simple version of the formalism (for unique $\ell$) is implemented in the code STARA, incorporation of the more general formalism is planned.

## Acknowledgements

Valuable discussions with M. Stefanon, G. Reffo and E. Menapace and a communication from H. Gruppelaar are gratefully acknowledged.

## References

/1/ D.D. Slavinskas and T.J. Kennett, Nucl. Phys. 85 (1966) 641

/2/ C.E. Porter and R.G. Thomas, Phys. Rev. 104 (1956) 483

/3/ F.H. Fröhner, Report KFK 2669 (1978)

/4/ H. Weigmann, G. Rohr and J. Winter, Neutron Cross Sections and Technology, Knoxville 1971 (CONF-710301), Vol.2 p. 749

/5/ G. Rohr and L. Maisano, contribution to these proceedings

/6/ C. Coceva and M. Stefanon, Nucl. Phys. A315 (1979) 1

/7/ H.A. Bethe, Rev. Mod. Phys. 9 (1937) 69

/8/ F.E. Dyson and M.L. Mehta, J. Math. Phys. 4 (1963) 701

/9/ H. Derrien and B. Lucas, Nucl. Cross Sections and Technology, Washington 1975 (NBS SP 425) vol.2, p. 637

/10/G.A. Keyworth and M.S. Moore, Neutron Physics and Nuclear Data, Harwell 1978, p.241

/11/S.F. Mughabghab and D.I. Schenter, BNL 325, 3rd ed. (1973)

/12/F.H. Fröhner, Report KFK 2889 (1980)

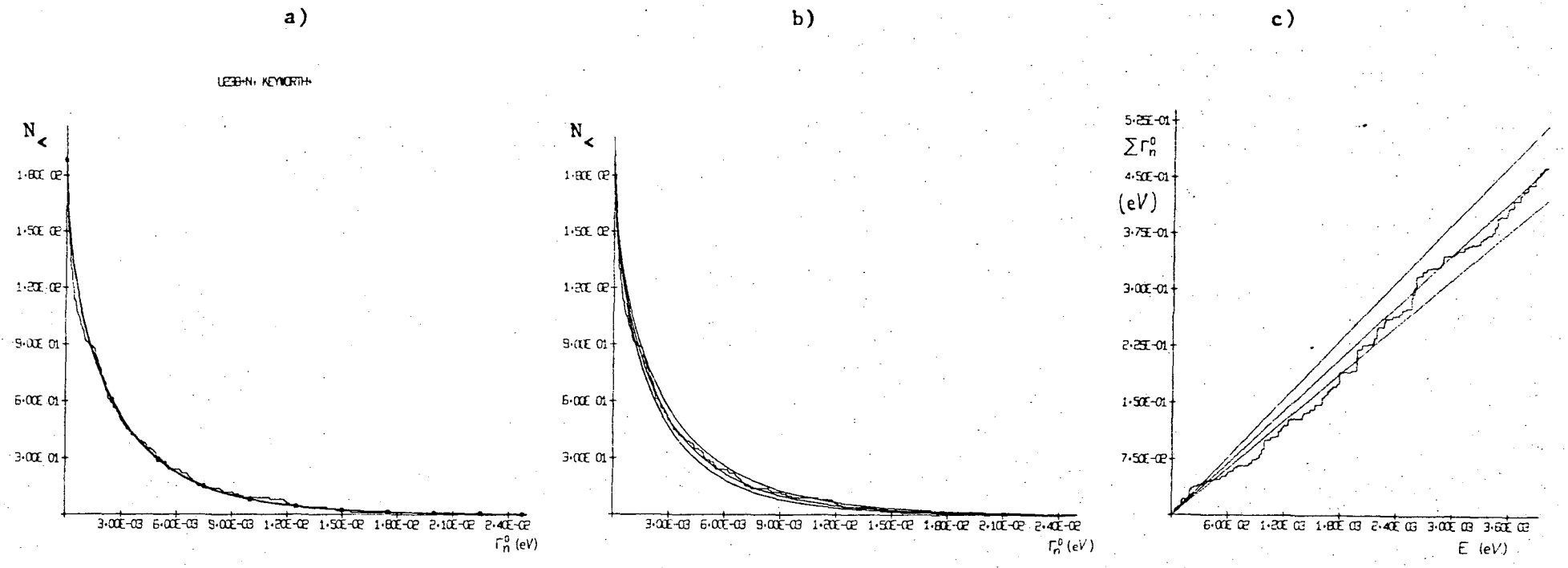


Fig. 3 - Example (s-wave levels of $^{238}$U+n below 4 keV, |10|) of graphical STARA output, first three plots:
a) experimental (histogram) and calculated (smooth) distribution of observed reduced widths,
b) observed reduced-width distribution (histogram) and undistorted (smooth) integral Porter-Thomas distributions calculated from best estimate of $\langle\Gamma_n^0\rangle$ and from its confidence limits,
c) experimental level strength staircase curve and straight lines corresponding to best estimate of $S_0$ and its confidence limits.

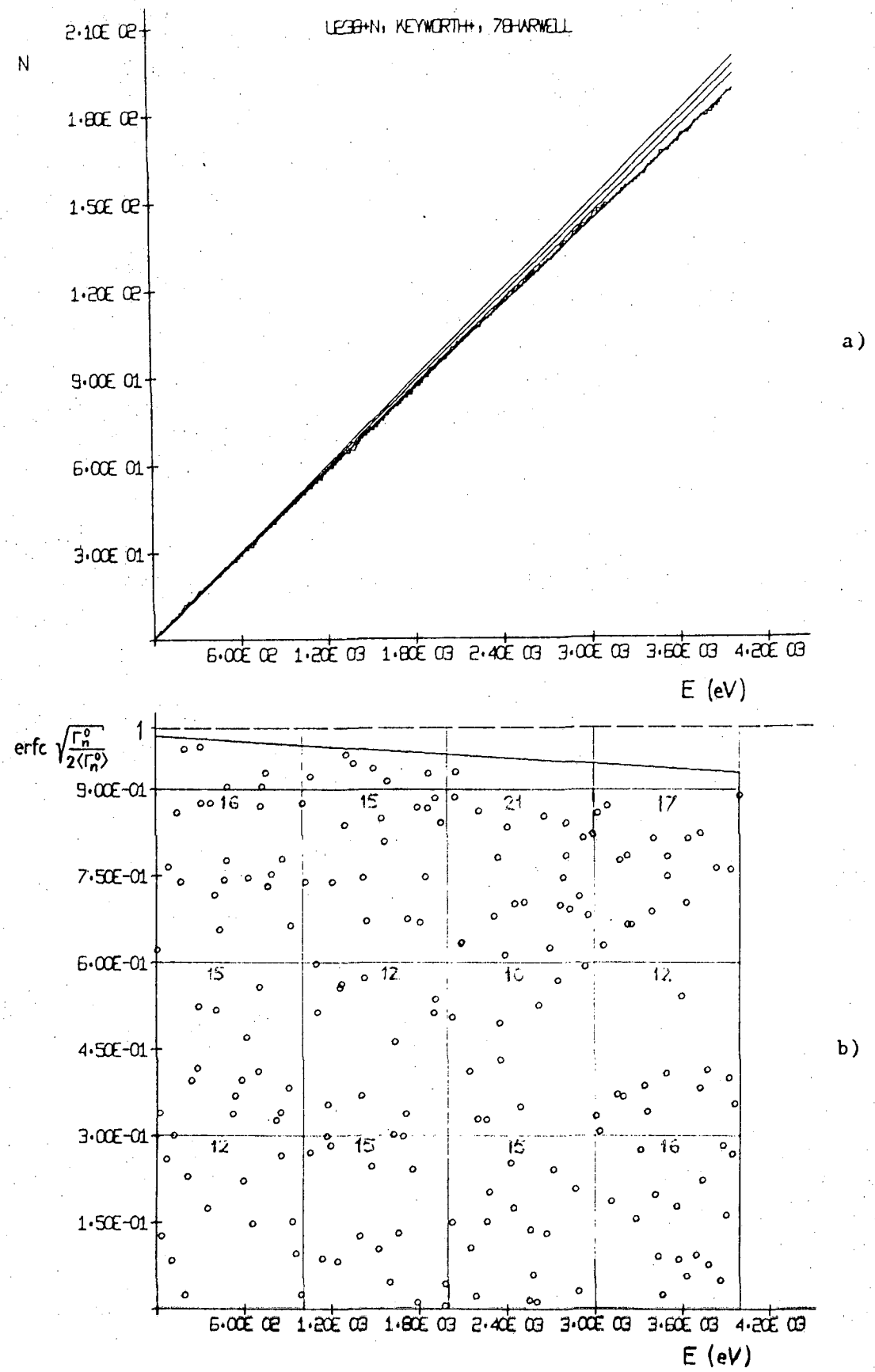


Fig. 4 - Example of graphical STARA output (continuation of Fig. 3), last two plots: a) level number staircase curve with parabolic fit and straight lines corresponding to best estimate of $\rho_0$ and its confidence limits, b) plot showing uniform distribution of levels in the E-u plane (see text) and estimated observability threshold. The figures in the equal rectangles give the number of levels, the theoretical estimate is 14.7±3.8.

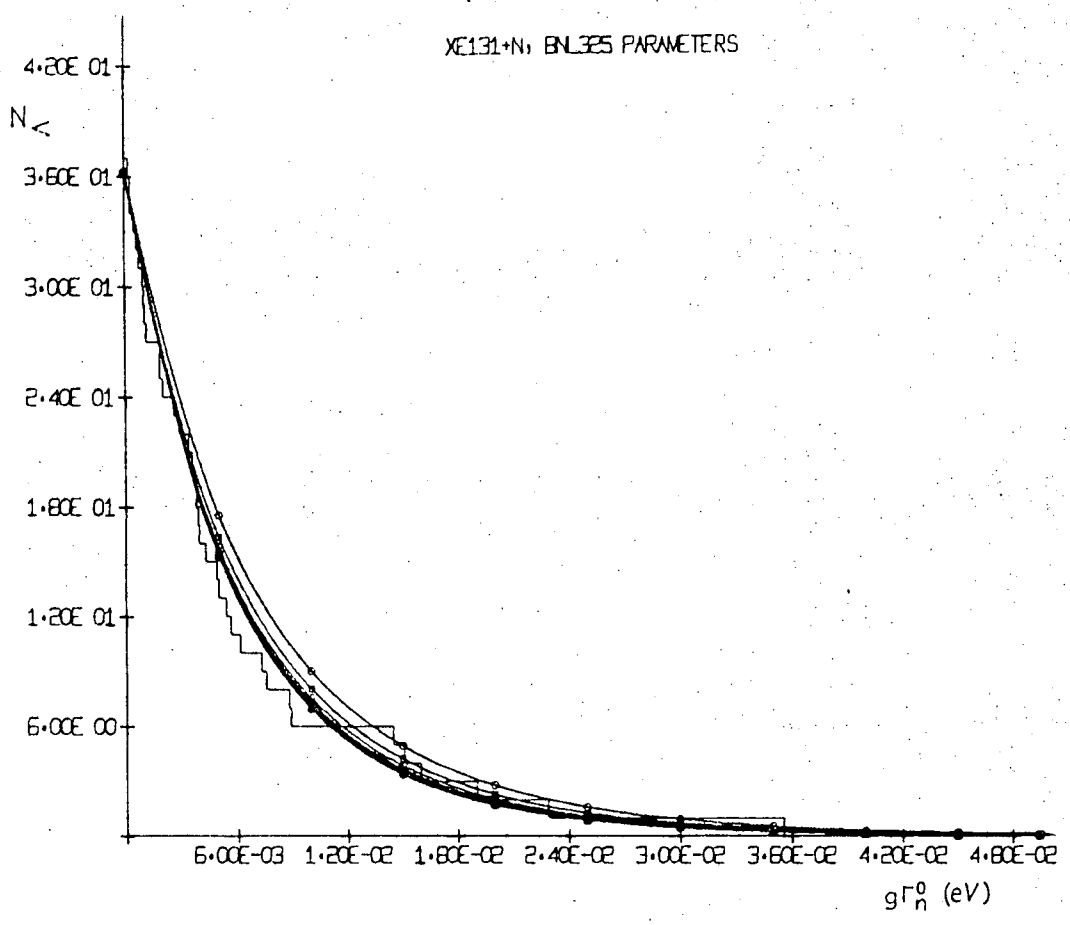


Fig. 5 - First plot of graphical STARA output for $^{131}$Xe+n showing integral reduced-width distributions as observed (histogram) and calculated (smooth curves) in each step of the iterative solution of the maximum-likelihood equations (33) and (34).

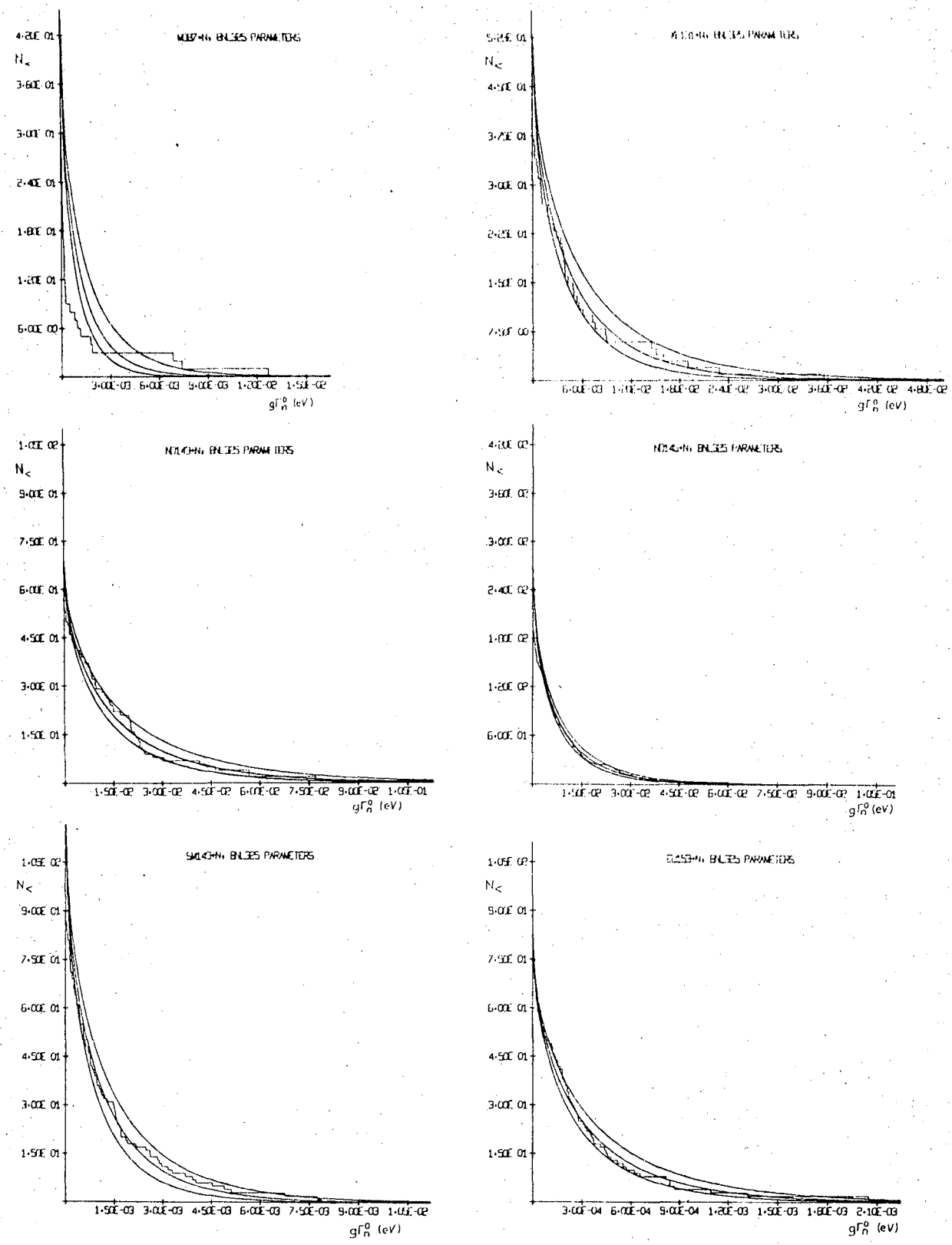


Fig. 6 - Second plots of graphical STARA output showing integral width distributions for six fission products. Note discrepancy between observation and calculation for $^{97}$Mo+n (upper left) due to mixed sample of s- and p-wave resonances.

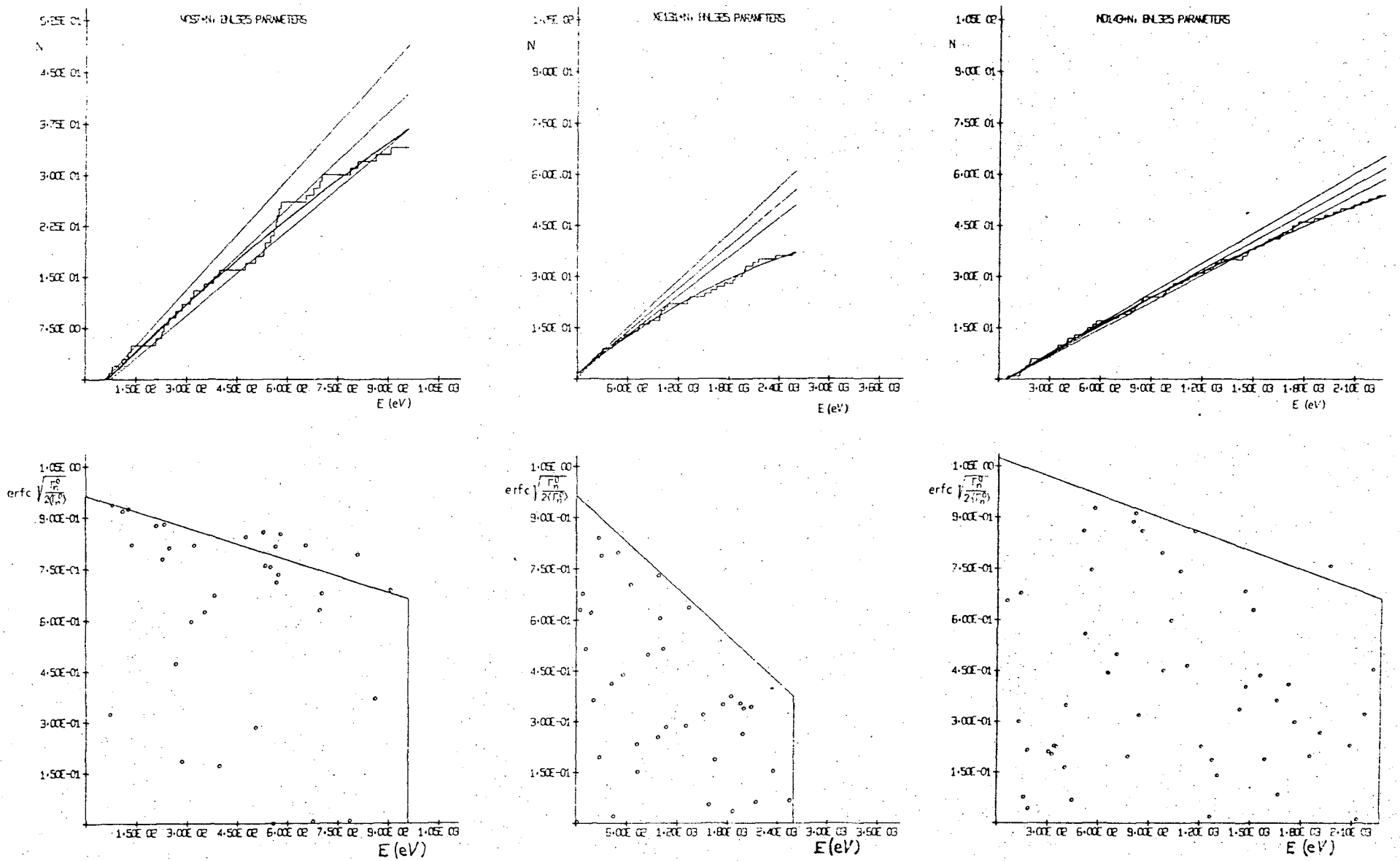


Fig. 7 - Last two plots of graphical STARA output for fission products. Note how well the parabolic fit to the level number staircase curves works. $^{97}$Mo+n with its mixture of s- and p-wave levels is again not tractable with STARA. In the lower plot its levels are unevenly distributed showing an excess of (p-wave) levels near the observability threshold.

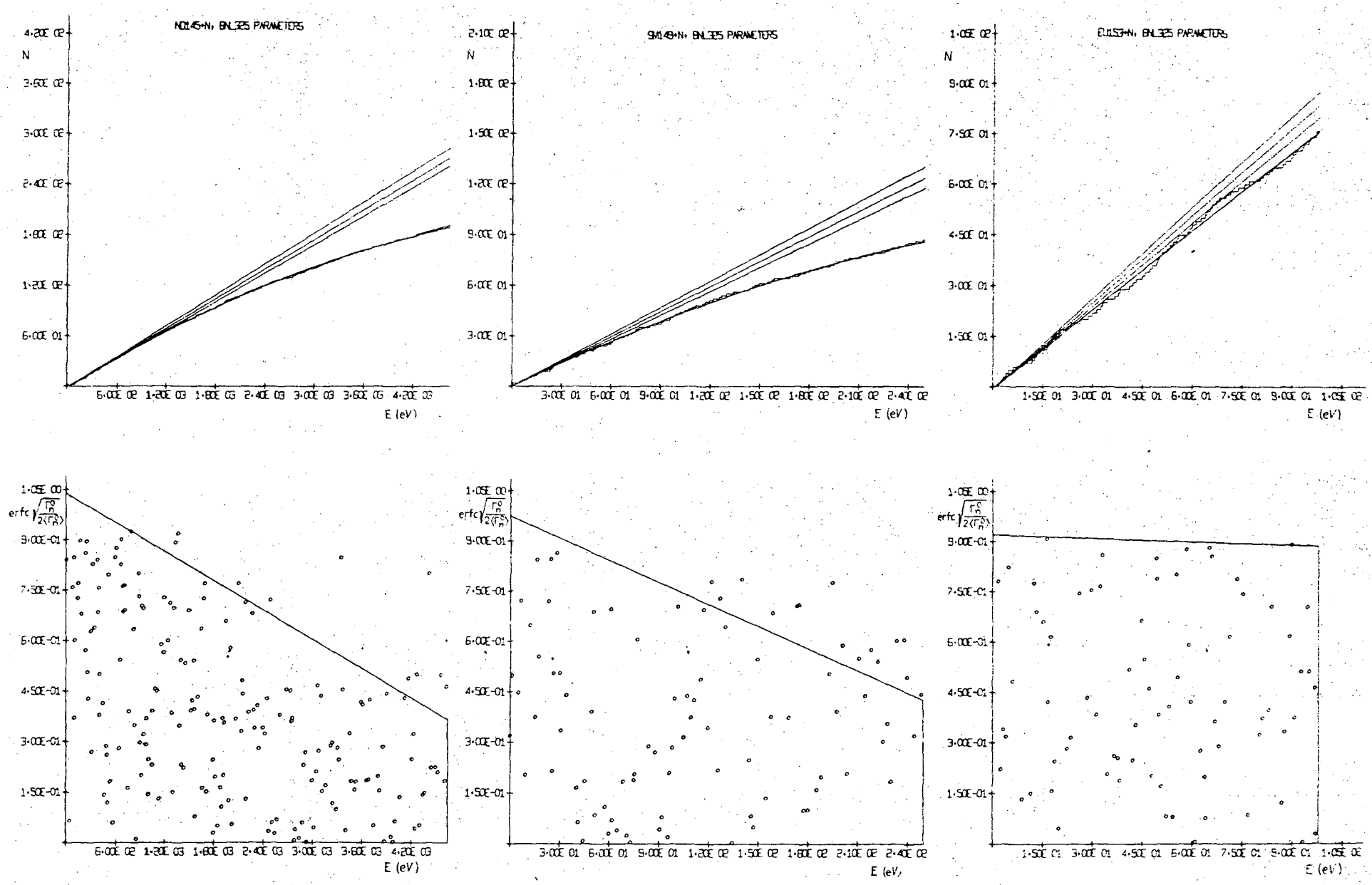


Fig. 8 - Last two plots of graphical STARA output for fission products. Note how well the parabolic fit to the level number staircase curves works. In all cases the assumption of practically pure s-wave samples is consistent with the STARA results.

# STATISTICAL ANALYSIS OF NEUTRON RESONANCE PARAMETERS

M. Stefanon
CNEN,Centro Studi e Ricerche "E.Clementel",Via Mazzini 2
40138 Bologna (Italy)

Abstract

A study is made of the problem of obtaining unbiased physical information from a statistical analysis of experimental sequences of neutron resonance parameters. It is shown that in particular conditions efficient analysis is possible which leads to simultaneous estimate of level density and of average s-wave and p-wave reduced neutron widths.

In many cases however, experimental uncertainties may severely limit the reliability of a statistical analysis.

## 1. Introduction

Statistical inference (both model testing and point estimation) involves peculiar complications in the case of measurements of resolved neutron resonances. This kind of experiment is, in fact, characterized by two different statistical aspects, one arising from the usually assumed theoretical scheme according to which resonances are considered to be sampled from a given population of statistical quantum states, and one coming from uncertainties in the measurement procedures. It is a difficult mathematical problem to combine the effects of these two statistical aspects and, furthermore, one has only a rough qualitative knowledge of the main sources of experimental uncertainties. The use of data whose statistical properties greatly depend on the detailed statistical features of experimental uncertainties should then be avoided as highly unreliable. In many cases a possible approach is that of using only a reduced set of data (or information) which can be reasonably considered as independent of the detailed distribution of errors. This idea was developed in the analysis of resonance capture gamma-rays /1/ and finds also a natural application in the case of statistical analysis of the parameters of well--resolved neutron resonances. The more favourable conditions in this case are usually met in high-resolution low-energy neutron-capture or total-cross-section measurements with even-even target nuclei where the probability of finding close doublets is low and one can often assume that there exist a threshold $\eta(E)$, for the $g\Gamma_n$ values, above which all resonances are observed, and $g\Gamma_n$ is sufficiently well measured.

A method of analysis which takes this threshold function into account and is based only on resonances for which $g\Gamma_n > \eta(E)$, is in principle able to avoid the biases induced by the uncertain statistical mechanism which governs the observability and the measurement of "weak" resonances. This was accomplished (ref. 2,3,4) by means of a Montecarlo simulation of experimental sets of parameters and a Maximum Likelihood estimation procedure including both s-and p-wave resonances. In the following we describe this method as far as the estimate of average spacing and reduced s-and p-wave neutron widths is concerned, with a few comments about the problem of guessing the "observability" threshold $\eta(E)$ only from the given parameter set. The method is here described in the case of even-even target nuclei; the extension to the general case is formally quite easy and has already been employed for the analysis of some

fission-product nuclei /5/. In this case however, particular care must be taken to avoid the effects of overlapping resonances and, furthermore, there is a theoretical uncertainty about the number of degrees of freedom of reduced neutron widths of p-wave resonances with spin values which are obtained by two possible channel spins.

## 2. Estimate of average level spacing and reduced neutron widths

The following simplifying assumptions are justified in the case of even--even nuclei:

i) There is one sequence of s-wave resonances having $J^{\pi}=1/2^{+}$ and two sequences of p-wave resonances with $J^{\pi}=1/2^{-}$ and $J^{\pi}=3/2^{-}$ respectively.

ii) The level spacing is proportional to $1/(2J+1)$ so that if $D$ is the spacing of s-wave resonances, $p_{1/2}$ resonances will also have spacing $D$, and $p_{3/2}$ resonances spacing $D/2$.

iii) The neutron strength function does not depend on the spin or, equivalently, due to assumption ii), $p_{1/2}$ and $p_{3/2}$ resonances will have the same average value $\langle g\Gamma_n^1\rangle$.

iv) A function of neutron energy $\eta(E)$ is given such that all resonances having $g\Gamma_n > \eta(E)$ are measured.

The general expression of the likelihood function restricted to all resonances having $g\Gamma_n > \eta(E)$ is proportional to the probability density that, given $D$, $\langle\Gamma_n^o\rangle$ and $\langle g\Gamma_n^1\rangle$, there are $N_{obs}$ resonances having the measured $g\Gamma_{ni}$ and $E_i$, while all remaining resonances in the given energy range have $g\Gamma_n < \eta(E)$.

This may be written:

$$L(D,\langle\Gamma_n^o\rangle, \langle g\Gamma_n^1\rangle, \nu) =$$

$$(E_i, g\Gamma_{n,i}, i=1,\ldots N_{obs} | N_{obs}, D, \langle\Gamma_n^o\rangle, \langle g\Gamma_n^1\rangle, \nu, \eta(E)) \times \qquad (1)$$

$$(N_{obs} | D, \langle\Gamma_n^o\rangle, \langle g\Gamma_n^1\rangle, \nu, \eta(E))$$

where the symbol $(A|B)$ indicates the probability of $A$ once $B$ is given and $\nu$ is the number of degrees of freedom of the distribution of reduced widths which is left unspecified in order to allow a test /3/ of the Porter-Thomas distribution ($\nu=1$).

The likelihood function (1) is too complicated to be calculated. A simpler likelihood function is obtained by disregarding part of the information contained in the measurement of energies $E_i$, keeping only that deriving from the observed energy variation of the local level density. This gives useful information especially if both $\langle\Gamma_n^o\rangle$ and $\langle g\Gamma_n^1\rangle$ are to be fitted. This is obtained by dividing the full energy range into subintervals $\varepsilon_o, \varepsilon_1, \ldots \varepsilon_m$ and considering the likelihood function as due to independent contributions from each subinterval. For simplicity let "list" indicate the whole set $\langle\Gamma_n^o\rangle$, $\langle g\Gamma_n^1\rangle$, $\nu$, $\eta(E)$.

Then one obtains /4/

$$L(D,\langle\Gamma_n^o\rangle, \langle g\Gamma_n^1\rangle, \nu) = \prod_{i=1}^{N_{obs}} (g\Gamma_{n,i} | \text{list}) \times \prod_{k=1}^{m} (n_k | D, \text{list}) \qquad (2)$$

where $n_k$ is the number of resonances with $g\Gamma_n > \eta(E)$ in the k-th interval. The calculation of the different factors appearing in eq.(2) is performed by standard techniques based essentially on expansions into sums over mutually excluding events and on the inversion of the probability brackets by means of Bayes formula. The calculation may be summarized as follows

a) Terms like $(g\Gamma_n|\text{list})$

One has /4/

$$(g\Gamma_n|\text{list}) = \sum_{\ell=0,1} (g\Gamma_n|\text{list},\ell)(\ell|\text{list})$$

$$= \frac{\sum_{\ell=0,1}(\text{meas}|g\Gamma_n)(g\Gamma_n|\langle g\Gamma_n^{\ell}\rangle,\nu)(\ell|)}{\sum_{\ell=0,1}\int dg\Gamma_n'(\text{meas}|g\Gamma_n')(g\Gamma_n'|\langle g\Gamma_n^{\ell}\rangle,\nu)(\ell|)} \tag{3}$$

where $(\text{meas}|g\Gamma_n)=(g\Gamma_n > \eta(E)|g\Gamma_n)=0,1$ according to $g\Gamma_n \lessgtr \eta(E)$, and is the probability that a resonance of given $g\Gamma_n$ is measured. The probability density $(g\Gamma_n|\langle g\Gamma_n^{\ell}\rangle,\nu)$ is the $\chi^2_\nu$ probability density transformed to an average $\langle g\Gamma_n\rangle = \sqrt{E}\,P_\ell(E)\,\langle g\Gamma_n^{\ell}\rangle$ i.e. if $t=g\Gamma_n$

$$(t\,|\,\langle t\rangle,\nu) = \frac{\frac{\nu}{2\langle t\rangle}}{\Gamma(\frac{\nu}{2})}\, e^{-\frac{\nu t}{2\langle t\rangle}} \left(\frac{\nu t}{2\langle t\rangle}\right)^{\nu/2-1} \tag{4}$$

The symbol $(\ell|)$ represents the *a priori* probability for a resonance to have a given $\ell$ value, and then from assumption ii) it follows $(\ell=0|)=1/4$ and $(\ell=1|)=3/4$.

b) Terms like $(n|D,\text{list})$

With simple calculations one obtains /4/

$$(n|D,\text{list}) = \sum_{N_s N_p} (N_s|D)(N_p|D)\left[\sum_{N_s}\binom{N_s}{n_s}P_s^{n_s}(1-P_s)^{N_s-n_s}\binom{N_p}{n-n_s}P_p^{n-n_s}(1-P_p)^{N_p+n_s-n}\right] \tag{5}$$

where $N_s$ and $N_p$ are the number of all s-and p-wave resonances in the given range and $n_s$ is the number of s-wave resonances above threshold ($n-n_s=n_p$ is then the number of p-wave resonances above threshold). The quantities $P_s$ and $P_p$ are, respectively, the probability that an s-wave or a p-wave resonance is above threshold:

$$P = \int_{\eta(E)}^{\infty} (t|\langle t\rangle,\nu)dt = \Gamma\left(\frac{\nu}{2}, \frac{\nu\eta(E)}{2\langle t\rangle}\right)/\Gamma\left(\frac{\nu}{2}\right) \tag{6}$$

where $\Gamma(a)$ and $\Gamma(a,X)$ are the complete and incomplete Gamma functions. The probabilities $(N|D)$ entering equation (5) are approximated by a gaussian shape with the correct average value and standard deviation as given by Dyson and Mehta /5/ (see also /4/ eqs.(17) and (18)); this approximation is justified

for $N \gtrsim 8$ as the calculation in practical cases depends but slightly on the shape of $(N|D)$.

Maximization of the likelihood function is performed numerically with a simple tabulation algorithm /4/ , leading to maximum likelihood estimates of $\langle\Gamma_n^o\rangle$ , $\langle g\Gamma_n^1\rangle$ , D and, possibly, also of $\nu$ (test of P.T. distribution) (see /3/).

The probability distributions of the maximum likelihood estimates necessary to give the errors in the final results cannot be calculated analytically. A Montecarlo simulation of experimental sets of parameters was developed, based on sampling eigenvalues of matrices from the Gaussian orthogonal ensemble and the analysis was applied, with the same experimental threshold $\eta(E)$ , to each generated sequence. This allows calculation of all statistical properties of the estimates and gives good control of the correctness and efficiency of the procedure. Furthermore, it is possible to introduce into the simulation small departures from the basic assumptions on which the analysis is based as, e.g. errors in $g\Gamma_n$ values, missed resonances due to overlapping etc.. This gives some idea of the corresponding effects on the final estimates.

An application example of the method, with assumed $\nu=1$ , is given in fig. 1. Open circles represent the result of the analysis of a measurement of $^{156}Gd$ resonances for different threshold functions $\eta_\alpha(E)$ represented in increasing order by the parameter $\alpha$ /3/ . Full lines and dotted lines represent, respectively, average values and stand. dev. calculated with Montecarlo simulation. The analysis was extended also to threshold functions slightly lower than a sure conservative estimate; in fact, a systematic trend in the experimental points is evident at low $\alpha$ values due, probably, to missing resonances above threshold. For large thresholds $(\alpha > 0.45)$ the maximum likelihood estimate of $\langle g\Gamma_n^1\rangle$ loses meaning as the probable number of p-wave resonances above threshold vanishes; a fixed $\langle g\Gamma_n^1\rangle$ value must then be employed. A more careful discussion of the results can be found in /3/.

The most important facts appearing from fig. 1 are that, at least in the case of good experiments, a simultaneous estimate of D , $\langle\Gamma_n^o\rangle$ and $\langle g\Gamma_n^1\rangle$ is possible, and that the described maximum likelihood procedure leads to unbiased estimates if the basic assumptions are followed. A semiempirical formula was found to reproduce roughly the correct variance in D estimate:

$$\frac{\mathrm{var}\ D}{D^2} \simeq \frac{0.8+m_s+n_p}{N_{obs}}$$

where $m_s$ and $n_p$ are respectively the expected number of missed s-wave and spurious p-wave resonances. The approximation can only be used if $m_s$ , $n_p < 0.3\ N_{obs}$ (see ref. 3). The fairly constant behaviour of the experimental estimates of $\langle\Gamma_n^o\rangle$ and D shown in fig. 1 for large thresholds, suggests that the consistency of the results for different thresholds $\eta_\alpha(E)$ may be an indication that the basic assumptions of the calculation are followed, in particular that only a negligible number of resonances are missed above threshold.

In favourable cases, when there is a large number of s-wave resonances with $g\Gamma_n$ above a sure cut-off threshold, sufficiently high to exclude p-wave resonances, the consistency of results for different, increasing threshold functions $\eta_\alpha(E)$ seems a possible empirical way to obtain a conservative estimate of the threshold only from resonance parameters, avoiding analysis of the experimental conditions (see G. Delfini and H. Seuppelaar, ref. 6). In the case of only s-wave resonances, a different method, which combines a maximum likelihood estimate with an authomatic threshold fitting was developed by F. Fröhner /7/. It seems however that all procedures devised to determine a realistic threshold function from the distribution of resonance parameter data can hardly be employed to the simultaneous determination of both s-and p-wave average reduced widths and, if properly used, should always include *a priori* information on the measuring process.

Indeed the formal generalisation of the present method to include threshold fitting is easy obtained. We briefly outline the changes this would imply in our likelihood function in order to clarify the meaning and limits of the procedure.

First, a different definition of the threshold must be given, as comparison of the values of the likelihood function (eq. 1 or eq. 2) obtained with two different $\eta(E)$ has no statistical meaning. In fact, due to the esclusion from the analysis of resonances with $g\Gamma_n < \eta(E)$ , one would in this case compare likelihood functions of different sets of experimental data. Otherwise, retaining all values of $g\Gamma_n$ is not consistent with the use of a sharp step-threshold function, which assigns zero probability to any $g\Gamma_n < \eta(E)$. The problem can be faced by considering a more general "smoothed-edge", threshold defined as the probability of measuring a resonance having an assigned value of $g\Gamma_n$

$$\eta(g\Gamma_n, E, \alpha) \equiv (\text{meas}\,|\,g\Gamma_n)$$

Here $(\text{meas}\,|\,g\Gamma_n)$ is the probability that a resonance of given $g\Gamma_n$ is included in the set of measured resonances, and $\alpha$ represents one or more continuous parameters.

It must be assumed that varying of $\alpha$ in an assigned range describes all reasonable thresholds consistent with our knowledge of the experimental conditions.

With this definition, the likelihood function eq.(2) becomes

$$L(D, \langle\Gamma_n^o\rangle, \langle g\Gamma_n^1\rangle, \nu, \alpha) = \prod_{i=1}^{N'_{obs}} (g\Gamma_{n,i}\,|\,\text{list}') \times \prod_{k=1}^{m} (n'_k\,|\,D, \text{list}') \qquad (2')$$

where all effectively measured resonances are counted in $N'_{obs}$ and $n'_k$ , and

$$\text{list}' \equiv \{\langle\Gamma_n^o\rangle, \langle g\Gamma_n^1\rangle, \nu, \alpha\} \quad .$$

The term given by Eq.(3) is formally unchanged with the only difference that $(\text{meas}\,|\,g\Gamma_n) = \eta(g\Gamma_n, E, \alpha)$ is no longer a step function.

Also eq.(5) remains the same except for a difference in the probability of measuring a resonance which is now

$$P = \int_0^\infty \eta(t, E, \alpha)(t\,|\,\langle t\rangle, \nu)\,dt$$

It appears that in the threshold-dependent likelihood function, the $g\Gamma_n$ probability distribution is always multiplied by the unknown function $\eta(t,E,\alpha)$. It is then evident that it is possible to exploit the information arising from the assumed validity of Porter-Thomas distribution only if we are able to place strong constraints on the parametrisation and the variation range of $\eta(t,E,\alpha)$ ; this can only arise from corresponding assumptions about the experimental process of measurement. We then get the impression that it is rather illusory to believe that an automatic maximum likelihood fitting of the threshold function allows to avoid, except in very favourable cases analysis of the experimental conditions. However, a reliable answer to this problem can only be obtained by a Montecarlo test including automatic threshold fitting, and simulation of different experimental conditions.

## 3. Conclusions

The characteristic features of the described estimation procedure are, first, the inclusion of the D-depending part of the likelihood function (see eq. 2), which allows a correct maximum likelihood estimation of D and, second, the possibility to deal with mixed sequences of p-and s-wave resonances. The Montecarlo simulation, which must be considered as an essential part of the estimation, showed that, if the basic assumptions of the calculation are followed, the estimates are very efficient and unbiased, allowing determination of p-wave neutron strength function also when only a small fraction of p-wave resonances can be experimentally measured.

Furthermore, it was possible to give an approximate formula for the statistical error of the D estimate which should represent also a lower limit for other estimation algorithms due to the efficiency of the maximum likelihood estimator. Application of the method (as of any other method based on the same theoretical model) is critical if the basic assumptions are not followed by the experimental data; analysis of the experimental conditions and a Montecarlo study of the sensitivity of the estimates to additional statistical uncertainties or biases seems to be the only possible way to face this problem.

References

1) C. Coceva, F. Corvi, P. Giacobbe and M. Stefanon, Nucl. Phys. A 170(1971)153

2) C. Coceva and M. Stefanon, Proc. Int. Conf. on the Interaction of Neutrons with Nuclei. Lowell 1976, CONF-760715-P2, p. 1456

3) C. Coceva and M. Stefanon, Nucl. Phys. A 315(1979)1

4) M. Stefanon, to be published

5) F.J. Dyson and M.L. Mehta, J. Math. Phys. 4(1963)701

6) G. Delfini and H. Gruppelaar, this meeting

7) F. Fröhner, this meeting

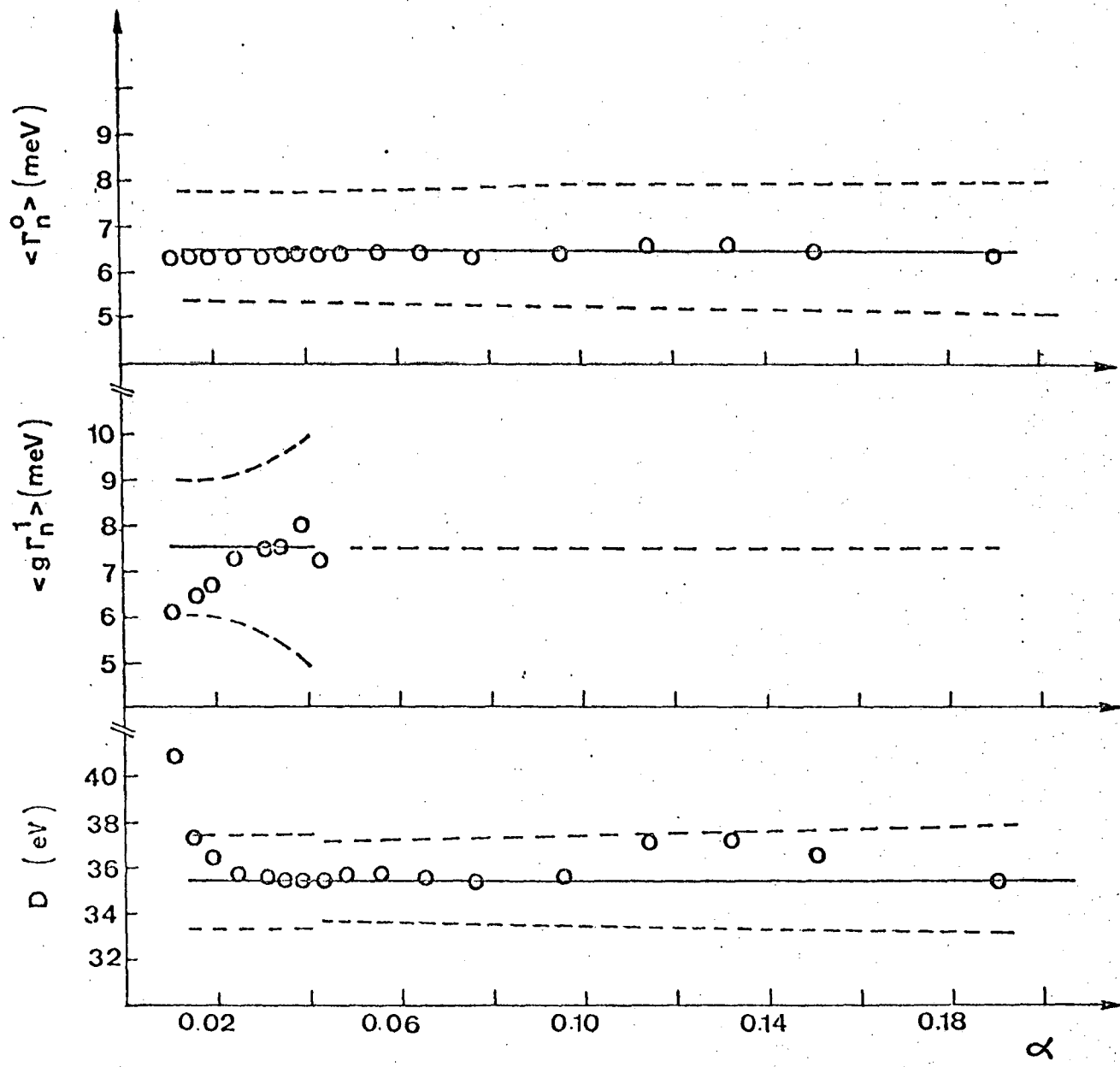


Fig. 1 Comparison between the maximum likelihood analysis of Montecarlo simulated sequences and the results obtained from a measurement of $^{156}$Gd resonances.

# MAXIMUM-LIKELIHOOD ANALYSIS OF RESOLVED RESONANCE PARAMETERS FOR SOME FISSION-PRODUCT NUCLIDES

G. Delfini and H. Gruppelaar
Netherlands Energy Research Foundation (ECN),
P.O. Box 1, 1755 ZG Petten, The Netherlands.

Abstract

The recently developed maximum-likelihood method of Coceva and Stefanon was slightly extended to facilitate the analysis of resolved resonance parameters for a large class of fission-product nuclides. This analysis was performed on a set of resolved resonance parameters, which has been used previously in the RCN-2 evaluation of neutron cross sections for fission products. A serious difficulty was that in many cases the quality of the experimental data was rather poor, which made it difficult to utilize the full power of the adopted method. For some nuclides the analysis revealed inconsistencies in the data; for other nuclides useful results were obtained, mostly in agreement with the values adopted in the RCN-2 evaluation. The estimated statistical uncertainties turned out to be quite high for most nuclides. A general conclusion is that without the use of high-quality experimental data it is quite difficult to obtain significant improvements, even when a sophisticated maximum-likelihood method is used.

## 1. INTRODUCTION

In the evaluation of neutron cross sections of fission-product (f.p.) nuclides the resolved resonance parameters play an important role. Their importance is not restricted to the resolved resonance range, because at higher neutron energies the cross sections are often calculated with a statistical model, using average parameters such as the s-wave level spacing $D_{obs}$, the s- and p-wave neutron strength functions $S_0$ and $S_1$ and the average radiation width. These average parameters have been used, for instance, in the RCN-2 f.p. cross section evaluation /1/. The determination of average parameters in the f.p. mass range can be difficult, mainly because of the often strong mixing of unassigned s- and p-wave levels, combined with the possibility of missed levels. Furthermore, for some nuclides non-statistical effects play an important role. In fact, most of the uncertainties in f.p. capture cross sections at neutron energies above a few keV are due to uncertainties in average parameters, which are enhanced by discrepancies between various determinations given in the literature. For this reason it was recommended at the 1977 FPND Advisory Group Meeting /2/ to improve the methods of determining these average parameters.

In this paper a recently developed maximum-likelihood method is used to determine $D_{obs}$, $S_0$ and $S_1$. This method was previously applied by Coceva and Stefanon /3/ for the analysis of neutron resonances of $^{156}$Gd. These authors have carefully checked this maximum likelihood method by means of Monte-Carlo simulation of resonance parameters, using random-matrix theory and Porter-Thomas

statistics for the distribution of level energies and level widths, respectively. The results turned out to be quite satisfactory. Therefore, and in view of the important application mentioned in the first paragraph, it was thought worthwhile to use a similar method for the analysis of a large class of f.p. neutron resonances, as compiled in the RCN-2 evaluation /1/. For this purpose the above-mentioned method was slightly generalized and a procedure was developed for the analysis of a large class of evaluated data. The adopted method is shortly reviewed in sect. 2., whereas in sect. 3 some examples are given of the analysis. A more extended discussion of the results will be given in a laboratory report /4/. This paper concludes with some general observations and recommendations, given in sect. 4.

## 2. METHOD OF ANALYSIS

The calculations were performed with an extended version /4/ of the code CAVE, written by Stefanon /5/ for the analysis of resonance parameters of even-even nuclides. Since the method has been described elsewhere /3,5/ we mention only a few basic principles in this paper.

### 2.1. Zero-spin target nuclides

The likelihood of the $N_{obs}$ measured resonance energies $E_i$ and neutron widths $(g\Gamma_n)_i$ is a function of the requested average s- and p-wave reduced neutron widths $\langle g\Gamma_n^0\rangle$ ,$\langle g\Gamma_n^1\rangle$ and the average level spacing $D_o$. The factor g is the usual statistical factor; $D_o$ follows from the approximative relation for the average spacing of levels with spin J: $D_J = D_o/(2J+1)$. The mean s-wave level spacing $D_{obs}$ and the neutron strength functions are calculated from the relations $D_{obs} = D_o/2(2I+1)$ and $S_\ell = \langle g\Gamma_n^\ell\rangle/D_{obs}$. It is assumed that all resonances above a certain known threshold function $\eta(E)$ have been measured (and resolved) and that all resonances are distributed according to the Porter-Thomas distributions for s- and p-waves (no higher $\ell$-waves are considered). The likelihood function is written as a product of probability functions over energy subintervals /3/. These subintervals are chosen such that within each subinterval the variation in the probability for a resonance to have a width above or below the threshold can be neglected. Furthermore, each subinterval must be large enough to allow a Gaussian approximation of the distribution function of the number of levels for each sequence. Actually, no use has been made of the spacing distributions for resonances with the same quantum numbers. The exponential energy dependence of $D_o$ over the total analysed range is also neglected. Another assumption is that the average reduced neutron widths are independent of spin, so that the two p-wave sequences of resonances are distributed according to the same Porter-Thomas distribution. This independence of spin follows from the assumption that both $S_\ell$ and $D_o$ are independent of the spin.

The maximum-likelihood method based upon these assumptions was checked with results of Monte-Carlo calculations, simulating the resonance parameters of $^{156}$Gd /3/. Coceva and Stefanon also proposed approximative expressions for the uncertainties in $\langle g\Gamma_n^0\rangle$ and $D_{obs}$, assuming that the numbers of missed s-wave and spurious p-wave resonances are each less than about 30% of the observed number of resonances. These expressions have been adopted in this work.

### 2.2. Non-zero spin target nuclides

The extension to nuclei with target spin I larger than 0 (i.e. for the most important f.p.) was made /4/ by assuming that all above-mentioned assumptions remain valid. However, for high values of J the simple (2J+1)-dependence of the spin distribution is not correct, because the exponential spin cut-off parameter f(J) can no longer be considered as a constant. Therefore, it is likely that $\langle g\Gamma_n^0\rangle$ and $\langle g\Gamma_n^1\rangle$ depend on the possible J-values. Still, we have assumed that these quantities are spin-independent and thus there

are only two different Porter-Thomas distributions, one for s-waves and one for p-waves. However, for p-wave resonances measured at non-zero spin targets, this assumption is already invalidated, since level widths for certain spin sequences are distributed according to a $\chi^2$-distribution with two degrees of freedom, instead of a Porter-Thomas distribution. For these reasons, one can apply this extension only in those cases where the number of p-waves is a small fraction of the resonances above the threshold. For s-wave resonances the above-mentioned approximations still seem to be reasonable. It has been shown by Tran Quoc Thuong /6/ that when a difference of less than 20% exists between the two values of $\langle g\Gamma_{nJ}^0\rangle$ the reduced neutron widths can still considered to belong to one Porter-Thomas distribution.

## 2.3. Threshold function

The threshold function $\eta(E)$ plays a very important role in the calculation procedure, since it is assumed that above $\eta(E)$ there are no missed resonances at all. In the present analysis of a large number of f.p. nuclides it is difficult to trace back the experimental threshold functions. Therefore, the following standard procedure was used. From each ten resonances the resonance with the smallest value of $g\Gamma_n/\sqrt{E}$ was selected. Through these weak resonances a function $\eta_o(E) = aE^b+c$ was fitted (cf. ref. /7/). The constants a and b were determined from a least-squares fit: c was the minimum observed value of $g\Gamma_n/\sqrt{E}$ of all resonances in the sample. In Fig. 1 an example of such a fit is given. In the calculations the threshold function was varied by multiplication with a factor t to find the dependence of the results on $\eta(E) = t\eta_o(E)$. For low values of t mostly there still is a significant number of missed resonances, which usually leads to decreasing values of $D_{obs}$ as a function of t, see Fig.2. Above a certain value of $t(t>t_1)$ constant values of $D_{obs}$ are found; for large values of t $(t>t_2)$ the statistical fluctuations in $D_{obs}$ may become quite high, see Fig. 2. The final outcomes for $D_{obs}$ and $S_\ell$ are deduced from the range $t=t_1$ to $t_2$, where their values are reasonably constant.

## 2.4. Limitations of the method

In the previous sections the main assumptions used in the analysis have been mentioned. Evidently, when the set of experimental data does not follow the assumed distribution laws, or when the data sample is too small, no useful averages can be obtained. This may occur, for instance, when results of several authors are combined to one "evaluated set of data", when so-called "non-statistical effects" occur or when there is a large fraction of unresolved doublets. For these reasons the data should be checked carefully before the maximum likelihood procedure is followed.

In order to meet the condition of a not too high fraction of p-wave resonances above threshold, the energy range could be reduced or the value of t could be increased. Both methods have been used. However, if the level-spacing is large (even-mass nuclides) the energy range cannot be reduced too much and it may occur that the mixing of s- and p-wave resonances remains too strong to obtain a sharp maximum in the likelihood function. In those cases quite large uncertainties for the average parameters are obtained. It is also possible that the data sample contains only a very small number of p-wave resonances. In these cases the value of $\langle g\Gamma_n^1\rangle$ has to be fixed in the analysis. The dependence of the final results on the value of $\langle g\Gamma_n^1\rangle$ could be checked by varying $\langle g\Gamma_n^1\rangle$ over a large range.

For the above-mentioned reasons it is often quite difficult to determine $S_1$ from resolved resonance parameters with the above-mentioned maximum-likelihood method. Therefore, it may be better to determine $S_1$ from optical-model analysis of average total or elastic scattering cross sections at low neutron energies. Unfortunately there are not many of these measurements in the range 10 to 500 keV for f.p. nuclides. It would also be helpful if more experimental information, e.g. the value of $\ell$, was available. A possible ex-

perimental method of determining $\ell$ has recently been applied by Rohr et al. /8/ in the measurement of $^{127}$I-resonance parameters.

## 3. RESULTS

### 3.1. Example: analysis of $^{127}$I resonance parameters

For each f.p. nuclide which was analysed a separate discussion is given in ref. /4/, together with figures and tables. As an example we discuss here only the results of the analysis performed for $^{127}$I in some detail. In Fig. 1 the values of $g\Gamma_n/\sqrt{E}$ have been plotted as a function of neutron energy, together with the fitted threshold function $\eta_0(E)$. The experimental data plotted in Fig. 1 are from Rohr et al. /8/. In the analysis the threshold was multiplied with factors t ranging from 1 to 14. For each value of t a maximum-likelihood calculation was performed of which the results are given in Table I and Fig. 2.

In the analysed energy range from 0 to 2 keV the p-wave penetration factor was small enough to prevent a strong mixing of s- and p-wave resonances. On the other hand, there were enough measured p-wave resonances to determine the p-wave neutron strength function, at least at low values of t. At threshold multiplication factors of more than t=5 the value of $\langle g\Gamma_n^1\rangle$ was fixed according to the initial values of $S_1$ and $D_{obs}$ /8/. The final results, obtained by averaging the data over the range $t_1 = 2$ to $t_2 = 5$ are: $D_{obs} = 14.5\pm0.6$ eV, $S_0 = (0.8\pm0.1)\times10^{-4}eV^{-\frac{1}{2}}$ and $S_1 \approx 3.1\times10^{-4}eV^{-\frac{1}{2}}$. These results are quite close to the values previously given by Rohr et al. /8/, i.e. $D_{obs} = 13.3\pm1.0$ eV, $S_0 = (0.80\pm0.09)\times10^{-4}eV^{-\frac{1}{2}}$ and $S_1 = (3.4\pm1.4)\times10^{-4}eV^{-\frac{1}{2}}$, which were analysed by using additional information from experimental s- and p-wave discrimination. The p-wave neutron strength function obtained by Camarda /9/ from an analysis of total cross section measurements is much lower: $S_1 = (1.6\pm0.5)\times10^{-4}eV^{-\frac{1}{2}}$. Fortunately, the results for $D_{obs}$ and $S_0$ are not very sensitive to the value of $S_1$. This follows from results obtained at t>5, where the number of spurious p-waves can be neglected (see Table I).

### 3.2. Survey of all results obtained

A survey of the results obtained in ref. /4/ is given in Table II. All resolved resonance parameters were taken from the RCN-2 evaluation /1/. The first five columns of Table I list the nuclide symbol, the number of resonances in the sample, the analysed energy range $\Delta E$, the target spin I and the spin cut-off parameter $\sigma$. Mostly, the initial guess parameters for $D_{obs}$, $S_0$ and $S_1$ were taken from the RCN-2 evaluation as well. The final parameters given in Table II result from the present analysis. When $S_1$ is not given in Table II, the value of $\langle g\Gamma_n^1\rangle$ was kept constant in the analysis at the initial value of the product $D_{obs} \times S_1$. In most cases there is good consistency between the initial and final results.

As far as the p-wave strength function is concerned, only for five odd-mass nuclides $S_1$ could be estimated; in these cases $S_1$ was much larger than $S_0$ (such that enough p-waves were included in the data) and $\Delta E$ was large with respect to $D_{obs}$. For $^{93}$Nb the value of $S_1$ was not estimated, because it was felt that for this nuclide with high target spin (I = 9/2) the condition that $\langle g\Gamma_n^1\rangle$ is only slightly dependent of spin was not fulfilled. In the case of even-even nuclides the values of $S_1$ were determined only for $^{92}$Mo and $^{98}$Mo. However, these values are not very certain as a result of non-statistical effects in the p-wave neutron widths; see e.g. /10/. The recent experimental data of Musgrove et al. /11/ for the Nd isotopes at E>2.5 keV were not analysed, because many of the neutron widths for the weak resonances were obtained from capture areas $g\Gamma_n\Gamma_\gamma/\Gamma$ with inserted mean values for g and $\Gamma_\gamma$, leading to large uncertainties in the deduced $g\Gamma_n$-values, probably with a distribution different from the Porter-Thomas one.

With regard to $D_{obs}$ and $S_0$ the results are more useful, except for nuclides where strong non-statistical effects have been observed, either in the s-wave neutron strengths (e.g. $^{142}$Nd /11/) or in the p-wave neutron strengths (e.g. $^{98}$Mo /11/). Typical uncertainties in $D_{obs}$ and $S_0$ are about ± 10% and ± 30%, respectively. The most accurate results (± 4% in $D_{obs}$; ± 12% in $S_0$) were obtained for $^{127}$I, where the recent data of Rohr et al. /8/ were used in the analysis. Apart from the listed nuclides, many other nuclides were analysed but no results were achieved; for some of these nuclides too few data were available whereas for others the fluctuations in the results were too large. Using the resonance parameters from the RCN-2 file no satisfactory average data were obtained for $^{94}$Mo, $^{96}$Mo, $^{100}$Mo, $^{101}$Ru, $^{102}$Ru, $^{104}$Ru, $^{102}$Pd, $^{104}$Pd, $^{105}$Pd, $^{107}$Pd, $^{108}$Pd, $^{110}$Pd, $^{129}$I, $^{141}$Pr, $^{147}$Pm, $^{148}$Sm, $^{150}$Sm, $^{152}$Sm and $^{154}$Sm. It should be mentioned that meanwhile for many of these nuclides improved data are available.

## 4. CONCLUSIONS

The maximum-likelihood method of Coceva and Stefanon /3/ for the determination of the average resonance parameters $D_{obs}$, $S_0$ and $S_1$ was slightly extended and used for the analysis of resonance parameters of a large number of f.p. nuclides, as contained in the RCN-2 evaluation. The basic principles of the method were shortly summarized. The extension to target nuclides with spin larger than zero has been discussed in some detail. For target nuclides with high spins the assumption that $\langle g\Gamma_n^0 \rangle$ and $\langle g\Gamma_n^1 \rangle$ are independent of the compound-state spins is not valid. This means that in particular the adopted estimation of $\langle g\Gamma_n^1 \rangle$ becomes doubtful. For this reason the above-mentioned method can be applied only in those cases where the number of p-wave resonances is a small fraction of the resonances above the threshold.

In the determination of the threshold function $\eta(E)$ for this large class of data a standard procedure was followed. By varying $\eta(E)$ with a factor t the dependence of the average parameters on the threshold was investigated. The final results were adopted at values of t for which $D_{obs}$ and $S_0$ could assumed to be constant.

The limitations of this method were also discussed. In general, high-quality data are required to obtain good results. Still, the determination of $S_1$ is often quite difficult and it is recommended to use additional experimental data to find $S_1$, e.g. s- and p-wave discrimination, or optical-model analysis of total cross sections.

As an example of the application of the maximum-likelihood method the analysis of resonance parameters of $^{127}$I was discussed. For this nuclide the recent accurate data of Rohr et al. /8/ were used. The results are consistent with the analysis performed by the experimenters, which was partly based upon experimental s- and p-wave level discrimination.

A survey of all results obtained has been given in Table II. In most cases a good consistency between initial and final values of average parameters was obtained. The value of $S_1$ could only be estimated for five odd-mass nuclides and two even-even nuclides. Some additional uncertainties in the results are due to so-called "non-statistical effects", e.g. for $^{98}$Mo and $^{142}$Nd. Typical uncertainties in $D_{obs}$ and $S_0$ are about ± 10% and ± 30%, respectively. The most accurate results were obtained for $^{127}$I, i.e. ± 4% in $D_{obs}$ and ± 12% in $S_0$. For many other nuclides given in the RCN-2 file no satisfactory results could be obtained due to poor quality of the data.

For some of these nuclides better measurements are already available; for many other nuclides high-quality data are still needed (particularly for a few long-lived f.p. like $^{107}$Pd, $^{151}$Sm and $^{147}$Pm). In general, significant improvements could be obtained when good data are available; for some nuclides, however, a statistical analysis can hardly yield good results because of more fundamental reasons such as "non-statistical effects" or strong mixture of s- and p-waves.

The required uncertainty in $D_{obs}$ for use in statistical-model calcu-

lations of the most important f.p. nuclides is in the order of ± 5%; a similar request exists for the average radiation width $\langle\Gamma_\gamma\rangle$. It is clear that mostly this accuracy is not reached and that for many important f.p. nuclides high-quality data in the resonance range are still needed. Accurate values of $D_{obs}$ are also required to provide data for further development of the level-density parameter systematics, which is important to predict capture cross sections of (short-lived) radioactive f.p. nuclides.

## 5. REFERENCES


/1/ H. Gruppelaar, Tables of RCN-2 fission-product cross section evaluation, vol. 1, ECN-13, (1977), vol. 2, ECN-33 (1977) and vol. 3, ECN-65 (1979).

/2/ Conclusions and recommendations of the Second Advisory Group Meeting on Fission Product Nuclear Data (FPND) - 1977 organized by the I.A.E.A. at Petten, Sept. 1977, IAEA-213, vol. 2 (1978) p. 811.

/3/ C. Coceva and M. Stefanon, Experimental aspects of the statistical theory of nuclear spectra fluctuations, Nucl. Phys. A315 (1979) 1.

/4/ G. Delfini, Maximum-likelihood analysis of resolved resonance parameters for some fission-product nuclides, ECN-report, to be published.

/5/ M. Stefanon, to be published; see also contribution to this meeting.

/6/ Tran Quoc Thuong, Analyse statistique des distributions des largeurs reduites partielles, Thesis, University of Paris-VII (1973).

/7/ T. Fuketa and J.A. Harvey, Nucl. Instr. Meth. 33 (1965) 107.

/8/ G. Rohr, R. Shelley and A. Brusegan, Neutron resonances studies of $^{127}I$, to be published; see also contr. to Lowell conf. 1976, CONF-760715-P2, p. 1249.

/9/ H.S. Camarda, Phys. Rev. C9 (1974) 28.

/10/ A.R. de L. Musgrove et al., Nucl. Phys. A270 (1976) 108.

/11/ A.R. de L. Musgrove et al., Non-statistical effects in the radiative capture cross sections of the Neodymium isotopes, AAEC/E401 (1977), supplemented at the Int. Conf. on Neutron Physics and Nuclear Data for Reactors, Harwell (1978) p. 449.

Table I. Analysis of resonance parameters of $^{127}I$ for different thresholds.

| Multipl. factor a) | $\langle g\Gamma_n^o \rangle$ (meV) | $\langle g\Gamma_n^1 \rangle$ (meV) b) | $D_{obs}$ (eV) | N c) | % missed s-waves d) | | % spurious p-waves d) | |
|---|---|---|---|---|---|---|---|---|
| 1 | 1.20 | 4.18 | 16.2±.8 | 179 | 3 | 11 | 22 | 25 |
| 2 | 1.18 | 3.95 | 14.6±.6 | 150 | 5 | 16 | 8 | 11 |
| 3 | 1.18 | 4.49 | 14.5±.6 | 136 | 6 | 19 | 4 | 6 |
| 4 | 1.18 | 4.76 | 14.6±.7 | 126 | 6 | 22 | 2 | 4 |
| 5 | 1.16 | 4.15 | 14.5±.7 | 117 | 7 | 25 | <1 | 1 |
| 6 | 1.17 | *(4.4) | 14.6±.7 | 113 | 8 | 28 | <1 | |
| 7 | 1.17 | * | 14.7±.7 | 109 | 8 | 30 | | |
| 8 | 1.16 | * | 14.4±.7 | 109 | 9 | 32 | | |
| 9 | 1.15 | * | 14.4±.8 | 107 | 9 | 34 | | |
| 10 | 1.15 | * | 14.3±.8 | 106 | 10 | 35 | | |
| 11 | 1.17 | * | 14.6±.8 | 103 | 11 | 36 | | |
| 12 | 1.16 | * | 14.4±.9 | 103 | 11 | 38 | | |
| 13 | 1.16 | * | 14.3±.9 | 102 | 12 | 39 | | |
| 14 | 1.14 | * | 14.2±.9 | 102 | 12 | 41 | | |

a) The coefficients of the threshold function are $a = 0.36 \times 10^{-5}$ and $b = 1.15$; see Fig. 1.

b) An asterisk means that the width was fixed in the calculations at the value given in brackets.

c) Total number of resonances above threshold.

d) The two columns indicate the percentages at the beginning and at the end of the energy range.

Table II. Summary of results.

| Nuclide | $N_{obs}$ | ΔE (keV) | I | σ | Initial | | | Final | | |
|---|---|---|---|---|---|---|---|---|---|---|
| | | | | | $D_{obs}$ (eV) | $S_0$ ($\times 10^{+4} eV^{-\frac{1}{2}}$) | $S_1$ ($\times 10^{+4} eV^{-\frac{1}{2}}$) | $D_{obs}$ (eV) | $S_0$ ($\times 10^{+4} eV^{-\frac{1}{2}}$) | $S_1$ ($\times 10^{+4} eV^{-\frac{1}{2}}$) |
| Nb93 | 94 | 0-3.0 | 9/2 | 5.3 | 100±10 | 0.36±0.06 | 5.16±2.4 | 90±20 | 0.4 ±0.1 | – |
| Mo92 | 43 | 0-32 | 0 | 5 | 3920±800 | 0.65±0.25 | 3.3 ±1.1 | 3600±700 | ≈0.34 | ≈ 6.8 |
| Mo95 | 55 | 0-2.25 | 5/2 | 5.5 | 87±10 | 0.48±0.1 | 5.9 ±1.8 | 91±11 | 0.38±0.13 | ≈11 |
| Mo98 | 122 | 0-53 | 0 | 5.3 | 1080±200 | 0.44±0.12 | 6.1 ±2 | 1180±200 | ≈0.32 | ≈ 3.9 |
| Rh103 | 280 | 0-4.0 | 1/2 | 6.0 | 26.1±0.8 | 0.47±0.07 | 6.5 ±2.0 | 31±3 | 0.53±0.05 | ≈ 9 |
| Ag107 | 81 | 0-0.9 | 1/2 | 6.1 | 19 ±4 | 0.37±0.10 | 3.8 ±0.6 | 25±3 | 0.40±0.18 | – |
| Ag109 | 69 | 0-1.0 | 1/2 | 6.1 | 16.3±1.5 | 0.64±0.16 | 3.8 ±0.6 | 18.7±1.3 | 0.68±0.22 | ≈ 3.2 |
| I127 | 189 | 0-2.0 | 5/2 | 6.3 | 13.3±1.0 | 0.80±0.09 | 3.4 ±1.4 | 14.5±0.6 | 0.8 ±0.1 | ≈ 3.1 |
| Cs133 | 165 | 0-3.5 | 7/2 | 6.4 | 24.2±2.0 | 0.8 ±0.1 | 3.9 ±1.0 | 22.7±2.9 | 0.67±0.20 | – |
| La139 | 77 | 0-10 | 7/2 | 5.9 | 286 ±25 | 0.64±0.15 | 2.0 ±1.0 | 283 ±50 | 0.66±0.22 | ≈ 1.2 |
| Nd142 | 61 | 0-22.5 | 0 | 6.2 | 680 ±130 | 2.0 ±0.4 | 1.0 ±0.4 | 663 ±70 | 1.2 ±0.3 | – |
| Nd143 | 49 | 0-2.5 | 7/2 | 6.4 | 35 ± 4 | 2.7 ±0.5 | 1.2 ±0.5 | 36.5±4.0 | 2.7 ±0.8 | – |
| Nd144 | 50 | 0-11.5 | 0 | 6.3 | 450 ±110 | 3.0 ±1.0 | 0.9 ±0.5 | 432 ±70 | 5.1 ±1.6 | – |
| Nd145 | 113 | 0-2.25 | 7/2 | 6.5 | 19.0±2.0 | 3.3 ±0.9 | 0.86±0.4 | 17.0±1.6 | 3.3 ±0.6 | – |
| Nd148 | 74 | 0-8 | 0 | 6.5 | 170 ±35 | 2.7 ±0.8 | 0.6 ±0.2 | 167 ±21 | 3.2 ±0.9 | – |
| Nd150 | 63 | 0-10 | 0 | 6.5 | 160 ±20 | 2.7 ±0.6 | 0.88±0.5 | 164 ±17 | 3.0 ±0.7 | – |
| Sm147 | 85 | 0-0.6 | 7/2 | 6.8 | 6.3±0.7 | 4.3 ±1.3 | 1.8 ±0.6 | 4.7±1.2 | 4.7 ±1.5 | – |
| Sm149 | 63 | 0-0.16 | 7/2 | 7.0 | 2.0±0.3 | 5.1 ±0.9 | 1.8 ±0.6 | 1.9±0.3 | 7.5 ±2.2 | – |

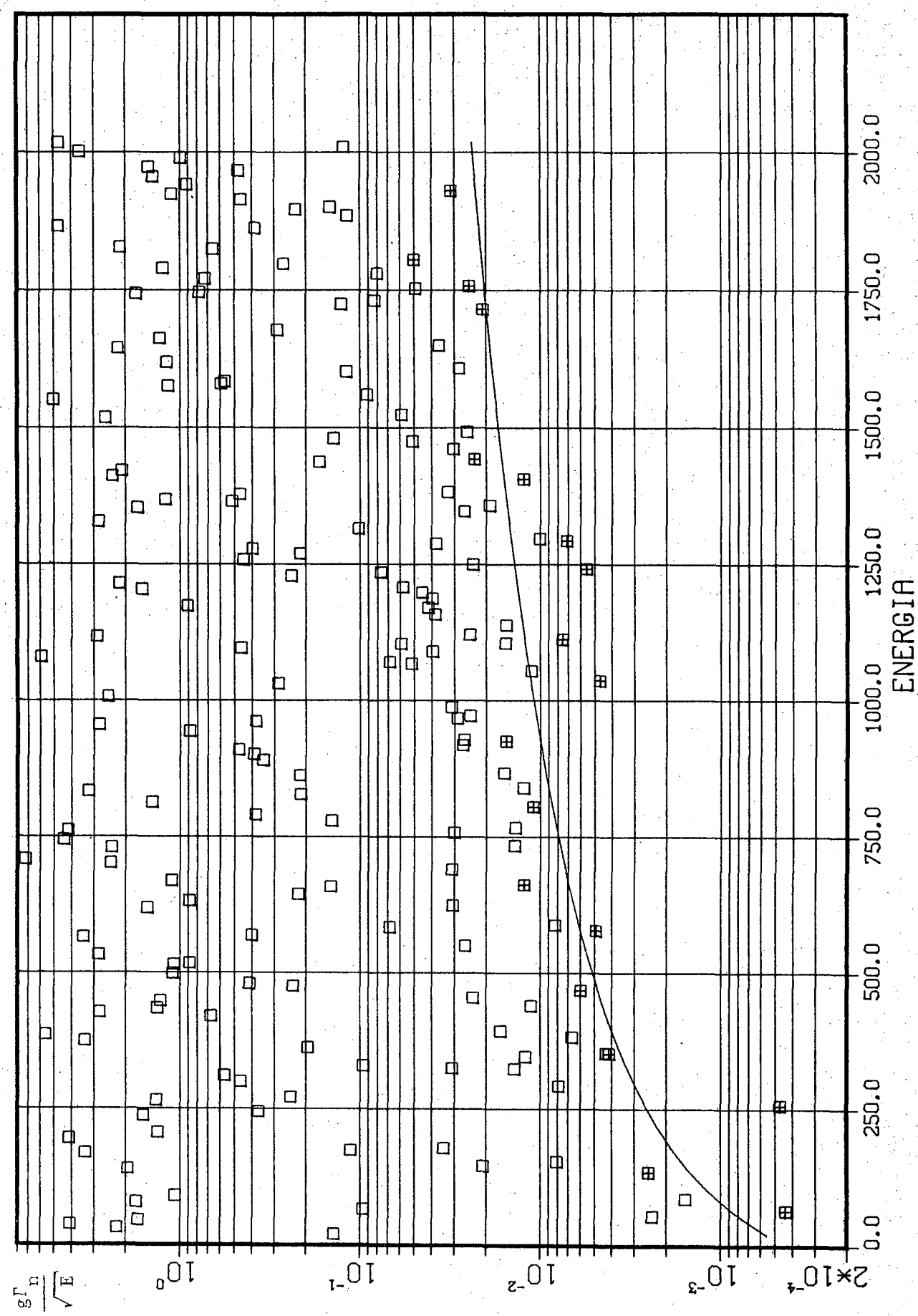


Fig. 1. Values of $g\Gamma_n/\sqrt{E}$ for $^{127}I$. The threshold function was fitted through the points indicated with a cross.(Energy in eV, $g\Gamma_n$ in meV).

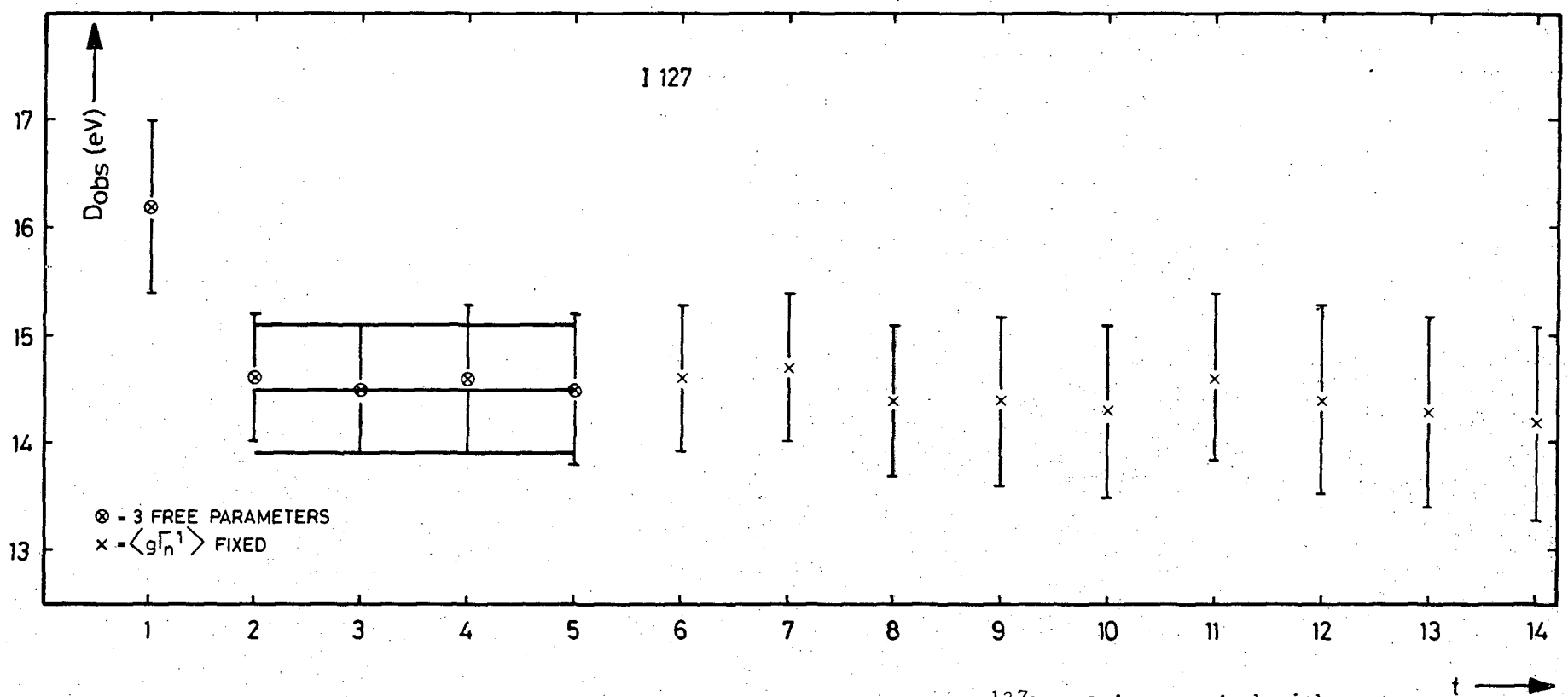


Fig. 2. $D_{obs}$ as a function of the threshold multiplication factor E for $^{127}I$. Points marked with a circle were obtained without a fixed value of $g\Gamma_n^1$.

# STATUS OF RADIATIVE WIDTHS, NEUTRON STRENGTH FUNCTIONS AND IMPROVED EVALUATION USING THE LANE-LYNN THEORY*

S. Mughabghab
National Nuclear Data Center
Brookhaven National Laboratory
Upton, N.Y. 11973

ABSTRACT

The s- and p-wave neutron strength functions and average radiative widths of fission product nuclides are reviewed.

The direct capture mechanism of Lane and Lynn is quantitatively verified for the two reactions $^{42}Ca(n,\gamma)\,^{43}Ca$ and $^{136}Xe(n,\gamma)\,^{137}Xe$. Thermal capture cross sections of $^{132}Te$ and $^{126}Sn$, are estimated with the aid of the Lane-Lynn theory.

## Introduction

The investigation of the average parameters of neutron resonances ($S_0$, $S_1$, $\Gamma_{\gamma 0}$, $\Gamma_{\gamma 1}$, $D_0$, $D_1$, $R'$) is of primary importance because these quantities play a major role in:

1) the optical model

2) reactor cycle and burn-up calculations

3) understanding the neutron reaction mechanisms of thermal and resonance neutrons.

For the prediction of the efficient and safe performance of thermal and fast reactors, it is necessary to have a knowledge of the capture cross sections in the thermal and fast regions of the various fission product (FP) nuclides produced in a reactor cycle. In some cases, either these FP isotopes are radioactive and/or experimental information is not available. Because of these difficulties, one has to resort to calculations of the capture cross section with the aid of average resonance parameters derived from theory (such as the optical model) and/or systematics of neighboring nuclides. Such a procedure is applied in the unresolved energy region. In the thermal

* Research supported by the U.S. Department of Energy.

region, in some favorable cases, one can predict the thermal capture cross section with the aid of the Lane and Lynn theory /1,2/.

Within the past five years, a great deal of experimental data on the individual resonance parameters has become available. In addition, numerous average capture and total cross section data from which average resonance parameters can be extracted have been carried out. This situation warranted a reexamination of the neutron resonance parameters and their average properties. The results of this study will be published in a fourth edition of BNL-325, Vol. 1.

The average neturon resonance parameters which I wish to cover here are the s- and p-wave neutron strength functions and average total radiative widths. The average level spacings are discussed by other speakers at this conference. In the last section, I would like to disucss the applicability of the Lane-Lynn theory /1/ in the calculations of thermal capture cross sections for two radioactive fission product nuclides, $^{132}$Te and $^{126}$Sn.

S- and P-Wave Neutron Strength Functions

The s- and p-wave neutron strength functions are defined by the relations:

$$S_0 = \frac{(g\Gamma_n^0)}{D_0} = \frac{\sum_j g\Gamma_{nj}^0}{\Delta E}, \tag{1}$$

$$S_1 = \frac{(g\Gamma_n^1)}{3\ D_1} = \frac{\sum_j g\Gamma_{nj}^1}{3\Delta E} \tag{2}$$

where the summation is carried out over N resonances in an energy interval $\Delta E$. Two methods have been exploited in the determination of the strength functions $S_0$ and $S_1$:

1) In the region where resonances are well resolved and thus individual resonance parameters are available, $S_0$ and $S_1$ are determined by Eqs. 1 and 2, respectively.

2) In the unresolved region, the behavior of the average cross section, yields values of the strength functions.

It can be shown that on the assumption that only s- and p-wave resonance contributions are significant, the average total cross section in the keV energy range can be written in the form

$$\langle\sigma_T\rangle = 4\pi(R')^2 + 2\pi^2\lambda\!\!\!^{-2} \sqrt{E}\ (S_0 + 3k^2R^2S_1) + 0\ (S_0)^2 \tag{3}$$

Usually, the contribution of higher order terms $0(S_0)^2$ in the keV energy region

is small and can be neglected. The accuracy in determining the strength functions by this method depends largely on the accuracy of the average cross section and on our knowledge of R' in the keV energy region. In addition, Gibbons et al. /3/ applied the theory of Lane and Lynn /4/ to derive s- and p-wave strength functions from their extensive average capture measurements through the relation

$$\langle\sigma_{J\ell}\rangle = \frac{2\pi^2}{k^2} \langle\Gamma_\gamma\rangle S_\ell P_\ell \sqrt{E} \frac{g_J \varepsilon^\ell_{IJ} F(\alpha_{\ell J})}{\langle\Gamma_J\rangle} \tag{4}$$

All the symbols have their usual meaning and are defined in Ref. /3/. It is important to recall here that certain assumptions were made in the derivation of Eq. 4.

1) The strength functions $S_\ell$, are independent of J and are $\ll 1$.
2) $D_J = Dobs/g_J$
3) $\Gamma_\gamma$ is independent of J, $\ell$, and energy.
4) $\Gamma = \Gamma_n + \Gamma_\gamma$. This indicates that inelastic channel is considered closed.

As is very well known at the present time, the first condition is satisfied. On the other hand, the third condition may not be fulfilled particularly in the 3s and 3p giant resonances where differences exist between s- and p-radiative widths. The nature of these differences arise because of nonstatistical effects, such as valence neutron capture and doorway state formation, and mode of decay of $\gamma$-rays to low lying states. Consequently, such differences in the radiative widths must be taken into account in applying Eq. 4.

The results which will be presented here are based largely on the evaluation of the experimental data which are compiled at the National Nuclear Data Center at Brookhaven National Laboratory and stored on magnetic tapes of the CSISRS library. At the present time, a major effort is devoted in the examination of the individual resonance parameter data for the purpose of coming up with recommended values which will be published in the report BNL-325, Vol. 1, 4th Edition. Before presenting the results, I would like to describe briefly our techniques. The various experimental data of measurers are transformed into a standard form (such as $g\Gamma_n$ values), are grouped according to resonance energy, and then a weighted average of the same quantities is computed. In addition internal and external errors are calculated. The evaluator then examines the results and makes any changes he may deem necessary. With the aid of another computer code, the recommended values are transformed into an ENDF format. Resonances with unknown spins and/or radiative widths

are assigned spins and/or average $\Gamma_\gamma$ with the provision that the (2J+1) law for the level density is satisfied. Subsequently, these recommended parameters are automatically fed into another program (BNLPSY) which performs calculations of the following quantities:

a) thermal capture and fission cross sections for each resonance

b) capture and fission resonance integrals for each resonance

c) coherent scattering amplitudes (the real and the imaginary parts) for each spin state

d) incoherent scattering cross sections for targets with $I \neq 0$

e) s- and p-wave strength functions

f) average radiative widths for s- and p-wave resonances.

Consequently, the evaluator examines the results and may make additional adjustments in the first few resonances or add bound levels in order to achieve agreement with the thermal cross sections and resonance integrals. Finally, a staircase plot is produced for s- and p-wave strength functions and level spacings. This is illustrated in Figs. 1-4 for $^{70}Zn$.

The preliminary evaluated strength functions, $S_0$ and $S_1$ in units of $10^{-4}$ are presented in Columns 3 and 4 of Table I. For the most part, these are based on the individual resonance parameters. In some cases, because of a lack of $g\Gamma_n$ values, the recommended values are based on average cross section data. These are designated by an asterisk. In Column 2, the status of the strength function values is described by the letters a,b,c,d; the significance of which is as follows:

(a) = resonance parameter data are available after 1973

(b) = new measurements of resonance parameters have not been carried out after 1973

(c) = recent measurements carried out but the results of the analysis have not yet been published

(d) = parameters for 7 resonances of $^{134}Cs$ are available. However the result of the calculation of strength function for this isotope may not be satistically meaningful.

An examination of the status column indicates that improvements in our knowledge of the strength functions of the isotopes in the mass region A = 87-110 have been achieved. This is largely due to measurements carried out at ORELA and GEEL. Note that the average resonance parameters of the rare earth isotopes are not included here because their evaluation have not been completed.

At this point it is noteworthy to mention that Murty et al. /5/ reported capture measurements of nuclei in the mass region 63-140 using the activation technique and an Sb-Be photoneutron source ($E_n \approx 25$ keV). From these

measurements these authors derived p-wave strength functions. On the basis of these determinations, they arrived at the conclusion that there is a splitting of the 3p size resonance with a minimum at A = 100 with $S_1 = 1.5\times10^{-4}$. This would require that the spin-orbit force is twice the normal value. This conclusion is at variance with the present results and with our present knowledge of the spin-orbit potential.

S- and P-Wave Total Radiative Widths

As pointed out previously, of particular importance in the calculations of capture cross section is an accurate determination of the radiative width of individual resonances in order to study its variation with mass number, excitation energy, spin and parity of the resonances. As is very well established now /6-8/, nonstatistical effects play an important role in the capture reaction mechanism particularly in the 3p size resonance, i.e., in the mass region 90-100. Because of this, the partial radiative decay amplitude (from an initial, j, state to a final state, f) can be written as a sum of several contributions

$$\Gamma^{\frac{1}{2}}_{\gamma jf} = \Gamma^{\frac{1}{2}}_{\gamma jf}\,(cn) + \Gamma^{\frac{1}{2}}_{\gamma jf}\,(ds) + \Gamma^{\frac{1}{2}}_{\gamma jf}\,(sp) \tag{5}$$

where the successive terms on the right-hand side correspond respectively to compound-nucleus, doorway state, and single particle effects. Therefore, the total radiative width of resonance j can be written as

$$\Gamma^{\frac{1}{2}}_{\gamma j} = \sum_{f} \Gamma^{\frac{1}{2}}_{\gamma jf} \tag{6}$$

If one assumes that the sign of the interference terms between direct capture and the statistical components is random, then:

$$\Gamma_{\gamma j} = \Gamma_{\gamma j}(cn) + \Gamma_{\gamma j}(ds) + \Gamma_{\gamma j}(sp) \tag{7}$$

It has been demonstrated in Ref. /6,7/ that the valence components in $^{90}Zr$ and $^{98}Mo$ can be as large as the statistical component particularly for resonances with large reduced neutron widths. Therefore, nonstatistical effects should be taken into consideration in the evaluation of capture cross sections in this mass region as well as in the 3s giant resonance region. For isotopes with A > 150, nonstatistical effects are negligible and can be ignored in the calculations of capture cross sections. Gruppelaar /9/ applied the valence neutron model in the evaluation of the capture cross sections of $^{90}Zr$ and $^{98}Mo$.

Other methods which are based on the Brink-Axel representation and thermodynamics considerations have been applied with some success. Dr. Benzi

will present at this meeting some results of total radiative widths based on the thermodynamical model. Moore /10/ presented at the Harwell conference calculations of total radiative widths for transactinium isotopes based on the Brink-Axel theory. Some success was achieved in these calculations. Finally, we note the recent theoretical calculations by Zaretskii and Sirotkin /11/ of the total radiative widths, which are carried out, in the framework of the shell approach using the theory of Fermi systems. A simple estimate is derived for the total radiative width which is given by:

$$\Gamma_\gamma = 3.1\text{x}10^{-2} \left(\frac{U}{a} A^{2/3}\right)^{7/2} \qquad (7)$$

where U and $a^{-1}$ are the excitation energy and level density, respectively, expressed in MeV units. The radiative width $\Gamma_\gamma$ is expressed in meV.

Next, let us turn our attention to the experimental values of the radiative widths of FP nuclides. The evaluated numbers are listed in Columns 5 and 6. Two features are readily evident from an examination of the numbers:

1) In the mass region spanning mass numbers 88 to 100, there are differences between the s- and p-wave radiative widths. Specifically, the p-wave radiative widths are larger than the s-wave radiative widths.

2) There is a general trend of a decrease of $\Gamma_\gamma$ with mass number for both s- and p-wave resonances.

This dependence of $\Gamma_\gamma$ on A has been known for some time. Recently, Malecky et al. /12/ analyzed the experimental data and deduced the following relation:

$$\Gamma_\gamma = 8.7\ U^{0.9}\ A^{-0.9} a^{-0.57} \qquad (8)$$

As an approximateion, a $\alpha$ A, therefore, $\Gamma_\gamma \alpha A^{-1.47}$. This dependence of $\Gamma_\gamma$ on mass number is in satisfactcory agreement with Zaretskii and Sirotkin's theory /11/.

The Potential Capture of Lane and Lynn

In the past few years a large body of thermal capture data in the mass regions around A=40 and 140 which exhibit positive correlation between "reduced" gamma ray intensities and (d,p) spectroscopic strengths has accumulated /13/. This indicates that the Lane and Lynn /1/ theory of channel capture plays a major role in the interactions of thermal neutrons with nuclear matter in these mass regions. At this point let us review briefly the expression for direct capture and discuss its validity and limitations. The capture of an s-wave neutron with energy $E_n$ by a target nucleus of spin I to a final p orbit of spin $J_f$ and spectroscopic factor $S_{dp}$ is described by

$$\sigma_{\gamma f} = \frac{0.062}{RE_n^{1/2}} \left(\frac{Z}{A}\right)^2 \mu \frac{(2J_f + 1)}{6(2I + 1)} S_{dp} y_f^2$$

$$X \left[\frac{(y_f + 3) + (y_f - y_{fs})(y_f + 2)}{(y_f + 1)}\right]^2 , \qquad (9)$$

where

$$y_f^2 = R^2 k_f^2 = R^2 2mE_\gamma/\hbar^2,$$

$$y_{fs}^2 = a_{coh}^2 \; 2mE_\gamma/\hbar^2.$$

The interaction radius R is set equal to 1.35 $A^{1/3}$. It is assumed that for an odd target nucleus, there are equal contributions from channel spins I + 1/2 and I - 1/2. The variable $\mu$ takes into account the multiplicity due to the incident-neutron channel spin. For I=0, $\mu$=1; however, for a target nucleus with nonzero spin, I,

$$\mu = 1 \quad \text{for } J_f = I \pm 3/2,$$

$$\mu = 2 \quad \text{for } J_f = I \pm 1/2.$$

It is emphasized that the resonance contribution, due to compound nucleus formation is assumed to be negligible, i.e., positive and/or negative neutron energy resonances, are not located close to thermal energy. Note that for the cases where $\Gamma_{nj}/E_j \ll 1$, $a_{coh} = R'$. As a result, the partial direct capture cross section can be written as

$$\sigma_{\gamma f} = \frac{0.062}{R \; E_n} \left(\frac{Z}{A}\right)^2 \mu \frac{2J_f+1}{6(2I_t+1)} S_{dp} \left(\frac{y_f+3}{y_f+1}\right)^2 y_f^2$$

$$X \left[1 + \frac{R-R'}{R} \; y_f \frac{y_f+2}{y_f+3}\right]^2 \qquad (10)$$

The total direct capture corss section is a summation of terms carried out over final states, f.

$$\sigma_\gamma \text{ (direct)} = \sum_f \sigma_{\gamma f}$$

It is interesting to note the following features;

1) There is a strong variation of the direct capture cross section with mass number through the term (R-R')/R. This can be shown by examination of Fig. 5 where the scattering radius R' is plotted versus mass number. Note that two minima occur at mass numbers 40 and 142. The minimum at 142 is important for our purposes here since it represents a maximum in the fission product yield.

2) Since the direct capture cross section is directly proportional to the (d,p) spectroscopic strength, it will be enhanced for those nuclei near magic numbers, for example at mass numbers near A = 138.

At this stage, let us turn our attention to the verification of the theory by presenting two examples; $^{42}$Ca and $^{136}$Xe for which $\gamma$-ray spectra measurements have been carried out.

The results of the calculations for $^{42}$Ca via expression /10/ are summarized in Fig. 6. On the right-hand side are shown the calculations for each transition, while on the left-hand side are presented the experimental partial capture cross sections obtained with the aid of the relation $\sigma_\gamma = I_{\gamma f}\sigma_\gamma$. As indicated, there is very good agreement between the experimental and calculated values for each partial capture cross section and consequently for the summation of the partial capture cross sections.

The comparison between theory and experiment for the reaction $^{136}$Xe (n,$\gamma$) $^{137}$Xe is illustrated in Fig.7. Again very good agreement is observed between calculations and measurements.

In WRENDA 76/77, two requests (No. 428, 420) for the thermal capture cross sections $^{132}$Te(n,$\gamma$) $^{133}$Te and $^{126}$Sn(n,$\gamma$) $^{127}$Sn are noted for the object of calculations of fission product poisons. Both of these nuclides are radioactive with half lives of 78h and 12.4d, respectively. Because of the well known experimental difficulties of obtaining samples for these isotopes, such data is not readily available as yet. Since both of these nuclides are even-even and they are situated in the vicinity of the mass region where the p-wave strength function peaks, it is expected that s-wave resonances are not situated close to thermal energy. Because of these considerations, one can carry out the calculations in the framework of the Lane-Lynn theory on the assumption that the single particle (d,p) spectroscopic strengths in $^{132}$Te and $^{126}$Sn are the same as in $^{130}$Te and $^{124}$Sn for which experimental data are available. The results of the calculations are:

$^{132}Te(n,\gamma)\ ^{133}Te \qquad \sigma_\gamma = 0.135$ b,

$^{126}Sn(n,\gamma)\ ^{127}Te \qquad \sigma_\gamma = 0.120$ b

We emphasize that if low-lying resonances are located near thermal energies, these values then would represent a lower limit for the capture cross section.

## CONCLUSION

In summary, the s- and p-wave strength functions of FP nuclei in the mass region 85-150 were surveyed. Improvements in our knowledge of these quantities have resulted because of the extensive capture and transmission measurements carried out at ORELA and GEEL. It will be useful to carry out transmission measurements on enriched samples of the Ru isotopes in order to combine with the ORELA capture measurements /14/ for the purpose of determining the parity of the resonances and hence the average s- and p-wave radiative widths.

Finally, the Lane-Lynn capture theory was applied to the two fission product nuclides $^{126}Sn$ and $^{132}Te$;estimates of their thermal capture cross sections were derived.

## REFERENCES


1. A.M. Lane and J.E. Lynn, Nucl. Phys. 17, 563, 586 (1961).
2. S.F. Mughabghab, Phys. Lett. 81B, 93 (1979).
3. J.H. Gibbons, R.L. Macklin, P.D. Miller, and J.H. Neiler, Phys. Rev., 122, 182 (1961).
4. A.M. Lane and J.E. Lynn, Proc. Phys. Soc. (London) A70, 557 (1957).
5. M.S. Murty, K. Siddapa, J. Rama Rao, Nucl. Phys. A213, 35 (1973).
6. S.F. Mughabghab, R.E. Chrien, O.A. Wasson, G.W. Cole, and M.R. Bhat, Phys. Rev. Lett. 26, 1118 (1971).
7. R.E. Toohey and H.E. Jackson, Phys. Rev. C9,346 (1974).
8. S.F. Mughabghab, III International School on Neutron Physics, p.328, Alushta (1978).
9. H. Gruppelaar, Internal Report FSR-Gr-42, Petten (1976).
10. M.S. Moore, Neutron Physics and Nuclear Data, p. 313, Harwell, Sept. 1978.
11. D.F. Zaretskii and V.K. Sirotkin, Yad. Fiz, 27, 1534 (1978).
12. H. Malecky, L.B. Pikelner, I.M. Salamatin, and E.I. Sharapov, Yad. Fiz. 13, 240 (1971).
13. J. Kopecky and C. Plug, RCN-75-004 (1974).
14. R.L. Macklin and J. Halperin (private communication) (1979). (To be published in Nucl. Sci. Eng.)

Table I. Summary of the s- and p-Wave Strength Functions and Average Radiative Widths of Fission Product Nuclides in the Mass Region 85-147

| Isotope | Status | $S_0$ | $S_1$ | $\Gamma_{\gamma 0}$(eV) | $\Gamma_{\gamma 1}$(eV) |
|---|---|---|---|---|---|
| Rb-85 | b | 1.0 ± 0.4 | | 0.205 | |
| Rb-87 | b | 1.6 ± 0.9 | | | |
| Sr-86 | | | | | |
| Sr-87 | a | 0.30 ± 0.07 | | 0.310 | |
| Sr-88 | a | 0.45 ± 0.23 | 5.0 ± 0.8 | 0.225 | 0.720 |
| Y-89 | a | 0.27 ± 0.05 | 2.64 ± 0.03 | 0.130 | 0.300 |
| Zr-90 | a | 0.7 ± 0.2 | 4.0 ± 0.6 | 0.240 | 0.440 |
| Zr-91 | a | 0.36 ± 0.08 | 6.7 ± 1.3 | 0.140 | 0.240 |
| Zr-92 | a | 0.5 ± 0.1 | 7.0 ± 1.3 | 0.140 | 0.360 |
| Zr-94 | a | 0.50 ± 0.15 | 9.8 ± 2.0 | 0.130 | 0.185 |
| Zr-96 | a | 0.34 ± 0.14 | 6.0 ± 1.8 | | |
| Nb-93 | a | 0.89 ± 0.10 | 4.7 ± 1.0 | 0.160 | 0.200 |
| Mo-95 | a | 0.40 ± 0.06 | 4.0 ± 2.0 | 0.160 | 0.250 |
| Mo-96 | a | 0.5 ± 0.2 | | 0.110 | |
| Mo-97 | a | 0.29 ± 0.02 | | 0.140 | 0.180 |
| Mo-98 | a | 0.5 ± 0.1 | 7.3 ± 1.1 | 0.085 | 0.125 |
| Mo-100 | a | 0.7 ± 0.2 | 5.0 ± 1.1 | 0.088 | 0.098 |
| Tc-99 | a | 0.45 ± 0.05 | | | |
| Ru-99 | b | 0.72 ± 0.16 | | | |
| Ru-100 | a | | 6.5 ± 0.9* | | |
| Ru-101 | a | 0.59 ± 0.04* | 6.1 ± 0.4* | | |
| Ru-104 | a | | 5.0 ± 0.4* | | |
| Ru-106 | a | | 5.7 ± 0.9* | | |
| Rh-103 | a | 1.04 ± 0.13* | 7.9 ± 0.7* | | |
| Pd-105 | a | 0.60 ± 0.10* | 5.8 ± 0.6 | 0.145 | |
| Pd-106 | a | 0.50 ± 0.05* | 6.7 ± 0.6* | | |
| Pd-108 | a | 0.78 ± 0.17* | 5.9 ± 0.6* | | |
| Pd-110 | a | 0.40 ± 0.06* | 8.1 ± 0.9* | | |
| Ag-107 | b | 0.38 ± 0.07 | 3.8 ± 0.6 | 0.140 | |
| Ag-108 | b | 0.46 ± 0.15 | 3.8 ± 0.6 | 0.130 | |
| Cd-111 | b | 0.45 ± 0.06 | | | |
| Cd-112 | b | 0.58 ± 0.08 | | | |
| Cd-113 | b | 0.32 ± 0.07 | | | |
| Cd-114 | b | 0.54 ± 0.11 | | | |
| Cd-116 | b | 0.21 ± 0.06 | | | |
| In-115 | b | 0.26 ± 0.03 | 2.5 ± 0.5 | | |
| Sn-115 | b | | | | |
| Sn-117 | b | 0.19 ± 0.02 | 3.0 ± 1.6 | | |
| Sn-118 | b | 0.40 ± 0.15 | | | |
| Sn-119 | b | 0.08 ± 0.03 | 3.8 ± 1.5 | | |
| Sn-120 | a | 0.14 ± 0.02 | 2.1 ± 0.2 | | |
| Sn-122 | b | | | | |
| Sn-124 | b | | | | |
| Sb-121 | b | 0.29 ± 0.05 | 1.1 ± 0.10 | | |
| Sb-123 | b | 0.22 ± 0.07 | 2.0 ± 1.5 | | |
| Te-125 | b,c | 0.49 ± 0.10 | | | |
| Te-126 | b,c | 0.30 ± 0.10 | | | |
| Te-128 | b,c | 0.25 ± 0.15 | | | |
| Te-130 | b,c | 0.14 ± 0.05 | | | |

Table I. (cont.)

| Isotope | Status | $S_0$ | $S_1$ | $\Gamma_{\gamma 0}$(eV) | $\Gamma_{\gamma 1}$(eV) |
|---|---|---|---|---|---|
| I-127 | a | 0.76 ± 0.06 | | 0.090 | |
| Xe-129 | b,c | 1.0 ± 0.2 | | | |
| Xe-130 | b,c | 1.3 ± 0.5 | | | |
| Xe-131 | b,c | 0.70 ± 0.16 | | | |
| Xe-132 | b,c | | | | |
| Xe-134 | b,c | | | | |
| Xe-136 | b,c | | | | |
| Cs-133 | a | 0.70 ± 0.08 | | 0.120 | |
| Cs-134 | d | | | | |
| Ba-135 | a | 0.39 ± 0.07 | | 0.141 | |
| Ba-136 | a | 1.2 ± 0.5 | | 0.126 | |
| Ba-137 | a | 1.4 ± 0.4 | | 0.084 | |
| Ba-138 | a | 2.0 ± 0.5 | | 0.108 | |
| La-139 | b | 0.75 ± 0.11 | | 0.060 | |
| Ce-140 | b | 1.1 ± 0.2 | 0.34 ± 0.05 | | |
| Ce-142 | a | | | | |
| Pr-141 | b | 1.5 ± 0.2 | | 0.086 | |
| Nd-143 | a | 3.3 ± 0.4 | | 0.081 | |
| Nd-144 | a | 4.4 ± 1.0 | | 0.055 | |
| Nd-145 | a | 4.0 ± 0.4 | | 0.075 | |
| Nd-146 | a | 2.3 ± 0.5 | | 0.054 | |
| Nd-148 | a | 3.1 ± 0.5 | 0.3 ± 0.1 | 0.051 | |
| Nd-150 | a | 2.9 ± 0.3 | | 0.067 | |

(a) Resonance parameter data available after 1973.
(b) Measurements have not been carried out after 1973.
(c) Recent measurements carried out but results are unavailable.
(d) Recent results of 7 resonances available for this radioactive isotope.

* Results derived from average cross section data.

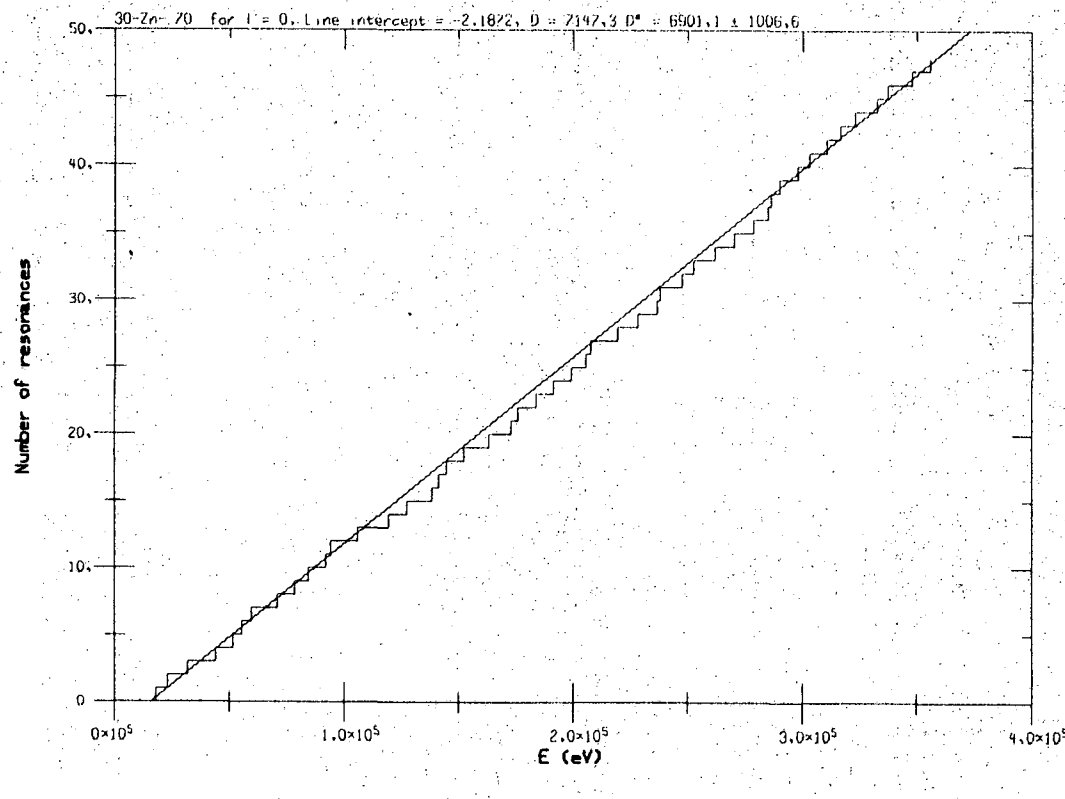


Fig. 1 Cumulative number of s-wave resonances of $^{70}Zn$ as a function of neutron energy. The data are based on measurements by Garg et al. (private communication).

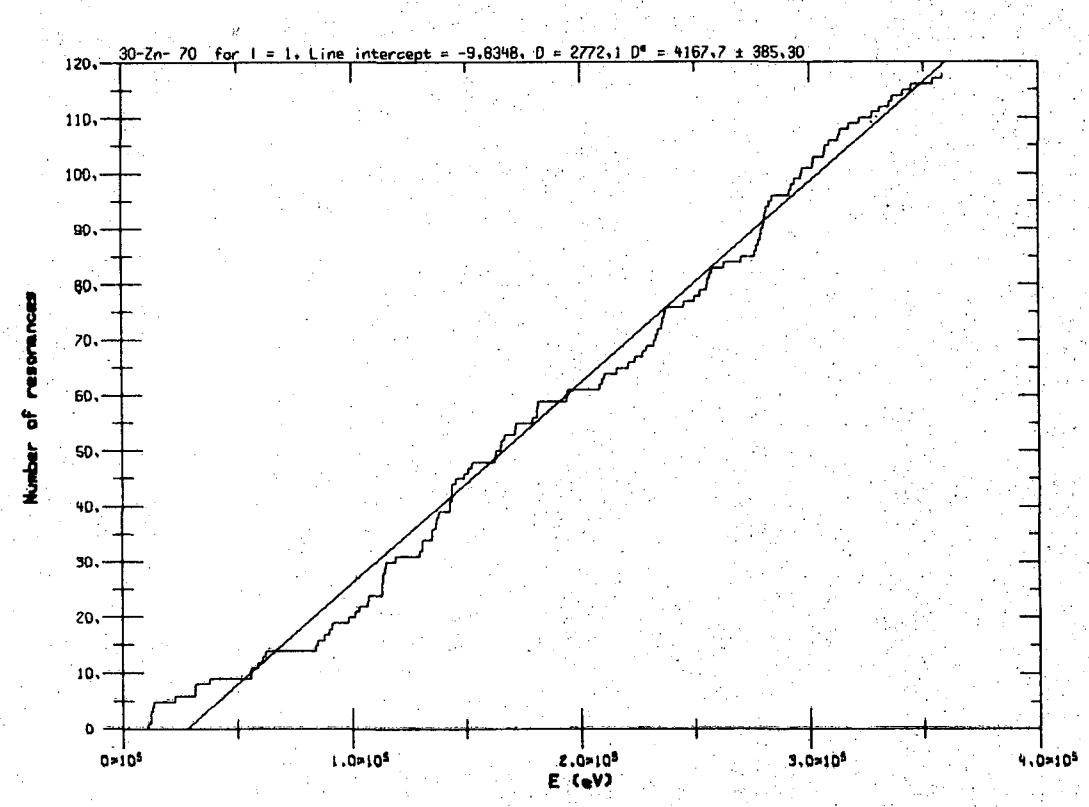


Fig. 2 Cumulative number of p-wave resonances of $^{70}Zn$ as a function of neutron energy. The data are based on measurements by Garg et al. (private communication).

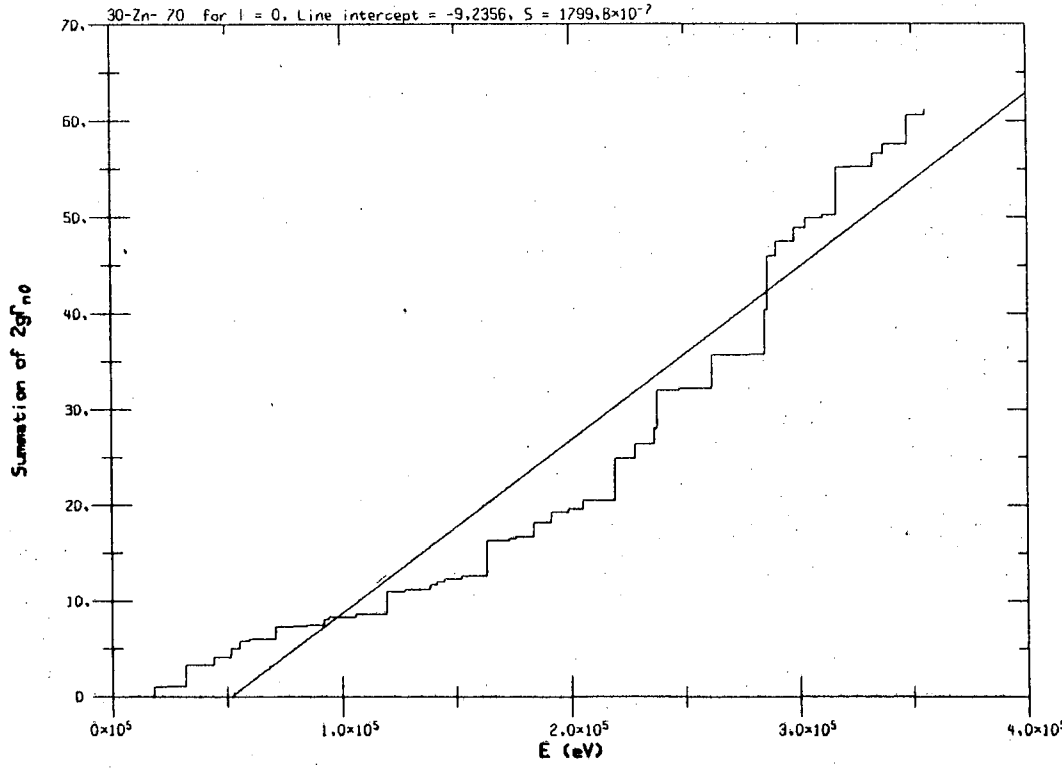


Fig. 3 Staircase plot of the s-wave reduced neutron widths of $^{70}Zn$ versus neutron energy. From such plots the s-wave neutron strength function is deduced.

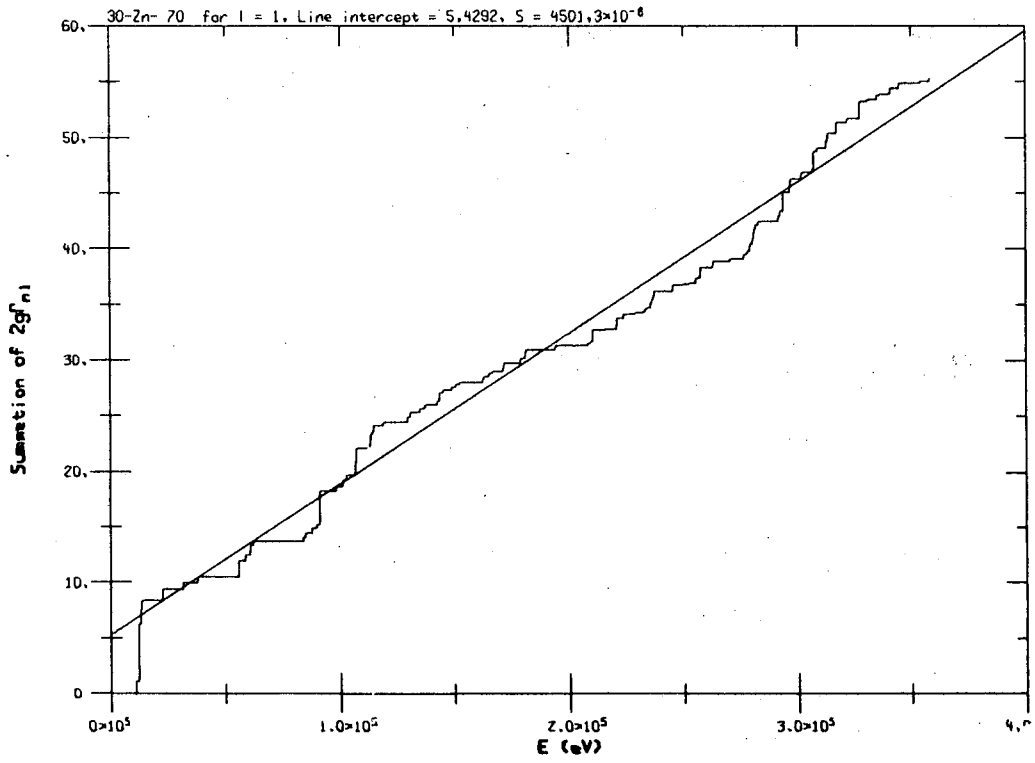


Fig. 4 Staircase plot of the p-wave reduced neutron widths of $^{70}Zn$ versus neutron energy.

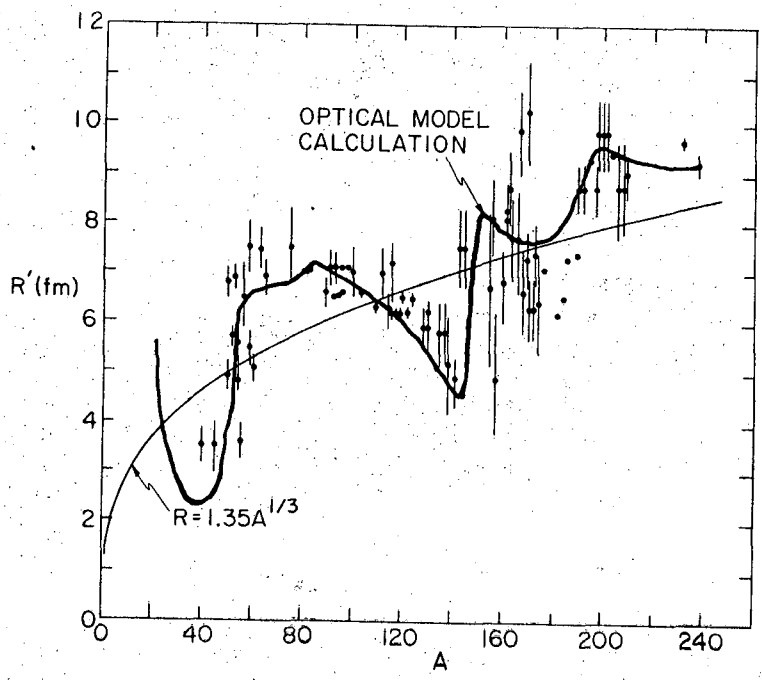


Fig. 5 Variation of the scattering radius as a function of mass number. Note the deep minima at mass numbers 40 and 140. The solid curve passing through the points is an optical model calculation.

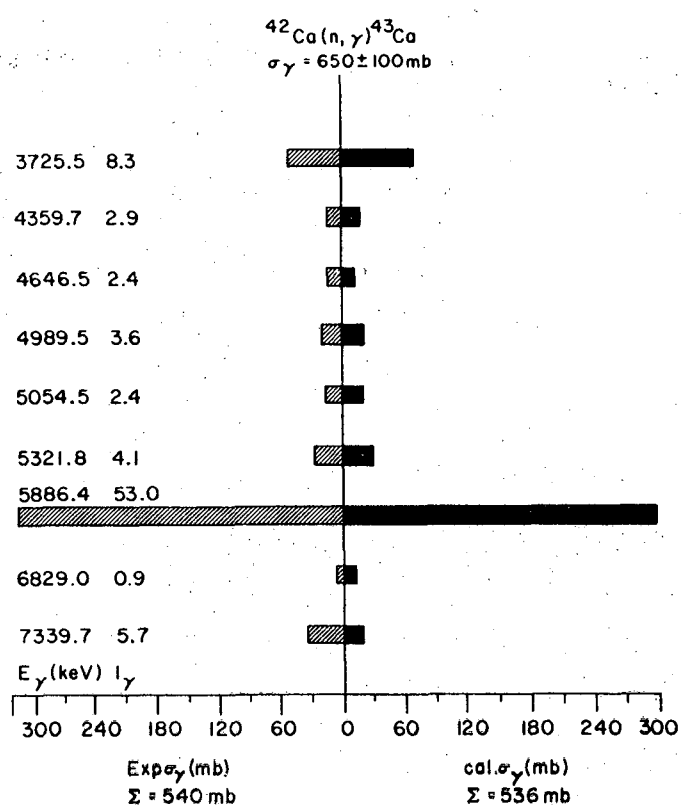


Fig. 6 Comparison of partial capture cross sections with the Lane-Lynn predictions for $^{42}Ca(n,\gamma)\ ^{43}Ca$.

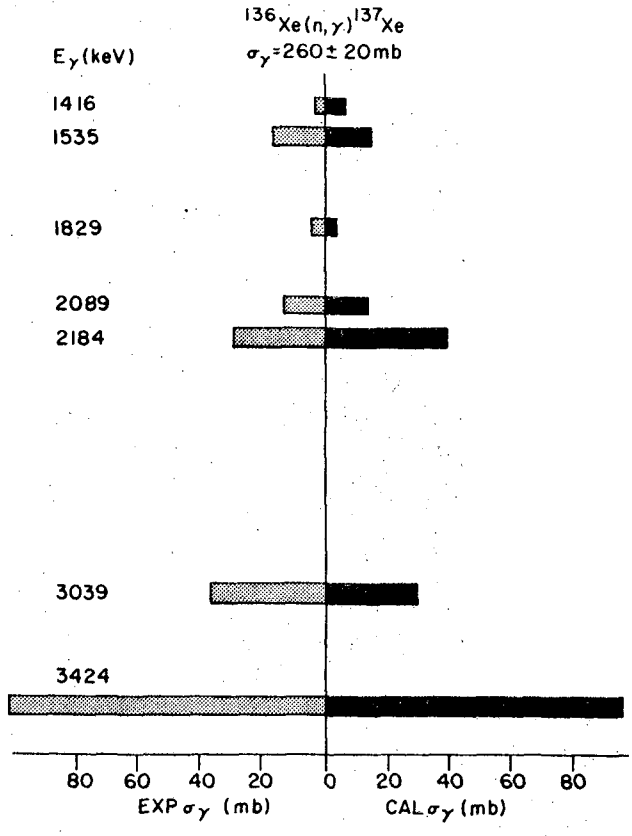


Fig. 7 Comparison of measured and calculated partial cross sections for $^{136}Xe$ $(n,\gamma)$ $^{137}Xe$.

NEANDC SPECIALISTS' MEETING ON NEUTRON
CROSS SECTIONS OF FISSION PRODUCT NUCLEI
(Bologna, Dec. 12-14, 1979)

# Phenomenological and Theoretical Basis for the Parameterization of Nuclear Models Used in Reactor Data Evaluation.

(G. Reffo)
Centro Ricerche "E.Clementel",CNEN
Via Mazzini,2 - 40138 Bologna-Italia

The problem of the parameterization of the various models involved in reactor nuclear data evaluation is reviewed from the practical application view point.
Procedures are discussed for extraction of parameters from available experimental quantities.
Parameter systematics have been determined which lend themselves to interpolations where experimental information is not available.

(oral presentation only)

# EVALUATION OF AVERAGE LEVEL SPACING AND S-WAVE STRENGTH FUNCTION PERFORMED FOR MORE THAN 240 NUCLEI

G. Rohr, L. Maisano* and R. Shelley
CEC, JRC, Central Bureau for Nuclear Measurements
B.2440 - Geel, Belgium

A method to evaluate the level spacing obtained from resonances at neutron separation energy is developed which is simple, experimentally orientated and incorporates very few assumptions for the resonance data. It separates large s-wave resonances from all other resonances by means of the Bayes' theorem. The number of small s-wave resonances lost in this procedure is estimated assuming a Porter Thomas distribution for the reduced widths. With small modifications, depending on the number of resonances available and on the p-wave to s-wave strength function ratio, this method has been applied to more than 240 nuclei. The uncertainty of the method is determined using a large number of different resonance parameter data sets produced in a statistical fashion using Porter Thomas and Wigner distributions for the widths and level spacings respectively. The method is applied to an intermediate structure (indicated by strong energy dependence of the strength function) with resonance data from $^{177}$Hf.

## Introduction.

The level density is the most important quantity used to describe highly excited nuclei at excitation energies where the statistical average of nuclear properties become important. That holds beyond the neutron separation energy for nuclei $A > 40$ where the cross section formula, based on statistical nuclear models, depends directly on the level spacing D and other average values such as the strength functions and the total radiative widths, which also depend on D. Furthermore the pairing energy and shell effects can be studied at high excitation energy and the level spacing of single particle states at Fermi surface energy can be determined by means of the level density obtained in the resonance region /1/.

Below the separation energy for low excitations the microscopic properties of the individual levels themselves have been used extensively to study nuclear properties and have served as tests for microscopic nuclear models. However at higher excitation energies the number of excited bound levels increases and can also be considered as a statistical set of levels.

In general three methods can be distinguished to measure the level density; they are listed as follows with increasing excitation energy: counting of bound states, measuring resolved neutron resonances at neutron separation energy and measuring evaporation spectra.

---

* Euratom boursier

The only method which is suited to evaluate the level spacing for almost all stable target nuclei is the measurement of resolved resonances. In this case the number of individual levels is high enough for nuclei with $A > 20$. One can extract a clean set of resonances with definite spin and parity and the energy shift of states towards lower excitation energies due to collective excitations and pairing energy is small compared to the neutron separation energy. On the other hand, due to the interest of applied nuclear physics (reactor technology) in this energy region, there exists an enormous amount of data for nearly all stable nuclei.

Based on this data, we develope a method to determine the s-wave level density and we obtain the s-wave strength function as a by-product. The level density will be used to study nuclear correlations and single particle effects by means of the newly developed level density systematics /1/.

A simple method to evaluate D.

The determination of the average level spacing D at neutron separation energy is, in principle, quite simple; it requires only the neutron resonance energies. D is then calculated from the number of resonances N in a given energy range $\Delta E$ by $D = \Delta E/N$, but the determination is complicated mainly by two facts:

1) The finite resolution of the neutron spectrometer results in a loss of small resonances.
2) The neutron has a spin $i = 1/2$ and may carry an angular momentum ($\ell$). If the target nucleus has a spin $I \neq 0$ then the total angular momentum J is a combination of three angular momenta, which leads to neutron resonances with different total spin and angular momentum. Introducing the channel spin $\vec{S} = \vec{I} + \vec{i}$, then J can take all values which are obtained by vectorially combining S and $\ell$;

$$\vec{J} = \vec{S} + \vec{\ell} .$$

The spin determination of resonances is often not performed (or sometimes not possible) and only the $g\Gamma_n$, which is proportional to the area below the resonance, can be determined. Therefore we define the level spacing and the strength function per compound spin state and use the definition of the spin independent strength function

$$S(\ell) = \frac{1}{2\ell+1} \cdot \frac{\sum_{\lambda=1}^{N} g\Gamma_{n\lambda}^{(\ell)}}{\Delta E} \qquad (1)$$

with the reduced neutron width given by

$$\Gamma_n^{(\ell)} = \Gamma_{n\ell}/[\, v(\ell) \cdot \sqrt{\frac{E(eV)}{1(eV)}}\, ] \qquad (2)$$

where $v(\ell)$ is the probability of a neutron to pass through the centrifugal barrier.
The denominator describes the energy dependence of the average neutron width $< \Gamma_{n\ell} >$ and ensures that the reduced average width $< \Gamma_n^{\ell} >$ in (2) and the strength functions in (1) are independent from energy.

The angular momentum of resonances has been assigned by experimental methods /2/ in only a few cases. Statistical considerations, sometimes used to assign p-wave resonances and determine missed levels, such as the $\Delta_3$- and F-statistics based on Deyson-Metha theory will not be used (so as to keep the evaluation procedure tangable). A possibility for separating large s-wave

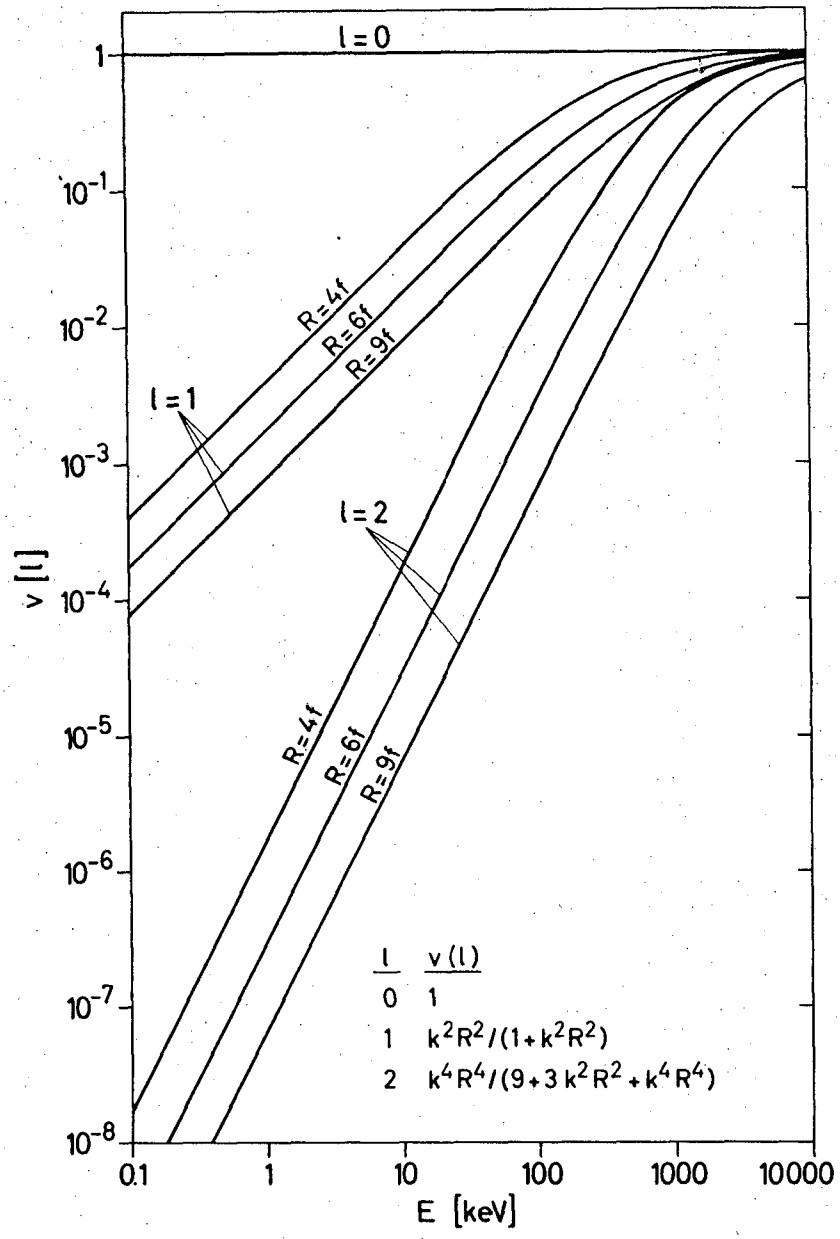


FIG. 1 : The probability $v(\ell)$ of a neutron to pass through the centrifugal barrier plotted against neutron energy for different radii and angular momenta.

resonances from small ones and resonances with $\ell \geqslant 1$ is offered by the different energy behaviour of $v(\ell)$ which is plotted in Figure 1 for three different nuclear radii and angular momenta. Below 100 KeV neutron energy this value for s-wave resonances is much larger than for p-wave resonances; the same holds for the average neutron widths (see (2)). Assuming that both populations, s- and p-wave resonances, obey the Porter Thomas distribution for the neutron widths we can calculate the probabilities:

$$p_s \; d(g\Gamma_n) = \frac{1}{\sqrt{2\pi x_s}} \cdot \exp(-x_s/2)\; dx_s \qquad x_s = g\Gamma_n / \langle g\Gamma_{no} \rangle$$

and (3)

$$p_p \; d(g\Gamma_n) = \frac{1}{\sqrt{2\pi x_p}} \cdot \exp(-x_p/2)\; dx_p \qquad x_p = g\Gamma_n / \langle g\Gamma_{n1} \rangle$$

for an observed value $g\Gamma_n$ in the interval $d(g\Gamma_n)$. The probability of a resonance with a given $g\Gamma_n$ being a p-wave resonance can be determined using the Bayes' theorem /3/

$$P(p,g\Gamma_n) = \frac{\pi_p \cdot p_p}{\pi_s \cdot p_s + \pi_p \cdot p_p}$$

where $\pi_s$ and $\pi_p$ are the 'a priory' probabilities that the resonance is excited by an s and a p-wave respectively.

Re-writing we get

$$P(p,g\Gamma_n) = (1 + \frac{\pi_s}{\pi_p} (\frac{p_s}{p_p}))^{-1} \qquad (4)$$

where the ratio $\pi_s/\pi_p$, which is the same as $D_{\ell=o}/D_{\ell=1}$, depends on the spin of the target nucleus I.
Assuming that the level density $\rho_J = 1/D_J$ is proportional to (2J + 1) independent of the parity then the ratio $\pi_s/\pi_p$ = 1/3, 4/9 and 1/2 for I = 0, 1/2, and $\geqslant$ 1 respectively.

From (3) and (4) we obtain:

$$P(p,g\Gamma_n) = \left\{ 1 + \frac{\pi_s}{\pi_p} \left( \frac{\langle g\Gamma_{no}\rangle}{\langle g\Gamma_{n1}\rangle} \right)^{1/2} \cdot \exp\left[ \frac{1}{2} \frac{(g\Gamma_n)}{\langle g\Gamma_{n1}\rangle} - \frac{1}{2} \frac{(g\Gamma_n)}{\langle g\Gamma_{no}\rangle} \right] \right\}^{-1} \qquad (5)$$

The separation function is finally obtained taking $P(p,g\Gamma_n)$ = const and solving (5) for $g\Gamma_n$, which we call $(g\Gamma_n)_{bias}$.

In our Fortran programme this value is calculated for each resonance (N) at its energy $E_o$ and the reduced widths are fitted by the following function:

$$\delta(E) = \frac{(g\Gamma_n)_{bias}}{\sqrt{E(eV)}} = a \cdot E^b$$

where the parameters a and b are obtained by a linear least square method. All resonances with $g\Gamma^o_n > \delta(E_o)$ are selected as large s-wave. This number of resonances $N_{bias}$ depends mainly on the probability P (normally ~ $10^{-3}$) and the p-wave strength function $(S_1)_{bias}$. However to determine the correct (best suited) energy dependence of $\delta(E)$, preliminary values of D and $S_o$ are also needed.

The $\delta(E)$ we consider as a suitable tool, producing a clean set of large s-wave resonances. The main part of the procedure to evaluate the level spacing consists of a missed level routine, which estimates in an iterative way the number of small resonances which have been lost using the bias function /4/.

The final results depend on the following assumptions:

1) The s-wave resonances obey a Porter Thomas distribution in $g\Gamma^o_n$.
2) The average reduced width $\langle g\Gamma^o_n\rangle_J$ is independent of the spin J.
3) The resonance parameter consists of a statistical set of resonance data.

Results.

Resonance parameters have been compiled up to the end of 1971 in the BNL 325, and are available on magnetic tape /2/. This data has formed the basis of our evaluation although more recently published data have been included.

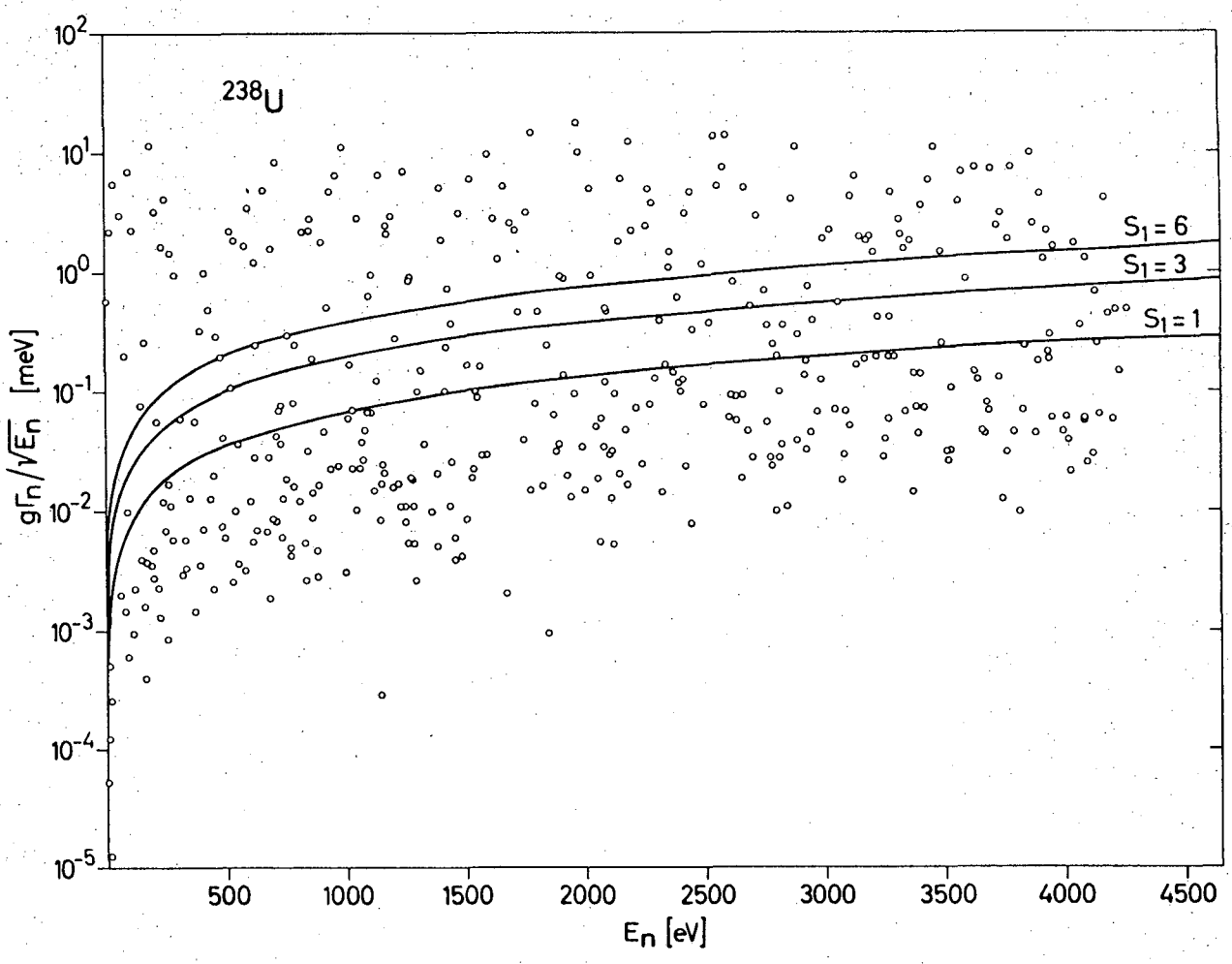


FIG. 2 : The reduced neutron widths plotted against neutron energy. The $S_1$ values correspond to those of $(S_1)_{bias}$ in the text.

The method described has been used for nuclei in the mass region $40 < A < 250$ with a few exceptions, namely for nuclei with $A \approx 100$ where the ratio $S_0/S_1$ is too small and for nuclei at closed shells. Normally we have started the procedure with $P = 10^{-3}$ and three different $(S_1)_{bias}$ values at once ($S_1/3$, $S_1$, and $2 \cdot S_1$ ; $S_1$ taken from optical model calculation /2/), in order to check whether the results are influenced by p-wave resonances.

The results of the procedure gives three D-values, which have been taken as final results if all three do not differ. In cases where the D-values had the tendency to become smaller for a lower bias, a new trio of bias values have been added.

In Figure 2 the reduced neutron width for

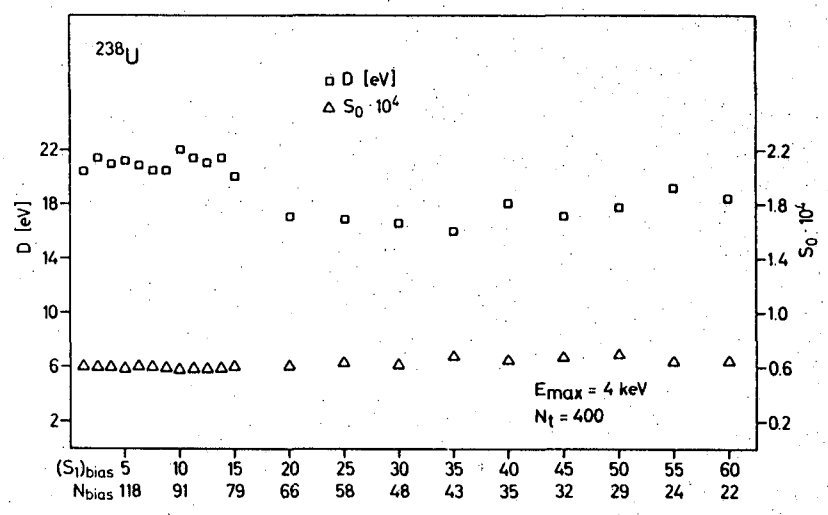


FIG. 3 : Level spacing D and strength function $S_0$ calculated for different bias values.

$^{238}U$ resonances is plotted against the neutron energy /5/. The influence of the bias on the results are shown in Figure 3.

The data of a low resolution measurement (low sensitivity) are shown in Figure 4 using Pa as an example. Here the $(S_1)_{bias}$ has to be increased to $36 \cdot 10^{-4}$, to discard a few resonances spread over the whole energy range, in order to ensure that no resonances are lost above the bias function $\delta$.

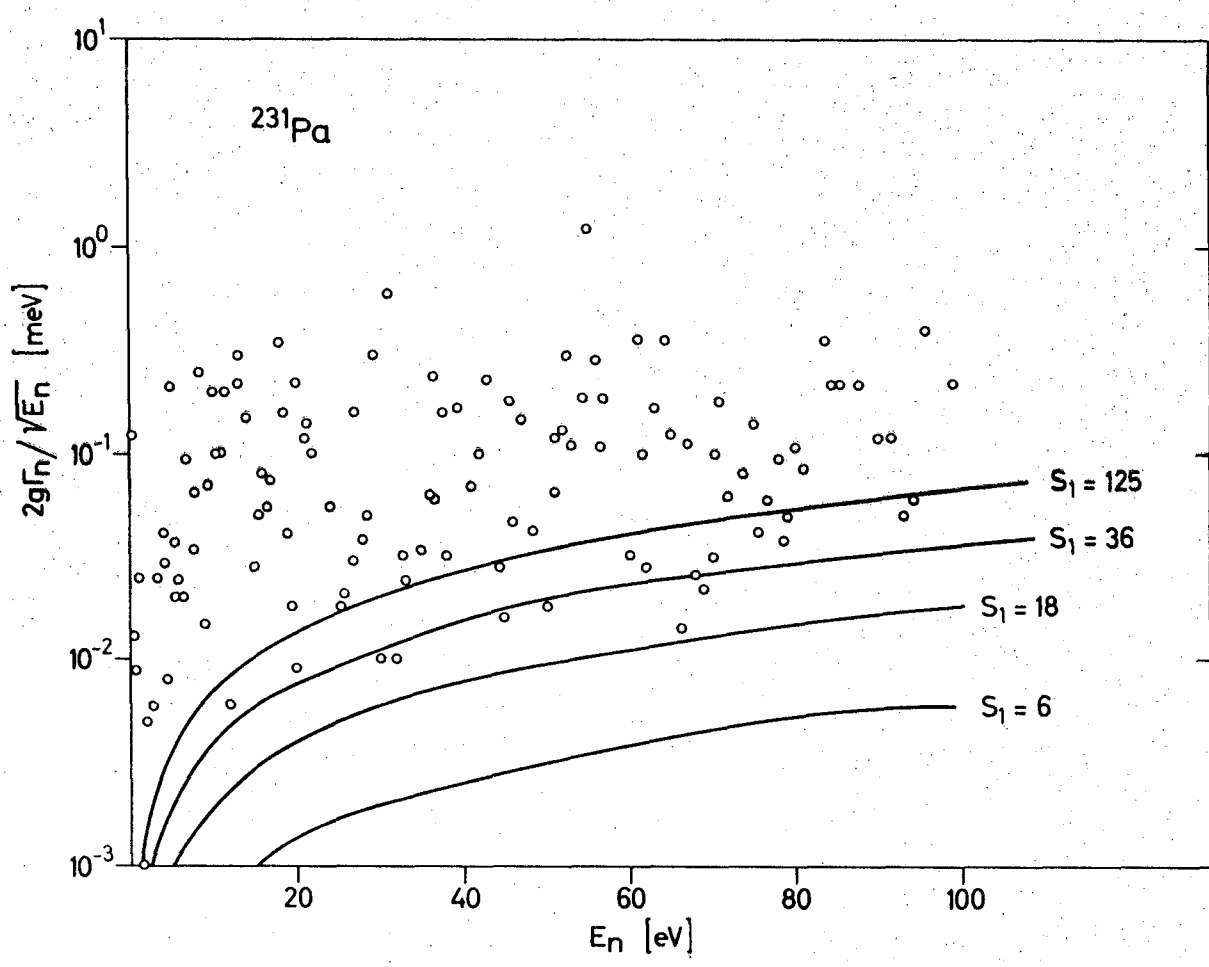


FIG. 4 : See caption Fig. 2.

The $^{56}Fe$ resonance data, angular momentum included, are shown in Figure 5 /6/. This example demonstrates the limitations of the method above 500 keV where a separation of large s-wave resonances is not possible.

The same holds for $^{93}Nb$ resonances which are shown in Figure 6 /7/. In this case where the parity of resonances is known from experimental work, only s-wave resonances have been used together with the missed level procedure to determine D and $S_0$.

The level spacing of closed shell nuclei and nuclei in the mass region $20 < A < 40$ have been determined directly by counting resonances with $\ell = 0$ and/or $\ell = 1$, using the assumption that $\rho_J \propto 2J + 1$ to determine the number of spin states.

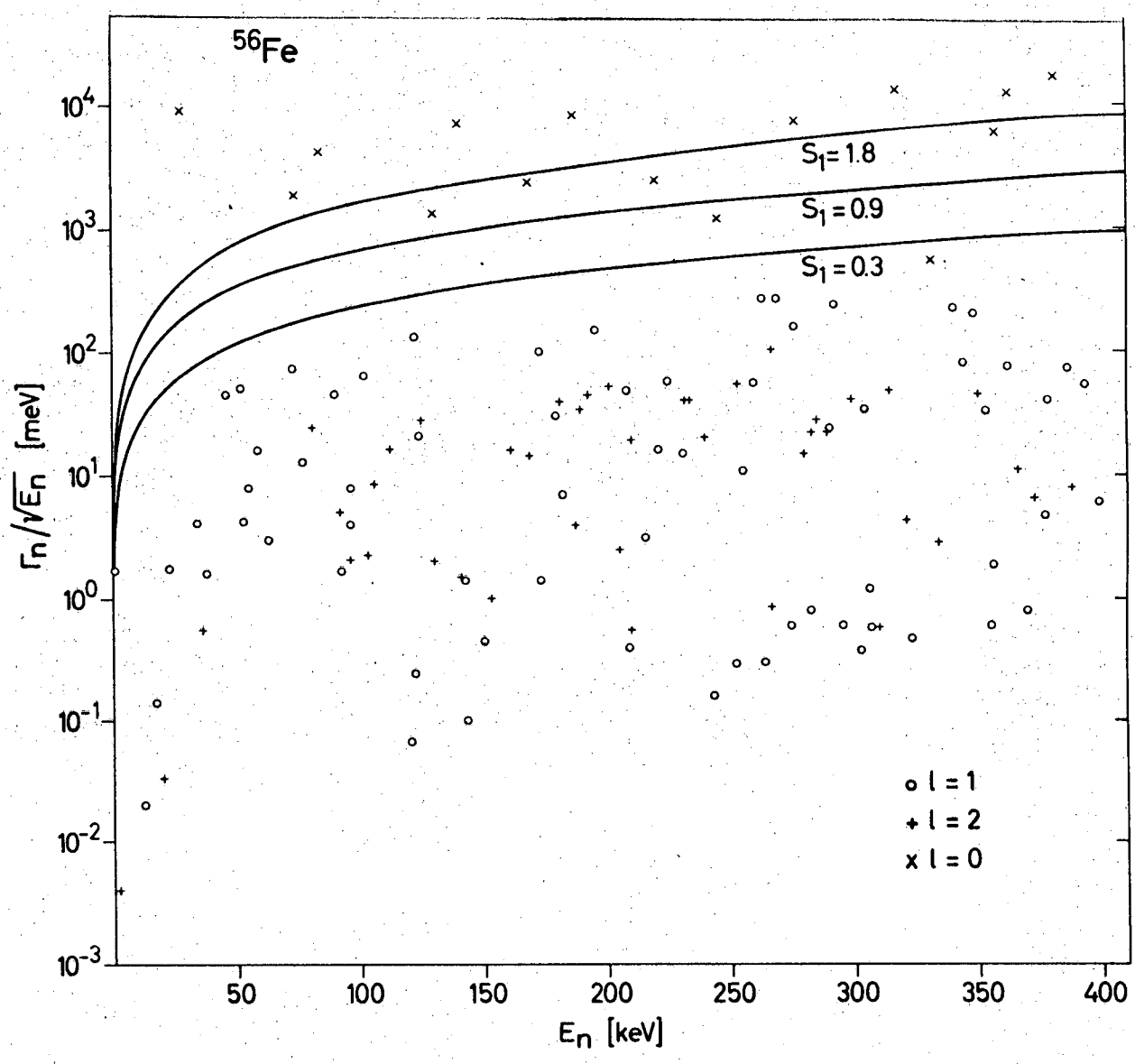


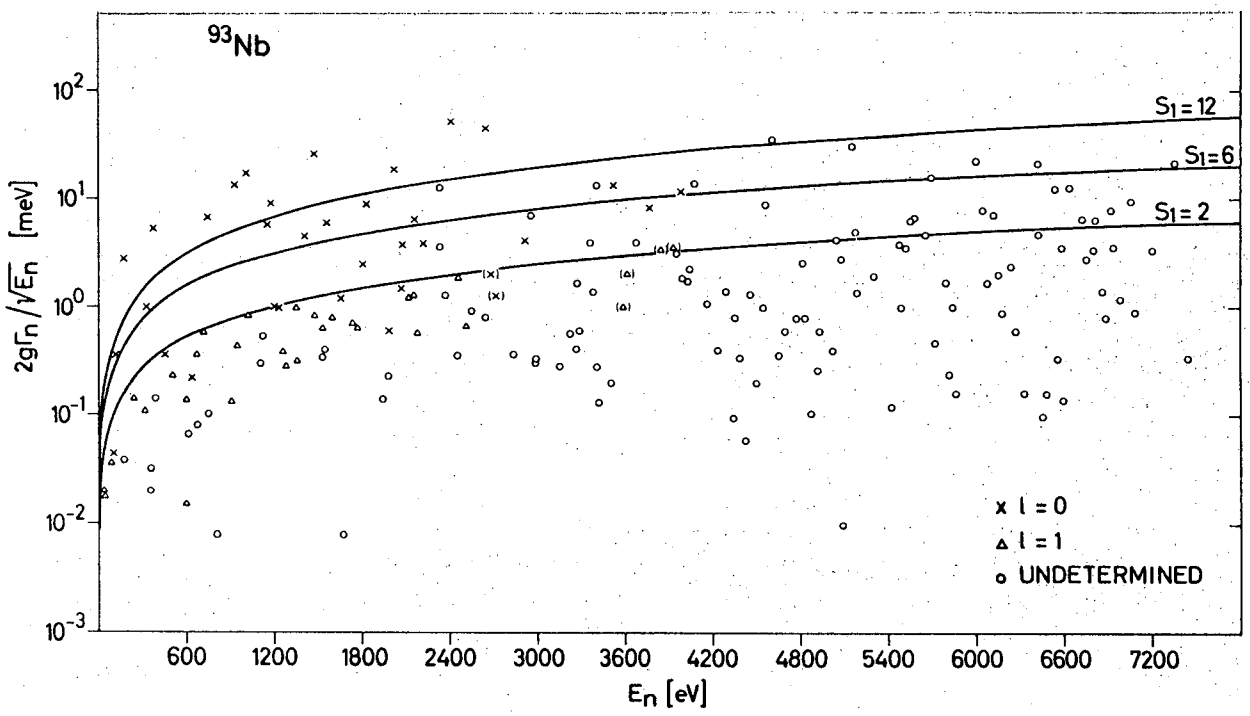


FIG. 5 (UPPER) and FIG. 6 (LOWER): See caption Fig. 2.

A missed level procedure has not been used for these nuclei since the resonances at neutron separation energy are doorway-resonances and it is very questionable that these resonances obey a Porter Thomas distribution.

In total more than 240 nuclei have been analysed covering the atomic weight range $20 < A < 200$. The level spacing results will be used in the contribution to this meeting titled 'The level density systematics applied to fission product nuclei'.

Uncertainty of the method.

In a recent paper /8/, where we have used the same method to determine the average resonance parameters for structural materials, the uncertainty of the final average parameters has been estimated by changing $(S_1)_{bias}$ in the limits $S_1/3 \leqslant S_1 \leqslant 2S_1$.

Here the uncertainty will be determined using resonance parameter sets for s- and p-wave resonances generated from level spacing and width parameters chosen randomly from Wigner and Porter Thomas distributions. Average resonance parameters similar to the $^{238}U$ data ($D = 22.4$ eV, $S_0 = 10^{-4}$, $S_1 = 2.5 \times 10^{-4}$, $R = 9.4 \times 10^{-13}$ cm) were taken in order to cover a large range of $N_{bias}$ values. This was done by using different values of $(S_1)_{bias}$ and $E_{max}$ the maximum resonance energy. For each case 10000 resonance data sets have been generated yielding a distribution of $N_{bias}$ values. For the most probable $N_{bias}$ value, where we have actually less than 10 % of the total number of sets, we describe the distribution of D and S.

The level spacing distribution is almost symmetric, its peak corresponds to $D = 22.4$ eV, and the half width at half maximum is plotted in Figure 7 against $N_{bias}$ for the two ratios $(S_1)_{bias}/S_1 = 1$ and 3. For a very high bias value the peak of the D-distribution $D_{av}$ is shifted to smaller values. The correction factor $22.4/D_{av}$ is about 1.2 for $(S_1)_{bias}/S_1 = 40$ and is considerable smaller than the $\delta D/D$ (%) which is plotted in Figure 8.

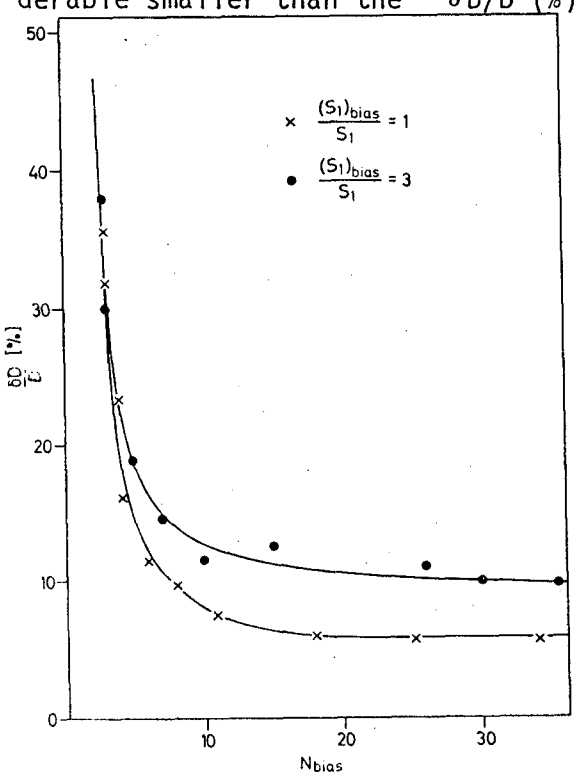


FIG. 7 : Percentage level spacing uncertainty against $N_{bias}$

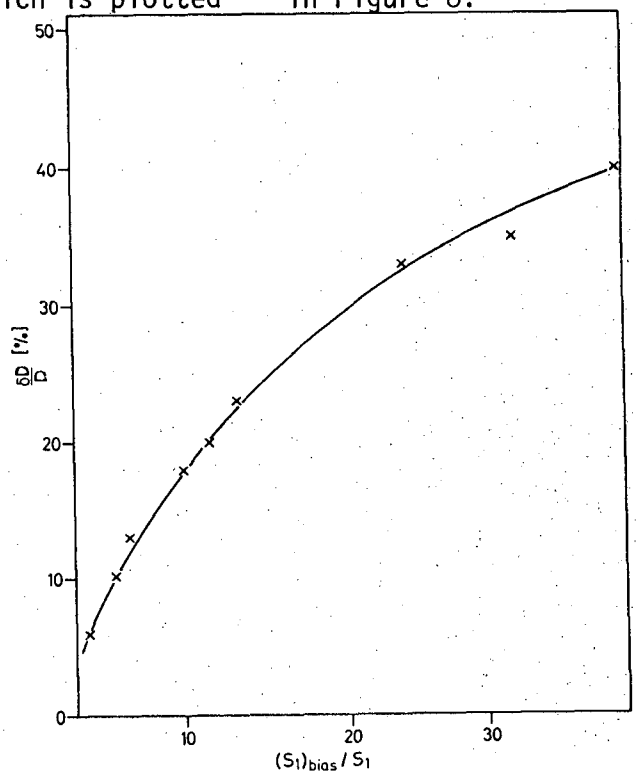


FIG. 8 : Percentage level spacing uncertainty against ratio $(S_1)_{bias}/S_1$

It is intended to check whether the uncertainty also depends on the strength function ratio $S_0/S_1$, with which the resonance set has been determined.

## Application to intermediate structure

Cross section measurements often show deviations from the statistically distributed resonance parameters, indicated by a strong energy dependence of the strength function, which are interpreted as intermediate structure. As an example the $^{177}$Hf-data are shown in Figure 9, where the strength function in the energy range 0-100 eV is a factor of three larger than that in the range 100-300 eV for J = 4 resonances /9/.
For resonances with J = 3 no change of the strength function in the energy range 0-300 eV is observed.

Our method of determining D has been applied in two ways for each spin. In the first case we take all resonances from 0-300 eV and in the second we have divided the range in three parts and applied the procedure separately to each interval.

Using $(S_1)_{bias} = 30 \cdot 10^{-4}$ and $P = 10^{-3}$ we calculate $N = \Delta E/D$ and obtain the values collected in Table I.

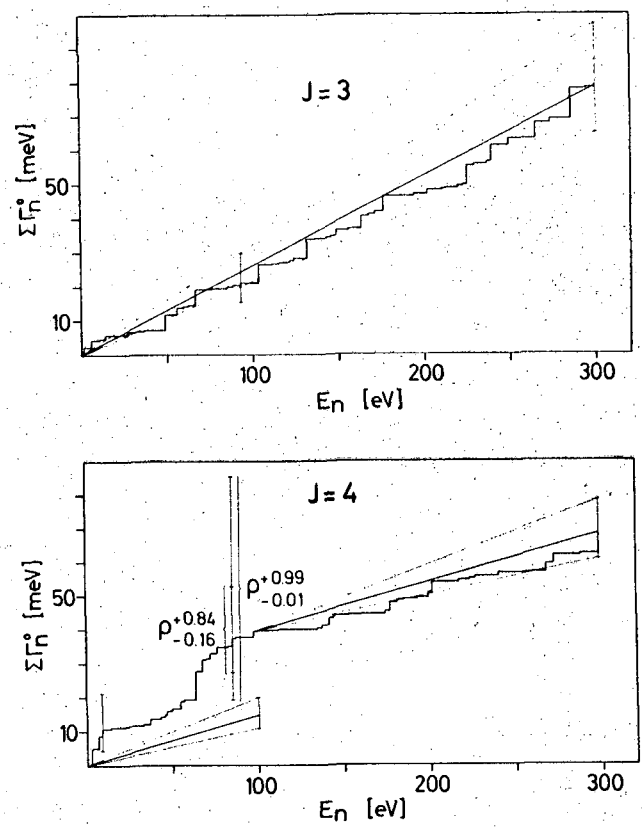


FIG. 9 : Cumulative sum of reduced neutron widths as a function of energy for $^{177}$Hf resonances.

TABLE I.

| J | | 0-300 | 0-100 | 100-200 | 200-300 | 0-300 |
|---|---|---|---|---|---|---|
| $3^+$ | $N_{Bias}$ | 48 | 19 | 15 | 14 | 48 |
| | missed levels | 13 | 4 | 5 | 4 | 13 |
| | $N_{Total}$ | 61 | 23 | 20 | 18 | 61 |
| | | == | | | | == |
| $4^+$ | $N_{Bias}$ | 43 | 22 | 12 | 9 | 43 |
| | missed levels | 13 | 4 | 7 | 5 | 16 |
| | $N_{Total}$ | 56 | 26 | 19 | 14 | 59 |
| | | == | | | | == |

The total number of resonances $N_{tot}$ = 61 is the same for the two ways for J = 3 resonances; but for J = 4 we get $N_{tot}$ = 56 taking all resonances at once and $N_{tot}$ = 59 dividing the range into 3 intervals.

The last value is increased by 5% towards the value for J = 3 resonances, which we would expect for a spin cut off factor of $\sigma = 4$ ($N_{J=3} \sim N_{J=4}$). There is an indication that the level spacing D evaluated in intermediate structure can be improved by dividing the energy range into regions where the strength function is almost constant.

References.

/1/ G. Rohr, L. Maisano and R. Shelley, contribution to this meeting.

/2/ S.F. Mughabghab and D.I. Garber, BNL 325 Neutron Cross Sections Vol. I, Third Edition 1973.

/3/ L.M. Bollinger and G.E. Thomas, Phys. Rev. 171 (1968) 1293.

/4/ T. Fuketa and J.A. Harvey, Nucl. Instr. Meth. 33 (1965) 107.

/5/ F. Poortmans et al., 4th Int. Conf. on Nuclear Physics, Kiev, 1977, to be published.

/6/ F.G. Perey, G.T. Chapman, W.E. Kinney and C.M. Perey, Neutron Data of Structural Materials for Fast Reactors. GEEL/Belgium (1977) p. 530.

/7/ J. Winter et al., Int. Conf. on Neutron Physics and Nuclear Data for Reactors and other applied purposes, Harwell, 1978, p. 696

/8/ G. Rohr, Neutron Data of Structural Materials for Fast Reactors. GEEL/Belgium (1977) p. 614.

/9/ G. Rohr and H. Weigmann, Nucl. Phys. A264 (1976) 93.

Acknowledgments.

The authors wish to thank Dr. C. Bastian and Mr. C. Cervini of CBNM for their help in making the large amount of data available from the B.N.L. magnetic tape library.

# THE LEVEL DENSITY SYSTEMATICS APPLIED TO FISSION PRODUCT NUCLEI

G. Rohr, L. Maisano* and R. Shelley
CEC-Joint Research Centre, Central Bureau for Nuclear Measurements
CEC-JRC, Central Bureau for Nuclear Measurements, Steenweg op Retie,
B-2440 GEEL, Belgium

A level density systematics based on the newly evaluated level spacing obtained at CBNM, Geel for more than 240 nuclei will be interpreted as proposed at the Harwell Conference 1978. The deviation of the level density parameter $a$ from a linear dependence on the atomic number A, indicates two types of structures :

1) the usual shell effects with "dips and bumps" at specific N and Z values, reflecting changes of the level density of single particle states at Fermi energy.
2) distinct steps (three in total) of the level density parameter $a$ at certain A values, which can be explained by the addition of two extra quasi particles participating in the excitation process of the compound nucleus, at each step.

The lines in between successive structures are defined by using odd-odd compound nuclei, where no pairing energy is expected. Based on this interpretation of the level density systematics (S) the following aspects are being considered : influence of the spin cut off factor on S, determination of pairing energy $\Delta$, possibility of adjusting Nilsson single particle states.

## Introduction

This contribution is concerned with the intermediate (or weak) coupling compound model which treats the excitation of a compound nucleus in steps produced by successive collisions of two nucleons. Throughout this paper the term 'doorway states' will refer to the excited state corresponding to the first of these steps.

The interpretation of the level density systematics as proposed in ref./1/ is performed with two sets of level density data:

1) An evaluation of the level density of compound resonances observed at neutron separation energy, based on one procedure used for nearly all nuclei in the atomic mass range $20 < A < 250$ /2/
2) The level density of doorway states calculated at neutron separation energy for more than 200 nuclei spread over nearly the whole atomic weight range, based on the single particle shell model including the pairing force/1,3/.

The results for the doorway level density and the experimentally determined level density of the compound states have been reduced to the level density parameter $a$ at excitation energy $U = E_S + E_{max}/2$ by means of the Fermi

* Euratom boursier

gas level density expression[4] :

$$\rho(U,J) = \frac{1}{24\sqrt{2}} \cdot \frac{2J+1}{\sigma^3 \cdot a^{1/4}} \cdot \frac{\exp\left[2(a(U-\Delta))^{1/2} - J(J+1)/2\sigma^2\right]}{(U-\Delta)^{5/4}} \qquad (1)$$

where $E_B$ is the binding energy of the neutron and $E_{max}$ the largest energy of a neutron resonance used in the evaluation. The parameters in expression (1) are :

| | |
|---|---|
| spin of the compound resonance | $J$ |
| spin cut off factor | $\sigma = \sqrt{(0.0888 \cdot a \cdot t \cdot A^{2/3})}$ |
| nuclear temperature | $t = \sqrt{(U-\Delta)/a}$ |
| pairing energy | $\Delta$ taken from [4] |

The level density parameter $a$ is proportional to the level density of single particle states at Fermi surface energy $g_0 = a\,(6/\pi^2)$.

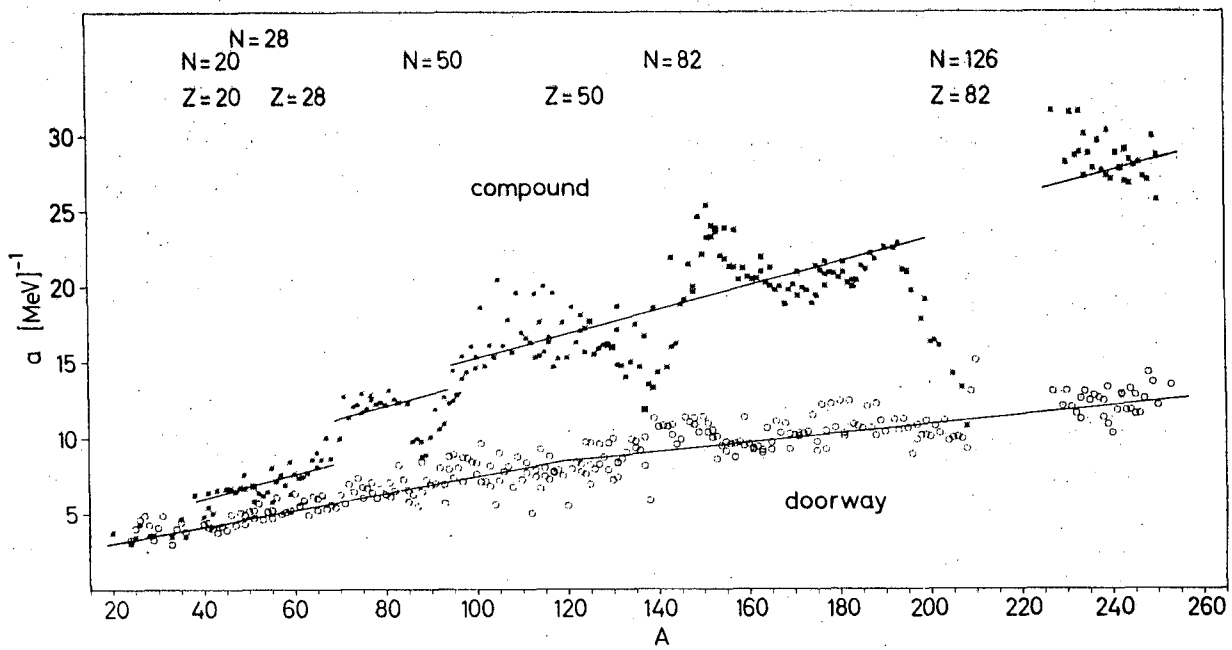


FIG.1 : The level density parameter $a$ appearing in the Fermi gas level density expression obtained from compound and doorway state level densities as a function of mass number A.

## Level Density Systematics

Fig. 1 shows the plot of $a$ against atomic number A; the stars correspond to the compound states and the circles to the doorway states. The deviation of the level density parameter $a$ from a linear dependence on the atomic number A indicates two types of structure : ($a$ shall refer to $a_{compound}$ from now)

1) The usual closed shell effects at specific numbers of neutrons N and protons Z, reflecting a decrease in the level density of single particle states at Fermi surface energy and a pronounced hump at A ~ 155(N = 90) indicating an increase of $g_0$.

2) Distinct steps (three in total) of the level density parameter $a$ at certain A values (A = 38, 69, 94), caused by changes of the compound level density (not $g_0$) at neutron separation energy, which can be explained by an addition of two extra quasiparticles participating in the excitation process of the compound nucleus at each step. Since $g_0 \propto A$, the successive steps with increasing A describes the changes of the hierarchy of the compound states. The highest hierarchy in the excitation of the compound nuclei for A < 38 is the doorway state ( $a_{doorway} = a_{compound}$) which corresponds to the first

step of the compound excitation. At A > 38, A > 69 and A > 94 the second, third and fourth steps respectively in the compound process become important. As the level density of compound states with an hierarchy larger than four becomes considerably smaller (because the energy per particle is too small) the linear dependence does not change to any great extent.

Between these structures the level density parameter $a$ should be linear with A, as indicated by the lines in Fig. 1 which will be defined later. Considerable fluctuation is observed in the mass range $100 < A < 130$ and $220 < A < 250$. To explain this we shall study the parameters in expression (1) in more detail.

## Sensitivity of $a$ to the parameters in the level density expression

Fig. 2 shows the variation of $a$ for all considered odd-odd nuclei, resulting from changes in D and U of + 50% and + 5% respectively. Similarly in Fig. 3 $\delta a/a$ is obtained by doubling the value of $\sigma^2$ and is plotted showing the influence of different target spins I.

The fluctuation in $a$ values between $220 < A < 250$ is approximately 10% and would represent almost a factor of two deviation in the level density. This is highly improbable and a deviation of 30% should be the maximum. The spin cut off factor $\sigma$ is directly dependent on the moment of inertia and should not vary significantly from one isotope to the next. This leaves only the effective excitation energy ($U_{(eff)} = E_B + E_{max}/2 - \Delta$) as a parameter able to cause such fluctuations and, as $E_B$ and $E_{max}$ are known accurately, the pairing energy term $\Delta$ (which is obtained by mass differences) becomes suspect. It is generally accepted that $\Delta$ has no influence for odd-odd nuclei so in this case the fluctuation is expected to be greatly reduced. The level density systematics for these nuclei are given in Fig. 4 showing a reduction in the fluctuation at the highest atomic weight range except for the peak at Z = 90. The deviation of the two points at Z = 90 (A = 235) from the straight line corresponds to a shell effect hump similar to the more pronounced hump seen at N = 90. This plot has been used to define the linear behaviour of $a$ between the previously mentioned structures.

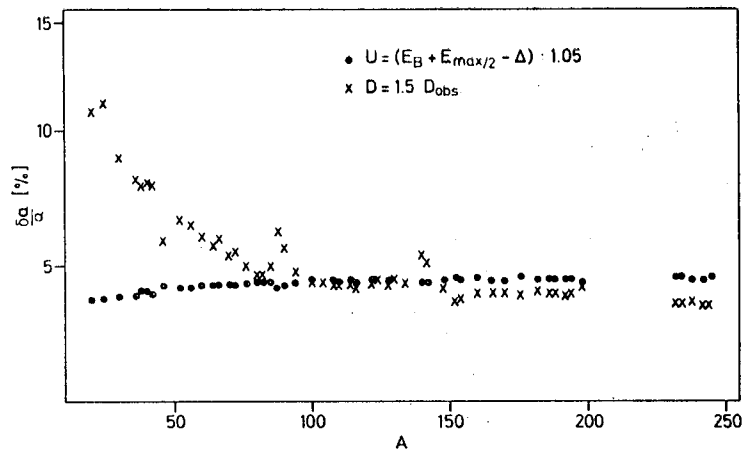


Fig. 2 : Percentage change in $a$ (for odd-odd nuclei) resulting from changes in level spacing D and excitation energy U.

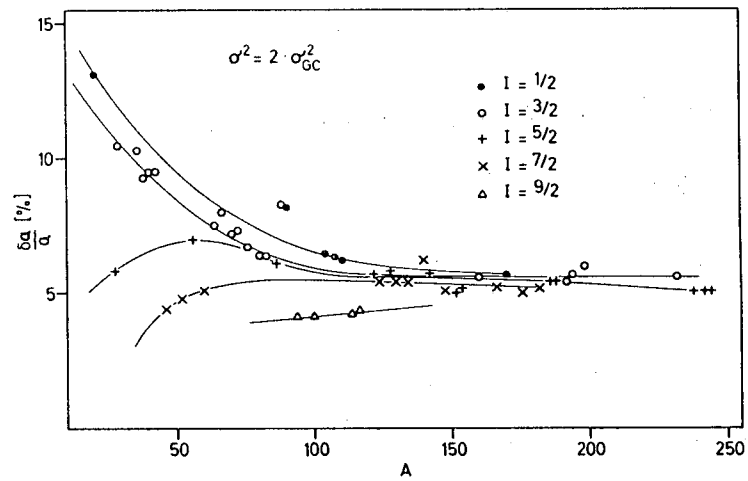


Fig. 3 : Percentage change in $a$ obtained by doubling $\sigma^2$ ($\sigma$ = spin cut off factor).

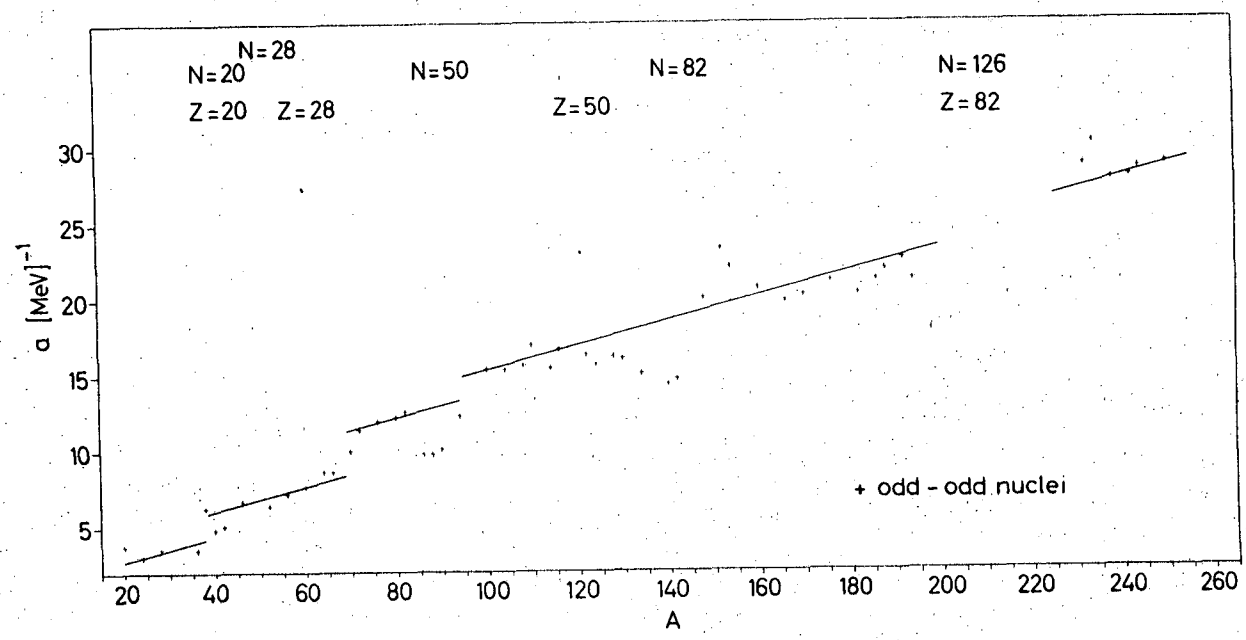


Fig. 4 : Level density parameter $a$ for odd-odd nuclei only.

Five regions have been fitted with straight lines of equal slope, namely :

$$
\begin{aligned}
a &= 0.08A + 1.2 && 20 < A < 38 \\
a &= 0.08A + 2.8 && 38 \leqslant A < 69 \\
a &= 0.08A + 5.8 && 69 \leqslant A < 94 \\
a &= 0.08A + 7.4 && 94 \leqslant A < 210 \\
a &= 0.08A + 8.64 && 220 \leqslant A < 250
\end{aligned}
\qquad (2)
$$

In fact it would be better to describe the last A range by a slight change in the slope instead of using the small step. This would not effect the results obtained in this range.

In Fig. 5 we have plotted groups of odd-odd nuclei where within each group nuclei of different target spin I are considered. For each nuclei $a$ has been calculated for the three spin cut off factors shown. By checking which of the values falls on the best straight line we conclude $\sigma^2$ must certainly be larger than $\frac{1}{4}\sigma^2_{rigid}$ and at higher A values the tendency suggests that $\sigma^2 > \frac{1}{2}\sigma^2_{rigid}$, although we see in Fig. 3 that the sensitivity of $\sigma$ to I is much larger at low A values ($A < 100$).

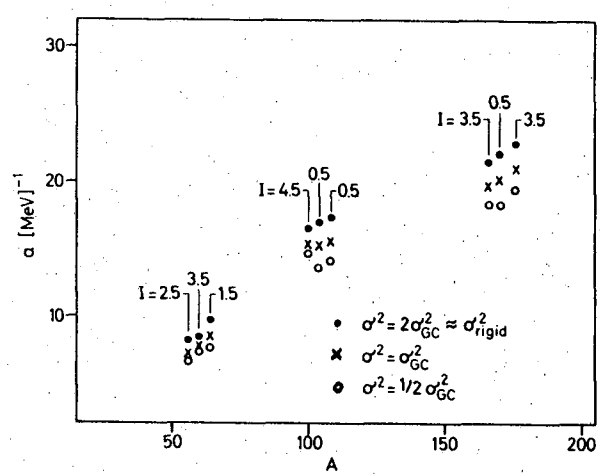


Fig. 5 : Dependence of $a$ on the spin cut off factor ($\sigma$) for different target spins I.

## Determination of the Pairing Energy

The procedure described in the previous chapter defined the linear behaviour of $a$ with atomic number (2) for odd-odd nuclei where we can take the pairing energy $\Delta = 0$. For all other nuclei we determine $\Delta$ in order that the corresponding $a$ parameter is also described by eq. (2). The circles in Fig. 6 give the resulting $\Delta_p$ values for even-odd actinide nuclei plotted

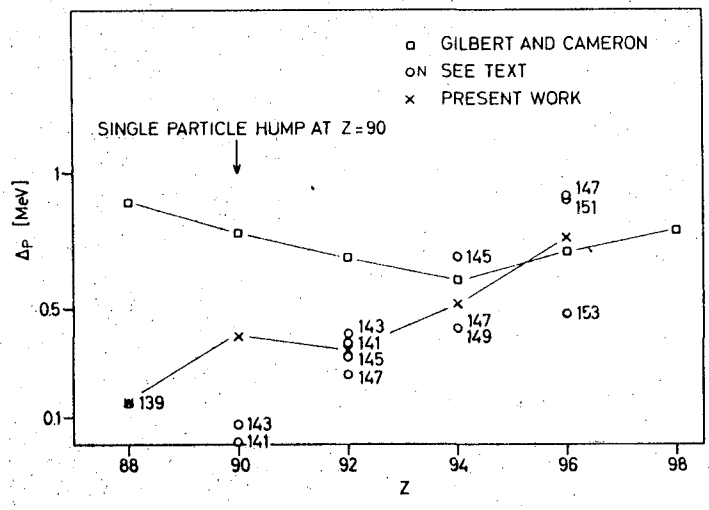


Fig. 6 : Proton pairing energy $\Delta_P$ plotted against proton number Z in the range $220 < A < 250$

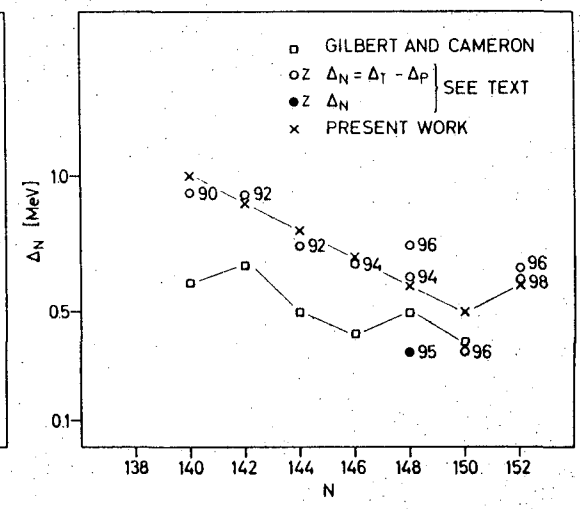


Fig. 7 : Neutron pairing energy $\Delta_N$ plotted against neutron number N in the range $220 < A < 250$

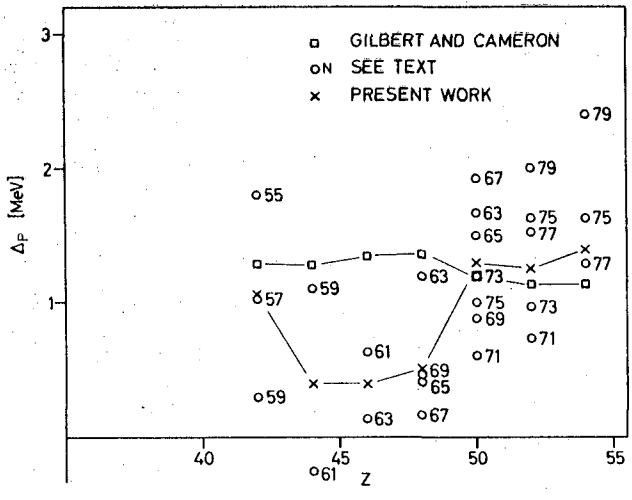


Fig. 8 : Proton pairing energy $\Delta_P$ plotted against proton number Z in the range $100 < A < 130$

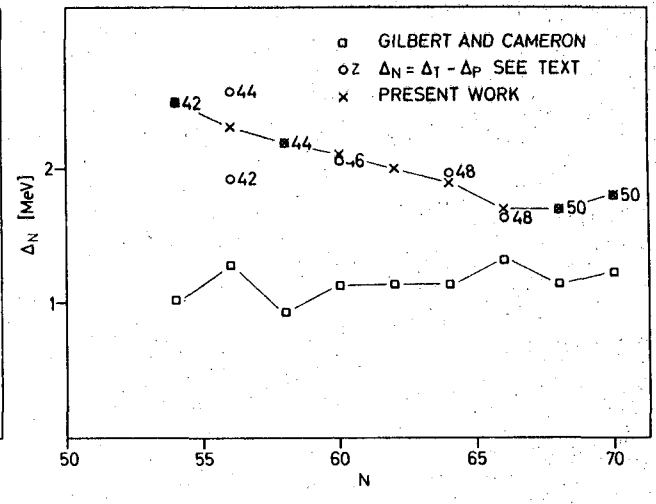


Fig. 9 : Neutron pairing energy $\Delta_N$ plotted against neutron number N in the range $100 < A < 130$

against Z. The neutron number is shown alongside each circle and the crosses represent the average pairing energy for that particular element Z. For Z = 90 the average value has been increased by 0.35 MeV due to the single particle effect previously described. Assuming a $\delta$ force for the pairing energy $\Delta$ proportional to $(2j + 1)$ /5/, the reduction in $\Delta$ in the range immediately below Z = 92 could be explained by single particle states with a small value of j being important in this region. The pairing energy $\Delta_N$ is plotted against the neutron number N in Fig. 7 for even-odd and even-even actinides represented by closed and open circles respectively. The number given next to each circle is the corresponding Z. For even-even nuclei $\Delta_N = \Delta_T - \Delta_P$. The actual values of $\Delta_N$ taken for this work are shown as the continuous line.

Similarly for nuclei in the fission product range $100 < A < 130$, $\Delta_P$ and $\Delta_N$ are given in Figs. 8 and 9. When comparing these results with those of Gilbert and Cameron /4/ a considerable reduction in the value of $\Delta_P$ between Z = 44 and Z = 48 can be seen, whereas $\Delta_N$ is consistantly higher over the whole range plotted.

Over the complete atomic mass range covered by this paper, the pairing

energy has been determined as described above. These new values are used in the level density systematics plotted in Fig. 10 and result in a considerable reduction of the fluctuation in the ranges 100 < A < 130 and 220 < A < 250.

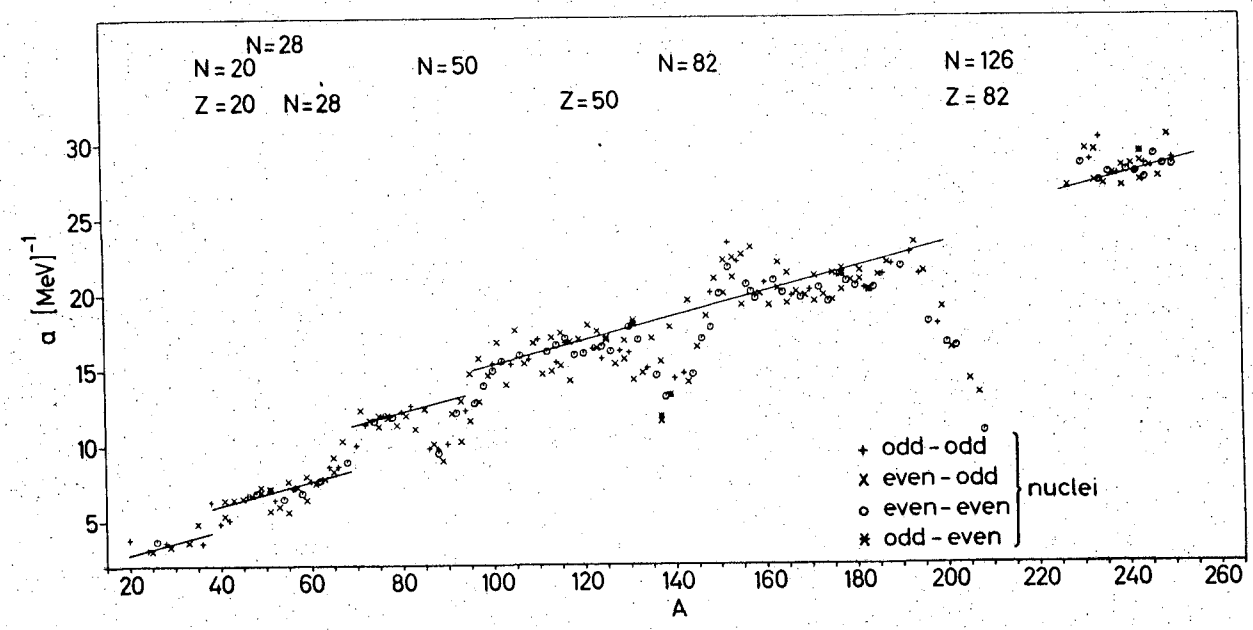


Fig. 10 : Level density systematics determined with pairing energies defined in this paper.

## Prediction of level density at neutron separation energy

The determination of the level spacing at neutron separation energy is most accurate in the actinide range of nuclei where the assumptions used are most valid. Therefore in the atomic number range 234 < A < 250 we have determined the theoretical value of the neutron resonance density $\rho_c$ from eqs. 1 and 2 and compared it with $\rho_{obs}$. The ratio $\rho_c/\rho_{obs}$ is plotted in Figs. 11 and 12 for the old (pairing energy $\Delta$ taken from ref./4/) and the new ($\Delta$ taken from present work) systematics respectively. Using the definitions defined in /4/ we have

$$\ell = \log(\rho_c/\rho_{obs})$$

and a figure of merit $F = \exp\sqrt{(\Sigma\ell^2/n)}$ where n is the number of nuclei. For n = 24 we obtain F = 1.6 and F = 1.22 for the old and the new systematics respectively. In order to determine how much of this error is attributed to experimental uncertainties in $\rho_{obs}$, another figure of merit F′ can be defined :

$$F' = \exp\sqrt{(\Sigma\Delta\ell^2/n)}$$

with $\Delta\ell = \log(\Delta\rho_{obs}/\rho_{obs})$. We obtain F′ = 1.21, showing that the error in the new systematics consists mainly of experimental errors.

## Refinement possibilities for nuclear models

It has been shown that the level density parameter $a$, between structures, can be described by equation (2). Then the level density at Fermi surface energy (reflecting shell effect structure but not the steps) is given by $g_0 = 0.049$ A. Below A = 150 and at closed shells, $g_0$ reproduces the shell structure predicted by the shell model. Above A = 150 the nuclei are strongly deformed between shell structures but the deformation does not seem to increase the level density. However, it rearranges the single particle states, producing humps in $g_0$ after closed shells and creates subshell structure indicated in Fig. 1 at A = 175 and

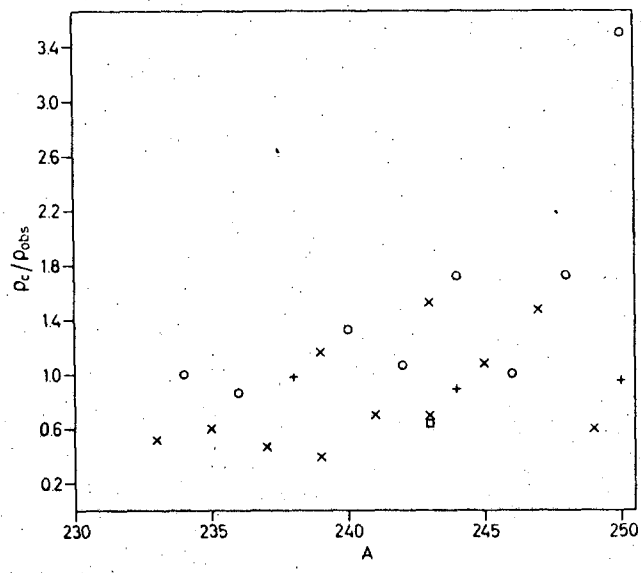


Fig. 11 : Ratio of calculated to observed neutron resonance density for actinide nuclei plotted against A. Pairing energies taken from ref./4/

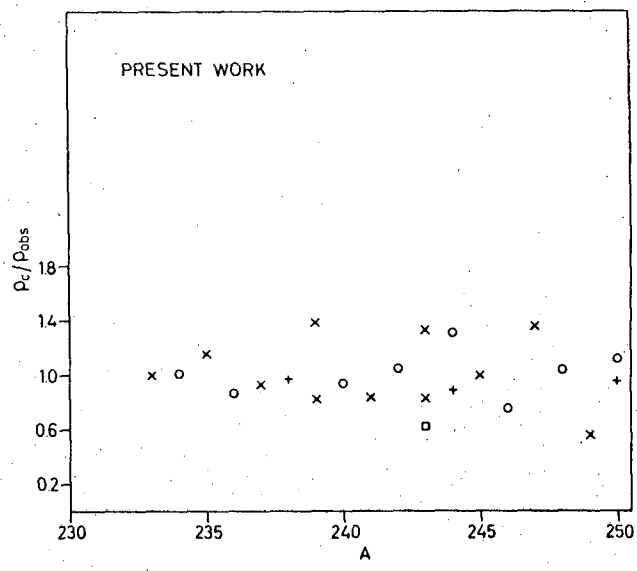


Fig. 12 : Ratio of calculated to observed neutron resonance density for actinide nuclei plotted against A. Pairing energies taken from this work.

and A = 183, as would be expected from the Nilsson model (deformation included).

To reproduce the dependence of $g_0$ (and also $a$) on A (and N and Z) in detail and to check nuclear models, calculations of the level density of states corresponding to higher steps in the compound process are required. These calculations should be based on a similar procedure to that used for determining the level density of doorway states. This would allow a study of the energy dependence of the level density and to interprete observed structures in resonance data (cross section data) such as doorway structure/1/ and intermediate structure caused by a higher hierarchy of the compound process/6/.

Until now we have assumed that the pairing energy exists only in nuclei with an even number of N and/or Z and it has been linked directly to this even number of N or Z. This assumption seems to be somewhat too simple ; for instance, the pairing energy at Z = 50 (Fig. 8) has been determined as the average pairing energy for seven different isotopes with rather different $\Delta p$. To study effects such as pairing energy dependence on the number of pairs and n-p correlations more carefully, the level density at neutron separation energy has to be improved. We hope to do this by means of the very accurate (experimental) values of the neutron binding energy as follows :

The sum $\Delta + S$ (S = shell effect energy) will be determined separately for each isotope using $U_{eff} = E_B + E_{max}/2 - \Delta - S$ and $a$ values defined by equation 2. These values will be taken together with the weakly A dependent terms (e.g. volume, surface), of the liquid drop model, whose free parameters will be determined by a least square fit of binding energy giving a'semi- emperical binding energy formula'. The difference between this predicted binding energy and the experimental value will be used to correct ( $\Delta + S$ ) allowing a new calculation of the level density at neutron separation energy to be done.

## References


1. G. Rohr and R. Shelley, International Conference on Neutron Physics and Nuclear Data for Reactors and other Applied Purposes, Harwell 1978, p.478
2. G. Rohr, L. Maisano and R. Shelley, contribution to this meeting
3. K.N. Müller and G. Rohr, Nucl. Phys. Vol. A164 p. 97 (1971)
4. A. Gilbert and A.G.W. Cameron, Cand. J. Phys., Vol. 43, p. 1446 (1965)
5. M.G. Mayer, Phys. Rev. 78 p. 22 (1950)
6. G. Rohr, International Conference on Neutrons with Nuclei, Lowell 1976, PG1/B12 p. 1258

# BCS LEVEL DENSITY CALCULATIONS AND CONSISTENT ESTIMATE OF RADIATIVE WIDTHS BY MEANS OF A THERMODYNAMIC MODEL

V. Benzi, G. Maino(°), E. Menapace, A. Ventura
Comitato Nazionale Energia Nucleare
Bologna (Italy)

Microscopic calculations of average s-wave level spacings $\bar{D}$ at neutron binding energy $B_n$ were performed for a number of nuclei in the mass number range $40<A<250$. The temperature corresponding to excitation energy $B_n$ was utilized for radiative width calculations through a thermodynamic approach (black-body model). Theoretical results were compared with experimental data.

## INTRODUCTION

The calculation of cross sections via a statistical model calls for knowledge of the average level spacings, $\bar{D}$, and radiation widths, $\bar{\Gamma}_\gamma$, together with the energy dependence of the above-mentioned parameters. However, in several cases of interest for reactor technology (e.g. fission product cross section estimates), these parameters are not known and have to be estimated by means of a model, which, in turn, requires knowledge of some empirical parameters, the values of which are frequently estimated on the basis of their systematic behaviour from nucleus to nucleus.

In the present paper, $\bar{D}$ and $\bar{\Gamma}_\gamma$ are consistently estimated on the basis of the Bardeen-Cooper-Schrieffer (BCS) approximation and a simple "black-body" model, respectively.

## 1. LEVEL DENSITY FORMALISM

As mentioned in the Introduction, the BCS approximation was adopted in order to estimate the $\bar{D}$-values, within the framework of the grand partition function method (see, e.g., ref./1/) and microscopic information is introduced through single-particle levels generated in a Nilsson potential with the quadrupole and hexadecapole deformations and the shell-dependent parameters of ref./2/. Separate residual pairing interactions for neutrons and protons are treated in the BCS approximation with constant pairing strengths $G_N$ and $G_Z$. The Bogolyubov-Valatin transformations applied to the BCS Hamiltonian allow us to deal with an approximate independent-quasiparticle model.

The collective degrees of freedom, which do not appear in the Hamiltonian of our model, are directly introduced into the level density $\rho$ (U,J) (levels per MeV with angular momentum J at the excitation energy U) in the approximate form

(°) Guest researcher

of ref./3/ . The nuclei of our sample are distributed in three classes:

(S): spherical nuclei without collective enhancements of the level density; in this case:

$$\rho_S(U,J) \simeq \frac{2J+1}{\sqrt{8\pi}\,\sigma^3(U)} \exp\left[-\frac{J(J+1)}{2\sigma^2(U)}\right] \rho_{intr.}(U) \qquad (1.1)$$

where $\rho_{intr.}$ is the density of intrinsic states and $\sigma^2$ the spin cutoff factor, both given by BCS calculations (see details in ref./1/);

(V): spherical, or slightly deformed nuclei with vibrational enhancements of the level density:

$$\rho_V(U,J) \simeq [1-\exp(-\hbar\omega/T)]^{-g}\, \rho_S(U,J) \qquad (1.2)$$

where $\hbar\omega$ is a characteristic phonon energy and $g$ the corresponding vibrational degeneracy (for multipole vibrations of order $\lambda$, $g=2\lambda+1$), $T$ the thermodynamic temperature in energy units;

(R): deformed nuclei, with axial and reflection symmetry and rotational spectra, while vibrational contributions are neglected:

$$\rho_R(U,J) \simeq \frac{1}{\sqrt{8\pi}\,\sigma_{\parallel}(U)} \sum_{-J}^{+J}{}_K \exp\left[-\frac{K^2}{2\sigma_{\parallel}^2(U)} - \frac{J(J+1)-K^2}{2\sigma_{\perp}^2(U)}\right] \rho_{intr.}(U) \qquad (1.3)$$

$K$ is here the projection of the angular momentum $J$ on the nuclear symmetry axis; the perpendicular spin cutoff factor $\sigma_{\perp}^2$ is related to the moment of inertia $I_{\perp}$ about an axis perpendicular to that of symmetry by the formula $\sigma_{\perp}^2 = I_{\perp} T/h^2$ . $\sigma_{\perp}^2$ should be calculated in the frame of the BCS theory (/4/) , just like $\sigma_{\parallel}^2$ ; however, since the calculation is rather cumbersome and formula (1.3) is not very sensitive to the exact value of $\sigma_{\perp}^2$ if $J$ is not much greater than 1 , we used the rigid-body value for $I_{\perp}$ , thus overestimating the true moment of inertia at low temperature, where the nucleus is in a "superfluid" state.

Finally, the average s-wave level spacing $\bar{D}$ (at $U=B_n$) is given by:

$$\bar{D}(eV) \simeq 2\cdot 10^6 \Big/ \left[\rho\left(B_n, I_t-\tfrac{1}{2}\right) + \rho\left(B_n, I_t+\tfrac{1}{2}\right)\right] \qquad (1.4)$$

where $I_t \neq 0$ is the ground state spin of the target nucleus, while, for $I_t=0$ , formula (1.4) is replaced by:

$$\bar{D}(eV) \simeq 2\cdot 10^6 / \rho\left(B_n, \tfrac{1}{2}\right) \qquad (1.5)$$

In both formulae (1.4) and (1.5) it is assumed that positive and negative parity states are equiprobable at the neutron binding energy, an assumption which seems to be good for deformed nuclei, while it might be less valid for spherical ones (/5/).

In our approach, the input parameters we have to adjust in order to reproduce the experimental $\bar{D}$'s are the ground state correlation functions (or "gap" parameters) $\Delta_N$ and $\Delta_Z$ for neutrons and protons, respectively. The same functional dependence on the corresponding nucleon number was assumed for both parameters.

## 2. RADIATION WIDTH FORMALISM

For a given excitation energy U the BCS equations allow us to work out the corresponding temperature T according to the procedure of ref./1/. The value of T corresponding to $U=B_n$ may be utilized to estimate the average radiation width $\overline{\Gamma}_\gamma$ at $B_n$ if we adopt the simple black-body model reported in ref./6/. In such a model, an excited nucleus is represented as an assembly of A independent oscillators, confined within a spherical region of radius $R=r_0A^{1/3}$ (we neglect nuclear deformations, because of the oversimplifications of the model), in thermodynamic equilibrium with the emitted radiation.

The number of photons with frequency between $\nu$ and $\nu+d\nu$ emitted by the nucleus per unit time turns out to be, approximately:

$$n(\nu)\,d\nu \simeq \pi S w \frac{c}{4\pi}\frac{u(\nu)}{h\nu}\,d\nu \quad \text{photons/sec} \tag{2.1}$$

Here $S=4\pi R^2$ is the nuclear surface, c the velocity of light and $u(\nu)$ a modified Planck energy density per unit frequency:

$$u(\nu) = \frac{1}{3A}\frac{8\pi h\nu^3}{c^3}\left[\exp\left(\frac{h\nu}{T}\right)-\frac{1}{3A}\right]^{-1} \quad \text{erg}/(\text{cm}^3\,\text{Hz}) \tag{2.2}$$

The term 1/(3A) derives from the fact that the number of allowed transitions up for a given specific energy density is 3A times the number of induced transitions down, as explained in ref./6/. The quantity $w$ is a weight factor due to the selection rules of angular momentum: if $J_i$ is the initial spin of the compound nucleus and $\{J_f\}$ the set of allowed final spins, then, approximately:

$$w \simeq (2J_i+1)/\left[\sum_f (2J_f+1)\right] \tag{2.3}$$

Electric dipole radiation usually plays the main rôle, so that $w=1/3$. Therefore, the total radiative width turns out to be:

$$\overline{\Gamma}_\gamma = h\int_0^{\nu_{max}} n(\nu)\,d\nu \simeq \frac{4\pi}{9}\left(\frac{r_0}{hc}\right)^2\frac{T^3}{A^{1/3}}\int_0^{h\nu_{max}/T}\frac{x^2\,dx}{e^x-\frac{1}{3A}} \tag{2.4}$$

and with the approximations $3A \gg 1$ and $h\nu_{max}/T > 1$ ($h\nu_{max}$ is of the order $B_n$, i.e. 5-10 MeV, and T of the order 0.5-1 MeV) one obtains:

$$\overline{\Gamma}_\gamma \simeq \frac{8\pi}{9}\left(\frac{r_0}{hc}\right)^2\frac{T^3}{A^{1/3}} \tag{2.5}$$

The radius parameter $r_0$ is adjustable, within reasonable limits: our best fit of experimental data is obtained with $r_0 = 1.2$ fm ; thus

$$\overline{\Gamma}_\gamma(\text{eV}) \simeq \frac{7.32\,T^3_{(\text{MeV})}}{(22A)^{1/3}} \tag{2.6}$$

## 3. RESULTS AND COMMENTS

The choice of a reliable set of experimental $\bar{D}$'s and $\bar{\Gamma}_\gamma$'s was the first step of the present study. To this end recent literature values were taken into account. Moreover, for many nuclei, the spacing $\bar{D}$ was deduced from resonance parameters by means of the missing level estimator as in ref./7/ , or by the maximum likelihood method as in ref./8/, and the width $\bar{\Gamma}_\gamma$ obtained as weighted average of experimental values of single resonances.

The order of magnitude of the gap parameters $\Delta_N$ and $\Delta_Z$ was estimated at first from the average trend of the pairing energies $\delta_N$ and $\delta_Z$ versus N and Z , respectively (/9/,/10/). Subsequently, since the correlation functions $\Delta$ do not coincide with the pairing energies, their values were adjusted so as to reproduce as near as possible the experimental $\bar{D}$'s. In order to have only one adjustable parameter, the same dependence of $\Delta_N$ and $\Delta_Z$ on the corresponding nucleon number (N or Z) was assumed (figures 1 and 2).

The comparison of experimental data and calculated values is given in table I and in figures 3 and 4.

Odd-Z and odd-odd compound nuclei are not included in the present analysis because a more consistent treatment of the blocking effect due to unpaired nucleons seems to be necessary in these cases. The study of such an effect is currently in progress.

As for collective enhancements of the level density, the rotational formalism seems to work rather well,while the vibrational formalism needs to be improved mainly for odd-mass nuclei, for which the phonon energy in formula (1.2) was assumed to be that of an adjacent even-even nucleus, on the hypothesis of a weak coupling between the excited core and the valence particle.

Moreover, we would point out that for the majority of our nuclei at $U=B_n$ neutrons,or protons,or both turn out to be below their critical temperature, i.e. in a superfluid state. Therefore, the use of simple formulae like those based on the Fermi gas model would not be realistic at such excitation energies unless allowance is made for energy (or temperature) dependence of some important parameters like "a" and $\sigma^2/T$ (/11/). As an illustration of discrepancies, fig. 5 shows the trend of the level density $\rho$ (U,J=1/2) of the compound nucleus Gd 157 from BCS approximation and Fermi gas formulae, normalized at $U=B_n$ .

In conclusion, the results of this preliminary work encourage us to improve our formalism; we list here some planned improvements:

1) parity dependence of level densities, as in ref./5/ ;
2) proper treatment of odd nucleon systems;
3) more rigorous inclusion of collective effects, mainly the vibrational ones, as in ref./12/;
4) study of changes of nuclear shape with excitation energy.

Hopefully, these improvements will give us a reliable and accurate instrument for studies of nuclear structure and reactions over a wider range of masses and excitation energies.

## ACKNOWLEDGMENT

We thank Dr. M. Stefanon for providing us with his "CAVE" program for resonance analysis and for useful discussions on this subject.

## REFERENCES


/1/ G.Maino,E.Menapace,and A.Ventura: Nuovo Cimento 50A,1(1979)

/2/ P.A.Seeger and W.M.Howard:Nucl.Phys.A238,491(1975)

/3/ S.Bjørnholm,A.Bohr and B.R.Mottelson: 3rd Int.Symp.on the Phys. and Chem. of Fission, Rochester,1973,IAEA,1,367(1974)

/4/ M.Brack,T.Ledergerber,H.C.Pauli,and A.S.Jensen: Nucl.Phys.A234,185(1974)

/5/ A.V.Ignatyuk and A.I.Blokhin:Sov.Journ.of Nucl.Phys.23,31(1976)

/6/ V.Benzi: Conf.on Neutr.Phys.and Nucl.Data,Harwell,288(1978)

/7/ G.A.Keyworth,M.S.Moore,and J.D.Moses: Spec.Meet.on Fast Neutr.Fiss.Cross Sect.of $^{233}U$,$^{235}U$,$^{238}U$,$^{239}Pu$, Argonne, rep. ANL-76-90,353(1976)

/8/ C.Coceva and M.Stefanon: Nucl.Phys.A315,1(1979)

/9/ P.E.Nemirowsky: Kurchatov rep.IAE-2530(1975) (in Russian)

/10/ J.W.Truran,A.G.W.Cameron,and E.Hilf: Int.Conf.on the Prop.of Nuclei far from the region of β-stability, Leysin,CERN 70-30,1,275(1970)

/11/ A.V.Ignatyuk,G.N.Smirenkin,and A.S.Tishin: Sov.J.of Nucl.Phys.21,255(1975)

/12/ A.R.de L.Musgrove,B.J.Allen,J.W.Boldeman,D.M.H.Chan,and R.L.Macklin: Nucl.Phys.A259,365(1976)

/13/ S.F.Mughabghab and D.I.Garber: Neutr.Cross Sect.: I-Resonance Parameters, Brookhaven, rep.BNL 325,3rd ed.(1973)

/14/ W.Dilg,W.Schantl,H.Vonach and M.Uhl:Nucl.Phys.A217,269(1973)

/15/ A.R.de L.Musgrove,B.J.Allen,J.W.Boldeman,D.M.H.Chan,and R.L.Macklin: Nucl. Phys.A279,317(1977)

/16/ F.H.Fröhner: Neutr.Data of Struct.Materials for Fast Reactors, Geel,1977, K.H.Böckhoff ed.,Pergamon Press,138(1979)

/17/ J.B.Garg,S.Jain,and J.A.Harvey: Phys.Rev.C18,1141(1978)

/18/ A.R.de L.Musgrove,B.J.Allen,J.W.Boldeman,and R.L.Macklin: Int.Conf.on Neutr.Phys. and Nucl.Data, Harwell,449(1978)

/19/ Hvan Cher Gu,A.B.Popov and K.Trzeciak: Int.Conf.on Neutr.Phys. and Nucl. Data, Harwell, 327(1978)

/20/ R.W.Hockenbury,W.R.Koste,and R.A.Shaw: Bull.Am.Phys.Soc.20,560(1975)

/21/ P.Staveloz,E.Cornelis,L.Mewissen,F.Poortmans,G.Rohr,R.Shelley,and T.van der Veen: Int.Conf.on Neutr.Phys.and Nucl.Data, Harwell,701(1978)

/22/ B.J.Allen and A.R.de L.Musgrove: Neutr.Data of Struct.Materials for Fast Reactors, Geel, 1977, K.H.Böckhoff ed., Pergamon Press, 447(1979)

/23/ F.H.Fröhner: Conf.on Nucl.Cross Sect.and Technology, Washington, R.A.Schrack and C.D.Bowman ed.,2,929(1975)

/24/ J.E.Lynn: The theory of neutron resonance reactions, Clarendon Press, Oxford,112(1968)

/25/ R.F.Carlton,S.Raman,J.A.Harvey,and G.G.Slaughter: Phys. Rev. C14,1439(1976)

/26/ H.S.Camarda: Phys.Rev.C18,1254(1978)

/27/ H.J.Liou,J.Rainwater,G.Hacken and U.N.Singh: Phys.Rev.C11,2022(1975)

TABLE I

Experimental and calculated parameters for nuclei in the mass range $40 < A < 190$

| TARGET NUCLEUS | $\Delta_N$ (MeV) | $\Delta_Z$ (MeV) | CLASS | $T(B_n)$ (MeV) | $\bar{D}_{exp}$ (eV) | $\bar{D}_{calc.}$ (eV) | $\bar{\Gamma}_{\gamma exp}$ (meV) | $\bar{\Gamma}_{\gamma calc.}$ (meV) |
|---|---|---|---|---|---|---|---|---|
| Ca 40 | 1.35 | 1.36 | S | 1.186 | (37±4)K (a) | 36.2 K | | 1263 |
| Ca 42 | 1.33 | 1.36 | S | 1.162 | (23±6)K (b) | 27.7 K | 1100±200 (d) | 1171 |
| | | | | | 28 K (c) | | | |
| | | | | | (8.6±1.0)K (d) | | | |
| Ca 43 | 1.32 | 1.36 | S | 1.303 | (1.5±0.2)K (d) | 2.0 K | 700±40 (d) | 1638 |
| Cr 50 | 1.29 | 1.32 | S | 1.250 | (15.4±1.3)K (e) | 16.5 K | (1.7±1.0)K (j) | 1373 |
| Cr 52 | 1.27 | 1.32 | S | 1.142 | (34.2±6.1)K (e) | 35.8 K | | 1034 |
| Cr 53 | 1.26 | 1.32 | S | 1.156 | (6.0±0.5)K (e) | 4.8 K | (1.4±0.8)K (j) | 1071 |
| Fe 54 | 1.27 | 1.30 | S | 1.200 | (17±2)K (e) | 17.8 K | | 1190 |
| | | | | | (22±4)K (d) | | | |
| Fe 56 | 1.25 | 1.30 | S | 1.063 | (25±5)K (a) | 25.1 K | 920±220 (m) | 816 |
| | | | | | (19.3±1.6)K (e) | | | |
| Fe 57 | 1.24 | 1.30 | S | 1.075 | (5.4±0.6)K (e) | 5.7 K | | 837 |
| Fe 58 | 1.23 | 1.30 | S | 0.921 | (24±5)K (e) | 29 K | | 524 |
| | | | | | (32±12)K (f) | | | |
| Ni 58 | 1.25 | 1.28 | S | 1.079 | (16.7±1.6)K (e) | 16.1 K | 1820±570 (m) | 844 |
| Ni 60 | 1.23 | 1.28 | S | 0.980 | (15.1±1.7)K (e) | 15.5 K | 962±277 (e) | 624 |
| Ni 61 | 1.22 | 1.28 | S | 1.013 | (1.61±0.10)K (e) | 1.5 K | 1380±400 (m) | 685 |
| Ni 62 | 1.21 | 1.28 | S | 0.874 | (16.6±3.3)K (b) | 23.6 K | | 437 |
| | | | | | (14.6±0.8)K (e) | | | |
| Sr 84 | 1.10 | 1.18 | S | 0.775 | 305±92 (b) | 440 | | 276 |
| Sr 86 | 1.08 | 1.18 | S | 0.810 | (1.5±0.4)K (b) | 970 | 240±50 (g) | 313 |
| | | | | | (3±1)K (g) | | | |
| Sr 88 | 1.06 | 1.18 | S | 0.679 | (10.1±1.8)K (b) | 8.1 K | 220±50 (g) | 183 |
| | | | | | 40 K (g) | | 125±24 (u) | |

(a): ref./12/; (b): value obtained from parameters of ref./13/ by the method of ref./7/; (c): quoted in ref./14/; (d): ref./15/; (e): obtained from parameters of ref./16/ by the method of ref./7/; (f): ref./17/; (g): quoted in ref./18/ (the radiative widths are for s-wave neutrons); (h): ref./19/; (i): ref./20/; (j): weighted average of (s-wave) data in ref./22/; (l): ref./21/; (m): weighted average of s-wave parameters in ref./23/; (n): quoted in ref./24/; (o): ref./25/; (p): ref./26/; (q): quoted in ref./1/; (r): quoted in ref./6/; (s): ref./27/; (t): obtained from parameters of ref./13/ by the method of ref./8/; (u): weighted average of data in ref./13/.

TABLE I (continued)

| TARGET NUCLEUS | $\Delta_N$ (MeV) | $\Delta_Z$ (MeV) | CLASS | $T(B_n)$ (MeV) | $\bar{D}_{exp}$ (eV) | $D_{calc.}$ (eV) | $\bar{\Gamma}_{\gamma exp}$ (meV) | $\bar{\Gamma}_{\gamma calc.}$ (meV) |
|---|---|---|---|---|---|---|---|---|
| Zr 91 | 1.05 | 1.16 | S | 0.730 | 378±112 (b) | 251 | 140±8 (g) | 226 |
| | | | | | 640±120 (g) | | 202±45 (u) | |
| Zr 92 | 1.05 | 1.16 | S | 0.637 | (2.7±0.6) K(b) | 1.98 K | 135±25 (g) | 149 |
| | | | | | (3.1±1.0) K(g) | | | |
| Zr 94 | 1.04 | 1.16 | S | 0.604 | (3.8±1.0) K(g) | 4.47 K | 85±20 (g) | 126 |
| | | | | | (3.3±0.6) K(b) | | | |
| | | | | | | | | |
| Mo 94 | 1.05 | 1.14 | S | 0.705 | (1.15±0.35)K(g) | 0.94 K | 184±27 (u) | 200 |
| Mo 95 | 1.04 | 1.14 | S | 0.727 | 80±25 (g) | 63.8 | 153±53 (u) | 220 |
| Mo 100 | 1.03 | 1.14 | R | 0.550 | 420+100 (g) | 560 | 85±11 (g) | 93 |
| Ru 99 | 1.04 | 1.12 | S | 0.722 | 25±2 (h) | 29.7 | 198±20 (h) | 211 |
| Ru 101 | 1.03 | 1.12 | S | 0.637 | 18±2 (h) | 25.1 | 175±18 (h) | 145 |
| Ru 102 | 1.03 | 1.12 | R | 0.588 | 110±16 (i) | 132 | | 114 |
| Ru 104 | 1.025 | 1.12 | R | 0.569 | 125±20 (i) | 155 | | 101 |
| Pd 105 | 1.03 | 1.11 | S | 0.672 | 10.6±0.4 (l) | 15.9 | 166.7±1.6 (l) | 167 |
| Cd 111 | 1.02 | 1.08 | V(octupole) | 0.668 | 24.0±1.5 (t) | 30 | 103±23 (u) | 162 |
| | | | $\hbar\omega$=1.97 MeV | | 20±4 (g) | | | |
| Cd 114 | 1.015 | 1.08 | V(quadrupole) | 0.568 | 235±35 (g) | 291 | 104±24 (u) | 99 |
| | | | $\hbar\omega$=0.558 MeV | | | | | |
| Cd 116 | 1.005 | 1.08 | R | 0.565 | 368±75 (b) | 246 | 125±30 (u) | 96 |
| Sn 112 | 1.02 | 1.07 | V(quadrupole) | 0.679 | 157±52 (b) | 183 | 110±21 (u) | 169 |
| | | | $\hbar\omega$=1.257 MeV | | | | | |
| Sn 114 | 1.02 | 1.07 | S | 0.656 | 283±106 (b) | 378 | | 152 |
| | | | | | 300 (c) | | | |
| Sn 115 | 1.015 | 1.07 | S | 0.699 | 50±30 (n) | 50 | | 183 |
| Sn 116 | 1.015 | 1.07 | S | 0.626 | 629±98 (t) | 660 | | 131 |
| | | | | | 464±147 (b) | | | |
| Sn 117 | 1.010 | 1.07 | S | 0.689 | 55.5±4.2 (b) | 56 | 73±30 (u) | 174 |
| Sn 118 | 1.005 | 1.07 | V(quadrupole) | 0.603 | 478±148 (b) | 519 | | 116 |
| | | | $\hbar\omega$=1.23 MeV | | | | | |
| Sn 120 | 1.0 | 1.07 | S | 0.598 | (1.8±0.2)K (o) | 1.66 K | | 113 |

TABLE I (continued)

| TARGET NUCLEUS | $\Delta_N$ (MeV) | $\Delta_Z$ (MeV) | CLASS | $T(B_n)$ (MeV) | $\bar{D}_{exp}$ (eV) | $D_{calc.}$ (eV) | $\bar{\Gamma}_{\gamma exp}$ (meV) | $\bar{\Gamma}_{\gamma calc.}$ (meV) |
|---|---|---|---|---|---|---|---|---|
| Te 124 | 0.995 | 1.05 | V(quadrupole) | 0.590 | 147±12 (b) | 178 | 119±49 (u) | 107 |
| | | | $\hbar\omega$=0.603 MeV | | 138±22 (t) | | | |
| Te 125 | 0.995 | 1.05 | S | 0.657 | 48±6 (t) | 65 | 142±51 (u) | 147 |
| | | | | | | | | |
| Te 126 | 0.990 | 1.05 | V(quadrupole) | 0.595 | 470±114 (b) | 416 | 149±45 (u) | 109 |
| | | | $\hbar\omega$=0.667 MeV | | 512±69 (t) | | | |
| Te 128 | 0.985 | 1.05 | V(quadrupole) | 0.625 | 992±350 (b) | 1246 | 87±40 (u) | 126 |
| | | | $\hbar\omega$=0.743 MeV | | | | | |
| Xe 129 | 0.990 | 1.045 | S | 0.633 | 32±3 (b) | 27.4 | 121±63 (u) | 131 |
| Xe 131 | 0.985 | 1.045 | V(octupole) | 0.668 | 74±19 (b) | 84 | 114±37 (u) | 153 |
| | | | $\hbar\omega$=2.58 MeV | | | | | |
| Ba 136 | 0.975 | 1.04 | S | 0.623 | 920±200 (g) | 866 | 100±20 (g) | 123 |
| Ba 137 | 0.970 | 1.04 | S | 0.600 | 157±47 (b) | 115 | 80±15 (g) | 109 |
| Ba 138 | 0.970 | 1.04 | V(quadrupole) | 0.508 | 4606±461 (t) | 5340 | 55±20 (g) | 66 |
| | | | $\hbar\omega$=0.62 MeV | | 6300±1700 (g) | | | |
| Ce 140 | 0.970 | 1.035 | S | 0.508 | 4900 (p) | 6200 | | 66 |
| | | | | | 3200±800 (g) | | | |
| Nd 142 | 0.970 | 1.03 | V(quadrupole) | 0.512 | 1040±329 (b) | 1365 | 66±33 (u) | 67 |
| | | | $\hbar\omega$=1.57 MeV | | 790±25 (g) | | | |
| Nd 144 | 0.965 | 1.03 | V(quadrupole) | 0.484 | 413±60 (b) | 508 | 78±12 (u) | 56 |
| | | | $\hbar\omega$=0.695 MeV | | 525±100 (g) | | | |
| Nd 145 | 0.960 | 1.03 | V(octupole) | 0.494 | 20.6±3.6 (b) | 31 | 48±6 (u) | 60 |
| | | | $\hbar\omega$=1.198 MeV | | 144±2.0 (i) | | | |
| Nd 146 | 0.955 | 1.03 | V(quadrupole) | 0.477 | 281±78 (b) | 179 | 55±8 (u) | 54 |
| | | | $\hbar\omega$=0.453 MeV | | 290±80 (g) | | | |
| Nd 148 | 0.950 | 1.03 | R | 0.478 | 106±22 (b) | 155 | 64±9 (u) | 54 |
| | | | | | 170±35 (g) | | | |
| | | | | | | | | |
| | | | | | | | | |
| | | | | | | | | |

TABLE I (continued)

| TARGET NUCLEUS | $\Delta_N$ (MeV) | $\Delta_Z$ (MeV) | CLASS | $T(B_n)$ (MeV) | $\bar{D}_{exp}$ (eV) | $D_{calc.}$ (eV) | $\bar{\Gamma}_{\gamma exp}$ (meV) | $\bar{\Gamma}_{\gamma calc.}$ (meV) |
|---|---|---|---|---|---|---|---|---|
| Sm 150 | 0.95 | 1.025 | R | 0.476 | 46+8 (b) | 42 | 60±6 (u) | 53 |
| | | | | | 68±10 (b) | | | |
| Sm 151 | 0.95 | 1.025 | R | 0.552 | 1.20±0.17 (t) | 0.97 | 69±10 (r) | 82 |
| | | | | | 1.72±0.07 (q) | | | |
| Sm 154 | 0.94 | 1.025 | R | 0.518 | 115+114 (q) | 101 | 79+16 (r) | 68 |
| | | | | | 117±17 (b) | | | |
| Gd 154 | 0.945 | 1.02 | R | 0.510 | 14.5+1.5 (q) | 16 | 65+21 (r) | 64 |
| Gd 155 | 0.945 | 1.02 | R | 0.563 | 1.5+0.3 (q) | 1.23 | 108±28 (r) | 87 |
| Gd 156 | 0.94 | 1.02 | R | 0.522 | 35.5±2.0 (q) | 30.5 | 82+12 (r) | 69 |
| | | | | | 31.0±4.4 (b) | | | |
| Gd 157 | 0.935 | 1.02 | R | 0.548 | 4.91±1.25 (q) | 3.31 | 91±22 (r) | 80 |
| | | | | | 4.8±0.6 (b) | | | |
| Gd 158 | 0.935 | 1.02 | R | 0.513 | 71±11 (b) | 67 | 90±13 (r) | 65 |
| Dy 160 | 0.935 | 1.015 | R | 0.524 | 27.3±1.7 (q) | 29.7 | | 69 |
| Dy 161 | 0.93 | 1.015 | R | 0.571 | 2.67±0.13 (q) | 2.58 | | 89 |
| Dy 162 | 0.93 | 1.015 | R | 0.530 | 64.6±1.9 (q) | 55.3 | | 71 |
| | | | | | 66±13 (b) | | | |
| Er 164 | 0.93 | 1.01 | R | 0.536 | 23+4 (q) | 23.7 | | 73 |
| Er 166 | 0.925 | 1.01 | R | 0.535 | 52+7 (q) | 50.6 | 88±20 (r) | 73 |
| Er 167 | 0.925 | 1.01 | R | 0.548 | 4.6±0.7 (q) | 4.0 | 91±12 (r) | 78 |
| Er 168 | 0.92 | 1.01 | R | 0.529 | 110±16 (q) | 135 | 81±15 (r) | 70 |
| | | | | | 101±32 (b) | | | |
| Er 170 | 0.915 | 1.01 | R | 0.521 | 170±24 (q) | 220 | | 66 |
| Yb 168 | 0.925 | 1.005 | R | 0.480 | $22.58^{+1.30}_{-1.26}$ (q) | 20.3 | | 73 |
| Yb 170 | 0.92 | 1.005 | R | 0.535 | 36±6 (b) | 39 | | 72 |
| Yb 171 | 0.92 | 1.005 | R | 0.543 | 7.0±0.8 (b) | 8.8 | 79+10 (r) | 75 |
| Yb 172 | 0.915 | 1.005 | R | 0.526 | 64±12 (b) | 52 | 80±20 (r) | 68 |
| Yb 173 | 0.915 | 1.005 | R | 0.526 | 6.8±1.2 (b) | 7.1 | 68±8 (r) | 88 |
| | | | | | | | | |
| | | | | | | | | |

TABLE I (continued)

| TARGET NUCLEUS | $\Delta_N$ (MeV) | $\Delta_Z$ (MeV) | CLASS | $T(B_n)$ (MeV) | $\bar{D}_{exp}$ (eV) | $D_{calc.}$ (eV) | $\bar{\Gamma}_{\gamma exp}$ (meV) | $\bar{\Gamma}_{\gamma calc.}$ (meV) |
|---|---|---|---|---|---|---|---|---|
| Hf 174 | 0.915 | 1.00 | R | 0.526 | 16±3 (q) | 15.8 | | 68 |
| Hf 176 | 0.91 | 1.00 | R | 0.508 | 32±7 (q) | 31.2 | | 61 |
| Hf 177 | 0.91 | 1.00 | R | 0.509 | 2.22±0.13 (q) | 2.15 | 64±18 (s) | 61 |
| | | | | | 2.44±0.2 (q) | | | |
| Hf 178 | 0.905 | 1.00 | R | 0.494 | 39.9±9.4 (s) | 30 | | 56 |
| W 186 | 0.890 | 0.995 | R | 0.467 | 90±7 (q) | 91 | 59±11 (u) | 47 |
| Os 188 | 0.890 | 0.99 | R | 0.482 | 47±10 (q) | 50 | | 51 |

# FIGURE CAPTIONS

1. Ground state neutron correlation function $\Delta_N$ versus neutron number $N$ ; dots: neutron pairing energies from ref./9/; crosses: neutron pairing energies from ref./10/.

2. Ground state proton correlation function $\Delta_Z$ versus proton number $Z$ ; dots: proton pairing energies from ref./9/; crosses: proton pairing energies from ref./10/.

3. Histogram of the ratios $\overline{D}_{exp}/\overline{D}_{calc.}$ for 96 nuclei in the mass number range $40<A<250$.

4. Histogram of the ratios $\overline{\Gamma}_{\gamma exp}/\overline{\Gamma}_{\gamma calc.}$ for 87 nuclei in the mass number range $40<A<250$.

5. Density of spin 1/2 levels of given parity versus excitation energy $U$ for the compound nucleus $Gd^{157}$ ; continuous curve: BCS approximation; dashed curve: back-shifted Fermi gas formula with parameters $a=18.65\ MeV^{-1}$, $\Delta=-0.67$ MeV, $\sigma^2/T=0.015\ A^{2/3}\ MeV^{-1}$ (ref./14/). Dot-dashed curve: Gilbert-Cameron formula, with parameters $a=27.57\ MeV^{-1}$, $\Delta=1.803$ MeV, $\sigma^2=0.0888\sqrt{aU}\ A^{2/3}$. The three curves were normalized at $\overline{D}_{1/2}(B_n)=31$ eV.

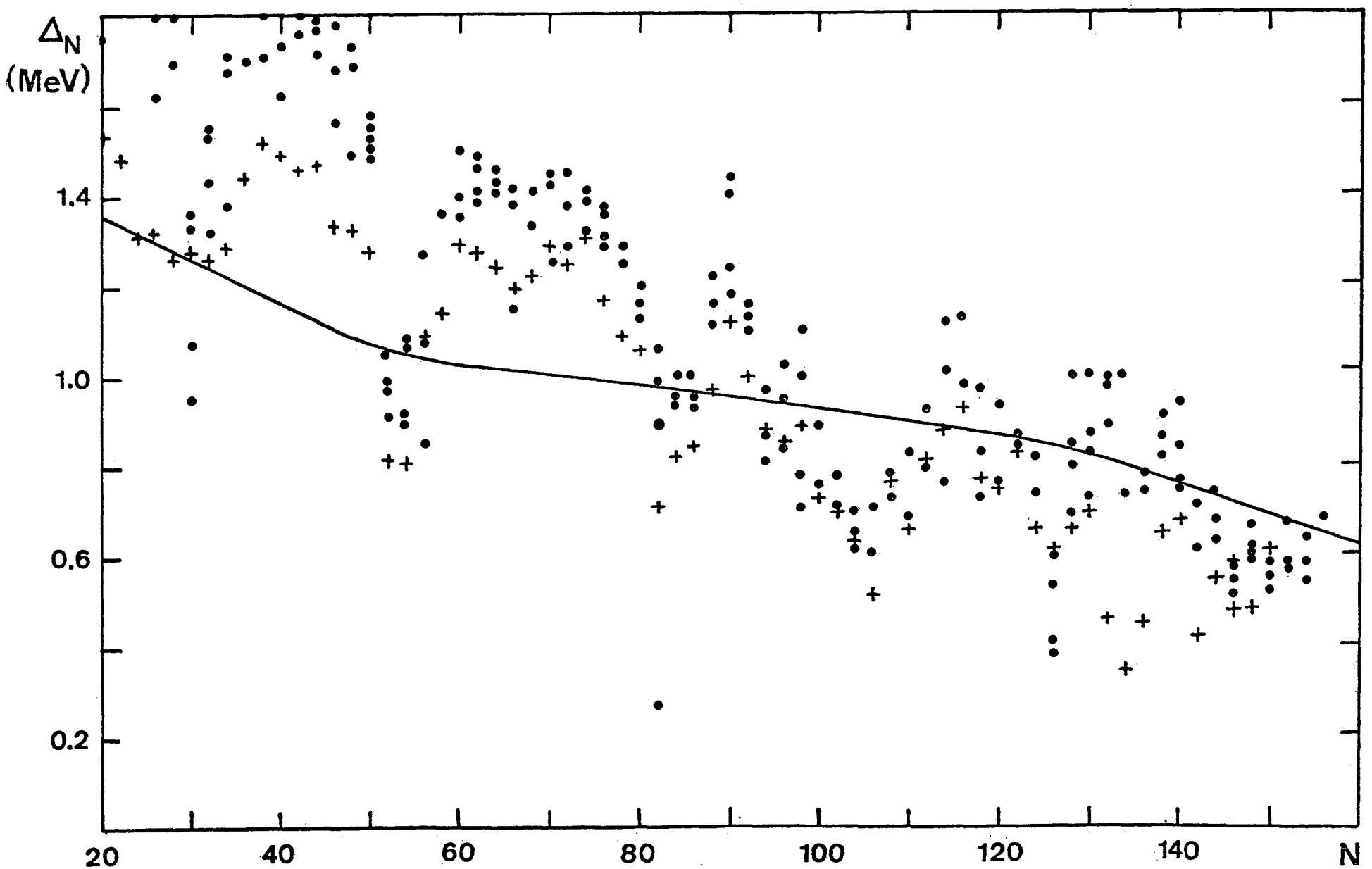


Fig.1

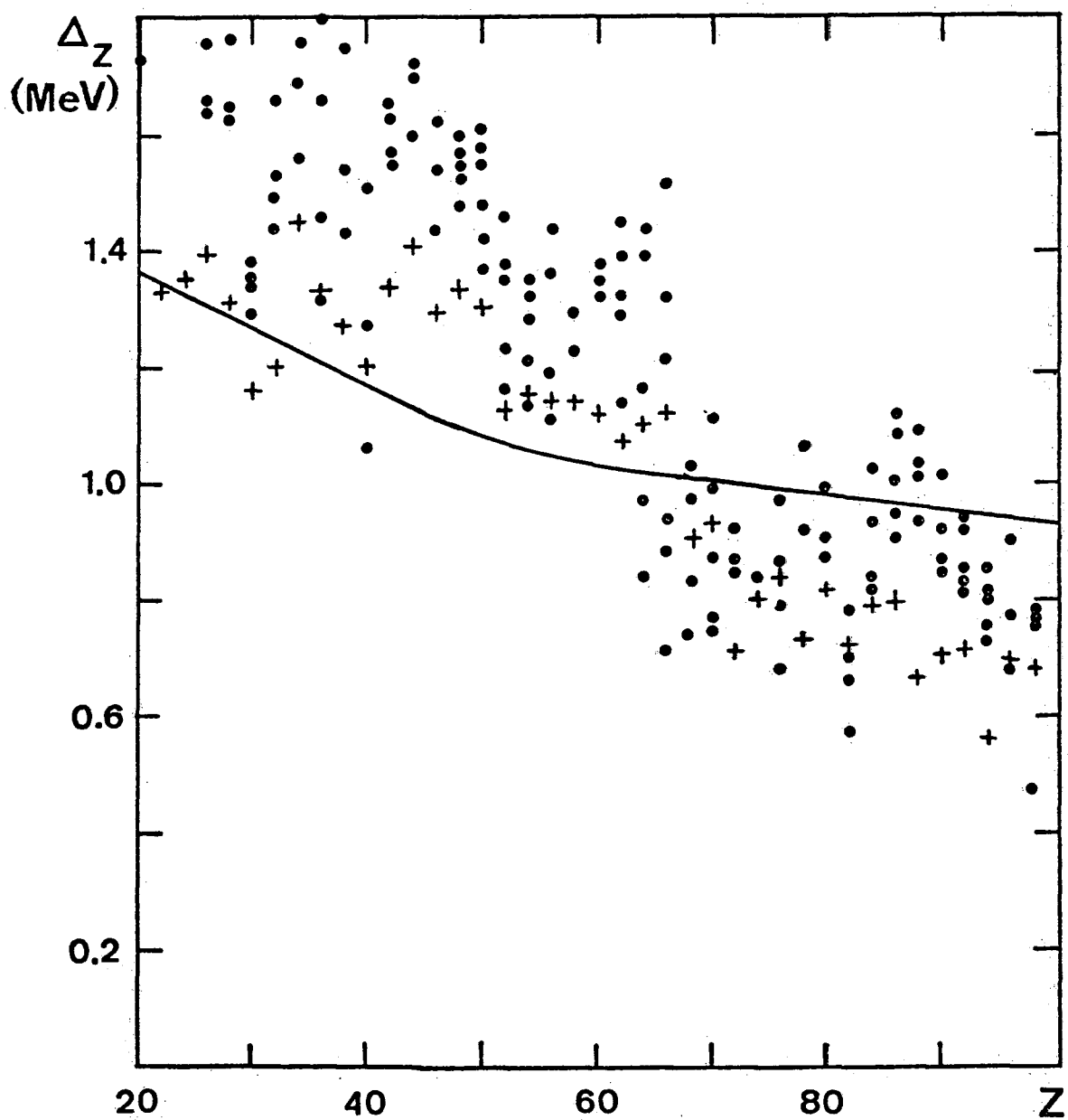

Fig.2

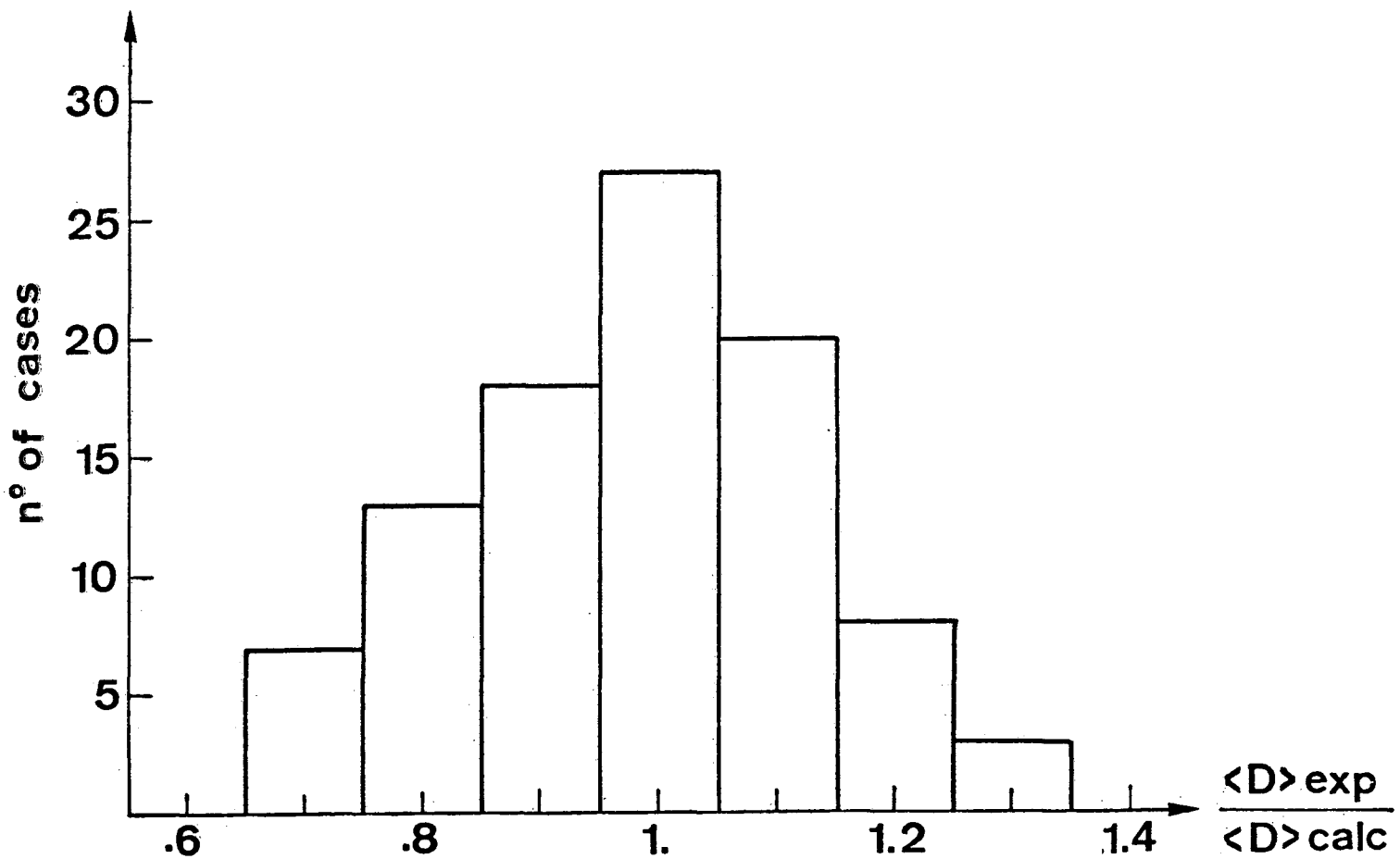


Fig.3

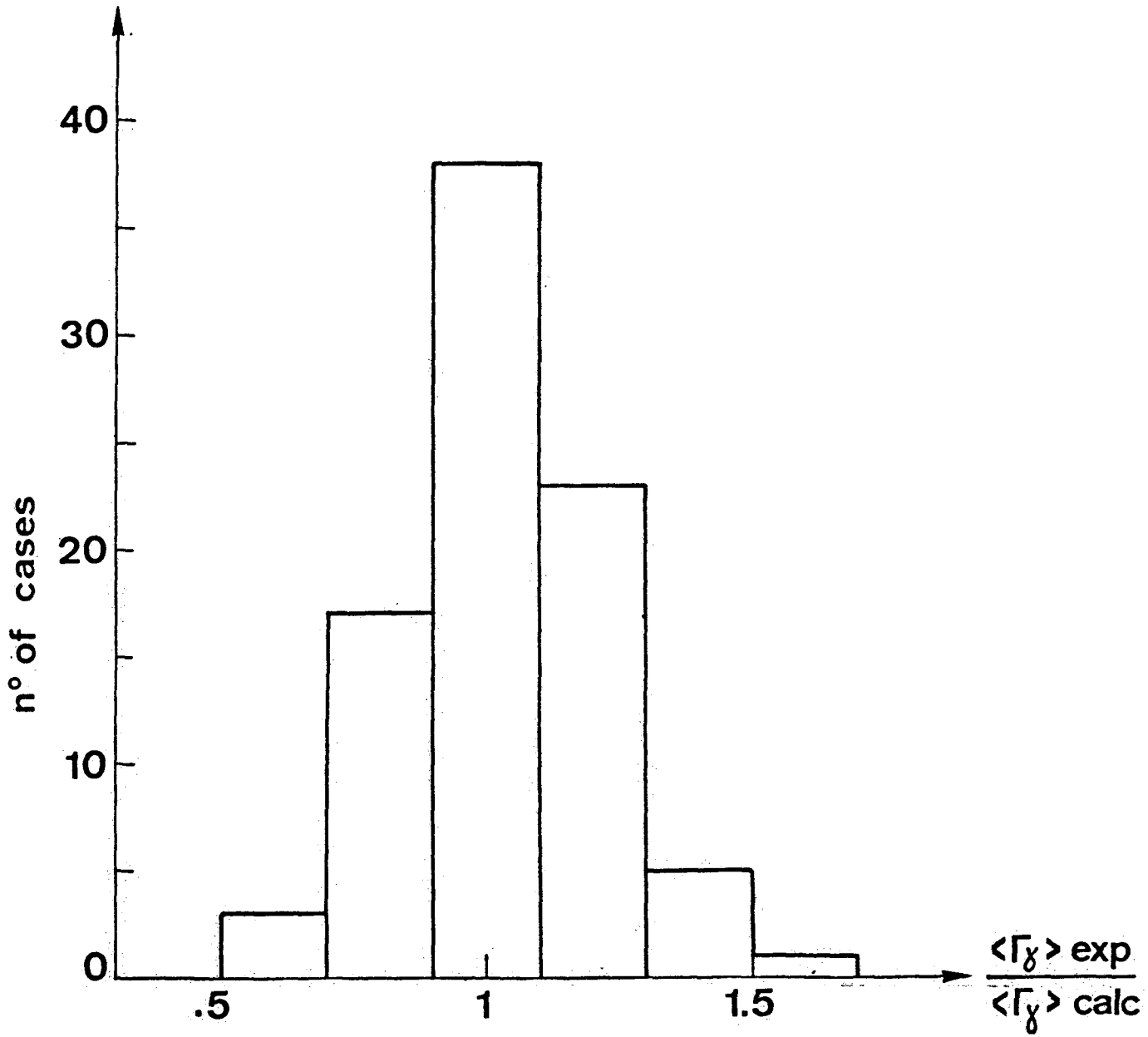
40
30
20
10
0
n° of cases
.5
1
1.5
$\frac{\langle\Gamma_\gamma\rangle \text{ exp}}{\langle\Gamma_\gamma\rangle \text{ calc}}$

Fig.4

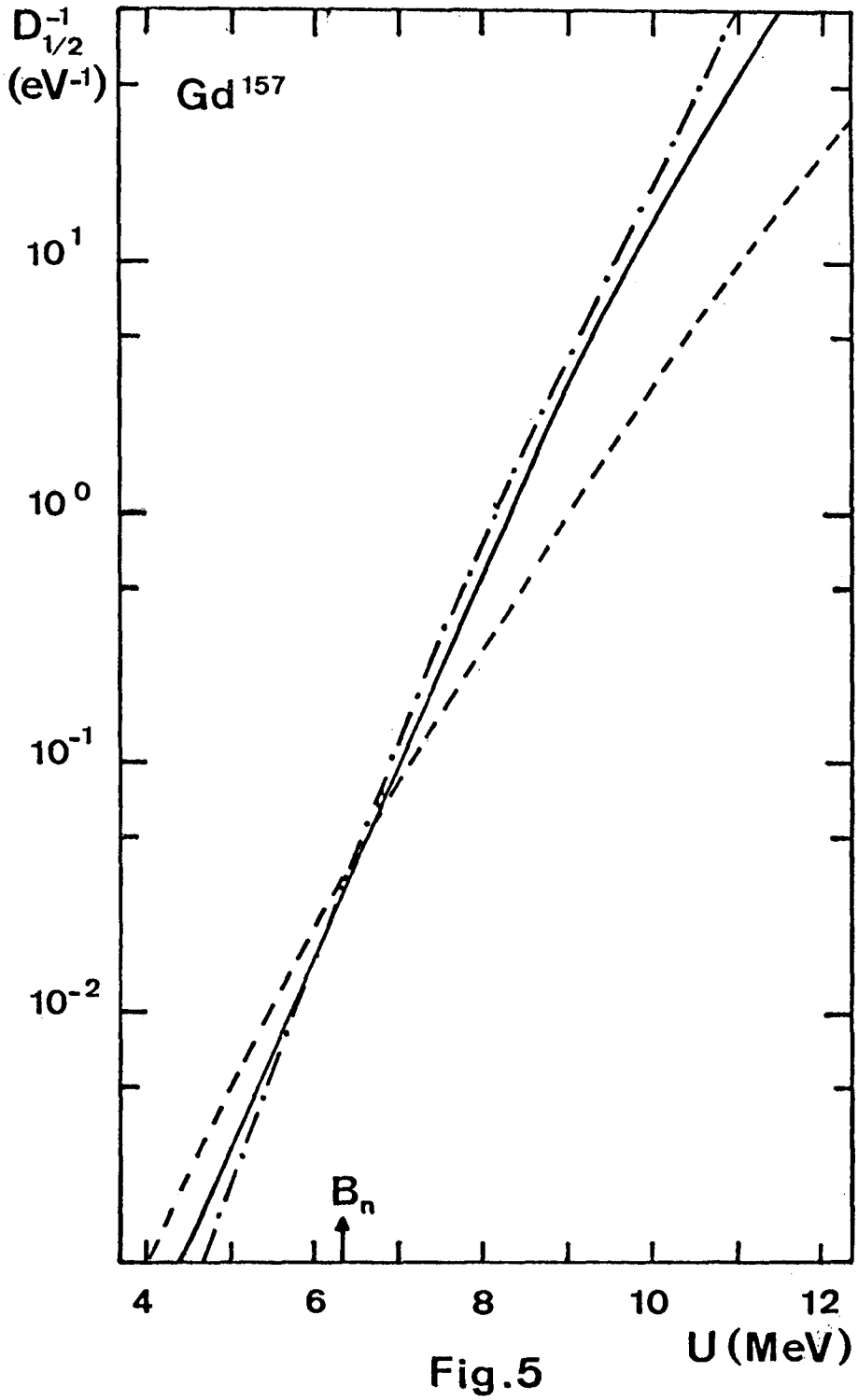


Fig.5

Chairman's Summary of Major Results of Session III:

Neutron Cross Sections: Theory and Evaluations

at the NEANDC Specialists' Meeting on Neutron Cross Sections of Fission Product Nuclei, Bologna (1979)

In the first invited paper Ch. Lagrange indicated that accuracy of optical model calculations can be improved provided the model parametrization is obtained from the fit of a wide experimental data basis containing appropriate information (strength functions, scattering radius, $\sigma_T$ , $\sigma_{el}(\theta)$ etc..) in the whole energy range. In addition such parameters can be taken to hold pretty well also locally in neighbouring nuclei.

The importance has been stressed of the projectile-target state coupling also in certain nuclei of reactor importance.

In the 2nd invited paper R. Schenter illustrated the main characteristics of ENDFB/V version.

Results were shown obtained by means of new evaluation techniques applied to recent information on differential and integral (namely STEK and CERMF) measurements.

A recent HEDL maximum likelihood analysis code FERRET, was used in order to make least squares adjustments of cross sections.

In the third invited paper H. Gruppelaar reviewed the results of an intercomparison of adjusted data sets (Carnaval IV and RCN-2). The main discrepancies were indicated. Methods adopted to produce the adjustements were discussed.

In the last invited paper S. Iijima presented some of the JENDL data file revisions and the results of integral tests of JENDL-1 fission product neutron cross sections with STEK reactivity and CFRMF activation data for selected nuclei.

In a contributed paper H. Gruppelaar summarized the results of his investigation on the contribution of $\sigma_{n,p}$ and $\sigma_{n,\alpha}$ to neutron capture.

In his contribution Y. Harker presented the results of integral capture measurements in Nd, Sm, Eu isotopes which were used for the adjustments of the ENDF/B-IV multigroup cross sections.

W. Osterhage in his contributed paper gave a useful outline of the NEA Data Bank activities concerned with the status of F.P. capture data (both experimental and evaluated) available since Petten 77.

A new computational output format giving "best value" group cross sections and a simplified error covariance analysis were also briefly presented.

In the last contributed paper R. Heijboer reported studies on the sensitivity to F.P. cross section of the sodium void reactivity effects in fast power reactors.

# ON OPTICAL MODEL CALCULATIONS IN THE MASS REGION A = 80 to A = 170

Ch. Lagrange

Service de Physique Neutronique et Nucléaire
Centre d'Etudes de Bruyères-le-Châtel
B.P. n° 561
92542 MONTROUGE CEDEX, France

Abstract

Optical model calculations may be used successfully to provide us with sets of neutron data for practical applications in cases where no experimental data are available. The degree of confidence in such predictions is related to our knowledge of the optical model in the energy range and mass region of interest. For this purpose the model parameterization is based on a fit to all available nucleon-nucleus data. Since the usual model employed is a gross approximation of the reaction mechanism, this parameterization is also based on results of more fundamental "microscopic" developments of the optical potential. Special emphasis will be given on recent efforts carried out in several laboratories for the "empirical" determination of the energy and isospin dependences of the potential strengths, as well as more precise information about nucleon scattering from low-lying collective states. Some limitations and failures of the model are presented together with necessary improvements needed for more accurate neutron cross section predictions.

## 1. INTRODUCTION

The theoretical aspects of the optical model have been presented in lectures given recently at the ICTP Trieste by Mahaux /1/. In these lectures meaningful theoretical constraints on the empirical parameters were explained. Therefore I shall focus my attention on phenomenological optical model potentials (OMP) analyses of nucleon experimental data. For practical reasons only local equivalent OMP are here considered.

The phenomenological OMP is a basic calculational tool for interpolation and extrapolation in the provision of nucleon data. These data include neutron strength functions and total cross sections, as well as elastic and inelastic nucleon scattering cross sections.

Moreover calculated quantities such as compound nucleus formation cross sections and nucleon transmission coefficients are needed for statistical model calculations of nucleon cross sections. These appear to be rather sensitive to the choice of transmission coefficients near the reaction threshold energies.

It is convenient to distinguish between "global" and "local" OMP parameter sets. The first ones which depend smoothly on mass number, energy and neutron excess are quite useful in providing us with general trends of the

empirical parameters. The second ones are tailored for specific nuclei in a limited mass region and thus they are more adapted for accurate extrapolations or interpolations in this mass region. In a review paper given at the last Fission Product Nuclear Data Meeting, IIJIMA /2/ observed that none of the "global" OMP parameter sets proposed by MOLDAUER /3/, IGARASI et al. /4/, ROSEN /5/, BECCHETTI and GREENLEES /6/, or WILMORE and HODGSON /7/, gives satisfactory fits simultaneously to all the neutron experimental data in the mass region A = 80 - 160. Therefore I shall only consider the "local" optical parameter sets and their determination methods.

The main emphasis in this paper will be :

i) to briefly review the phenomenological OMP parameters, the knowledge of which is obtained from theoretical calculations or empirical determinations.

ii) to mention only a few examples of OMP parameter set determination for nucleon data evaluation or analysis purposes.

iii) to present recent results obtained in several laboratories about the empirical determination of the isospin dependence of the OMP and nucleon scattering from low-lying collective states.

## 2. OPTICAL MODEL PARAMETERS

The phenomenological OMP currently employed are of the following form :

$$U(r) = - Vf(x_R) - i\,(W_v f(x_v) - 4a_D\, W_D \frac{d}{dr} f(x_D)) + V_c + 2\,(V_{so} + iW_{so})\,(\frac{1}{r}\frac{d}{dr} f\,(x_{so}))\,\vec{\ell}.\vec{\sigma} \qquad (1)$$

where $f(x_j) = \left[1 + \exp\,[(r-R_j)/a_j]\right]^{-1}$ is the Woods-Saxon form factor and $a_j$ is the diffuseness and $R_j$ the radius of the potentials. V, W and $W_D$ are, respectively, the attractive real, the imaginary volume-absorptive and imaginary surface-absorptive parts of the OMP. Their dependence on energy charge and mass are often written as :

$$V = V_o - b_o E \pm V_1\,\varepsilon + \Delta_c,\; W_v = W_{vo} + b_1 E,\; W_D = W_{Do} + b_2 E \pm W_{D1}\,\varepsilon \qquad (2)$$

where $\varepsilon$ is the neutron excess ($\varepsilon = [N-Z]/A$), $\Delta_c$ the Coulomb correction coefficient ($\Delta_c = 0$ for neutrons and $\Delta_c = b_3\, Z/A^{1/3}$ for protons). The plus signs refer to protons and the minus ones to neutrons. Although theoretical considerations suggest the inclusion of an imaginary spin-orbit component ($iW_{so}$) most of the practical analyses employ only a real component ($V_{so}$). In case of proton scattering the Coulomb potential ($V_c$) is of the homogeneously-charged-sphere form :

$$V_c(r) = \frac{Ze^2}{2R_c}\left[3 - \left(\frac{r}{R_c}\right)^2\right] \text{ if } r < R_c \text{ and } V_c(r) = \frac{Ze^2}{r} \text{ if } r \geqslant R_c \qquad (3)$$

I note that the surface imaginary term is sometimes written as :

$$W_G.\ \exp - \left[(r - R_G)/a_G\right]^2 \qquad (4)$$

The volume integral per nucleon, $J_x/A$, and the root mean square radius, $\langle r_x^2\rangle^{1/2}$, of the various components of the OMP are more significant

quantities in view of comparisons than the depths, radii and diffusenesses. I report, for example, in Table I such values obtained from different phenomenological analyses of neutron scattering data for Mo isotopes and calculated at $E_n$ = 0.0 MeV. Calculations of such quantities facilitate comparisons between theoretical and phenomenological OMP. Such comparisons have recently been made by KAILAS and GUPTA /12/, WIEDLING /13/, LAGRANGE and DELAROCHE /14/.

2.1. Functional forms for the potential radii on mass number. (spherical nuclei)

From their analyses of neutron differential elastic scattering (at $E_n$ = 11 MeV and 26 MeV) and total cross sections data (in the energy ranges 5.0 - 10.6 MeV and 20.0 - 26 MeV) for the even Sn isotopes and $^{nat}Sn$, RAPAPORT et al./15/ have deduced for the real potential the following functional forms on mass number :

$$R_R = r_R A^{1/3} \tag{5}$$

$$R_R = r_R A^{1/3} + C \tag{6}$$

In these analyses the diffuseness of the real potential was kept fixed : $a_R$ = 0.668 fm. Best results were obtained with the following values: $r_R$ = 1.2 fm (eq.5) and $r_R$ = 1.158 fm, C = 2.0 fm (eq.6). From their theoretical calculations of the OMP, JEUKENNE et al. /16/ deduced for the real potential the functional form given by equation 5 with the value : $r_R$ = 1.21 fm, whereas the computed diffuseness was .62 fm. From these empirical and theoretical findings I suggest to adopt the functional form given by equation 5 for all the nuclear components of the OMP. This has the further advantage of reducing the number of parameters to be dealed with. In the following that functional form is implicitly assumed.

For the Coulomb radius I suggest the use of the semi-empirical formula given by ELTON /17/ :

$$R_c = 1.149\ A^{1/3} + 1.788\ A^{-1/3} - 1.163/A \tag{7}$$

2.2. Energy dependence of real and imaginary potential depths

The energy dependence of the real potential well is assumed to be linear in the energy range 10 keV - 40 MeV. From the empirical determinations carried out in several laboratories the value of $J_R/A$ can be expressed as :

$$J_R/A = J_R\ (E = 0)/A - (2.5 \pm 0.6)\ E \tag{8}$$

Most of the empirical analyses of nucleon scattering data are made with only a surface absorptive term at lower energies ($E < E_x$), and with a mixture of volume and surface absorptive terms at higher energies ($E > E_x$). The values of $E_x$ are scattered between 7 MeV /6/ and 15 MeV /8/. In these analyses $W_D$ increases with energy between a few keV and $E_x$. The results may be parametrized as follows :

$$J_{WD}/A = J_{WD}\ (E = 0)/A + (4.0 \pm 1.0)\ E \tag{9}$$

At higher energies $W_V$ increases and $W_D$ decreases with energy both linearly. The coefficients of the energy dependence scatter very much following various analyses. For example the energy dependence of the volume integral per nucleon $J_W/A$ of the imaginary potential has been determined by RAPAPORT et al. for

Mo isotopes /8/ in the energy range 20 - 26 MeV to be : $J_W/A = J_W(E=E_x)/A - (1 \pm 0.4)E$. For the Sn isotopes in the energy range 15 MeV - 26 MeV they give : $J_W/A = J_W(E=E_x)/A - (0.6 \pm 0.2)E$, whereas I have found for $^{93}$Nb in the energy range 11 MeV - 50 MeV the following expression : $J_W/A = J_W(E=E_x)/A - 0.23\ E$. From the theoretical calculations by JEUKENNE et al./19/ of $J_W/A$ for protons on $^{120}$Sn it appears that $J_W/A$ increases between low energies and 37 MeV, and then decreases sligthly. More precise proton reaction cross sections are needed at higher energies (E > 25 MeV) in order to determine more precisely the energy dependence of the absorptive part of the OMP.

## 2.3. The spin-orbit dependence of the OMP (spherical nuclei)

H.C. VOLKIN has shown /20/ that in order to obtain an acceptable fit to polarization measurements it was necessary to adopt the following value of the spin-orbit potential radius $R_{so} \simeq 1.1\ A^{1/3}$, which is smaller than the one adopted for the real central potential. WIEDLING /13/ has demonstrated in case of neutron scattering that the slopes of the differential scattering cross sections curve increase quite drastically at the backward angles with decreasing numerical value of the spin-orbit term. Moreover he suggested a value of $V_{so}$ equal to 6 MeV that appeared to him as a good choice.

In order to avoid having to choose a radius and a diffuseness for the spin-orbit potential I suggest to adopt the form currently used in shell model calculations :

$$V_{so}(r) = -\frac{1}{3}\pi\ V_{so}\ \frac{1}{r}\frac{d}{dr}\ \left[\rho_U + 2\rho_L\right]\ \vec{\ell}.\vec{\sigma} \qquad (10)$$

where $\rho_U$ (and $\rho_L$) refer to unlike (and like) projectile-target nucleon density distributions. I present in Fig. 1 such a potential ($V_{so}$ = - 61 MeV fm$^5$) calculated by using the nucleon densities obtained from Hartree-Fock-Bogolyubov calculations by DECHARGE /21/ (full line) together with phenomenological forms calculated with the following parameters : $V_{so}$ = 7.7 MeV (for neutrons), $V_{so}$ = 6.4 MeV (for protons), $a_{so}$ = 0.47 fm, $r_{so}$ = 1.12 fm (dashed curve). We think that it is sufficient, concerning that potential, to assume the density distributions of neutrons and protons have the same geometry and are given according to the semi-empirical expression proposed by NEGELE /22/.

# 3. PARAMETERIZATIONS OF THE OMP

Optical model calculations of nucleon cross sections can be employed as an extrapolational tool when the OMP parameter set used has been previously tailored on all the available nucleon experimental data in the energy range or mass region of interest. We try and explain below the expected aid of experimental data in the empirical parameterization of the OMP.

## 3.1. Neutron strength functions, scattering radius and total cross section

At very low energies the neutron absorption cross sections can be expressed in terms of neutron strength functions ($S_0$,$S_1$), the experimental data of which can be used for the determination of the absorptive part of the OMP. Moreover the "potential scattering radius" R' which determines the off resonance scattering cross section and is defined by :

$$R' = \lim_{(E\to 0)} (\sigma^{SE}/4\pi)^{1/2} \qquad (11)$$

(where SE is for "shape elastic scattering cross section") can also be used

for the determination of the real part of the OMP. From the example shown in Table II it appears that an adjustment on $S_0$, $S_1$, R' fixes the value of V within 1%, whereas the less satisfying determination of $W_D$ (30%) is due to the large experimental uncertainties associated to the strength functions. These calculations were performed by PERRIER /24/, using the spherical optical model code SOMC2 /25/. As can be shown in Table III a small variation of V (2%) changes the value of the calculated ratio $S_0/S_1$ drastically (80%).

I share with the Argonne Laboratory Group /26/ the belief that "a first criteria for an energy-averaged model is consistency with the measured total cross section over a wide energy range". It is important to note that the calculated values of the total cross sections cannot describe the experimental ones in detail at lower energies (resonances, fluctuations) but only the energy averaged data. However at lower energies the broad structure in the total cross section observed in the mass region A = 93 can be reproduced by the model as can be seen in Fig. 2. Differences of 10% between calculated values are obtained at an energy of 0.5 MeV when only the parameter V is varied by 2%. From that result and those presented in Table II the real well of the OMP can be fairly determined. The sensibilities of the calculated total ($\sigma_t$) and shape elastic ($\sigma_s$) cross sections to a small variation of V (1%) are presented for $^{89}Y$ in Fig. 3.

3.2. Proton reaction cross sections (lower energies)

It was pointed out by JOHNSON et al. /27/ that (p,n) cross sections in energy region where the cross sections are nearly equal to the total absorption cross sections could be a useful tool for the determination of proton OMP parameters. More recent measurements of sub-coulomb proton absorption for isotopes of zirconium and molybdenum were performed by FLYNN et al. /28/ in the energy range 1.7 - 6.7 MeV. Experimental strength functions were there defined as :

$$SF = R\ \sigma(p,n)/[4\pi^2\ k^{-2} \sum_{\ell} (2\ell+1)P_\ell] \qquad (12)$$

where $P_\ell$ is the Coulomb penetration factor evaluated at the radius $R = 1.45\ A^{1/3}$. Their results are in Fig. 4 for $^{92}Zr$ together with predictions from various OMP parameters : BECCHETTI and GREENLEES (dotted line), JOHNSON et al. (dashed curve), and those they obtained (full line). These authors also pointed out that "the quantity $VR_R^2$ is determined by causing the maximum and minimum to occur at the correct energies".

3.3. Nucleon elastic scattering data

When experimental data are fitted with an optical potential search code it is possible to obtain a good $\chi^2$ with parameters which do not satisfy the theoretical constraints. Moreover in order to avoid well known parameter ambiguities such as "$Vr_R^x$" or "$W_D\ a_D$" the search has to be guided. For these reasons I suggest to adopt the prescription described in Ref. 29.

As noted in Ref. 26 "Energy averaged interpretations of elastic distributions have meaning only in the context of broad averages transcending local and intermediate structure fluctuations". Moreover at low energies the theoretical cross section is the incoherent sum of direct and compound cross sections. These compound components are calculated using the statistical model, and it still remains many uncertainties in the practical applications of this model : width fluctuation factors, spin and parity assignments for the discrete levels, level density for the continuum... . An exemple of such difficulties is shown in Fig. 5. The two calculated curves differ from each other in the practical treatment of the width fluctuation factor (cf. Ref. 11). For

these reasons it seems to me difficult to obtain meaningful OMP parameter sets from a fit to elastic scattering at low energies. At higher energies the compound contribution to the elastic cross sections vanishes and the model can be applied with great confidence. Nevertheless other experimental constraints such as total or reaction cross sections should be included in the OMP determination procedure in order to avoid ambiguities arising from experimental normalization uncertainties.

. Neutron OMP parameters were obtained for the even Molybdenum isotopes by RAPAPORT et al. in the energy range 7 - 26 MeV. The analysis of their elastic scattering data was done in two steps : "first the individual searches were carried out by varying the maximum number of parameters. Then the average geometry was obtained and kept fixed while searches were conducted on the potential strengths" as clearly explained in Ref. 8.

### 3.4. (p,n) isobaric analog state data

The obvious way to test the isovector components of the OMP is by studying quasi-elastic scattering to the ground state isobaric analog. Theoretical calculations of the (p,n) transition amplitudes can be made by solving the coupled equations derived by LANE /30/. I mention that the formalism for (p,n) reaction to analogs of ground and excited state has been recently developed by MADSEN and collaborators. Investigations of such reactions for even Samarium isotopes have been presented by them in a recent paper /20/. In the following I consider the case of (p,n) reaction to the ground state isobaric analog. I have recently /18/ made comparisons of calculated values with experimental data, obtained for $^{93}$Nb, between 18 MeV and 50 MeV, and the results for 49.4 MeV protons are shown in Fig. 6. The dashed curve has been obtained with a surface absorptive term only in the diagonal potentials and the isovector components as determined from a fit on (p,n) data for 18 MeV protons. Further calculations were done by including volume absorption in the diagonal potential (dot-dashed curve), and finally by reducing the depth of the real isovector term (solid curve). From the shape of the experimental angular distribution it is clear that both volume and surface absorptive terms are needed in the diagonal part of the OMP.

### Remark on some experimental data

Nucleon reaction data are needed at high enough energies as a guide to the determination of the absorptive terms of the OMP. Unfortunately the experimental values scatter too much and have large uncertainties. Polarization data which are a guide for the determination of the spin-orbit potential are too sparse.

### 3.5. The "SPRT" parameter determination procedure

The determination of a set of OMP parameters is carried out in three stages.

The first one consists of a fitting of the model parameters to the neutron strength functions and scattering radius. The parameters involved are $V$, $a_R$, $r_R$, $W_D$, $a_D$, $r_D$, whereas the depth and the geometry part of the spin-orbit potential have the values given in Ref. 6 or in Ref. 33.

In the second stage, in order to test the parameters obtained, comparisons are done between calculated and experimental values of the total cross section assuming a reasonable energy dependence of the potential depths ($b_0 = 0.3$, $b_2 = 0.4$, Eq. 2). These comparisons are for a few carefully chosen neutron energies, at the minima and maxima of the cross section for example, and in a limited energy range : 10 keV - 15 MeV. If the agreement is not satisfactory the depths and (or) the geometric parameters are varied and

search is started again at the first stage.

If a good agreement cannot be obtained we must explore the necessity of coupled channel calculations or the possible effect of a modification of the coupling basis and (or) the deformation parameters.

Final adjustments of all the parameters are made in the third stage by considering neutron elastic and inelastic scattering, total cross sections at higher energies, proton scattering data... . If the agreement with nucleon inelastic scattering data is not satisfactory, the deformation parameters or the coupling basis are modified and search is started again at the first stage.

This procedure was clearly explained by PERRIER in Ref. 24, and some results obtained by him are here briefly reported on. An example of the method employed in the second stage is presented in Table IV. The values of $V_0$ and $W_{D0}$ obtained from the first stage of the procedure were : $V_0 = 49.59$ and $W_{D0} = 2.907$, with uncertainties of 1% and 30% respectively. Assuming $b_0 = 0.3$ and $b_2 = 0.4$ (cf Eq. 2) a chi-square fitting of $V_0$ and $W_{D0}$ to the total cross sections at various energies was undertaken. The values obtained : $V_0 = 48.63 \pm 0.7$, $W_{D0} = 4.64 \pm 2$ differed from those resulting from the first stage, nevertheless a good reasonable agreement to the experimental data considered in the first and second stages was obtained with $V_0 = 49.0$, $W_{D0} = 3.3$. With these starting values a chi-square fitting of $V_0$ and $W_{D0}$ has been made to the neutron elastic scattering data at various energies /34/ (cf. Table V). From all these results the final values deduced are : $V_0 = 49.0$, $W_{D0}$ : 3.600, $b_2 = 0.500$.

It is clear that a reasonable agreement is finally obtained with all the experimental data, and that it is not the best one possible for each case individually ; for example the final calculated values of the strength functions and scattering radius, namely $S_0 \doteq 0.40\ 10^{-4}$, $S_1 = 3.59\ 10^{-4}$, $R' = 6.76$ fm, are less satisfactory than those presented in Table II.

In this mass number region I have employed this procedure in the case of $^{89}Y$, $^{93}Nb$, $^{103}Rh$ and for the even-A isotopes of Neodynium, Samarium and Gadolinium.

## 4. DETERMINATION OF THE ISOVECTOR COMPONENTS OF THE OMP

A review paper was recently written by J. RAPAPORT and R.W. FINLAY /35/ on that subject and thus I present only some particular aspects of that problem.

Empirical informations in the isovector parts of the OMP can be obtained from comparisons of neutron and proton scattering data from the same nuclei. Unfortunately these informations are ambiguous for the following reasons :

- In the theoretical calculations of JEUKENNE et al. /16/ the real coulomb correction has the form : $\Delta V = V(r,E-V_C) - V(r,E)$, whereas the empirical form is : $\Delta V = b_3\ f(x_R)\ Z/A^{1/3}$. The value of $b_3$ is currently calculated using the prescription of SATCHLER /36/ : $b_3 = 1.17\ b_0/r_C$ ($b_3 \sim 0.4$). An empirical determination of this coefficient was performed by RAPAPORT et al. /37/ from their analyses of nucleon scattering for T = 0 nuclei. The value quoted in Ref. 37 is $b_3 = 0.46 \pm 0.07$. Comparisons between theoretical and empirical determinations are unrealistic, and proper comparisons of various empirical ones can be made only if the values of the volume integral per nucleon ($J_{bC}/A$) of $b_3\ f(x_R)$ are almost the same. It is the case for the determinations of $J_{V_1}/A$ carried out in Ref. 38 and Ref. 18 :

$\varepsilon\ J_{V_1}/A = 20.9 - 0.17E,\quad J_{bc}/A = 3.812$ for $^{90}Zr$ /38/

$\varepsilon\ J_{V_1}/A = 21.48 - 0.16E,\quad J_{bc}/A = 3.713$ for $^{93}Nb$ /18/

$\varepsilon\ J_{V_1}/A = 25.48 - 0.21E,\quad J_{bc}/A = 3.734$ for $^{116}Sn$ /38/.

From these calculated values I recommend to adopt the mean value of $J_{bc}/A$ : 3.75. Moreover in the mass region in consideration the empirical values of $J_{V_1}/A$ increase slightly with the mass number /38/, as predicted by the theoretical calculation /16/.

- In empirical calculations it is assumed that the imaginary Coulomb correction term $\Delta W$ is equal to zero, whereas it has been found by JEUKENNE et al. that this term, $\Delta W = W(r, E - V_C) - W(r,E)$, was greatly energy dependent (greater at lower energies than at higher energies) and of a sign opposite to the one of the absorptive term, hence a possible cancellation, near the Coulomb barrier, with the imaginary isospin term. The fact that the imaginary Coulomb correction term is not taken into account in the empirical proton OMP determinations could explain the abnomalous energy dependence of some parameters observed in the neighbourhood of the Coulomb barrier. In these determinations, for example, the energy dependence of the potential depths are much more rapid than at higher energies /39/, /40/, or the diffuseness of the surface absorptive potential is energy dependent /41/.

The effects of such inadequacies in the empirical treatment of the Coulomb correction terms can be illustrated by the following example :

To test my nucleon OMP set of parameters /18/, I have recently made /42/ comparisons of calculated and experimental /27/ values of sub-Coulomb proton strength functions for $^{89}Y$, $^{93}Nb$, $^{103}Rh$. The agreement was within 20% for $^{93}Nb$ and $^{103}Rh$, but within 50% for $^{89}Y$. A sligth modification of $V_R$ and a drastic decrease of $W_D$ was necessary so as to obtain a good agreement. In these last calculations the absorptive term was the same for neutrons and sub-Coulomb protons. Moreover the fit on the neutron and proton strength functions indicates a strong A-dependence of $W_D$ ($W_D = 2.6$ for $^{89}Y$, $W_D = 5.4$ for $^{103}Rh$). This A-dependence is nevertheless smaller than the one observed by JOHNSON et al. /27/ ($W_D = 6.0$ for $^{89}Y$ and $W_D = 97.0$ for $^{103}Rh$) from their fit to only proton strength functions.

## 5. NUCLEON SCATTERING FROM COLLECTIVE STATES

Recent efforts carried out in several laboratories for more precise information about nucleon scattering from collective states were recently reported by HAOUAT /43/ with a special emphasis on experimental difficulties. Thus I present only the main problems generally met in the calculations.

### 5.1. Coupled channels or spherical optical model calculations ?

The experimental evidence of the coupling projectile-target states comes from analyses of experimental data in inelastic scattering and in the variations of the strength functions with the mass number. Theoretical guides come from analyses of the excited states spectra ; in this paper I distinguish, as usual, between "vibrational" and "rotational" nuclei.

As can be seen in Fig. 7 there is no important discrepancies between statistical model calculations /11/ and experimental data /10/ (cf Ref. 11). However near neutron energy of 6.0 MeV the statistical model indicates inelastic scattering cross sections, for the two states in consideration, near zero, whereas the experimental value /44/ of the sum is 137 millibarns.

The low lying spectra of the stable even A Mo isotopes show many characteristics of a vibrational nucleus but the marked decreases in the first $0^+$ excitation energy as neutrons are added to $^{92}$Mo, indicate that the collective wave functions for these nuclei are of a complex nature. A reasonable agreement with all the experimental data, except inelastic scattering cross sections at energies greater than 4 MeV, can be obtained using only spherical model calculations /11/. I think that for the mass region A = 89 - 103, spherical model calculations and D.W.B.A. calculations are sufficient in most of the cases. On the other hand coupled channel calculations are needed in the mass region A = 144 - 170. As can be seen in Fig. 8, the coupling between elastic and inelastic channels is quite strong : a small variation of the deformation parameter induces a change in the inelastic as well as elastic scattering distributions /45/.

5.2. Deformation parameters

It is clear that :

1) For "vibrational" nuclei, deformation parameters obtained from neutron inelastic scattering data and electromagnetic excitations data are almost equal. MADSEN, BROWN and ANDERSON /46/ have presented some theoretical explanations of the small differences between deformation parameters obtained using various probes. An example of such differences is shown in Table VI, where experimental determinations are reported from Ref. 35 and Ref. 47.

2) For rotational nuclei, instead of comparing the deformation parameters $\beta_2$ $\beta_4$, comparisons have to be made using the multipole moments of the OMP which are defined as :

$$q_\lambda = Z\int V(r)\, Y_\lambda^0(\theta)\, r^\lambda\, \vec{dr} \,/\, \int V(r)\, \vec{dr} \qquad (13)$$

From the results presented in Ref. 48 and Ref. 14 the quadrupole moments obtained from nucleon scattering and electromagnetic excitations are in a very good agreement.

Another problem is that the empirical calculations of neutron inelastic scattering cross sections are in rather poor agreement with the experimental pronounced structure. As reported in Fig. 9 BRIEVA and GEORGIEV /49/ have shown that a much better agreement could be obtained if a more realistic scattering potential is employed.

5.3. The problem of odd-A nuclei

For vibrational nuclei the coupling scheme can be chosen following the prescription derived from the weak coupling model of De-SHALIT /50/. The optical model potential used in such a case can be extrapolated from that obtained for neighbouring even-A nuclei. The problem is more complex for rotational nuclei :

The diagonal potential for the ground state of an even-A nucleus is defined as :

$$V_{g.s}(r) = V_{\lambda=0}(r)\, g_\lambda \text{ , whereas for an odd-A nucleus :}$$

$$V_{g.s}(r) = \sum_{\lambda=0}^{2I} \langle I \,\|\, Q_\lambda \,\|\, I \rangle\, g_\lambda\, V_\lambda(r).$$

In these expressions the $g_\lambda$ are geometrical coefficients, $V_\lambda$ corresponds to the term of order $\lambda$ in the Legendre expansion of the potential, and I is the spin of the ground state. Except the case of I = 1/2, the definition of the potential

for odd-A nuclei is not the same than for even A nuclei and therefore parameters have to be determined in each individual case.

### 5.4. The problem of transitional nuclei

Wave functions more elaborate than those currently employed in the "vibrational" or "rotational" model are needed for these nuclei. An example of the calculated inelastic cross section leading to the first $2^+$ state of $^{150}Sm$ is given in Fig. 10. Comparisons of experimental data and results of rotational model calculations are given together with results of more elaborate calculations based on the wave functions obtained by KUMAR /51/ from his dynamic deformation theory of spherical and deformed nuclei.

## CONCLUSION

I believe that optical model calculations of neutron cross sections can be usefully employed for practical applications. When a very limited amount of experimental data is available the optical model parameterization can be based on an adequate readjustment of a parameter set previously tailored for a neighbouring nucleus. For this purpose more accurate experimental values of strength functions are required. As for the theoretical tools, more precise informations are needed concerning the deformation parameters for odd-A nuclei, and the collective wave functions.

## Aknowledgments

I would like to thank Dr J. SALVY for many discussions and comments and for the preparation of the paper. I am thankful to the many scientists from whom I received papers and informations.

## REFERENCES


/1/ C. MAHAUX, Lectures given at the "Course on Nuclear Theory for Applications" ICTP Trieste, 17 January - 18 February 1978 (IAEA, Vienna, to be published).

/2/ S. IIJIMA, Review paper 9, Fission product Nuclear Data, Petten 5-9 September 1977 (IAEA-213).

/3/ P.A. MOLDAUER, Nucl. Phys. 47 (1963) 65.

/4/ S. IGARASI et al., Japanese Nuclear Data Committee, Evaluation of fission product nuclear data for fast reactor, JAERI-M-57, (1974).

/5/ L. ROSEN, J.G. BEERY, A.S. GOLDHABER and E.H. AUERBACH, Ann. Phys. 34 (1965) 96.

/6/ F.D. BECCHETTI and G.W. GREENLEES, Phys. Rev. 182 (1969) 1190.

/7/ D. WILMORE and P.E. HODGSON, Nucl. Phys. 55 (1964) 673.

/8/ T.S. CHEEMA, Ph. D. Thesis Ohio University (1976).

J. RAPAPORT, T.S. CHEEMA, D.E. BAINUM, R.W. FINLAY and J.D. CARLSON, Nucl. Phys. A313 (1979) 1.

/9/ F.D. McDANIEL, J.D. BRANDENBERGER, G.P. GLASGOW, W.H. LEIGTHON, Phys. Rev. C10 (1974) 1807.

/10/ A. SMITH, P. GUENTHER, J. WHALEN, Nucl. Phys. A244 (1975) 215.

/11/ Ch. LAGRANGE, Contributed paper in Neutron data of structural materials for fast reactors. Pergamon Press (1978) 756.

/12/ S. KAILAS, S.K. GUPTA, Phys. Lett. 71B (1977) 271 and Phys. Rev. C17 (1978) 2236.

/13/ T. WIEDLING, Invited paper in Proc. of the III$^{th}$ Int. Symposium on the interactions of fast neutrons with nuclei (Gaussig GDR 21-25 November 1977)- ZFK 376

/14/ Ch. LAGRANGE, J.P. DELAROCHE, Proc. of an Int. Conf. on Neutron Physics and Nuclear Data (Harwell U.K. 1978) p. 355.

/15/ J. RAPAPORT, M. MIRZAA, H.HADIZADEH, D.E. BAINUM and R.W. FINLAY, to be published and private communication.

/16/ J.P.JEUKENNE, A. LEJEUNE, C. MAHAUX, Phys. Rev. C16 (1977) 80.

/17/ L.R.B. ELTON, in Nuclear radii, ed. H. Schopper (Springer-Verlag, Berlin, 1967) p.5.

/18/ Ch. LAGRANGE, Bull. Am. Phys. Soc. 24 (1979) 876.

/19/ J.P. JEUKENNE, A. LEJEUNE and C. MAHAUX, Phys. Rev. 16 (1977) 80.

/20/ H.C. VOLKIN, Bull. Am. Phys. Soc. 9 (1964) 439.

/21/ J. DECHARGE, private communication.

/22/ J.W. NEGELE, Phys. Rev. C1 (1970) 1260.

/23/ S.F. MUGHABGHAB and G.I. GARBER, BNL-325, Third edition, volume 1 EANDC(US) 183 "L" - INDC(US) 3816.

/24/ R. PERRIER, Thèse C.N.A.M., Paris (1978).

/25/ Ch. LAGRANGE and R. PERRIER, Note CEA-N-2088 , NEANDC(E) 205 "L", INDC(FR) 35/L (1979).

/26/ A. SMITH, R. McKNIGHT and D. SMITH (cf. Ref. 11 p. 374).

/27/ Ch. JOHNSON and R.L. KERNELL, Phys; Rev. Lett. 39 (1977) 1606.

C.H. JOHNSON, A. GALONSKY and R.L. KERNELL, to be published in Phys. Rev. C, and private communication.

/28/ D.S. FLYNN, R.L. HERSHBERGER and F. GABBARD, to be published in Phys. Rev. C and private communication.

/29/ J. RAPAPORT, T.S. CHEEMA, D.E. BAINUM, R.W. FINLAY and J.D. CARLSON, Nucl. Phys. A296 (1978) 95.

/30/ A.M. LANE, Phys. Rev. Lett. 8 (1962) 17.

/31/ C. WONG, V.R. BROWN, V.A. MADSEN and S.M. GRIMES, Phys. Rev. C 20 (1979) 59.

/32/ C.J. BATTY, B.E. BONNER, E. FRIEDMAN, C. TSCHALAR, L.E. WILLIAMS, A.S. CLOUGH and J.B. HUNT, Nucl. Phys. A116 (1968) 693.

/33/ F.G. PEREY, Phys. Rev. 131 (1963) 745.

/34/ F.G. PEREY, W.E. KINNEY, Report ORNL-4552 (1970).

/35/ J. RAPAPORT and R.W. FINLAY, IEEE Transactions on Nuclear Science, Vol. NS-26, n° 1 (February 1979).

/36/ G.R. SATCHLER, Isospin in nuclear physics (1969) Ch. 9 (D.H. Wilkinson, Ed.) North Holland Publishing Company, Amsterdam.

/37/ J. RAPAPORT, J.D. CARLSON, D. BAINUM, T.S. CHEEMA, R.W. FINLAY, Nucl. Phys. A286 (1977) 232.

/38/ J. RAPAPORT, to be published and private communication.

/39/ J.S. ECK and J.W. THOMSON, Nucl. Phys. A237 (1975) 83.

/40/ B. GYARMATI, T.VERTSE, L. ZOLNAI, A.I. BARYSHNIKOV, A.F. GURBICH, N.N. TITARENKO and E. YADROVSKY, J. Phys. G5 (1979) 1225.

/41/ W. DRENCKHAHN, A. FEIGEL, E. FINCK, R. KEMPF, M. KOENNER, P. KRÄMMER and H.K. UEBEL, to be published.

/42/ Ch. LAGRANGE, to be submitted as a comment on Physical Review C.

/43/ G. HAOUAT, Invited paper - The second International Symposium on Neutron induced reactions, Smolenice June 25-29 (1979).

/44/ M.T. McELLISTREM, Private communication.

/45/ Ch. LAGRANGE, J. LACHKAR, G. HAOUAT, R.E. SHAMU and M.T. McELLISTREM, to be submitted in Nuclear Physics.

/46/ V.A. MADSEN, V.R. BROWN and J.D. ANDERSON, Phys. Rev. Lett. 34 (1975) 1388.

/47/ J. RAPAPORT, T.S. CHEEMA, D.E. BAINUM, R.W. FINLAY and J.D. CARLSON, Nucl. Phys. A296 (1978) 95.

/48/ R.S. MACKINTOSH, Nucl. Phys. A266 (1976) 379.

/49/ F.A. BRIEVA and B.Z. GEORGIEV, Nucl. Phys. A308 (1978) 27.

/50/ A. De SHALIT, Phys. Rev. 122 (1961) 1530.

/51/ K. KUMAR, Invited paper at the Conference on the Structure of Medium-Heavy Nuclei, 1-4 May 1979, Rhodos, Greece.

TABLE I

Values of volume integral per nucleon and root mean square radius of the real central potential obtained from various studies

| TARGET | $J_V/A$ | | | | $\langle r_V^2 \rangle^{1/2}$ | | | |
|---|---|---|---|---|---|---|---|---|
| | CHEEMA• Ref.8 | SMITH et al. Ref.10 | McDANIEL•• et al. Ref.9 | LAGRANGE Ref.11 | CHEEMA• Ref.8 | SMITH et al. Ref.10 | McDANIEL et al. Ref.9 | LAGRANGE Ref.11 |
| $^{92}Mo$ | 439.6 | 407 | 450 | 441 | 4.854 | 4.889 | 4.996 | 4.912 |
| $^{100}Mo$ | 415.7 | 390 | 448 | 428 | 4.957 | 4.991 | 5.103 | 5.018 |

• Calculated with the following average geometry : $a_R = 0.66$, $r_R = 1.20$
•• Calculated with : $V = V_o - 0.22\ E_n$

TABLE II

Uncertainties in the fitting parameters induced by the experimental uncertainties. Application to $^{89}Y + n$.

| | | $S_0 . 10^{+4}$ | $S_1 . 10^{+4}$ | R'(fm) |
|---|---|---|---|---|
| Evaluated values (BNL-325 Réf.23) | | 0.32±0.11 | 4.4±1.6 | 6.7±0.1 |
| Best fit parameters | $V = 49.6 \pm 0.500$<br>$W_D = 2.9 \pm 0.9$ | 0.347 | 3.287 | 6.684 |

The fixed parameters are : $r_R = 1.25$, $a_R = 0.65$, $r_D = 1.25$, $a_D = 0.47$
$V_{so} = 6.2$, $r_{so} = 1.12$, $a_{so} = 0.47$ (depth in MeV, lengths in Fermis).

TABLE III

Evaluated and calculated neutron strength functions ($S_0$,$S_1$) and scattering radius for $^{93}$Nb.

| | EVALUATED BNL-325 | CALCULATED | | |
|---|---|---|---|---|
| | | V = 4.90 | V = 49.5 | V = 50.0 |
| $S_0 . 10^{+4}$ | 0.36±0.06 | 0.447 | 0.433 | 0.423 |
| $S_1 . 10^{+4}$ | 5.16±0.24 | 3.840 | 4.567 | 5.456 |
| R'(fm) | 7.00±0.2 | 6.713 | 6.628 | 6.544 |

The fixed parameters are : $a_R$ = 0.62, $r_R$ = 1.24, $W_D$ = 3.4, $a_D$ = 0.58 $r_D$ = 1.26, $V_{so}$ = 7.7, $a_{so}$ = 0.47, $r_{so}$ = 1.12 (depths in MeV, lengths in Fermis).

TABLE IV

Parameter set obtained by searching the real and surface potential depths so as to optimize the fit to neutron total cross section for $^{89}$Y at various energies.

| $E_n$(MeV) Exp. $\sigma_T$ (barns) | 2.5 4.140±0.166 | 5.0 3.740±0.150 | 8.0 4.300±0.172 | 10.0 4.240±0.180 | 15.0 3.780±0.150 |
|---|---|---|---|---|---|
| Best fit $V_0$= 48.63±0.7 $W_{DO}$ = 4.64±2.06 | 4.208 | 3.800 | 4.232 | 4.248 | 3.728 |

The fixed parameters are : $a_R$ = 0.673, $r_R$ = 1.248, $a_D$ = 0.469, $r_D$ = 1.262, $V_{so}$ = 6.2 $a_{so}$ = 0.47, $r_{so}$ = 1.12 (depths in MeV, lengths in Fermis).

TABLE V

Parameter sets obtained by searching the real and surface potential depths so as to optimize the fit to $^{89}Y$ proton scattering at various energies.

| E (MeV) | $V_0$ | $W_{DO}$ | $\chi^2/N$ |
|---|---|---|---|
| 6.44 | 49 | 3.3 | 5.22 |
| | 48.77 ± 0.13 (0.26%) | 3.87 ± 0.12 (3%) | 2.2 |
| 7.6 | 49 | 3,3 | 7.92 |
| | 48.96 ± 0.24 (0.5%) | 4.38 ± 0.19 (4.4%) | 2.3 |
| 8.56 | 49 | 3.3 | 4.7 |
| | 49.1 ± 0.22 (0.44%) | 4.28 ± 0.19 (4.38%) | 1.6 |

The fixed parameters are the same than those presented in Table IV.

TABLE VI

Quadrupole deformation parameters for N = 50 and Z = 50 single-closed shell nuclei.

| β | Nuclei N = 50 | | | Nuclei Z = 50 | | | | |
|---|---|---|---|---|---|---|---|---|
| | $^{88}Sr$ | $^{90}Sr$ | $^{92}Mo$ | $^{116}Sn$ | $^{118}Sn$ | $^{120}Sn$ | $^{122}Sn$ | $^{124}Sn$ |
| $\beta_{nn'}$ | 0.133(7) | 0.085(8) | 0.099(5) | 0.120(10) | 0.109(7) | 0.106(5) | 0.100(6) | 0.092(6) |
| $\beta_{pp'}$ | 0.110 | 0.070(5) | 0.080(6) | 0.133 | 0.134(10) | 0.119(10) | 0.112(7) | 0.108(7) |
| $\beta_{em}$ | 0.14 (2) | 0.094(5) | 0.116(8) | 0.118(7) | 0.108(2) | 0.106(2) | 0.102(2) | 0.096(2) |

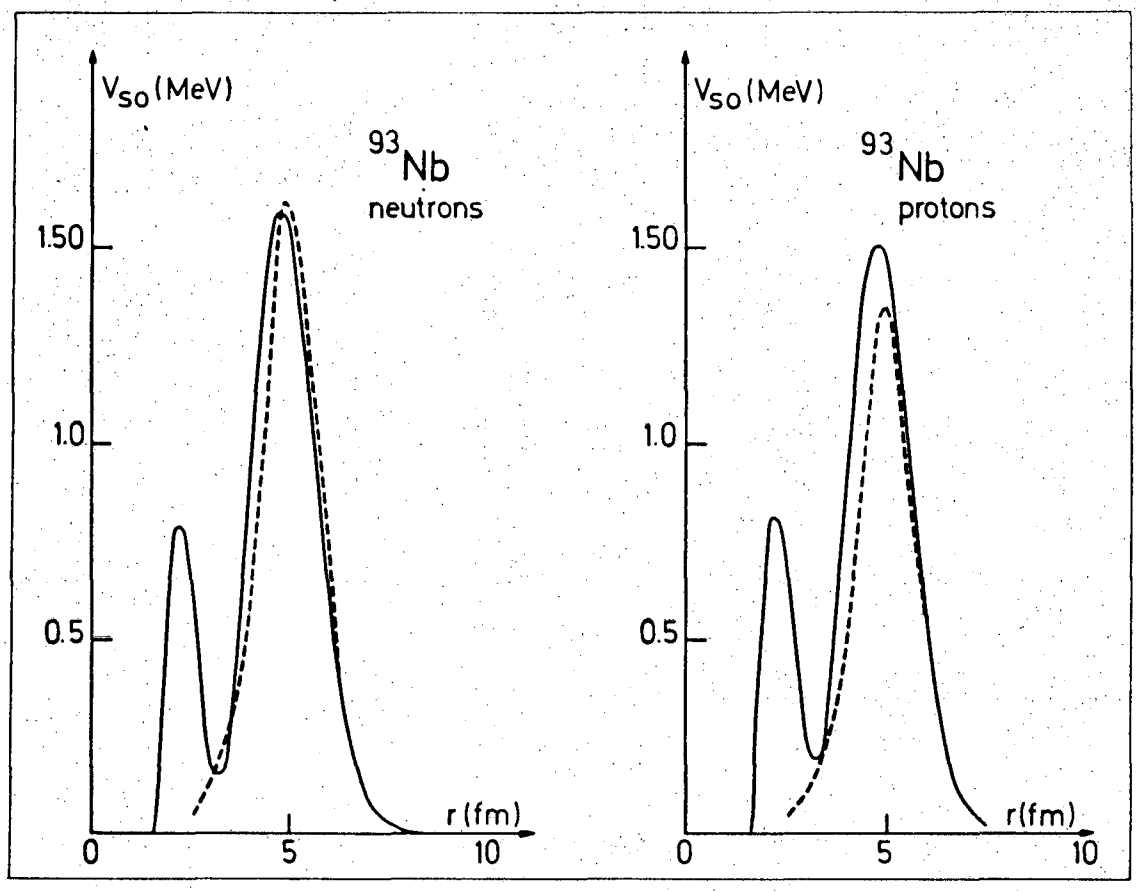


Fig. 1 - Radial variations of the nucleon spin-orbit potential for $^{93}Nb$

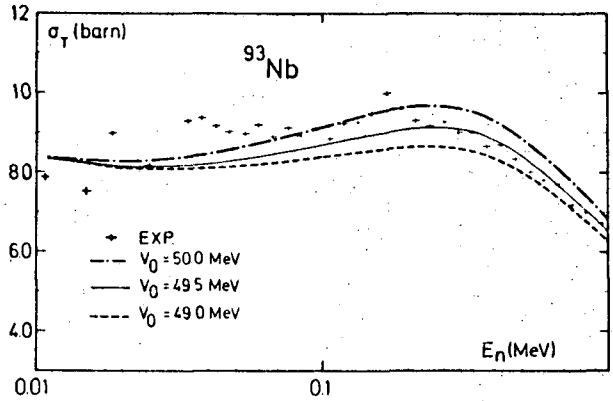


Fig. 2

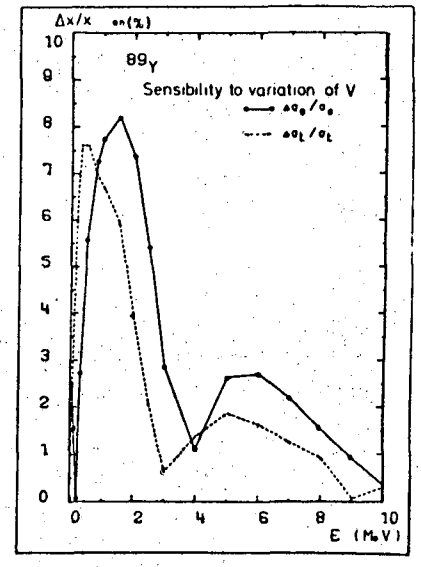


Fig. 3

Sensibilities of the calculated total cross section to small variations of the real potential depth -(Total cross section Fig. 2, total and shape elastic scattering Fig. 3).

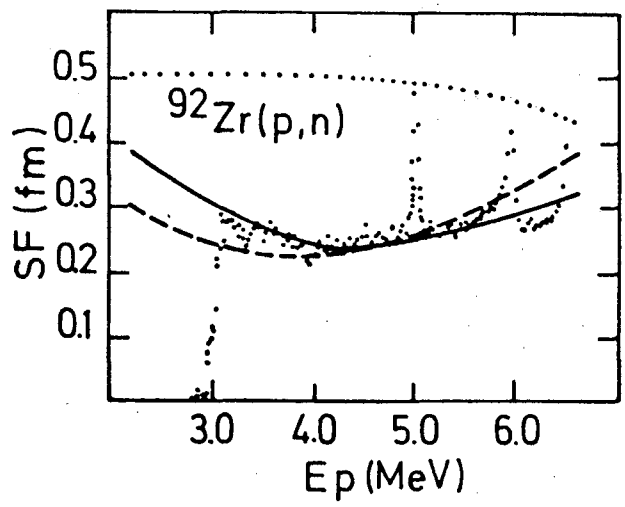


Fig. 4

$^{92}$Zr (p,n) strength functions

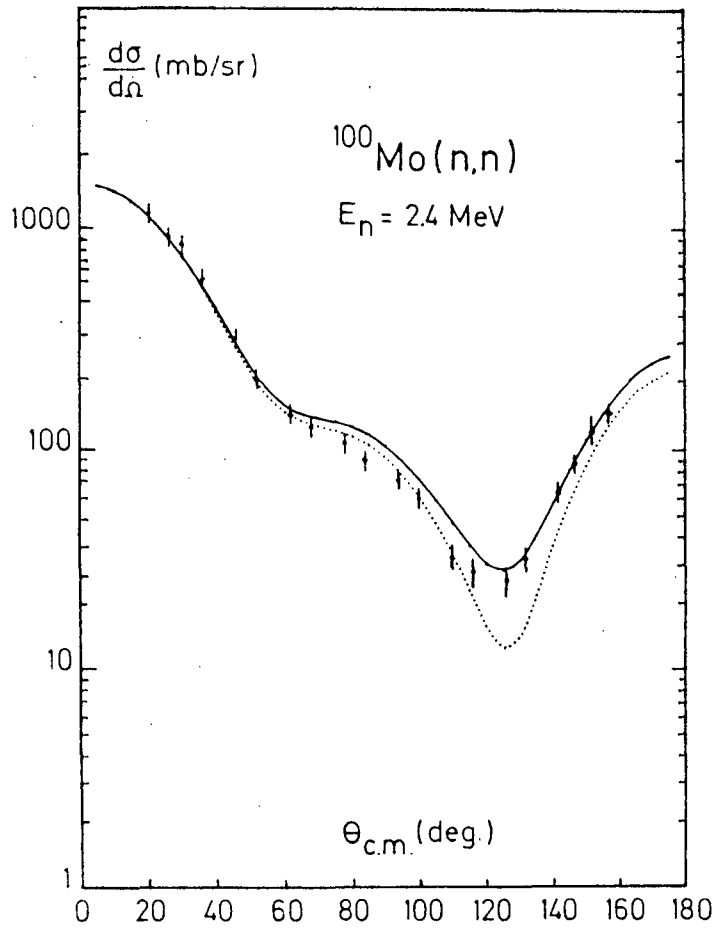


Fig. 5

Differential elastic scattering cross sections for 2.4 MeV neutrons on $^{100}$Mo.

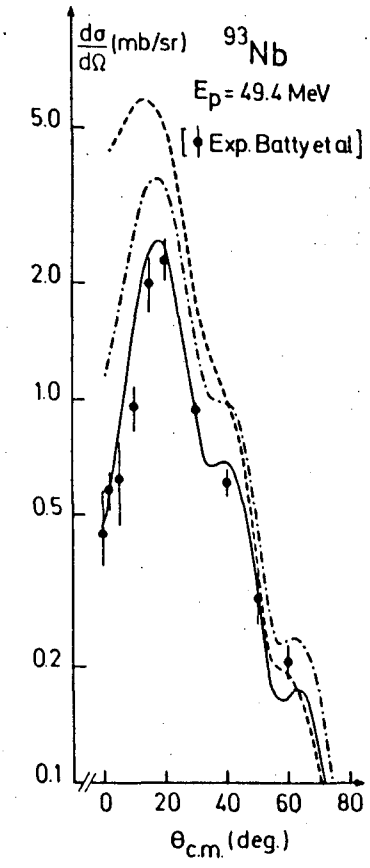


Fig. 6

Comparisons of coupled channel calculations with (p,n) IAS differential cross section data.

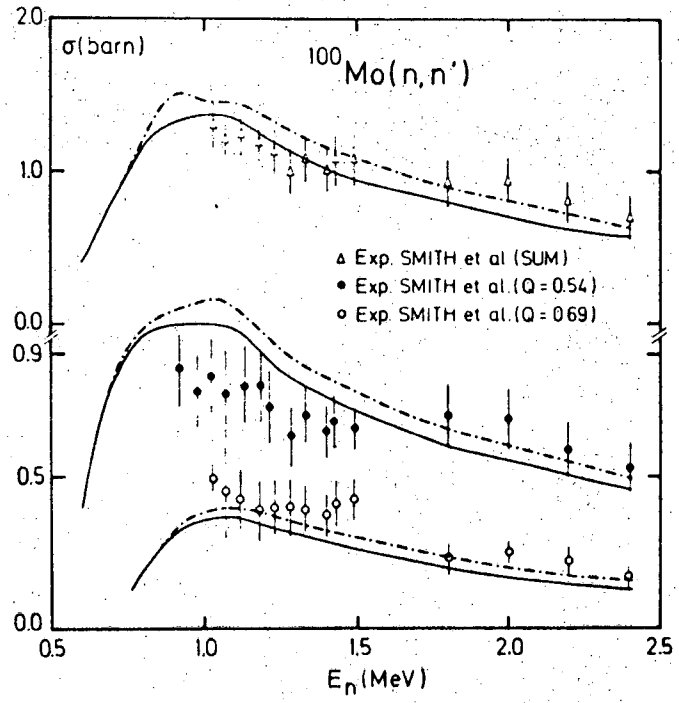


Fig. 7

Excitation functions for the reactions $^{100}Mo$ (n,n').

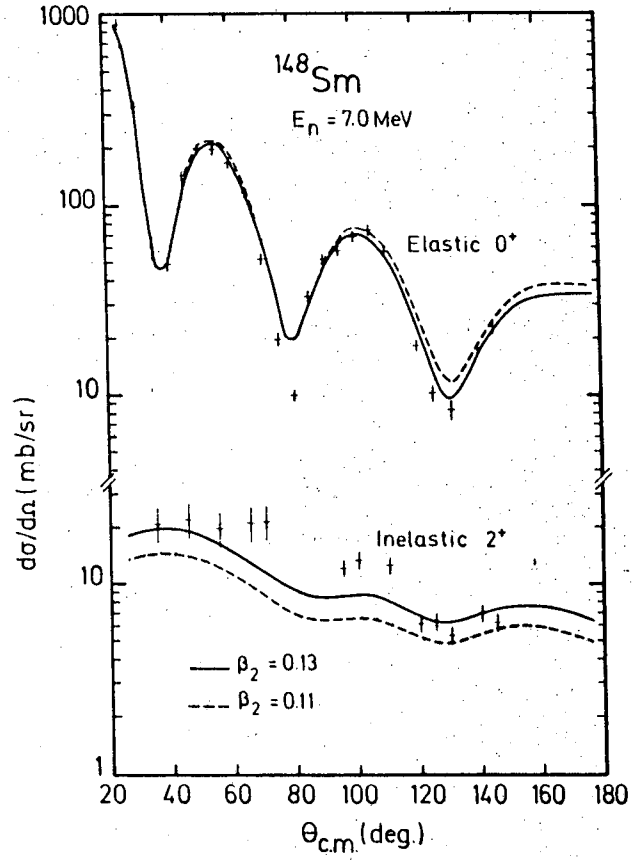


Fig. 8

Differential elastic and inelastic cross section for 7.0 MeV neutron on $^{148}Sm$.

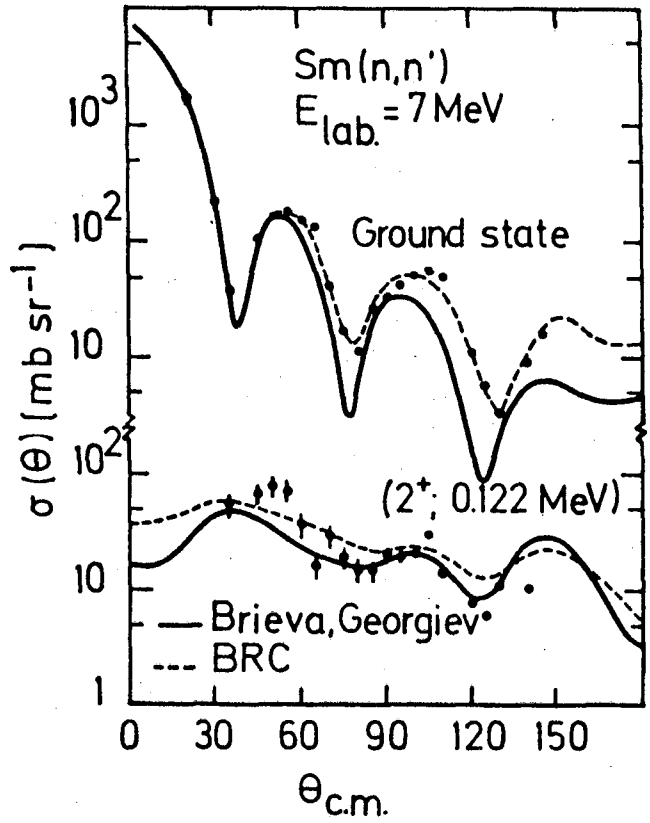


Fig. 9

Elastic and inelastic cross sections for 7.0 MeV neutrons on $^{152}Sm$

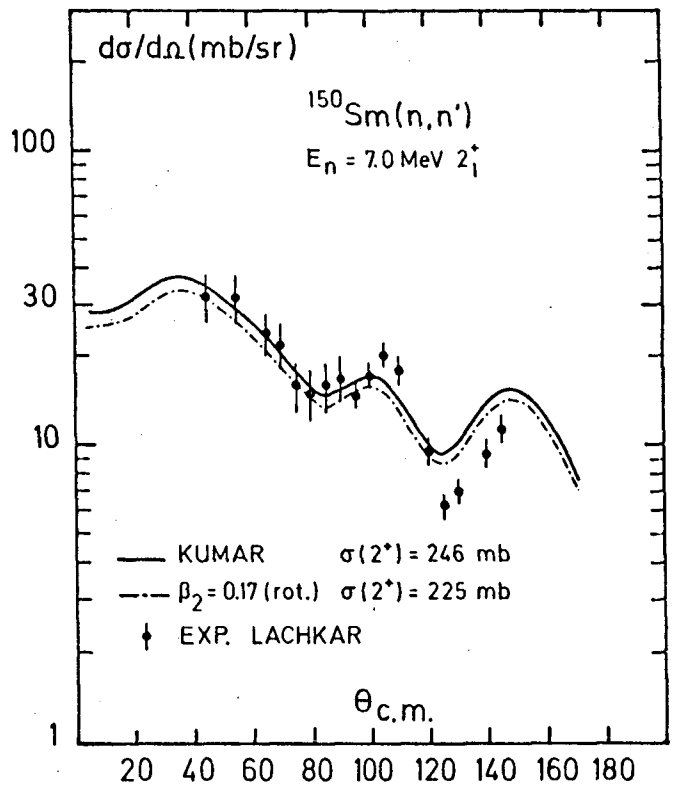


Fig. 10

Differential cross sections for 7.0 MeV neutron inelastic scattering

# ENDF/B-5 FISSION PRODUCT CROSS SECTION EVALUATIONS*

R. E. Schenter
Hanford Engineering Development Laboratory
P.O.Box 1970
Richland, Washington 99352

T. R. England
Los Alamos Scientific Laboratory
P.O.Box 1663
Los Alamos, New Mexico 87545

## ABSTRACT

Cross section evaluations have been made for the 196 fission product nuclides on the ENDF/B-5 data files. Most of the evaluations involve updating the capture cross sections of the important absorbers for fast and thermal reactor systems. This included updating thermal values, resonance integrals, resonance parameter sets and fast capture cross sections. For the fast capture results generalized least-squares calculations were made using the computer code FERRET. Input for these cross section adjustments included nuclear models calculations and both integral and differential experimental data results. The differential cross sections and their uncertainties were obtained from the CSIRS library. Integral measurement results came from CFRMF and STEK Assemblies 500, 1000, 2000, 3000, 4000. Comparisons of these evaluations with recent capture measurements will be presented.

## Introduction

The ENDF/B-5 fission product file consists of 877 nuclide evaluations. Of these, 196 have full cross section data sets which contain values for total, elastic, inelastic, capture and angular distributions for the energy range $10^{-5}$ev to 20 MeV. Table I lists the 196 nuclides. The file is basically an update of ENDF/B-4, where most of the changes occur for the fast and thermal capture cross sections. These changes involve the use of important new evaluation techniques and recent experimental results from both integral and differential measurements.

In this paper we present typical results illustrating these new techniques where use was made of a generalized least-squares adjustment procedure/1/ to obtain a nominal cross section curve and uncertainty information

*Work supported by DOE contract DE-AC14-FF02170.

Table I. Fission Product Nuclides with Cross Section Data for ENDF/B-5.

| | | | | | | | | | | | | | | |
|---|---|---|---|---|---|---|---|---|---|---|---|---|---|---|
| 1. | 32 | Ge | 72 | 51. | 43 | Tc | 99 | 101. | 51 | Sb | 125 | 151. | 60 | Nd 142 |
| 2. | 32 | Ge | 73 | 52. | 44 | Ru | 96 | 102. | 51 | Sb | 126 | 152. | 60 | Nd 143 |
| 3. | 32 | Ge | 74 | 53. | 44 | Ru | 98 | 103. | 52 | Te | 120 | 153. | 60 | Nd 144 |
| 4. | 32 | Ge | 76 | 54. | 44 | Ru | 99 | 104. | 52 | Te | 122 | 154. | 60 | Nd 145 |
| 5. | 33 | As | 75 | 55. | 44 | Ru | 100 | 105. | 52 | Te | 123 | 155. | 60 | Nd 146 |
| 6. | 34 | Se | 75 | 56. | 44 | Ru | 101 | 106. | 52 | Te | 124 | 156. | 60 | Nd 147 |
| 7. | 34 | Se | 76 | 57. | 44 | Ru | 102 | 107. | 52 | Te | 125 | 157. | 60 | Nd 148 |
| 8. | 34 | Se | 77 | 58. | 44 | Ru | 103 | 108. | 52 | Te | 126 | 158. | 60 | Nd 150 |
| 9. | 34 | Se | 78 | 59. | 44 | Ru | 104 | 109. | 52 | Te | 127M | 159. | 61 | Pm 147 |
| 10. | 34 | Se | 80 | 60. | 44 | Ru | 105 | 110. | 52 | Te | 128 | 160. | 61 | Pm 148 |
| 11. | 34 | Se | 82 | 61. | 44 | Ru | 106 | 111. | 52 | Te | 129M | 161. | 61 | Pm 148M |
| 12. | 35 | Br | 79 | 62. | 45 | Rh | 103 | 112. | 52 | Te | 130 | 162. | 61 | Pm 149 |
| 13. | 35 | Br | 81 | 63. | 45 | Rh | 105 | 113. | 52 | Te | 132 | 163. | 61 | Pm 151 |
| 14. | 36 | Kr | 78 | 64. | 46 | Pd | 102 | 114. | 53 | I | 127 | 164. | 62 | Sm 144 |
| 15. | 36 | Kr | 80 | 65. | 46 | Pd | 104 | 115. | 53 | I | 129 | 165. | 62 | Sm 147 |
| 16. | 36 | Kr | 82 | 66. | 46 | Pd | 105 | 116. | 53 | I | 130 | 166. | 62 | Sm 148 |
| 17. | 36 | Kr | 83 | 67. | 46 | Pd | 106 | 117. | 53 | I | 131 | 167. | 62 | Sm 149 |
| 18. | 36 | Kr | 84 | 68. | 46 | Pd | 107 | 118. | 53 | I | 135 | 168. | 62 | Sm 150 |
| 19. | 36 | Kr | 85 | 69. | 46 | Pd | 108 | 119. | 54 | Xe | 124 | 169. | 62 | Sm 151 |
| 20. | 36 | Kr | 86 | 70. | 46 | Pd | 110 | 120. | 54 | Xe | 126 | 170. | 62 | Sm 152 |
| 21. | 37 | Rb | 85 | 71. | 47 | Ag | 107 | 121. | 54 | Xe | 128 | 171. | 62 | Sm 153 |
| 22. | 37 | Rb | 86 | 72. | 47 | Ag | 109 | 122. | 54 | Xe | 129 | 172. | 62 | Sm 154 |
| 23. | 37 | Rb | 87 | 73. | 47 | Ag | 111 | 123. | 54 | Xe | 130 | 173. | 63 | Eu 151 |
| 24. | 38 | Sr | 84 | 74. | 48 | Cd | 106 | 124. | 54 | Xe | 131 | 174. | 63 | Eu 152 |
| 25. | 38 | Sr | 86 | 75. | 48 | Cd | 108 | 125. | 54 | Xe | 132 | 175. | 63 | Eu 153 |
| 26. | 38 | Sr | 87 | 76. | 48 | Cd | 110 | 126. | 54 | Xe | 133 | 176. | 63 | Eu 154 |
| 27. | 38 | Sr | 88 | 77. | 48 | Cd | 111 | 127. | 54 | Xe | 134 | 177. | 63 | Eu 155 |
| 28. | 38 | Sr | 89 | 78. | 48 | Cd | 112 | 128. | 54 | Xe | 135 | 178. | 63 | Eu 156 |
| 29. | 38 | Sr | 90 | 79. | 48 | Cd | 113 | 129. | 54 | Xe | 136 | 179. | 63 | Eu 157 |
| 30. | 39 | Y | 89 | 80. | 48 | Cd | 114 | 130. | 55 | Cs | 133 | 180. | 64 | Gd 152 |
| 31. | 39 | Y | 90 | 81. | 48 | Cd | 115M | 131. | 55 | Cs | 134 | 181. | 64 | Gd 154 |
| 32. | 39 | Y | 91 | 82. | 48 | Cd | 116 | 132. | 55 | Cs | 135 | 182. | 64 | Gd 155 |
| 33. | 40 | Zr | 90 | 83. | 49 | In | 113 | 133. | 55 | Cs | 136 | 183. | 64 | Gd 156 |
| 34. | 40 | Zr | 91 | 84. | 49 | In | 115 | 134. | 55 | Cs | 137 | 184. | 64 | Gd 157 |
| 35. | 40 | Zr | 92 | 85. | 50 | Sn | 112 | 135. | 56 | Ba | 134 | 185. | 64 | Gd 158 |
| 36. | 40 | Zr | 93 | 86. | 50 | Sn | 114 | 136. | 56 | Ba | 135 | 186. | 64 | Gd 160 |
| 37. | 40 | Zr | 94 | 87. | 50 | Sn | 115 | 137. | 56 | Ba | 136 | 187. | 65 | Tb 159 |
| 38. | 40 | Zr | 95 | 88. | 50 | Sn | 116 | 138. | 56 | Ba | 137 | 188. | 65 | Tb 160 |
| 39. | 40 | Zr | 96 | 89. | 50 | Sn | 117 | 139. | 56 | Ba | 138 | 189. | 66 | Dy 160 |
| 40. | 41 | Nb | 93 | 90. | 50 | Sn | 118 | 140. | 56 | Ba | 140 | 190. | 66 | Dy 161 |
| 41. | 41 | Nb | 94 | 91. | 50 | Sn | 119 | 141. | 57 | La | 139 | 191. | 66 | Dy 162 |
| 42. | 41 | Nb | 95 | 92. | 50 | Sn | 120 | 142. | 57 | La | 140 | 192. | 66 | Dy 163 |
| 43. | 42 | Mo | 92 | 93. | 50 | Sn | 122 | 143. | 58 | Ce | 140 | 193. | 66 | Dy 164 |
| 44. | 42 | Mo | 94 | 94. | 50 | Sn | 123 | 144. | 58 | Ce | 141 | 194. | 67 | Ho 165 |
| 45. | 42 | Mo | 95 | 95. | 50 | Sn | 124 | 145. | 58 | Ce | 142 | 195. | 68 | Er 166 |
| 46. | 42 | Mo | 96 | 96. | 50 | Sn | 125 | 146. | 58 | Ce | 143 | 196. | 68 | Er 167 |
| 47. | 42 | Mo | 97 | 97. | 50 | Sn | 126 | 147. | 58 | Ce | 144 | | | |
| 48. | 42 | Mo | 98 | 98. | 51 | Sb | 121 | 148. | 59 | Pr | 141 | | | |
| 49. | 42 | Mo | 99 | 99. | 51 | Sb | 123 | 149. | 59 | Pr | 142 | | | |
| 50. | 42 | Mo | 100 | 100. | 51 | Sb | 124 | 150. | 50 | Pr | 143 | | | |

in the form of a covariance matrix which linked energy points. This procedure involves calculations which use the finite element representation of the FERRET /2/ data adjustment code. Also presented in this paper will be a study of thermal reactor absorption sensitivity to capture cross section changes in important fission products.

## FAST CAPTURE

Table II lists the 25 most important fission product absorbers in a fast reactor core with their percent contribution to total absorption. Emphasis for ENDF/B-5 has been on updating the capture cross sections of these top absorbers plus an additional 50 more. Typical results of these evaluations are shown in Figures 1-14, where the "Adjusted" curves will be used for ENDF/B-5. Also shown is the data used as input to the FERRET code. This includes both differential and integral data and their uncertainties. Also inputted to the calculation was an "a priori" description which combined multi-group average cross sections obtained from resonance parameters for the resolved resonance region with "smooth" average cross section from ENDF/B-4 for the higher energy region. The resonance parameters used were from ENDF/B-4 or BNL-325 /3/ as indicated. The histogram or multi-group cross section description in the resonance region is required for the FERRET least-squares calculation because following the exact resonance structure takes too many points for the standard computer calculations, especially for the covariance matrix part.

The integral data came from reaction rate measurements in STEK Assemblies 500, 1000, 2000, 3000, 4000 /4/ and CFRMF /5/. ENDF/B-4 evaluations also used earlier CFRMF measurements which helped normalize nuclear models calculations made with the Hauser-Feshbach computer code NCAP /6/.

This type of approach which quantitatively combines three evaluation sources, diverges somewhat from the usual ENDF/B philosophy which is to rely essentially on differential results with some adjustment due to integral results. This method also differs from the Japanese and European procedures in which either only differential or only integral values are exclusively used. For individual fission products, however, it is felt that this approach has substantial promise since many of the problems associated with the use of integral data are greatly simplified in dealing with a single nuclide. As can be seen in Table II, for most of the nuclides which have experimental measurements, the differential data is discrepant. Consequently, it is hoped that use of the integral results will supplement our information and help resolve these discrepancies. Another advantage of the procedure is that it provides quantitative uncertainty information in the form of covariance matrices which can be easily translated into ENDF/B formats. Obviously there are problems associated with using integral data such as self shielding effects, mixtures of isotopes for the same element, flux and adjoint flux determinations and uncertainty assignments and these will have to be examined carefully to have a viable method.

Figure 1 shows results for the important absorber Sm149. As can be seen from the curves, significant changes occur in going from ENDF/B-4 to ENDF/B-5. The ENDF/B-4 result was made with nuclear model calculations where no previous experimental data existed in 1973. Also shown in Figure 1 are "Adjusted" cross sections using the FERRET code, comparing various results when only integral data is used or differential data is used. For the Sm149 case, the results are consistent with each other. For some of the other cases shown in Figures 5-14 this does not necessarily occur.

Table II. Twenty five most "important" fission product absorbers in fast reactor cores. Also shown are fast integral and differential experiments which have published results as of November 1979. The CFRMF, STEK and differential data were used in the HEDL-PETTEN evaluations for ENDF/B-5.

| | Nuclide | Percent Contribution to Total Absorption | EBR-2 | CFRMF | STEK | Differential Data* | Discrepant Diff. Data |
|---|---|---|---|---|---|---|---|
| 1. | Pd 105 | 9.9 | - | - | ✓ | M,S, •• | - |
| 2. | Tc 99 | 8.6 | - | ✓ | ✓ | S,•• | ✓ |
| 3. | Ru 101 | 7.7 | - | - | ✓ | M,S | ✓ |
| 4. | Pd 107 | 6.2 | - | - | - | - | no data |
| 5. | Rh 103 | 5.5 | - | ✓ | ✓ | M,S,•• | - |
| 6. | Cs 133 | 4.9 | - | ✓ | ✓ | •• | ✓ |
| 7. | Pm 147 | 3.5 | - | ✓ | - | - | no data |
| 8. | Sm 149 | 3.4 | ✓ | - | ✓ | S | one data set |
| 9. | Nd 145 | 3.4 | ✓ | - | - | S | one data set |
| 10. | Ru 102 | 3.3 | - | ✓ | ✓ | M,S,•• | ✓ |
| 11. | Cs 135 | 3.0 | - | - | - | - | no data |
| 12. | Mo 97 | 2.9 | - | - | ✓ | Mu,•• | - |
| 13. | Ag 109 | 2.7 | - | ✓ | ✓ | •• | ✓ |
| 14. | Ru 106 | 2.3 | - | - | - | - | no data |
| 15. | Nd 143 | 2.3 | ✓ | - | - | Mu | one data set |
| 16. | Xe 131 | 1.9 | - | - | - | - | no data |
| 17. | Sm 151 | 1.9 | - | - | ✓ | - | no data |
| 18. | Mo 95 | 1.5 | - | - | ✓ | Mu,•• | - |
| 19. | Ru 104 | 1.3 | - | ✓ | ✓ | M,S | ✓ |
| 20. | Eu 153 | 1.3 | - | ✓ | - | •• | - |
| 21. | Mo 98 | 1.2 | - | ✓ | ✓ | Mu,•• | ✓ |
| 22. | Ce 144 | 1.1 | - | - | - | - | no data |
| 23. | I 129 | 1.0 | - | ✓ | ✓ | - | no data |
| 24. | Mo 100 | 0.9 | - | ✓ | ✓ | Mu,•• | ✓ |
| 25. | Pr 141 | 0.9 | - | ✓ | ✓ | •• | ✓ |
| | | 82.6 | | | | | |

* M=Macklin (79)ORL, S=Shaw(75)RPI, Mu=Musgrove(77)AUA,

••=Additional differential data

Error estimates are outputted from the FERRET code and Figure 2 shows fractional uncertainty versus energy for the Sm149 case, where the final uncertainty changes from about 60% to 10% (1σ) in going from ENDF/B-4 to ENDF/B-5. Figures 3 and 4 show the cases of adjusted curves using STEK measurements compared to recent integral results at EBR-II adjusted by Anderl et al., /7/ for Sm149 and Sm147. The full energy region (1 ev - 10 MeV) evaluation is shown in Figure 5 for Mo97. Comparisons to recent differential measurements by Macklin, et al., /8/ is shown in Figures 6-10 for Ru101, Ru102, Ru104, Pd104, and Pd108. Finally, results for four of the top twenty-five fission product absorbers (Tc99, Rh103, Ag109 and Cs133) are given in Figures 11-14.

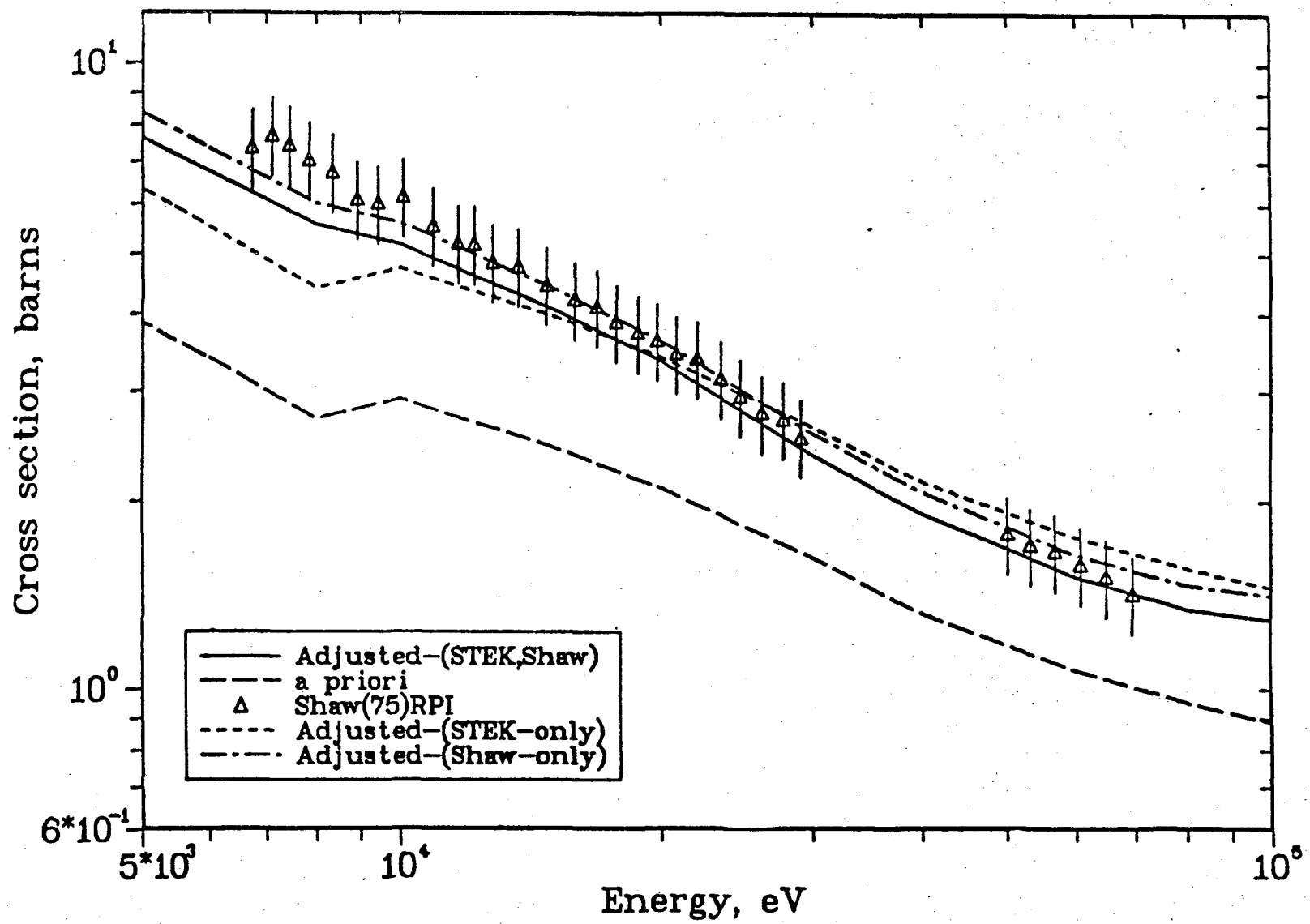


FIGURE 1. SM 149 CROSS SECTION EVALUATIONS. ENDF/B4+BNL - APRIORI.

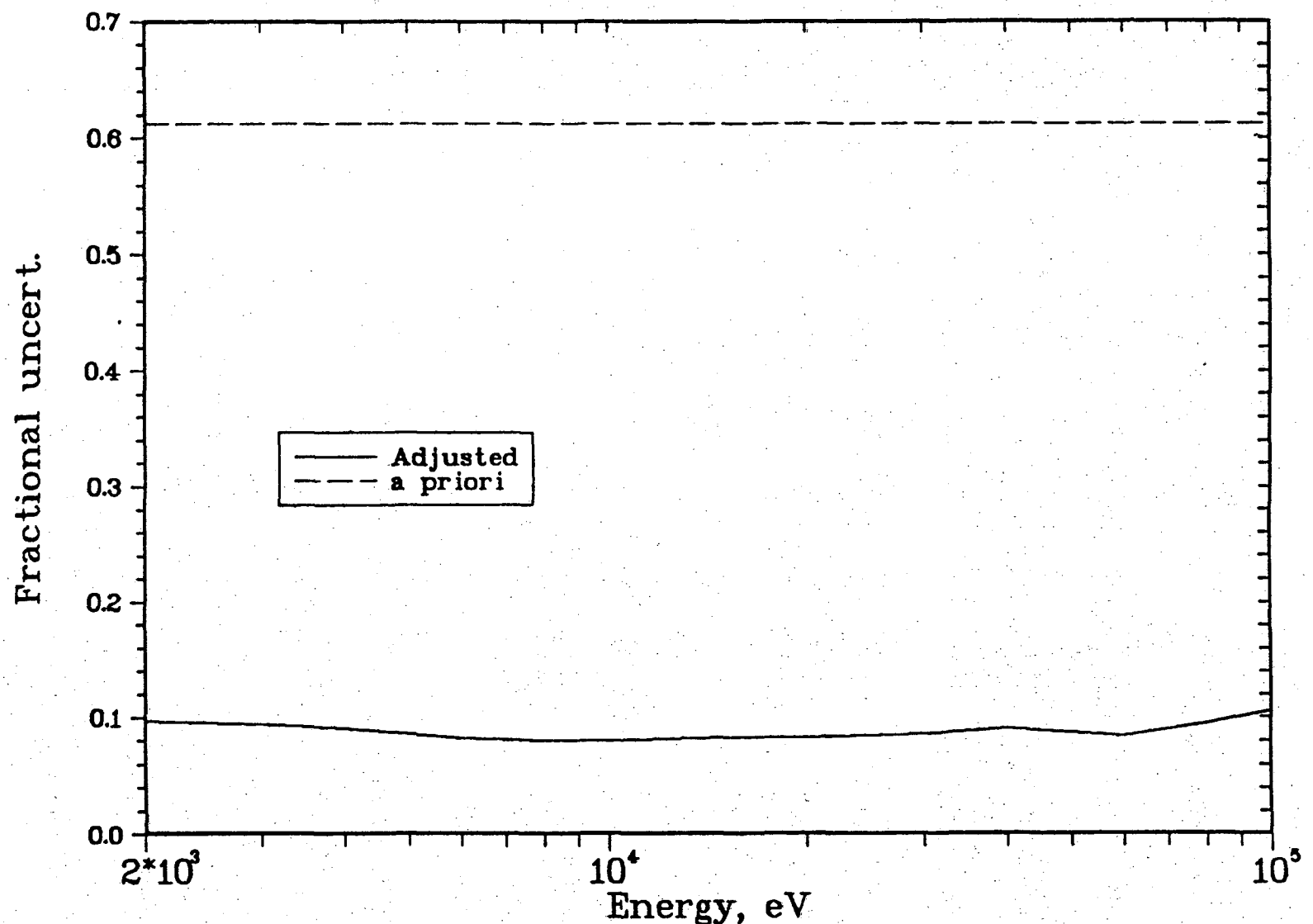


FIGURE 2. SM 149 UNCERTAINTY EVALUATION. ENDF/B4+BNL - APRIORI.

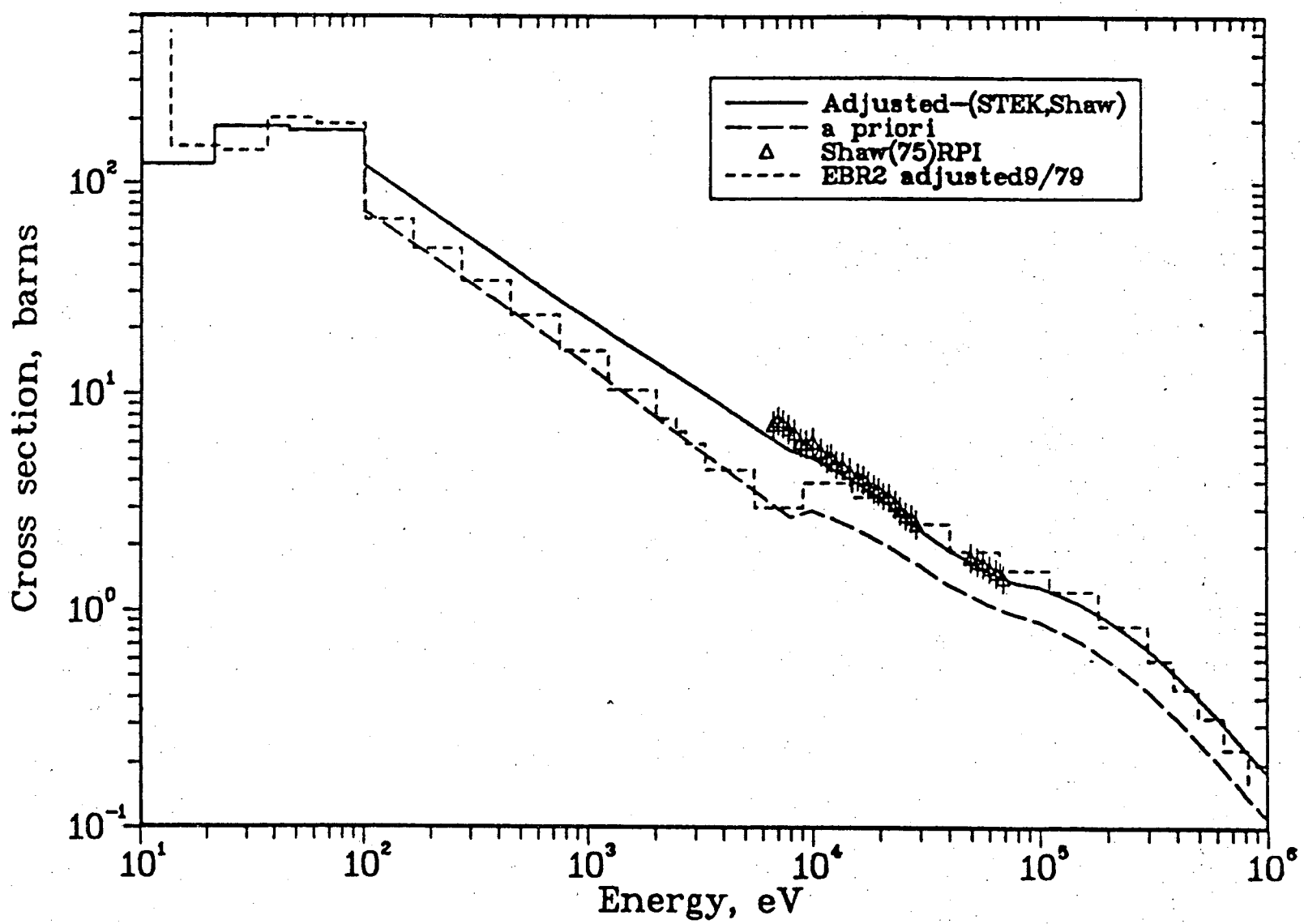


FIGURE 3. SM 149 CROSS SECTION EVALUATIONS. ENDF/B4+BNL - APRIORI.

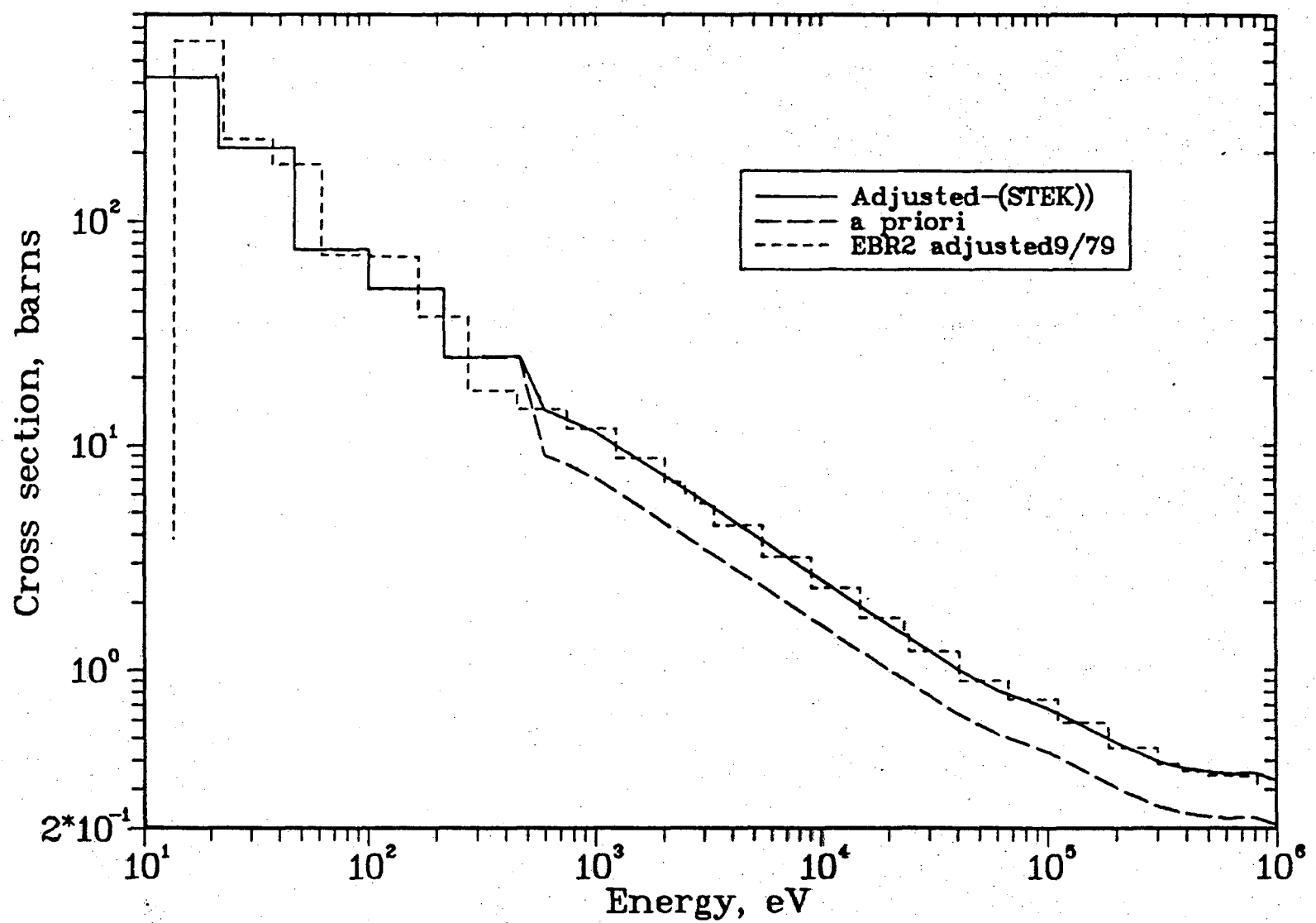


FIGURE 4. SM 147 CROSS SECTION EVALUATION. ENDF/B4+BNL - APRIORI.

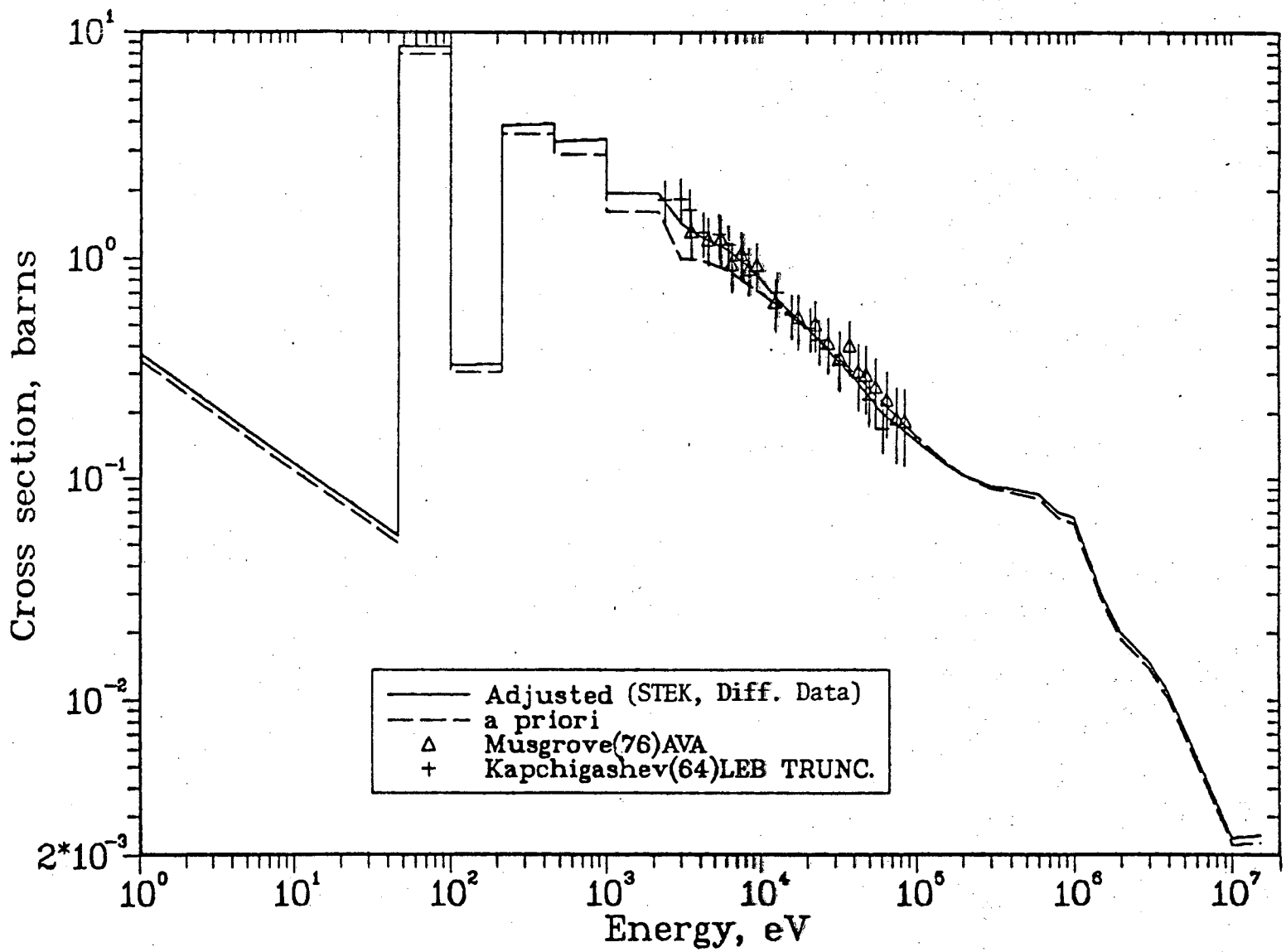


FIGURE 5. MO 97 CROSS SECTION EVALUATION. ENDF/B4 - APRIORI.

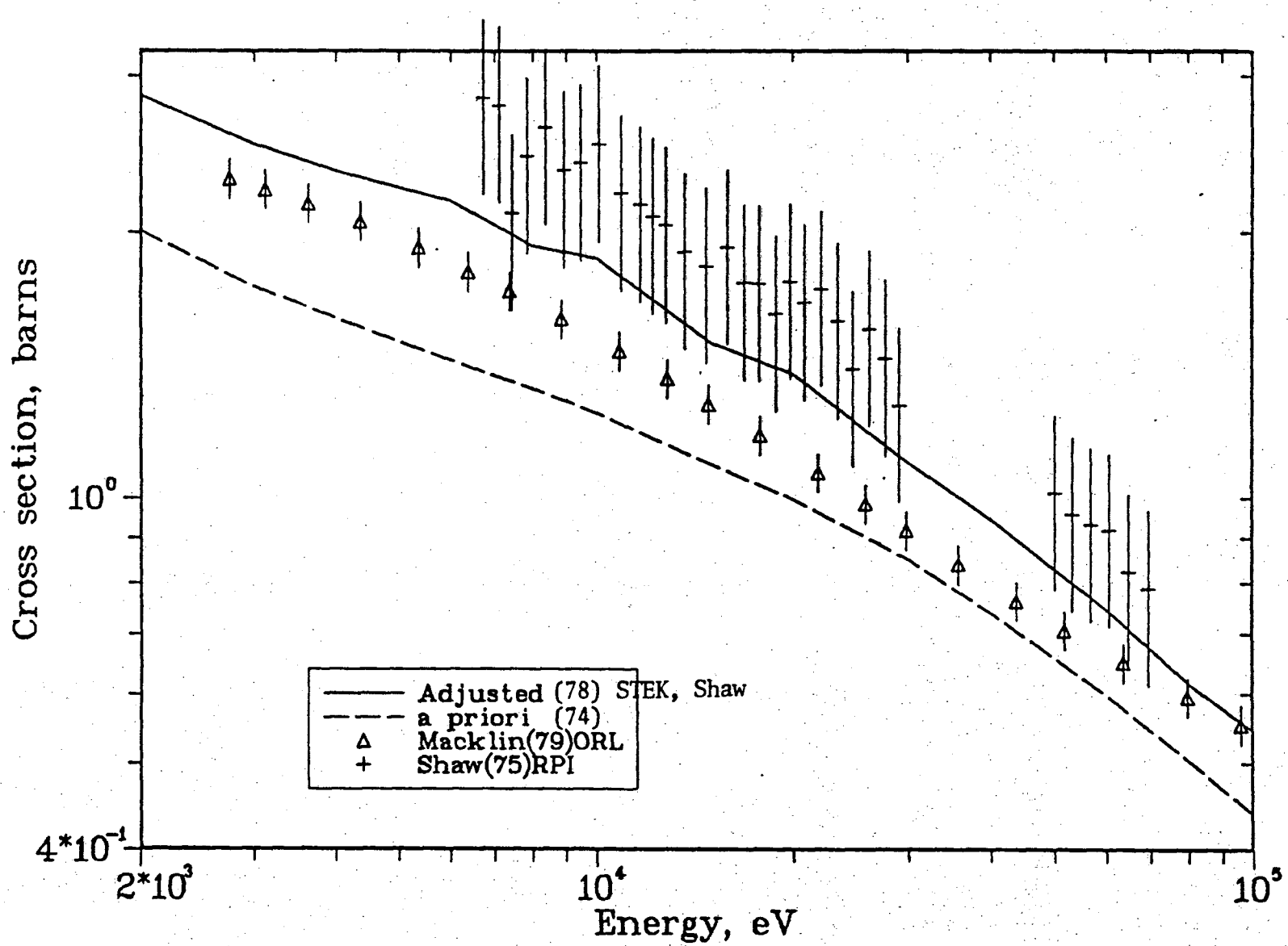


FIGURE 6. RU 101 CROSS SECTION EVALUATION. ENDF/B4 - APRIORI.

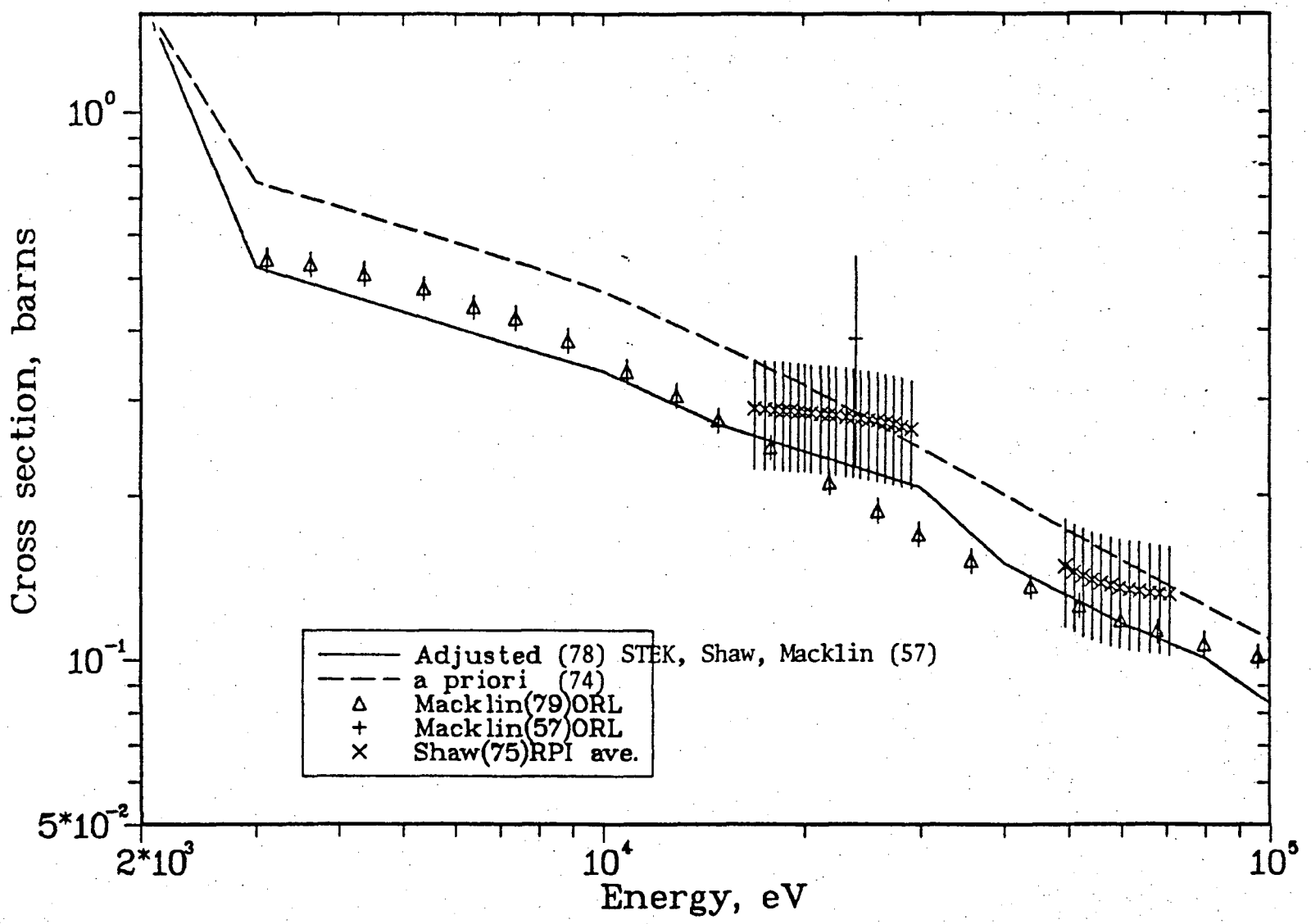


FIGURE 7. RU 102 CROSS SECTION EVALUATION. ENDF/B4 - APRIORI.

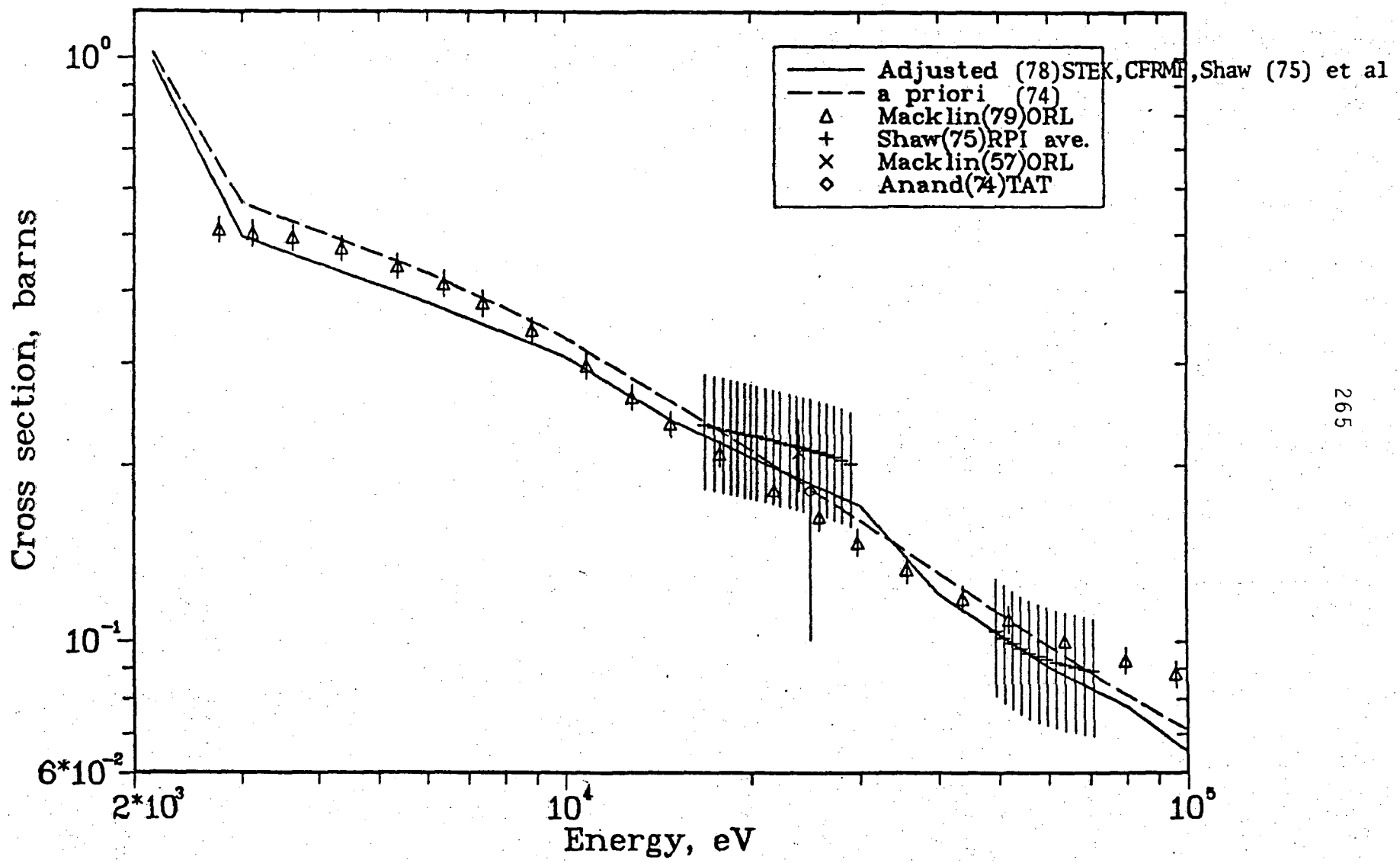


FIGURE 8. RU 104 CROSS SECTION EVALUATION. ENDF/B4 - APRIORI.

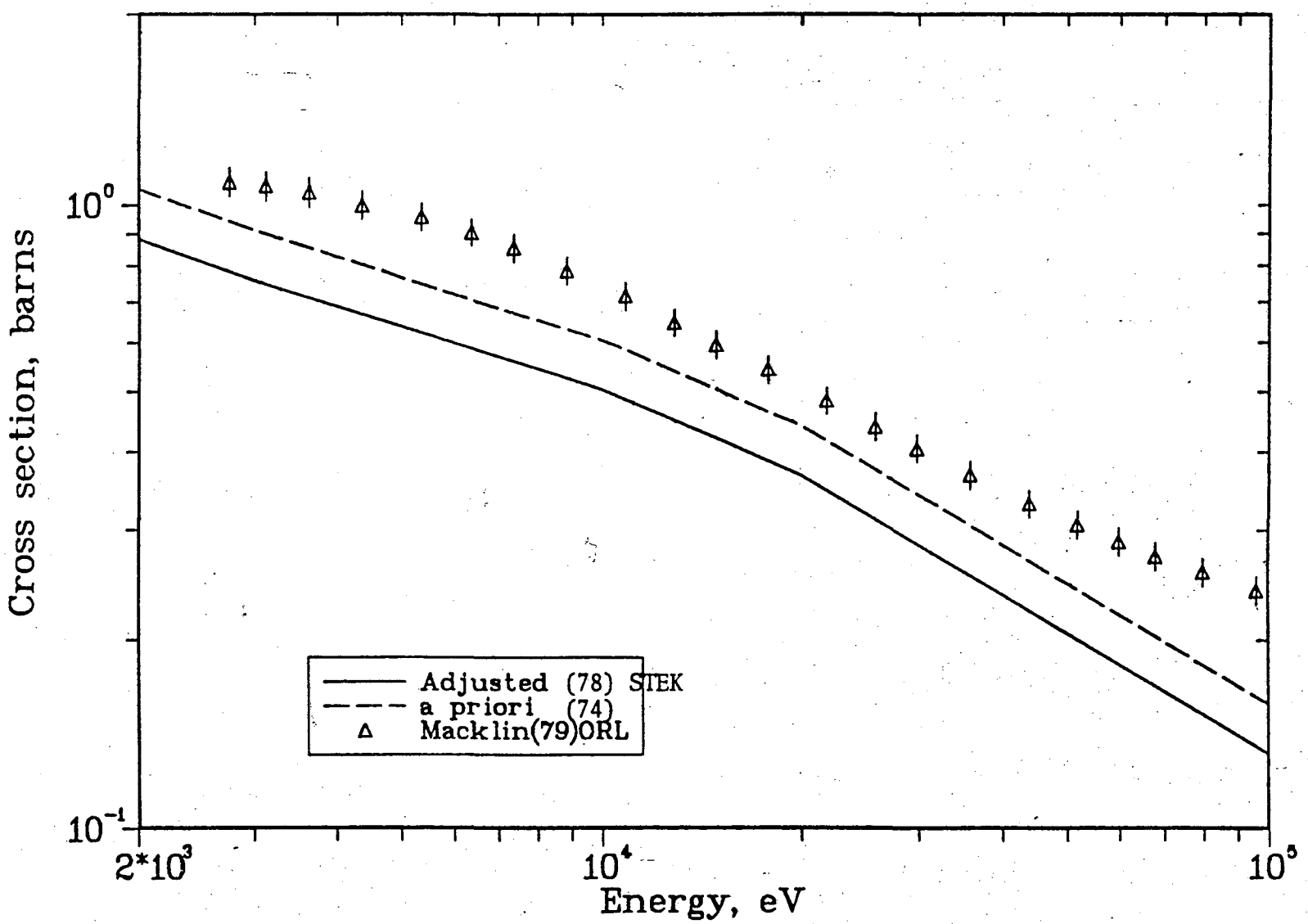


FIGURE 9. PD 104 CROSS SECTION EVALUATION. ENDF/B4 - APRIORI.

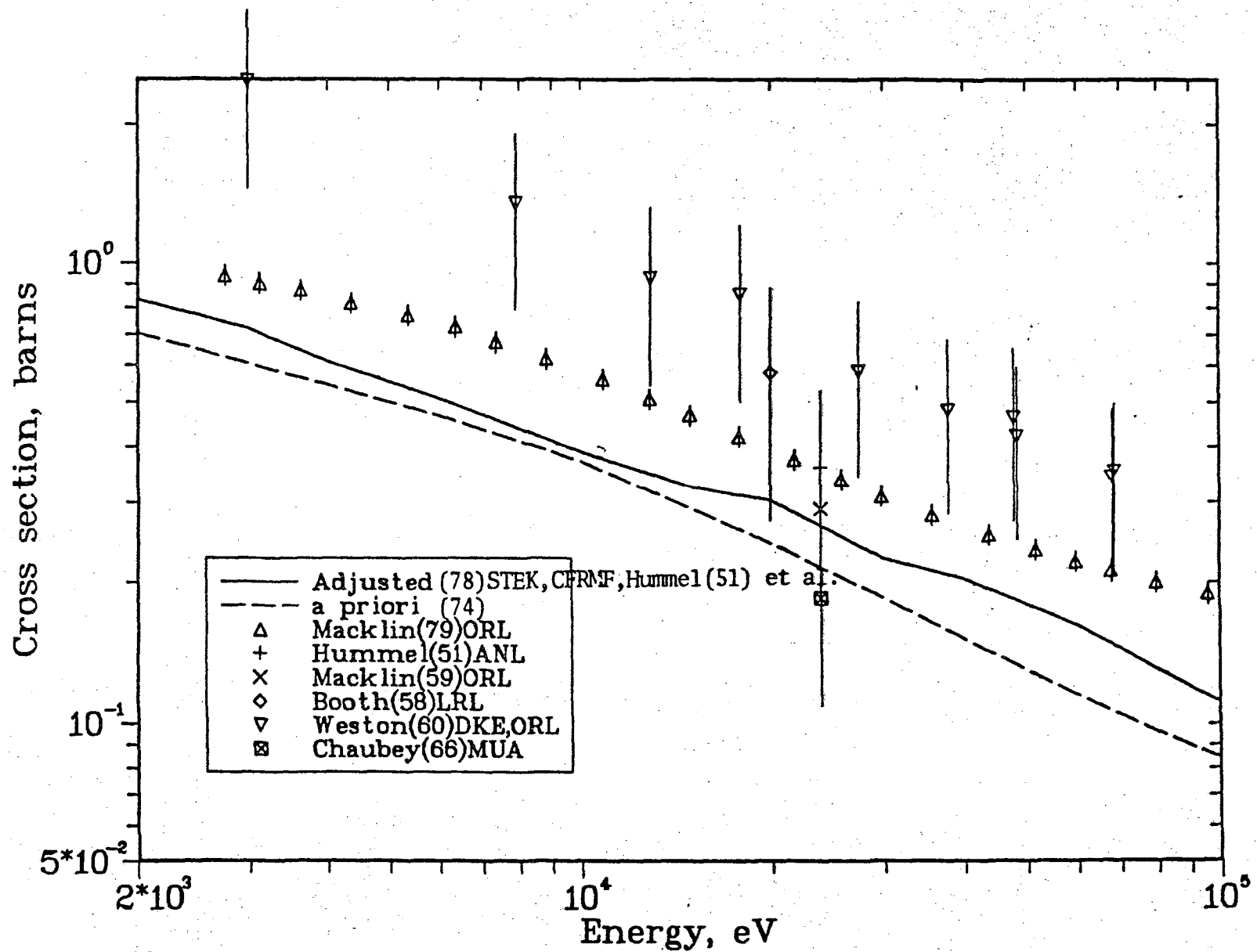


FIGURE 10. PD 108 CROSS SECTION EVALUATION. ENDF/B4.

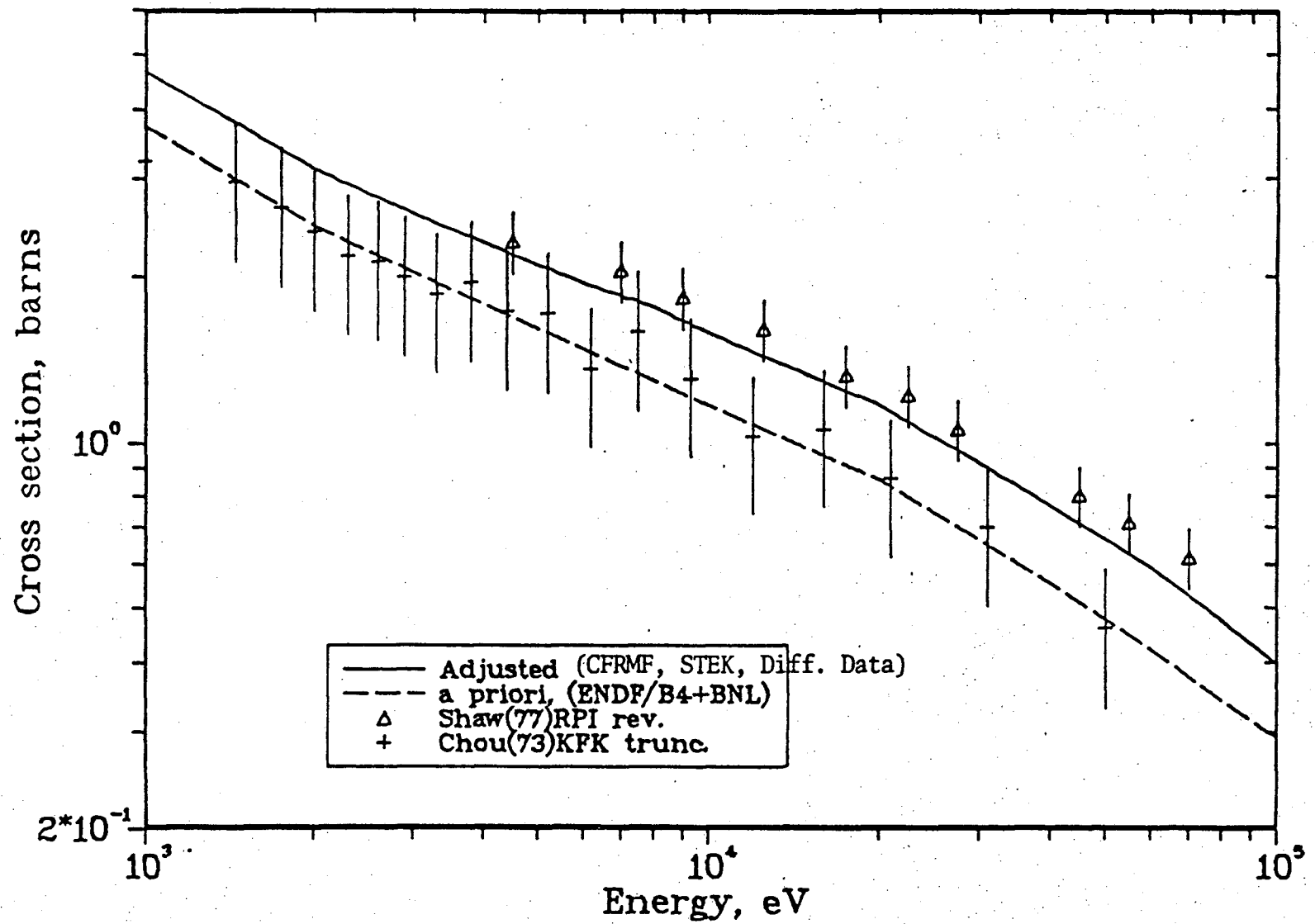


FIGURE 11. Tc 99 EVALUATION. ENDF/B4+BNL - APRIORI.

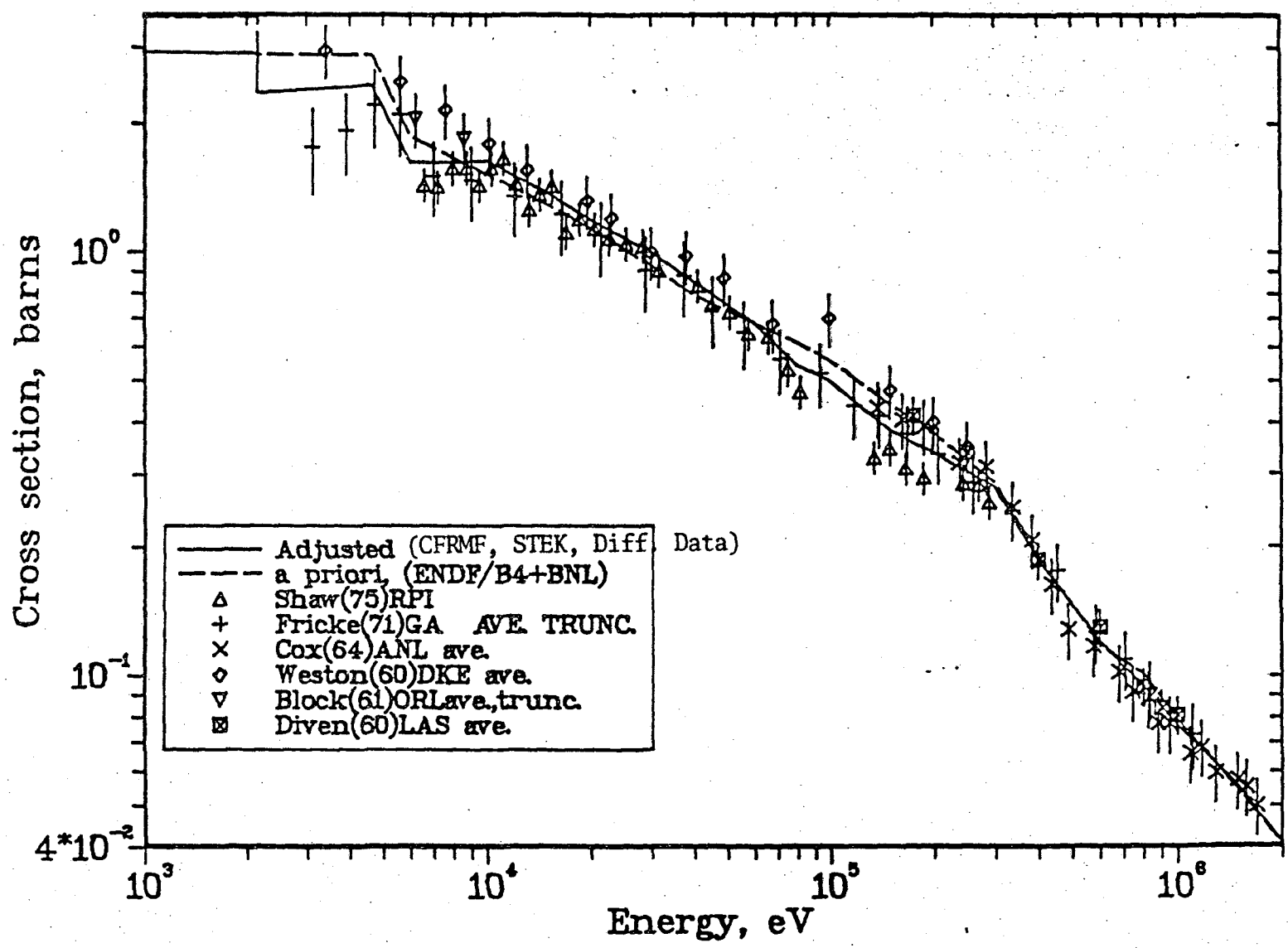


FIGURE 12. RH 103 EVALUATION. ENDF/B4+BNL - APRIORI.

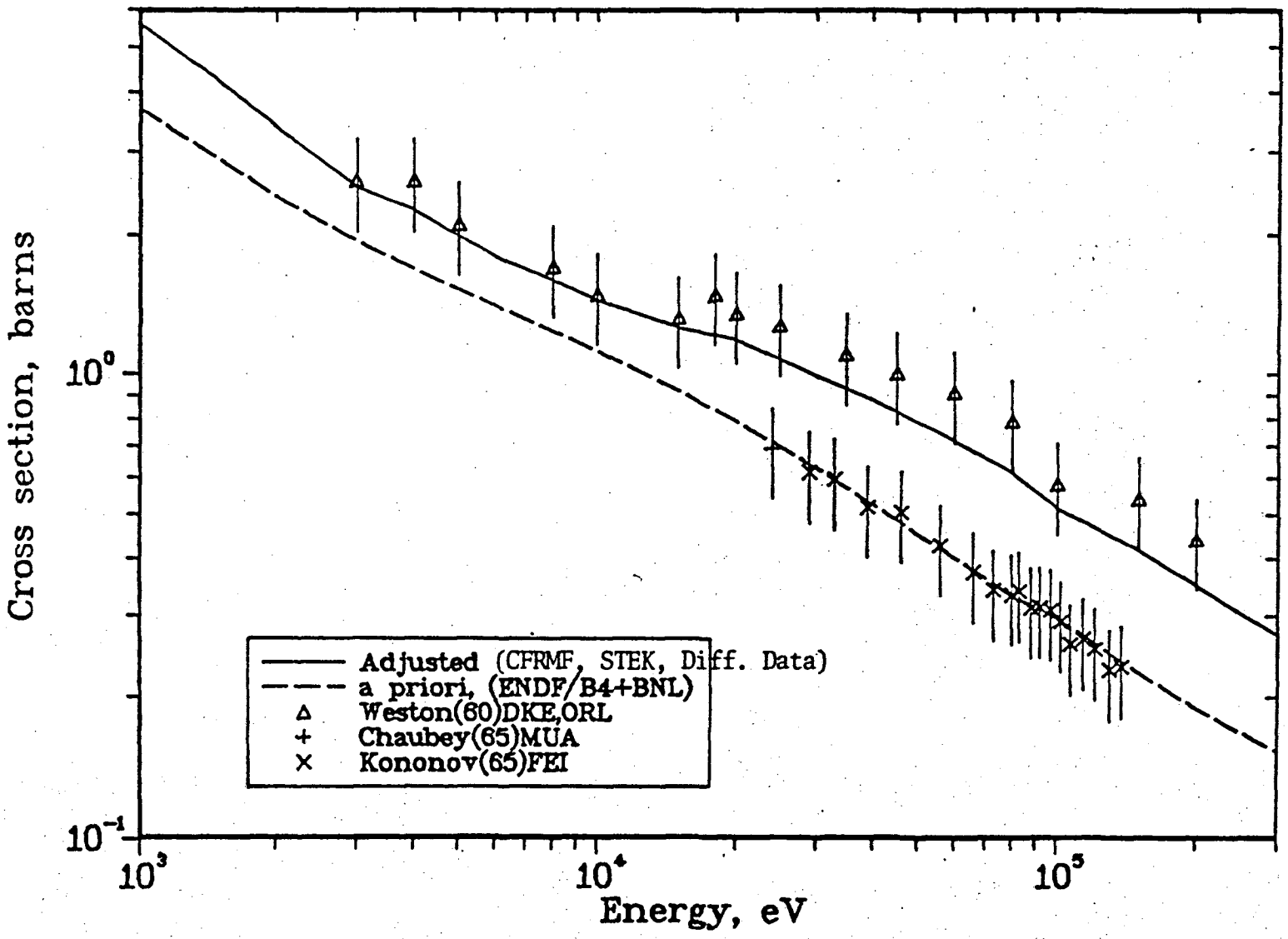


FIGURE 13. AG 109 EVALUATION. ENDF/B4+BNL - APRIORI.

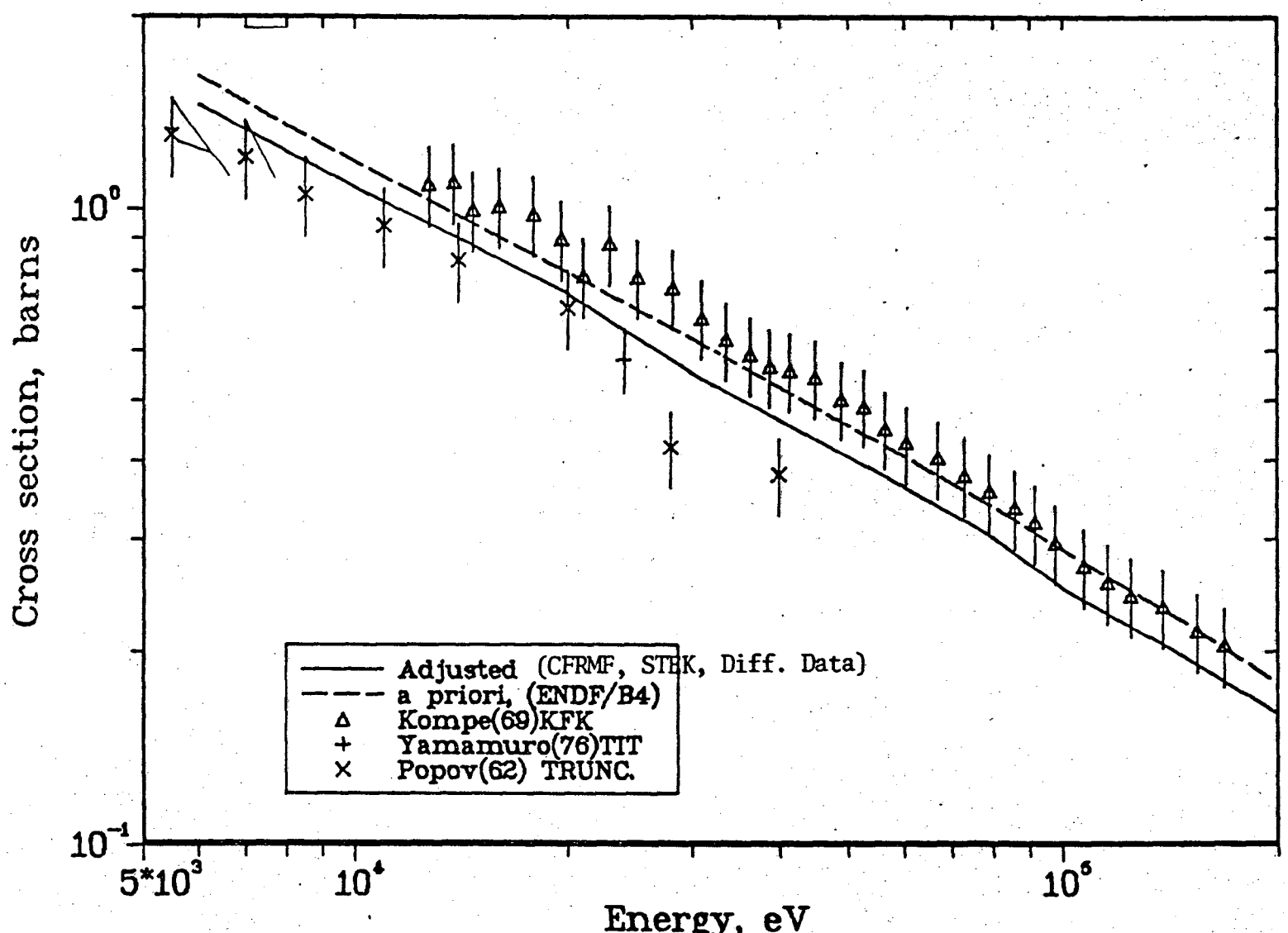


FIGURE 14. Cs 133 EVALUATION. ENDF/B4 - APRIORI.

## THERMAL AND RESONANCE CAPTURE

Table III gives the results of calculations of ENDF/B-4 resonance integrals (Ecut=0.5, T=0°k) and thermal cross sections for the major fission product absorbers in thermal reactors. These will form the basis of the ENDF/B-5 evaluations. Also shown in Table III are the values given in BNL-325 /3/ which for most cases are identical or very close to, the ENDF/B-4 results. Most of the ENDF/B-5 "196 nuclides" with cross section data will have "File 2" resonance parameter descriptions. The "File 3" smooth background cross section will then be adjusted consistent with experimental results to give measured resonance integrals (within 1$\sigma$) and measured thermal cross sections. The main source of experimental resonance integrals and thermal values was BNL-325 which has almost identical agreement with the "Chart of the Nuclides". For those cases which BNL-325 did not list measured values, other sources of data were from Clayton /9/, Ribon and Krebs /10/, Pope and Story /11/, and Kirouac /12/.

Appendix A provides thermal reactor absorption sensitivity analysis.

Table III. Resonance Integrals and Thermal Cross Sections of Major FP Absorbers in Thermal Reactors.

| | Resonance Integrals (barns) | | Thermal Capture Cross Sections (barns) | |
|---|---|---|---|---|
| Nuclide | ENDF/B-4* | BNL-325 | ENDF/B-4 | BNL-325 |
| Xe135 | 7645. | 7634. | $2.64 \times 10^6$ | $(2.65 \pm 0.20) \times 10^6$ |
| Sm149 | 3200. | 3183. | 41190. | 41000.±2000. |
| Pm147 | 2283. | 2300.±350. | 182. | 181.±7. |
| Xe131 | 879. | 870. | 90. | 90.±10. |
| Cs133 | 381. | 415.±15. | 29.5 | 31.5±1.5 |
| Nd143 | 205. | 140. | 325. | 325.±10. |
| Sm151 | 3357. | 3300.±700. | 15000. | 15000.±1200. |
| Rh103 | 1050. | 1100.±50. | 148. | 150.±5. |
| Tc99 | 354. | 340.±35. | 19. | 19.±2. |
| Nd145 | 226. | 240.±35. | 42. | 42.±2. |
| Sm152 | 3008. | 3000.±200. | 206. | 206.±6. |
| Pm148M | 3608. | 3600. | 10600. | 22000.±2500. |
| Mo95 | 113. | 105.±7. | 14.5 | 14.5±0.5 |
| Eu153 | 1590. | 1635.±200. | 453. | 390.±30. |
| Kr83 | 192. | 230. | 208. | 200.±30. |
| Rh105 | 15850. | 15800.±1500 | 16000. | 16000.±1500. |
| Sm150 | 320. | 310.±15. | 102. | 102.±5. |
| Pm148 | 40010. | 40000. | 2000. | 2000.±1000 |
| Cs135 | 61.6 | 62. | 8.7 | 8.7±0.5 |
| Ru101 | 95.2 | 85. | 3.1 | 3.1±0.9 |
| Eu155 | 1856. | -- | 4040. | 4040.±125. |
| La139 | 13.0 | 12.2±0.6 | 9.0 | 9.0±0.3 |
| Pr141 | 19.4 | 14.1±0.2 | 11.5 | 11.5±0.3 |
| Eu154 | 2700. | -- | 1500. | 1500.±400. |
| Pr143 | 190. | 190.±25. | 89. | 89.±10. |
| Xe133 | 356. | -- | 190. | 190.±90. |
| Cd113 | 405. | -- | 19880. | 19910.±300. |
| Nd146 | 3.3 | 3.2±0.5 | 1.4 | 1.4±0.1 |
| Cs134 | 213. | -- | 140. | 140.±12. |
| Mo97 | 16.1 | 13.±3. | 2.2 | 2.2±0.7 |

*ECUT=0.5 eV, T=0°k

## REFERENCES


1. F. Schmittroth, "Generalized Least-Squares for Data Analysis", HEDL-TME 77-51. (March 1978).

2. F. Schmittroth, "FERRET Data Analysis Code", HEDL-TME 79-40, (Sept.1979).

3. S.F. Mughabghab and D.I. Garber, "Neutron Cross Sections, Vol. I., Resonance Parameters", BNL 325, June 1973.

4. J.W.M. Dekker, ECN-14, February 1977.

5. Y.D. Harker, et al., EGG Report 1977, Kiamesha Lake Talk, 1972.

6. F. Schmittroth, "Theoretical Calculations of Fast Neutron Capture Cross Sections", HEDL-TME 71-106, (August 1971).

7. R.A. Anderl, et al., "Neodymium, Samarium and Europium Capture Cross Section Adjustments Based on EBR-II Integral Measurements", International Conference on Nuclear Cross Sections for Technology, Knoxville, Tennessee, October 22-26, 1979.

8. R.L. Macklin, et al., "$^{100, 101, 102, 104}Ru(n,\gamma)$ and $^{103}Rh(n,\gamma)$ Cross Sections above 2.6 KeV" and "$^{104, 105, 106, 108, 110}Pd(n,\gamma)$ Cross Sections" to be published and Nucl. Sci. Eng. 71, p. 182-191 (1979).

9. E. Clayton, AAEC/TM 619 (Sept. 1972).

10. P. Ribon and J. Krebs, Bologna Panel Report (April 1974).

11. A. L. Pope and J.S. Story, AEEW-M 1234 (1973).

12. G.J. Kirouac, et al., Nuc. Sci. and Eng., 52, 310 (1973).

# APPENDIX A

## FISSION-PRODUCT ABSORPTION IN THERMAL REACTORS: MAJOR CONTRIBUTORS AND CROSS-SECTION SENSITIVITIES

All sensitivity data in this appendix are based on ENDF/B-IV; the ENDF/B-V files were not complete in time for a processing and sensitivity study before this meeting. However for thermal reactors, the cross-section changes are not likely to be significant to aggregate absorption buildup, and the sensitivities in this appendix can be used to predict the results of specific cross-section changes between Version IV and V.

The cross sections used in this study are listed in Refs. 1 and 2. These were first processed using NJOY/3/ in 154 energy groups and then spectrum weighted into the 4-group structure defined in Table A-I using a typical mid-life spectrum for LWR's. The function is illustrated in Fig. A-1 and listed in Ref. 1. A detailed listing of the 4-group cross sections will be available for this meeting, and differences in $\sigma_{2200}$ and RI between Versions IV and V noted.

The depletion and buildup calculations also require decay and yield data. Decay parameters are listed in Ref. 4; ENDF/B-IV yields are essentially those listed in Ref. 5, except for minor changes in independent yields that are of no significance to this study. The basic depletion calculations use a 3.3 w/% U-235 enriched fuel at a constant power level of 30 Mw/MT for a total burnup of 33 GWd/MT. Power and fission-product production was from the constantly changing production of Pu-239 and concomitant depletion of U-235 and U-238. The content and 4-group macroscopic absorption of each fission product was calculated at 33 times in increments of 800 h (1 GWd/MT) out to 26 400 h (approximately 3 yr). A large number of such calculations were required for the sensitivity studies.

All parameters affecting the major nuclides contributing to the aggregate absorption were examined./6/ Space limits this appendix to a condensed summary of the results at two times in reactor life and to cross-section data. However, those readers interested in fission-product absorption in thermal reactors should remember that, depending on the nuclide, cross sections are not always the most important parameter. For example, at approximately 20 GWd/MT depletion, the yields, branching fractions, and decay constants account for 26 of the largest 40 sensitivities. Furthermore, those nuclides having very large cross sections such as Sm-149 have relatively small cross-section sensitivities in LWR's. The reason for this behavior is simply that the products are both produced and depleted, and therefore those stable nuclides having large cross sections tend to reach an equilibrium macroscopic value determined only by the production (yield) rate; at constant power, the cross section determines the time of equilibrium, not the ultimate absorption rate. It is also true that an <u>increase</u> in the cross sections of some nuclides (e.g., Nd-147) can <u>decrease</u> the aggregate absorption, an effect due to the reduction of the decay branching to daughters having large cross sections. These statements are not intended to reduce the importance of cross sections. In fast reactors and in transient phenomena in LWR's, the cross sections are of dominate importance.

### IMPORTANT NUCLIDE ABSORBERS IN LWR's

Table A-II lists 64 nuclides that contribute >0.1% to the aggregate thermal, epithermal, or total absorption at some time during the 33 Gwd/MT depletion. The specific contribution at 33 times of 10 of the most important contributors is listed in Table A-III.

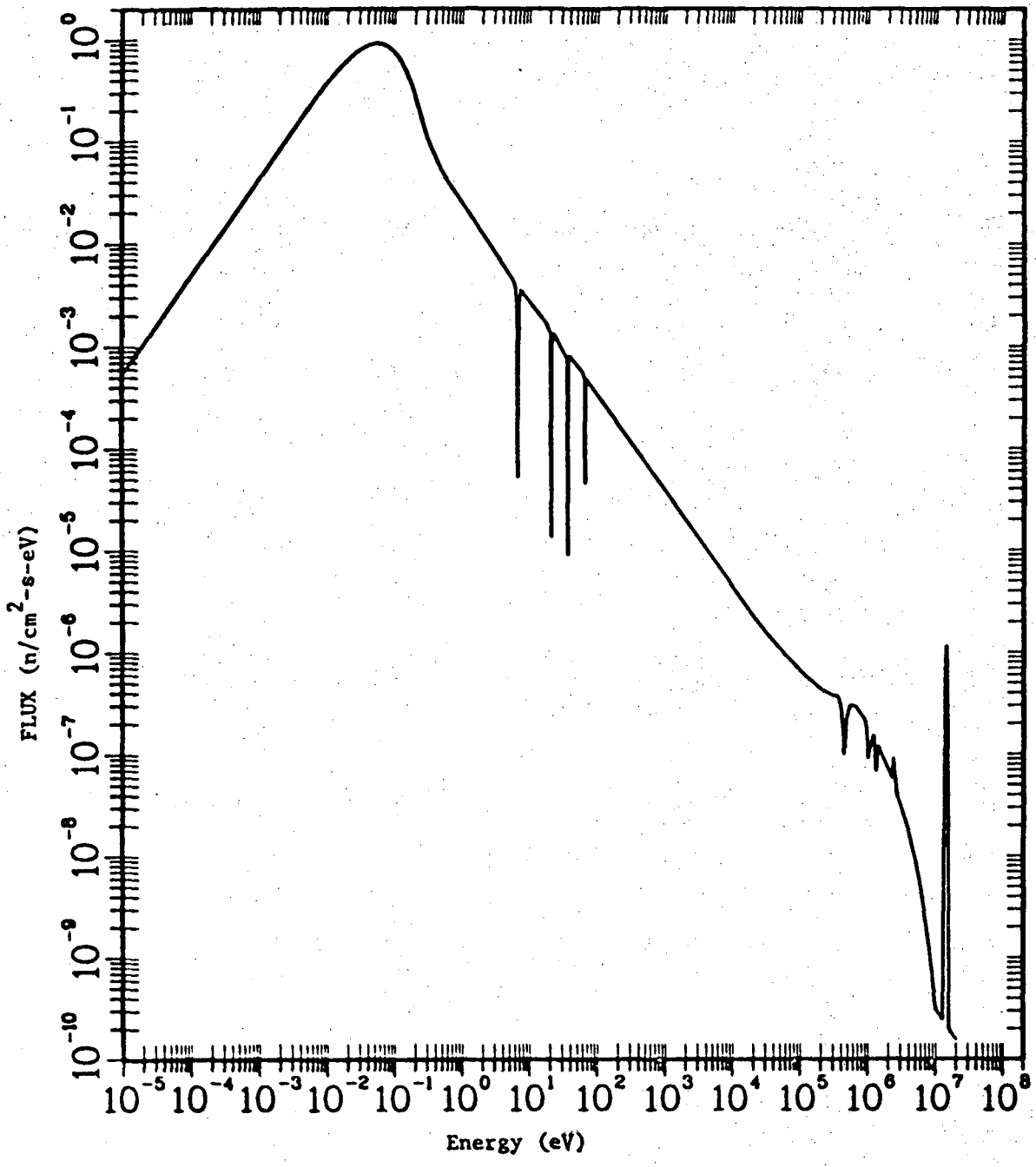


**Fig. A-1**
Flux weighting function.

The chain systematics of each of the 64 nuclides was examined to determine the most important parameters (291) affecting their total absorption, and sensitivites were calculated./6/

SENSITIVITIES

Thermal and epithermal cross sections were individually increased by 10%, one at a time, and the change in aggregate absorption calculated. The tabulated sensitivity, S, of the aggregate absorption rate, $R_T$, was calculated from the change, $\Delta R_T$, where $R_T$ is a sum over all groups and nuclides.

$$S \equiv \frac{\Delta R_T / R_T}{\Delta X / X} , \qquad \text{(A-1)}$$

where $\Delta X$ is the 10% increase in either a thermal or epithermal (resonance) cross section X. Values of S thus represent the direct change in the aggregate absorption per unit change in one of these cross sections. Values of $S < 10^{-5}$ are listed as $\sim 0$.

Table A-IV lists the resulting sensitivities at two depletion times, 5 GWd/MT and 33 GWd/MT (4000 and 26 400 h). A total of 78 nuclides were examined; that is, the list includes sensitivities for cross sections coupled to the initial 64 in Table A-II. An ordered list of the largest 15 sensitivities at both depletion times is given in Table A-V.

Sensitivities do not show the actual importance of the major contributors. Tables A-VI and A-VII show the percent contribution to the total, thermal, and resonance absorption, ordered on the total absorption for the major contributors.

REFERENCES

1. W. B. Wilson and T. R. England, "Multigroup and Few-Group Cross Sections for ENDF/B-IV Fission Products: The TOAFEW Collapsing Code and Data File of 154-Group Fission-Product Cross Sections," LA-7174-MS (1978).

2. T. R. England, W. B. Wilson, and M. G. Stamatelatos, "Fission-Product Data for Thermal Reactors, Part 1, A Data Set for EPRI-CINDER Using ENDF/B-IV," LA-6745-MS (1976) and "Fission Product Data for Thermal Reactors, Part 2, Users Manual for EPRI-CINDER Code and Data," LA=6746-MS (1976). [Also published by Electric Power Research Institute as EPRI-NP-356 (Dec. 1976)].

3. R. E. MacFarlane et al., "The NJOY Nuclear Data Processing System: User's Manual," LA-7584-MS (Dec. 1978).

4. Fission-Product Decay Library of the Evaluated Nuclear Data Files, Version IV (ENDF/B-IV, available from and maintained by the National Nuclear Data Center at the Brookhaven National Laboratory. For a list of decay parameters, see T. R. England and R. E. Schenter, "ENDF/B-IV Fission-Product Files: Summary of Major Nuclide Data," LA-6116-MS [ENDF-223] (Oct. 1975).

5. M. E. Meek and B. F. Rider, "Compilation of Fission Product Yields," NEDO-12154-L (Jan. 1974).

6. W. B. Wilson and T. R. England, "Status of Fission-Product Data for Absorption Calculations," in Symposium Proceedings: Nuclear Data Problems for Thermal Reactor Applications, EPRI NP-1098 (June 1979).

TABLE A-I

4-GROUP ENERGY STRUCTURE AND FLUX RATIOS

| Group | Energy Boundary eV | Lethargy Width | LWR Flux Ratios to Thermal* |
|---|---|---|---|
| | $10^7$ | | |
| 1 | | 2.5 | 1.4759 |
| | $8.2085 \times 10^5$ | | |
| 2 | | 5.0 | 2.3401 |
| | $5.5308 \times 10^3$ | | |
| 3 | | 9.088 | 1.7833 |
| | $6.2506 \times 10^{-1}$ | | |
| 4 | | 8.412 | 1.0 |
| | $1.0 \times 10^{-5}$ | | |

*The degree of spectrum hardness used is indicated by the average value, 0.554018, of a unit 1/v cross section at 0.0253 eV.

TABLE A-II

NUCLIDES CONTRIBUTING GREATER THAN 0.1% OF THERMAL, EPITHERMAL OR TOTAL FISSION-PRODUCT ABSORPTION RATE AT SOME TIME DURING FUEL HISTORY (to 33 000 MWd/MT)

| Z SYM | Thermal | Epithermal | Total |
|---|---|---|---|
| 36 Kr | $^{83}Kr$ | $^{83}Kr$ | $^{83}Kr$ |
| 40 Zr | $^{93}Zr$ | $^{91,93,95,96}Zr$ | $^{91,93}Zr$ |
| 41 Nb | | $^{95}Nb$ | |
| 42 Mo | $^{95,97}Mo$ | $^{95,97,98,99,100}Mo$ | $^{95,97,98}Mo$ |
| 43 Tc | $^{99}Tc$ | $^{99}Tc$ | $^{99}Tc$ |
| 44 Ru | $^{101}Ru$ | $^{101,102,103,104}Ru$ | $^{101,102,103}Ru$ |
| 45 Rh | $^{103,105}Rh$ | $^{103,105}Rh$ | $^{103,105}Rh$ |
| 46 Pd | $^{105,107,108}Pd$ | $^{104,105,107,108}Pd$ | $^{105,107,108}Pd$ |
| 47 Ag | $^{109}Ag$ | $^{109}Ag$ | $^{109}Ag$ |
| 48 Cd | $^{113}Cd$ | | $^{113}Cd$ |
| 49 In | | $^{115}In$ | |
| 53 I | $^{129}I$ | $^{127,129}I$ | $^{129}I$ |
| 54 Xe | $^{131,133,135}Xe$ | $^{131,133,135}Xe$ | $^{131,133,135}Xe$ |
| 55 Cs | $^{133,134,135}Cs$ | $^{133,134,135}Cs$ | $^{133,134,135}Cs$ |
| 56 Ba | | $^{140}Ba$ | |
| 57 La | $^{139}La$ | $^{139,140}La$ | $^{139}La$ |
| 58 Ce | $^{141}Ce$ | $^{141,143}Ce$ | $^{141}Ce$ |
| 59 Pr | $^{141,143}Pr$ | $^{141,143}Pr$ | $^{141,143}Pr$ |
| 60 Nd | $^{143,144,145}Nd$ | $^{143,144,145,147,148}Nd$ | $^{143,144,145,147,148}Nd$ |
| 61 Pm | $^{147,148,148m,149}Pm$ | $^{147,148,148m,149,151}Pm$ | $^{147,148,148m,149}Pm$ |
| 62 Sm | $^{147,149,150,151,152}Sm$ | $^{147,148,149,150}Sm$ $^{151,152,153}Sm$ | $^{147,149,150,151,152}Sm$ |
| 63 Eu | $^{153,154,155,156}Eu$ | $^{153,154,155}Eu$ | $^{153,154,155,156}Eu$ |
| 64 Gd | $^{155,157}Gd$ | $^{156}Gd$ | $^{157}Gd$ |

TABLE A-III

CONTRIBUTIONS OF TEN MAJOR NUCLIDES TO THE TOTAL NEUTRON ABSORPTION RATE OF FISSION PRODUCTS

| Elapsed Time, hours | Burnup GWd/MT | Percent of Total Fission-Product Absorption Rate | | | | | | | | | | |
|---|---|---|---|---|---|---|---|---|---|---|---|---|
| | | $^{99}Tc$ | $^{103}Rh$ | $^{131}Xe$ | $^{135}Xe$ | $^{133}Cs$ | $^{143}Nd$ | $^{147}Pm$ | $^{149}Sm$ | $^{151}Sm$ | $^{152}Sm$ | All Others |
| 800 | 1 | 0.49 | 0.29 | 0.55 | 72.97 | 0.52 | 0.76 | 0.79 | 16.98 | 2.46 | 0.30 | 3.89 |
| 1600 | 2 | 0.94 | 0.88 | 1.21 | 65.87 | 1.12 | 1.97 | 1.82 | 16.05 | 3.79 | 0.64 | 5.71 |
| 2400 | 3 | 1.32 | 1.56 | 1.77 | 60.25 | 1.61 | 3.05 | 2.66 | 15.11 | 4.46 | 0.98 | 7.23 |
| 3200 | 4 | 1.64 | 2.24 | 2.24 | 55.60 | 2.03 | 3.96 | 3.32 | 14.33 | 4.77 | 1.29 | 8.58 |
| 4000 | 5 | 1.91 | 2.89 | 2.64 | 51.67 | 2.39 | 4.73 | 3.85 | 13.65 | 4.88 | 1.58 | 9.81 |
| 4800 | 6 | 2.16 | 3.49 | 3.00 | 48.28 | 2.70 | 5.39 | 4.27 | 13.04 | 4.88 | 1.84 | 10.95 |
| 5600 | 7 | 2.37 | 4.04 | 3.31 | 45.32 | 2.99 | 5.96 | 4.61 | 12.50 | 4.83 | 2.08 | 11.99 |
| 6400 | 8 | 2.57 | 4.55 | 3.59 | 42.69 | 3.24 | 6.46 | 4.88 | 12.01 | 4.75 | 2.29 | 12.97 |
| 7200 | 9 | 2.75 | 5.02 | 3.84 | 40.34 | 3.48 | 6.90 | 5.10 | 11.56 | 4.65 | 2.48 | 13.88 |
| 8000 | 10 | 2.91 | 5.45 | 4.07 | 38.21 | 3.69 | 7.29 | 5.27 | 11.14 | 4.55 | 2.65 | 14.77 |
| 8800 | 11 | 3.07 | 5.84 | 4.27 | 36.27 | 3.89 | 7.63 | 5.41 | 10.74 | 4.44 | 2.80 | 15.64 |
| 9600 | 12 | 3.21 | 6.21 | 4.46 | 34.50 | 4.07 | 7.94 | 5.51 | 10.38 | 4.34 | 2.94 | 16.44 |
| 10400 | 13 | 3.34 | 6.55 | 4.63 | 32.87 | 4.24 | 8.22 | 5.59 | 10.03 | 4.25 | 3.06 | 17.22 |
| 11200 | 14 | 3.46 | 6.87 | 4.79 | 31.36 | 4.39 | 8.47 | 5.64 | 9.71 | 4.16 | 3.17 | 17.98 |
| 12000 | 15 | 3.58 | 7.16 | 4.93 | 29.96 | 4.54 | 8.69 | 5.67 | 9.40 | 4.07 | 3.27 | 18.73 |
| 12800 | 16 | 3.69 | 7.43 | 5.06 | 28.65 | 4.68 | 8.89 | 5.69 | 9.11 | 3.99 | 3.36 | 19.47 |
| 13600 | 17 | 3.79 | 7.68 | 5.18 | 27.43 | 4.81 | 9.06 | 5.69 | 8.83 | 3.91 | 3.44 | 20.18 |
| 14400 | 18 | 3.89 | 7.92 | 5.29 | 26.28 | 4.94 | 9.22 | 5.67 | 8.57 | 3.84 | 3.51 | 20.87 |
| 15200 | 19 | 3.98 | 8.14 | 5.39 | 25.20 | 5.05 | 9.36 | 5.65 | 8.31 | 3.77 | 3.57 | 21.58 |
| 16000 | 20 | 4.07 | 8.34 | 5.48 | 24.19 | 5.17 | 9.48 | 5.61 | 8.07 | 3.71 | 3.62 | 22.26 |
| 16800 | 21 | 4.16 | 8.53 | 5.56 | 23.24 | 5.27 | 9.59 | 5.56 | 7.84 | 3.65 | 3.67 | 22.93 |
| 17600 | 22 | 4.24 | 8.70 | 5.64 | 22.34 | 5.37 | 9.68 | 5.51 | 7.62 | 3.60 | 3.71 | 23.59 |
| 18400 | 23 | 4.31 | 8.86 | 5.71 | 21.48 | 5.47 | 9.76 | 5.45 | 7.41 | 3.55 | 3.75 | 24.25 |
| 19200 | 24 | 4.39 | 9.00 | 5.77 | 20.68 | 5.56 | 9.82 | 5.38 | 7.21 | 3.50 | 3.78 | 24.91 |
| 20000 | 25 | 4.46 | 9.14 | 5.82 | 19.91 | 5.65 | 9.87 | 5.30 | 7.01 | 3.46 | 3.81 | 25.57 |
| 20800 | 26 | 4.53 | 9.26 | 5.87 | 19.19 | 5.73 | 9.91 | 5.23 | 6.82 | 3.42 | 3.83 | 26.21 |
| 21600 | 27 | 4.59 | 9.37 | 5.91 | 18.51 | 5.81 | 9.94 | 5.14 | 6.64 | 3.39 | 3.85 | 26.85 |
| 22400 | 28 | 4.66 | 9.47 | 5.94 | 17.86 | 5.89 | 9.96 | 5.06 | 6.47 | 3.35 | 3.86 | 27.48 |
| 23200 | 29 | 4.72 | 9.56 | 5.97 | 17.25 | 5.96 | 9.97 | 4.97 | 6.30 | 3.32 | 3.87 | 28.11 |
| 24000 | 30 | 4.78 | 9.64 | 6.00 | 16.66 | 6.03 | 9.96 | 4.88 | 6.14 | 3.30 | 3.88 | 28.73 |
| 24800 | 31 | 4.83 | 9.71 | 6.02 | 16.11 | 6.09 | 9.95 | 4.78 | 5.99 | 3.28 | 3.89 | 29.35 |
| 25600 | 32 | 4.89 | 9.77 | 6.03 | 15.59 | 6.16 | 9.93 | 4.69 | 5.84 | 3.26 | 3.89 | 29.95 |
| 26400 | 33 | 4.94 | 9.82 | 6.04 | 15.10 | 6.22 | 9.90 | 4.59 | 5.70 | 3.24 | 3.89 | 30.56 |

TABLE A-IV

SENSITIVITY OF TOTAL LWR FISSION-PRODUCT ABSORPTION RATE TO THERMAL AND EPITHERMAL (RESONANCE) CROSS SECTIONS*

| Nuclide | 5 GWd/MT (n,γ) Epithermal | 5 GWd/MT (n,γ) Thermal | 33 GWd/MT (n,γ) Epithermal | 33 GWd/MT (n,γ) Thermal |
|---|---|---|---|---|
| Br-81 | --- | .00001 | --- | .00004 |
| Kr-82 | ~0 | ~0 | .00003 | .00002 |
| Kr-83 | .00076 | .00256 | .00105 | .00352 |
| Sr-90 | --- | .00013 | --- | .00031 |
| Zr-91 | .00018 | .00009 | .00072 | .00035 |
| Zr-92 | --- | .00004 | --- | .00010 |
| Zr-93 | .00193 | .00041 | .00479 | .00103 |
| Mo-95 | .00224 | .00081 | .01431 | .00519 |
| Mo-96 | --- | ~0 | --- | .00002 |
| Mo-97 | .00068 | .00035 | .00244 | .00097 |
| Mo-98 | .00039 | .00002 | .00125 | .00007 |
| Tc-99 | .01552 | .00307 | .03526 | .00705 |
| Mo-100 | .00025 | .00003 | .00076 | .00011 |
| Ru-100 | --- | .00001 | --- | .00036 |
| Ru-101 | .00421 | .00044 | .01169 | .00122 |
| Ru-102 | .00014 | .00018 | .00060 | .00070 |
| Ru-103 | .00073 | .00024 | .00026 | .00009 |
| Rh-103 | .01709 | .01029 | .03486 | .02122 |
| Ru-104 | .00015 | .00003 | .00066 | .00013 |
| Rh-105 | .00126 | .00496 | .00104 | .00409 |
| Pd-105 | .00114 | .00054 | .00527 | .00250 |
| Pd-106 | .00001 | ~0 | .00022 | .00002 |
| Pd-107 | .00028 | .00012 | .00222 | .00098 |
| Pd-108 | .00054 | .00009 | .00548 | .00094 |
| Ag-109 | .00153 | .00035 | .00718 | .00167 |
| Cd-112 | ~0 | ~0 | .00003 | .00002 |
| Cd-113 | ~0 | .00004 | ~0 | ~0 |
| Te-128 | .00001 | ~0 | .00003 | .00001 |
| I -129 | .00022 | .00050 | .00081 | .00183 |
| Xe-130 | --- | ~0 | --- | .00003 |
| Xe-131 | .01906 | .00612 | .02765 | .00906 |
| Xe-132 | .00006 | .00006 | .00025 | .00022 |
| Xe-133 | --- | .00155 | --- | .00050 |
| Cs-133 | .01851 | .00612 | .04657 | .01298 |
| Xe-134 | .00006 | .00009 | .00014 | .00028 |
| Cs-134 | .00015 | .00032 | .00258 | .00642 |
| I -135 | ~0 | ~0 | ~0 | ~0 |
| Xe-135 | .00006 | .13693 | .00001 | .02363 |
| Cs-135 | .00073 | .00046 | .00182 | .00114 |

| Nuclide | 5 GWd/MT (n,γ) Epithermal | 5 GWd/MT (n,γ) Thermal | 33 GWd/MT (n,γ) Epithermal | 33 GWd/MT (n,γ) Thermal |
|---|---|---|---|---|
| La-139 | .00069 | .00156 | .00185 | .00418 |
| Ce-140 | .00001 | .00009 | .00005 | .00027 |
| Ce-141 | .00032 | .00124 | .00013 | .00051 |
| Pr-141 | .00077 | .00133 | .00279 | .00478 |
| Ce-142 | --- | .00018 | --- | .00064 |
| Pr-142 | ~0 | ~0 | ~0 | ~0 |
| Nd-142 | --- | ~0 | --- | .00020 |
| Ce-143 | .00003 | .00001 | .00001 | ~0 |
| Pr-143 | .00104 | .00152 | .00020 | .00029 |
| Nd-143 | .00491 | .04026 | .00672 | .05337 |
| Ce-144 | --- | .00012 | --- | .00015 |
| Nd-144 | .00006 | .00012 | .00060 | .00153 |
| Nd-145 | .00737 | .00432 | .01560 | .00917 |
| Nd-146 | .00009 | .00013 | .00049 | .00072 |
| Nd-147 | .00084 | .00021 | -.00022 | -.00006 |
| Pm-147 | .04775 | .01391 | .03069 | .00927 |
| Sm-147 | .00064 | .00017 | .00467 | .00123 |
| Nd-148 | .00067 | .00023 | .00227 | .00078 |
| Pm-148 | .00281 | .00163 | .00585 | .00366 |
| Pm-148m | .00022 | .00697 | .00021 | .00649 |
| Sm-148 | .00005 | .00001 | .00107 | .00029 |
| Pm-149 | .00001 | .00005 | .00001 | .00005 |
| Sm-149 | .00001 | .00105 | ~0 | .00028 |
| Nd-150 | .00019 | .00004 | .00112 | .00023 |
| Sm-150 | .00181 | .00478 | .01118 | .02939 |
| Pm-151 | .00001 | .00002 | -.00005 | -.00006 |
| Sm-151 | .00174 | .01462 | .00039 | .00330 |
| Sm-152 | .01242 | .00299 | .02945 | .00735 |
| Sm-153 | .00010 | .00004 | -.00006 | -.00003 |
| Eu-153 | .00318 | .00266 | .02055 | .01721 |
| Sm-154 | .00005 | .00002 | .00028 | .00012 |
| Eu-154 | .00043 | .00054 | .00742 | .00822 |
| Gd-154 | ~0 | ~0 | .00014 | .00015 |
| Eu-155 | .00024 | .00193 | .00038 | .00290 |
| Gd-155 | ~0 | .00002 | ~0 | .00001 |
| Eu-156 | ~0 | ~0 | ~0 | ~0 |
| Gd-156 | .00006 | ~0 | .00168 | .00006 |
| Eu-157 | ~0 | ~0 | ~0 | ~0 |
| Gd-157 | ~0 | ~0 | ~0 | .00001 |

*Listed values are the fractional change in the aggregate total absorption rate (summed over all energies) per unit change in the thermal or epithermal cross section for the listed nuclides.

## TABLE A-V

### ORDERED LIST OF THE FIRST 15 MOST IMPORTANT CROSS SECTION SENSITIVITIES AT 5 AND 33 GWd/MT

| 5 GWd/MT | | | 33 GWd/MT | | |
|---|---|---|---|---|---|
| Nuclide | X-sec type | Sensitivity | Nucide | X-sec type | Sensitivity |
| Xe-135 | Thermal | .13693 | Nd-143 | Thermal | .05337 |
| Pm-147 | Epithermal | .04775 | Cs-133 | Epithermal | .04657 |
| Nd-147 | Thermal | .04025 | Tc-99 | Epithermal | .03526 |
| Xe-131 | Epithermal | .01906 | Rh-103 | Epithermal | .03486 |
| Cs-133 | Epithermal | .01851 | Pm-147 | Epithermal | .03069 |
| Rh-103 | Epithermal | .01709 | Sm-152 | Epithermal | .02945 |
| Tc-99 | Epithermal | .01552 | Sm-150 | Thermal | .02939 |
| Sn-151 | Thermal | .01462 | Xe-131 | Epithermal | .02765 |
| Pm-147 | Thermal | .01391 | Xe-135 | Thermal | .02363 |
| Sm-152 | Epithermal | .01242 | Rh-103 | Thermal | .02122 |
| Rh-103 | Thermal | .01029 | Eu-153 | Epithermal | .02055 |
| Nd-145 | Epithermal | .00737 | Eu-153 | Thermal | .01721 |
| Pm-148m | Thermal | .00697 | Nd-145 | Epithermal | .01560 |
| Xe-131 | Thermal | .00612 | Mo-95 | Epithermal | .01431 |
| Cs-133 | Thermal | .00512 | Cs-133 | Thermal | .01298 |

TABLE A-VI

SUMMARY OF MAJOR FISSION-PRODUCT TOTAL ABSORBERS AT 4000 HOURS

| NUCLIDE | PERCENT OF TOTAL ABSORPTION (GROUPS 1-4) | PERCENT OF THERMAL ABSORPTION (GROUP 4) | PERCENT OF EPITHERMAL ABSORPTION (GROUP 3) | PERCENT OF RESONANCE ABSORPTION (GROUPS 1-3) |
|---|---|---|---|---|
| XE135 | 51.66877 | 62.25804 | .11979 | .11758 |
| SM149 | 13.64641 | 16.28261 | .82427 | .81274 |
| SM151 | 4.87625 | 5.28924 | 2.89994 | 2.86568 |
| ND143 | 4.72617 | 5.06554 | 3.05532 | 3.07406 |
| PM147 | 3.84727 | 1.03728 | 17.74753 | 17.52700 |
| RH103 | 2.88576 | 1.29927 | 10.71796 | 10.60918 |
| XE131 | 2.64281 | .77094 | 11.94299 | 11.75554 |
| CS133 | 2.38660 | .61488 | 11.04344 | 11.01176 |
| TC 99 | 1.91200 | .37562 | 9.41367 | 9.39149 |
| SM152 | 1.58060 | .36688 | 7.61827 | 7.48928 |
| PM148M | 1.26102 | 1.47567 | .21755 | .21607 |
| ND145 | 1.19667 | .52806 | 4.47278 | 4.45166 |
| RH105 | .65107 | .62619 | .78595 | .77220 |
| EU153 | .53709 | .29189 | 1.73731 | 1.73080 |
| RU101 | .49444 | .05294 | 2.52978 | 2.64382 |
| SM150 | .41197 | .35620 | .66846 | .68346 |
| EU155 | .38497 | .41294 | .24903 | .24883 |
| KR 83 | .34854 | .32251 | .46944 | .47526 |
| MO 95 | .31201 | .09792 | 1.34417 | 1.35424 |
| PR143 | .27672 | .19653 | .66838 | .66711 |
| XE133 | .25333 | .19356 | .55340 | .54433 |
| PM148 | .24959 | .11543 | .91820 | .90268 |
| CD113 | .24338 | .29297 | .00195 | .00195 |
| ZR 93 | .23937 | .04997 | 1.15644 | 1.16140 |
| LA139 | .22821 | .18864 | .41419 | .42088 |
| PR141 | .21542 | .15979 | .46206 | .48621 |
| AG109 | .19883 | .04410 | .96633 | .95210 |
| GD157 | .18819 | .22641 | .00215 | .00213 |
| PD105 | .18198 | .06566 | .68771 | .74826 |
| CE141 | .15961 | .15063 | .19272 | .20334 |
| ND147 | .14174 | .03452 | .67001 | .66372 |
| MO 97 | .13916 | .04204 | .52592 | .61199 |
| CS135 | .11925 | .05473 | .43583 | .43334 |
| PM149 | .10907 | .11192 | .09292 | .09522 |
| RU103 | .10723 | .03021 | .46006 | .48218 |
| ALL OTHERS | 1.17850 | .51830 | 3.93406 | 4.39249 |

TABLE A-VII

SUMMARY OF MAJOR FISSION-PRODUCT TOTAL ABSORBERS AT 26400 HOURS

| NUCLIDE | PERCENT OF TOTAL ABSORPTION (GROUPS 1-4) | PERCENT OF THERMAL ABSORPTION (GROUP 4) | PERCENT OF EPITHERMAL ABSORPTION (GROUP 3) | PERCENT OF RESONANCE ABSORPTION (GROUPS 1-3) |
|---|---|---|---|---|
| XE135 | 15.09836 | 26.77836 | .01371 | .01342 |
| ND143 | 9.90337 | 15.62377 | 2.50825 | 2.51536 |
| RH103 | 9.81659 | 6.50558 | 14.28416 | 14.09282 |
| CS133 | 6.21505 | 2.35690 | 11.26709 | 11.19792 |
| XE131 | 6.03893 | 2.59298 | 10.69177 | 10.48944 |
| SM149 | 5.69759 | 10.00653 | .13483 | .13251 |
| TC 99 | 4.93791 | 1.42788 | 9.52478 | 9.47118 |
| PM147 | 4.59155 | 1.82217 | 8.29825 | 8.16826 |
| SM152 | 3.89481 | 1.33069 | 7.35464 | 7.20642 |
| SM151 | 3.23823 | 5.17014 | .75449 | .74313 |
| EU153 | 3.21177 | 2.56920 | 4.07021 | 4.04165 |
| ND145 | 2.88226 | 1.87209 | 4.22063 | 4.18692 |
| EU154 | 2.23714 | 2.19512 | 2.31606 | 2.29140 |
| EU155 | 2.18896 | 3.45605 | .55475 | .55249 |
| MO 95 | 2.09987 | .97005 | 3.54423 | 3.55906 |
| PM148M | 1.83657 | 3.16345 | .12413 | .12288 |
| SM150 | 1.54143 | 1.96175 | .97988 | .99859 |
| AG109 | 1.44728 | .47249 | 2.75572 | 2.70625 |
| RU101 | 1.42170 | .22404 | 2.84980 | 2.96850 |
| CS134 | .91132 | 1.08947 | .68118 | .68123 |
| PD105 | .87408 | .46420 | 1.29412 | 1.40344 |
| SM147 | .79702 | .28738 | 1.47167 | 1.45524 |
| PR141 | .77187 | .84276 | .64865 | .68031 |
| KR 83 | .66512 | .90590 | .35097 | .35416 |
| LA139 | .61911 | .75325 | .44022 | .44586 |
| ZR 93 | .60368 | .18550 | 1.14261 | 1.14376 |
| RH105 | .58694 | .83091 | .27759 | .27184 |
| PD108 | .51431 | .13153 | 1.02206 | 1.00867 |
| PM148 | .49921 | .33984 | .71952 | .70504 |
| MO 97 | .38887 | .17290 | .57576 | .66779 |
| PD107 | .32190 | .16308 | .49077 | .52702 |
| CS135 | .30709 | .20745 | .43972 | .43578 |
| I129 | .28230 | .33702 | .19489 | .21162 |
| ND144 | .22832 | .24854 | .17046 | .20221 |
| GD157 | .21670 | .38375 | .00097 | .00096 |
| ND148 | .14303 | .05925 | .22772 | .25123 |
| CD113 | .13790 | .24433 | .00043 | .00043 |
| MO 98 | .13324 | .01024 | .25971 | .29209 |
| RU102 | .12987 | .09197 | .10409 | .17882 |
| ZR 91 | .11696 | .06208 | .17006 | .18784 |
| XE133 | .11005 | .12376 | .09418 | .09234 |
| PR143 | .10586 | .11066 | .10017 | .09965 |
| EU156 | .10472 | .11108 | .09860 | .09651 |
| ALL OTHERS | 2.13118 | 1.34390 | 2.77646 | 3.14797 |

# THE CONTRIBUTION OF (n,p) AND (n,α) REACTIONS TO FISSION-PRODUCT CAPTURE CROSS SECTIONS

H. Gruppelaar and B.P.J. van den Bos
Netherlands Energy Research Foundation (ECN),
P.O. Box 1, 1755 ZG Petten, The Netherlands.

Abstract

In recent fission-product cross section libraries evaluated (n,p) and (n,α) cross sections are lacking for most of the nuclides. To estimate these cross sections, calculations with a semi-empirical model of Pearlstein have been performed. The calculated excitation functions were renormalized at 14.5 MeV to experimental data, recently compiled by Qaim, or to data from recent systematics of Kumabe and Fukuda. The shapes of the excitation functions were checked against available experimental data. Group cross sections of pseudo fission products for a fast power reactor at a burn-up of 41 MWd/kg have been calculated. It was found that only in the highest energy-group (6.5 to 10.5 MeV) the (n,p) and (n,α) cross sections give important contributions to the absorption cross section. However, this group contributes only marginally to the total spectrum-averaged fission-product absorption. Most of the remaining discrepancies between various evaluated capture cross sections in the energy range above 1 MeV have to be ascribed to differences in nuclear models used for the calculation of $\sigma_{n\gamma}$.

## 1. INTRODUCTION

A large number of fission-product nuclides is accumulated during burn-up of fuel in a fast power reactor. An important effect of these fission products (f.p.) is the decrease of reactivity caused by in-growing parasitic absorption. The sodium-void effect /1/ in a fast power reactor is also significantly influenced by the presence of parasitic absorption of the fission products.

To calculate the above-mentioned effects, the neutron cross sections of a large number of fission products are required. Some recent evaluations of f.p. neutron cross sections are: ENDF/B-IV /2/, JENDL-1 /3/, CNEN/CEA /4/ and RCN-2 /5/. Intercomparisons of these data files show rather large discrepancies for capture cross sections of some individual f.p. isotopes. However, for the lumped fission products ("pseudo" f.p.) there is quite good agreement, in particular between results of the last three data files mentioned. The more serious discrepancies, partly of systematic nature, occur at neutron energies above about 1 MeV. For this reason it was thought worthwhile to investigate the contribution of $\sigma_{np}$ and $\sigma_{n\alpha}$ to the capture cross sections.

Inspection of the contents of the above-mentioned data files revealed that (n,p) and (n,α) cross sections are not given for many nuclides.

In this paper an estimate is given of the contributions of these and other charged-particle emission cross sections to the absorption cross section of a mixture of fission products in a fast power reactor. A more extended report of this work is given in ref. /6/.

## 2. SYSTEMATICS OF CHARGED-PARTICLE EMISSION CROSS SECTIONS

In the calculation of pseudo f.p. cross sections a large number of nuclides is involved. Since experimental data of charged-particle emission cross sections in the full energy range from threshold to 15 MeV are rather scarce, model calculations have to be performed. For this purpose the statistical model is widely used. However, this model requires level-density parameters of the compound and residual nuclides, most of which are rather uncertain. This seems to be the main reason that quite often the calculated cross sections have to be renormalized to values at 14.5 MeV, which are relatively well-known from activation experiments or from systematics. In order to avoid time-consuming statistical-model calculations, we have followed the semi-empirical approach of Pearlstein, with a renormalization to recent 14.5 MeV data.

Pearlstein's code THRES-2 has been described in refs. /7-9/. This code estimates neutron-induced cross sections from 0 to 20 MeV for 19 different reactions with one or two outgoing particles. An empirical model with approximate formulas, e.g. for the shapes of the excitation functions, is employed. In a first trial, we have applied this model without any renormalization to experimental data. In tables I and II the results of these calculations are shown for those f.p. nuclides having an atomic abundance of more than 0.5% in the $^{239}$Pu f.p. mixture (calculated for a 1300 MWe fast power reactor at a burn-up of 41 MWd/kg /10/). The second columns of tables I and II list the most recent experimental data, compiled by Qaim /11/. It appears that for the light fragments ($A \leq 114$) the THRES-2 values for $\sigma_{np}$ are about a factor of 3 too high; for the heavier fragments $\sigma_{np}$ is predicted a factor of 2 too high. The corresponding factors for $\sigma_{n\alpha}$ are 1.6 and 0.8. The reason for these large systematical discrepancies is that the model parameters were fitted primarily to data in an other mass range /8/.

In order to improve the results, it was decided to renormalize the cross sections to values at 14.5 MeV obtained from experimental data, supplemented with data from systematics. Quite recently, Kumabe and Fukuda /12/ have improved the systematics of $\sigma_{np}$ and $\sigma_{n\alpha}$ at about 14 MeV by introducing the following formulae, where the parameters have been fitted to experimental data by means of a least-squares method:

$$\sigma_{np} = \begin{cases} 21.8\ A\ \exp[-34.0\ s]\text{mb} & (40 \leq A \leq 62), \\ 0.75\ A^2\ \exp[-43.2\ s]\text{mb} & (63 \leq A \leq 89), \\ 0.75\ A^2\ \exp[-45.0\ s]\text{mb} & (90 \leq A \leq 160), \end{cases}$$

$$\sigma_{n\alpha} = \begin{cases} 51.0\sqrt{A}\ \exp[-30\ s]\text{mb} & (30 \leq A \leq 60), \\ 55.0\sqrt{A}\ \exp[-33\ s]\text{mb} & (61 \leq A \leq 105), \\ 7.6\times10^{-4}A^3\ \exp[-40\ s]\text{mb} & (106 \leq A \leq 150). \end{cases}$$

In these expressions the asymmetry parameter is defined as $s = (N-Z)/A$. In columns 4 of tables I and II the values calculated by means of these formulae are listed for the most important f.p. From figs. 1 and 2 it follows that there is quite good agreement for most of these nuclides, without notable systematic deviations.

It is also interesting to compare the experimental data or the data from systematics with those given in *evaluated* data files, as listed in the last two columns of tables I and II. The CNEN/CEA data were obtained from statistical-model calculations without any renormalization. The results appear to be much too low, in contrast with most of the given ENDF/B-IV data.

Other possible reactions below 15 MeV are the (n,d), (n,t) and (n,$\tau$)

reactions† and those in which more than one particle is emitted. From the last-mentioned class of reactions the important ones are those in which one or more of the emitted particles is a neutron, thus giving no contribution to the absorption cross section. For the (n,t) and (n,τ) cross sections at 14.5 MeV we have adopted estimates given in a recent review of Qaim /13/. Cross sections for a few other residual capture reactions, such as $\sigma_{n2p}$, were taken from the calculations with THRES-2, without renormalization.

The *shapes* of the excitation functions were calculated with the code THRES-2. In order to check these calculations for nuclides in the f.p. mass range, comparisons have been made with experimental excitation functions as compiled in ref. /14/. Only for a small number of nuclides sufficient data for $\sigma_{np}$ and $\sigma_{n\alpha}$ have been measured. In fig. 3 an example of a comparison between experimental /15,16/ and calculated data is given for the $^{90}Zr(n,p)^{90}Y$ reaction. In this figure the calculated curve has been renormalized to the experimental values at 14.5 MeV recommended by Qaim /11/. More examples are given in ref. /6/. From these intercomparisons it follows that the calculated curves predict the shape of the excitation functions reasonably well. However, the number of nuclides for which these data exist is too small to detect possible systematic deviations between the calculated and measured shapes.

## 3. CALCULATION OF CROSS SECTIONS

The code THRES-2 has been extended with an option to compute group cross sections in the Russian ABBN scheme /17/. The boundaries of the first five groups of this scheme are at 0.8, 1.4, 2.5, 4.0, 6.5 and 10.5 MeV. The group cross sections $\sigma_g^i$ were calculated, using as weighting function a Cranberg fission spectrum. The calculations with THRES-2 were performed for all 162 f.p. nuclides, given in ref. /10/ with normalization to 14.5-MeV systematics or to 14.5-MeV experimental data as discussed before.

The pseudo fission-product group cross sections were calculated according to

$$\sigma_g^p = \sum_{i=1}^{162} c_i \, \sigma_g^i \quad \text{with} \quad \sum_{i=1}^{162} c_i = 2.$$

The isotopic concentrations $c_i$ (in atoms per fission) were taken from /10/. The results presented in this paper refer to fission of $^{239}Pu$ in a 1300 MWe fast power reactor at a burn-up of 41 MWd/kg. In columns 3 to 5 of table III the calculated charged-particle emission cross sections or "residual" capture cross sections for this pseudo f.p. are given. We recommend to use these group cross sections which are partly based upon experimental values. In fact, for 38% of the nuclides $\sigma_{np}$ is known; for $\sigma_{n\alpha}$ this percentage is 28%. These nuclides cover the whole f.p. mass range from A = 76 to 164. However, the light fission fragments ($A \leq 114$) give the major contribution (of about 90%) to $\sigma_{np}$ and $\sigma_{n\alpha}$ of a pseudo-fission product. From these light fragments there are about 24 important nuclides, with concentrations of more than 0.5% (see tables I and II). There are experimental 14.5-MeV data for about 50% of these important nuclides, with uncertainties mostly less than 15%. Therefore, we expect that our estimates for the pseudo f.p. cross sections are quite accurate at energies near 14.5 MeV. At lower energies uncertainties could be affected by unknown systematic errors in the shapes of the excitation curves.

In table IV the calculated pseudo f.p. absorption group cross sections are given as calculated from four different sets of cross section libraries. Each library contains a "main library", consisting of f.p. isotopes from RCN-2A, CNEN/CEA, JENDL-1 or ENDF/B-IV, supplemented with isotopes from other libraries, mostly ENDF/B-IV and the Australian f.p. library /18/. The

† The symbol τ is used for $^3He$-particles.

exact composition of the *adjusted* RCN-2A set has been given in /10/. Each "main library" contains the most important nuclides, predicting at least 82% (RCN-2A set) of the average capture rate in a fast power reactor.

The absorption cross sections in the f.p. libraries of RCN-2(A) and JENDL-1 are pure radiative capture cross sections, those of CNEN/CEA and ENDF/B-IV include $\sigma_{np}$ and $\sigma_{n\alpha}$ for 28 and 29 nuclides, respectively. We have corrected the four libraries for the remaining contributions by performing THRES-2 calculations with renormalizations to the *evaluated* data. The final corrections to be applied to the data in table IV are listed in table III. The corrected absorption cross sections are indicated in between brackets in table IV. These corrections are only important in ABBN-group 1 (energy interval from 6.5 to 10.5 MeV). In fig. 4 the corrected absorption cross sections at energies above 0.1 MeV have been plotted. The relative differences between the various curves are always less than 35%. At lower energies these differences are much smaller, see fig. 5. In table V the average (one-group) absorption cross sections in the flux spectrum of a fast power reactor are given. The applied corrections are only very small.

## 4. INTERCOMPARISON OF PSEUDO F.P. CROSS SECTIONS

Although it is not the purpose of this paper to discuss in detail the differences between pseudo f.p. cross sections calculated from various f.p. data files, a few remarks will be made. From fig. 5 it follows that the differences between the pseudo's of the more recent f.p. libraries RCN-2A, CNEN/CEA and JENDL-1 are very small; the ENDF/B-IV results are on the average about 10% lower. The small differences between the absorption cross sections of the first three data files could be the result of the use of more recent data and the application of similar nuclear models.

At energies above a few hundred keV somewhat more serious discrepancies occur. It is easily concluded from fig. 5 and table V that these discrepancies cannot be ascribed to uncertainties in the evaluated residual absorption cross sections $\sigma_{np}$ and $\sigma_{n\alpha}$. Therefore, it is most likely that the systematic differences near 1 MeV in the absorption cross sections are due to systematic differences in the nuclear models used to predict the *radiative* capture cross sections in the MeV range.

Inspection of these models revealed that possible systematic differences might occur in the energy range where there is a large competition due to inelastic scattering to levels in the continuum. In these "continuum models" a quite sensitive parameter is the spin cut-off parameter $\sigma^2$, for which different expressions are used by various authors. This has been discussed previously in ref. /20/. The basic point is that at low excitation energies $\sigma^2$ should agree with the experimental distribution of the spins of low-lying levels of the target nucleus /21/, a condition which is fulfilled in all RCN-2 evaluations and in the more recent CNEN/CEA evaluations, performed since 1976. In the past quite often too large values of $\sigma^2$, based upon theoretical predictions at high energies /22/ were used over the whole energy range. This generally leads to too high values of $\sigma_{n\gamma}$ above about 1 MeV. It is our impression that for many nuclides in JENDL-1, ENDF/B-IV and CNEN/CEA too high values of $\sigma^2$ have been used at energies from about 1 to 5 MeV. For further details we refer to ref. /20/.

## 5. ACKNOWLEDGEMENTS

The authors like to thank Dr. Pearlstein for his suggestion to use the code THRES-2 for the calculation of the contribution of $\sigma_{np}$ and $\sigma_{n\alpha}$ to lumped fission-product absorption cross sections. They are also grateful to Drs. Qaim and Kumabe for the possibility to use their data prior to publication.

## 6. REFERENCES


/1/ Heijboer, R.J., A.J. Janssen and F. Lekkerkerk, Status of pseudo fission-product cross sections for fast reactors; sensitivity studies for sodium void effects, invited paper, contributed to this meeting.

/2/ Evaluated Nuclear Data File B, version IV, National Neutron Cross Section Center, Brookhaven National Laboratory, 1974.

/3/ Iijima, S. et al., Evaluation of neutron cross section of 27 fission product nuclides important for fast reactor, J. Nucl. Sci. Technol. 14 (1977) 161 and data file (extended to 68 nuclides), available from NEA Data Bank, Saclay (1977).

/4/ Centro di Calcolo del CNEN (Bologna) and Commissariat à l'Energie Atomique CEA (Cadarache), Fission product library for 63 nuclides, available from NEA Data Bank, Saclay (1977).

/5/ Gruppelaar, H. Tables of RCN-2 fission product cross section evaluation, vol. 1, ECN-13 (1977), vol. 2, ECN-33 (1977) and vol. 3, ECN-65 (1979).

/6/ Gruppelaar, H. and B.P.J. van den Bos, The contribution of (n,p) and (n,α) reactions to fission-product capture cross sections, ECN-78 (1979).

/7/ Pearlstein, S. Neutron-induced reactions in medium mass nuclei, J. of Nuclear Energy 27 (1973) 81.

/8/ Pearlstein, S. Neutron cross sections and their uncertainties obtained from systematics, Proc. Conf. on Nuclear Cross Sections and Technology, Washington D.C., 1975, NBS Special Publication 425, vol. 1 (1975) 332 and private communication (1979).

/9/ Pearlstein, S. Program THRES-2, December 1975, code available from NEA Data Bank, Saclay.

/10/ Heijboer, R.J. Pseudo fission-product cross sections for a 1300 MWe fast breeder reactor (status July 1978), ECN-52 (1978).

/11/ Qaim, S.M. 14 MeV neutron activation cross-sections, Handbook of Spectroscopy, vol. 3, The Chemical Rubber Company (CRC) Press, Inc., West Palm Beach, Florida, USA, to be published.

/12/ Kumabe, I. and K. Fukuda, Empirical formulae for the (n,p) and (n,α) reactions for 14 MeV neutrons, Progress Report (July 1977 to June 1978 Inclusive) of the Japan Atomic Energy Research Institute, NEANDC(J)-65/U (1978) 45.

/13/ Qaim, S.M. Recent advances in the study of some neutron threshold reactions, Proc. Int. Conf. on Neutron Physics and Nuclear Data for Reactors and other Applied Purposes, Harwell (1978), p. 1088.

/14/ Garber, D.I. and R.R. Kinsey. Neutron cross sections, vol. II, Curves, BNL-325 (1976), third edition.

/15/ Carroll, E. and R.W. Stooksherry, Zirconium (n,p) cross-section measurements, Nucl. Sci. and Eng. 25 (1966) 285.

/16/ Bayhurst, B.P. and R.J. Prestwood, (n,p) and (n,α) excitation functions of several nuclei from 7.0 to 19.8 MeV, J. Inorg. Nucl. Chem. 23 (1961) 173.

/17/ Abagyan, L.P., N.O. Bazazyants, I.I. Bondarenko and H.N. Nikolaev, Group constants for nuclear reactor calculations, New York, Consultants Bureau, 1964.

/18/ Rose, E.K. The AAEC fission product cross section libraries FISPROD, POINTXSL and FISPROD.GROUPXSL, AAEC/TM-587 (1971).

/19/ Kiefhaber, E. The KFK-INR set of group constants; Nuclear data basis and first results of its application to the recalculation of fast zero-power reactors, KFK-1572 (1972).

/20/ Gruppelaar, H., A.J. Janssen and J.W.M. Dekker, Radiative capture cross section in the MeV range, App. 1 of ECN-12 (1976) p. 113.

/21/ Schmittroth, F. Neutron capture calculation for $E_n$ = 100 keV to 4 MeV, HEDL-TME-73-79 (1973).

/22/ Gilbert, A. and A.G.W. Cameron, A composite nuclear-level-density formula with shell corrections, Can. J. of Phys. 43 (1965) 1446.

Table I. $\sigma_{np}$ of important[a)] fission-product nuclides (in mb)

| Nuclide identification (Z,A) | experimental[b)] (14-15 MeV) Qaim /11/ | 14.5 MeV systematics | | evaluation | |
|---|---|---|---|---|---|
| | | Pearlstein /9/ (Thres-2) | Kumabe and Fukuda /12/ | CNEN/ CEA /4/ (15 MeV) | ENDF/B-IV /2/ (14 MeV) |
| 37087 | 12 ±1.3 | 38 | 8.9 | - | - |
| 38088 | 13.5±1.5 | 50 | 16.1 | - | - |
| 38090 | | 33 | 5.5 | - | - |
| 39089 | 28 ±6 | 67 | 28.5 | - | - |
| 40091 | 43.2±4 | 93 | 26.9 | 21.7 | - |
| 40092 | 19.5±2.5 | 63 | 17.9 | 14.0 | - |
| 40093 | | 69 | 12.0 | 1.21 | - |
| 40094 | 11 ±1 | 38 | 8.1 | 1.81 | - |
| 40096 | | 15 | 3.8 | - | - |
| 42095 | (31 ±4 ) | 87 | 36.9 | 34.5 | - |
| 42097 | 21 ±2 | 68 | 17.0 | 4.35 | - |
| 42098 | ( 2.6±0.7) | 29 | 11.6 | 2.43 | - |
| 42100 | | 13 | 5.6 | 0.096 | - |
| 43099 | 15 ±2.3 | 56 | 20.0 | 0.68 | - |
| 44101 | | 66 | 23.3 | 4.20 | - |
| 44102 | ( 4.4±1.5) | 31 | 16.2 | 0.57 | - |
| 44104 | 7 ±1.5 | 16 | 8.0 | 0.057 | - |
| 44106 | | 7.7 | 4.0 | - | - |
| 45103 | 17 ±3 | 46 | 27.2 | 0.29 | - |
| 46105 | 54 ±9 | 73 | 31.5 | 3.37 | - |
| 46106 | 22 ±4.5 | 39 | 22.1 | - | - |
| 46107 | | 54 | 15.6 | - | - |
| 46108 | ( 8.3±1.5) | 20 | 11.1 | - | - |
| 47109 | (10 ±3 ) | 61 | 18.2 | 0.25 | 10.2 |
| 52130 | 1.7±0.14 | 2.9 | 1.6 | - | - |
| 53129 | | 19 | 4.1 | - | - |
| 54131 | 6.1±0.6 | 31 | 4.8 | - | 4.86 |
| 54132 | ( 3.2±0.3) | 10 | 3.7 | - | 2.04 |
| 54134 | ( 2.0±0.5) | 7.0 | 2.2 | - | 1.69 |
| 54136 | | 2.4 | 1.3 | - | 0.028 |
| 55133 | 15.3±2.4 | 22 | 5.5 | 3.61 | 11.6 |
| 55137 | | 15 | 2.0 | - | - |
| 56138 | ( 2.6±0.4) | 6.1 | 3.0 | - | - |
| 57139 | 4.4±0.8 | 16 | 4.4 | - | - |
| 58140 | 6.5±0.7 | 7.9 | 6.6 | - | - |
| 58142 | 4.8±0.8 | 2.5 | 4.0 | - | - |
| 58144 | | 1.1 | 2.5 | - | - |
| 59141 | 4.5±1.5 | 29 | 9.7 | 2.08 | 5.8 |
| 60143 | 11 ±2 | 31 | 11.0 | 1.00 | 5.7 |
| 60144 | ( 9.8±1.5) | 6.5 | 8.6 | - | - |
| 60145 | 7 ±1.3 | 15 | 6.7 | 0.53 | 2.9 |
| 60146 | 4.7±0.7 | 3.0 | 5.3 | - | 0.86 |
| 60148 | 3.5±0.5 | 1.1 | 3.3 | - | 0.36 |
| 61147 | | 13.3 | 7.7 | 0.23 | 3.75 |
| 62149 | | 6.4 | 8.8 | 0.40 | 16.0 |

a) Nuclides with concentrations of more than 0.5% in the $^{239}Pu$ pseudo fission product at a burn-up of 41 MWd/kg /10/.

b) Activation cross sections compiled by Qaim /11/, summed over ground and metastable states. Data in between brackets refer to only part of the total activation cross section, as given in ref. /11/.

Table II. $\sigma_{n\alpha}$ of important[a)] fission-product nuclides (in mb)

| Nuclide identification (Z,A) | experimental[b)] (14-15 MeV) Qaim /11/ | 14.5 MeV systematics | | evaluation | |
|---|---|---|---|---|---|
| | | Pearlstein /9/ (Thres-2) | Kumabe and Fukuda /12/ | CNEN/ CEA /4/ (15 MeV) | ENDF/B-IV /2/ (14 MeV) |
| 37087 | 3.8±0.4 | 3.6 | 3.7 | - | - |
| 38088 | (75 ±30 ) | 3.7 | 5.7 | - | - |
| 38090 | | 3.1 | 3.1 | - | - |
| 39089 | 6.5±0.6 | 6.4 | 8.8 | - | - |
| 40091 | | 33.8 | 9.7 | 11.4 | - |
| 40092 | 8.5±1.0 | 17.2 | 7.1 | 24.1 | - |
| 40093 | | 18.8 | 5.3 | 0.64 | - |
| 40094 | 4.0±0.3 | 12.7 | 3.9 | 0.46 | - |
| 40096 | 2.3±0.3 | 5.3 | 2.2 | - | - |
| 42095 | | 23.3 | 11.7 | 14.6 | - |
| 42097 | | 20.4 | 6.5 | 2.5 | - |
| 42098 | 5.5±0.7 | 11.2 | 4.9 | 1.08 | - |
| 42100 | 2.8±0.3 | 7.2 | 2.8 | 0.24 | - |
| 43099 | 7 ±1 | 9.4 | 7.2 | 1.82 | - |
| 44101 | | 11.4 | 7.9 | 0.94 | - |
| 44102 | 6.2±0.7 | 4.0 | 6.0 | 0.29 | - |
| 44104 | 2.6±1.0 | 4.6 | 3.5 | 0.057 | - |
| 44106 | | 0.96 | 1.0 | - | - |
| 45103 | 11 ±2 | 6.0 | 8.7 | 0.55 | - |
| 46105 | | 11.4 | 9.5 | 0.737 | - |
| 46106 | 5.6±0.7 | 5.2 | 4.6 | - | - |
| 46107 | | 8.9 | 3.4 | 0.285 | - |
| 46108 | 2.6±0.4 | 3.6 | 2.6 | - | - |
| 47109 | (12 ±3 ) | 4.5 | 4.0 | 0.66 | 10.2 |
| 52130 | ( 0.4±0.1) | 0.42 | 0.56 | - | - |
| 53129 | | 0.66 | 1.3 | - | - |
| 54131 | | 3.4 | 1.5 | - | 0.38 |
| 54132 | | 0.73 | 1.2 | - | 0.07 |
| 54134 | | 0.64 | 0.78 | - | 0.05 |
| 54136 | | 0.47 | 0.51 | - | 0.05 |
| 55133 | 1.6±0.2 | 0.95 | 1.8 | 0.48 | 1.2 |
| 55137 | | 0.70 | 0.74 | - | - |
| 56138 | 2.5±0.2 | 1.1 | 1.1 | - | - |
| 57139 | 1.6±0.2 | 1.6 | 1.5 | - | - |
| 58140 | 1.4±0.2 | 2.1 | 2.2 | - | - |
| 58142 | 2.3±0.6 | 3.2 | 1.4 | - | - |
| 58144 | | 2.0 | 0.95 | - | - |
| 59141 | | 3.0 | 3.1 | 0.61 | 4.7 |
| 60143 | | 12.7 | 3.6 | 0.46 | 6.3 |
| 60144 | 10 ±1 | 5.6 | 2.9 | - | - |
| 60145 | | 8.9 | 2.3 | 0.67 | 4.2 |
| 60146 | 3.4±0.5 | 2.2 | 1.9 | - | 2.5 |
| 60148 | 4.8±0.6 | 1.5 | 1.3 | - | 1.4 |
| 61147 | | 3.4 | 2.7 | 0.58 | 3.5 |
| 62149 | | 1.7 | 3.1 | 0.29 | - |

a) Nuclides with concentrations of more than 0.5% in the $^{239}Pu$ pseudo fission product at a burn-up of 41 MWd/kg /10/.

b) Activation cross sections compiled by Qaim /11/, summed over ground and metastable states. Data in between brackets refer to only part of the total activation cross section, as given in ref. /11/.

Table III. Residual capture group cross sections for a pseudo fission-product of $^{239}Pu$ at 41 MWd/kg burn-up.

| ABBN group nr. | $\Delta E$ a) (MeV) | Total contribution | | | Correction to RCN-2A | | | Correction to CNEN/CEA | | |
|---|---|---|---|---|---|---|---|---|---|---|
| | | $\sigma_{np}$ | $\sigma_{n\alpha}$ | $\sigma_{res}$ b) | $\Delta\sigma_{np}$ | $\Delta\sigma_{n\alpha}$ | $\Delta\sigma_{res}$ b) | $\Delta\sigma_{np}$ | $\Delta\sigma_{n\alpha}$ | $\Delta\sigma_{res}$ b) |
| 1 | 6.5-10.5 | 2.7 | 0.64 | 3.4 | 2.7 | 0.63 | 3.3 | 2.1 | 0.39 | 2.5 |
| 2 | 4.0- 6.5 | 0.52 | 0.11 | 0.63 | 0.51 | 0.10 | 0.62 | 0.40 | 0.065 | 0.47 |
| 3 | 2.5- 4.0 | 0.15 | 0.033 | 0.18 | 0.15 | 0.033 | 0.18 | 0.11 | 0.020 | 0.13 |
| 4 | 1.4- 2.5 | 0.062 | 0.015 | 0.077 | 0.061 | 0.015 | 0.076 | 0.047 | 0.009 | 0.056 |
| 5 | 0.8- 1.4 | 0.025 | 0.0069 | 0.032 | 0.025 | 0.0068 | 0.032 | 0.018 | 0.004 | 0.023 |
| - | 0 - 15 | 0.16 | 0.038 | 0.20 | 0.16 | 0.038 | 0.20 | 0.12 | 0.023 | 0.15 |

| ABBN group nr. | $\Delta E$ a) (MeV) | Correction to JENDL-1 | | | Correction to ENDF/B-IV | | |
|---|---|---|---|---|---|---|---|
| | | $\Delta\sigma_{np}$ | $\Delta\sigma_{n\alpha}$ | $\Delta\sigma_{res}$ b) | $\Delta\sigma_{np}$ | $\Delta\sigma_{n\alpha}$ | $\Delta\sigma_{res}$ b) |
| 1 | 6.5-10.5 | 2.7 | 0.64 | 3.4 | 2.5 | 0.55 | 3.1 |
| 2 | 4.0- 6.5 | 0.51 | 0.11 | 0.62 | 0.49 | 0.097 | 0.58 |
| 3 | 2.5- 4.0 | 0.15 | 0.033 | 0.18 | 0.14 | 0.029 | 0.17 |
| 4 | 1.4- 2.5 | 0.062 | 0.015 | 0.077 | 0.058 | 0.013 | 0.071 |
| 5 | 0.8- 1.4 | 0.025 | 0.0069 | 0.032 | 0.021 | 0.0068 | 0.028 |
| - | 0 - 15 | 0.16 | 0.038 | 0.20 | 0.15 | 0.033 | 0.18 |

a) Averaged over a Cranberg fission spectrum.

b) Sum of $\sigma_{np}$, $\sigma_{n\alpha}$, $\sigma_{nd}$, $\sigma_{nt}$ and $\sigma_{n\tau}$.

Table V. Average absorption cross sections in mb/fission of pseudo fission product of $^{239}Pu$ at a burn-up of 41 MWd/kg in a fast power reactor a).

| Main f.p. library b) | $\sigma_{abs}$ c) | $\sigma_{res}$ d) |
|---|---|---|
| RCN-2A | 438.3 | 0.20 |
| CNEN/CEA | 437.9 | 0.15 |
| JENDL-1 | 442.4 | 0.20 |
| ENDF/B-IV | 398.6 | 0.18 |

a) Flux spectrum of a 1300 MWe fast power reactor /19/.

b) See table IV.

c) Corrected for residual capture cross sections.

d) See table III.

Table IV. Absorption cross sections[a)] in b/fission of pseudo fission product of $^{239}Pu$ at 41 MWd/kg burn-up, calculated from different f.p. cross section libraries.

| f.p. libraries | Number of f.p. nuclides | | | |
|---|---|---|---|---|
| RCN-2 | 1 | - | - | - |
| RCN-2A | 37 | - | - | - |
| CNEN/CEA | 1 | 62 | - | - |
| JENDL-1 | - | - | 59 | - |
| ENDF/B-IV | 116 | 93 | 90 | 155 |
| Australian | 7 | 7 | 7 | 7 |

| ABBN group nr. | ΔE | Main libraries: | | | |
|---|---|---|---|---|---|
| | | RCN-2A[b,c)] | CNEN/CEA[c)] | JENDL-1[c)] | ENDF/B-IV[c)] |
| 1 | 6.5 -10.5 MeV | 0.0030(6.3) | 0.0054(7.9) | 0.0037(7.1) | 0.0058(8.9) |
| 2 | 4.0 - 6.5 | 0.013 (14) | 0.020 (20) | 0.018 (19) | 0.017 (18) |
| 3 | 2.5 - 4.0 | 0.034 | 0.042 | 0.047 | 0.041 |
| 4 | 1.4 - 2.5 | 0.058 | 0.064 | 0.080 | 0.068 |
| 5 | 0.8 - 1.4 | 0.084 | 0.082 | 0.103 | 0.088 |
| 6 | 0.4 - 0.8 | 0.119 | 0.117 | 0.131 | 0.109 |
| 7 | 0.2 - 0.4 | 0.180 | 0.180 | 0.186 | 0.158 |
| 8 | 0.1 - 0.2 | 0.255 | 0.256 | 0.256 | 0.229 |
| 9 | 46.5-100 keV | 0.381 | 0.382 | 0.384 | 0.349 |
| 10 | 21.5-46.5 | 0.586 | 0.600 | 0.595 | 0.545 |
| 11 | 10.0-21.5 | 0.872 | 0.895 | 0.891 | 0.827 |
| 12 | 4.65-10.0 | 1.30 | 1.31 | 1.31 | 1.23 |
| 13 | 2.15-4.65 | 1.93 | 1.88 | 1.91 | 1.75 |
| 14 | 1.00-21.5 | 3.04 | 2.94 | 2.95 | 2.62 |
| 15 | 465 -1000 eV | 4.59 | 4.47 | 4.44 | 3.99 |
| 16 | 215 -465 | 9.58 | 8.89 | 8.66 | 7.57 |
| 17 | 100 -215 | 12.5 | 12.5 | 12.1 | 10.4 |
| 18 | 46.5-100 | 18.1 | 18.5 | 17.9 | 16.6 |
| 19 | 21.5-46.5 | 34.5 | 37.9 | 37.5 | 33.0 |
| 20 | 10.0-21.5 | 50.5 | 52.6 | 50.5 | 51.6 |
| 21 | 4.65-10.0 | 99.4 | 100. | 98.4 | 104.0 |
| 22 | 2.15-4.65 | 24.3 | 25.4 | 25.8 | 20.4 |
| 23 | 1.00-2.15 | 68.5 | 54.5 | 56.0 | 53.3 |
| 24 | 0.465-1.00 | 98.1 | 94.4 | 87.6 | 87.4 |
| 25 | 0.215-0.465 | 52.9 | 60.5 | 60.2 | 55.6 |
| 26 | $10^{-3}$ - 0.215 | 1013. | 1035. | 1055. | 1040. |

a) Flux weighting spectrum from KFK-INR-1 set /19/.

b) In ref. /10/ a slightly different flux weighting spectrum has been used.

c) Data in between brackets are cross sections in mb per fission, corrected for $\sigma_{n\alpha}$, $\sigma_{np}$, etc.; see table V.

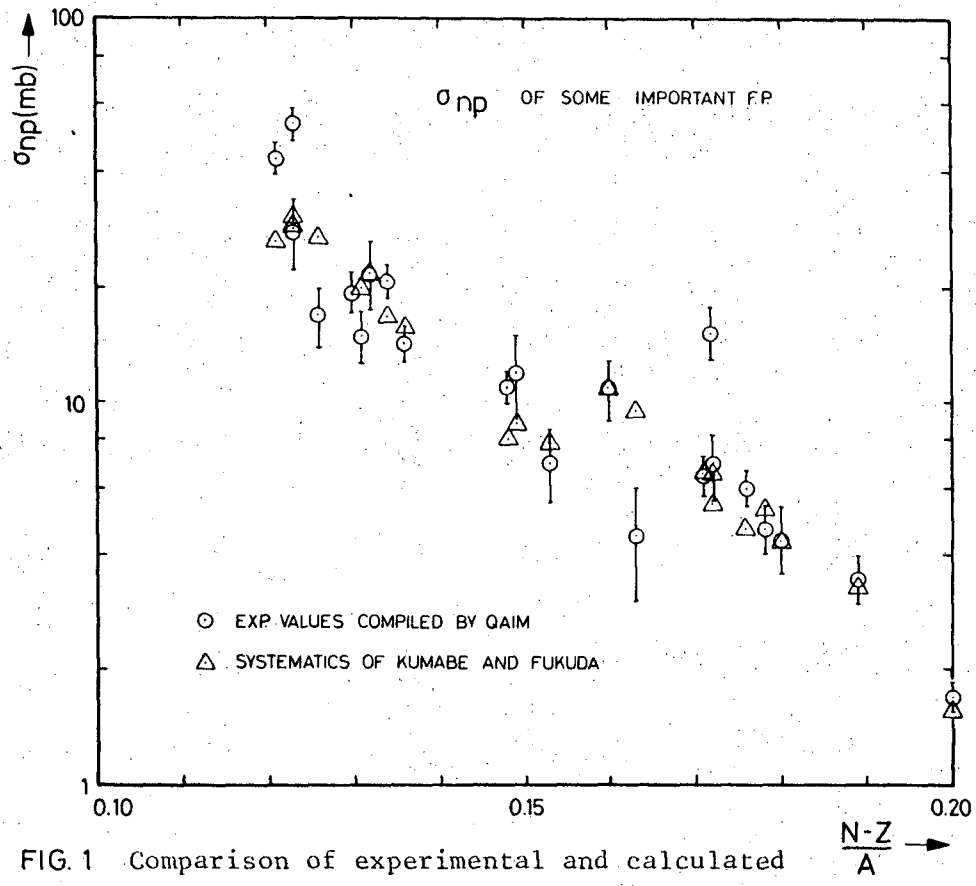


FIG. 1 Comparison of experimental and calculated 14.5-MeV values of $\sigma_{np}$.

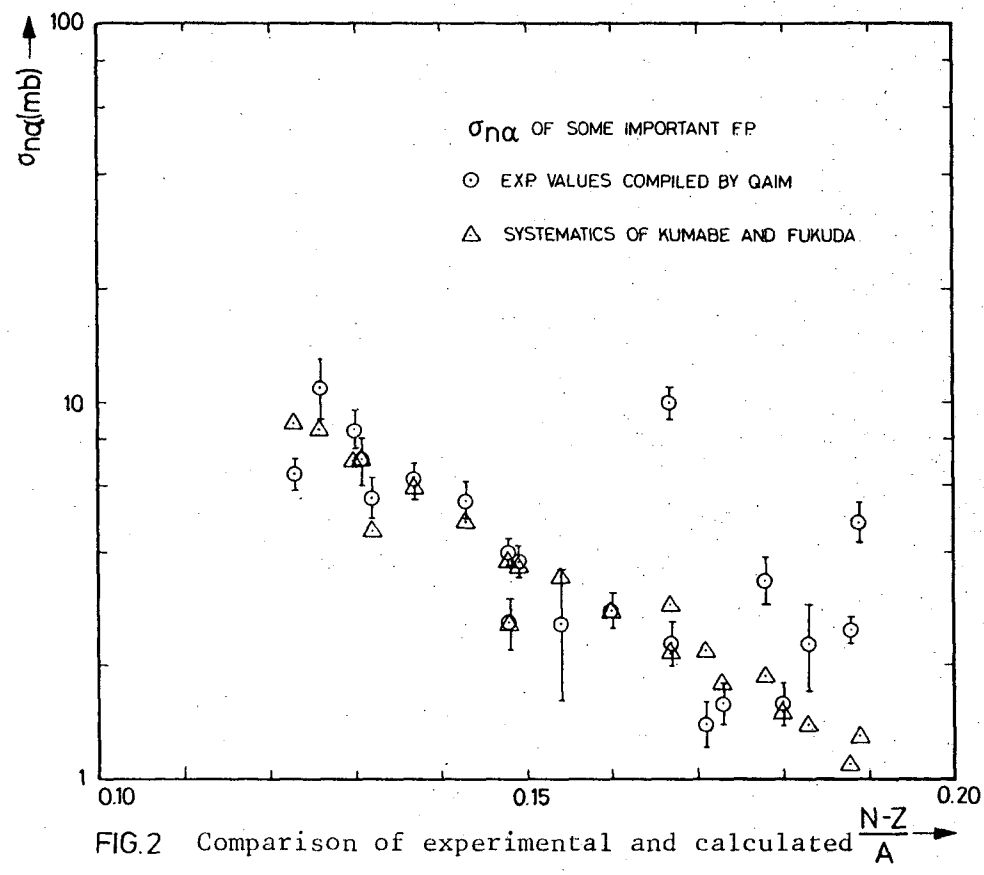


FIG. 2 Comparison of experimental and calculated 14.5-MeV values of $\sigma_{n\alpha}$.

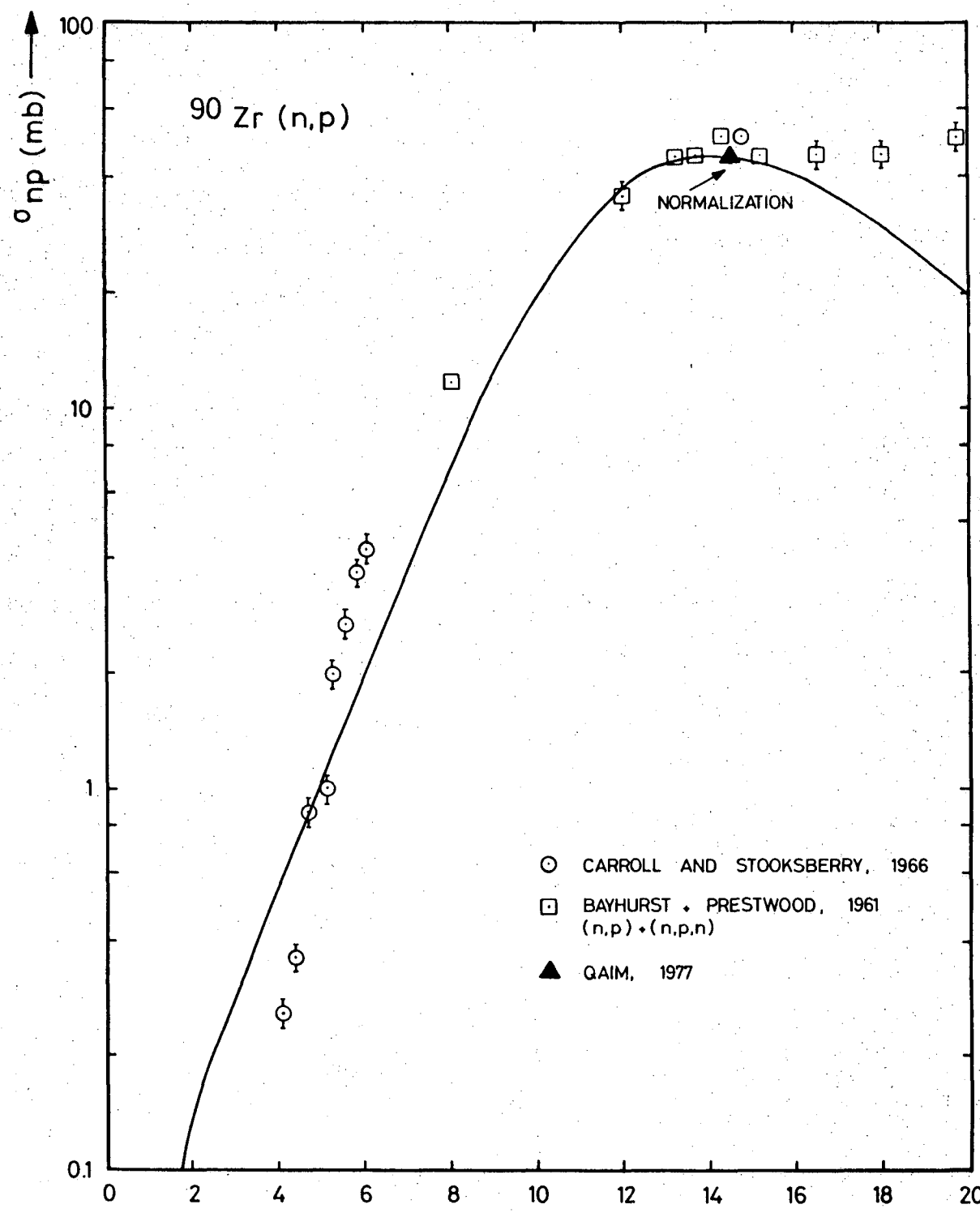


Fig. 3. Comparison of experimental and calculated excitation functions for the $^{90}Zr(n,p)^{90}Y$ reaction.

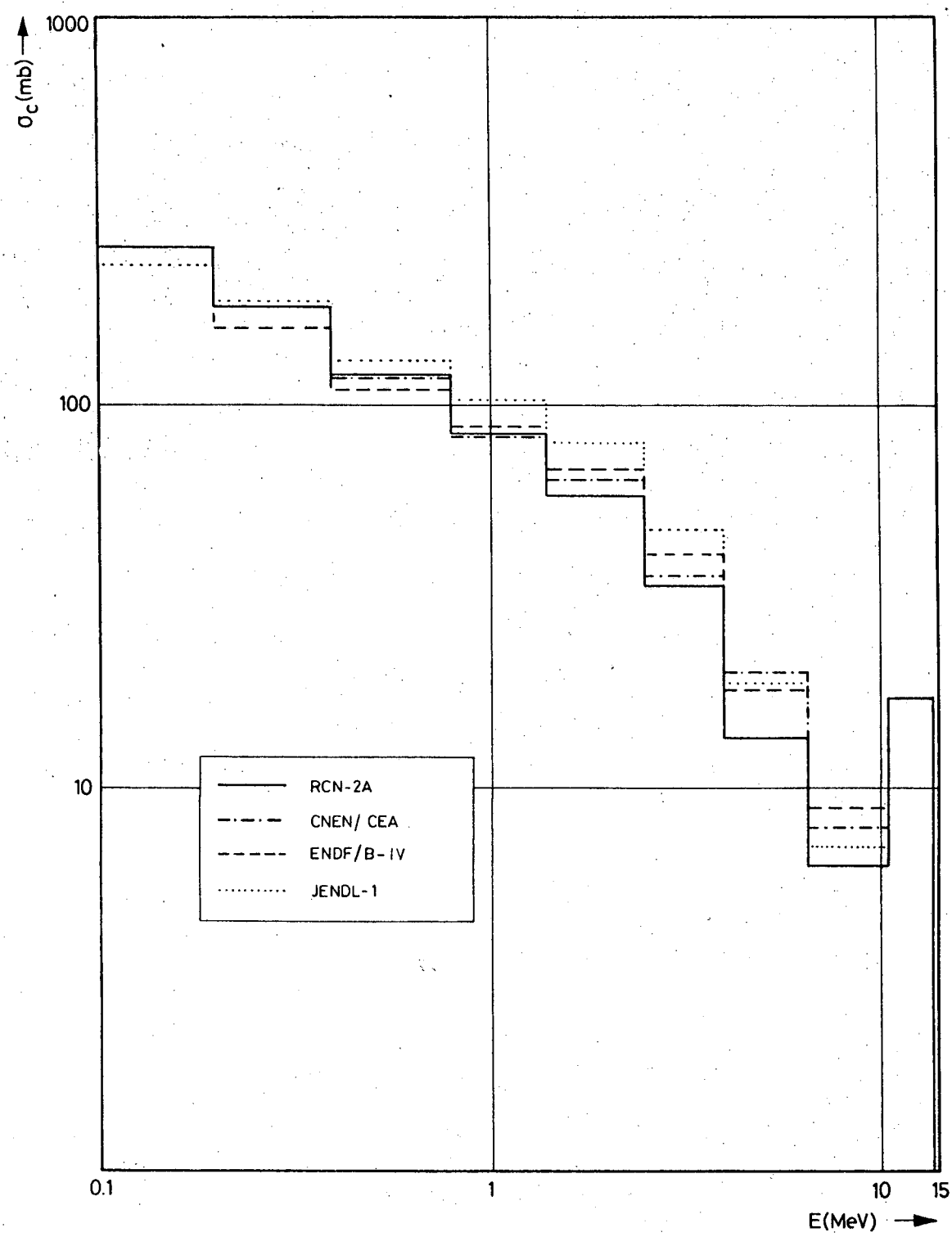


Fig. 4. Absorption group cross sections for a pseudo fission product, calculated from various data libraries; see also table IV.

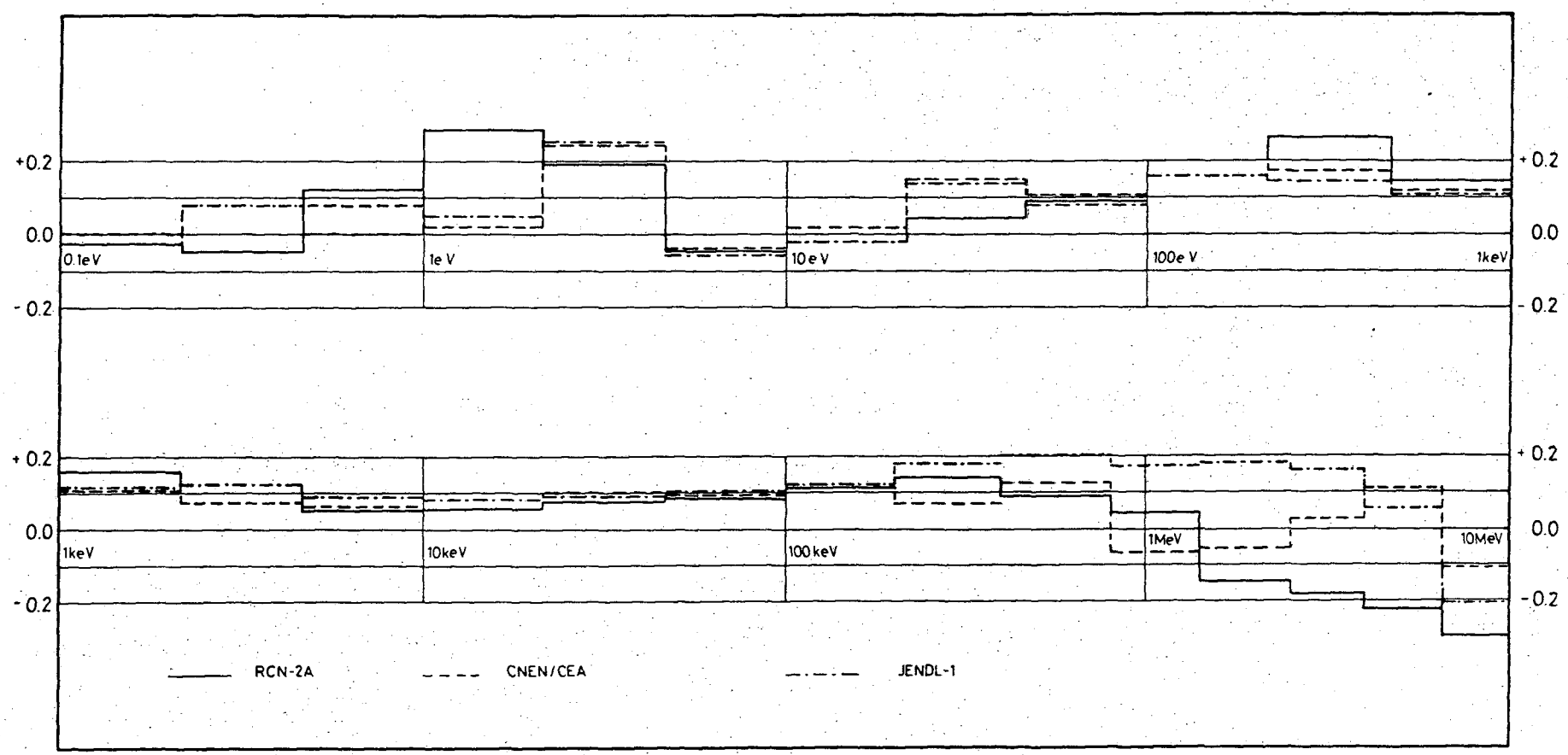


Fig. 5. Relative differences of pseudo fission-product absorption cross sections calculated from RCN-2A, CNEN/CEA and JENDL-1 with respect to ENDF/B-IV, see also table IV.

# INTERCOMPARISON OF ADJUSTED DATA SETS FOR CAPTURE CROSS SECTIONS OF FISSION PRODUCTS

H. Gruppelaar
Netherlands Energy Research Foundation (ECN),
P.O. Box 1, 1755 ZG Petten, The Netherlands,
P. Hammer† and L. Martin-Deidier*
Centre d'Etudes Nucléaires de Cadarache,
B.P. No.1, 13115 Saint Paul lez Durance, France.

Abstract

Integral measurements of capture cross-sections of fission products in fast reactor assemblies have been performed at various laboratories in France, The Netherlands, Sweden and the U.S.A. These measurements have been analysed extensively both at CEA and ECN during the last decade, in order to obtain adjusted group cross-sections for a large number of fission-product nuclides playing a major part in the reactivity loss per cycle of fast breeders.
In this paper, the adopted methods to derive these adjusted data are shortly discussed. The adjusted group constant sets, CARNAVAL-IV and RCN-2A have recently been intercompared by means of the calculation of average (one-group) capture cross-sections in a representative fast spectrum. The results of this intercomparison are given in this paper, together with a discussion of the major discrepancies between the two sets. An encouraging result is that the one-group capture cross-sections for the lumped fission products in a fast reactor spectrum, calculated with the two data sets, differ not more than by 5%.

## 1. INTRODUCTION

Integral measurements of capture cross sections of fission products (f.p.) in fast-reactor assemblies have been performed at various laboratories in France (ERMINE, PHENIX /1/), The Netherlands (STEK /2/), Sweden (FRO /3/) and the USA (CFRMF /4/, EBR-2 /5/). Part of these measurements has been reviewed at the second IAEA advisory meeting on fission-product nuclear data in 1977 /6,7/. There are three types of integral measurements: central reactivity measurements (ERMINE,MASURCA, STEK, FRO), activation measurements (ERMINE, CFRMF) and irradiation (or transmutation) measurements (PHENIX, EBR-2). In all these measurements a good knowledge of the neutron flux spectrum is required. Provided that the flux is well-known, the most accurate information comes from the transmutation measurements. Also the activation data may yield

†Département des Réacteurs à Neutrons Rapides (DRNR/SEDC)
*Département des Réacteurs à Eau (DRE/SEN).

quite accurate results. The reactivity worth measurements, however, are much more difficult to interprete /6/. In sect. 2 the characteristics of these experiments are shortly reviewed, with emphasis on the data used in this intercomparison.

A rather important aspect of the analysis of the data is the determination of the neutron flux spectrum at the sample position /1,8/. For reactivity worths also the adjoint neutron flux is important. The neutron spectra were mostly obtained from calculations, eventually with adjustments /8/ based upon integral spectrum information. Other aspects of the data analysis concern various corrections to the data, the choice of a standard and the discussion of errors /1,6/. Some comments with regard to the differences in the applied methods of data analysis are given in sect. 3.

Once the neutron spectra and integral data and their (co-)variances have been analysed, adjustments /9,10/ can be applied to the f.p. capture cross sections. For this purpose evaluated data are first converted into a multi-group scheme, and (co-)variances are estimated. Next, the group constants are adjusted, taking into account the uncertainty margins and correlation, to obtain optimal agreement between calculated and measured integral data. Essentials of the French and Dutch adjustment methods are compared in sect. 4.

In the adjustments performed at CEA, a large number of different experiments were used, including the Dutch STEK data. At ECN, so far only STEK and CFRMF measurements were utilized. The a-priori data files used for adjustments of f.p. nuclides were the CARNAVAL-III system, of which the f.p. data were derived from various evaluations performed at CEA and CNEN /11-13/, and the RCN-2 library /14/. The final adjusted multi-group systems are known as CARNAVAL-IV /15/ and RCN-2A /16,17/. These two data sets have recently been intercompared as part of a cooperation between DeBeNe and CEA/CNEN. Some results of this intercomparison are discussed in sect. 5, where the average cross sections in a fast reactor spectrum, calculated from both sets are given.

In sect. 6 the conclusions from this preliminary intercomparison are summarized. Also some recommendations for future evaluations and measurements are presented.

## 2. SUMMARY OF INTEGRAL DATA

In Table I a survey of some characteristics of the adopted integral data is given. Table II gives a listing of all integral data used for adjustments discussed in this paper. All uncertainties mentioned in this paper refer to standard deviations ($1\sigma$).

### 2.1. Data used at CEA

The experimental results on individual or global f.p. capture have been obtained at CEA through three complementary kinds of measurements /1,7/:

#### a. Reactivity worths by the oscillation technique

These measurements were performed in the fast-thermal coupled reactor ERMINE and in the fast critical experiment MASURCA. The correponding spectra are close to the SUPER-PHENIX core-zone spectra. The experiments concern isotopes for which a sufficient amount of sample material was available (some grams) : $^{99}$Tc, $^{102}$Ru, $^{103}$Rh, $^{105}$Pd, $^{109}$Ag, $^{133}$Cs, $^{141}$Pr, $^{147}$Pm and $^{147}$Sm. The results were in every case normalized to the $^{235}$U reactivity effect. Due to important correction factors (selfhielding, scattering), the global accuracy remains around about 5% to 15%.

#### b. Activation technique

This method, used also in ERMINE, provides directly the effective capture cross section, but has only been applied to some isotopes for which

the capture products can be measured by γ-ray spectrometry: $^{98}Mo$, $^{100}Mo$, $^{102}Ru$, $^{104}Ru$, $^{108}Pd$ and $^{141}Pr$. The capture rates are normalized to the $^{238}U$ capture rate and the accuracies are between ± 3% and ± 4%.

c. Irradiation technique

This technique has been applied to samples irradiated in a special pin located at the PHENIX core-center during three cycles /18/ with the $^{238}U$ capture rate used as a standard. The mass-spectrometry measurements which were performed on the irradiated samples provide a quite good accuracy: ≈ 2%. Moreover, information could be deduced for some isotopes from the original ones (e.g. $^{150}Sm$, $^{151}Sm$ from $^{149}Sm$). These results have a higher uncertainty (≈ 5%). With this technique capture cross sections were measured for: $^{95}Mo$, $^{96}Mo$, $^{97}Mo$, $^{101}Ru$, $^{105}Pd$, $^{106}Pd$, $^{133}Cs$, $^{134}Cs$, $^{145}Nd$, $^{149}Sm$, $^{150}Sm$ and $^{151}Sm$.

d. Global measurements

The reactivity effect of the bulk fission products has been measured in ERMINE for irradiated fuel pins coming from RAPSODIE or PHENIX: such measurements have been used to adjust the global f.p. effect of the CARNAVAL-IV system with an accuracy close to ± 5% /19/.

In addition to the French data the results of STEK, CFRMF and FRO were reanalysed at CEA to obtain adjusted group constants.

## 2.2. Data used at ECN

At ECN so far only STEK reactivity worths /2/ and CFRMF activation /4/ measurements were used. The STEK data set forms the largest source of integral data for f.p., see Table I. For all nuclides discussed in this paper these measurements were used (Table II). All worths were normalized to a quantity $\rho_0$ /2/, defined in a footnote to Table I. The smallest statistical uncertainty in $\rho/\rho_0$ was about 2% for samples which gave large signals. In worse cases the accuracy could be 10% or more. By using samples with various thicknesses an impression of the amount of self-shielding was obtained. This self-shielding can be important for worths measured in these STEK-cores with relatively soft neutron spectra; in the harder STEK-spectra the inelastic scattering may give significant contributions.

Some reactivity measurements with irradiated (thermal) fuel samples have also been performed at ECN. The results have been discussed in ref. /21/. They show consistency with calculated RCN-2A data within the experimental uncertainty (≈ 3-8%).

The CFRMF activation data were also obtained for a large class of nuclides (see Table II). Initially these data were normalized to a gold standard; in ref. /4/ all values were renormalized to the measured fission rate of $^{235}U$. Typical uncertainties in the activation ratios are about 10%; the major contribution to these uncertainties comes from uncertainties in the decay data. In most cases a small self-shielding correction was needed.

## 3. ANALYSIS OF INTEGRAL DATA AND FLUX SPECTRA

A summary of important corrections applied to the experimental integral data is given in Table III. The most important sources of uncertainties which have to be accounted for in the comparison of experimental and a-priori integral capture data are listed in Table IV.

At CEA the following procedure was adopted. In order to adjust the f.p. cross-sections calculated corrections have been applied to the measurements to get the fundamental-mode values corresponding to the fuel zone of a two-zones cell as it is described by the cell code HETAIRE /9/.

The main corrections /1/ concern:

a. Spatial effects, which induce a spectrum variation in the sample with res-

pect to the fundamental-mode spectrum. The corresponding corrections, taken into account by 1D-transport calculations, generally remain small (1 to 5%).

b. Local perturbations of spectrum and flux-level, which are associated to the measurement devices, were calculated with specific options of the cell code HETAIRE; the correction amount about 1 to 3%.

c. Self-shielding effects are important for the oscillated samples: up to now these effects (10% to 40%) were deduced from the STEK measurements by extrapolating the data obtained at various sample sizes to infinite dilution. This leads to supplementary uncertainties in the corrected results.

d. Inelastic (and elastic) scattering: the associated reactivity effects may reach 40% of the measured total reactivity, and the corresponding calculated corrections induce important uncertainties in the final results (≈ 5%).

Finally, the supplementary uncertainty due to all the calculated corrections amounts about 1% for the irradiation measurements, about 2% for the activation measurements and about ≈3 to 15% for the oscillation measurements.

In the CEA-procedure it is supposed that no uncertainties result from the calculation method of the fundamental-mode spectra in the adopted 25-group structure. It was also assumed that spectrum uncertainties due to nuclear-data uncertainties of the fissile nuclides can be neglected in the calculation of integral quantities. This assumption is based upon the fact that for the fissile nuclides group cross sections were used which had been adjusted to a large series of integral data in various fast reactor cores, using the CARNAVAL-III system of nuclear data and cell codes /9/.

At ECN the STEK integral data were not reduced to a fundamental mode "reference spectrum", but the actual flux and adjoint spectra for the five STEK-cores were calculated at the sample position. For these spectra the covariance matrices based upon uncertainties in the nuclear data used were evaluated as well /8/. The finally adopted spectra were slightly adjusted to fit a selected set of reaction rate and reactivity measurements /8/.

Another difference between the ECN- and CEA-approaches was that at ECN no corrections were applied for self-shielding and for isotopic admixtures in the STEK-samples (Table III). Instead, sets of measured and calculated worths for samples of various sizes and isotopic compositions were directly intercompared, taking into account uncertainties and possible correlations. This procedure /10/ was followed because the above-mentioned effects are functions of the cross sections which are to be adjusted.

For the analysis of the CFRMF activation data the flux spectrum of Millsap et al. /20/ was transformed into 26-groups and supplied with a covariance matrix /17/. Small self-shielding corrections were applied to most of the data, see tables in ref. /17/.

## 4. COMPARISON OF ADJUSTMENT METHODS

Some differences between the CEA and ECN adjustment methods are indicated in Table V.

The f.p. capture cross sections of the CARNAVAL-IV set have been adjusted in most cases according to the BARRACA-method described in /9/. In this method it is assumed that in each energy range the cross sections to be adjusted can take any value with the same probability, within the uncertainty margins deduced from differential measurements or evaluations. This implies that for each f.p. nuclide a number of available integral data is required which is higher than the number of parameters to be adjusted. To perform the adjustment, the a-priori cross sections having the CARNAVAL 25-group structure were first collapsed into 6 groups using the fundamental-mode spectrum associated with each experiment. This 6-group structure is the one used for all CARNAVAL-adjustments /9/; for the f.p. capture cross sections only 4 groups

were adjusted, covering the energy range from 0.5 keV to 1.35 MeV. Strong correlation coefficients (≈ 0.9) between the group constants were taken into account, in order to limit the variation in the shape of the cross sections. After adjustment the data were transformed again into the 25-group structure, using the a-priori 25-group constants to retain the detailed cross section shape within each coarse group.

The adjustment method adopted at ECN has been described in ref. /10/. It may be characterized as a least-squares minimization of the quantity

$$q^2 = \underline{\delta R}^T \, \underline{\underline{C(R)}}^{-1} \, \underline{\delta R} + \underline{\delta \Sigma}^T \underline{\underline{C(\Sigma)}}^{-1} \, \underline{\delta \Sigma}$$

with

$$\underline{\delta R} = \underline{\underline{F}} \, \underline{\delta \Sigma} \, ,$$

where $\underline{\delta \Sigma}$ and $\underline{\delta R}$ are vectors of variations in capture group constants and integral data, respectively and $\underline{\underline{C(R)}}$ and $\underline{\underline{C(\Sigma)}}$ are the covariance matrices of experimental integral data (STEK+CFRMF) and a-priori cross sections (RCN-2 /14/). The sensitivity matrix $\underline{\underline{F}}$ contains the group fluxes and adjoint fluxes. The co-variance matrix of $\underline{\underline{F}}$ is used to increase the uncertainties in the adjusted data vectors $\underline{\Sigma}$ and $\underline{\overline{R}}$. These vectors usually contain data for composite samples in various dilutions, including that for a (hypothetical) sample of a pure isotopic composition in infinite dilution /10/.

From this survey it follows that the a-priori group cross sections and their covariances play a much more important role at ECN than at CEA. Roughly speaking, the ECN-procedure leads to a kind of "weighted average" between a-priori and experimental integral data, whereas the CEA-adjusted values are generally much closer to the "weighted average" of the experimental integral data. For this reason a large effort was devoted at ECN to determine co-variance matrices of integral data, flux and adjoint flux spectra and capture cross sections /10,22/. Another important difference is the treatment of self-shielding and mixtures of isotopes, see previous section.

## 5. COMPARISON OF ADJUSTED GROUP CROSS SECTIONS

### 5.1. Group constant scheme

The adjusted group cross sections are given in the CARNAVAL-IV system and the RCN-2A /16,17/ library. The group structures of these libraries are not the same, which complicates the intercomparison of the data. A possible way of comparing the data is to calculate average (one-group) cross sections of both sets in a representative fast reactor spectrum. For this purpose a 25-group flux spectrum was adopted, which was also transformed into 26 groups. This transformation was checked by calculating average capture cross sections from the (unadjusted) CNEN/CEA evaluation /12,13/ in the two group-constant schemes. The observed differences were always less than 1.5%.

### 5.2. Over-all comparison

In Table VI the values of the average (one-group) cross sections are given for all 38 nuclides of which at present adjusted data are available both in RCN-2A and CARNAVAL-IV. For comparison the results of the unadjusted RCN-2 and CNEN CEA data files are shown as well. The uncertainties in the data refer to standard deviations, which were calculated previously for average cross sections in slightly different flux spectra (i.e. SNR-300 for RCN-2, RCN-2A /16,17/ and PHENIX for CARNAVAL-IV /7/). In the last column the relative differences between the averages calculated from the two adjusted sets are given. When this difference is larger than its standard deviation one or two asterisks were printed (18 nuclides); two asterisks mean that the difference exceeds twice its standard deviation (10 nuclides). Assuming a normal distribution for these differences, the number of times an excess of one or two standard deviations is obtained should be 12 and 2, respectively. Thus,

there are serious discrepancies which have to be investigated.

Of the twenty most important f.p. nuclides there are discrepancies for $^{105}Pd$, $^{151}Sm$, $^{147}Pm$, $^{109}Ag$, $^{104}Ru$, $^{143}Nd$, $^{95}Mo$ and $^{100}Mo$, which are discussed in sect. 5.4.

## 5.3. Pseudo fission products

Another over-all comparison follows from the calculation of pseudo f.p. cross sections for $^{239}Pu$ in a fast reactor. For such a calculation we have used the isotopic concentrations of 162 nuclides which correspond to a burn-up of 41 MWd/kg /21/. The full libraries of CARNAVAL-IV, CNEN/CEA, RCN-2 and RCN-2A were used. The last three libraries were supplemented with cross sections from other sources, mainly ENDF/B-IV. In all calculations the major contribution to the average capture cross section of the pseudo f.p. came from the above-mentioned data libraries. For instance, 82% of the average pseudo f.p. capture cross section is calculated from the adjusted RCN-2A data set. The results, given on the last line of Table VI indicate a difference between RCN-2A and CARNAVAL-IV of only 5%, which is in agreement with the estimated standard deviations. This small difference must be due to partial compensation of the deviations between the two sets. The unadjusted data files lead to about the same average capture cross sections /21/, however, with higher uncertainties, estimated to be of the order of ± 15% (CARNAVAL-III /23/).

## 5.4. Discrepancies for the 20 most important f.p.

### $^{105}Pd$

The adopted integral values for $^{105}Pd$ are reactivity and irradiation data, with uncertainties of about 3 to 7% and 2%, respectively. The unadjusted RCN-2 and CNEN/CEA average cross sections given in Table VI are appreciably lower than the adjusted CARNAVAL-IV value. The RCN-2 and CNEN/CEA evaluations are in agreement with recent differential capture cross sections in the unresolved resonance range /24-26/ and with model calculations based upon recent average resonance parameters /27-28/. The adjusted RCN-2A data are still within the range of uncertainty of the differential measurements. However, the CARNAVAL-IV data are too high compared with these measurements. This discrepancy is under investigation at CEA and ECN in order to identify possible systematic errors in the integral data.

### $^{151}Sm$ (93 a)

The STEK-measurements for this nuclide were performed with a Sm f.p. sample containing only 6.13% $^{151}Sm$, so that no accurate results could be expected. Therefore, the adjusted RCN-2A value heavily depends on the a-priori evaluation (RCN-2), which was based upon model calculations using average resonance parameters of Kirouac et al. /29/. Meanwhile, it was found /30,31/ that the value of $D_{obs}$ determined by Kirouac et al. was estimated a factor of 1.4 to 1.7 too high.Correcting for this leads to an average capture cross section which is much closer to the CARNAVAL-IV value.

The CARNAVAL-IV value is based upon an irradiation measurement with a sample of $^{149}Sm$ containing minor quantities of other stable Sm-isotopes. The measured quantity of $^{152}Sm$ was formed via multiple capture. Therefore, the analysis of these data was rather involved, leading to a relatively large uncertainty in the capture cross section of $^{151}Sm$. More integral and differential measurements, with enriched $^{151}Sm$ samples are recommended. At present a highly enriched $^{151}Sm$ sample is being irradiated in PROFIL-2 of PHENIX.

### $^{147}Pm$ (2.62 a)

For this nuclide there are several reactivity measurements performed at FRO, STEK, ERMINE and a CFRMF activation measurement. The STEK worths have good

accuracies (3 to 5%), but the other reactivity worths are less certain; the CFRMF-value has an uncertainty of ±12%. Though the STEK reactivity measurements have small uncertainties, they were difficult to interprete because there were large fractions of the decay product $^{147}$Sm in the samples. In the data analysis performed at ECN the worths of $^{147}$Pm (with 30% to 40% $^{147}$Sm) and highly enriched $^{147}$Sm (98%) were used in one adjustment calculation. Moreover, the CFRMF-result was added to this adjustment run. It was shown that the CFRMF-value (of which the uncertainty is quite high) is consistent with the STEK-data /17/.

The adjusted RCN-2A and CARNAVAL-IV data do not agree. This may be partly due to the fact that also other integral data (ERMINE, FRO) with larger uncertainties were used. The discrepancy could also be ascribed to differences in the adopted methods of analysis as discussed before. More integral (e.g. activation) and differential measurements are recommended. At present there are only resolved resonances known up to 316.5 eV /32/.

$^{109}$Ag

The available reactivity worths and CFRMF activation data have uncertainties of 3 to 16% and 11%, respectively. The STEK-data for the cores with the hardest spectra are quite uncertain (9 to 16%). Moreover, these results are about 13% lower than the CFRMF data. The RCN-2A data are mainly based upon STEK. In the French analysis the same data were used with some additional reactivity worths. The discrepancy between RCN-2A and CARNAVAL-IV cannot be resolved by means of existing differential data, because there are two quite discrepant series of rather old data /33,34/. The CARNAVAL-IV value is close to the data of Weston et al. /33/. We conclude that high-accuracy integral and differential measurements have to be recommended. At present oscillation measurements with a natural silver sample are being performed at ERMINE, but integral data for $^{109}$Ag are not foreseen.

$^{104}$Ru

For $^{104}$Ru there are reactivity worths (STEK, FRO) and activation data (CFRMF, ERMINE). The STEK reactivity worths in the hardest spectra are quite uncertain due to high scattering corrections. There is no consistency between the adjusted data. There are also large differences between various evaluations. The recent differential measurements of Hockenbury /35/ at 15 to 70 keV show large fluctuations and have large uncertainties. Therefore, the shape of the cross section curve is rather uncertain. This may be a reason for the large discrepancies in the adjusted data. More differential measurements both in the resolved and unresolved resonance regions for $^{104}$Ru are recommended. Similar remarks apply to $^{102}$Ru, although there are no discrepancies between RCN-2A and CARNAVAL-IV for this nuclide (Table VI).

$^{143}$Nd

The integral data used in the adjustment calculations were the STEK reactivity worths, which, however, show rather large uncertainties (4 to 26%), particularly in the hard cores /36/. This may be the reason for the discrepancy between the adjusted RCN-2A and CARNAVAL-IV data in Table VI. The adjusted RCN-2A curve is in good agreement /14/ with recent differential measurements upto about 100 keV /37,26,38/. It seems that there is also reasonably good agreement between RCN-2A results and EBR-2 transmutation data /5/. Therefore the CARNAVAL-IV value will be corrected. In the near future the results of an ongoing irradiation measurement in PROFIL-2 of PHENIX will be used for further improvements.

Mo-isotopes

In recent evaluations of the capture cross sections for the Mo-isotopes there

are large differences in the high-energy range, above about 50 keV. Differential measurements exist upto about 200 keV for most stable Mo-isotopes /39, 40/. Above that energy there are a few (discrepant) series of data only for $^{98}$Mo and $^{100}$Mo /41/. Differential measurements are very important for the Mo-isotopes, because model calculations seem to be not very reliable, possibly as a result of non-statistical effects /42/. Since the adopted a-priori cross sections are heavily based on statistical-model calculations, the failure of these predictions is probably the main reason for the discrepancies in the Mo-results, observed from Table VI.

Another point is that the reactivity measurements for the even-mass nuclides in the fast-spectrum cores are rather uncertain, due to large inelastic scattering corrections. In this respect the irradiation measurements (for $^{95}$Mo and $^{97}$Mo) and activation measurements (for $^{98}$Mo and $^{100}$Mo) are much easier to interprete. The CFRMF activation data for $^{98}$Mo and $^{100}$Mo have somewhat larger uncertainties. Since the RCN-2A set is only based upon STEK and CFRMF data, it is expected that the average cross sections given in Table VI calculated from CARNAVAL-IV are better than the RCN-2A values. However, the shape of the capture cross section is still not known well enough. For this reason high-quality differential measurements of the capture cross sections still have to be requested for $^{95}$Mo and $^{97}$Mo at energies upto about 500 keV.

## 6. CONCLUSIONS

Both at ECN and at CEA f.p. capture cross sections were adjusted to fit integral data, in order to meet the ±5% design target accuracy /23/ in the global capture effect of f.p. in a fast reactor. Such an accuracy cannot be achieved by using evaluated data only (this uncertainty was estimated to be ± 15% for the unadjusted CEA data). It was shown in this paper that the adjusted sets RCN-2A and CARNAVAL-IV are consistent with regard to the lumped f.p. within ± 5%. This is in agreement with the estimated accuracy of ± 8%. Nevertheless, significant differences were observed for some individual f.p. isotopes, which need further consideration.

In the two institutes the available STEK and CFRMF integral data have been used. Additional French data were used at CEA only. In particular the French irradiation data lead to smaller uncertainties in adjusted capture cross sections than the reactivity worths, which were affected by self-shielding and scattering contributions. So far, the recent EBR-2 irradiation data have not been used.

Some differences in the data analyses applied at CEA and ECN concern the calculation of flux and adjoint flux spectra and the treatment of corrections to the data, e.g. for self-shielding. The adopted multi-group cross-section adjustment procedures are also quite different, in particular with regard to the role of the a-priori capture cross sections and their (co)-variances, which are given much less weight at CEA than at ECN. For this reason it is expected that the adjusted French CARNAVAL-IV data are much closer to the integral data than the adjusted Dutch RCN-2A data. Another important difference is that at ECN self-shielded data in various dilutions and isotopic concentrations were introduced in the adjustment calculations. In summary: deviations between the two adjusted data sets could be ascribed to various origins, such as differences in: the adopted integral data, methods of analyses, a-priori cross sections, estimation of (co-)variances of the data and adjustment techniques.

A complicating factor in the intercomparison of the CARNAVAL-IV and RCN-2A data sets is that different group structures were used. For this reason a first comparison was made by calculating average (one-group) capture cross sections in a representative fast reactor spectrum. The preliminary results of this intercomparison were discussed in the previous section (Table VI). For 18 out of 38 nuclides the differences between the one-group cross

sections of the two adjusted sets exceed one standard deviation; for 10 of these nuclides the differences are even more than two standard deviations.

From the ten most important f.p. listed in Table VI there are discrepancies for $^{105}$Pd, $^{151}$Sm and $^{147}$Pm. For the last two mentioned nuclides more, new high-quality integral data are required, with improved sample material. Differential measurements would also be very useful for these nuclides. The discrepancies for $^{105}$Pd are still under investigation at CEA and ECN.

Of the next ten important f.p. in the intercompared data sets there are discrepancies for $^{109}$Ag, $^{104}$Ru, $^{143}$Nd, $^{95}$Mo and $^{100}$Mo. For three of these nuclides (i.e. $^{104}$Ru, $^{143}$Nd and $^{100}$Mo) the reactivity worths in the hardest spectrum cores are quite uncertain due to large scattering corrections, which could explain part of the differences. For most of these nuclides (except for $^{143}$Nd) the shape of the a-priori cross sections is not well-established. For this reason more high-quality differential data are needed for these nuclides in the unresolved resonance range. New integral activation or irradiation measurements would be useful for $^{109}$Ag and $^{143}$Nd.

More detailed intercomparisons will be made in the near future, in order to remove most discrepancies. At CEA the main effort will be to improve the adjustments, where necessary, through a more refined analysis of the available experimental data and the use of recent differential data. These results will be included in the CARNAVAL-V system. At ECN more integral data (PHENIX, ERMINE, EBR-2) will be used in the adjustment process and the number of nuclides in the RCN-2A library will be increased. In addition the differential data reviewed at this meeting will be utilized. Furthermore, the results will be presented in a more general form, by including adjustments in a point cross section file. So far, this has been achieved for 20 nuclides (RCN-3 file). The new ENDF/B-V f.p. data file will also be partially based upon integral data /43/.

## 7. REFERENCES


/1/ L. Martin-Deidier, Mesure intégrale de la capture des produits de fission dans les réacteurs à neutrons rapides, Rapport CEA-R-5023 (1979).

/2/ J.J. Veenema and A.J. Janssen, Small-sample reactivity worths of fission product isotopes and some other materials measured in STEK, ECN-10 (1976).

/3/ T.L. Anderson, Integral measurements of fission product reactivity worths in some fast reactor spectra, AE-428 (1971).

/4/ Y.D. Harker, J.W. Rogers and D.A. Millsap, Fission product and reactor dosimetry studies at coupled fast reactivity measurements facility, TREE-1259 (1978).
See also contr. of Y.D. Harker and F. Schmittroth to this meeting.

/5/ R.A. Anderl, Y.D. Harker, R.L. Tromp and J.E. Delmore, EBR-II irradiation of enriched isotopes of Neodymium, Samarium and Europium. Trans. Am. Nucl. Soc. 28 (1978) 745. See also contr. of R.A. Anderl, Y.D. Harker and F. Schmittroth to Knoxville Conf. 1979 and contr. of Y.D. Harker and R.A. Anderl to this meeting.

/6/ M. Bustraan, J.W.M. Dekker, R.J. Heijboer and A.J. Janssen, Integral determination of fission product capture cross sections, Proc. Second I.A.E.A. Advisory Group meeting on Fission Product Nuclear Data (FPND)-1977, IAEA-213, vol. 2, p. 627.

/7/ G. Langlet and L. Martin-Deidier, The French programme on the determination of the effect of fission products in fast reactors, Sec. I.A.E.A. Advisory Group Meeting on Fission Product Nuclear Data, Petten 1977, Annexes and selected contributions to the review papers, INDC(NDS)-87/Go+Sp. (1978), p. 293.

/8/ J.W.M. Dekker, J.B. Dragt, A.J. Janssen, R.J. Heijboer and H.Th. Klippel, Adjusted neutron spectra of STEK cores for reactivity calculations, ECN-35 (1978).

/9/ J. Chaudat, J. Barré and A. Khairallah, Proc. Int. Symp. Physics of Fast Reactors (Tokyo, 1973) p. 1207 (IAEA, Vienna).
/10/ J.B. Dragt, J.W.M. Dekker, H. Gruppelaar and A.J. Janssen, Nucl. Sci. Eng. 62 (1977) 117.
/11/ P. Ribon, E. Fort, J. Krebs, Tran Quoc Thuong, Evaluation des sections efficaces de capture et de diffusion inélastique de 26 produits de fission, CEA-N-1832, NEANDC(E)-167L.
/12/ E. Fort, J. Krebs, P. Ribon, Tran Quoc Thuong, E. Menapace, M. Motta and G. Reffo, Neutron cross sections for 22 most important fission products, Proc. Nat. Sov. Conf. on Neutron Physics (Kiev) vol. 4 (1977) 3.
/13/ M. Darrouzet et al., An evaluated fission product data library for Super Phenix project, Proc. Int. Conf. on Neutron Physics and Nuclear Data, Harwell, 1978, p. 1146, OECD (1978).
/14/ H. Gruppelaar, Tables of RCN-2 fission-product cross section evaluation, vol. 1, ECN-13 (1977), vol. 2, ECN-33 (1977) and vol. 3, ECN-65 (1979).
/15/ J.P. Chaudat et al., Data adjustments for fast reactor design, Trans. Am. Nucl. Soc. 27 (1977) 877.
/16/ J.W.M. Dekker, Tables and figures of adjusted and unadjusted capture group cross sections based on the RCN-2 evaluation and integral measurements in STEK, vol. 1, ECN-14 (1977), vol. 2, ECN-30 (1977), and vol. 3, ECN-54 (1979).
/17/ J.W.M. Dekker and H.Ch. Rieffe, Adjusted cross sections of fission product nuclides from STEK reactivity worths and CFRMF activation data, vol. 1, ECN-28 (1977) and vol. 2, ECN-55 (1979).
/18/ A. Giacometti et al., Mesure de sections intégrales de capture par l'irradiation PROFIL dans PHENIX, Contr. to Int. Symp. on Physics of Fast Reactors (Aix-en-Provence, 1979).
/19/ L. Martin-Deidier et al., Mesures intégrales de la capture des produits de fission dans les spectra de réacteurs à eau et de réacteurs à neutrons rapides, Proc. Int. Conf. on Neutron Physics and Nuclear Data, Harwell, 1978, p. 1016, OECD (1978).
/20/ J.W. Rogers, Y.D. Harker and D.A. Millsap, The Coupled Fast Reactivity Measurements Facility, Proc. IAEA Consultants Meeting on Integral Cross Section Measurements in Standard Neutron Fields for Reactor Dosimetry, Vienna, November 1976.
/21/ R.J. Heijboer, Pseudo fission-product cross sections for a 1300 MWe fast breeder reactor (status July 1978), ECN-52 (1978) and contribution to this meeting.
/22/ H. Gruppelaar, Proc. Symp. on Neutron Capture Gamma-Ray Spectroscopy, Petten 1974, p. 760, Reactor Centrum Nederland (1975) and H. Gruppelaar, Proc. IAEA Consultants meeting on the use of Nuclear Theory in Nuclear Data Evaluation, 1975, Trieste, IAEA-190, vol. 2 (1976) 61.
/23/ P. Hammer, Besoins en données nucleaires des produits de fission et actinides pour les calculs de réacteurs de puissance à neutron rapides. Proc. Int. Conf. on Neutron Physics and Nuclear Data, Harwell, 1978, p. 551, OECD (1978).
/24/ R.W. Hockenbury, H.R. Knox and N.N. Kaushal, Proc. Conf. Nuclear Cross Sections and Technology, Washington, D.C., March 3-7, 1975, CONF-750303, NBS Special Publication 425, vol. 2, p. 905. National Bureau of Standards (1975).
/25/ R.L. Macklin, J. Halperin and R.R. Winters, Nucl. Sc. and Eng. 71 (1979) 182.
/26/ A.R. de L. Musgrove et al., Proc. Conf. on Neutron Physics and Nuclear Data, Harwell, Sept. 1978, p. 449, OECD (1978).
/27/ A.V. Popov, K. Trzeciak and Khvan Cher Gu, Neutron resonances of Pd isotopes, P3-11013, Communication of the Joint Institute for Nuclear Research, Dubna (1977).
/28/ P. Staveloz et al., Proc. Conf. on Neutron Physics and Nuclear Data, Harwell, Sept. 1978, p. 701, OECD (1978).
/29/ G.J. Kirouac and H.M. Eiland, Phys. Rev. C11 (1975) 895.

/30/ E. Menapace, private communication, CNEN, 1979.
/31/ E. Fort, private communication, CEA, 1979.
/32/ G.J. Kirouac et al., Nucl. Sci. Eng. 52 (1973) 310.
/33/ L.W. Weston et al., Annals of Physics 10 (1960) 477.
/34/ V.N. Kononov et al., IAEA Conf. on Nuclear Data for Reactors, Paris, vol. 1 (1966) 469.
/35/ R.W. Hockenbury et al., ERDA/NDC-3/U (1976) 255.
/36/ H. Gruppelaar et al., Proc. Int. Conf. on Neutron Physics and Nuclear Data for Reactors, Harwell, Sept. 1978, p. 1167, OECD (1978).
/37/ A.R. de L. Musgrove et al., Non-statistical effects in the radioactive capture cross sections of the Neodymium isotopes, AAEC/E401 (1977).
/38/ Y. Nakajima et al., Proc. Int. Conf. on Neutron Physics and Nuclear Data for Reactors, Harwell, Sept. 1978, p. 438, OECD (1978).
/39/ S.V. Kapchigashev et al., Sov. J. Atomic Energy 15 (1964) 808.
/40/ A.R. de L. Musgrove et al., Nucl. Phys. A270 (1976) 108, supplemented in Proc. Conf. on Neutron Physics and Nuclear Data, Harwell, Sept. 1978, p. 449, OECD (1978).
/41/ D.I. Garber and R.R. Kinsey, Neutron Cross Sections, vol. 2 (curves), BNL-325, third ed. (1976).
/42/ H. Gruppelaar, Evaluated neutron cross sections of natural molybdenum, ECN-40 (1978).
/43/ R.E. Schenter et al., Evaluations of fission product capture cross sections for ENDF/B-V, Contr. to Int. Conf. on Nuclear Cross Sections and Technology, Knoxville 1979 and contr. to this meeting.

Acknowledgements

This work was performed in the framework of a cooperation between DeBeNe and CEA/CNEN on fission-product nuclear data, in which Dr. E. Fort (CEA), Dr. E. Menapace (CNEN) and the authors were involved. The authors are indebted to Drs. Fort and Menapace for useful discussions with regard to microscopic data evaluations. They also thank Mr. B.P.J. van den Bos and Mr. H.Ch. Rieffe (ECN) for performing the calculations leading to Table VI.

Table I

Some characteristics of integral measurements

| Subject | STEK | CFRMF | ERMINE MASURCA | ERMINE | PHENIX | FRO |
|---|---|---|---|---|---|---|
| Type | reactivity | activation | reactivity | activation | transmutation | reactivity |
| Normalization | $\rho_o$ a) | $^{235}U(n,f)$ b) | $^{235}U$ c) | $^{238}U(n,\gamma)$ d) | $^{238}U(n,\gamma)$ e) | $^{235}U$ c) |
| Self-shielding | yes | small | yes | no | no | yes |
| Scattering effect | yes | no | yes | no | no | yes |
| Typical uncertainty f) | 3-10% | 10% g) | 3-10% | 3-4% | 2% | 10-15% |
| Nr. of core | 5 | 1 | 4 | 2 | 1 | 3 |
| Nr. of isotopes | 57 | 48 | 10 | 6 h) | 12 h) | 10 |

a) Apparent reactivity worth of a calibrated $^{252}Cf$ source, multiplied by the measured fission rate of $^{235}U$ |2|.

b) Absolute NBS fission chamber.

c) Reactivity worth of 1 gram of $^{235}U$.

d) Measured by γ-ray spectroscopy with Ge(Li) detectors.

e) $^{239}Pu$ / $^{238}U$ ratio by isotopic dilution and mass spectrometry.

f) Standard deviation in experimental data (including uncertainty due to normalization) estimated by authors of this paper.

g) Mainly due to decay data.

h) To be extended in near future.

Table II

Number of data in different spectra used for adjustments at CEA and ECN[a)]

| Nuclide [b)] | Reactivity | | | Activation | | Irradiation |
|---|---|---|---|---|---|---|
| | STEK | FRO | ERMINE/ MASURCA | CFRMF | ERMINE | PHENIX |
| $^{95}$Mo | 5 | 3 | - | - | - | 1 |
| $^{96}$Mo | 5 | - | - | - | - | 1 |
| $^{97}$Mo | 5 | 3 | - | - | - | 1 |
| $^{98}$Mo | 5 | - | - | 1 | 2 | - |
| $^{100}$Mo | 5 | - | - | 1 | 1 | - |
| $^{99}$Tc | 5 | 3 | 6 | 1 | - | - |
| $^{101}$Ru | 5 | 3 | - | - | - | 1 |
| $^{102}$Ru | 5 | 3 | 3 | 1 | 1 | - |
| $^{104}$Ru | 5 | 3 | - | 1 | 2 | - |
| $^{103}$Rh | 5 | 3 | 6 | 1 | - | - |
| $^{104}$Pd | 5 | - | - | - | - | - |
| $^{105}$Pd | 5 | - | 3 | - | - | 1 |
| $^{106}$Pd | 5 | - | - | - | - | 1 |
| $^{107}$Pd | 5 | - | - | - | - | - |
| $^{108}$Pd | 5 | - | - | 1 | 1 | - |
| $^{110}$Pd | 5 | - | - | 1 | - | - |
| $^{107}$Ag | 5 | - | - | - | - | - |
| $^{109}$Ag | 5 | - | 2 | 1 | - | - |
| $^{127}$I | 5 | - | - | 1 | - | - |
| $^{129}$I | 5 | - | - | 1 | - | - |
| $^{133}$Cs | 5 | - | 5 | 1 | - | 1 |
| $^{139}$La | 5 | - | - | 1 | - | - |
| $^{141}$Pr | 5 | - | 4 | 1 | 1 | - |
| $^{142}$Nd | 5 | - | - | - | - | - |
| $^{143}$Nd | 5 | - | - | - | - | - |
| $^{144}$Nd | 5 | - | - | - | - | - |
| $^{145}$Nd | 5 | - | - | - | - | 1 |
| $^{146}$Nd | 5 | - | - | 1 | - | - |
| $^{148}$Nd | 5 | - | - | 1 | - | - |
| $^{150}$Nd | 5 | - | - | 1 | - | - |
| $^{147}$Pm | 5 | 3 | 2 | 1 | - | - |
| $^{147}$Sm | 5 | - | 4 | - | - | - |
| $^{148}$Sm | 5 | - | - | - | - | - |
| $^{149}$Sm | 5 | 3 | - | - | - | 1 |
| $^{150}$Sm | 5 | - | - | - | - | 1 |
| $^{151}$Sm | 5 | - | - | - | - | 1 |
| $^{152}$Sm | 5 | - | - | 1 | - | - |
| $^{154}$Sm | 5 | - | - | 1 | - | - |

a) Only STEK and CFRMF data were used at ECN.

b) Nuclides for which both at ECN and CEA adjusted data have been obtained.

Table III

Corrections applied to experimental integral data

| Type of correction | CEA | ECN |
|---|---|---|
| Chemical admixtures | reactivity data | reactivity data |
| Isotopic admixtures | reactivity data | - |
| Self-shielding | reactivity data | activation data only |
| Scattering effects | reactivity data | reactivity data |
| Correction to reference spectrum | all data | - |

Table IV

Sources of uncertainties which have to be accounted for in the comparison of experimental and a-priori integral capture data.

| Type of measurement | Nr. | Source of uncertainty |
|---|---|---|
| All | 1 | Measurement of sample worths, activation rates or transmutation rates. |
| All | 2 | Composition of sample (chemical or isotopic). |
| Mainly in reactivity | 3 | Self-shielding in sample. |
| All | 4 | Measurement of standard, including possible self-shielding. |
| All | 5 | Nuclear data of standard (small when adjusted set is used). |
| All | 6 | A-priory nuclear data for measurements. |
| All | 7 | Spectra, or corrections to reference spectrum. |
| Reactivity | 8 | Correction for scattering. |
| Activation | 9 | Decay data. |
| Transmutation | 10 | Corrections for capture in other isotopes in target and multiple capture. |

Table V

Differences between adjustment methods applied at ECN and CEA.

| Item | ECN | CEA |
|---|---|---|
| Group constant scheme | 26 groups (ABBN) | 25 groups |
| Experimental data (see Tables I, II) | STEK, CFRMF | MASURCA, ERMINE, PHENIX, STEK, CFRMF, FRO |
| Self-shielding | STEK uncorrected | corrected |
| Flux+adjoint flux | actual spectra | fundamental mode spectrum |
| A-priory cross sections | RCN-2 \|14\| | CARNAVAL-III + CNEN/CEA \|11-13\| |
| (Coarse) groups in adjustment | 26 groups ($10^{-3}$ eV to 10.5 MeV) | 4 groups (0.5 keV to 1.35 MeV) |
| Covariances in cross sections | 26 x 26 covariance matrices | uncertainty limits + high correlations neighbouring coarse groups |
| Role of a-priori cross sections | data adjustment to both integral data and a-priori cross sections | data adjustment only to integral data; a-priori cross sections used for transformation coarse-groups to 25 groups |
| Adjustment method | Dragt et al. \|10\| (self-shielded data, isotopic admixtures) | Barraca \|9\| (corrected data in infinite dilution) |
| Uncertainties in spectra | a-posteriori added to adjusted data | included only in corrections to integral data |

Table VI

Comparison of average (one-group) cross sections (mb) in a representative fast reactor spectrum.

| Nuclide[a] | RCN-2 [b] (26 groups) | RCN-2A [b] (26 groups) | CARNAVAL-IV[c] (25 groups) | CNEN/CEA (26 groups) | 2A-IV / 2A [d] (%) |
|---|---|---|---|---|---|
| $^{105}$Pd | 653. (16) | 704. (7) | 822. (4.5) | 688. | - 16* |
| $^{101}$Ru | 536. (16) | 527 (8) | 522. (4.4) | 592. | + 1 |
| $^{103}$Rh | 507. (9) | 510. (6) | 525. (4.2) | 504. | - 3 |
| $^{99}$Tc | 425. (16) | 463. (6) | 471 (4.9) | 424. | - 2 |
| $^{107}$Pd | 791. (55) | 761 (10) | 752. (7) | 637. | + 1 |
| $^{151}$Sm | 1526. (9) | 1303. (14) | 2897. (10) | 1491. | -122** |
| $^{149}$Sm | 1662. (15) | 1659. (9) | 1672. (4.5) | 1272. | - 1 |
| $^{147}$Pm | 779. (24) | 964. (7) | 781 (6) | 800. | + 19** |
| $^{97}$Mo | 238. (17) | 238. (9) | 231 (4.5) | 217. | + 3 |
| $^{145}$Nd | 347. (9) | 361. (7) | 344. (5) | 272. | + 5 |
| $^{133}$Cs | 393. (12) | 374. (6) | 404. (5) | 385. | - 8 |
| $^{109}$Ag | 552. (12) | 590. (6) | 693. (7) | 515. | - 17** |
| $^{102}$Ru | 168. (37) | 129. (8) | 132. (6) | 190. | - 2 |
| $^{104}$Ru | 139. (30) | 109. (7) | 128. (6) | 147. | - 17* |
| $^{143}$Nd | 247. (8) | 228. (7) | 175. (6) | 254. | + 23** |
| $^{95}$Mo | 239. (18) | 222. (8) | 194. (5) | 214 | + 13* |
| $^{100}$Mo | 80.2 (27) | 55.2 (8) | 73.6 (6) | 64.2 | - 33** |
| $^{141}$Pr | 90.6 (12) | 87.5 (7) | 89.4 (7) | 91.3 | - 2 |
| $^{98}$Mo | 65.7 (9) | 66.3 (6) | 64.9 (6) | 81.0 | + 2 |
| $^{108}$Pd | 145. (84) | 132. (17) | 127. (5) | 155. | + 4 |
| $^{106}$Pd | 151. (61) | 176. (12) | 223. (9) | 167. | - 26* |
| $^{129}$I | 254. (25) | 251 (8) | 318. - | - | - 37** |
| $^{152}$Sm | 322. (12) | 341 (5) | 260. (9) | 312. | + 23** |
| $^{146}$Nd | 80.6 (15) | 78.2 (9) | 86.2 (8) | 59.8 | - 10 |
| $^{127}$I | 396. (9) | 431 (7) | 458. | - | - 6 |
| $^{139}$La | 24.5 (16) | 23.8 (7) | 28.3 (12) | 21.7 | - 19* |
| $^{148}$Nd | 108. (11) | 107. (8) | 101. (7) | 117. | + 6 |
| $^{147}$Sm | 1003. (19) | 911. (9) | 797 (6) | 743. | + 13* |
| $^{150}$Nd | 140. (10) | 129. (9) | 101 (15) | 169. | + 22* |
| $^{144}$Nd | 60.8 (14) | 59.0 (14) | 65.0 (8) | 73.4 | - 10 |
| $^{150}$Sm | 331 (16) | 413. (9) | 359. (6) | 277. | + 13* |
| $^{154}$Sm | 163. (20) | 142. (6) | 202. (10) | - | - 60** |
| $^{104}$Pd | 146. (61) | 157. (21) | 318. - | 237. | -100** |
| $^{110}$Pd | 138. (88) | 56.8 (44) | 33.5 (11) | 84.3 | + 41 |
| $^{96}$Mo | 66.9 (44) | 45.7 (27) | 62.7 | - | - 37 |
| $^{148}$Sm | 228. (41) | 220. (15) | 177 - | - | + 20 |
| $^{107}$Ag | 505. (14) | 529. (10) | 577. | - | - 5 |
| $^{142}$Nd | 50.5 (17) | 39.0 (20) | 63.2 - | - | - 62** |
| pseudo[e] | 392. | 389. (6-9) | 410. (4-5) | 389. | - 5 |

a) In order of importance with respect to fast reactor reactivity effects.

b) Uncertainties in $\langle\sigma_{n\gamma}\rangle$ have been assumed to be the same as those for SNR-300. They are indicated in parenthesis (standard deviations in %).

c) Uncertainties (1 standard deviation) from Langlet and Martin-Deidier /7/

d) One or two asterisks mean discrepancies of more than one or two standard deviations of the difference respectively. In case the uncertainty for CARNAVAL-IV is not given, the same uncertainty as for RCN-2A was assumed.

e) Pseudo fission product of $^{239}Pu$ at a burn-up of 41 MWd/kg, as defined in /21/; cross sections in mb/fission.

# FISSION PRODUCT NEUTRON CROSS SECTION EVALUATIONS FOR JENDL AND THE INTEGRAL TESTS

S. Iijima*, T. Watanabe**, T. Yoshida*, Y. Kikuchi*** and H. Nishimura***

* NAIG Nuclear Research Laboratory, Nippon Atomic Industry Group Co., Ltd.
4-1 Ukishima-cho, Kawasaki, Japan

** Nuclear System Division, Kawasaki Heavy Industries, Ltd.
2-4-25 Minami-suna-cho, Koto-ku, Tokyo, Japan

*** Japan Atomic Energy Research Institute
Tokai-mura, Naka-gun, Ibaraki-ken, Japan

Results of integral tests of JENDL-1 fission products neutron cross sections with STEK reactivity and CFRMF activation data are presented for selected nuclides. Discrepancies between integral and differential capture data are extracted through this comparion. New evaluations of neodymium and samarium isotopes cross sections in keV - MeV region are presented which are based on the recent capture measurements at ORNL, FEI and JAERI and the re-investigation of theoretical model parameters. The effects of determination of these parameters on the capture cross section calculation are demonstrated and discussed.

## 1. Introduction

JENDL-1 FP data file contains the neutron cross sections of 67 nuclides in fission products mass region [1] Of these, cross sections of 28 nuclides [2,3] were evaluated in 1975, and those of other 34 nuclides (except Mo isotopes) in 1977. Files are available from NEA Data Bank. Since that time, there have been considerable progress in this field, both experimental work and evaluation methodology [4,5]. In view of these progress, a thorough examination and revision of JENDL-1 FP file toward JENDL-2 are planned and going on in FPND working group of Japanese Nuclear Data Committee. Present paper describes the interim results of this activity.

In Sec. 2 the integral tests of JENDL-1 FP cross sections with STEK and CFRMF data are presented for selected nuclides. Discrepancies between integral and differential capture data are pointed out through this comparision. In Sec. 3 is described the re-evaluation of cross sections for Nd and Sm isotopes in keV-MeV region. The determination of theoretical model parameters and cross section calculation are given and discussed in comparison with RCN-2 evaluation. The effects of model parameters on cross section calculation is demonstrated.

## 2. Integral tests of JENDL-1 FP cross sections

Integral tests of JENDL-1 FP cross sections were performed with small sample reactivity data in STEK [Ve76] and activation data in CFRMF [Ha78].

### 2.1 Method of analysis [8]

JAERI-FAST set type 70-group cross sections were prepared with resonance self-shielding tables at 300 K using ETOA-1 code [9] (a version based on ETOE code [10]), which calculates the self-shielding factor in narrow resonance approximation in the scheme of Bondarenko et al. [11]. The neutron flux and adjoint flux spectra were taken from [De78] and [Ha78]. These flux spectra were interpolated and converted into the present 70-group structure spectra. The self-shielding factors for experimental samples were calculated by using the escape cross sections based on the equivalence theorem.

By the analyses of STEK data, U-235 fission cross section and californium fission spectrum were taken from [De78] to calculate the normalizing reactivity $\rho_0$. For the normalizing reaction rate of CFRMF activation, the ENDF/B-4 U-235 fission cross section was adopted.

As to the fission product cross sections, those for the following nuclides were taken from ENDF/B-4*:

Ru-99,100, Pd-106,108, Xe-132,134,136, Nd-142,145,
Eu-153, Gd-154,158,160.

Cross sections for C, N, Al, O, Cl and Pb, which form the chemical compounds with fission product isotopes, were also taken from ENDF/B-4.

### 2.2 Results

Results of calculation of activation rate ratios in CFRMF are shown in Table 1, in comparison with experimental data and the calculation by ENDF/B-4 [Ha78]. Both self-shielded and infinite dilution calculations are listed in the table.

Fig. 1 shows the results of analyses of STEK data for relatively strong absorbing materials. Calculation is compared with measured data as a function of the "effective average energy" of the neutron spectrum of STEK cores with sample size (ld value) fixed, where l is the mean chord length and d the density of sample. The effective average energy is defined here as follows.

$$1/\sqrt{E_{av}} = \int (1/\sqrt{E})\, F\, dE \Big/ \int F\, dE ,$$

| | STEK-4000 | STEK-3000 | STEK-2000 | STEK-1000 | STEK-500 |
|---|---|---|---|---|---|
| $E_{av}$: with $F = \phi^*\phi$ | 3.0keV | 9.0keV | 15.5keV | 29keV | 70keV |
| $E_{av}$: with $F = \phi$ | 3.2 | 9.2 | 16 | 33 | 80 |

We have assumed $\phi^*\phi$ weighted $E_{av}$ in the plot of Fig. 1. The CFRMF neutron spectrum gives $E_{av}$=110 keV with $\phi$ weight, indicating a little bit harder neutron spectrum than STEK-500 with regard to neutron capture.

In Fig. 1 only the results for samples of relatively large ld values or large weights are shown.

---

*) JENDL-1 contains cross sections for Pd-108, Nd-145 and Eu-153, but we encountered with trouble by processing the file, the occurrence of negative self-shielding factor for elastic scattering in unresolved resonance region.

---

Discrepancies between integral and differential capture data

From intercomparison of integral data and differential data using the calculated values as media and with allowance of experimental uncertainties, the following discrepancies may be noted.

Tc-99 : STEK results (C/E = 0.85 -0.9) and CFRMF result (C/E = 1.21 ± 15%) are not mutually consistent. RPI capture data seem to support STEK data.

Pd-108: STEK data indicate smaller cross section than ENDF/B-4 (C/E = 1.2 -1.3). CFRMF data indicate slightly opposite direction (C/E = 0.82 ± 6.7%). Substantially high capture cross section at ORELA are probably not in agreement with either of integral data.

I-127: STEK results (C/E = 0.85 -1.0) and CFRMF result (C/E = 1.23 ± 10%) are not consistent.

Sm-149: Recent capture data at FEI and JAERI are significantly higher than that expected from STEK measurements.

For other important, strongly absorbing nuclides, the integral data studied here are not inconsistent with each other, nor with recent differential capture data.

Comments

The case of Rh reactivities (and probably of Ag-109 and Sm-149) in STEK needs some comments. Fig. 2 shows the comparison of calculation and experiment of Rh sample reactivity as a function of ld values. The calculation is in significant overprediction for STEK-4000 and -3000, while RCN-2 calculation is in good agreement with experiment. In STEK-4000, about 60% of calculated reactivity of Rh sample comes from the absorption by a strong resonance at 1.26 eV. The resonance self-shielding for this resonance was re-calculated by using sophisticated methods. Firstly, pointwise cross sections were generated in eV region and self-shielding factor was calculated numerically without rendering the semi-analytical method used in ETOA-1 code. In the second method, the space energy neutron slowing down spectrum was solved by TIMS-2 code [13] for simulated geometrical arrangement of Rh pin in carbon or hydrogen medium to obtain a precise effective absorption rate. Both trials were not successful to improve the disagreement mentioned above. The same tendency for overprediction of reactivity for soft spectrum core is observed for other materials which possess strong neutron resonance near 1 eV, such as Ag-109 and Sm-149.

## 3. Re-evaluation of cross sections of Nd and Sm isotopes in keV - MeV region

JENDL-1 FP cross section evaluation is based on the experimental data prior to 1975 and on an old systematics of theoretical model parameters, especially of level density parameters. The motivation of re-evaluation is two-fold. One is to up-data and obtain the best-estimates of JENDL cross sections, utilizing the recent capture data at ORELA [Mu78], RPI [Sh75], FEI [Ko77,KO78] and JAERI [Na78,Na79], [Mi79]. Capture data for Nd and Sm isotopes have been quite scarce or absent at all until recently. The other motivation is to establish the method of evaluation and parameter determination. We have adopted closely the methods as discussed and, in a sense, recommended at the FPND meeting, Petten, 1977 [1,5,7]. We compare our results with RCN-2 evaluation, since we have largely followed the RCN-2 method of level density parameter determination, and therefore a detailed comparison may be possible.

### 3.1 Optical model parameters

Spherical optical model was assumed. Optical model parameters (OMP) at zero neutron energy were determined by SPR method as proposed by Lagrange and Delaroche [14]. Tables 2 through 5 show the input SPR data and obtained optical model parameters (derivative Woods-Saxon type surface absorption). The calculated total cross sections of natural Nd and Sm isotopes are shown in Fig. 3 in comparison with experimental values which were read roughly from graphs in BNL-325, 3rd ed., Vol. 2. Disagreement of Nd total cross section in 70 - 400 keV is due to that the assumed scattering radii data of Nd-144, 145 and 146 were too small.

Compound nucleus formation cross sections are shown in Figs. 4 and 5 together with RCN-2 values*. Differences between two evaluations are significant for most nuclides under study. It is also noted that the discrepancy of compound nucleus formation cross section at low energy persists up to MeV region. Comparison of inelastic scattering cross section for Sm-154 as an example shows the disagreement of about a factor of 2 between the present calculation and RCN-2 values up to 1 MeV.

### 3.2 Level density parameters

Composite level density formula of Gilbert and Cameron [17] was used. For the sake of later discussions the precise formulae are given in Appendix.

The a parameter of Fermi-gas level density was obtained from the observed average s-wave resonance level spacing, Dobs. When this is not available, a was determined by interpolation or extrapolation from a values for neighboring nuclides. Figs. 6 and 7 show respectively the plot of a versus neutron number and Cameron's shell correction energy. The latter way of plot was adopted for inter- or extrapolation.

The parameters C and T of constant temperature level density formula were determined from the staircase plot of lowlying levels. Adjustment was made to obtain a smooth continuation with Fermi-gas level density. The dividing energy $E_x$ is determined at the same time. Frequently, we have encountered with difficulty to obtain a smooth continuation without violating too much the trend indicated from the staircase plot of low levels. The case of Sm-151 is shown in Figs. 7 and 8, which was the most difficult case. In some other cases we had to abandon the

---

*) In RCN-2 evaluations, the OMP of Igarasi et al. [15] and Rosen et al. [16] were adopted for Nd and Sm isotopes, respectively. [5]

smooth continuation, thus resulting in an abrupt change of nuclear temperature at dividing energy. These are the cases of Nd-142, 146, 148, Sm-153 and 154. An interesting point to note is that the staircase plot of lowlying levels of odd isotopes of Nd and Sm show almost invariably a sudden level-off at excitation energy somewhere around a few hundred keV to 1 MeV.

Tables 6 and 7 show the present level density parameters together with RCN-2 values. The C and T parameters of RCN-2 are the ones calculated here from a and $E_x$ with smooth continuity condition.

3.3 Other parameters

The adopted a priori values of $D_{obs}$ and $\Gamma_\gamma$ are listed in Tables 9 and 10. The giant dipole resonance parameters were taken from Berman's compilation [18] of photo-reaction cross sections of the form,

$$\sigma_\gamma(\varepsilon_\gamma) = \sum_{i=1,2} \frac{\sigma_i}{1 + (\varepsilon_\gamma^2 - E_i^2)^2/\Gamma_i^2 \varepsilon_\gamma^2} .$$

The parameter values are shown in Table 8. Finally, level schemes were taken from Table of Isotopes, 7-th ed. (1978).

3.4 Calculation of capture cross sections

Cross sections were calculated by the spherical optical model and the statistical theory with neutron width fluctuation correction. The parameter $S_\gamma = \Gamma_\gamma/D_{obs}$ was adjusted to fit the calculation with available capture data at 30 keV. In Tables 9 and 10 are shown the a priori values and adjusted values of $S_\gamma$ together with cross section values assumed for normalization. Calculated capture cross sections are displayed in Figs. 9 through 21, incomparison with experimental data, JENDL-1 and RCN-2 evaluations. Some of old experimental data are plotted after re-normalization of flux and cross section standards [19], with comment "renormalized".

3.5 Effect of model parameters on capture cross section

From Figs. 9 - 21 we see that there exist often considerable disagreement between RCN-2 and present calculation for neutron energies above a few hundred keV. In order to clarify the origin of these disagreements, the effects of model parameters on capture cross sections of Sm-151 and Sm-152 were investigated.

Effect of level density

The lower part of Fig. 22 shows the effect of the target nucleus level density on Sm-151 cross section through the competition due to inelastic scattering. Level density was altered from the present value ($C = 7.46\ MeV^{-1}$, $T = 0.456$ MeV) to RCN-2 value ($C = 37.9\ MeV^{-1}$, $T = 0.519$ MeV). The modified calculation (dot-dash line) has come to agree well with RCN-2 evaluation.

The upper part of Fig. 22 shows the effect of compound nucleus level density on Sm-152 cross section. In this case the target nucleus level densities of both evaluations are very similar. The modified present calculation (dot-dash line) with RCN-2 compound nucleus level density agrees fairly well with RCN-2 curve, the agreement being caused by the change of energy variation of $S_\gamma$. Fine dotted line shows the calculation using the spin-cut-off expression $\sigma^2 = 0.0888\sqrt{aU}\ A^{2/3}$

($\underline{a}$ = 23.74 $MeV^{-1}$ with same Dobs) instead of the present expression, $\sigma^2 = 0.146\sqrt{au}\ A^{2/3}$. It is seen that the cross section shape is again affected substantially by the change of $\underline{a}$ value (with same Dobs) through the change of energy variation of $S_\gamma$.

From these sensitivities of capture cross section shape with target and compound nucleus level densities, we may speculate that a meaningful information concerning level densities may be obtained if the shape of capture cross sections were measured in 100 keV to MeV region, provided that reasonable optical model parameters were used.

Effect of optical model parameter

Fig. 23 shows the effect on capture cross section of Sm-152 when OMP is changed from the present values to the OMP of Igarashi et al, which was adopted in JENDL-1 evaluation. The effect can not be neglected in 0.1 - 1 MeV region. The same calculation was performed for all isotopes of Nd and Sm. Sm-152 was the most remarkable case. For all other nuclides, the effect on the shape of capture cross section (after normalization at 30 keV) was about 10% or less in the energy range of a few keV to 3 MeV, although the inelastic scattering cross sections were affected considerably.

Effect of giant dipole resonance parameters

Giant dipole resonance parameters of Berman for Nd-148, 150, Sm-152 and 154 were replaced by the Brink-Axel estimates. After the same normalization of capture cross section at 30 keV, the effect on the shape of capture cross section was found as within a few percent.

## 4. Conclusions

STEK and CFRMF integral data of relatively strong absorbing materials are generally consistent with each other and with recent differential capture data. Some exceptional discrepant cases were remarked.

As to the evaluation, the choice of optical model parameters does not affect much in general the shape of capture cross section, though there are exceptional cases. The level density parameters, both of target and compound nuclei, affect the shape of capture cross section strongly. There is sometimes considerable difficulty in obtaining all level density parameters in a straightforward manner, as described in Section 3.2, at least in the scheme of Gilbert-Cameron' formula. The determination of level density parameters, in particular C, T and $E_x$ is apt to depend on subjective judgement. On the other hand, direct information of level density may be obtained from the analysis of shape of capture cross section in MeV region. Good agreement of RCN-2 evaluation with experiments of MeV capture cross sections for Sm-152 and 154 (Figs. 20,31) seems to support this possiblility.

Acknowledgement

We are thankful to Dr. Y. D. Harker for sending us the report of CFRMF measurements, and to Dr. H. Gruppelaar the STEK measurements and RCN-2 evaluations. Prof. Kazachkowskii at Physico-Energetic Institute, USSR, kindly sent us the numerical data of capture measurements at FEI To many persons of JNDC and JAERI we owe discussions and helps including cross section calculations etc. They are : S. Igarasi, Y. Sekine, Z. Matsumoto, T. Asami, T. Nakagawa and T. Narita at Nuclear Data Center, M. Mizumoto, Y. Nakajima and A. Asami at Physics-2 (Liniac) Laboratory, H. Takano and S. Ishiguro at Reactor System Laboratory, JAERI We owe also to R. Nakasima at Hosei University and H. Matsunobu at Sumitomo Atomic Energy Industries, Ltd. for discussions on level density and cross section renormalization. We wish to express our sincere gratitude to these persons.

References : General

[1] S. Iijima, Status of fast neutron reaction cross sections of fission products, Fission Product Nuclear Data [FPND] -1977, Proc. Second Advisory Group Meeting on Fission Product Nuclear Data, Petten, 1977, IAEA-213, RP9, p.279

[2] S. Iijima, T. Nakagawa, Y. Kikuchi, M. Kawai, H. Matsunobu, K. Maki, and S. Igarasi, J. Nucl. Sci. Technol. 14 (1977) 161

[3] Y. Kikuchi, T. Nakagawa, H. Matsunobu, M. Kawai, S. Igarasi, and S. Iijima, Neutron cross sections of 28 fission product nuclides adopted in JENDL-1, JAERI report (to be published, 1980)

[4] See for example, Progress in Fission Product Nuclear Data, collected by G. Lammer, No.2, 1976 (INDC(NDS)-55/G+P), No.3, 1977 (ibid. 86/G+P), No.4, 1978 (ibid. 95/G+P), No.5, 1979 (ibid. 102/G+P)

[5] H. Gruppelaar, Tables of RCN-2 fission-product cross section evaluation, Vol.1 (24 nuclides), ECN-13 (1977), Vol.2 (13 nuclides) ECN-33 (1977), Vol.3 (Nd and Pm isotopes), ECN-65 (1979).
H. Gruppelaar, Impact of integral measurements on the capture cross section evaluations of individual fission product isotope, IAEA-213 (1977), RP8, p.219

[6] M. Bustraan, J. W. M. Dekker, R. J. Heijboer and A. J. Janssen, Integral determination of FP neutron cross sections, IAEA-213 (1977), RP14, p.627

[7] G. Reffo, INDC(NDS)-87/GO+SP, Annexes and Selected Contributions to the Review Papers, Fission Product Nuclear Data [FPND]-1977, p.165.

[8] H. Nishimura, T. Watanabe, T. Nakagawa and Y. Kikuchi, Integral test of the JENDL FP data file, Proc. 1978 Seminar on Nuclear Data, Tokai, 20-21 Dec., 1978, JAERI-M 8163 (1979) p.136

[9] H. Nishimura, ETOA-1 code (1972), private communication

[10] D. R. Green and T. A. Pitterle, ETOE, A program for ENDF/B to $MC^2$ data conversion, APDA-219 (ENDF-120) (1968)

[11] Group Constants for Nuclear Reactor Calculation, Constants Bureau, N. Y., edited by I. I. Bondarenko

[12] J. W. M. Dekker, Tables and figures of adjusted and unadjusted capture group cross sections based on RCN-2 evaluations and integral measurements in STEK, Vol.1, ECN-14 (1977), Vol.2, ECN-30 (1977), and Vol.3, ECN-54 (1979)

[13] H. Takano et al., TIMS-2 code, JAERI report (to be published,1980)

[14] J. P. Delaroche, Ch. Lagrange and J. Salvy, RP5, IAEA Consultant Meeting, Trieste, December, 1975.
Ch. Lagrange, NEANDC(E)183L (1977), Determination du potential optique derivant l'interaction neutron - Mo-98

[15] Japanese Nuclear Data Committee, Evaluation of fission product nuclear data for fast reactor, JAERI-M 5752 (1974)

[16] L. Rosen, J. G. Beery, A. S. Goldhaber and E. H. Auerbach, Ann. Phys. 34 (1965) 96

[17] A. Gilbert and A. G. W. Cameron, Can. J. Phys. 43 (1965) 1446

[18] B. L. Berman, Atomic Data and Nucl. Data Tables 15 No.4 (1975)

[19] H. Matsunobu, private communication, 1979

References : Experimental data


[Be71] F. Bensch and H. Ledermann, EANDC(OR) 105L, p.1 (1971)

[Ch66] A. K. Chaubey and M. L. Sehgal, Phys. Rev. 152 (1966) 1055

[De78] J. W. M. Dekker, J. B. Dragt, A. J. Janssen, R. J. Heijboer and H. Th. Klippel, Adjusted neutron spectra of STEK cores for reactivity calculations, ECN-35 (1978)

[Ei74] H. M. Eiland, S. Weinstein and K. W. Seeman, Nucl. Sci. Eng. 54 (1974) 286

[Fa72] L. W. Faucett, A. K. Furr and J. G. Lindsay, Nucl. Sci. Eng. 49 (1972) 317

[Ha68] S. S. Hasan, A. K. Chaubey and M. L. Sehgal, Nuovo Cimento B58 (1968) 402

[Ha78] Y. D. Harker, J. W. Rogers and D. A. Millsap, Fission product and reactor dosimetry studies at coupled fast reactivity measurements facility, Preliminary report of ENDF-266, TREE-1259 (1978)

[Jo59] A. E. Johnsrud, M. G. Silbert and H. H. Barshall, Phys. Rev. 116 (1959) 927

[Ki75] G. J. Kirouac and H. M. Eiland, Phys. Rev. C11 (1975) 895

[Ko77] V. N. Kononov, B. D. Yurelov, E. D. Poletaev and V. M. Timokhov, Sov. J. Nucl. Phys. 26 (1977) 947

[Ko78] V. N. Kononov, B. D. Yurelov, E. D. Poletaev and V. M. Timokhov, Sov. J. Nucl. Phys. 27 (1978) 10

[La73] L. Lakosi and A. Beresh, Conf. on Neutron Physics, Kiev, Vol.4, p. 312, (1973)

[Ly59] W. S. Lyon and R. L. Macklin, Phys. Rev. 114 (1959) 1619

[Ma57] R. L. Macklin, N. H. Lazar and W. S. Lyon, Phys. Rev. 107 (1957) 504

[Ma63] R. L. Macklin, J. H. Gibbons and T. Inada, Nature 197 (1963) 369

[Mi79] M. Mizumoto, M. Sugimoto, Y. Nakajima, Y. Kawarasaki, Y. Furuta and A. Asami, Neutron radiative capture and transmission measurement of Sm-147 and Sm-149, a paper presented to Int. Conf. on Nuclear Cross Sections for Technology, Univ. Tennessee, Oct. 1979

[Mu77] A. R. de L. Musgrove, B. J. Allen, J. W. Boldeman and R. L. Macklin, AAEC/E401 (1977)

[Mu78] A. R. de L. Musgrove, B. J. Allen, J. W. Boldeman and R. L. Macklin, Proc. Int. Conf. on Neutron Physics and Nuclear Data for Reactors and other Applied Purposes, Harwell, Sept. 1978, p.438

[Na78] Y. Nakajima, A. Asami, Y. Kawarasaki, Y. Furuta, N. Yamamuro and Y. Kanda, Harwell conf.,1978,ibid. p.438

[Na79] Y. Nakajima, private communication, 1979

[Pe67] G. Petö, Z. Miligy and I. Hunyadi, J. Nucl. Energy 21 (1967) 797

[Pi74] W. F. E. Pineo, M. Divadeenam, E. G. Bilpuch and K. K. Seth, Ann. Phys. 84 (1975) 165

[Sh67] Shorin et al., INDC-187E (1967) 30

[Sh75] Shaw et al., Data in NEUDADA, NEA Data Bank.

[Si73] K. Siddapa, M. S. Murty and J. Rama Rao, Nuovo Cimento 18A (1973) 48

[Te71] H. Tellier, CEA-N-1459 (1971)

[Th72] B. V. Thirumala Rao, J. Rama Rao and E. Kondaiah, J. Phys. A5 (1972) 468

[Ve76] J. J. Veenema and A. J. Janssen, Small-sample reactivity worths of fission product isotopes and some other materials measured in STEK, ECN-10 (1976)

Appendix : Composite level density formula

$$\rho_{J\pi}(E) = p_\pi R_J \rho_0(E) \tag{1}$$

$$R_J = \frac{2J+1}{2\sigma^2} \exp\left[-(J+\tfrac{1}{2})^2/2\sigma^2\right] \tag{2}$$

$$\rho_0(E) = \frac{\exp(2\sqrt{aU})}{12\sqrt{2}\,\sigma\, a^{1/4} U^{5/4}}, \quad E > E_x \quad (U \equiv E-\Delta) \tag{3a}$$

$$= C \exp(E/T), \quad E < E_x \tag{3b}$$

Here, $p_\pi$ and $R_J$ are normalized parity and spin distributions, resp. $\Delta$ is paring energy. For $p_\pi$, the expression by Igarasi was assumed.

$$p_\pi(E) = \left\{ f_\pi + 0.5 \exp\left(\frac{U-U_0}{\delta}\right)\right\} \Big/ \left\{ 1 + \exp\left(\frac{U-U_0}{\delta}\right)\right\} \tag{4}$$

where $f_\pi$ is the fraction of lowlying levels with parity $\pi$. $U_0$ and $\delta$ are somewhat arbitrarily determined parameters so that $p_\pi$ approaches 1/2 at high excitation energy.

The spin cut-off parameter is expressed by

For $E > E_x$ $\quad \sigma^2(E) = c_1 \sqrt{aU}\, A^{2/3}$ (5)

For $E < E_x$ $\quad \sigma^2(E) = c_1 \sqrt{aU_x}\, A^{2/3}$ (6)

or $\quad = \sigma^2_{exp} + (\sigma^2(E_x) - \sigma^2_{exp}) E/E_x$ (7)

In JENDL-1 evaluation, $c_1$=0.0888 and eq. (6) was used. In the present evaluation, $c_1$=0.146 and eq. (7) was adopted as in RCN-2 and CNEN-2 evaluations. In eqs. (6) and (7), $\sigma^2_{exp}$ is expressed as (Schmittroth1973)

$$\sigma^2_{exp} = \frac{1}{2N} \sum_{i=1}^{N} (I_i + \tfrac{1}{2})^2 \tag{8}$$

where $I_i$ (i=1,2,---,N) are the spins of lowlying levels.

The dividing energy $E_x$ is usually considered as smaller than neutron separation energy $B_n$. If eqs. (3a) and (3b) continues smoothly at $E = E_x$, the parameters C and T are related with other parameters by

$$\frac{1}{T} = \sqrt{\frac{a}{U_x}} - \frac{3}{2U_x} \tag{9}$$

$$\rho_0(\text{eq. 3a}) = \rho_0(\text{eq. 3b}) \quad \text{at } E = E_x . \tag{10}$$

Table 1 Fission Product (n,γ) Reaction Rate in CFRMF

| Nuclide | $\sigma_{n\gamma}$ (FP) $\phi/\sigma_f$ ($^{235}U$) $\phi$ and (C/E) | | | |
|---|---|---|---|---|
| | Measured*** | ENDF/B-4 | JENDL-1 | JENDL-1 (inf. dilution) |
| 87 Rb | $7.52\times10^{-3}$ (±10%) | $7.46\times10^{-3}$ (0.99) | - | - |
| 89 Y | $2.12\times10^{-4}$ (±4.8%) | - | - | - |
| 99 Tc | 0.167 (±15%) | 0.174 (1.04) | 0.203 (1.21) | 0.209 (1.25) |
| 98 Mo | 0.0354 (±6.4%) | 0.0436 (1.23) | 0.0438 (1.24) | 0.0470 (1.33) |
| 100 Mo | 0.0345 (±17%) | 0.0311 (0.90) | 0.0306 (0.89) | 0.0321 (0.93) |
| 102 Ru | 0.0557 (±6.6%) | 0.0784 (1.41) | 0.0879 (1.58) | 0.0888 (1.59) |
| 104 Ru | 0.0518 (±6.3%) | 0.0550 (1.06) | 0.0609 (1.17) | 0.0627 (1.21) |
| 103 Rh | 0.235 (±24%) | 0.264 (1.12) | 0.231 (0.98) | 0.245 (1.04) |
| 108 Pd | 0.0903 (±6.7%) | - | 0.0741 (0.82)* | 0.0937 (1.04)* |
| 110 Pd | $3.18\times10^{-3}$ (±6.9%) | - | - | - |
| 107 Ag | 0.238 (±19%) | 0.265 (1.11) | 0.235 (0.99) | 0.242 (1.02) |
| 109 Ag | 0.318 (±9.7%) | 0.192 (0.60) | 0.328 (1.03) | 0.341 (1.07) |
| 115 In | 0.175 (±4.3%) | 0.192 (1.10) | - | - |
| 121 Sb | 0.157 (±8.3%) | 0.193 (1.23) | - | - |
| 123 Sb | 0.0966 (±7%) | 0.105 (1.09) | - | - |
| 127 I | 0.187 (±10%) | 0.214 (1.15) | 0.229 (1.23) | 0.232 (1.24) |
| 129 I | 0.115 (±6.6%) | 0.146 (1.27) | 0.172 (1.49) | 0.173 (1.50) |
| 132 Xe | 0.0275 (±7.7%) | - | 0.0306 (1.11)* | 0.0306 (1.11)* |
| 134 Xe | $9.15\times10^{-3}$ (±6.9%) | 0.0151 (1.65) | 0.0151 (1.65)* | 0.0151 (1.65)* |
| 133 Cs | 0.173 (±6.6%) | 0.189 (1.09) | 0.175 (1.01) | 0.183 (1.06) |
| 137 Cs | 0.056 (±25%) | - | - | - |
| 139 La | 0.0110 (±5.2%) | - | 0.0133 (1.21) | 0.0150 (1.36) |
| 140 Ce | $5.27\times10^{-4}$ (±6.7%) | $8.71\times10^{-3}$ (16.5) | 0.0143 (27.2) | 0.0149 (28.3) |
| 142 Ce | 0.0115 (±7.4%) | 0.0156 (1.35) | 0.0236 (2.05) | 0.0239 (2.07) |
| 141 Pr | 0.0458 (±15%) | 0.0639 (1.40) | 0.0422 (0.92) | 0.0516 (1.13) |
| 147 Pm | 0.402 (±13%) | 0.487 (1.21) | 0.455 (1.13) | 0.466 (1.16) |
| 146 Nd | 0.0364 (±6.5%) | 0.0572 (1.57) | 0.0363 (1.00) | 0.0367 (1.01) |
| 148 Nd | 0.0558 (±14%) | 0.102 (1.83) | 0.0834 (1.49) | 0.0882 (1.58) |
| 150 Nd | 0.0418 (±12%) | 0.0915 (2.19) | 0.0770 (1.84) | 0.0787 (1.88) |
| 152 Sm | 0.174 (±6.4%) | 0.188 (1.08) | 0.206 (1.19) | 0.226 (1.30) |
| 154 Sm | 0.733 (±4.5%) | 0.978 (1.33) | 0.0916 (0.12) | 0.0948 (0.13) |
| 151 Eu | 1.50 (±5.8%) | 1.43 (0.95) | 1.31 (0.87) | 1.33 (0.89) |
| 153 Eu | 0.909 (±7.04%) | 0.89 (0.98) | 0.870 (0.96)* | 0.886 (0.97)* |

Table 1 (cont'd)

| Nuclide | $\sigma_{n\gamma}$ (FP) $\phi/\sigma_f$ ($^{235}U$) $\phi$ and (C/E) | | | | | | | |
|---|---|---|---|---|---|---|---|---|
| | Measured | | ENDF/B-4 | | JENDL-1 | | JENDL-1 (inf. dil.) | |
| 158 Gd | 0.112 | (±12%) | 0.115 | (1.03) | 0.113 | (1.01)* | 0.116 | (1.03)* |
| 160 Gd | 0.0575 | (±8.5%) | 0.0897 | (1.56) | 0.0866 | (1.51)* | 0.0878 | (1.53)* |
| 169 Tm | 0.293 | (±12%) | - | | - | | - | |
| 181 Ta | 0.329 | (±9.0%) | 0.346 | (1.05) | - | | - | |
| 186 W | 0.0900 | (±13%) | - | | - | | - | |
| 239 Pu(n,f) | 1.165 | | 1.117 | (0.959) | - | | 1.130 | (0.970)** |
| 238 U (n,f) | 0.0488 | | 0.0481 | (0.986) | - | | 0.0509 | (1.043)** |
| 238 U (n,γ) | 0.144 | | 0.146 | (1.01) | - | | 0.154 | (1.07)** |
| <$^{235}$U (n,f)> | | | 1.595 barn | | | | 1.562 barn** | |

*ENDF/B-4 cross sections were used. **JENDL-2 preliminary version.
***Revised based on the report by Y.D. Harker and R.A. Anderl presented to this meeting.

Table 8. Giant dipole resonance parameters (from Berman [Be 75])

| Compound Nucleus | $E_1$ (MeV) | $\sigma_1$ (mb) | $\Gamma_1$ (Mev) | $E_2$ (MeV) | $\sigma_2$ (mb) | $\Gamma_2$ (Mev) | $\sigma_{int}$ (MeV-mb) |
|---|---|---|---|---|---|---|---|
| 142-Nd | 14.94 | 359 | 4.44 | | | | 1873 |
| 143 Nd | 15.01 | 349 | 4.75 | | | | 1901 |
| 144 Nd | 15.06 | 317 | 5.28 | | | | 1882 |
| 145 Nd | 14.95 | 296 | 6.31 | | | | 2037 |
| 146 Nd | 14.74 | 310 | 5.78 | | | | 1920 |
| 148 Nd | 12.76 | 107 | 3.97 | 15.48 | 220 | 5.30 | 1702 |
| 150 Nd | 12.30 | 175 | 3.38 | 16.04 | 223 | 5.17 | 2011 |
| nat Nd | 14.92 | 315 | 4.70 | | | | 1559 |
| 144 Sm | 15.32 | 383 | 4.45 | | | | 2001 |
| 147 Sm | | | | | | | |
| 148 Sm | 14.82 | 339 | 5.09 | | | | 1942 |
| 149 Sm | Assumed as for $^{148}$Sm | | | | | | |
| 150 Sm | 14.61 | 312 | 5.97 | | | | 1991 |
| 151 Sm | Assumed as for $^{150}$Sm | | | | | | |
| 152 Sm | 12.38 | 176 | 2.97 | 15.74 | 234 | 5.22 | 2026 |
| 154 Sm | 12.27 | 181 | 2.95 | 15.94 | 215 | 5.70 | 2059 |
| nat Sm | | | | | | | 2413 |

For $^{153}$Sm and $^{155}$Sm, the values as for $^{152}$Sm and $^{154}$Sm are assumed, resp.

Table 2. SPR data for Nd isotopes and the optical model fit

| | So ($10^{-4}$) | | $S_1$ ($10^{-4}$) | | R' (fm) | | $S_2$($10^{-4}$) |
|---|---|---|---|---|---|---|---|
| | Exp.[a] | Calc | Exp.[a] | Calc | Exp.[d] | Calc. | Calc |
| Nd-142 | 1.4 ±0.35 | 1.42 | 0.70 ±0.05 | 0.69 | 4.7 ±0.5 | 4.75 | 0.92 |
| 143 | 3.1 ±0.5 | 2.99 | 1.0 ±0.4 | 1.03 | 4.7 ±0.5 | 4.71 | 2.4 |
| 144 | 3.9 ±1.0 | 4.00 | 0.8 ±0.3 | 0.78 | 4.6 ±0.5 | 4.62 | 2.4 |
| 145 | 5.2 ±0.9 | 4.97 | 0.8 ±0.4 | 0.81 | 4.55±0.5 | 4.70 | 2.4 |
| 146 | 3.5 ±0.9 | 3.55 | 1.1 ±0.35 | 1.02 | 4.5 ±0.5 | 4.75 | 2.0 |
| 148 | 2.7 ±0.8 | 3.00 | 0.60 ±0.20 | 0.62 | 8,45±1.0 | 8.49 | 3.4 |
| 150 | 3.2 ±0.6[b] | 3.19 | 0.65 ±0.3[c] | 0.67 | 8.4 ±1.0 | 8.20 | 3.5 |

a) Musgrove et al. [Mu 78], b) Tellier [Te 71], c) Calculation by Moldauer's potential

d) Rough eye-guided interpolation from R' vs. A curve.

Table 3. SPR data for Sm isotopes and the optical model fit

| Target nucleus | $S_0$ ($10^{-4}$) | | $S_1$ ($10^{-4}$) | | R' (fm) | | $S_2$ ($10^{-4}$) |
|---|---|---|---|---|---|---|---|
| | Exp. | Calc. | Exp. | Calc. | Exp. | calc. | calc. |
| Sm-147 | 4.8 ±0.5[a] | 4.77 | 0.75 ±0.4[e] | 0.71 | 7.5 ±1.0[e] | 7.77 | 3.9 |
| 148 | 3.0 ±1.0[b] | 3.11 | | 0.73 | 7.5 ±1.0[e] | 7.80 | 3.4 |
| 149 | 4.6 ±0.6[a] | 4.78 | | 0.77 | 7.5 ±1.0[e] | 7.52 | 3.7 |
| 150 | 3.3 ±1.1[c] | 3.13 | | 0.755 | 8.0 ±1.0[e] | 8.08 | 3.4 |
| 151 | 3.65 ±0.48[b] | 3.51 | | 0.765 | 8.0 ±1.0[e] | 7.95 | 3.4 |
| 152 | 2.2 ±0.4[d] | 2.20 | | 0.85 | 8.2 ±0.7[d] | 8.20 | 2.6 |
| 154 | 1.8 ±0.5[d] | 2.02 | | 0.88 | 8.2 ±0.7[d] | 8.34 | 2.5 |

a) Mizumoto et al. [Mi 79], b) Kirouac et al. [Ki 75], e) Eiland et al. [Ei 74]

d) BNL-325, 3rd ed. [Mu 73], e) Rough estimation from systematics.

Table 4. Spherical optical model parameters for Nd isotopes

| Target nucleus | Real well | | | Imaginary surface well | | | Spin-orbit well | | |
|---|---|---|---|---|---|---|---|---|---|
| | $V_o$ | $r_o$ | $a_o$ | $W_s$ | $r_s$ | $a_s$ | $V_{so}$ | $r_{so}$ | $a_{so}$ |
| Nd-142 | 48.21 | 1.23 | 0.60 | 3.42 | 1.31 | 0.45 | 7.0 | 1.28 | 0.60 |
| 143 | 45.76 | 1.29 | | 6.97 | 1.23 | | | | |
| 144 | 45.75 | 1.30 | | 5.68 | 1.27 | | | | |
| 145 | 46.59 | 1.29 | | 6.43 | 1.17 | | | | |
| 146 | 45.657 | 1.29 | | 7.417 | 1.196 | | | | |
| 148 | 47.94 | 1.27 | | 9.13 | 1.43 | | | | |
| 150 | 47.94 | 1.27 | | 9.13 | 1.43 | | | | |

Table 5. Spherical optical model parameters for Sm isotopes

| Target Nucleus | Real well | | | Imaginary surface well | | | Spin-orbit well | | |
|---|---|---|---|---|---|---|---|---|---|
| | $V_o$ | $r_o$ | $a_o$ | $W_s$ | $r_s$ | $a_s$ | $V_{so}$ | $r_{so}$ | $a_{so}$ |
| Sm-147 | 47.08 | 1.291 | 0.60 | 8.364 | 1.352 | 0.45 | 7.0 | 1.28 | 0.60 |
| 148 | 44.878 | 1.294 | | 8.510 | 1.463 | | | | |
| 149 | 46.71 | 1.287 | | 8.674 | 1.334 | | | | |
| 150 | 45.395 | 1.297 | | 9.788 | 1.434 | | | | |
| 151 | 46.677 | 1.283 | | 10.078 | 1.382 | | | | |
| 152 | 52.75 | 1.188 | | 11.88 | 1.44 | | | | |
| 154 | 54.01 | 1.116 | | 11.36 | 1.483 | | | | |

Table 6. Level density parameters of Nd isotopes. Comparison of present and RCN-2 evaluation

| Compound nucleus | Bn (Mev) | Δ (MeV) | Dobs (eV) | | a ($MeV^{-1}$) | | $E_x$ (MeV) | | T (MeV) | | C ($MeV^{-1}$) | |
|---|---|---|---|---|---|---|---|---|---|---|---|---|
| | | | Present | RCN-2 | Present | RCN-2 | Present | RCN-2 | Present | RCN-2[a)] | Present | RCN-2[a)] |
| Nd-142 | 9.813 | 2.03 | - | - | 12.88 | 16.40 | 4.50 | 3.975 | 0.718 | 0.469 | 0.320 | 0.0451 |
| 143 | 6.125 | 1.18 | 680 | 680 | 18.26 | 18.28 | 4.00 | 3.859 | 0.480 | 0.487 | 0.598 | 0.695 |
| 144 | 7.817 | 1.94 | 35 | 35 | 17.71 | 17.72 | 4.65 | 5.512 | 0.585 | 0.553 | 0.593 | 0.397 |
| 145 | 5.760 | 1.18 | 450 | 450 | 20.54 | 20.56 | 4.50 | 5.199 | 0.514 | 0.530 | 2.52 | 3.44 |
| 146 | 7.565 | 2.10 | 19 | 19 | 20.19 | 20.20 | 3.35 | 6.536 | 0.768 | 0.557 | 1.30 | 0.930 |
| 147 | 5.302 | 1.18 | 270 | 270 | 23.93 | 23.99 | 3.80 | 5.185 | 0.502 | 0.482 | 5.68 | 5.22 |
| 148 | 7.324 | 2.17 | - | 8.6 | 23.59 | 23.60 | 4.00 | 6.813 | 0.606 | 0.518 | 1.68 | 1.43 |
| 149 | 5.068 | 1.18 | 170 | 170 | 26.57 | 26.75 | 5.00 | 6.097 | 0.479 | 0.493 | 12.45 | 20.22 |
| 150 | 7.357 | 2.28 | - | - | 24.15 | 24.10 | 5.50 | 7.418 | 0.550 | 0.534 | 2.10 | 2.16 |
| 151 | 5.309 | 1.18 | 120 | 160 | 26.18 | 25.25 | 5.30 | 5.996 | 0.480 | 0.506 | 11.50 | 14.57 |

a) Calculated by assuming continuity of level density at E = Ex.

Table 7. Level density parameters of Sm isotopes. Comparison of the present and RCN-2 evaluations

| Compound nucleus | Bn (MeV) | Δ (MeV) | Dobs (eV) | | a ($MeV^{-1}$) | | $E_x$ (MeV) | | T (MeV) | | C ($MeV^{-1}$) | |
|---|---|---|---|---|---|---|---|---|---|---|---|---|
| | | | Present | RCN-2 | Present | RCN-2 | Present | RCN-2 | Present | RCN-2[a)] | Present | RCN-2[a)] |
| Sm-147 | 6.373 | 1.22 | - | | 22.75 | 21.00 | 4.50 | 5.198 | 0.477 | 0.469 | 2.620 | 1.085 |
| 148 | 8.140 | 2.14 | 7.0 | 6.3 | 20.56 | 20.77 | 6.00 | 6.358 | 0.547 | 0.537 | 0.798 | 0.713 |
| 149 | 5.873 | 1.22 | - | 107 | 24.95 | 23.78 | 4.50 | 5.865 | 0.481 | 0.472 | 6.140 | 3.21 |
| 150 | 7.985 | 2.21 | 2.38 | 2.0 | 23.62 | 24.00 | 6.50 | 6.853 | 0.523 | 0.513 | 1.489 | 1.37 |
| 151 | 5.596 | 1.22 | 56.5 | 56.5 | 26.87 | 26.88 | 5.00 | 6.806 | 0.456 | 0.519 | 7.460 | 37.9 |
| 152 | 8.258 | 2.32 | 1.72 | 1.72 | 23.75 | 24.23 | 8.00 | 7.611 | 0.547 | 0.539 | 2.400 | 2.41 |
| 153 | 5.867 | 1.22 | 53.8 | 53.8 | 25.62 | 25.63 | 3.50 | 7.360 | 0.590 | 0.556 | 19.10 | 52.5 |
| 154 | 7.979 | 2.14 | - | - | 22.35 (21.90)[b)] | 22.80 | 4.75 (5.0)[b)] | 7.287 | 0.601 | 0.551 | 2.313 | 2.42 |
| 155 | 5.814 | 1.22 | 112.6 | 130 | 24.02 | 23.66 | 5.50 | 7.201 | 0.508 | 0.575 | 8.430 | 31.8 |

a) Calculated by assuming continuity of level density at E = Ex.

b) Revised value, not used in the present cross section calculation.

Table 9. Average s-wave neutron resonance level spacings and radiation widths of Nd isotopes

| Target nucleus | Dobs (exp), eV | | $\overline{\Gamma}_\gamma$(exp), mV | RCN-2 evaluation | | | Present evaluation | | | |
|---|---|---|---|---|---|---|---|---|---|---|
| | BNL-325 | [Mu78] | [Mu78] | Dobs, eV | $\Gamma_\gamma^s$, mV | $S_\gamma(10^{-4})$ | Dobs, eV | $\Gamma_\gamma$, mV | $S_\gamma(10^{-4})$ | $S_\gamma^*(10^{-4})$ |
| Nd-142 | 415±70 | 680±130 | 50±10 | 680 | 65 | 0.956 | 680 | 50 | 0.735 | 0.991 |
| 143 | 32±3 | 35±4 | 86±9 | 35 | 86 | 24.6 | 35 | 86 | 24.6 | 22.6 |
| 144 | 540±65 | 450±110 | 47±5 | 450 | 47 | 1.04 | 450 | 47 | 1.04 | 0.912 |
| 145 | 19±2 | 19±2 | 87±9 | 19 | 87 | 45.8 | 19 | 87 | 45.8 | 51.3 |
| 146 | 210±25 | 270±60 | 51±6 | 270 | 51 | 1.89 | 270 | 51 | 1.89 | 1.89 |
| 148 | 72±6 | 170±35 | 46±5 | 170 | 46 | 2.71 | 170 | 46 | 2.71 | 2.42 |
| 150 | 120±8 | | 72±10 | 160 | 72 | 4.50 | 120 | 72 | 6.0 | 3.02 |

*) $S_\gamma^*$ is the adjusted value to normalize the calculation to capture data at 30 keV as follows:

| | Nd-142 | Nd-143 | Nd-144 | Nd-145 | Nd-146 | Nd148 | Nd-150 |
|---|---|---|---|---|---|---|---|
| $\sigma_{n\gamma}$(30 keV), mb | 59 | 280 | 66 | 510 | 114 | 135 | 153 |

Table 10. Average S-wave neutron resonance level spacings and radiation widths of Sm isotopes

| Target nucleus | Dobs (exp), eV | | $\bar{\Gamma}_\gamma$, mV | RCN-2 evaluation | | | Present evaluation | | | |
|---|---|---|---|---|---|---|---|---|---|---|
| | BNL-325 | BNL-325 | Other exp. | Dobs, ev | $\Gamma_\gamma$, mV | $S_\gamma (10^{-4})$ | Dobs, ev | $\Gamma_\gamma$, mV | $S_\gamma (10^{-4})$ | $S_\gamma^* (10^{-4})$ |
| Sm-147 | 7.4±0.7 | 7.00[a], 5.7[b] | 66[a], 70[b] | 6.3 | 100 | 159 | 5.70 | 70 | 122.8 | 162.8 |
| 148 | | | | 107 | 60 | 5.6 | 79.0 | 70 | 8.86 | 6.19 |
| 149 | 2.3±0.3 | 2.38[c], 2.2[b] | 62[b] | 2.0 | 76 | 380 | 2.2 | 62 | 282 | 641 |
| 150 | 68±10 | 56.5[a] | 60[a] | 56.3 | 60 | 10.7 | 56.5 | 60 | 10.6 | 15.6 |
| 151 | 1.3±0.2 | 1.72±0.07[d] | 96[d] | 1.72 | 96 | 558 | 1.72 | 96 | 558 | — |
| 152 | 51.8±14 | 53.8[e] | 65[e] | 53.8 | 70 | 13.0 | 53.8 | 65 | 12.1 | 14.0 |
| 154 | 115±14 | 112.6[e] | 79[e] | 130 | 70 | 5.38 | 112.6 | 79 | 7.02 | 5.20 |

a) Eiland et al. [Ei 74], b) Mizumoto et al. [Mi 79], c) Karzhavina et al.

d) Kirouac and Eiland [Ki 75], e) Rahn et al [Ra 72]

*) $S^*$ is the adjusted value to normalize the calculation with capture data at 30 keV as follows:

| | Sm-147 | Sm-148 | Sm-149 | Sm-150 | Sm-151 | Sm-152 | Sm-154 |
|---|---|---|---|---|---|---|---|
| $\sigma_{n\gamma}$(30 kev), mb | 1080 | 235 | 2300 | 430 | - | 420 | 215 |

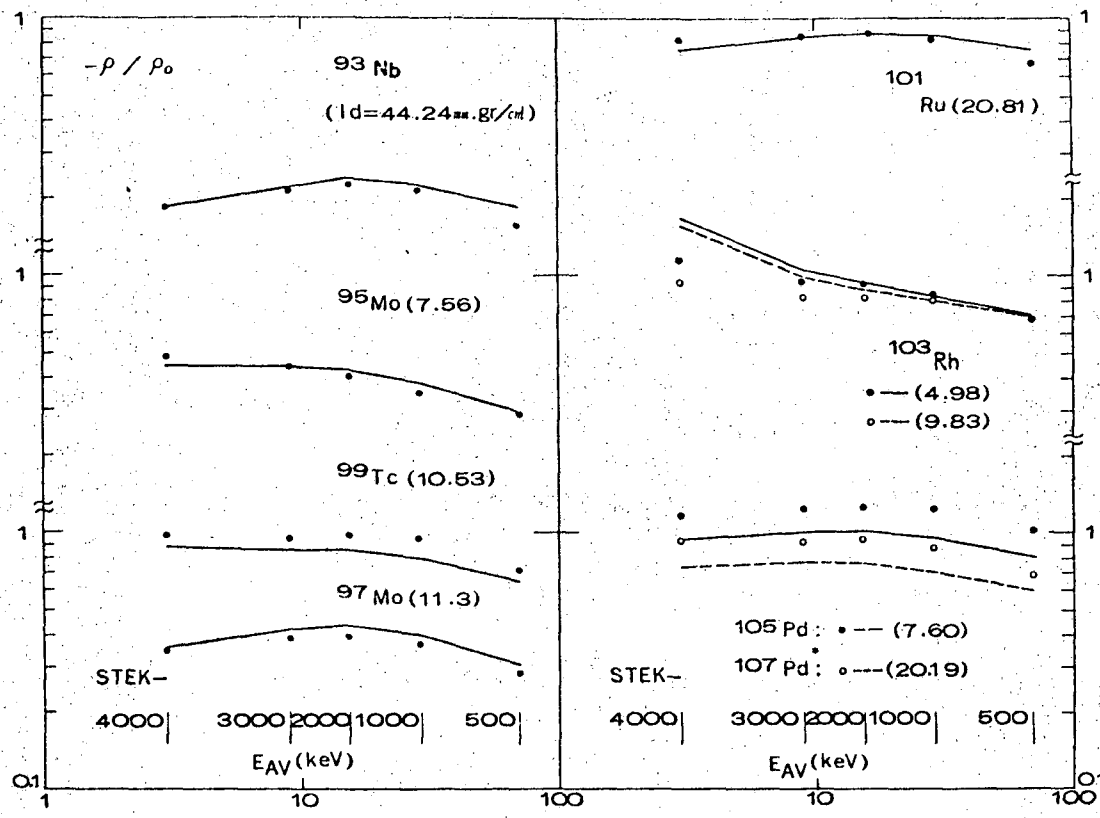


Fig. 1. Small sample reactivities in STEK cores (normalized reactivity per gram of chemical compound). Comparison of calculation (JENDL-1) and experiment. The number in parenthesis denotes the ld value (mm·gr/cm$^3$) of sample. Isotope marked with asterisk indicates the sample with low isotopic enrichment.

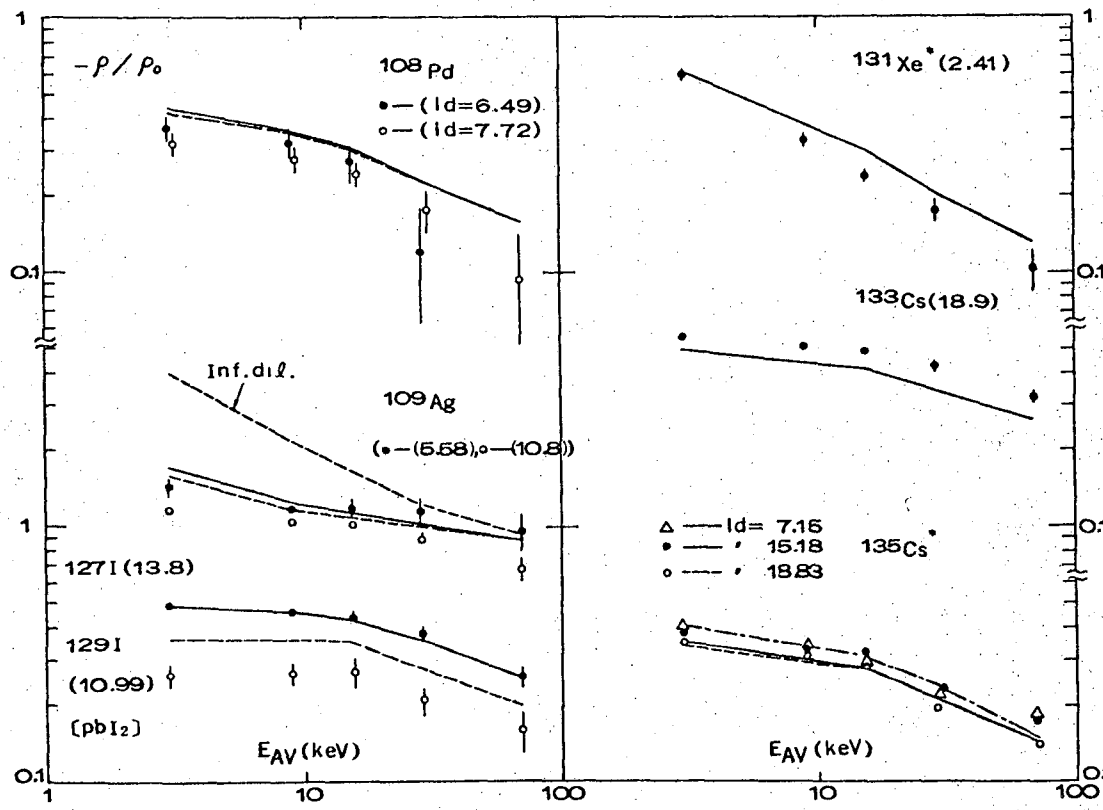


Fig. 1. (cont'd)

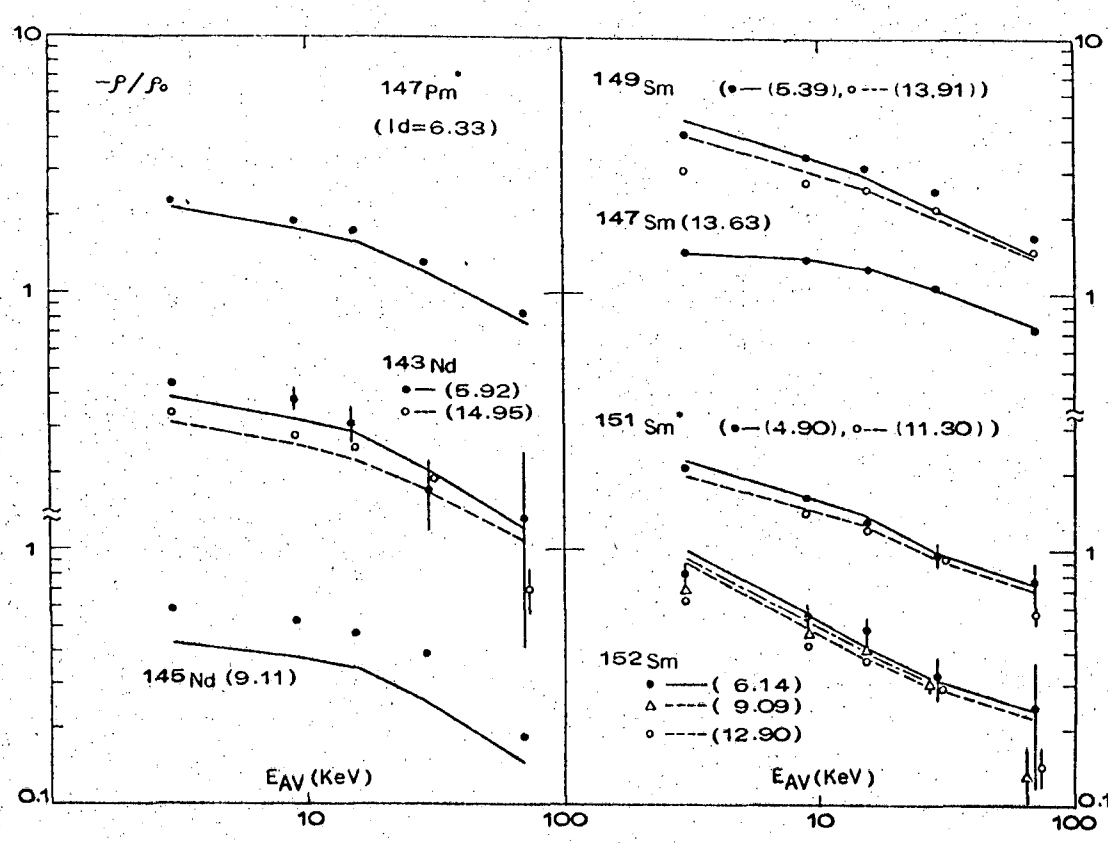


Fig. 1. (cont'd)

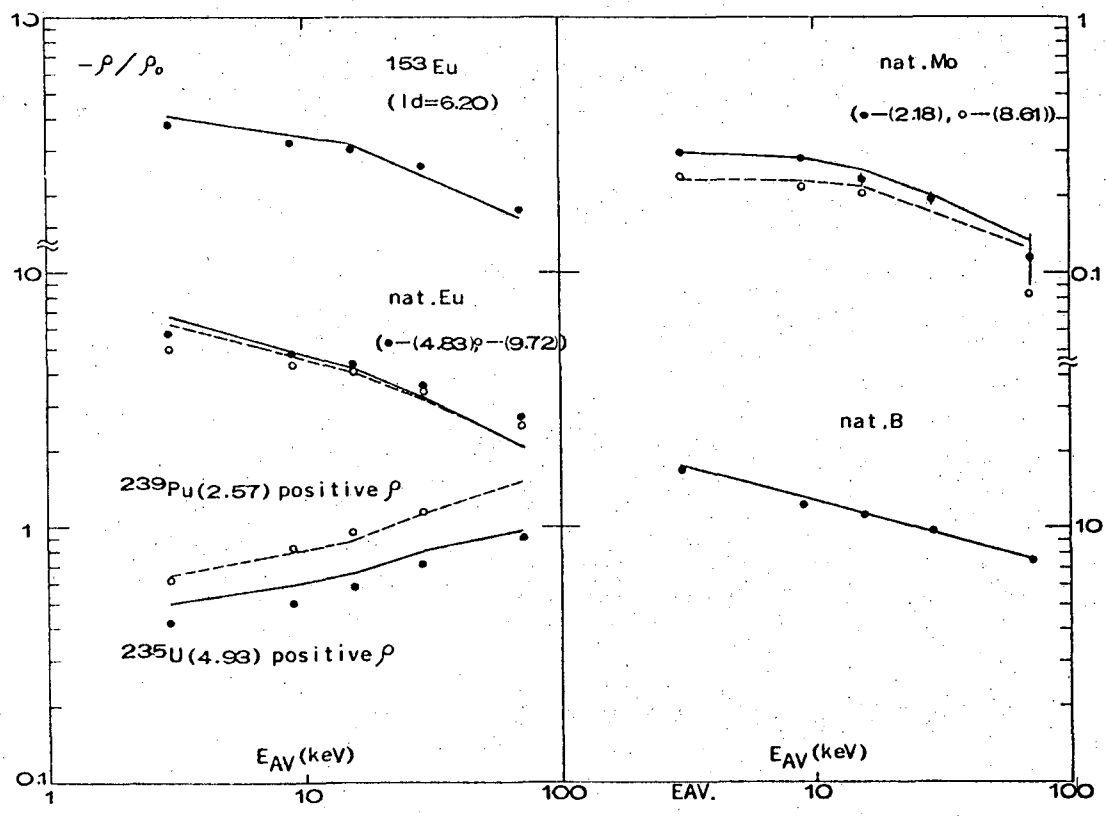


Fig. 1. (cont'd)

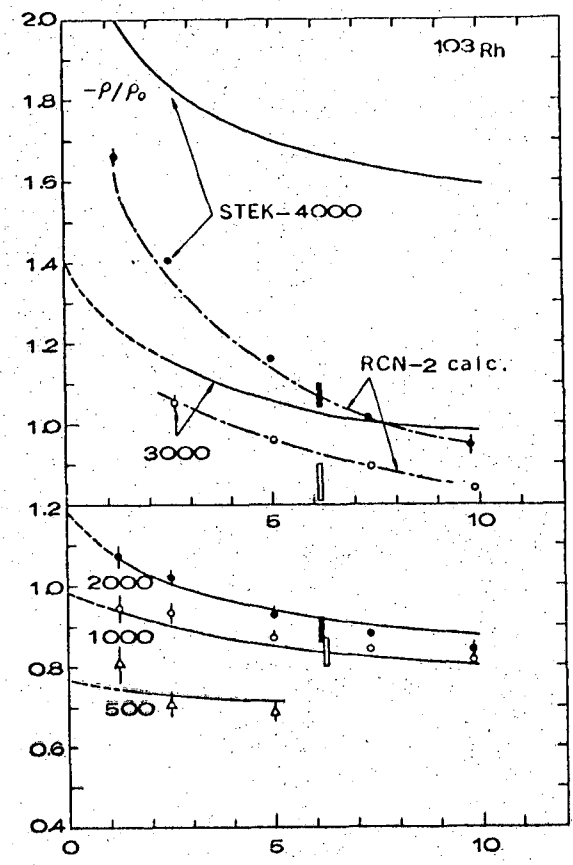


Fig. 2. Rh sample reactivity as a function of ld values. Comparison of calculation with experiment.

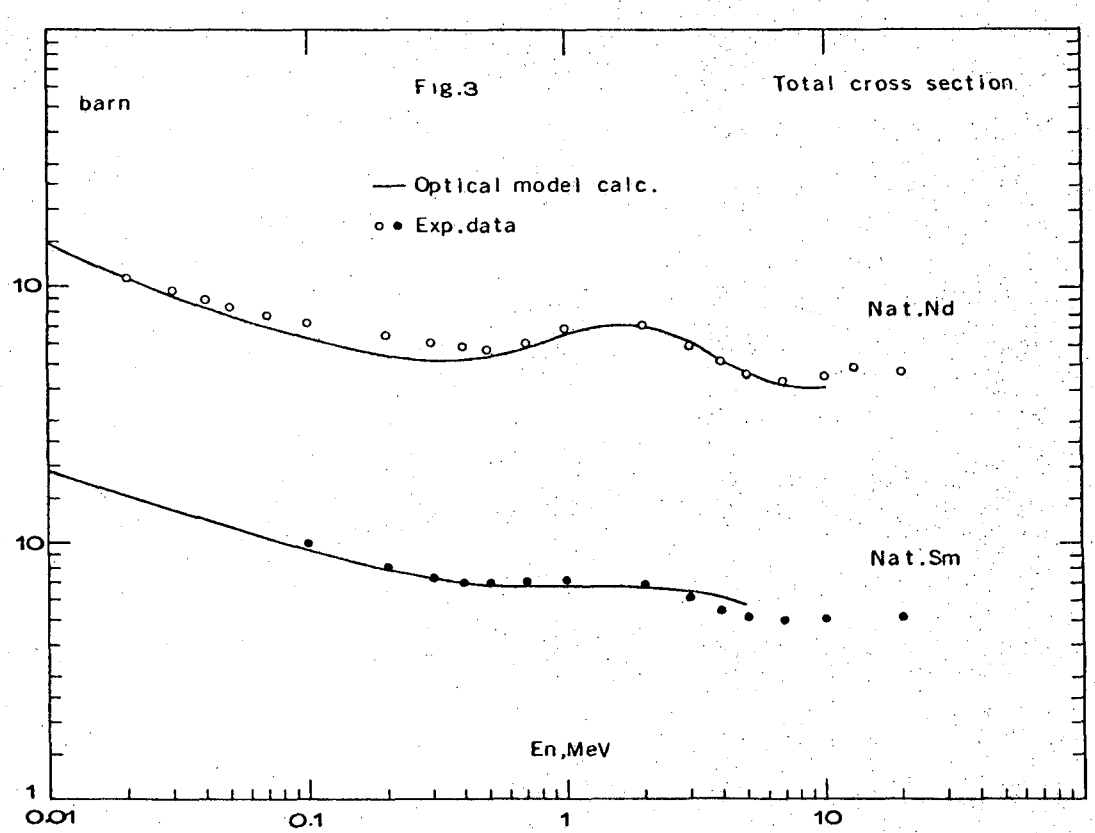


Fig. 3. Total cross sections of natural neodymium and samarium. Comparison of the present optical model calculation and experiment. Experimental data were read roughly from graphs in BNL-325, 3rd ed., vol. 2.

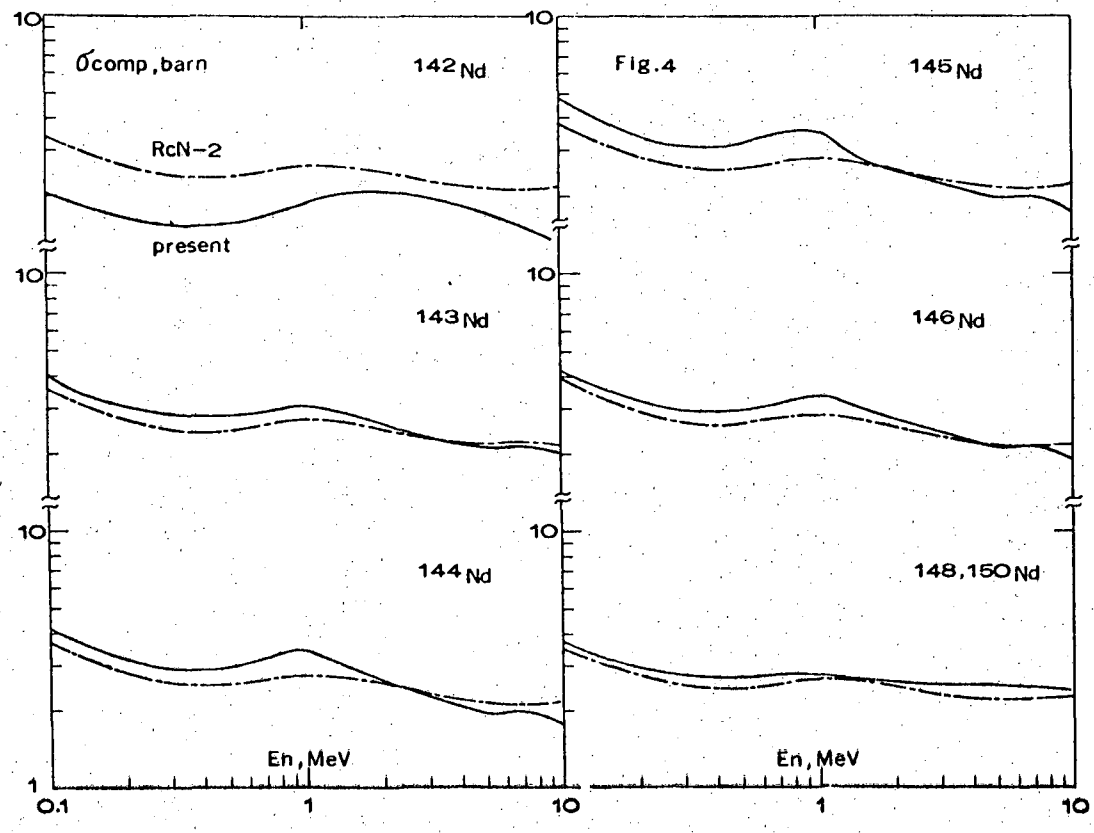


Fig. 4. Compound nucleus formation cross sections of Nd and Sm isotopes. Comparison of present optical model calculation with RCN-2 evaluated data.

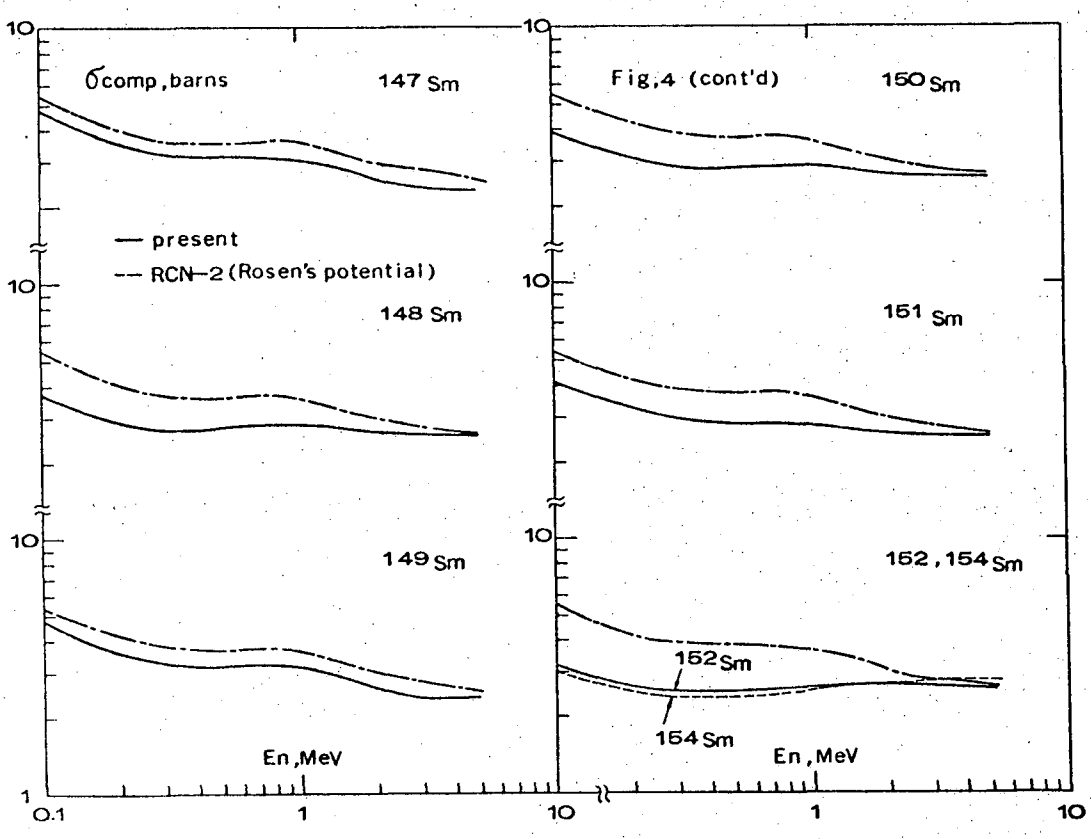


Fig. 4. (cont'd)

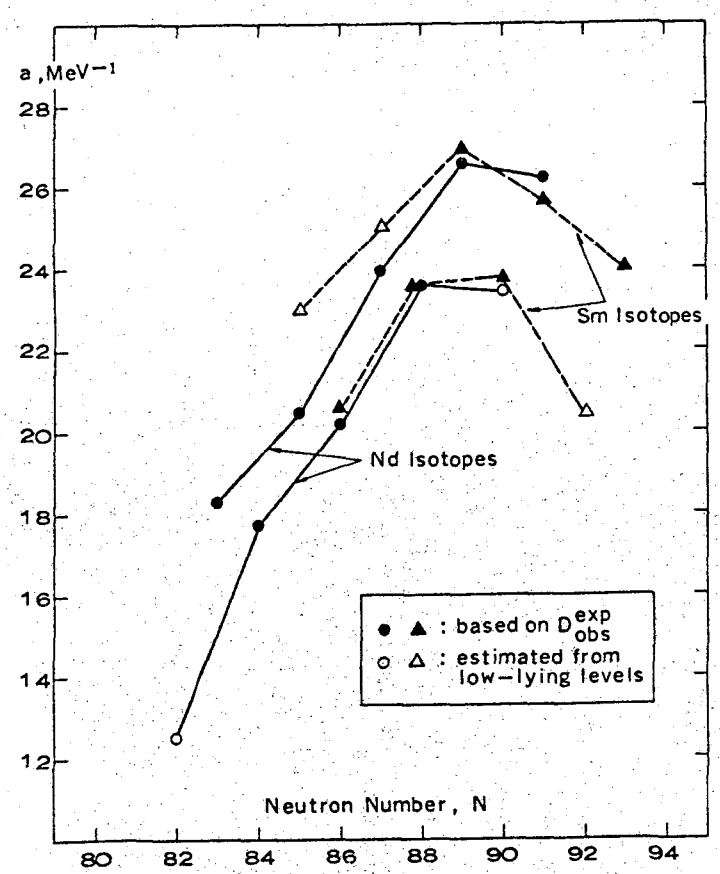


Fig. 5. Level density parameters a as a function of neutron number

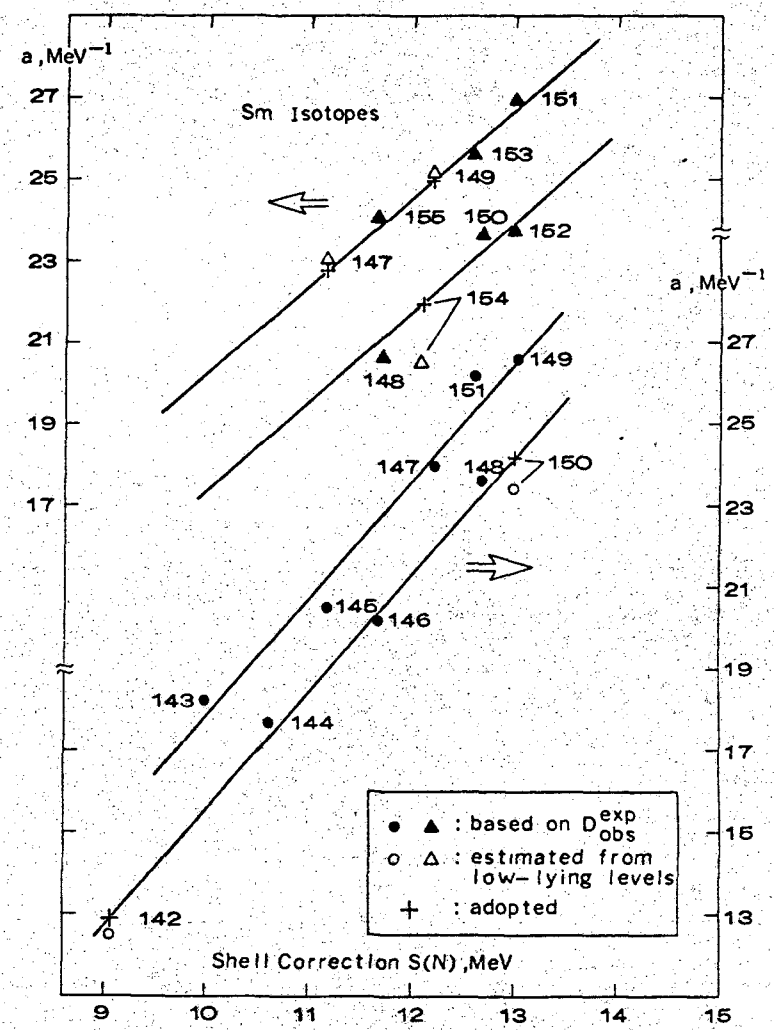


Fig. 6. Level density parameters a as a function of Cameron's shell correction energy

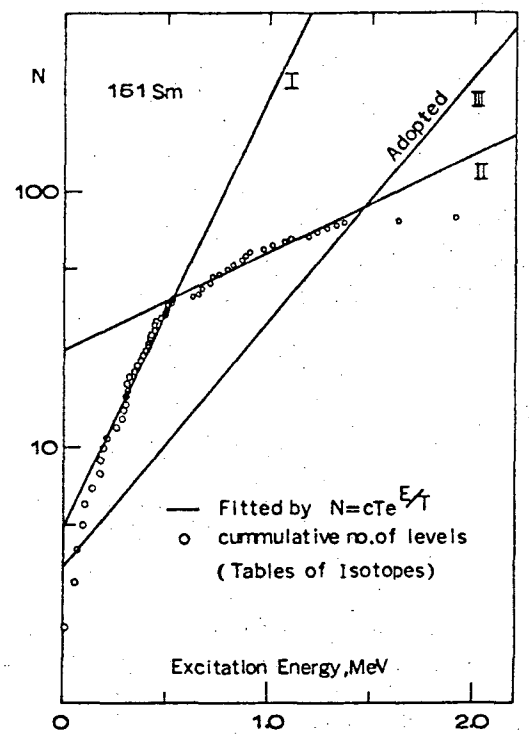


Fig. 7. Cumulative plot of number of low-lying levels of $^{151}$Sm with respect to excitation energy

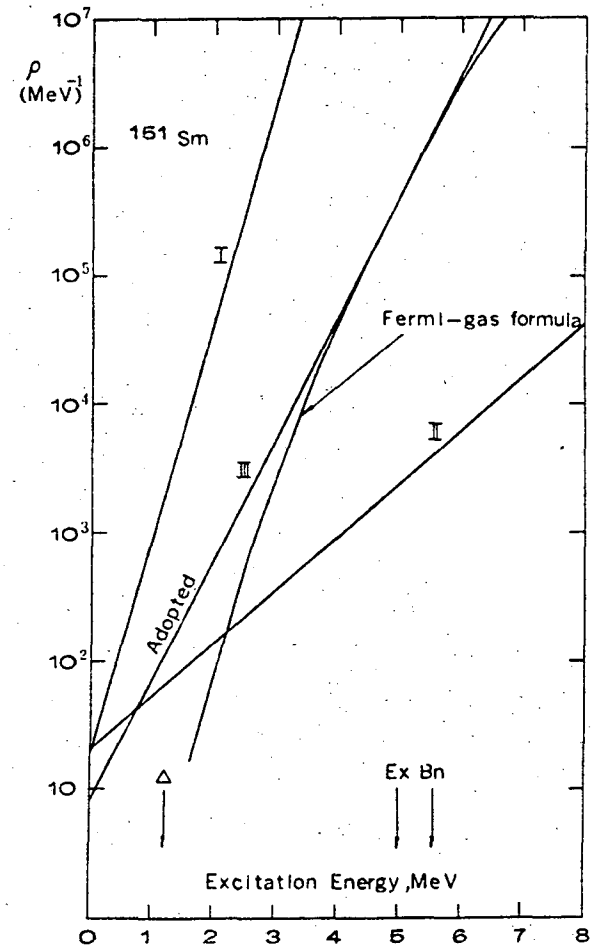


Fig. 8. Determination of level density of $^{151}$Sm. The most difficult case in obtaining smooth joining between constant temperature and Fermi-gas regions

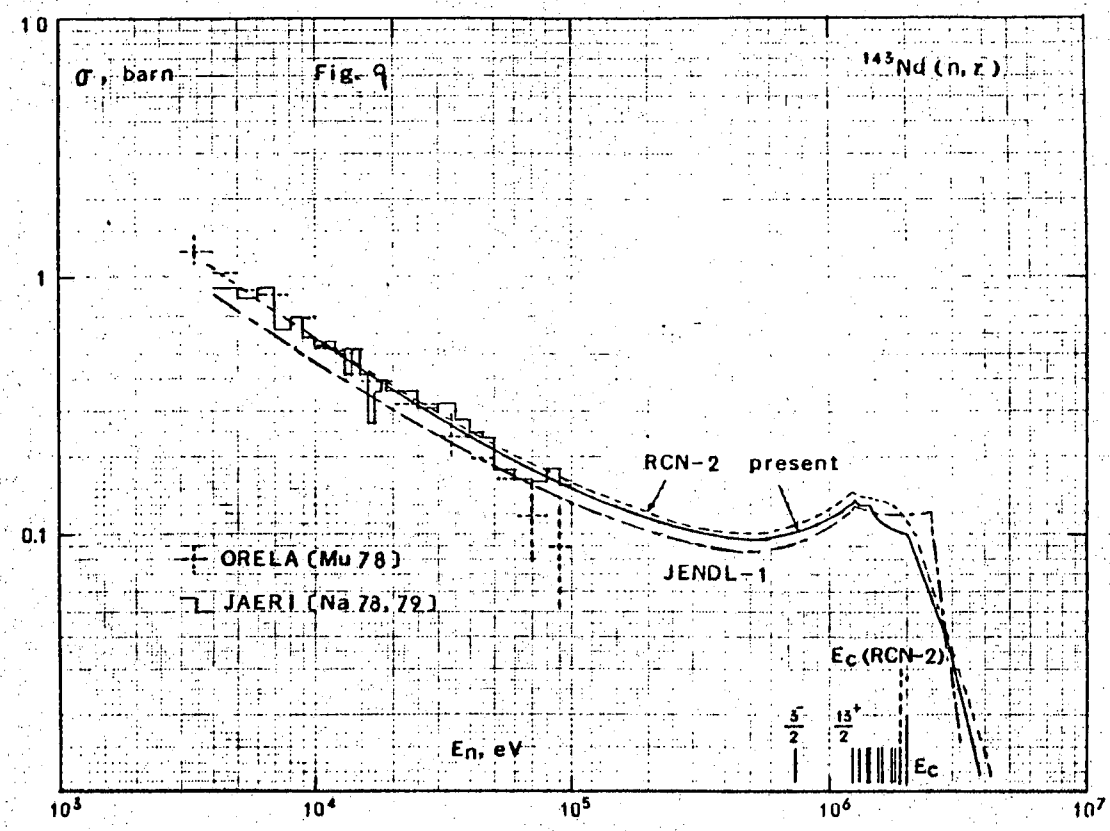
σ, barn
Fig. 9
$^{143}$Nd (n, γ)
RCN-2
present
JENDL-1
ORELA (Mu 78)
JAERI (Na 78, 79)
$E_c$ (RCN-2)
$E_c$
$E_n$, eV
10
1
0.1
$10^3$
$10^4$
$10^5$
$10^6$
$10^7$

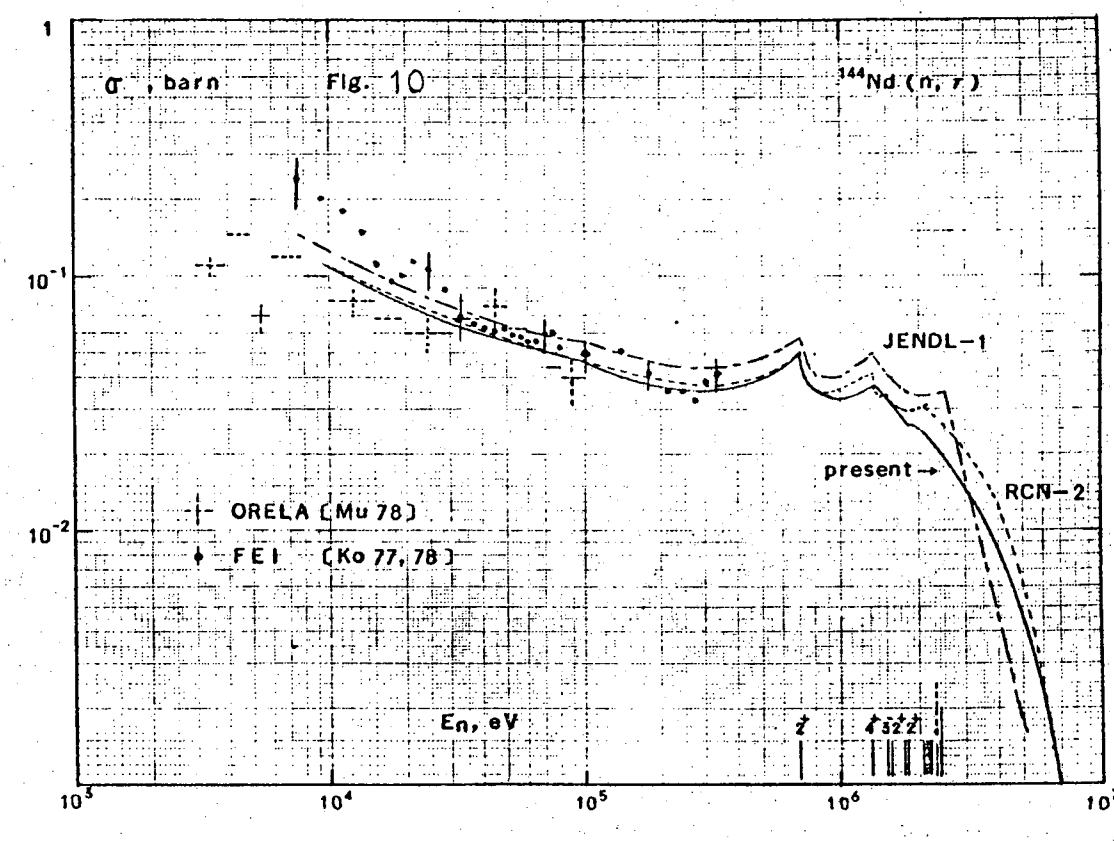
σ, barn
Fig. 10
$^{144}$Nd (n, γ)
JENDL-1
present
RCN-2
ORELA (Mu 78)
FEI (Ko 77, 78)
$E_n$, eV
1
$10^{-1}$
$10^{-2}$
$10^3$
$10^4$
$10^5$
$10^6$
$10^7$

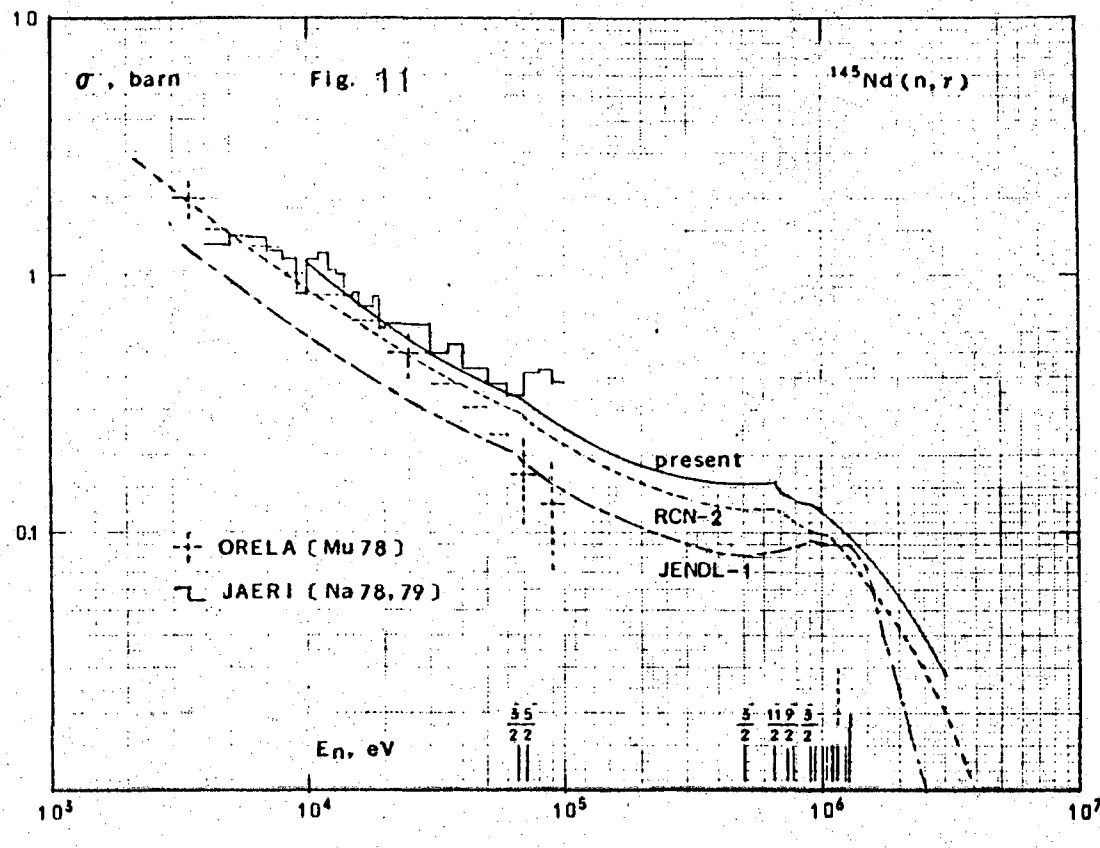
σ, barn
Fig. 11
145Nd (n, r)
present
RCN-2
JENDL-1
ORELA (Mu 78)
JAERI (Na 78, 79)
En, eV
10
1
0.1
10³
10⁴
10⁵
10⁶
10⁷

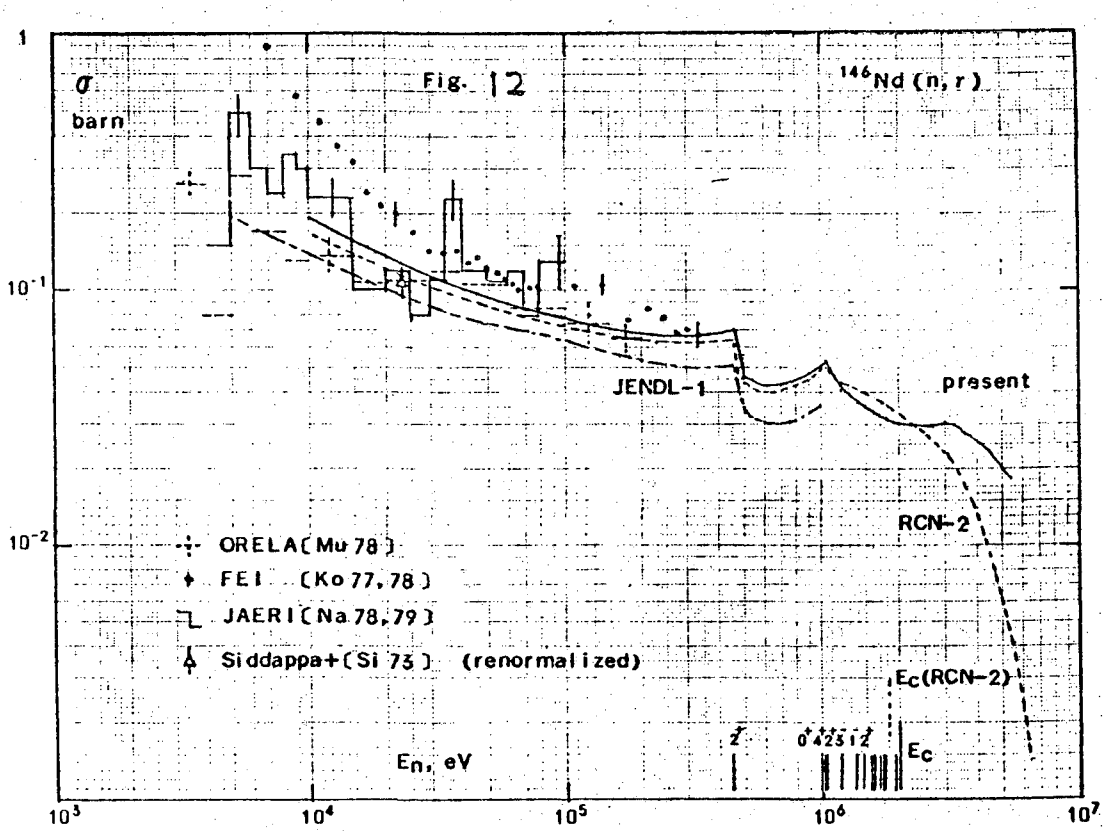
σ
barn
Fig. 12
146Nd (n, r)
JENDL-1
present
RCN-2
ORELA (Mu 78)
FEI (Ko 77, 78)
JAERI (Na 78, 79)
Siddappa+ (Si 73) (renormalized)
Ec(RCN-2)
Ec
En, eV
1
10⁻¹
10⁻²
10³
10⁴
10⁵
10⁶
10⁷

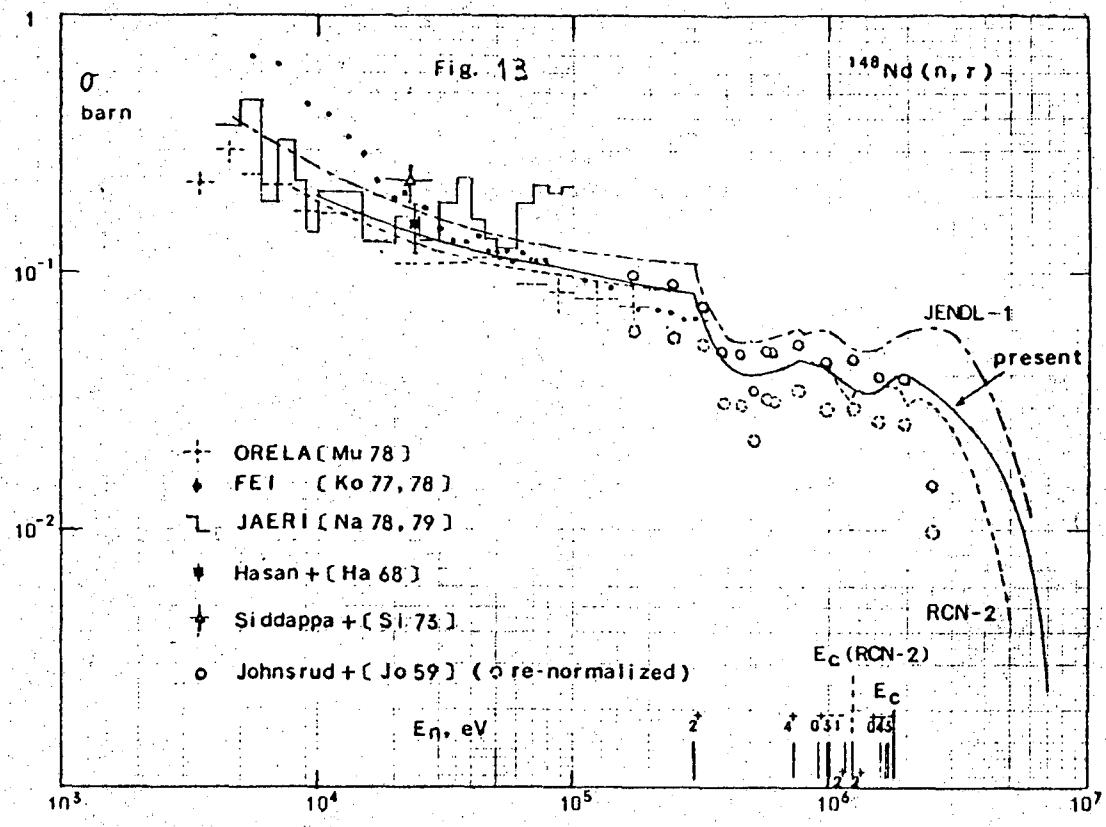
Fig. 13
$^{148}$Nd (n, γ)
σ
barn
JENDL-1
present
RCN-2
ORELA [Mu 78]
FEI [Ko 77, 78]
JAERI [Na 78, 79]
Hasan + [Ha 68]
Siddappa + [Si 73]
Johnsrud + [Jo 59] (○ re-normalized)
Ec (RCN-2)
Ec
En, eV

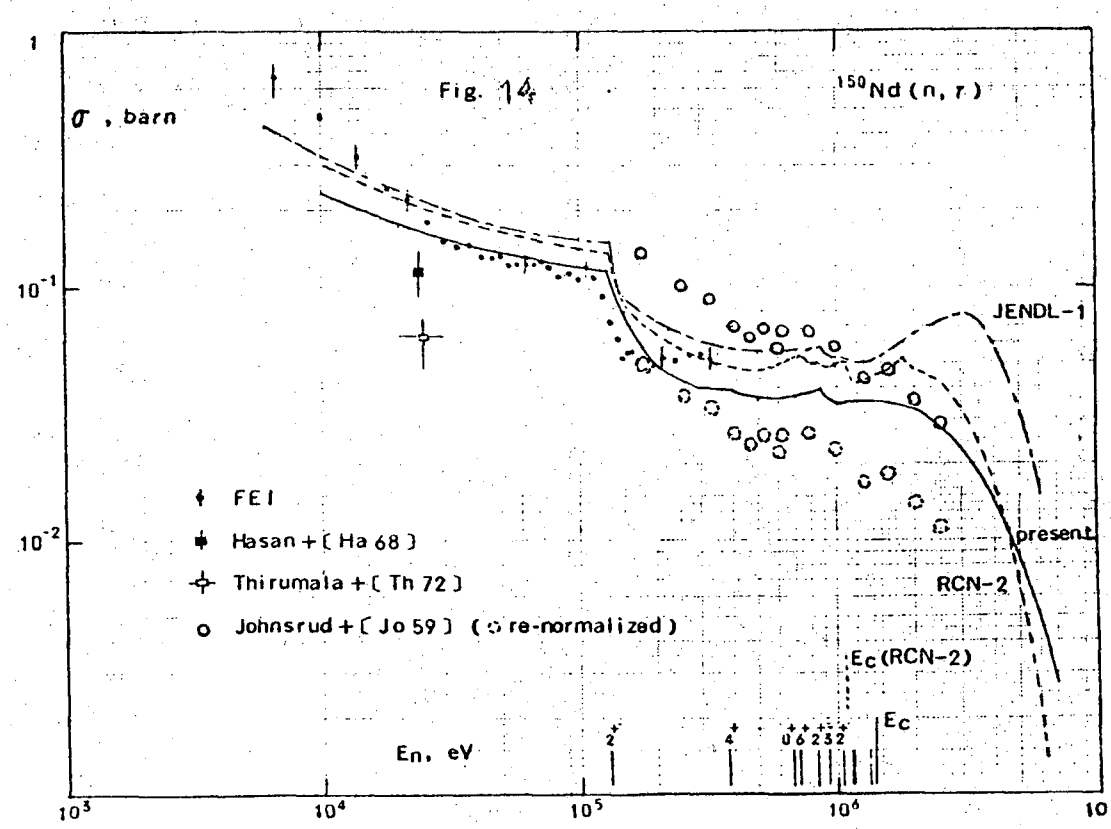
Fig. 14
$^{150}$Nd (n, γ)
σ , barn
JENDL-1
present
RCN-2
FEI
Hasan + [Ha 68]
Thirumala + [Th 72]
Johnsrud + [Jo 59] (○ re-normalized)
Ec (RCN-2)
Ec
En, eV

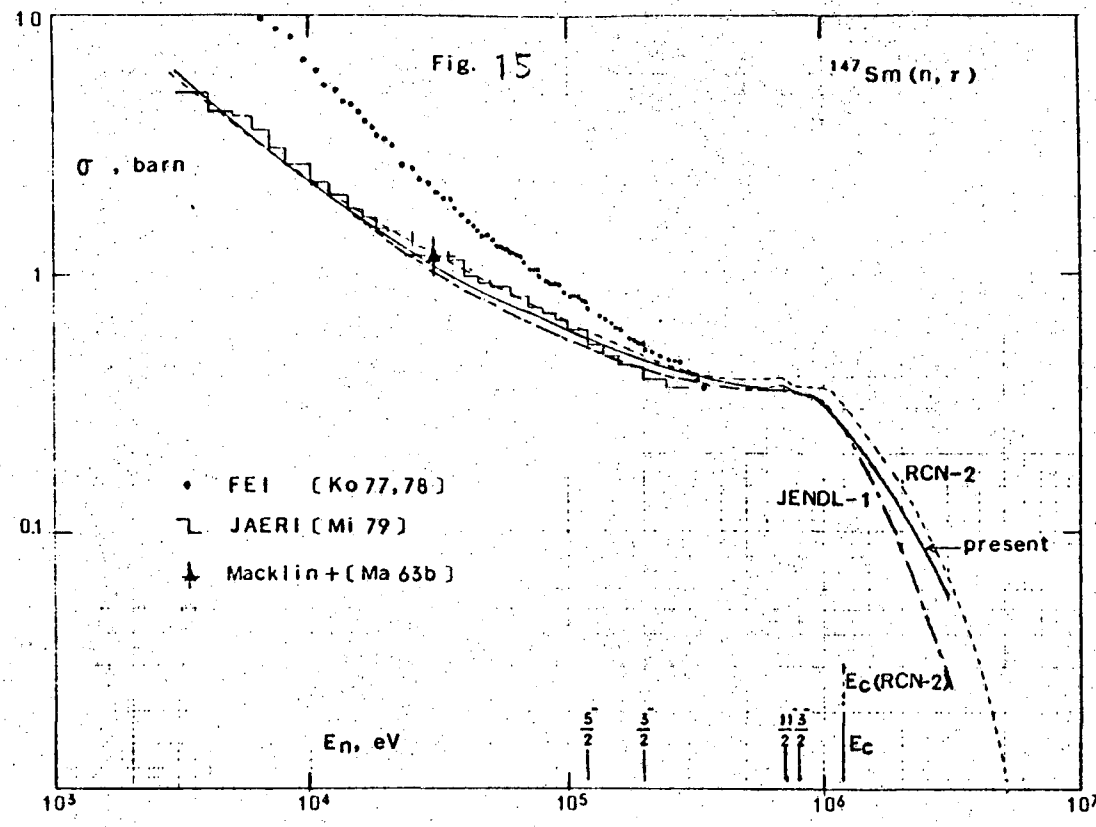
Fig. 15
$^{147}$Sm (n, γ)
σ , barn
FEI [Ko 77,78]
JAERI [Mi 79]
Macklin + [Ma 63b]
JENDL-1
RCN-2
present
Ec(RCN-2)
Ec
En, eV
10
1
0.1
10³
10⁴
10⁵
10⁶
10⁷

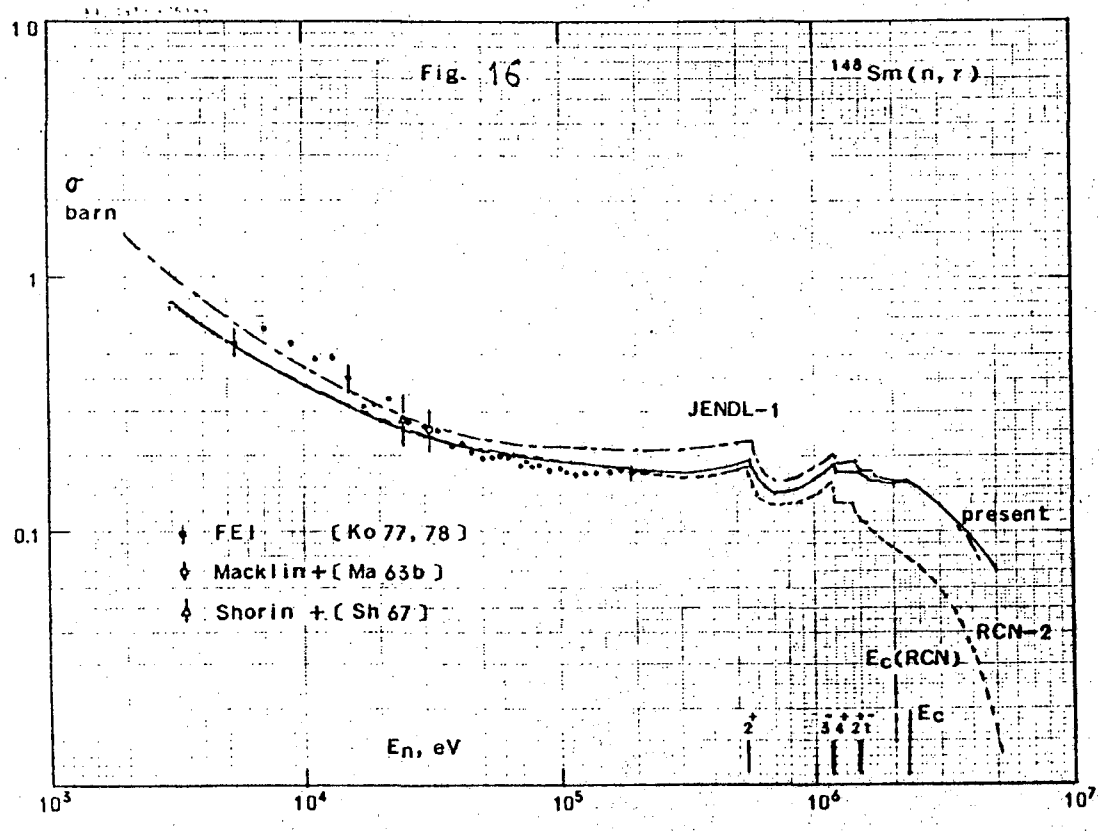
Fig. 16
$^{148}$Sm (n, γ)
σ
barn
JENDL-1
present
FEI [Ko 77, 78]
Macklin + [Ma 63b]
Shorin + [Sh 67]
RCN-2
Ec(RCN)
Ec
En, eV
10
1
0.1
10³
10⁴
10⁵
10⁶
10⁷

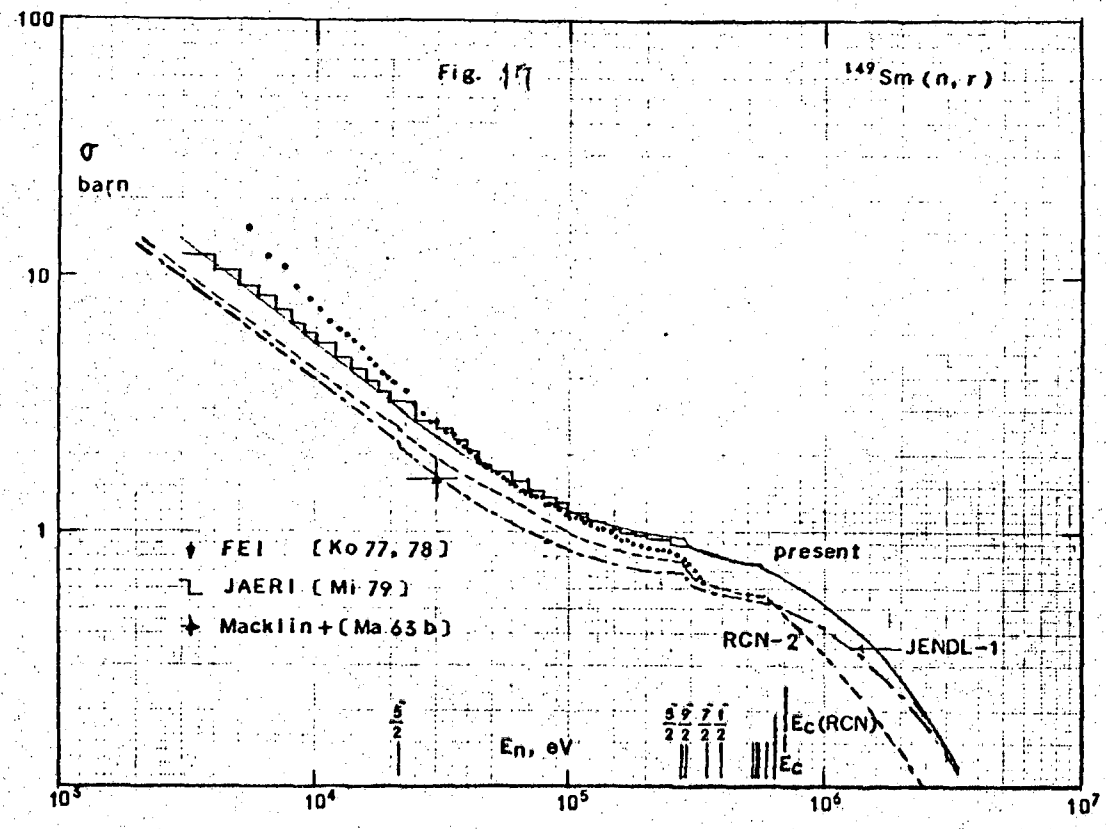
Fig. 17
$^{149}$Sm (n, r)
σ
barn
100
10
1
FEI [Ko 77, 78]
JAERI [Mi 79]
Macklin + [Ma 63 b]
present
RCN-2
JENDL-1
Ec(RCN)
Ec
En, eV
10³
10⁴
10⁵
10⁶
10⁷

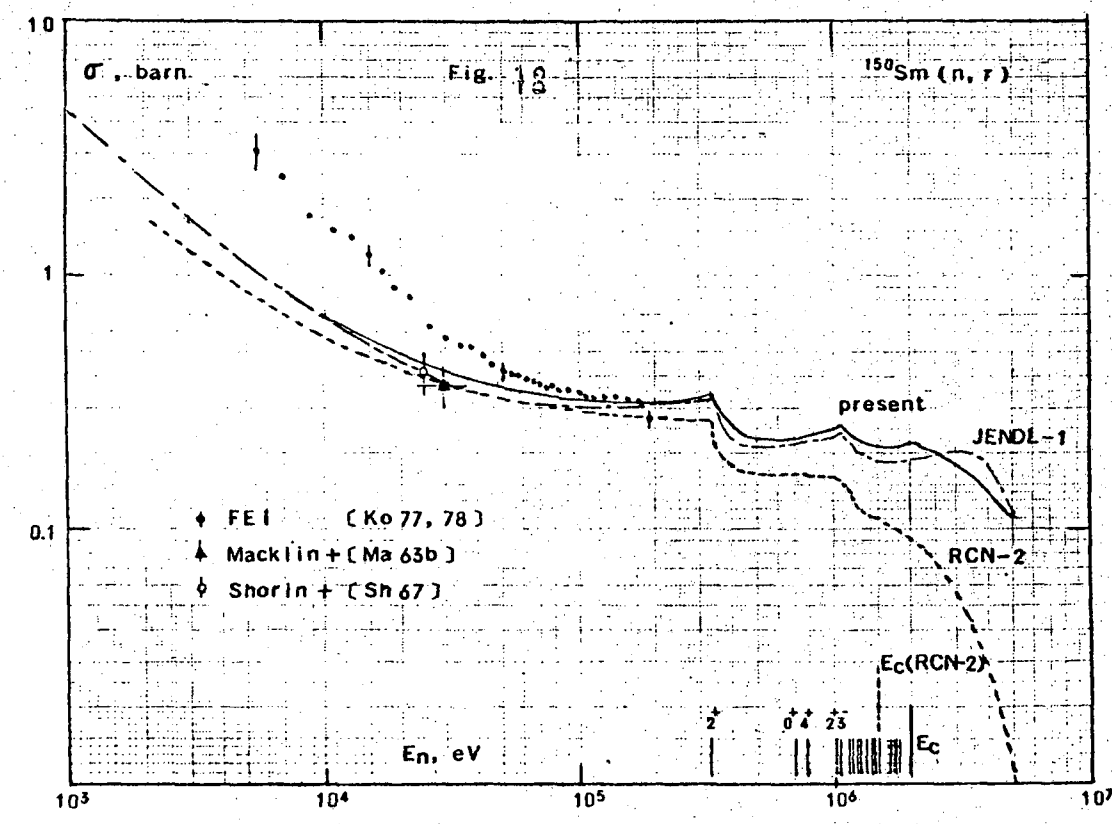
σ, barn
Fig. 18
$^{150}$Sm (n, r)
10
1
0.1
present
JENDL-1
RCN-2
FEI [Ko 77, 78]
Macklin + [Ma 63b]
Shorin + [Sh 67]
Ec(RCN-2)
Ec
En, eV
10³
10⁴
10⁵
10⁶
10⁷

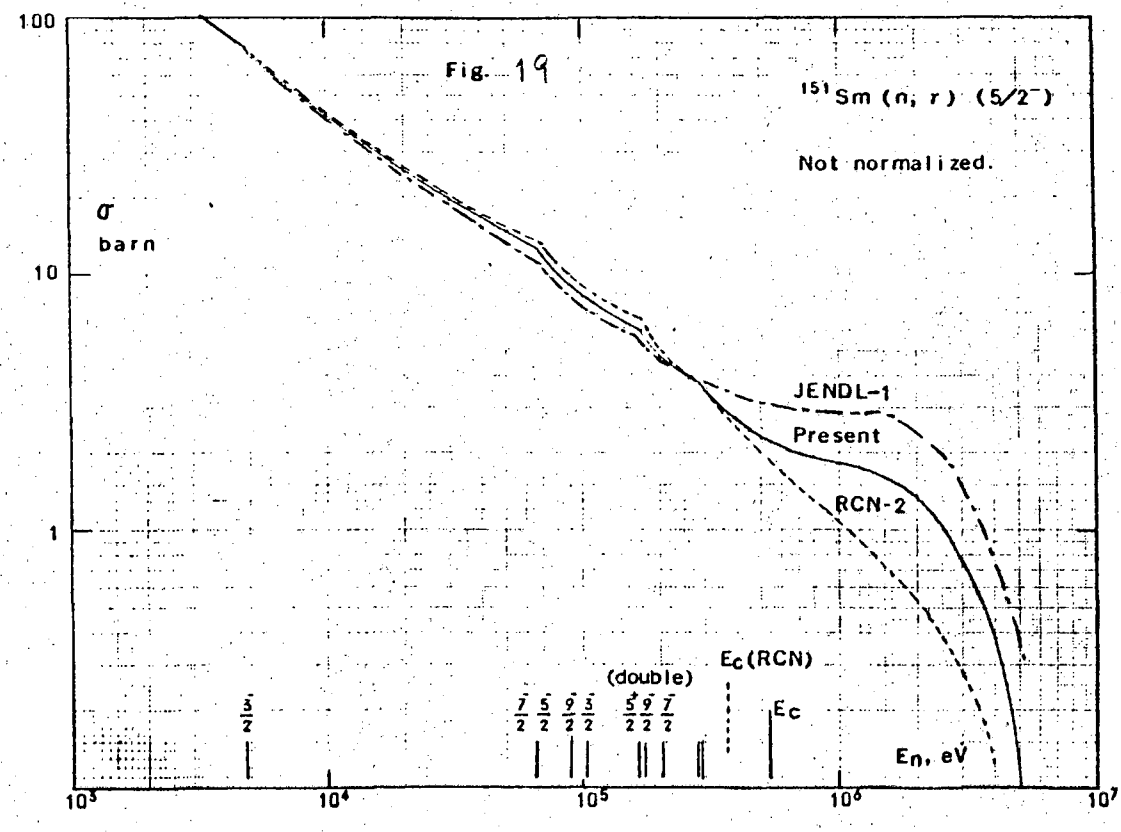
Fig. 19
$^{151}$Sm (n, r) (5/2$^-$)
Not normalized.
σ
barn
JENDL-1
Present
RCN-2
Ec(RCN)
(double)
Ec
En, eV
1.00
10
1
$10^3$
$10^4$
$10^5$
$10^6$
$10^7$

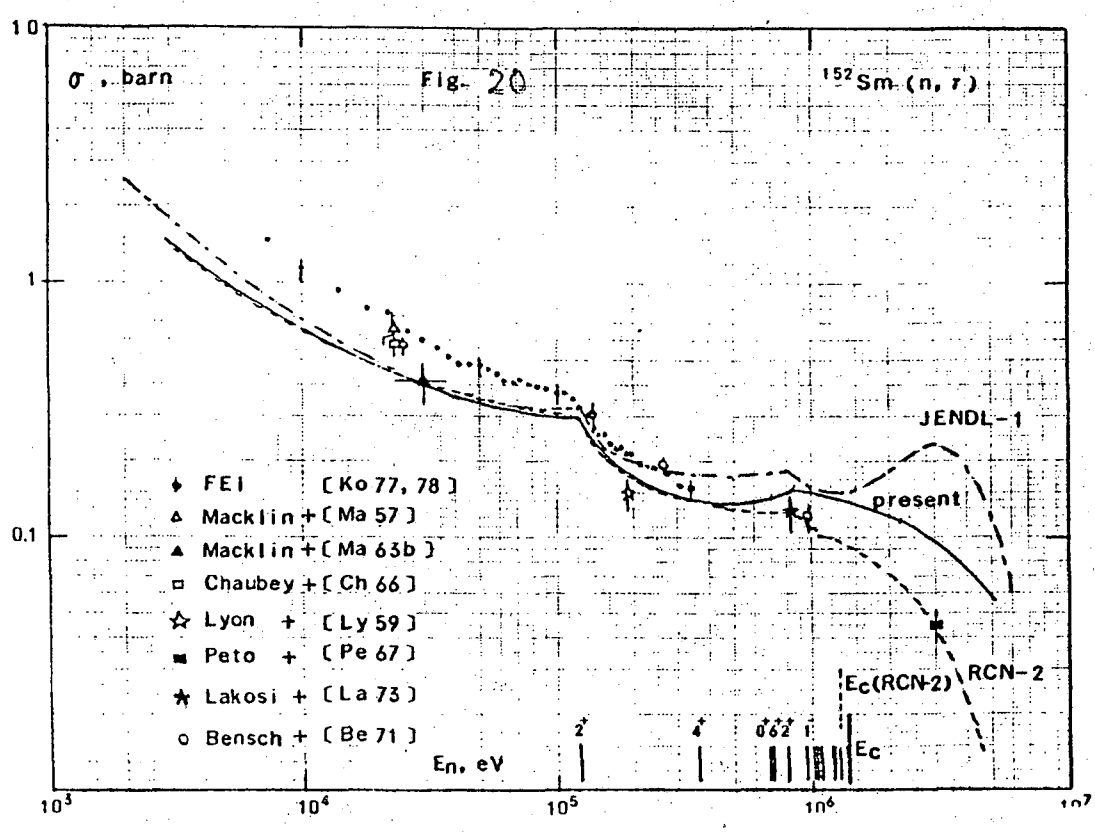
σ , barn
Fig. 20
$^{152}$Sm (n, r)
JENDL-1
present
RCN-2
Ec(RCN-2)
Ec
En, eV
FEI [Ko 77, 78]
Macklin + [Ma 57]
Macklin + [Ma 63b]
Chaubey + [Ch 66]
Lyon + [Ly 59]
Peto + [Pe 67]
Lakosi + [La 73]
Bensch + [Be 71]
10
1
0.1
$10^3$
$10^4$
$10^5$
$10^6$
$10^7$

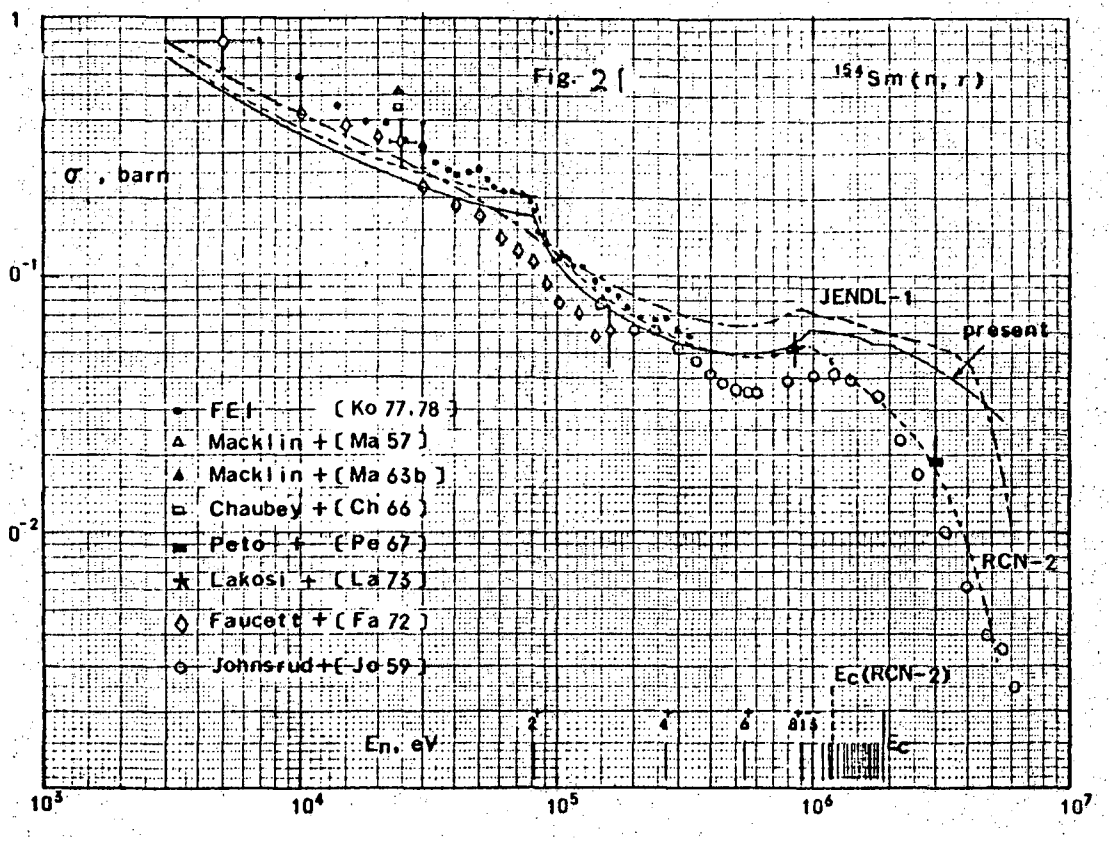
Fig. 2
$^{154}$Sm (n, γ)
σ , barn
1
$0^{-1}$
$0^{-2}$
JENDL-1
present
RCN-2
FEI (Ko 77.78)
Macklin + (Ma 57)
Macklin + (Ma 63b)
Chaubey + (Ch 66)
Peto + (Pe 67)
Lakosi + (La 73)
Faucett + (Fa 72)
Johnsrud + (Jo 59)
$E_c$(RCN-2)
$E_c$
$E_n$, eV
$10^3$
$10^4$
$10^5$
$10^6$
$10^7$

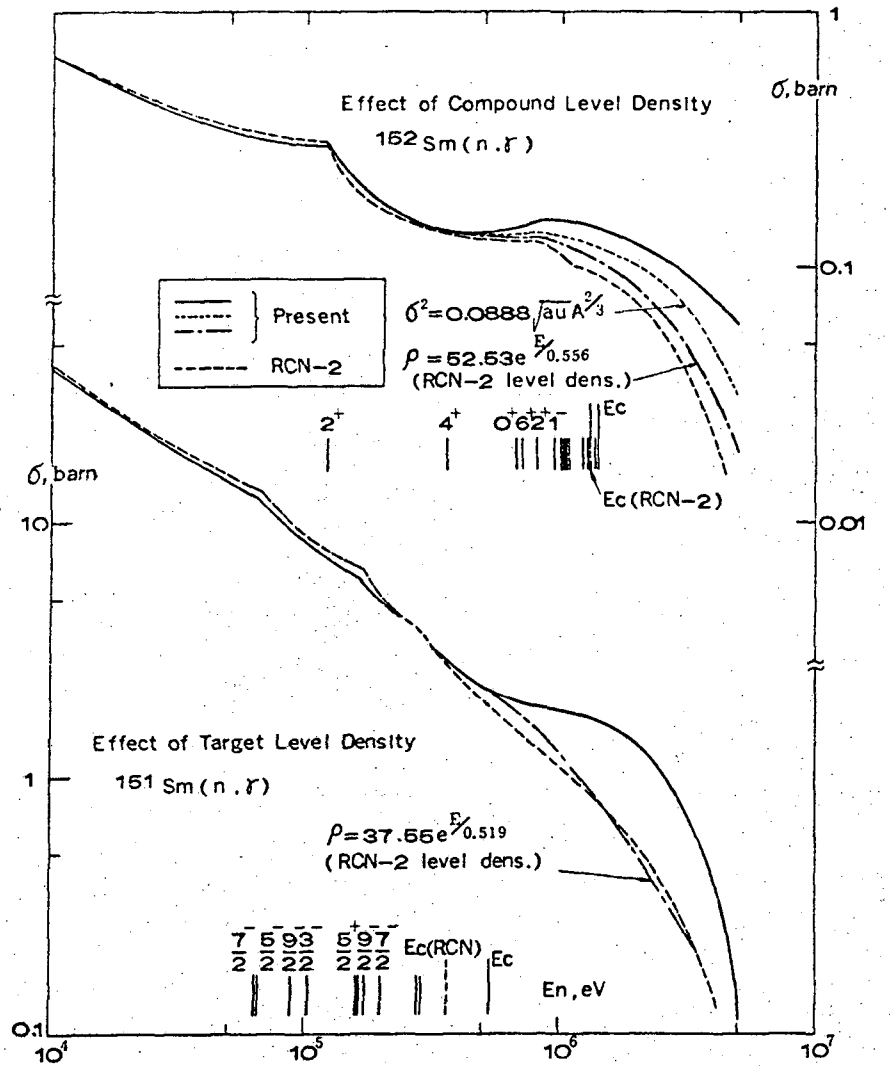


Fig. 22. The effect of level densities on capture cross section calculation. Upper figure shows the effect of compound nucleus level density on Sm-152 cross section. Lower figure shows the effect of target level density on Sm-151 cross section.

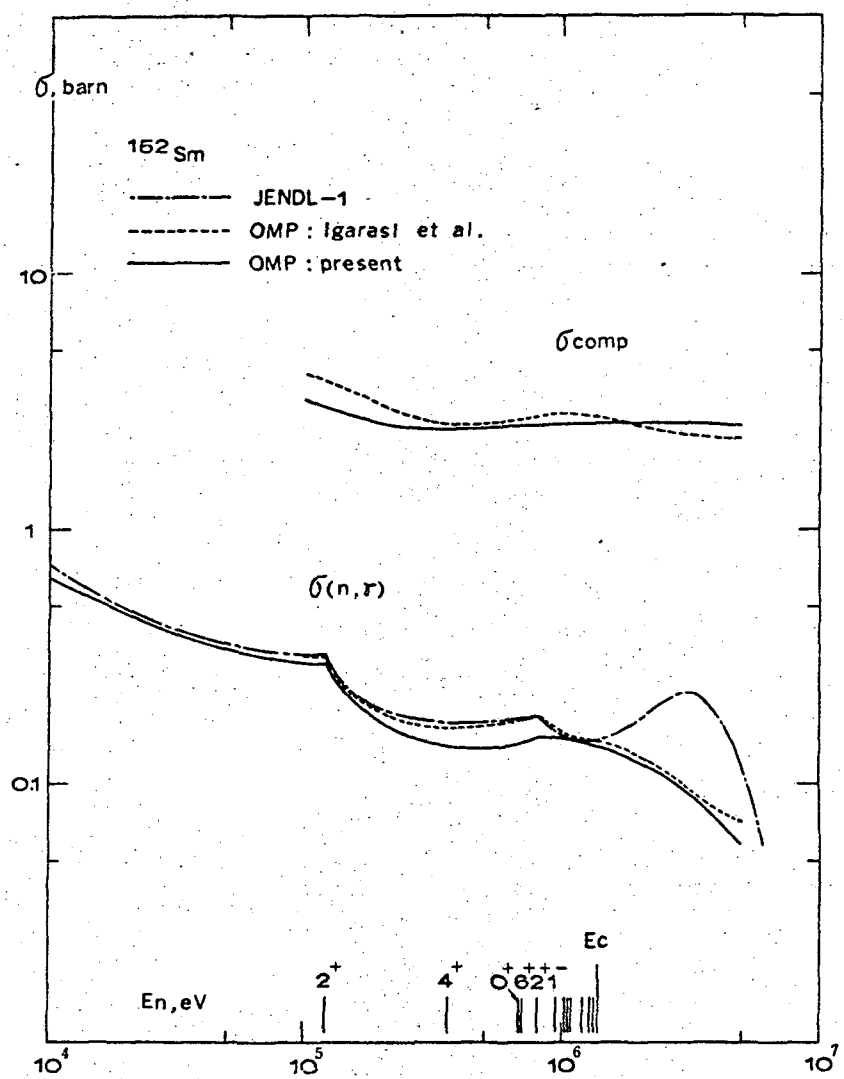


Fig. 23. The effect of optical model parameters on capture cross section calculation. Dotted line shows the calculation with optical potential of Igarasi et al.

# FISSION PRODUCT NUCLEAR DATA AT THE NEA DATA BANK

W.W. Osterhage, P.D. Johnston
NEA Data Bank/OECD
B.P. No.9(Bât.45)
F-91190 GIF sur YVETTE

The activities of the NEA Data Bank in storage and manipulation of nuclear data are briefly described with particular emphasis on recent neutron cross section data for fission products. The status and availability of evaluated and experimental data files is presented. The example of the 45-RH-103 (n, $\gamma$) cross section is used to illustrate a method of data condensation from the experimental data base to "best" values and the application of simplified covariance analysis. Comparison with available group cross sections is presented.

## INTRODUCTION

This presentation treats three different activities of the NEA Data Bank in the field of fission product cross sections data. Firstly, a brief introduction to our data centre is given with special regard to its history, the present role within the nuclear data community and the technical support available to it to fulfill its commitments.

In a second part we give a summary of the status of fission product capture cross section data, both experimental and evaluated, available from the Data Bank since the 1977 Petten meeting/1/. Our new computational output format will be described briefly.

A specific example, taking the 45-Rh-103 (n, $\gamma$) cross section, has been chosen to illustrate the possibilities of data condensation within our DBMS framework. "Best value" group cross sections are presented and compared with the corresponding data from LIB-IV.

Finally, the results of a simplified error covariance analysis will be given.

## THE NEA DATA BANK

In 1978 the NEA Data Bank of the OECD was created to take over the combined functions of the NDCC (Neutron Data Compilation Centre) in Saclay, France, and the CPL (Computer Program Library) in Ispra, Italy. The mandate of the Data

Bank includes the collection, compilation and distribution of nuclear data and the collection, verification and distribution of computer programs relevant to nuclear technology. Within the context of nuclear data activities, experimental and evaluated neutron data play the prominent role, although files containing charged particle induced reaction data, photonuclear and static nuclear data, such as decay - and nuclear structure data, are also available. In the neutron data field the most important single file is the EXFOR collection of experimental measurements with more than 3 million data points, jointly created according to geographic area, exchanged and continuously updated by the 4-Centre Network, comprising the Data Bank, NNDC in Brookhaven, the Nuclear Data Section of the IAEA and the CJD in Obninsk, USSR.

Among the evaluated files available from the Data Bank to laboratories in NEA member countries are ENDF/B-IV, parts of ENDF/B-V, UKNDL, KEDAK, JENDL-1, RCN-2 and the CNEN-CEA evaluations. A full list is available at this meeting.

With the creation of the NEA Data Bank a new computer system was installed on a DEC PDP-11/70, which serves as data base carrier and at the same time as satellite to the larger systems installed at the CISI (Compagnie Internationale de Service en Information) in Saclay. Bibliographic and numerical information is stored and administrated in a data base management system, DBMS-11.

## STATUS OF AVAILABLE FISSION PRODUCT CAPTURE CROSS SECTIONS

### a) Experimental data

Although the data collection at the Data Bank covers all types of neutron induced reactions, a selection has been made of only capture cross sections of fission product nuclei. Table I shows a general overview of the quantity of experimental fission product (n,$\gamma$) cross section data available in the Data Bank files. Priorities follow the assignments of Dr. S. Iijima at the 1977 Petten meeting/2/. Table II gives more detail of the new experimental data made available since the 1977 Petten meeting. Some of these data sets, although measured before 1977, have only recently been compiled and included in the EXFOR file. There are other data sets referenced in CINDA, but for which the numerical data has not yet been made available to the data centres; these are listed in Table V.

### b) Evaluated data

Table III lists briefly the main evaluated FPND-libraries made available to the Data Bank after 1977. The most recent material is the ENDF/B-V fission product data library.

### c) Computational format

Whereas the evaluated data will usually be presented and used in their format of origin, ENDF/B, UKNDL, KEDAK etc., the data from the EXFOR file is often inconvenient for manipulation and graphical display. A format more suited for the users has been developed, similar in philosophy and structure to the NEUDADA format, but improved to allow better handling of increasingly complex measured data. Computer printouts are always in the EXFOR - format itself, but for large quantities of data the user requires a "computational format" for data processing. Here the basic criteria are: single line with sorting keys, fixed data fields and a unique set of units. Although the number of fields is theoretically unrestricted, initially only cross section data are converted with the four main fields "Energy", "Energy-Error", "Cross Section" and "Cross Section Error". Additional fields are reserved for "Standard Cross Section", "Angle" and "Secondary Energy" to extend the scope of the format to more complex data sets, such as angular distributions and double differential cross sections. A detailed description of the format is available from the Data Bank.

## 45-Rh-103 (n, $\gamma$) GROUP CROSS SECTION CALCULATION AND ERROR COVARIANCE ANALYSIS

Part of the work of the NEA Data Bank includes the collection and distribution of computer codes used in many aspects of nuclear technology. This includes computer codes for nuclear model calculations and for the handling of both experimental and evaluated nuclear data. As the quantity of experimental data on nuclear cross sections increases year by year it becomes more important for the Data Bank to collect and distribute code packages providing convenient and acceptable mehtods for data evaluators and reactor physicists to manipulate and condense the large quantities of experimental data.

In recent years there has been a growing interest from reactor physics in a more complete description of uncertainties related to evaluated cross sections. This has been reflected in the extensive inclusion of data uncertainties and uncertainty covariances in the new ENDF/B-V file. The work in Europe is more diversive, with some uncertainty covariance information produced in connection with adjustment of differential data to integral experiments, in shielding studies and in fission product capture.

Differential cross section measurements do of course themselves contain correlations between uncertainties at different energies and to some extent between different reaction channels. Attempts have been made by Dr.Perey in ORNL and by Prof. Vonach in Vienna to prepare cross section uncertainty correlation matrices from a careful study of experimental data alone. The Data Bank has invited both Prof. Vonach and Dr.Perey to provide code packages for implementation at the Data Bank, and which will be made available to other users in our member countries. The code package of Prof. Vonach has been implemented at the Data Bank by Dr. Tagesen, and modified to accept input in the "computational format" produced directly by retrievals from the experimental data base. The techniques of data manipulation are described in detail for threshold reactions in PHY-D 13-1/3/, but are also applicable to any smoothly varying cross section. As an example we have chosen 45-Rh-103 (n, $\gamma$).

After retrieving all available data sets for this particular reaction from the data base, obviously wrong data and sets not carrying error columns are eliminated, and the remainder, if necessary, renormalised to improved standards. The group structure within the energy range available is dependent on data set overlap and cross section variation. The calculation proceeds in two steps: 1) Approximate derivation of excitation function by calculating the average within each group, weighted with the inverse of the squared errors. 2) The slope of this preliminary excitation function serves for the renormalisation of all cross section values to the respective group center, and the resulting new values for the calculation of the final evaluated cross section. Fig. 1 shows the graphical results without, fig. 2 the same cross section with error bands. Fig. 3 shows a comparison with the LIB-IV/4/ group cross sections.

A further stage in analysis allows a covariance matrix to be generated: Table IV. The correlations between energies are derived essentially from the degree to which the quoted uncertainties on each measurement reflect systematic and normalisation uncertainties. A documentation of these codes and the codes themselves are available from the Data Bank on request.

There are significant differences in the approaches of Prof. Vonach and Dr.Perey, not only in the mathematical approximations used, but also in the degree to which inter-reaction correlations are considered. We hope that it will be possible to provide both code packages from the Data Bank in the near future. Uncertainty correlations in differential cross section measurements are of course only one source of information; constraints from nuclear model calculations and integral measurements are equally important, but in the effort to meet the stringent uncertainty requirements in data requests all available information must be fully used.

## CONCLUSIONS

The activities of the NEA Data Bank in all areas, including that of fission product cross section data depend on the cooperation of data measures, evaluators and reactor physicists. The Data Bank is not only a distribution centre but also relys on feedback from data evaluators and reactor physicists, who use data and computer codes, and on data measurers to provide readily up-to-date information. Table V constitutes a "wish" list of new measurements for which data is not yet available at the data centres. This list is based partly on a selection from CINDA/5/ made by Dr. S. Igarasi/6/ and distributed to all data centres in July 1979: we count on your assistance to help us reduce the length of this list.

## ACKNOWLEDGEMENT

We gratefully appreciate the effort of Dr. E. Sartori, who extracted the required LIB-IV information for us from the main file.

## REFERENCES

/1/ 2nd IAEA Advisory Group Meeting on FPND, Petten, Netherlands, Sept.1977.

/2/ S. Iijima, IAEA-213, p.279, in /1/.

/3/ S. Tagesen et al. Physics Data, No. 13-1, 1979.

/4/ R.B. Kidman et al., LA-6260-MS, March 1976.

/5/ CINDA, An Index to the Literature on Microscopic Neutron Data, IAEA, 1979.

/6/ S. Igarasi, priv. communication, Memo 4-C 2/108 June 1979.

TABLE I

Experimental Fission Product (n, $\gamma$) Cross Section Data Sets, Currently Available in EXFOR.

| Isotope | No. of Data Sets | Priority |
|---|---|---|
| 33-As-75 | 20 | |
| 35-Br-79 | 14 | |
| 35-Br-81 | 15 | |
| 35-Kr-78 | 1 | |
| 36-Kr-80 | 5 | |
| 36-Kr-82 | 3 | |
| 36-Kr-83 | 1 | |
| 36-Kr-84 | 5 | 1 |
| 36-Kr-85 | 2 | |
| 36-Kr-86 | 3 | |
| 37-Rb-85 | 13 | |
| 37-Rb-87 | 8 | |
| 38-Sr-88 | 5 | |
| 39-Y-89 | 26 | |
| 40-Zr-90 | 4 | |
| 40-Zr-91 | 6 | 1 |
| 40-Zr-92 | 4 | 1 |
| 40-Zr-94 | 13 | |
| 40-Zr-96 | 9 | 1 |
| 41-Nb-93 | 15 | 1 |
| 41-Nb-94 | 5 | 3 |
| 41-Nb-95 | 1 | |
| 42-Mo-92 | 6 | |
| 42-Mo-94 | 3 | |
| 42-Mo-95 | 2 | |
| 42-Mo-96 | 4 | |
| 42-Mo-97 | 2 | 1 |
| 42-Mo-98 | 22 | |
| 42-Mo-100 | 15 | |
| 44-Ru-96 | 4 | |
| 44-Ru-98 | 1 | |
| 44-Ru-99 | 1 | |
| 44-Ru-100 | 2 | |
| 44-Ru-101 | 3 | 1 |
| 44-Ru-102 | 7 | |
| 44-Ru-104 | 10 | 1 |
| 44-Ru-105 | 1 | |
| 44-Ru-106 | 1 | |
| 45-Rh-103 | 28 | |
| 46-Pd-102 | 1 | |
| 46-Pd-104 | 1 | |
| 46-Pd-105 | 2 | 1 |
| 46-Pd-106 | 4 | |
| 46-Pd-108 | 15 | |
| 46-Pd-110 | 8 | |
| 47-Ag-107 | 17 | |
| 47-Ag-109 | 18 | |
| 48-Cd-106 | 2 | |
| 48-Cd-108 | 4 | |
| 48-Cd-110 | 7 | |
| 48-Cd-112 | 4 | |

Table I (Contd)

| Isotope | No. of Data Sets | Priority |
|---|---|---|
| 48-Cd-114 | 7 | |
| 48-Cd-116 | 11 | |
| 49-In-113 | 8 | |
| 49-In-115 | 43 | |
| 50-Sn-116 | 3 | |
| 50-Sn-117 | 2 | |
| 50-Sn-118 | 2 | |
| 50-Sn-119 | 2 | |
| 50-Sn-120 | 5 | |
| 50-Sn-122 | 9 | |
| 50-Sn-124 | 12 | |
| 51-Sb-121 | 21 | |
| 51-Sb-123 | 15 | |
| 52-Te-122 | 5 | |
| 52-Te-123 | 3 | |
| 52-Te-124 | 4 | |
| 52-Te-125 | 3 | |
| 52-Te-126 | 7 | |
| 52-Te-128 | 10 | |
| 52-Te-130 | 13 | |
| 53-I-127 | 42 | |
| 54-Xe-124 | 5 | |
| 54-Xe-125 | 1 | |
| 54-Xe-126 | 4 | |
| 54-Xe-128 | 4 | |
| 54-Xe-129 | 1 | |
| 54-Xe-130 | 4 | |
| 54-Xe-131 | 2 | 1 |
| 54-Xe-132 | 4 | |
| 54-Xe-133 | 1 | |
| 54-Xe-134 | 4 | |
| 54-Xe-135 | 4 | |
| 54-Xe-136 | 4 | |
| 55-Cs-133 | 26 | 1 |
| 55-Cs-134 | 1 | |
| 55-Cs-135 | 2 | 1 |
| 56-Ba-134 | 6 | |
| 56-Ba-135 | 3 | |
| 56-Ba-136 | 6 | |
| 56-Ba-137 | 1 | |
| 56-Ba-138 | 19 | |
| 57-La-139 | 25 | |
| 58-Ce-136 | 2 | |
| 58-Ce-138 | 5 | |
| 58-Ce-140 | 12 | |
| 58-Ce-141 | 1 | |
| 58-Ce-142 | 13 | |
| 58-Ce-144 | 1 | 1 |
| 59-Pr-141 | 23 | |
| 60-Nd-142 | 5 | |
| 60-Nd-143 | 5 | 1 |
| 60-Nd-144 | 4 | |
| 60-Nd-145 | 5 | 1 |
| 60-Nd-146 | 9 | |
| 60-Nd-147 | 2 | |

Table I (Contd)

| Isotope | No. of Data Sets | Priority |
|---|---|---|
| 60-Nd-148 | 10 | |
| 60-Nd-150 | 8 | |
| 61-Pm-147 | 8 | 1 |
| 61-Pm-148 | 4 | |
| 61-Pm-149 | 1 | |
| 61-Pm-151 | 1 | |
| 62-Sm-144 | 3 | |
| 62-Sm-145 | 1 | |
| 62-Sm-147 | 4 | 1 |
| 62-Sm-148 | 3 | |
| 62-Sm-149 | 6 | 1 |
| 62-Sm-150 | 3 | |
| 62-Sm-151 | 3 | 1 |
| 62-Sm-152 | 10 | |
| 62-Sm-153 | 1 | |
| 62-Sm-154 | 11 | |
| 63-Eu-151 | 18 | 1 |
| 63-Eu-152 | 1 | |
| 63-Eu-153 | 8 | 1 |
| 63-Eu-154 | 1 | |
| 63-Eu-155 | 1 | 2 |
| 64-Gd-152 | 1 | |
| 64-Gd-154 | 6 | |
| 64-Gd-155 | 4 | |
| 64-Gd-156 | 2 | 1 |
| 64-Gd-157 | 5 | |
| 64-Gd-158 | 10 | 1 |
| 64-Gd-160 | 7 | 1 |
| 65-Tb-159 | 13 | |

TABLE II

Fission Product Capture Cross Section Data made available to the NEA Data Bank after 1977 (Priority 1)

| Isotope | E-Range | No. Data Points | Author | Laboratory | Year of Publ. |
|---|---|---|---|---|---|
| 40-Zr-91 | 0.1-20KeV | resonance parameters | Brusegan + | Geel | 1978 |
| | 3-200KeV | 15 | Musgrove + | Lucas Heights | 1978 |
| 40-Zr-92 | 3-200KeV | 15 | Musgrove + | Lucas Heights | 1978 |
| 40-Zr-96 | 1MeV | 1 | Dezso + | Debrecen | 1977 |
| 41-Nb-93 | 2.6 - 700KeV | 521 | Macklin | ORNL | 1976 |
| | 24 KeV | 1 | Yamamuro + | Kyoto | 1978 |
| 42-Mo-97 | 3-200KeV | 15 | Musgrove + | Lucas Heights | 1978 |
| 44-Ru-101 | 6.6-71KeV | 434 | Hockenbury + | Rennsselaer | 1975 |
| 44-Ru-104 | 17-71KeV | 164 | Hockenbury + | Rennsselaer | 1975 |
| 46-Pd-105 | 6.3-300KeV | 562 | Hockenbury + | Rennsselaer | 1975 |
| | 3-200KeV | 15 | Musgrove + | Lucas Heights | 1978 |
| 55-Cs-133 | thermal | 1 | Takine + | JAERI | 1978 |
| | 24KeV | 1 | Yamamuro + | Kyoto | 1978 |
| 60-Nd-143 | 3-100KeV | 13 | Musgrove + | Lucas Heights | 1978 |
| 60-Nd-145 | 6.6-71KeV | 434 | Hockenbury + | Rennsselaer | 1975 |
| | 3-100KeV | 13 | Musgrove + | Lucas Heights | 1978 |
| 62-Sm-147 | thermal | 1 | Eiland + | Knolls | 1974 |
| 62-Sm-149 | 6.6-71KeV | 434 | Hockenbury + | Rennsselaer | 1975 |
| 63-Eu-151 | thermal | 1 | Ryves + | Teddington | 1971 |

TABLE III

Evaluated FPND - Libraries Available At the NEA Data Bank After 1977

1. CNEN-CEA Preliminary Fission Product Cross Sections in ENDF/B Format, 63 Nuclides, 73812 Log. Rec. (Bologna/Saclay, 1978)

2. CEN Fission Product Decay Data (Blachot et al.), 699 Nuclides, 21867 log. rec. (Grenoble, 1978)

3. Tobias Fission Product Decay Data in ENDF/B Format, 836 Nuclides, 25143 Data Records (CEGB/UK, 1978)

4. ENDF/B-V Fission Product Data, 32000 log. rec. (BNL, 1979)

5. JNDC-FFP-WG, Fission Product Cross Sections, 62 Nuclides, in ENDF/B Format (Japan, 1977)

6. RCN-2, Fission Product Cross Sections, 37 Nuclides, 149069 Data Records (ECN, 1977)

## TABLE IV

### Relative Covariance Matrix for 45-Rh-103 (n, $\gamma$)

Correlations given in %

| | | | | | | | | | | | | | | | | | | | | |
|---|---|---|---|---|---|---|---|---|---|---|---|---|---|---|---|---|---|---|---|---|
| 1 | 0 | 0 | 0 | 0 | 0 | 0 | 0 | 0 | 0 | 0 | 0 | 0 | 0 | 0 | 0 | 0 | 0 | 0 | 0 | 0 |
| 2 | | 100 | 35 | 37 | 38 | 38 | 39 | 38 | 39 | 38 | 37 | 29 | 4 | 7 | 9 | 7 | 6 | 0 | 0 | 0 |
| 3 | | | 100 | 40 | 39 | 37 | 38 | 39 | 39 | 40 | 40 | 39 | 12 | 21 | 25 | 20 | 17 | 0 | 0 | 0 |
| 4 | | | | 100 | 40 | 38 | 39 | 40 | 40 | 40 | 40 | 37 | 10 | 18 | 22 | 17 | 14 | 0 | 0 | 0 |
| 5 | | | | | 100 | 38 | 40 | 40 | 40 | 40 | 40 | 36 | 9 | 16 | 13 | 15 | 12 | 0 | 0 | 0 |
| 6 | | | | | | 100 | 38 | 38 | 38 | 38 | 38 | 32 | 7 | 12 | 15 | 12 | 10 | 0 | 0 | 0 |
| 7 | | | | | | | 100 | 40 | 40 | 40 | 39 | 34 | 7 | 14 | 16 | 13 | 11 | 0 | 0 | 0 |
| 8 | | | | | | | | 100 | 40 | 40 | 40 | 36 | 9 | 17 | 19 | 16 | 13 | 0 | 0 | 0 |
| 9 | | | | | | | | | 100 | 40 | 40 | 35 | 8 | 15 | 17 | 14 | 11 | 0 | 0 | 0 |
| 10 | | | | | | | | | | 100 | 40 | 37 | 9 | 17 | 20 | 17 | 14 | 0 | 0 | 0 |
| 11 | | | | | | | | | | | 100 | 37 | 10 | 18 | 22 | 17 | 14 | 0 | 0 | 0 |
| 12 | | | | | | | | | | | | 100 | 15 | 27 | 32 | 26 | 21 | 0 | 0 | 0 |
| 13 | | | | | | | | | | | | | 100 | 25 | 17 | 14 | 11 | 0 | 0 | 0 |
| 14 | | | | | | | | | | | | | | 100 | 35 | 28 | 26 | 0 | 0 | 0 |
| 15 | | | | | | | | | | | | | | | 100 | 32 | 28 | 0 | 0 | 0 |
| 16 | | | | | | | | | | | | | | | | 100 | 38 | 5 | 0 | 0 |
| 17 | | | | | | | | | | | | | | | | | 100 | 5 | 0 | 0 |
| 18 | | | | | | | | | | | | | | | | | | 100 | 28 | 0 |
| 19 | | | | | | | | | | | | | | | | | | | 100 | 0 |
| 20 | | | | | | | | | | | | | | | | | | | | 0 |

| | | | | | | | | | | | | | | | | | | |
|---|---|---|---|---|---|---|---|---|---|---|---|---|---|---|---|---|---|---|
| 0 | 0 | 0 | 0 | 0 | 0 | 0 | 0 | 0 | 0 | 0 | 0 | 0 | 0 | 0 | 0 | 0 | 0 | 0 |
| . | . | . | . | . | . | . | . | . | . | . | . | . | . | . | . | . | . | . |
| 1 | 1 | 1 | 2 | 2 | 3 | 3 | 4 | 4 | 5 | 5 | 6 | 6 | 1 | 2 | 4 | 8 | 2 | 1 |
| 0 | 4 | 3 | 0 | 5 | 0 | 5 | 0 | 5 | 0 | 5 | 0 | 5 | 2 | 1 | 0 | 0 | 0 | 3 |
| 0 | 7 | 6 | 1 | 1 | 0 | 1 | 1 | 1 | 1 | 1 | 1 | 0 | 3 | 9 | 0 | 0 | 0 | 6 |
| E | E | E | E | E | E | E | E | E | E | E | E | E | E | E | E | E | E | E |
| - | + | + | + | + | + | + | + | + | + | + | + | + | + | + | + | + | + | + |
| 0 | 0 | 0 | 0 | 0 | 0 | 0 | 0 | 0 | 0 | 0 | 0 | 0 | 0 | 0 | 0 | 0 | 0 | 0 |
| 4 | 4 | 5 | 5 | 5 | 5 | 5 | 5 | 5 | 5 | 5 | 5 | 5 | 6 | 6 | 6 | 6 | 7 | 8 |

TABLE V

Outstanding Requests for Capture Cross Section Data of Fission Products at the NEA Data Bank

| Isotope | Author | Laboratory |
|---|---|---|
| 36-Kr-84 | | KfK |
| 36-Kr-86 | | KfK |
| 37-Rb-87 | Murty | Waltair |
| 38-Sr-86 | Musgrove | Lucas Heights |
| 38-Sr-86 | Murty | Waltair |
| 38-Sr-86 | Vanpraet | ORNL |
| 38-Sr-87 | Vanpraet | ORNL |
| 38-Sr-88 | Vanpraet | ORNL |
| 39- Y -89 | Czirr | Livermore |
| 40-Zr-91 | Macklin | ORNL |
| 42-Mo-95 | Hockenbury | Rennsselaer |
| 42-Mo-97 | Hockenbury | Rennsselaer |
| 42-Mo-98 | Murty | Waltair |
| 42-Mo-98 | Scoville | Idaho Falls |
| 42-Mo-99 | Musgrove | Lucas Heights |
| 42-Mo-100 | Murty | Waltair |
| 42-Mo-100 | Weigmann | ORNL |
| 43-Tc-99 | Adamchuk | Kurchatov |
| 44-Ru-96 | Murty | Waltair |
| 44-Ru-102 | Murty | Waltair |
| 44-Ru-103 | Hasan | Aligarh (India) |
| 44-Ru-103 | Poenitz | Argonne |
| 44-Ru-103 | Tromp | Idaho Falls |
| 44-Ru-104 | Murty | Waltair |
| 46-Pd-105 | Macklin | ORNL |
| 46-Pd-107 | Singh | Rennsselaer |
| 47-Ag-107 | Muradjan | Kurchatov |
| 47-Ag-109 | Muradjan | Kurchatov |
| 48-Cd-110 | Thirumala | Waltair |
| 48-Cd-114 | Herman | Warsaw |
| 48-Cd-116 | Herman | Warsaw |
| 48-Cd-Isot. | Hla-Pe | Lucas Heights |
| 49-In-113 | Murty | Waltair |
| 49-In-115 | Grady | Michigan Univ. |

Table V (Contd)

| Isotope | Author | Laboratory |
|---|---|---|
| 49-In-115 | Konov | Obninsk |
| 49-In-115 | Murty | Waltair |
| 49-In-115 | Temperley | Aberdeen, USA |
| 49-In-115 | Thirumala | Waltair |
| 49-In-115 | Tromp | Idaho Falls |
| 50-Sn-122 | Murty | Waltair |
| 51-Sb-123 | Stamatelatos | Columbia Univ. |
| 52-Te-130 | Thirumala | Waltair |
| 53-I-127 | Chatuverdi | Vanarasi (India) |
| 53-I-127 | Hasan | Aligarh (India) |
| 53-I-127 | Rohr | Geel |
| 53-I-127 | Shorin | Obninsk |
| 54-Xe-124 | Kane | BNL |
| 55-Cs-133 | Murty | Waltair |
| 55-Cs-137 | Anderl | Idaho Falls |
| 56-Ba-138 | Potokar | Ljubljana |
| 56-Ba-138 | Sidappa | Waltair |
| 57-La-139 | Ngo-Quoc Buu | Dubna |
| 58-Ce-140 | Bergquist | Lund |
| 58-Ce-140 | Sidappa | Waltair |
| 58-Ce-141 | Chatuverdi | Waltair |
| 58-Ce-142 | Scoville | Idaho Falls |
| 59-Pr-141 | Feigenbaum | Rennsselaer |
| 60-Nd-142 | Kononov | Obninsk |
| 60-Nd-146 | Kononov | Obninsk |
| 60-Nd-146 | Sidappa | Waltair |
| 60-Nd-148 | Kononov | Obninsk |
| 60-Nd-148 | Sidappa | Waltair |
| 60-Nd-150 | Kononov | Obninsk |
| 60-Nd-Isot. | Nakajima | JAERI |

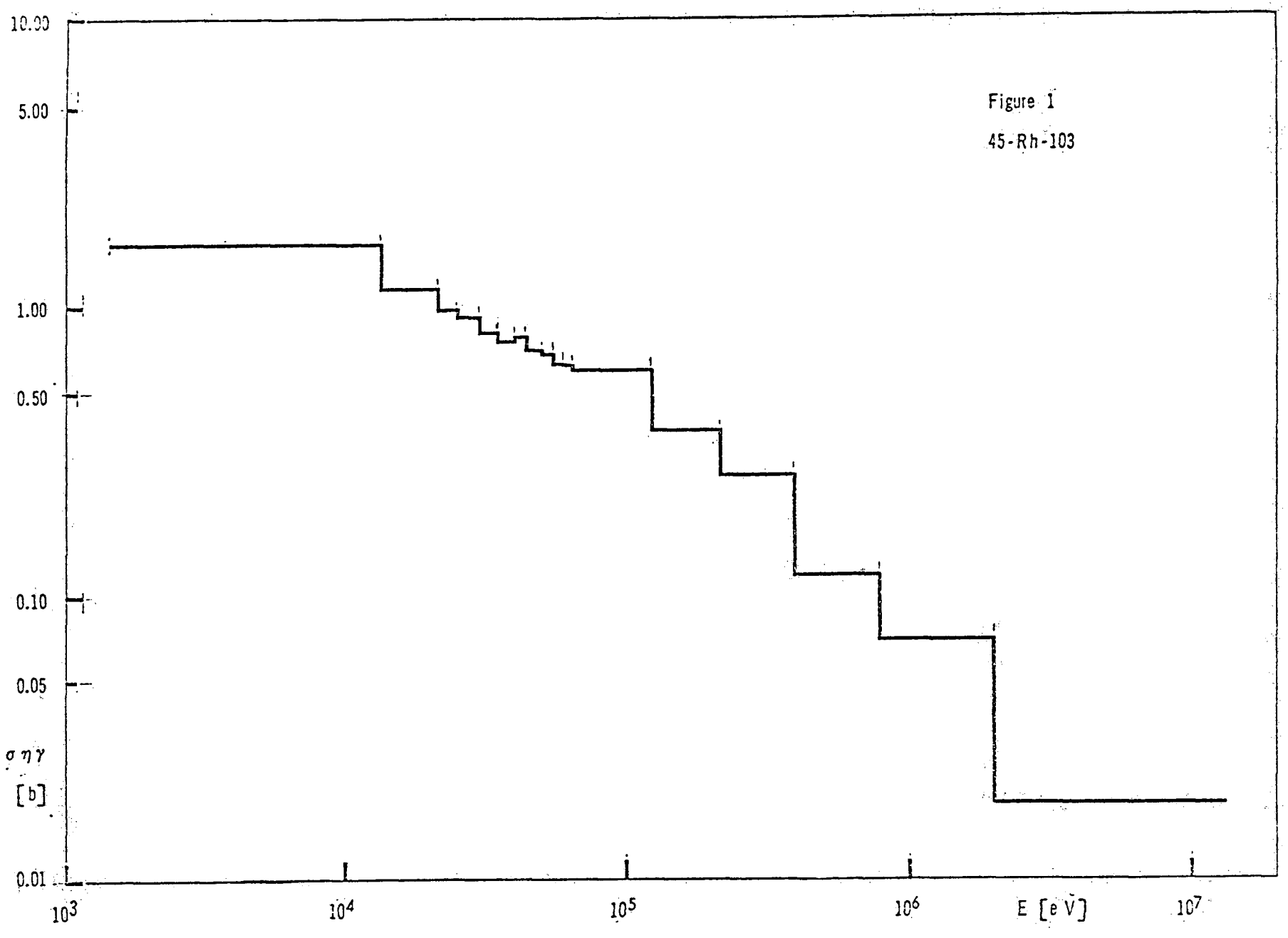
Figure 1
45-Rh-103
10.00
5.00
1.00
0.50
0.10
0.05
0.01
σ ηγ
[b]
10^3
10^4
10^5
10^6
10^7
E [eV]

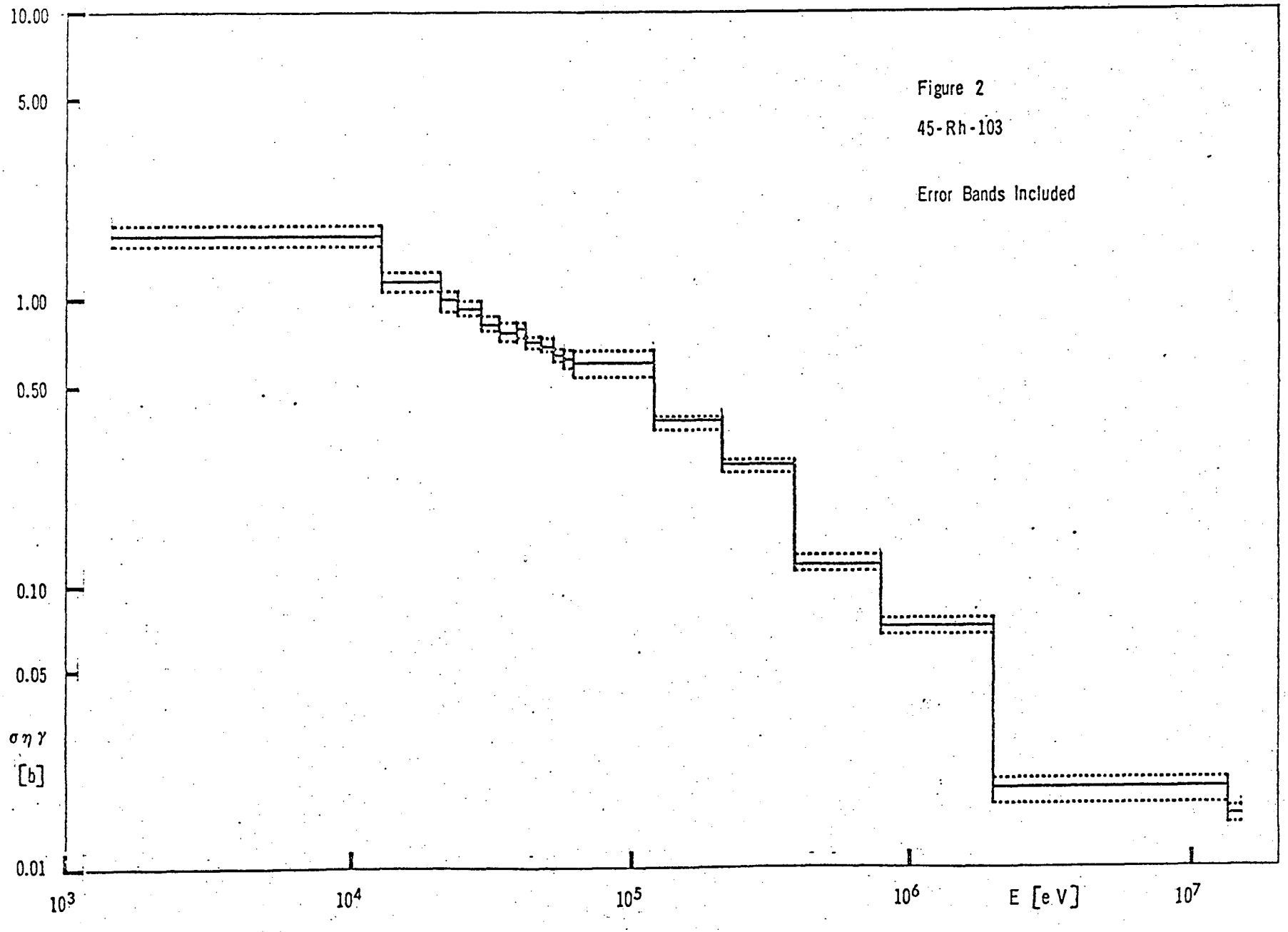
Figure 2
45-Rh-103
Error Bands Included
10.00
5.00
1.00
0.50
0.10
0.05
0.01
σηγ
[b]
10³
10⁴
10⁵
10⁶
10⁷
E [eV]

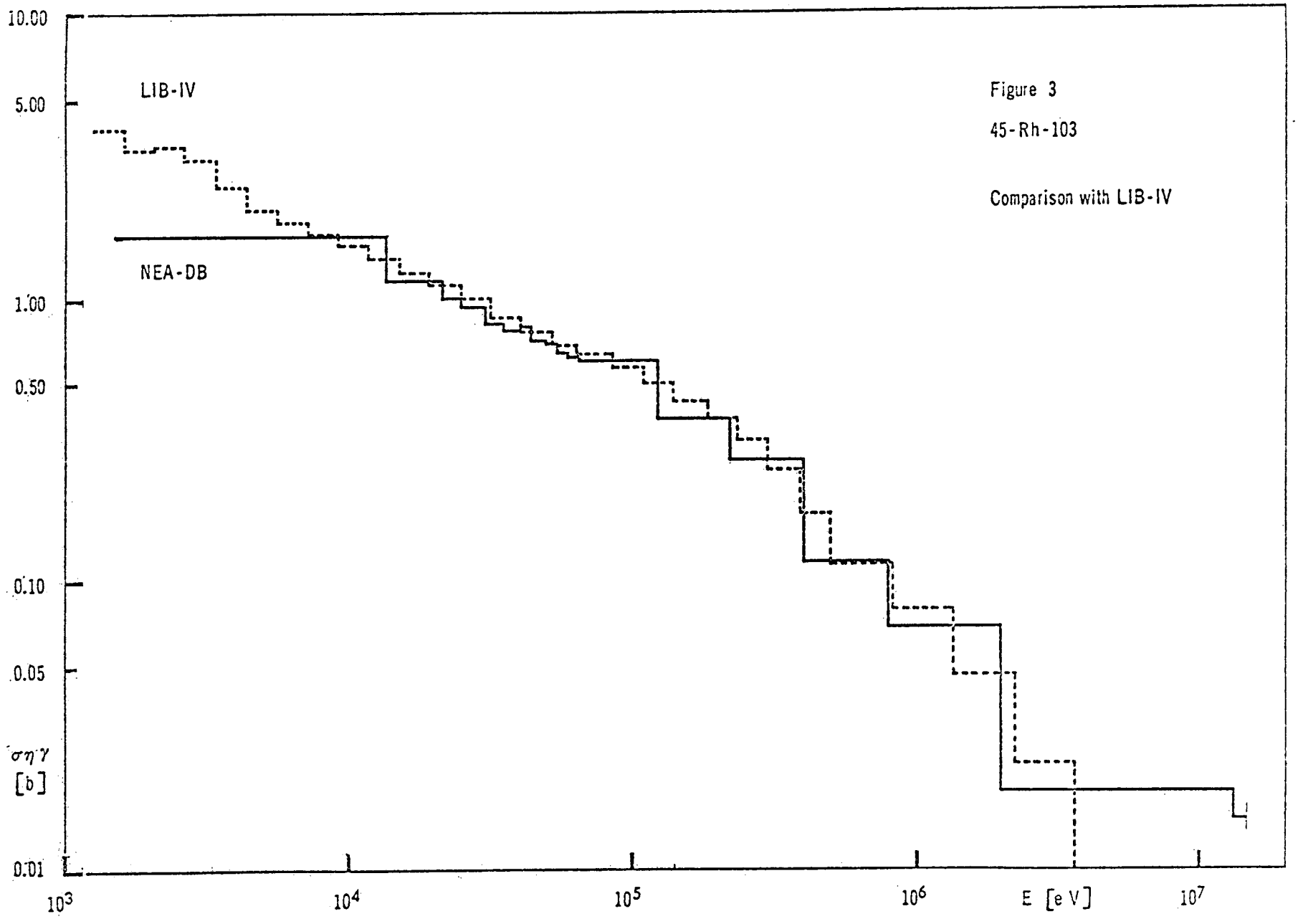
10.00
5.00
1.00
0.50
0.10
0.05
0.01
σηγ
[b]
LIB-IV
NEA-DB
Figure 3
45-Rh-103
Comparison with LIB-IV
10^3
10^4
10^5
10^6
E [eV]
10^7

# NEODYMIUM, SAMARIUM AND EUROPIUM CAPTURE CROSS-SECTION ADJUSTMENTS BASED ON EBR-II INTEGRAL MEASUREMENTS

R. A. Anderl and Y. D. Harker
Idaho National Engineering Laboratory
EG&G Idaho, P.O. Box 1625
Idaho Falls, Idaho USA 83415

F. Schmittroth
Hanford Engineering Development Laboratorty
P.O. Box 1970
Richland, Washington 99352

## Abstract

Integral capture measurements have been made for high-enriched isotopes of neodymium, samarium and europium irradiated in a row 8 position of EBR-II with samples located both at mid-plane and in the axial reflector. Broad response, resonance, and threshold dosimeters were included to characterize the neutron spectra at the sample locations. The saturation reaction rates for the rare-earth samples were determined by post-irradiation mass-spectrometric analyses and for the dosimeter materials by the gamma-spectrometric method. The HEDL maximum-likelihood analysis code, FERRET, was used to make a "least-squares adjustment" of the ENDF/B-IV rare-earth cross sections based on the measured dosimeter and fission-product reaction rates. Preliminary results to date indicate a need for a significant upward adjustment of the capture cross sections for $^{143}$Nd, $^{145}$Nd, $^{147}$Sm and $^{148}$Sm.

## Introduction

In recent years, integral data (capture reaction rates and reactivity worth measurements in fast-reactor fields) have played an important role in the evaluation of fission-product capture cross sections of importance to reactor technology, especially the development of fast reactor systems/1/. In the simplest evaluation application for isotopes with sparse or no measured differential data, integral measurements have been used to normalize capture cross sections based exclusively on nuclear model calculations. For isotopes with a more extensive base of measured differential data, integral measurements have been used to make integral tests of cross-section curves based on the differential measurements and nuclear model calculations. Such integral tests have been helpful to the evaluator in sorting out normalization problems between differential measurements. In a more sophisticated application, integral data obtained from measurements in different spectra have been used to adjust both multigroup and/or point-wise cross sections/1/. This latter application requires a realistic treatment of the uncertainties and correlations in the integral data and in the a-priori flux spectra and fission-product cross sections.

A significant fraction of the integral data used in the fission product cross-section evaluation process comprises reactivity worth measurements in the fast reactor spectra of the STEK cores/2/ and activation capture rates in the fast neutron field of the Coupled Fast Reactivity Measurements Facility (CFRMF) at the Idaho National Engineering Laboratory/3/. This paper presents the integral capture results for enriched isotopes of neodymium, samarium and europium irradiated in different spectra in the Experimental Breeder Reactor-II (EBR-II). The Nd and Sm cross sections are of importance to fission product poison effects in fast reactors and/or to the establishment of a reliable burnup monitor for fast reactor fuels. Cross sections for the Eu isotopes are needed in the evaluation of europium oxide as a control material. For most of the isotopes in the irradiation, some integral data exist as reactivity worths. Little, if any, integral capture data have been published. The EBR-II experiment differs significantly from experiments in the CFRMF and STEK facilities in terms of neutron spectrum characterization. The neutron fields in the latter two facilities are well characterized by means of neutronic calculations and active neutron dosimetry. Characterization of the neutron spectra in the EBR-II is dependent on the use of passive dosimeters (activation monitors).

Included in this paper are a brief description of the EBR-II irradiation experiment and a detailed presentation of the measured reaction rates for the rare-earth samples and for the neutron spectrum dosimeters. In addition, preliminary results of the application of the FERRET Code/4,5/ for spectrum unfolding and for the adjustment of ENDF/B-IV multigroup cross sections based on the measured integral data are presented.

## EBR-II Irradiation Experiment

### Irradiation Configuration

A detailed description of the irradiation experiment was presented earlier/6/. Only pertinent details will be given here. Shown in Figures 1 and 2 are the subassembly and axial loading patterns for this experiment. The irradiation package consisted of multiple samples (0.1 μg to 50 μg deposits on Ni or V foils) of the isotopically enriched isotopes shown in Figure 2 and dosimeter sets consisting of Co, Cu, Fe, Ni, Ti, Sc, $^{237}$Np, $^{235}$U, $^{238}$U monitors. Two B-7 capsules provided the primary containment of the eight experiment capsules. Each experiment capsule contained up to five subcapsules each of which contained the sample or dosimetry materials.

### Reaction-Rate Determination

Dosimeters. Saturation reaction rates for the dosimeters were determined by the radiometric technique/7,8/ using calibrated Ge(Li) spectrometers. Decay data for the analysis was taken from reference 8. The fission-rate determinations were based on the consensus fast reactor fission yields given in reference 9. Infinitely-dilute reaction rates for the dosimeters in each set for the irradiation are summarized in Table I. Accurate fission rates for $^{238}$U, not given in the table, are difficult to obtain because a large correction is required to account for fission-product activity due to fission of the "grown-in" $^{239}$Pu. Uncertainties in the reaction rates for the Co dosimeters reflect significant neutron self-shielding corrections (~factor of 2) required for these monitors.

Rare-Earth Samples. The saturation reaction rates summarized in Table II for the Nd, Sm and Eu samples are based on mass-spectrometric or gamma spectrometric measurements for the post-irradiation samples. For the Nd and Sm isotopes for which integral results are reported here, both the parent and the capture products are stable and the reaction rates are determined easily from mass spectrometer measurements of the (A+1)/A atom ratios for the samples/6/.

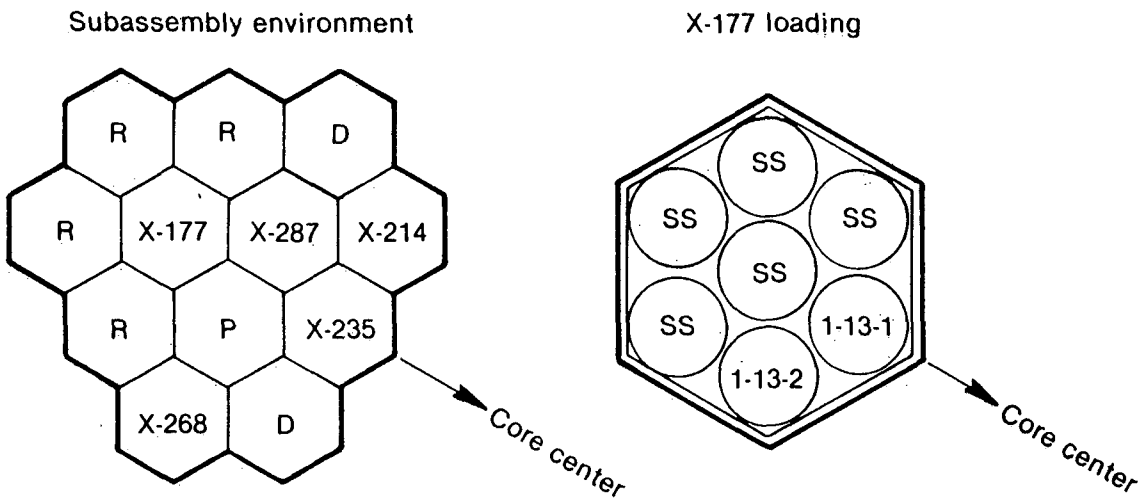


R: Stainless steel reflector
P: 1/2 driver fuel, 1/2 stainless steel
D: MARK II driver fuel
X-287: structural
X-214: oxide fuel
X-235: MARK II driver fuel
X-268: structural

Subassembly: X-177
Position: 8A4
Irradiation time: Cycles 87C-88B, 2504 MWd
Midplane fluence: $4.3 \times 10^{21}$ n/cm$^2$

INEL-A-13 718

Fig. 1 Subassembly loading pattern for EBR-II Irradiation.

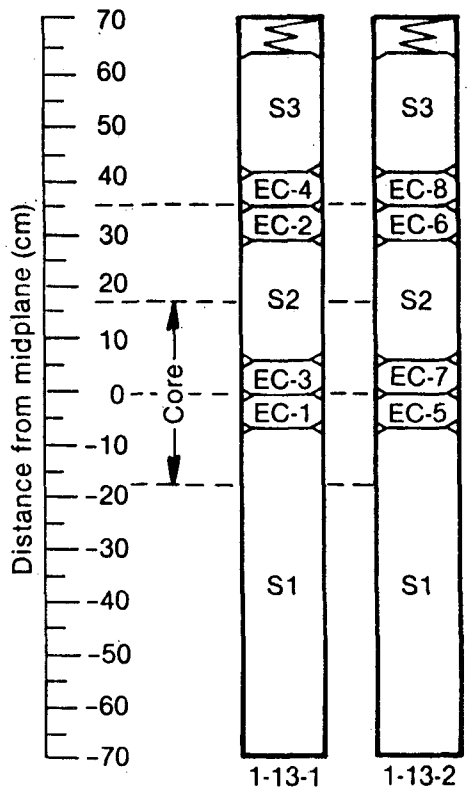


| Experiment capsule | Contents |
|---|---|
| EC-1 | $^{152}$Eu, $^{154}$Eu, XX-1 |
| EC-2 | $^{152}$Eu, $^{154}$Eu, XX-2 |
| EC-3 | $^{151}$Eu, $^{153}$Eu, $^{144}$Nd, $^{146}$Nd, $^{148}$Nd |
| EC-4 | $^{151}$Eu, $^{153}$Eu, $^{144}$Nd, $^{146}$Nd, $^{148}$Nd |
| EC-5 | $^{147}$Sm, $^{149}$Sm, $^{150}$Nd |
| EC-6 | $^{147}$Sm, $^{149}$Sm, $^{150}$Nd |
| EC-7 | $^{143}$Nd, $^{145}$Nd, XX-3 |
| EC-8 | $^{143}$Nd, $^{145}$Nd, XX-4 |

Dosimeter sets: XX-1, XX-2, XX-3, XX-4

Spacers: S1, S2, S3

INEL-A-13 717

Fig. 2 B-7 Axial Loading Pattern for EBR-II Irradiation.

TABLE I. Infinitely-dilute Reaction Rates for Dosimeters in EBR-II Experiment X-177

| Reaction | Reaction rate (reactions/sec-atom) x $10^{11}$ XX-1[a] | XX-3 | XX-2 | XX-4 |
|---|---|---|---|---|
| $^{59}Co(n,\gamma)^{60}Co$ | 20.2(9)[b] | 27.8(12) | 64.(5) | 70.(6) |
| $^{235}U(n,f)$ | 231.(7) | 234.(9) | 238.(9) | 230.(8) |
| $^{237}Np(n,f)$ | 63.(4) | 50.(2) | 19.3(10) | 11.0(5) |
| $^{45}Sc(n,\gamma)^{46}Sc$ | 3.75(9) | 3.72(8) | 3.99(9) | 4.07(8) |
| $^{54}Fe(n,p)^{54}Mn$ | 1.300(22) | 0.910(15) | 0.2162(37) | 0.1024(17) |
| $^{58}Fe(n,\gamma)^{59}Fe$ | 0.965(13) | 0.998(14) | 1.239(16) | 1.166(15) |
| $^{58}Ni(n,p)^{58}Co$ | 1.74(4) | 1.27(3) | 0.306(6) | 0.152(3) |
| $^{46}Ti(n,p)^{46}Sc$ | 0.1570(19) | 0.1142(14) | .02364(28) | 0.01169(14) |
| $^{63}Cu(n,\alpha)^{60}Co$ | 0.00728(12) | 0.00527(8) | .00212(3) | 0.00104(2) |

[a]Label for dosimetry set.

[b]Number in parenthesis is the 1-sigma error in the last significant digits.

TABLE II. Infinitely-dilute $(n,\gamma)$ Reaction Rates for Rare-Earth Samples in EBR-II Experiment X-177

| Isotope | Applicable[a] Dosimeter Set | Reaction Rate (rps/atom)x$10^{10}$ | $\frac{C}{M}$[c] |
|---|---|---|---|
| $^{143}Nd$ | XX-3 | 5.03(6)[b] | .822 |
| | XX-4 | 8.75(5) | .863 |
| $^{144}Nd$ | XX-1 | 1.06(2) | .997 |
| | XX-4 | 0.993(11) | .970 |
| $^{145}Nd$ | XX-3 | 7.64(8) | .653 |
| | XX-4 | 14.55(9) | .765 |
| $^{147}Sm$ | XX-3 | 23.11(14) | .658 |
| | XX-2 | 44.8(5) | .813 |
| $^{149}Sm$ | XX-3 | 40.9(10) | .721 |
| | XX-2 | 81.5(27) | 1.07 |
| $^{151}Eu$ | XX-1 | 54.(3) | .705 |
| | XX-4 | 113.(7) | .794 |
| $^{152}Eu$ | XX-1 | 52.(5) | .913 |
| | XX-2 | 75.(8) | 1.26 |
| $^{153}Eu$ | XX-1 | 29.6(15) | .804 |
| | XX-4 | 61.9(25) | .934 |
| $^{154}Eu$ | XX-1 | 38.(3) | .757 |
| | XX-2 | 62.(5) | 1.03 |

[a]Dosimeter set identification which relates rare-earth reaction rates to dosimeter rates in Table I.

[b]Number in parenthesis is the 1-sigma error in the last significant digits.

[c]Calculated-to-measured reaction-rate ratios based on the unadjusted fission-product cross sections and the multigroup fluxes obtained from spectrum unfolding analysis.

Prior to mass spectrometric analysis, the rare-earth deposits were chemically isolated from the backing foil. A minimum of three mass-spectrometric analyses were made for the Nd and Sm samples from each axial location. The quoted errors for the Nd and Sm isotopes result from averaging the isotopic data from each mass-spectrometric analysis and accounting for an estimated 0.5% systematic error in the mass-spectrometric determination.

For the Eu isotopes, which involve radioactive parent or capture products, the reaction-rate determination is more complicated. Because a significant fraction of the capture in $^{151}$Eu goes to the 9.6 h $^{152}$Eu metastable state (estimated to be 41% from the data in reference 3), chemical isolation of the Eu fraction from the Gd and Sm decay products from the 9.6 h activity was required prior to mass-spectrometric analysis for the 152/151 atom ratio. Consequently, the capture rates for $^{151}$Eu in the table were derived from decay-corrected measured-atom ratios divided by .59 to account for the isomer production. The errors in the measured capture rates for the $^{151}$Eu are dominated by a 5% uncertainty estimated for the isomer ratio.

Capture rates for $^{152}$Eu are based on decay corrected 153/152 atom ratios obtained from mass spectrometric measurements for Eu samples isolated from the nickel backing and from the Sm and Gd decay products from the decay of the 13.2y $^{152}$Eu. The sizable errors estimated for the quoted $^{152}$Eu capture rates result from uncertainties in the mass spectrometric determination of the 153/152 atom ratios in the unirradiated and irradiated samples. Similarly, the capture rates for $^{153}$Eu are based on decay-corrected 154/153 atom ratios obtained from mass-spectrometric measurements. The dominant contribution to the error for the $^{153}$Eu capture rate is due to uncertainties in the mass-spectrometric determination of the 154/153 atom ratios.

The capture rates for the $^{154}$Eu samples are based on decay-corrected atom ratios determined by the Ge(Li) spectrometric measurement of the relative gamma emission rates of the 123.14-keV and 105.3-keV lines in the $\beta$- decay of $^{154}$Eu and $^{155}$Eu, respectively. The dominant contributors to the uncertainty in the capture rates are errors in the gamma-ray branching ratios and half-lives used in the computation of the atom ratios from the relative gamma intensities. Decay data for these analyses were taken from the INEL Decay Data Master File .

## Data Analysis

### Neutron Spectrum Characterization

The FERRET data analysis code/4,5/, was used to obtain 47 group* representations of the neutron spectra based on the measured reaction rates for the dosimeters in Table I. A priori information for this analysis included the following:

1) 47 group fluxes derived from 29 group fluxes obtained from XY-geometry (for mid-plane) and RZ-geometry (for reflector) neutronics calculations for applicable core configurations of EBR-II/11/,

2) parametric representations for the flux covariance matrices,

3) 47 group dosimeter cross sections based on ENDF/B-IV, 620 group cross sections collapsed with a weighting function representative of the neutron spectra in EBR-II,

*Slightly modified version of the HEDL 42 group energy structure with maximum energy extended to 16.91 MeV.

4) parametric representations for the cross-section covariance matrices.

The covariance matrices generated for both the fluxes and cross sections are composed of two components: an overall fractional normalization uncertainty, c, and a second term, $r_i r_j \rho_{ij}$, that describes any additional uncertainties and correlations. The correlation matrix is parameterized by

$$\rho_{ij} = (1 - \Theta)\ \delta_{ij} + \Theta\ e^{-\frac{(i-j)^2}{2\gamma^2}}$$

where $\Theta$ denotes the strength of the short range correlations and $\gamma$ denotes their range. For example, completely uncorrelated data or a-priori values are described by $\Theta$=0 so that $\rho_{ij} = \delta_{ij}$. The values, $\{r_i\}$ are the group-by-group fractional uncertainties.

In the present analysis, a mid-plane a-priori flux was assumed to have a 10% normalization uncertainty, a group-by-group uncertainty of 20% with short-range correlations specified by $\Theta$= 0.9 and $\gamma$= 3.0 A reflector a-priori flux was assumed to have a 20% normalization uncertainty and a group-by-group uncertainty of 40%. A more extensive evaluation by one of the authors (F. Schmittroth) of the uncertainties and correlations for the dosimeter cross section is beyond the scope of this paper.

Two examples of the spectrum-unfolding analysis which simultaneously treated all four dosimeter sets are illustrated in Figures 3 and 4. In Figure 3, one notes that the adjusted multi-group flux appears to be somewhat softer than the a-priori flux. Group-to-group fractional uncertainties were reduced

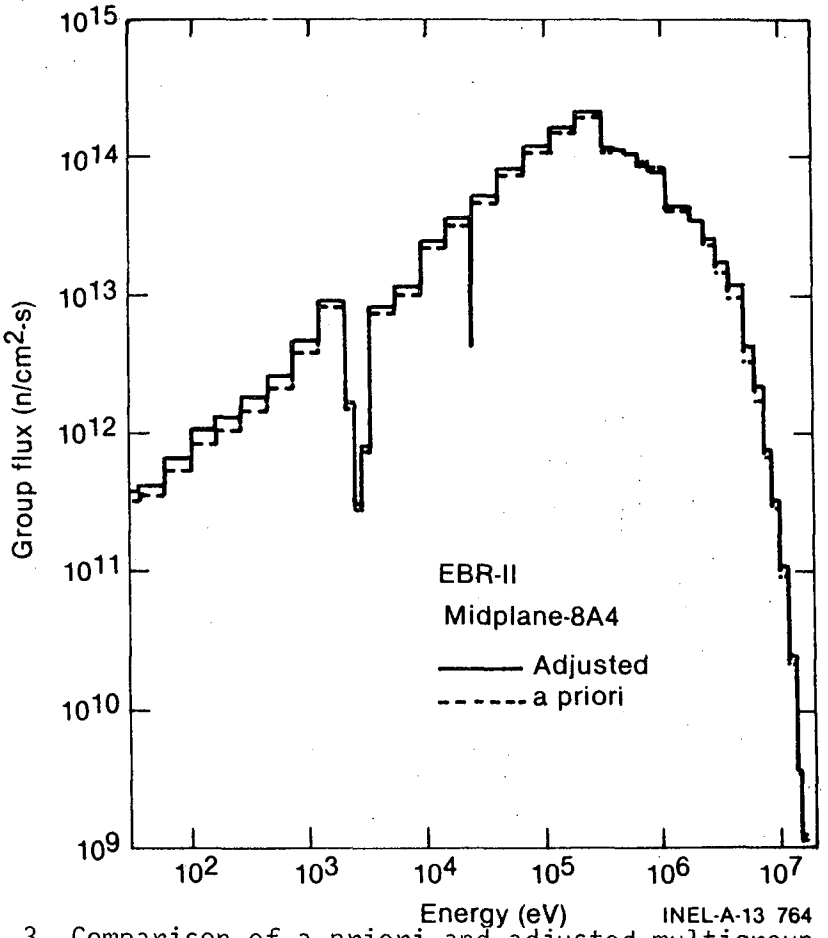


Fig. 3 Comparison of a-priori and adjusted multigroup fluxes for XX-1 dosimeter at mid-plane.

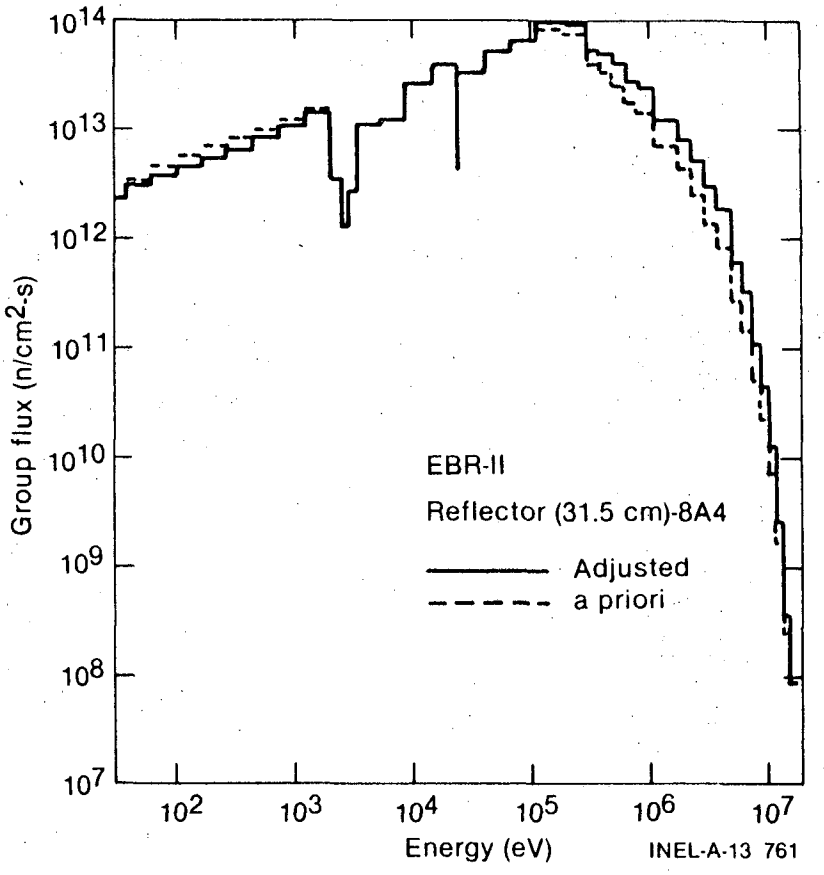


Fig. 4 Comparison of a-priori and adjusted multigroup fluxes for XX-2 dosimeter in the reflector.

to as low as 12% in the region of maximum response above the sodium dip (25 keV). Illustrated in Figure 4 is the overall hardening of the a-priori reflector neutron spectrum by the adjustment. The two figures illustrate the significant differences in the energy distribution of the neutron flux between a mid-plane and a reflector location and point to the sensitivity of the reflector reaction rates to resonance capture.

Cross-Section Adjustment

A least-squares adjustment of the fission-product multigroup cross sections was made with FERRET based on the following a-priori information:

1) Adjusted multigroup fluxes and adjusted flux covariance matrices from the spectrum unfolding analysis.

2) 47 group fission-product cross sections based on ENDF/B-IV.

3) parametric representations for the cross-section covariance matrices.

Summarized in the 4th column of Table II and illustrated by Figures 5-8 are some of the results of the FERRET analysis. The C/M ratios given in Table II present "conventional" integral tests of the fission-product cross sections. For example, both the mid-plane and reflector C/M ratios for $^{143}$Nd indicate the need for an upward adjustment in the cross section throughout the region of sensitivity of the fluxes. The C/M ratios based on the adjusted fission-product cross sections and fluxes were essentially 1 for all cases except those with large errors in the measured reaction rate, e.g., $^{152}$Eu.

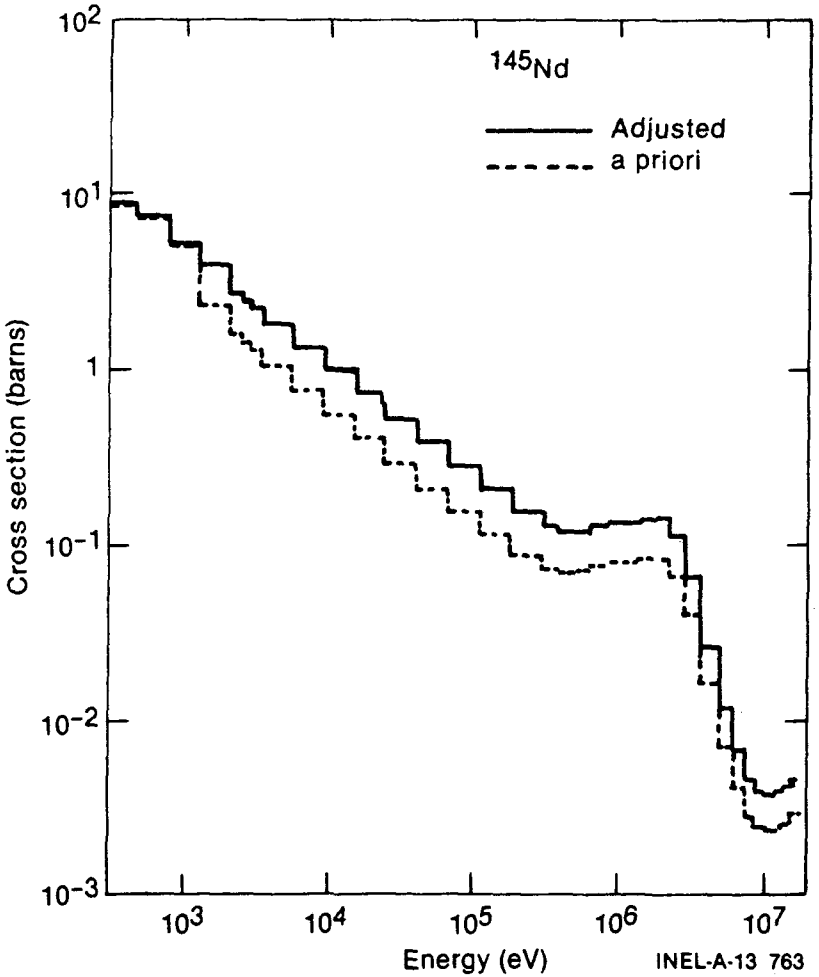


Fig. 6 Comparison of a-priori and adjusted multigroup cross sections for $^{145}$Nd

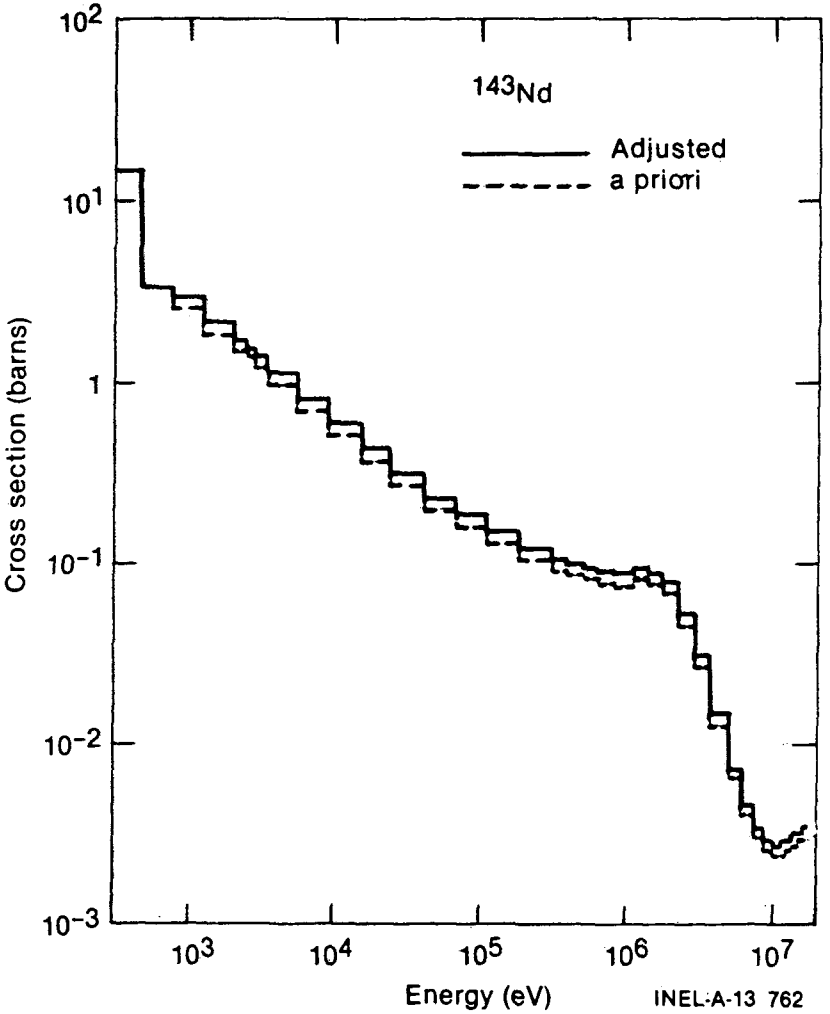


Fig. 5 Comparison of a-priori and adjusted multigroup cross sections for $^{143}$Nd

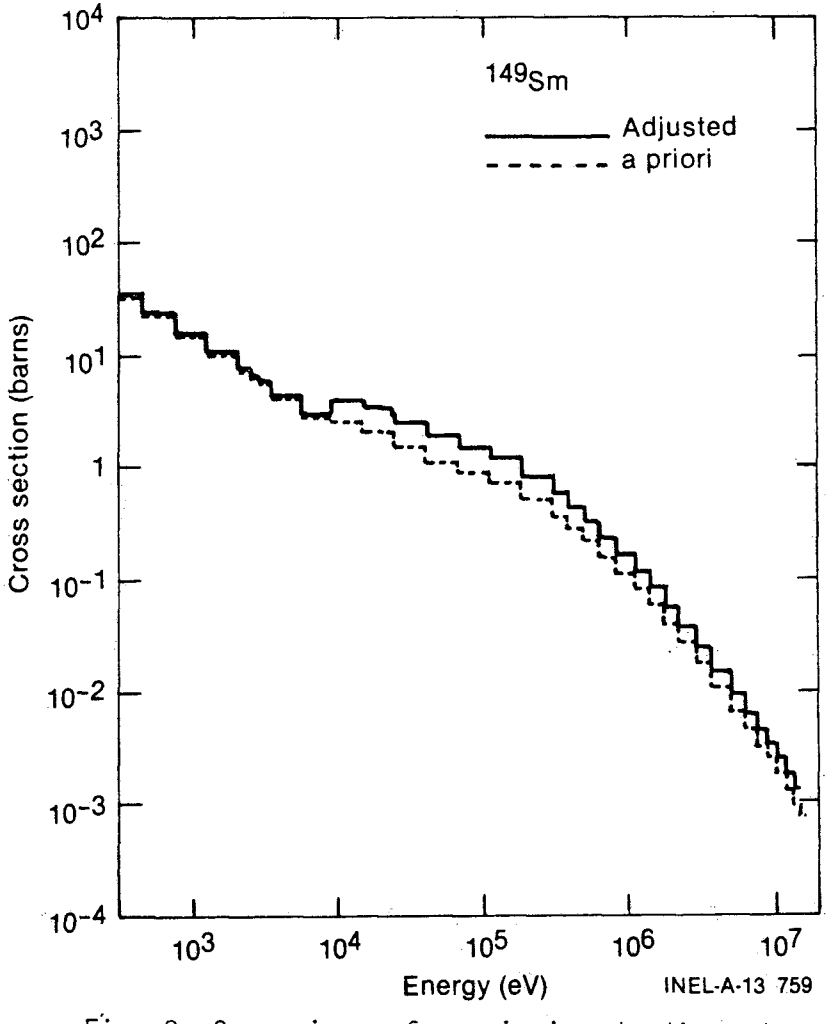


Fig. 8 Comparison of a-priori and adjusted cross sections for $^{149}Sm$

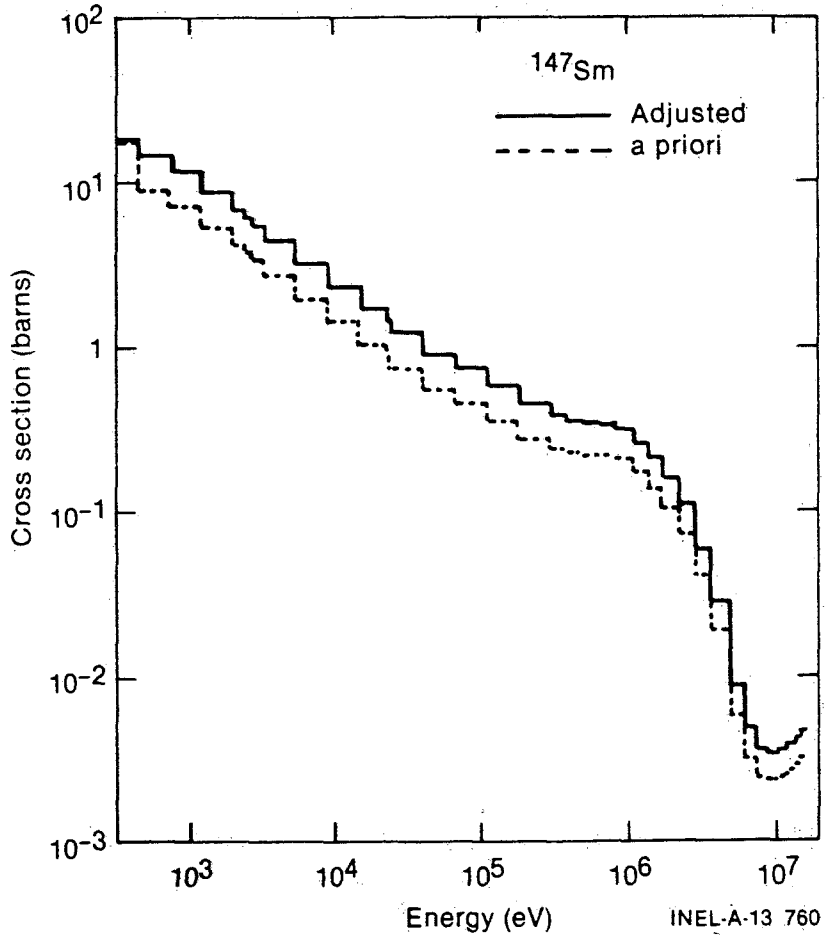


Fig. 7 Comparison of a-priori and adjusted cross sections for $^{147}Sm$

Shown in Figures 5-8 are comparisons of the a-priori and adjusted cross sections for $^{143}$Nd, $^{145}$Nd, $^{147}$Sm and $^{149}$Sm isotopes for which no previous integral capture data have been reported. As expected, the adjustment in the cross section is mainly over the region of maximum response in the neutron fields and the magnitude of the adjustment is approximately given by the inverse of the C/M ratios from Table II.

## Discussion

Some qualitative comparisons of the present integral results and cross section adjustments with other integral data, measured differential cross sections and/or evaluated cross sections were made. Integral checks of the ENDF/B-IV cross sections for $^{147}$Sm and $^{149}$Sm based on reactivity-worth measurements in the STEK cores has been reported as C/M ratios/2/. The C/M ratios from the present experiment are in good agreement with the STEK results. For $^{143}$Nd, $^{144}$Nd and $^{145}$Nd, Gruppelaar/13/ has reported adjusted cross sections (RCN-2A set) based on reactivity-worth measurements in the STEK cores. A comparison of the adjusted Nd cross sections from the present work with those of Gruppelaar indicates good agreement for $^{145}$Nd and reasonable agreement for $^{143}$Nd and $^{144}$Nd. A comparison of the preliminary EBR-II adjusted cross sections with recent differential data indicates reasonable agreement for $^{149}$Sm and $^{145}$Nd and good agreement for $^{143}$Nd and $^{144}$Nd/14/.

We consider the present integral results and FERRET analyses to be of more use in data evaluation that just for qualitative comparisons of C/M ratios and adjusted cross sections. Especially of use to the data evaluator are the adjusted cross sections and associated adjusted covariance matrices. The adjusted covariance matrices embody all the uncertainties and correlations associated with these integral experiments. The data could subsequently be used by the evaluator to adjust evaluated point cross sections based on nuclear model calculations and measured differential data/1/. Furthermore, with the advent and utilization of covariance files for ENDF/B cross sections, this approach to data evaluation will utilize in the most consistent way all the measured and calculated information important to determining point-wise cross sections for fission-product isotopes.

In summary, we would like to emphasize the unique features and contributions of the present experiment and analyses. From an experimental standpoint,

1) small sample sizes were required (μg quantities of highly enriched rare-earth samples were prepared with the INEL electromagnetic mass separator),

2) short-time (~30 days) irradiation of samples in different neutron fields of high flux test reactor,

3) spectral characterization of neutron fields by use of passive dosimetry,

4) capture reaction-rate measurements based on conventional mass spectrometric and Ge(Li) spectrometric techniques and capabilities at the INEL.

From an analysis standpoint, we have demonstrated the adjustment of cross sections based on the present integral results to be consistent with other evaluations and differential measurements.

## Acknowledgment

This work was performed under the auspices of the U. S. Department of Energy.

## References

1. H. Gruppelaar and J. W. M. Dekker, "Impact of Integral Measurements on the Capture Cross-Sections Evaluations of Individual Fission-Product Isotopes," ECN-24, (September 1977).

2. M. Bustrann, J. W. M. Dekker, R. J. Heigboer, A. J. Janssen, "Integral Determination of Fission Product Neutron Capture Cross Sections for Applications in Fast Reactors," ECN-27, (September 1977).

3. Y. D. Harker, J W Rogers and D. A. Millsap, "Fission-Product and Reactor Dosimetry Studies at Coupled Fast Reactivity Measurements Facility," U. S. DOE Report TREE-1259 (March 1978).

4. F. S. Schmittroth, "Varied Applications of a New Maximum-Likelihood Code with Complete Covariance Capability," ORNL-RSIC-42, 145 (February 1979).

5. F. Schmittroth, "FERRET Data Analysis Code," HEDL-TME 79-40 (September 1979).

6. R. A. Anderl, Y. D. Harker, R. L. Tromp, J. E. Delmore, "EBR-II Irradiation of Enriched Isotopes of Neodymium, Samarium and Europium," Trans. Am. Nucl. Soc. 28 745 (1978).

7. R. C. Greenwood, R. G. Helmer, J W Rogers, N. D. Dudy, R. J. Popek, L. S. Kellogg and W. H. Zimmer, Nucl. Tech 25, 275 (1975).

8. R. C. Greenwood, R. G. Helmer, J W Rogers, R. J. Popek, R. R. Heinrich, N. D. Dudy, L. S. Kellogg and W. H. Zimmer, "Radiometric Reaction-Rate Measurements in CFRMF and Big-10," NUREG/CP-0004, Vol. 3, 1207 (1978).

9. D. M. Gilliam, R. G. Helmer, R. C. Greenwood, J W Rogers, R. R. Heinrich, R. J. Popek, L. S. Kellog, E. P. Lippincott, G. E. Hansen, W. H. Zimmer, "Reference and Standard Benchmark Fission Yields for U. S. Reactor Dosimetry Programs," NUREG/CP-0004, Vol. 3, 1289 (1978).

10. Private communication from R. L. Bunting and C. W. Reich.

11. Private communication from G. H. Golden, EBR-II Project.

12. B. A. Magurno, Editor, "ENDF/B-IV Dosimetry File," BNL-NCS-50446 (April 1975).

13. H. Gruppelaar, J. W. M. Dekker, A. J. Janssen, H. Ch. Rieffe, "Adjustment of Evaluated Neutron Capture Cross Sections of Neodymium Isotopes to Integral STEK and CFRMF Data," paper presented at the Int. Conf. on Neutron Physics and Nuclear Data for Reactors and Other Applied Purposes, Harwell, 25-29 September, 1978.

14. Private communication from R. E. Schenter.

# STATUS OF PSEUDO FISSION-PRODUCT CROSS SECTIONS FOR FAST REACTORS; SENSITIVITY STUDY FOR SODIUM VOID EFFECT

R.J. Heijboer and A.J. Janssen
Netherlands Energy Research Foundation (ECN),
P.O. Box 1, 1755 ZG Petten, The Netherlands.

Abstract

The accuracy requirements and the status of the evaluated neutron capture cross sections of the nuclides, which together make up the total fission-product mixture in a fast power reactor, are reviewed. The most important fission-product neutron cross section data files are shortly discussed and compared. In order to define the accuracy needed for the cross sections of fission products in the calculation of the sodium-void reactivity effect in a fast power reactor a sensitivity study has been made using a simple reactor model. Some conclusions are presented.

## 1. INTRODUCTION

During burn-up of the fuel in a fast reactor a large number of fission-product nuclides is created. The greater part of these nuclides is unstable, decaying by β-decay. The easiest way of looking at the properties of this mixture of fission products is by normalizing on the number of fissions that has created them. The total number of the fission products then adds to a value of 2, and the distribution of the number of nuclides (generated per fission) over the mass range is then changing only slowly in the course of the burn-up of the fuel. During the first few months of irradiation, however, the many short-lived nuclides have not yet reached their equilibrium concentrations, and changes in composition are then therefore still large. At longer periods of irradiation the long-lived and stable nuclides dominate in this mixture, while also small changes in composition caused by neutron capture are going to play a role.

The concept of pseudo fission-products is introduced by calculating the summed microscopic capture (and other) cross sections of the mixture using the normalized concentrations (or so-called effective yields) mentioned above. Normally this is done on the level of group cross sections. For reaction x in group g (for fission in nuclide j) one gets:

$$\hat{\sigma}^{j}_{x,g}(t) = \sum_{i} y^{j}_{i}(t)\ \sigma^{i}_{x,g}\ ,$$

where $y^{j}_{i}(t)$ is the concentration of fission product i per fission in nuclide j at time t after reactor start-up, and $\sigma^{i}_{x,g}$ is the cross section for reaction x in group g for fission product i. For the concentrations the following relation holds: $\sum_{i} y^{j}_{i}(t) = 2.0$.

In practice the summation for $\hat{\sigma}$ is not made over all possible fission products, because the cross sections of the very short-lived ($T_{\frac{1}{2}} < 30$ hours) nuclides are generally unknown and assumed to vanish. Mostly 160 to 190 nuclides are taken into account, of which about 110 stable, 10 long-lived ($T_{\frac{1}{2}} > 3$ years) and 45 short-lived ($T_{\frac{1}{2}} > 30$ hours). However, for the capture cross section of the total mixture only 6 to 8 of the most important nuclides are needed to obtain 50% of the capture effect, 20 nuclides give about 80%, 40 nuclides about 95%, and with 50 nuclides more than 98% can probably be obtained.
In table I a list of the 20 most important fission products contributing to the pseudo product cross sections is given (from /1/).

## 2. ACCURACY REQUIREMENTS FOR FISSION PRODUCT CROSS SECTIONS

At the second IAEA advisory group meeting on fission-product nuclear data, held in 1977 at Petten, the needs and accuracy requirements for individual f.p. nuclides and for the total mixture of f.p. were reviewed /2/. Here we will only summarize the recommendations of that meeting concerning the cross section requirements in a fast reactor for the total mixture of fission products (ref. /2/, R.P. 3 by Rowlands, and the Conclusions and Recommendations, chapters III and IV) and add some additional recent views, mainly from the French /3,4/.

The target accuracy for the prediction of reactivity effects of the fission products was requested less than 10% /2/. In future, however, for the expected development of high-burn-up fast reactors a target accuracy of 7% would be appropriate. The 10% target implies that the bulk capture effect of f.p. is required to 10% accuracy. The reactivity effect due to inelastic scattering of lumped f.p. is 10% to 15% of the capture effect. An accuracy of ±30% in the bulk f.p. scattering effect is wanted.

The effect of f.p. on sodium void reactivity should be predicted to within 30% accuracy. The cross section requirements are not easily defined. The effect of f.p. on Doppler reactivity should be predicted to within 50% accuracy. For the resulting requirements on the bulk f.p. cross sections, it has to be taken into account that the effects of capture and inelastic scattering are of opposite sign and that therefore the requirements for these separate components may be more stringent than 50%.

At short times after reactor start-up the time behaviour of the lumped f.p. depends partly on the cross sections of some radioactive nuclides ($T_{\frac{1}{2}} > 30$ h) such as $^{99}$Mo, $^{103}$Ru, $^{105}$Rh and $^{149}$Pm. These cross sections are not well known and it was recommended to investigate the effect of their uncertainties on the total uncertainty of the time dependence of reactivity.

So far the conclusions of the 1977 FPND meeting. During that conference, however, the French already stated that in their opinion tighter accuracies on the bulk f.p. reactivity effect were needed, especially in future, for a 1200 MWe reactor (/10/, page 293). In more recent French papers /3,4/ this view is repeated and discussed. As a goal at the moment an accuracy of 5% ($1\sigma$; it has to be remarked that the figures given in the French publications refer to $2\sigma$) seems to be needed, while in future even a goal of 3.5% is considered as desirable. We will discuss this further in section 3.

Concerning the bulk capture effect of f.p. the following was stated at the 1977 Petten meeting:
Calculations, carried out in The Netherlands and in France suggested that, with the accuracies of individual cross sections as given in present evaluations, the required target accuracy (of 7%) was already reached. However, preliminary results of experiments performed in France on irradiated fuel from PHENIX showed integral data which were systematically about 15% lower than those calculated. On the other hand Dutch experiences with samples of irradiated thermal reactor fuel oscillated in STEK were in satisfactory

agreement with the calculations. It was felt that, before judgment was made, the final analysis of the French experiments had to be awaited. Only then it could be decided whether new experiments on bulk FP samples are required or not.

In the meantime the French results have been published /5/. Their conclusion is that the bulk f.p. capture as calculated with the CARNAVAL-IV cross section set should be reduced by about 18% (for the results of these measurements an accuracy of ±3.5% is claimed, 1σ). This conclusion seems to be in contradiction with the Dutch experiences with irradiated samples (see /2/, RP14, table 8, and /12/). There the high-irradiation sample HFR-101 showed a good agreement with calculations, while the (much less accurate) low irradiation sample HFR-102 could indicate that the cross sections should be enlarged somewhat.

So no final conclusions are at the moment possible. In the French program more irradiations are planned to obtain bulk f.p. samples /5/, with pure $^{239}$Pu fuel as well as with normal PHENIX plutonium fuel. As far as we know also the Japanese are contemplating irradiation of fuel to measure thereafter the f.p. reactivity effects.

In the final uncertainty of the reactivity effect of the bulk f.p. mixture the uncertainties in the cross sections of the individual nuclides take a large part. That is why a continued effort in improving the knowledge of these cross sections is needed. In RP14 of the Petten meeting it was discussed that when calculating the spectrum-averaged one-group cross section of the $^{239}$Pu pseudo fission product with different data files, one finds, when the old (1971) Australian library /6/ is used, a value which is quite near to the value calculated with an up-to-date library. However, when the same is done for the other pseudo's (say of $^{235}$U and $^{241}$Pu) large differences appear when compared with modern libraries. The reason is that the cross sections of some individual nuclides in the Australian set are out of date (for example the cross section for $^{101}$Ru is about 100% too high, etc.). So, to be sure that in all cases the right pseudo f.p. capture cross section will be calculated, it is necessary that also for the major individual nuclides certain accuracy requirements are met. There was some discussion at the 1977 Petten meeting about the individual accuracy that should be reached in order to safely fulfil the bulk requirements. Finally values were agreed upon which were mostly much lower than those requested at the 1973 Bologna Panel /7/. The main argument for accepting these thight requests was that possible systematic errors in the capture cross sections of individual f.p. in general do not cancel, unlike statistical errors.

The strong time dependence of the pseudo fission product capture cross section at short times ($t < 150$ days) after reactor start-up was shortly discussed at the 1977 Petten meeting. The four most important nuclides were mentioned in the Proceedings. The nuclides that may play a role in this effect are those with halflives between about 6 hours and 2 months. Involved are the cross sections of the short-lived nuclides and of their stable daughters. The growing into equilibrium concentration may give an increase or a decrease of the net cross section, or the net effect may be approximately zero. In table II we have listed the most important unstable nuclides involved in this effect. The cross sections of these nuclides have to be evaluated with reasonable degree of accuracy, say some 30-50%. However, no work has as yet been done to investigate more precisely the effect of their uncertainty on the total uncertainty of the time dependence of reactivity after start-up of the reactor at the beginning of a cycle.

Concerning the effect of f.p. on the sodium void reactivity some work has been done. In Japan measurements have been performed to determine this effect /8/. The bulk f.p. was simulated by a mixture of natural elements devised by Schröder /9/, and in other measurements by respectively boron, molybdenum, and niobium. Also a comparison was made with calculations.

Especially the KfK simulation material /9/ gave large and till now unexplainable deviations. The authors concluded that in order to estimate the effect on sodium worth the capture cross sections of the f.p. should be known more precisely, especially in the low energy range of 100 eV - 10 keV.
In section 5 we will report some results of a preliminary sensitivity study on the influence of f.p. cross sections on the sodium void reactivity.

## 3. OTHER FACTORS INFLUENCING THE ACCURACY OF THE PSEUDO FISSION PRODUCT CROSS SECTIONS.

Other factors determining the accuracy with which the cross sections of the pseudo fission products can be calculated are the following:

1. Uncertainties in the yields used.
2. Uncertainties in the leakage and migration of some gaseous and volatile f.p. towards the plenum.
3. Uncertainties arising from variations in reactor operations.
4. Uncertainties coming from variations in reactor or fuel element design.

In several French publications these points have been discussed (/1/, /3/, the paper by Langlet et al. in /10/), and partly also in Japanese reports /11/.

Hammer /3/ gives an estimate of the uncertainty in $\hat{\sigma}$ due to yields at present of about 4% (1$\sigma$). On the basis of new yield data /25/ he expects that in future this contribution in the f.p. error can be reduced to 1.5%. Although the error estimations for the yields in /25/ probably are somewhat optimistic, we also have the feeling that this error contribution is at the most some 1 or 2%. In some Dutch studies /12,13/ different existing yield sets were used to calculate the effective one-group pseudo f.p. cross section; the difference was found to be of the order of 0.5%. It has to be admitted, however, that if a large error in the yields of some important nuclides would be detected, the change in the pseudo cross section could be non-negligible. And it is perhaps questionable whether the detailed yield curve for $^{239}$Pu is known with good enough accuracy.

In the uncertainty due to migration effects it is probably mass chain 133, with $^{133}$Xe ($T_{\frac{1}{2}}$ ~5 days) $\rightarrow$ $^{133}$Cs, which gives the largest contribution /31/. If one assumes that the leakage of gaseous products as Br, Kr, I and Xe is taken correctly into account with a constant half-life decrease of about 10 days, a net uncertainty of about 1.5% (1$\sigma$) results /3/.
The uncertainties due to the other two factors mentioned only contribute about 1%.

In the opinion of the French /3/ the total uncertainty at the moment in the bulk f.p. reactivity effect is primarily caused by errors in the cross sections and yields. For the CARNAVAL-IV set the cross sections contribute 5%, the yields 4%, with the other errors mentioned a total uncertainty of 8% is estimated. For the near future it is expected that improvements are possible in the cross sections (error reducing to 4%) and especially in the yields (error reducing to 1.5%), the total uncertainty then becoming about 5% (1$\sigma$). The final goal is, however, 3.5%, which is in our opinion still a long way.

## 4. FISSION PRODUCT CROSS SECTION DATA FILES

In this section the status of the available fission product cross section libraries of recent evaluations (see table III) will shortly be discussed. The format of these data files is that of ENDF/B, except for the RCN-2 evaluation, which is stored in KEDAK format.

ENDF/B-IV: This file contains cross sections for 184 nuclides in the fission-product mass range, of which about 172 can be considered to occur as fission products; the other 12 are stable isotopes of the natural elements in this mass range /15/.

ENDF/B-V: This file contains 196 nuclides, including 12 more stable isotopes of the natural elements, so that now practically all natural elements are complete in this evaluation. Apart from this extention also a number of important f.p. nuclides has been adjusted to fit integral data and recent differential experiments /16/.

CNEN/CEA: Compared to the status in 1977 this evaluation has been extended from 50 to 63 nuclides. In 1978 an Italian report has been published /17/ in which this evaluation was compared with the other evaluations in table III. For that purpose a 25 group cross section set was calculated for each of the 63 nuclides. That report gives graphs and tables with numerical values of these multigroup cross sections.

RCN-2: This library has been extended from 29 f.p. nuclides (1977) towards 38 (1978). Apart from this extention also an evaluation has been made of the (n,p) and (n,α) cross sections of the nuclides in this library /18/. A further extention of this library is still in progress /32/.

JENDL-1: This library was extended from 28 nuclides (1977) towards 62. Recently full documentation for neutron cross sections of 28 f.p. nuclides has been completed /19/. There seems to exist plans for a further extention towards 96 nuclides.

Apart from these basic data evaluations, several group constant libraries for f.p. exist. We mention here the adjusted RCN-2A set /20,21/ and the CARNAVAL-IV system, which have been intercompared in a contribution to this meeting /14/. These two sets were obtained by applying adjustments using integral data measured in various fast reactor cores.

At ECN pseudo fission product cross sections have been calculated in the Russian 26-group scheme /23/ for $^{239}$Pu using the ENDF/B-IV, CNEN/CEA, RCN-2A and JENDL-1 libraries. The concentrations were taken from ref. /13/, table 3.2. These data sets were supplemented with data from other libraries, mostly ENDF/B-IV and the Australian data set /6/.

The calculated pseudo f.p. absorption group cross sections are listed in table IV. These data include corrections for (n,p) and (n,α) reactions /18/. The relative differences of the pseudo f.p. absorption cross sections calculated from RCN-2A, CNEN/CEA and JENDL-1 with respect to ENDF/B-IV are plotted in fig. 1. The differences between the cross sections of the first three libraries are very small; the ENDF/B-IV results are systematically about 10% lower. The deviation between RCN-2A and the other data files from 1 to 2.15 eV is mainly due to the cross section of one isotope ($^{107}$Pd), for which in RCN-2A a resonance was assumed to fit the thermal cross section /32/. Most other differences are found at higher neutron energies, possibly due to differences between the models used to evaluate the cross sections /18/.

To compare these libraries in a more global way with each other and with the situation of 1977 the one-group capture cross section averaged over an SNR-300 spectrum was calculated for each library (table IV). It was found that the deviation with 1977 was less than 1%; and as in 1977 all libraries agree within 1% except for ENDF/B-IV, which is 10% low, the main sources of this difference were already explained at the 1977 FPND meeting (RP 14 /2/). Unfortunately we can not yet indicate how the situation will be with respect to ENDF/B-V.

In ref. /14/ also a comparison between one-group cross sections calculated from the adjusted RCN-2A and CARNAVAL-IV has been made, though with another weighting spectrum. The results show that the CARNAVAL-IV set gives about 5% higher values, which can be ascribed mostly to discrepancies for $^{151}$Sm and $^{105}$Pd. The assumed uncertainties in the one-group cross sections calculated from the adjusted sets is about ±8% /3,13/. See sect. 2 for a discussion on comparison of these results with integral data measured with real f.p. mixtures from irradiated fuel.

## 5. SENSITIVITY OF SODIUM VOID EFFECTS TO FISSION PRODUCT CROSS SECTIONS

At the 1977 Petten FPND meeting a target accuracy of 30% for the effect of fission products on the sodium void reactivity effect was formulated /22/ (giving an uncertainty contribution to the central void term of about 3% and to the total core voidage of about 7%). A translation of this target into fission product cross section accuracies is not so easy because the sodium void effect consists of several, partly compensating, effects which have their main influence in different energy regions. Fig. 2 shows the terms contributing to the central void effect in a 1300 MWe FBR. For each energy group g (of the Russian ABBN 26 group scheme /23/) is given:

- the capture contribution : $\sigma_{c,g}\ \phi_g\ \phi_g^+$
- the elastic scattering contribution : $\sigma_{el,g\to g+1}\ \phi_g(\phi_g^+ - \phi_{g+1}^+)$
- the inelastic scattering contribution: $\sum_{g'} \sigma_{in,g\to g'}\ \phi_g(\phi_g^+ - \phi_{g'}^+)$

In order to get some insight into the sodium void sensitivity to the fission product capture cross section as a function of energy, a series of zero dimensional reactor calculations was performed, with perturbed capture cross sections in each of the 26 ABBN groups. The solid curve in fig. 3 shows the resulting total (= capture + scattering) sodium void sensitivities; for example, increasing $\Sigma_c$ of the fission product mixture (at 74 MWd/kg burn-up) in group 14 by 10% results in an increase of the reactivity effect of sodium, $\rho_{Na}$, of 1%. It can be seen that the effect is dominating in the energy region between 200 eV and 5 keV, which is clearly lower than the region in which the fission product poisoning effect is established (see the sensitivity curve in fig. 3 for the fission product capture rate; dotted line). It was found that capture cross section perturbations mainly affect $\rho_{Na}$ through the elastic scattering term, the capture and inelastic terms being much less sensitive. Also the leakage term in whole core voiding, in fundamental mode approximation proportional to $\sigma_{tr,g}^{Na} D_g^2 B^2 \phi_g \phi_g^+$ ($D_g$ and $B^2$ being the reactor diffusion coefficient and buckling, respectively), turned out to be rather insensitive to capture cross section variations.

The numerical values of fig. 3 should be used with some care, for several reasons.

1. The values depend on the way in which criticality is re-established in the calculations after a cross section perturbation ($B^2$ search, poison search or no criticality search). In particular above 5 keV relatively large differences were found between the sensitivities obtained with the different approaches. However, the region below 5 keV was always found to be dominating, with sensitivities of the same order of magnitude.
2. Apparently, the negative contribution to $\rho_{Na}$ of the sodium scattering resonance near 3 keV is most sensitive to fission product cross section perturbations. This negative contribution (see fig. 2) strongly depends on the neutron spectra $\phi$ and $\phi^+$ below 10 keV and was rather small in the fairly hard fundamental mode spectra used in our calculations. In more realistic FBR spectra this contribution could be larger, which would probably result in larger sensitivities of $\rho_{Na}$. On the other hand, infinite dilution sodium cross sections were used in the calculation of $\rho_{Na}$. The use of sodium cross sections appropriate to the unvoided core composition would result in a reduction of the contribution to $\rho_{Na}$ of group 13 by about 60%. The sensitivities near group 13 would also be reduced; thus, the important sensitivity in group 14 (0.10) turned out to become 0.065.
3. In realistic void situations the positive central term is partly compensated by the accompanying negative leakage term, which means that sensitivities of real void effects would be larger. This has been taken into account in the accuracy requirements mentioned above.

The sensitivities of $\rho_{Na}$ to fission product cross sections are more or less linearly dependent on core burn-up. For fig. 3 this burn-up was 74 MWd/kg, which is about the average core burn-up at the end of a two-batch equilibrium cycle expected in future FBR designs. Even at this burn-up the fission product capture cross sections do not play a dominant role in the total sodium void uncertainty. For comparison the sensitivities of $\rho_{Na}$ to the capture (absorption - fission) cross sections of the complete reactor material mixture have been inserted in fig. 3 (dashed curves). It can be seen that the fission product capture cross sections contribute at most 10-20% to the total $\Sigma_c$ sensitivities.

Finally, it may be mentioned that $\rho_{Na}$ was found to be much less sensitive to fission product cross sections other than capture.

In view of the above mentioned uncertainties is it hardly possible to formulate accuracy requirements of fission product cross sections for the prediction of sodium void effects. Further calculations, using more realistic reactor models, would be necessary. The most one can do is to say that, for the conditions appropriate to the calculations underlying fig. 3, a (correlated) error in $\sigma_c$ in the energy region 200 eV - 5 keV of 10-15% would be tolerable.

Table V might give an idea about the differences between present-day fission product cross section evaluations, as far as the effect on sodium void is concerned. A clean 1300 MWe FBR core was poisoned with various fission product mixtures to amounts which equalled the reactivity of the reference fission product mixture at 74 MWd/kg according to the adjusted RCN-2A data set. In the table the elements boron, niobium and molybdenum and the mock-up mixture KFK defined by Schröder /9/ are included because they have been used in several recent mock-up experiments /8/. The table gives the central sodium void reactivity effects $\rho_{Na}$ in the different fundamental mode spectra. For the fission product mixtures the $\rho_{Na}$ values are very close. Apparently, the relation between the reactivity invested in fission products and the effect on the sodium void worth is about the same for the three evaluations mentioned in the table. (It should be remembered, however, that the fission product reactivity per fission according to ENDF/B-IV is about 10% lower than the corresponding RCN-2A and JENDL-1 values. The fission product concentration was adjusted correspondingly to obtain the same reactivity investment). Formerly, much larger differences were found /22,30/, e.g. between the COOK /6/ and BENZI /29/ evaluations; but in /30/ the BENZI evaluation (which extends down to 1 keV) was not supplied with fission product capture data below 1 keV. For the three other fission product simulating elements in table V larger variations are found in the relation between invested reactivity and the effect on $\rho_{Na}$.

References

/1/ G. Langlet, P. Coppé and J.P. Doat, Uncertainties on a pseudo fission product for fast reactors, Cadarache, May 1977, NEACRP-L-190.
/2/ Fission product nuclear data (FPND) - 1977 (2 vols.), Proceedings of the second advisory group meeting on FPND, held at Petten, 5-9 September, 1977, IAEA-213 (1978).
/3/ Ph. Hammer, Besoins en données nucléaires des produits de fission et actinides pour les calculs de réacteurs de puissance à neutrons rapides, Proc. Int. Conf. on Neutron Physics and Nuclear Data for Reactors, Harwell, September 1978, p. 551, OECD (1978).
/4/ L. Martin-Deidier, Mesure intégrale de la capture des produits de fission dans les réacteurs à neutrons rapides, CEA-R-5023 (1979).
/5/ L. Martin-Deidier, M. Darrouzet, P. Hammer and E. Fort, Mesures intégrales de la capture des produits de fission dans les spectres de réacteurs à eau et de réacteurs à neutrons rapides, Proc. Int. Conf. on Neutron Physics and Nuclear Data for Reactors, Harwell, September, 1978, p. 1016, OECD (1978).
/6/ E.K. Rose, The AAEC fission product cross section libraries FISPROD. POINTXSL and FISPROD.GROUPXSL, AAEC/TM-587 (1971).
/7/ Proc. of a panel on fission product nuclear data organized by the IAEA, Bologna, November 26-30, 1973, IAEA-169 (1974).
/8/ K. Koyama, H. Mitani and H. Kuroi, Effect of Fission Product Accumulation on Sodium Void Worth, IAEA Int. Symp. on Fast Reactor Physics, Aix-en-Provence, September, 1979, IAEA-SM-244/2.
/9/ R. Schöder, Nukleonik 10.1, p. 18 (1967).
/10/ Second IAEA advisory group meeting on FPND, Petten, 5-9 September, 1977, Annexes and selected contributions to the Review Papers, INDC(NDS)-87/GO+Sp (1978).
/11/ Y. Kikuchi et al., INDC Fission product group constants - preliminary version, JAERI-M6001 (1975).
/12/ R.J. Heijboer and A.J. Janssen, Pseudo fission-product cross sections for a fast breeder reactor, ECN-11 (1976).
/13/ R.J. Heijboer, Pseudo fission-product cross sections for a 1300 MWe fast breeder reactor (status July 1978), ECN-52 (1978).
/14/ H. Gruppelaar, Ph. Hammer and L. Martin-Deidier, Intercomparison of adjusted data sets for capture cross sections of fission products, contribution to this meeting.
/15/ National Neutron Cross Section Center (Brookhaven), Evaluated Nuclear Data File B, version IV (1975).
/16/ R.E. Schenter et al., Evaluation of fission product capture cross sections for ENDF/B-V, Contr. to Int. Conf. on Nuclear Cross Sections and Technology, Knoxville 1979, and contr. to this meeting.
/17/ S. Montaguti, G.C. Panini and M. Vacari, Multigroup cross sections of 63 fission product nuclei from different nuclear data files, RT/FI(78) 16.
/18/ H. Gruppelaar and B.P.J. van den Bos, The contribution of (n,p) and (n,α) reactions to fission product capture cross sections, ECN-78 (1979), and contr. to this meeting.
/19/ Y. Kikuchi et al., Neutron cross sections of 28 fission product nuclides adopted in JENDL-1, JAERI-report to be published.
/20/ J.W.M. Dekker, Tables and figures of adjusted and unadjusted capture group cross sections based on the RCN-2 evaluation and integral measurements in STEK, vol. 1, ECN-14 (1977), vol. 2, ECN-30 (1977) and vol. 3, ECN-54 (1979).
/21/ J.W.M. Dekker and H.Ch. Rieffe, Adjusted cross sections of fission product nuclides from STEK reactivity worths and CFRMF activation data, vol. 1, ECN-28 (1977) and vol. 2, ECN-55 (1979).

/22/ J.L. Rowlands, Needs and accuracy requirements for fission product nuclear data in the physics design of power reactor cores, IAEA-213 (1978).
/23/ L.P. Abagyan et al., Group constants for nuclear reactor calculations, Consultants Bureau (1964)
/24/ S. Iijima, Evaluation of neutron cross section of 27 fission product nuclides important for fast reactor, J. Nucl. Sci. Techn. 14 (1977) 161, and data file (extended to 68 nuclides), available from NEA Data Bank.
/25/ M.E. Meek and B.F. Rider, Compilation of fission product yields, USERDA-NEDO/12154-2 (1977).
/26/ J.W.M. Dekker et al., Adjusted neutron spectra of STEK cores for reactivity calculations, ECN-35 (1978).
/27/ E. Kiefhaber, Private communication, June 1976.
/28/ E. Kiefhaber, The KFKINR set of group constants; nuclear data basis and first results of its application to the recalculation of fast zero-power reactors, KfK-1572 (1972).
/29/ V. Benzi and G. Reffo, Fast neutron radiative capture cross sections of stable nuclei with $32 \leq Z \leq 66$, CCDN-NW/10 Newsletter, Bulletin 10, ENEA (1969)
/30/ D. Ilberg, D. Saphier and S. Yiftah, Nuclear Technology 24 (Nov. 1974) 111-122.
/31/ L. Martin-Deidier, Capture des produits de fission dans un réacteur de puissance à neutrons rapides. Etude fundamentale et expérience préliminaire, Thesis, l'Université de Paris-Sud, Centre d'Orsay, (1974).
/32/ H. Gruppelaar, Tables of RCN-2 fission-product cross section evaluation, vol. 1, ECN-13 (1977), vol. 2, ECN-33 (1977) and vol. 3, ECN-65 (1979).
/33/ H. Gruppelaar, Evaluated neutron cross sections of natural molybdenum, ECN-40 (1978)

Table I

The 20 most important fission products in a fast reactor, in order of importance /1/.

| no. | nuclide | $T_{\frac{1}{2}}$ | no. | Nuclide | $T_{\frac{1}{2}}$ |
|---|---|---|---|---|---|
| 1 | Pd105 | | 11 | Cs133 | |
| 2 | Ru101 | | 12 | Cs135 | $2.10^6$ a |
| 3 | Rh103 | | 13 | Ag109 | |
| 4 | Tc99 | $2.10^5$ a | 14 | Ru103 | 39 d |
| 5 | Pd107 | $6.10^6$ a | 15 | Ru102 | |
| 6 | Sm149 | | 16 | Eu153 | |
| 7 | Sm151 | | 17 | Nd143 | |
| 8 | Pm147 | 2.6 a | 18 | Ru104 | |
| 9 | Mo97 | | 19 | Mo95 | |
| 10 | Nd145 | | 20 | Mo100 | |

Table II

Some important unstable fission products (with $T_{\frac{1}{2}}$ in between 6 h and 2 months)

| nuclide | $T_{\frac{1}{2}}$ | % contribution to bulk $\hat{\sigma}_{capt.}$ at t=1 day |
|---|---|---|
| $^{99}Mo$ | 66 h | 5.4 |
| $^{103}Ru$ | 39 d | 6.0 |
| $^{105}Rh$ | 36 h | 4.0 |
| $^{143}Ce$ | 33 h | 2.0 |
| $^{147}Nd$ | 11 d | 2.6 |
| $^{149}Pm$ | 53 h | 7.0 |

Table III

Recent fission product nuclear data files

| file name | number of f.p. nuclides with cross section data | year of release |
|---|---|---|
| ENDF/B-IV | ~172 | 1974 |
| ENDF/B-V | ~172 | 1979 |
| CNEN/CEA | 63 | 1978 |
| RCN-2 | 38 | 1978 |
| JENDL-1 | 62 | 1978 |

Table IV

Absorption cross sections[a)] in b/fission of pseudo fission product of $^{239}Pu$ at 41 MWd/kg burn-up, calculated from different f.p. cross section libraries.

| f.p. libraries: | Number of f.p. nuclides | | | |
|---|---|---|---|---|
| RCN-2 | 1 | - | - | - |
| RCN-2A | 37 | - | - | - |
| CNEN/CEA | 1 | 62 | - | - |
| JENDL-1 | - | - | 59 | - |
| ENDF/B-IV | 116 | 93 | 96 | 155 |
| Australian | 7 | 7 | 7 | 7 |

| ABBN group nr. | ΔE | Main libraries: | | | |
|---|---|---|---|---|---|
| | | RCN-2A[b,c)] | CNEN/CEA[c)] | JENDL-1[c)] | ENDF/B-IV[c)] |
| 1 | 6.5 -10.5 MeV | 0.0030(6.3) | 0.0054(7.9) | 0.0037(7.1) | 0.0058(8.9) |
| 2 | 4.0 - 6.5 | 0.013 (14) | 0.020 (20) | 0.018 (19) | 0.017 (18) |
| 3 | 2.5 - 4.0 | 0.034 | 0.042 | 0.047 | 0.041 |
| 4 | 1.4 - 2.5 | 0.058 | 0.064 | 0.080 | 0.068 |
| 5 | 0.8 - 1.4 | 0.084 | 0.082 | 0.103 | 0.088 |
| 6 | 0.4 - 0.8 | 0.119 | 0.117 | 0.131 | 0.109 |
| 7 | 0.2 - 0.4 | 0.180 | 0.180 | 0.186 | 0.158 |
| 8 | 0.1 - 0.2 | 0.255 | 0.256 | 0.256 | 0.229 |
| 9 | 46.5-100 keV | 0.381 | 0.382 | 0.384 | 0.349 |
| 10 | 21.5-46.5 | 0.586 | 0.600 | 0.595 | 0.545 |
| 11 | 10.0-21.5 | 0.872 | 0.895 | 0.891 | 0.827 |
| 12 | 4.65-10.0 | 1.30 | 1.31 | 1.31 | 1.23 |
| 13 | 2.15-4.65 | 1.93 | 1.88 | 1.91 | 1.75 |
| 14 | 1.00-21.5 | 3.04 | 2.94 | 2.95 | 2.62 |
| 15 | 465 -1000 eV | 4.59 | 4.47 | 4.44 | 3.99 |
| 16 | 215 -465 | 9.58 | 8.89 | 8.66 | 7.57 |
| 17 | 100 -215 | 12.5 | 12.5 | 12.1 | 10.4 |
| 18 | 46.5-100 | 18.1 | 18.5 | 17.9 | 16.6 |
| 19 | 21.5-46.5 | 34.5 | 37.9 | 37.5 | 33.0 |
| 20 | 10.0-21.5 | 50.5 | 52.6 | 50.5 | 51.6 |
| 21 | 4.65-10.0 | 99.4 | 100. | 98.4 | 104.0 |
| 22 | 2.15-4.65 | 24.3 | 25.4 | 25.8 | 20.4 |
| 23 | 1.00-2.15 | 68.5 | 54.5 | 56.0 | 53.3 |
| 24 | 0.465-1.00 | 98.1 | 94.4 | 87.6 | 87.4 |
| 25 | 0.215-0.465 | 52.9 | 60.5 | 60.2 | 55.6 |
| 26 | $10^{-3}$ - 0.215 | 1013. | 1035. | 1055. | 1040. |
| $\bar{\sigma}$ [d)] | | 0.497 | 0.496 | 0.500 | 0.451 |

a) Flux weighting spectrum from KFK-INR-1 set /28/.

b) In ref. /13/ a slightly different flux weighting spectrum has been used.

c) Data in between brackets are cross sections in mb per fission, corrected for $\sigma_{n\alpha}$, $\sigma_{np}$, etc. /18/.

d) One group capture cross section averaged over a SNR-300 neutron spectrum.

Table V

Central sodium void effects (in arbitrary units) in a 1300 MWe reactor containing various poisons with the same reactivity investment.

| poison | evaluation | weighting spectrum | $\rho_{Na}$ |
|---|---|---|---|
| no poison | - | - | 1.893 |
| f.p. (74 MWd/T) | RCN-2A /20,21/ | SNR-2 /27/ | 2.487 |
| f.p. | ENDF/B-IV /15/ | SNR-2 | 2.478 |
| f.p | JENDL-1 /24/ | SNR-2 | 2.465 |
| KFK mock-up | RCN-2A | SNR-300 /28/ | 2.549 |
| nat. boron | from ref. /26/ | STEK /26/ | 2.369 |
| Nb | RCN-2A | SNR-2 | 2.613 |
| Mo | RCN-3 /33/ | SNR-2 | 2.612 |

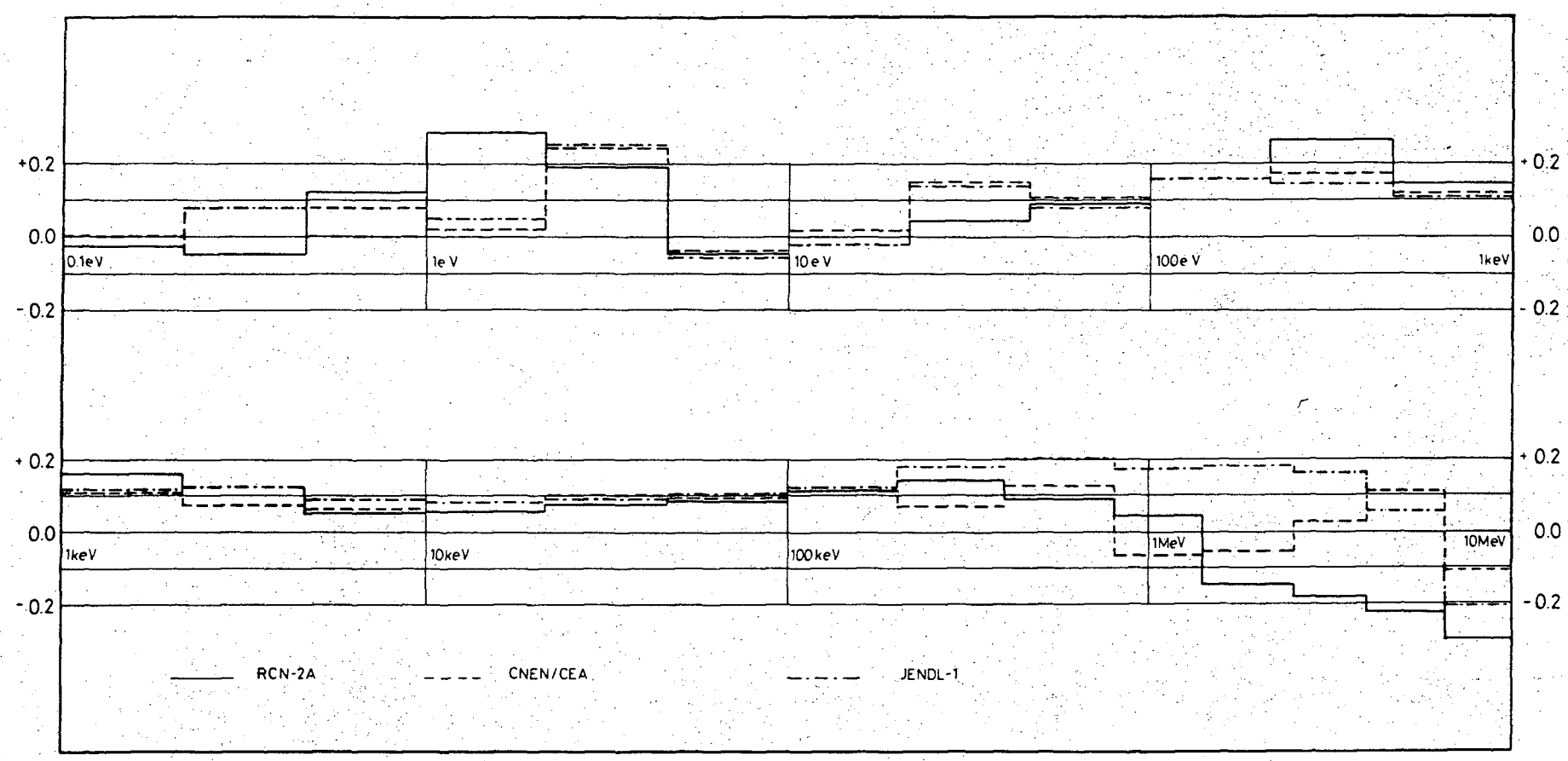


Fig. 1. RELATIVE DIFFERENCES OF PSEUDO F.P. ABSORPTION GROUP CONSTANTS WITH RESPECT TO ENDF/B-IV

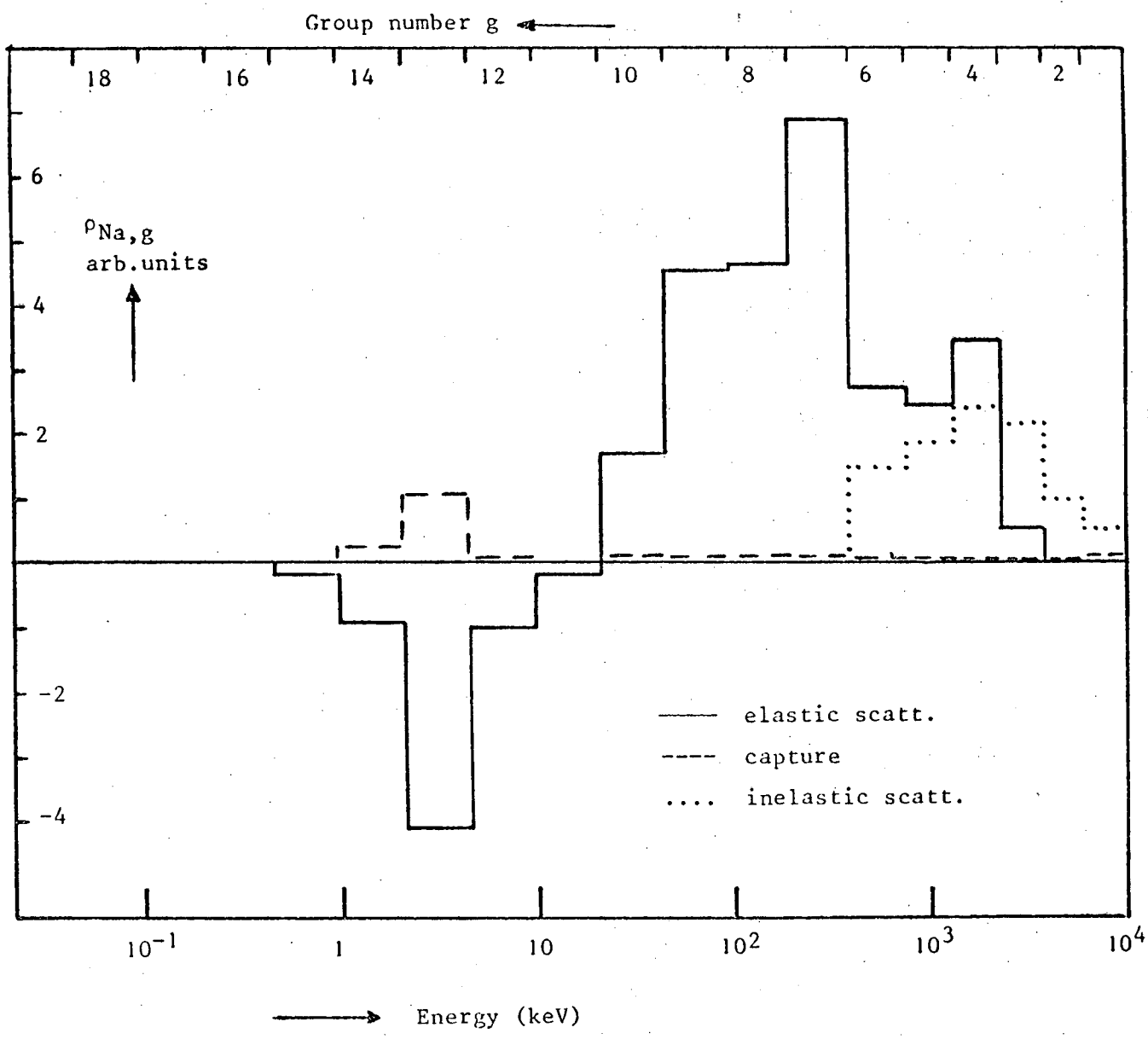


Fig. 2. Energy group break-down of central sodium void effects of elastic and inelastic scattering and capture in fundamental mode spectrum of a 1300 $MW_e$ FBR at 74 MWd/kg burn-up.

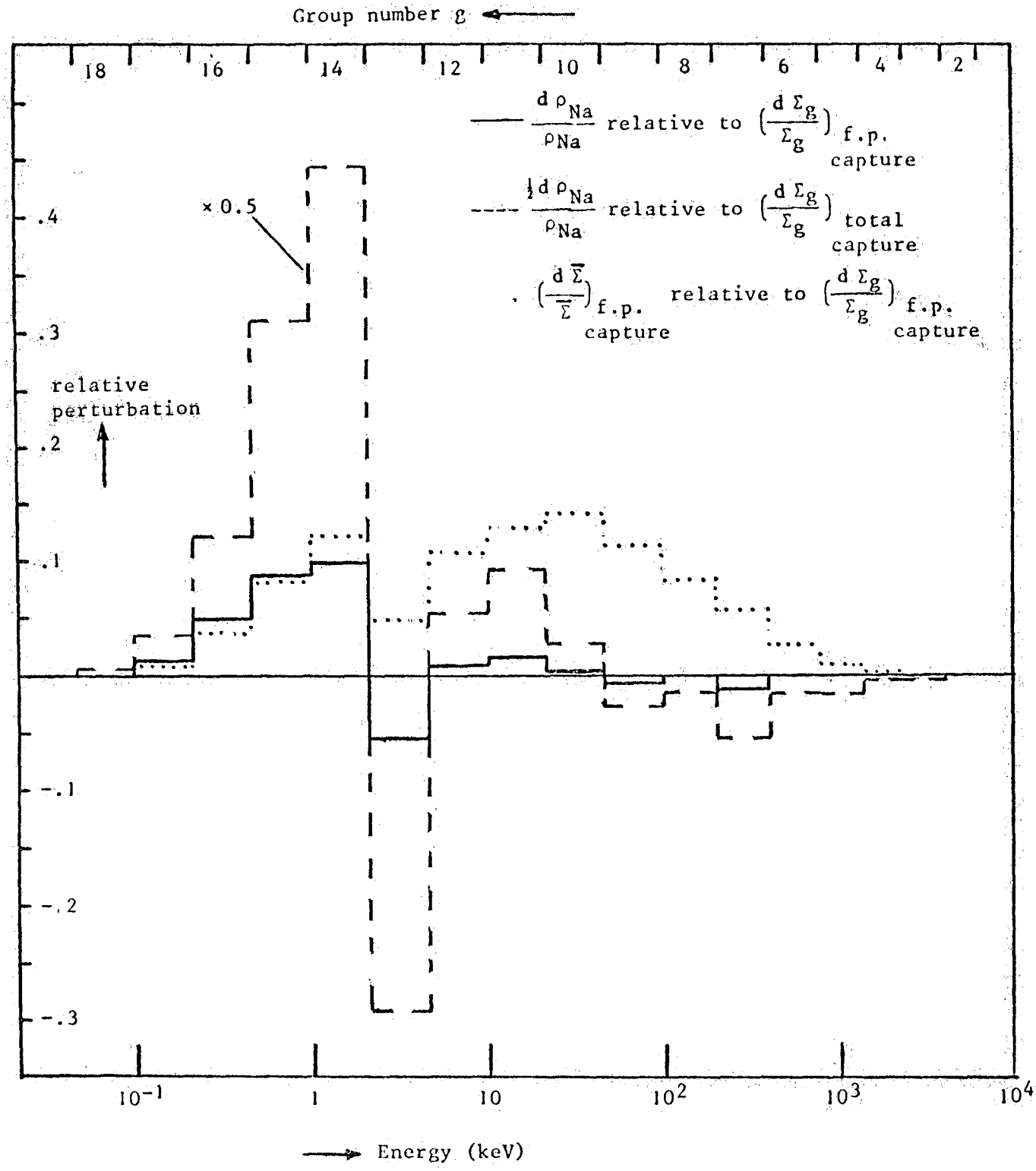


Fig. 3. Sensitivities of central sodium void effect $\rho_{Na}$ and fission product capture rate $\bar{\Sigma}$ to perturbations of capture group cross sections of total reactor mixture and fission product mixture.
Composition of 1300 $MW_e$ FBR at 74 MWd/kg burn-up.

# NEUTRON CROSS SECTION CALCULATIONS FOR FISSION-PRODUCT NUCLEI

E. D. Arthur and D. G. Foster, Jr.
Los Alamos Scientific Laboratory, University of California
Theoretical Division
Los Alamos, New Mexico 87545

ABSTRACT

To satisfy nuclear data requirements for fission-product nuclei, we performed Hauser-Feshbach statistical calculations with preequilibrium corrections for neutron-induced reactions on isotopes of Se, Kr, Sr, Zr, Mo, Sn, Xe, and Ba between 0.001 and 20 MeV. Spherical neutron optical parameters were determined by simultaneous fits to resonance data and total cross sections. Isospin coefficients appearing in the optical potentials were determined through analysis of the behavior of s- and p-wave strengths as a function of mass for a given Z. Gamma-ray strength functions, determined through fits to stable-isotope capture data, were used in the calculation of capture cross sections and gamma-ray competition to particle emission. The resulting (n,γ), (n,n'), (n,2n), and (n,3n) cross sections, the secondary neutron emission spectra, and angular distributions calculated for 19 fission products will be averaged to provide a resulting ENDF-type fission-product neutronics file.

---

To provide averaged neutronics information for fission-product nuclei we have performed nuclear-model calculations on a number of nuclei resulting from fast-neutron induced fission of U-235 and Pu-239. To approximate the sum over the constituents of yield curves for fission products, we have chosen a weighted average of the cross sections calculated for a few selected nuclides. These nuclei were chosen from the maximum and half-value points of the yield curves for both low- and high-mass fragments, using distinct sets for U-235 and Pu-239 fission. The resulting 19 nuclides are listed in Table I. We calculated, assuming each of these as a target, cross sections for the (n,γ), (n,n'), (n,2n), and (n,3n) reactions, together with elastic and inelastic angular distributions and neutron emission spectra in the incident neutron energy range beteen 0.001 and 20 MeV.

We relied upon use of the Hauser-Feshbach statistical model/1/ to which we applied preequilibrium corrections necessary at higher energies. This combination of nuclear models has generally worked well in the case of neutron cross-section calculations on stable nuclei, once suitable input parameters have been determined. We did not include direct-reaction effects since these contributions make up a comparatively small part of the total

TABLE I

NUCLIDES USED FOR FISSION PRODUCT CALCULATIONS

| | U-235 | Pu-239 |
|---|---|---|
| Lower Peak | | |
| Low | $^{87,88}Se$ | $^{92,93}Kr$ |
| Center | $^{94,95}Sr$ | $^{99,100}Zr$ |
| High | $^{102,103}Zr$ | $^{107,108}Mo$ |
| Higher Peak | | |
| Low | $^{131}Sn$ | $^{130}Sn$ |
| Center | $^{138,139}Xe$ | $^{137,138}Xe$ |
| High | $^{146}Ba$ | $^{145}Ba$ |

reaction cross section. We sought to improve the reliability of the calculated results obtained from these models through a careful determination of input parameters. Generally we fitted various types of stable-isotope experimental data and then tried to determine means by which to extrapolate these parameter sets for use with unstable target nuclei. We further checked the applicability of these input parameters through comparison of calculated cross sections, such as those for (n,2n) reactions, to experimental results.

Special attention was paid to the determination of spherical neutron optical parameters suitable for use over the major portion of the incident energy range. The use of optical parameters that simultaneously describe lower and higher energy data is important for the calculation of (n,xn) reactions where accurate compound-nucleus formation cross sections are needed at higher energies along with a reasonable description of the emission of low energy neutrons. We followed the "SPRT"/2/ approach in which total-cross-section data available over a wide energy range were used with low-energy resonance data in a simultaneous fit. For extrapolation to neutron-rich nuclei, we included isospin terms in both the real and imaginary potential. The coefficients $V_1, W_1$ multiplying the $\eta \equiv \frac{(N-Z)}{A}$ terms were determined through fits to the behavior of experimental s- and p-wave strength values as a function of $\eta$ for a given Z. As an example, Fig. 1 illustrates our fit to xenon total-cross-section data while Fig. 2 compares our calculated s-wave strength-function values to experimental data for xenon isotopes having differing $\eta$ values. The xenon optical parameters along with those determined for other nuclei involved in these calculations appear in Table II. The $V_1$ and $W_1$ coefficients shown in Table II are generally larger than those determined from fits to data such as elastic scattering from separated isotopes in the MeV region./3/ The cause for this discrepancy is not clear, but such values are in agreement with results obtained through similar analyses by Newstead and Delaroche./4/

For calculation of capture cross sections as well as to describe gamma-ray competition to particle emission, we chose to base gamma-ray transmission coefficients on determined values of the gamma-ray strength function rather than to normalize them to the ratio $\frac{2\pi\langle\Gamma_\gamma\rangle}{\langle D\rangle}$, where $\langle\Gamma_\gamma\rangle$ and $\langle D\rangle$ are the average gamma-ray width and spacing for s-wave resonances. For unstable nuclei the $\langle\Gamma_\gamma\rangle$ and $\langle D\rangle$ values would have to be deduced from their systematic behavior over the mass region of interest. Use of the gamma-ray strength function $f(\varepsilon_\gamma)$ defined by

TABLE II

SPHERICAL OPTICAL PARAMETERS[a]

| Element | $V_0$ | $V_1$ | $\alpha$ | $r_r$ | $a_r$ | $W_0$ | $W_1$ | $\beta$ | $r_i$ | $a_i$ | $W_0'$ |
|---|---|---|---|---|---|---|---|---|---|---|---|
| Se | 54.8 | 43 | -0.35 | 1.24 | 0.62 | 12.5 | 33 | 0.36 | 1.26 | 0.65 | 14.5 |
| Kr | 52.75 | 22 | -0.34 | 1.24 | 0.62 | 10.1 | 35 | 0.5 | 1.26 | 0.65 | 13.5 |
| Sr | 49.4 | 0 | -0.15 | 1.24 | 0.62 | 8.5 | 36 | 0.5 | 1.26 | 0.58 | 12.9 |
| Zr | 48.6 | 0 | -0.33 | 1.24 | 0.62 | 7.9 | 35 | 0.3 | 1.26 | 0.58 | 11 |
| Mo | 50.8 | 17 | -0.22 | 1.24 | 0.62 | 4.8 | 7 | 0.45 | 1.26 | 0.58 | 9.75 (Ref 5) |
| Sn | 56.3 | 50 | -0.28 | 1.25 | 0.57 | 4.4 | 15 | 0.5 | 1.25 | 0.56 | 9.5 |
| Xe | 55.4 | 50 | -0.35 | 1.25 | 0.65 | 12.8 | 50 | 0.4 | 1.25 | 0.56 | 17.1 |
| Ba | 49.0 | 22 | -0.15 | 1.25 | 0.74 | 7.8 | 32 | 0.48 | 1.25 | 0.58 | 13 |

[a]Real and imaginary (Saxon derivative) forms used were

$$V = V_0 - V_1\eta + \alpha E$$

$$W = W_0 - W_1\eta + \beta E$$

$$W_{max} = W_0' - W_1\eta,$$ with V and W in MeV: $r_r$, $a_r$, $r_i$, and $a_i$ in fm.

Spin orbit values used were

$V_{SO}$ = 6.2 MeV, $r_{SO}$ = 1.12 fm, $a_{SO}$ = 0.47 fm for Se, Kr, Sr, Zr, Mo isotopes.

$V_{SO}$ = 7.5 MeV, $r_{SO}$ = 1.25 fm, $a_{SO}$ = 0.65 fm for Sn, Xe, and Ba, isotopes.

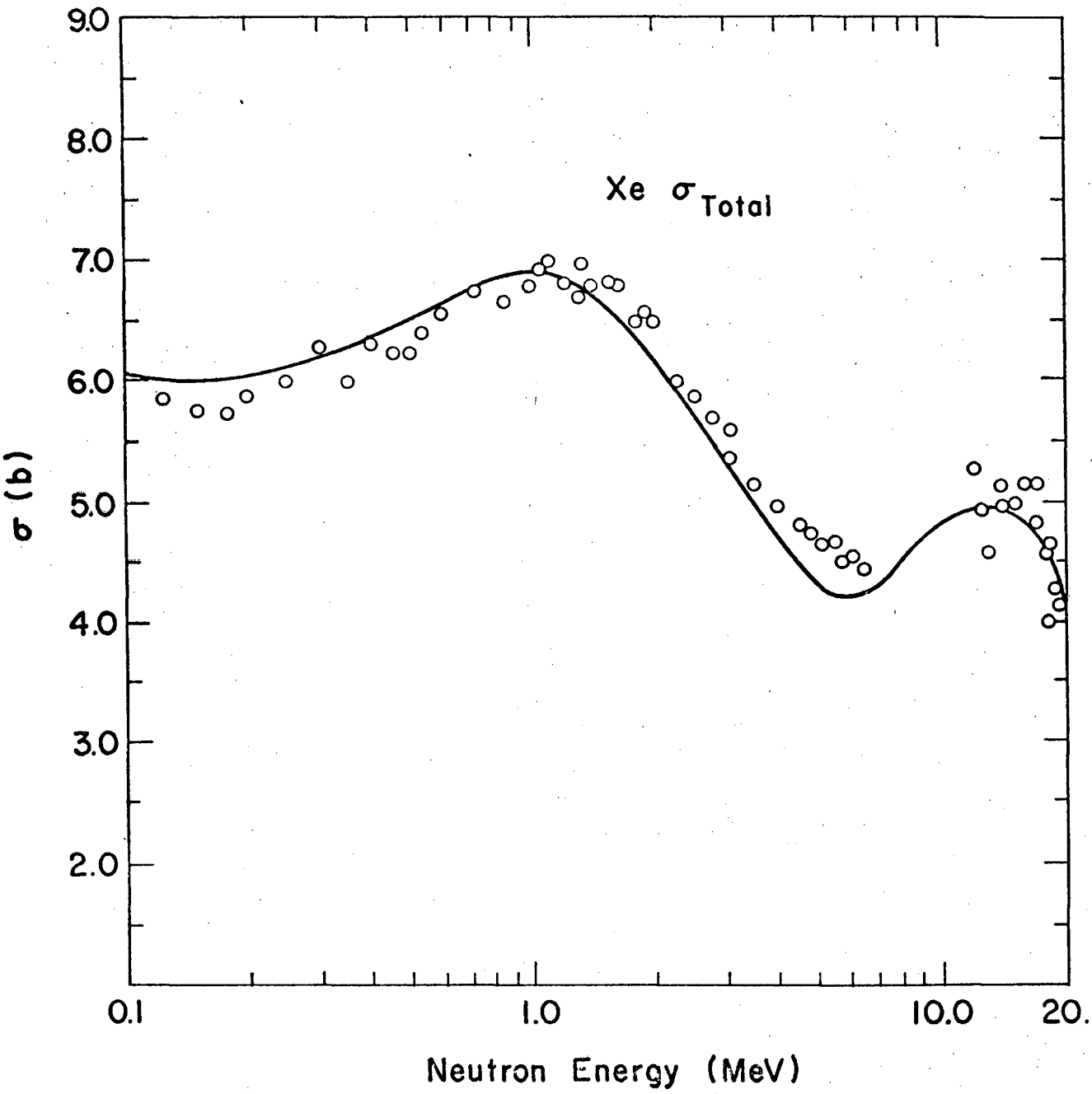


Fig. 1.

Comparison of calculated and experimental values for the xenon total cross section.

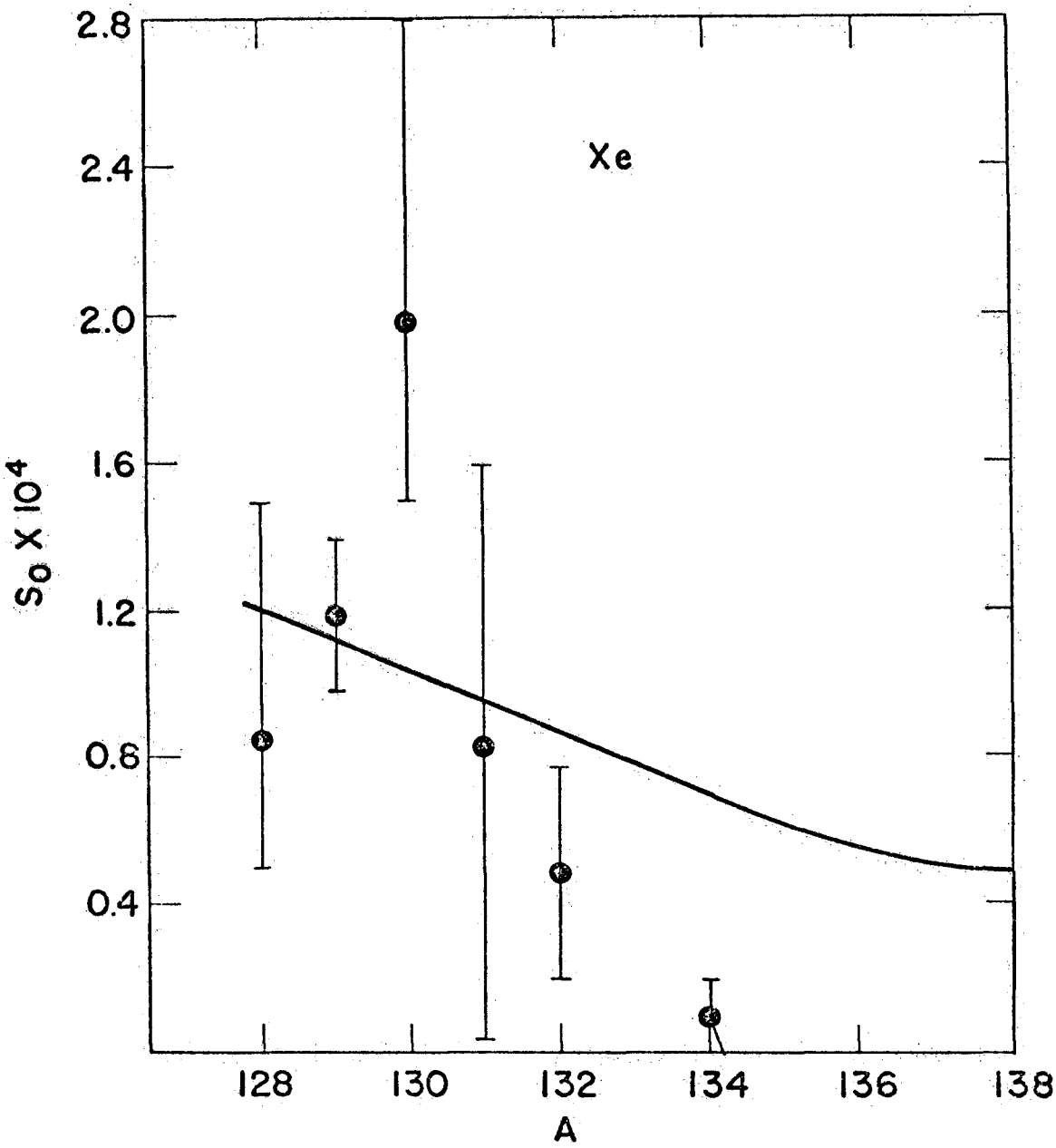


Fig. 2.

Calculated and experimental dependence of the s-wave strength function $S_0$ for isotopes of xenon.

$$\frac{\langle\Gamma_\gamma\rangle}{\langle D\rangle} = \int_0^{S_n} f(\varepsilon_\gamma)\ \varepsilon_\gamma^{\ 3}\ \rho(S_n-\varepsilon_\gamma)d\varepsilon_\gamma \quad , \tag{1}$$

where $S_n$ is the neutron separation energy and $\rho$ is the compound system level density, eliminates much of this uncertainty. If the strength function is assumed to have a giant dipole resonance form given by

$$f_{E1}(\varepsilon_\gamma) = \frac{k\varepsilon_\gamma\Gamma_{GDR}}{(\varepsilon_\gamma\Gamma_{GDR})^2 + (\varepsilon_\gamma^{\ 2}-E_{GDR}^2)^2} \quad , \tag{2}$$

then the constant appearing in Eq. (2) can be determined from fits to capture cross sections and spectra available for stable isotopes. This strength function should not vary as rapidly as $\frac{2\pi\langle\Gamma_\gamma\rangle}{\langle D\rangle}$ ; thus one can extrapolate its use to neutron-rich nuclei with greater confidence. As an example, Fig. 3 illustrates calculated gamma-ray strength functions for various Sn compound systems as determined from fits to capture data on Sn-116, Sn-118, Sn-119, and Sn-120. The extracted strength function varies at most by about 50%, a part of which may result from the fact that recent capture measurements in the keV region do not exist for these nuclei. On the other hand, the $\frac{2\pi\langle\Gamma_\gamma\rangle}{\langle D\rangle}$ ratios vary by a much larger amount, ranging from values of 0.0003 for n + Sn-120 to 0.013 for n + Sn-119. Figure 3 illustrates the range covered by strength functions determined for representative nuclei in this work.

Additional parameters needed for the present calculations included discrete level data, level-density information, and preequilibrium parameters. Some discrete level information was available from experimental measurements that was augmented in some cases by information based on shell model arguments./6/ To represent the continuum region where no discrete level information existed, we used the Gilbert-Cameron level density expressions/7/ with the Cook parameters/8/ as obtained from a systematic study of resonance spacings near the neutron binding energy. Preequilbrium corrections were applied using the Kalbach master equations model./9/

At low energies we used the COMNUC/10/ Hauser-Feshbach statistical code with the inclusion of width fluctuation corrections. At higher energies the preequilbrium-statistical model code GNASH/11/ was used to calculate cross sections and spectra resulting from multistep reactions. Figure 5 illustrates some of the preliminary calculations we made to further check our input parameter values. Here our calculated values are compared to experimental data for the Zr-90(n,2n) and Sn-112(n,2n) reactions.

Figures 6 and 7 illustrate calculated results for several major neutron reactions on Xe-138 and Xe-139 (solid and dashed curves, respectively). As shown in Table I, we calculated cross sections for both even and odd isotopes of a given element so that the final results, averaged over both cross section sets, would not be biased by such odd-even effects. The capture cross sections calculated in Fig. 6 used the same gamma-ray strength function. The principal reason for the different low-energy cross-section values is the differing neutron separation energies for these two isotopes. The capture cross section for Xe-139 becomes smaller than that for Xe-138 above 0.2 MeV because of competition from inelastic scattering off low-lying states in Xe-139. Most dissimilarities in cross-section shapes shown in Fig. 7 occur because of threshold differences resulting from the odd-even character of these two

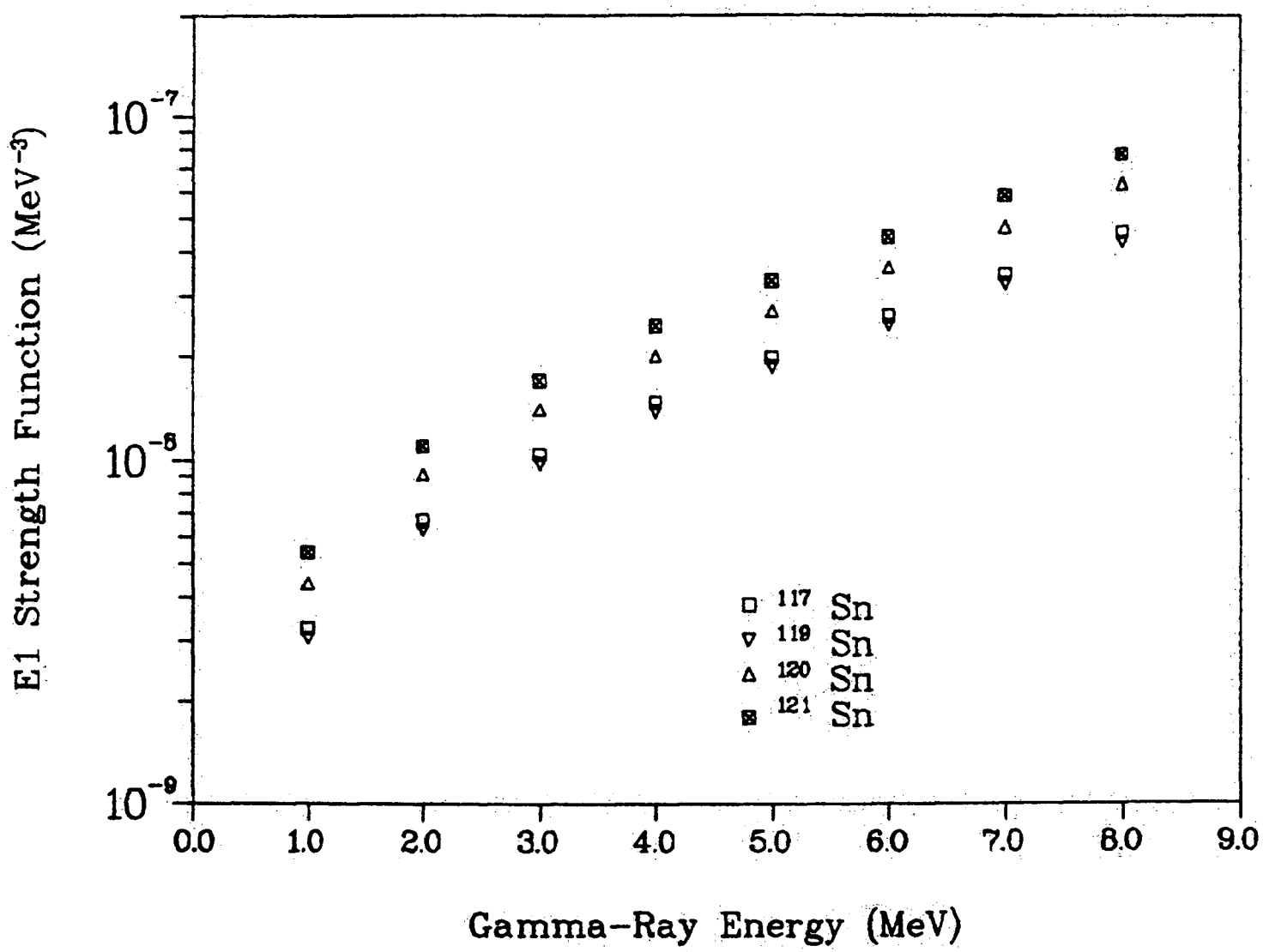


Fig. 3.

Gamma-ray strength functions determined from fits to capture data on tin isotopes.

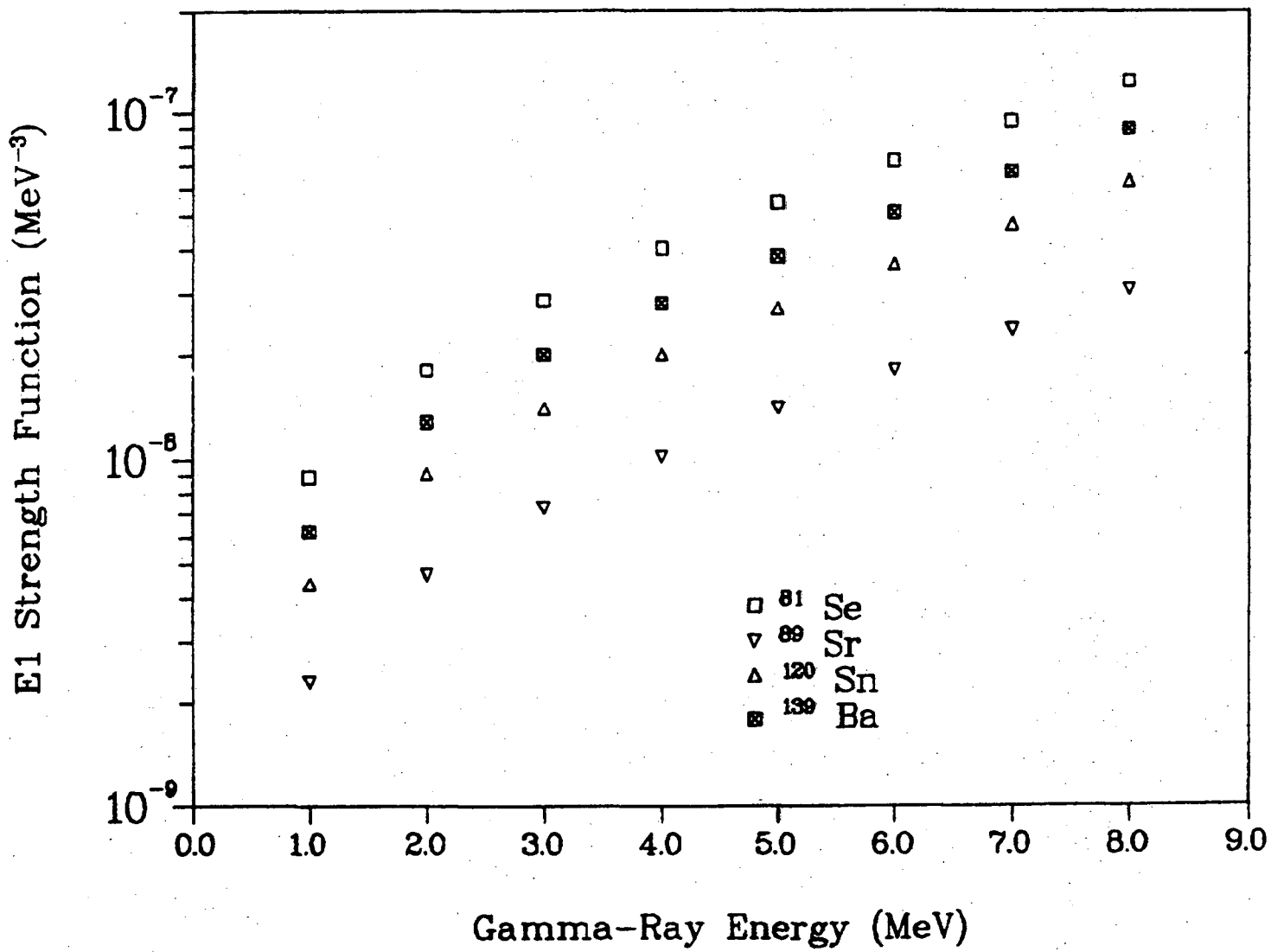


Fig. 4.

Representative gamma-ray strength functions used in this work.

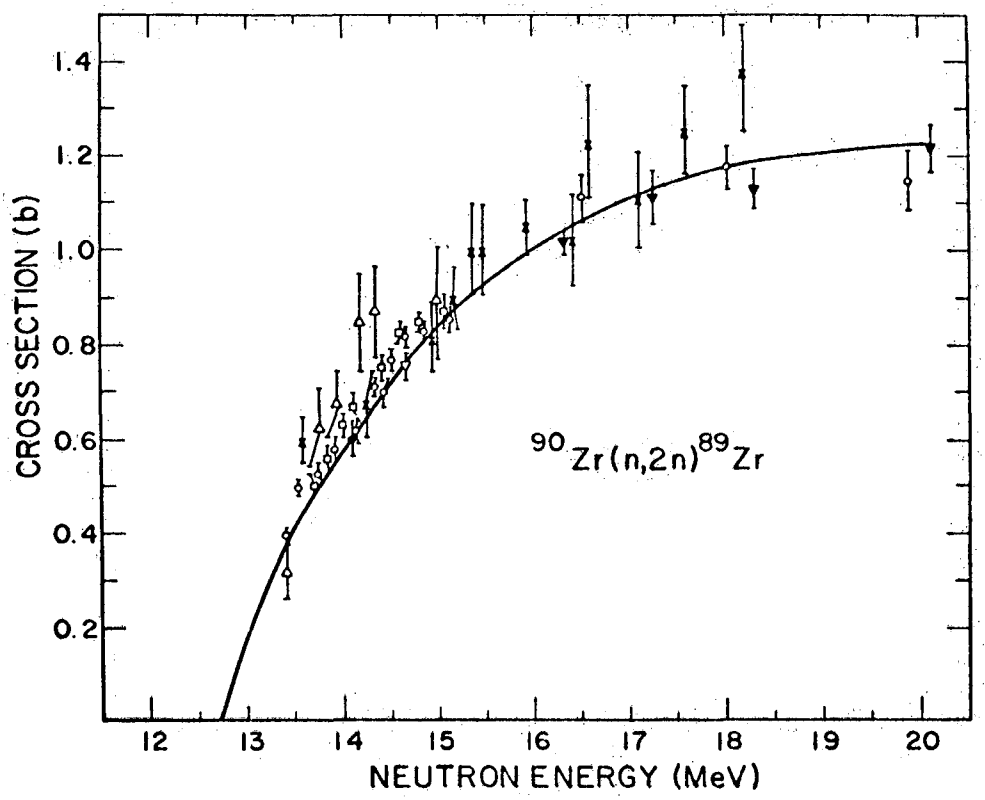


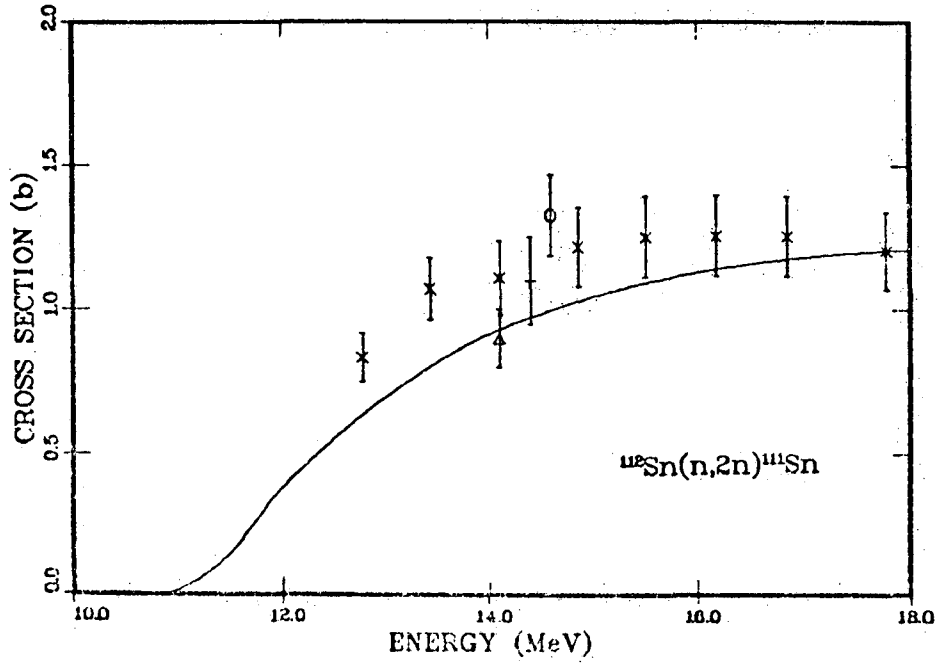


Fig. 5.

Comparison of calculated cross sections to experimental data for the Zr-90(n,2n) and Sn-112(n,2n) reactions.

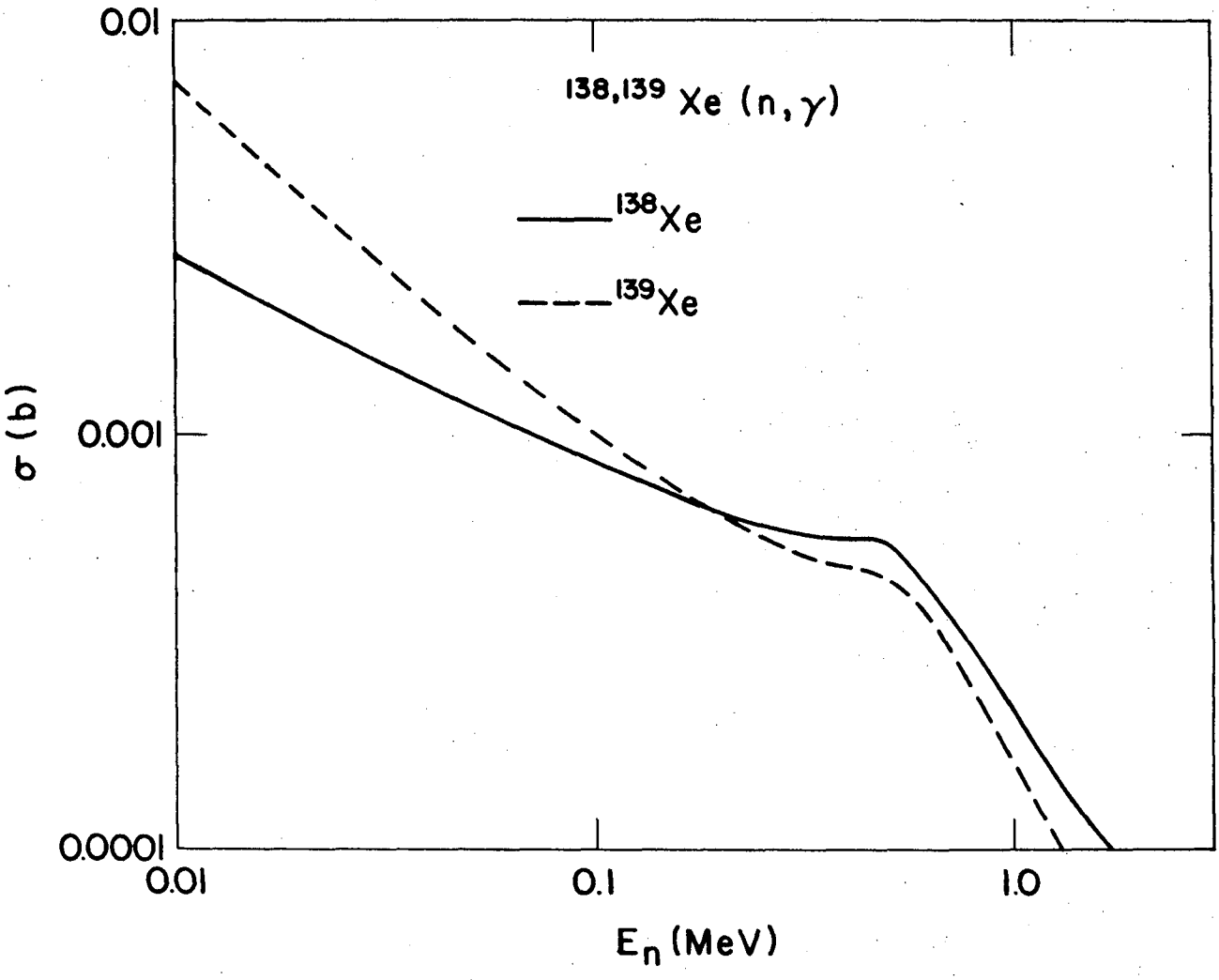


Fig. 6.

Predicted neutron capture cross sections for Xe-138 and Xe-139.

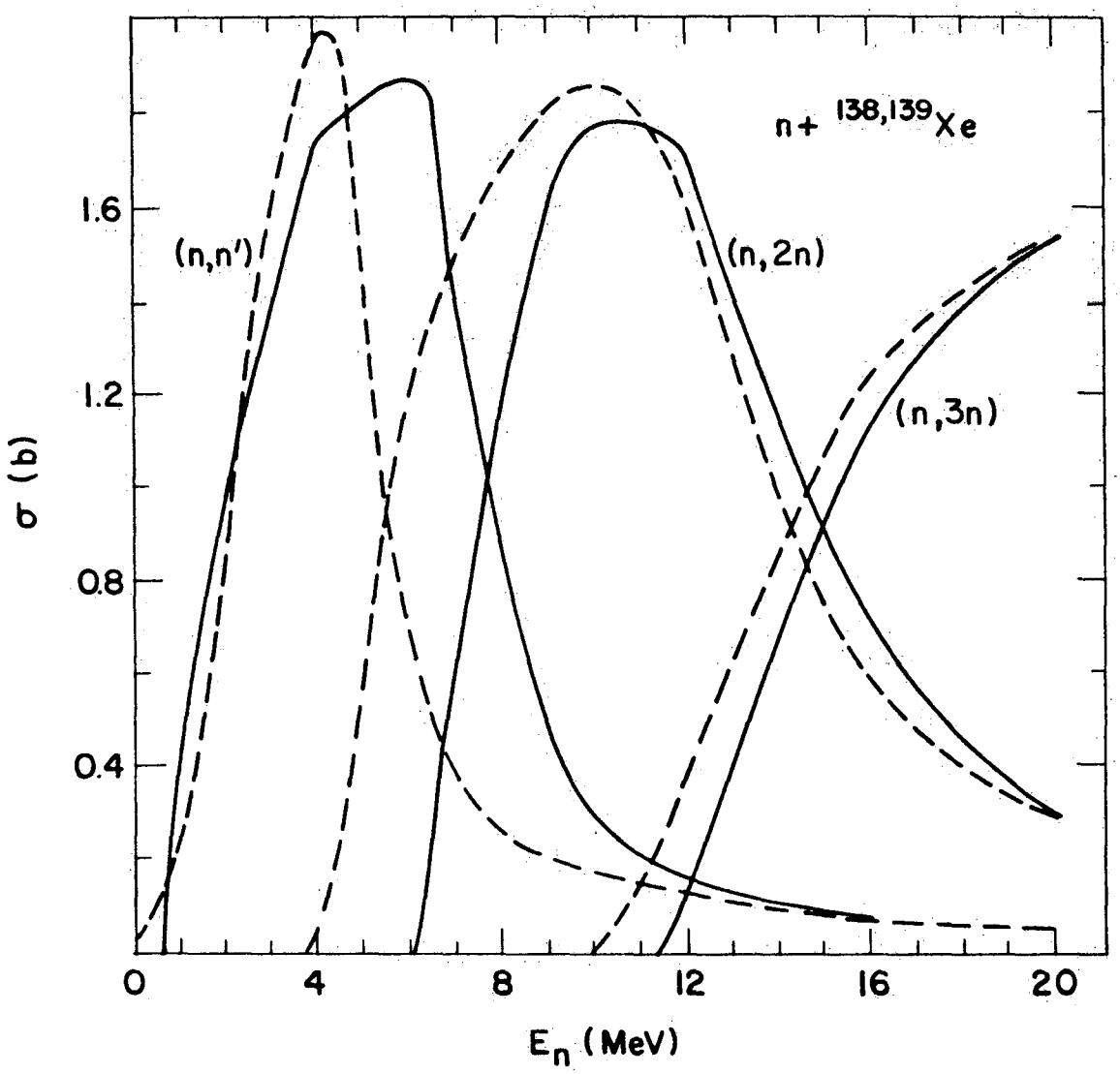


Fig. 7.

A comparison of (n,n'), (n,2n), and (n,3n) cross sections calculated for Xe-138 and Xe-139 (solid and dashed curves, respectively)

isotopes. Preequilibrium effects are apparent in that the higher energy portions of the (n,n') and (n,2n) cross sections have higher values than would be obtained from pure Hauser-Feshbach calculations. This in turn decreases the peak values obtained for the calculated (n,2n) and (n,3n) cross sections.

Similar calculations have been completed for all nuclei listed in Table I. Presently we are assembling cross sections, spectra, and angular distributions which will be averaged to produce an ENDF-like file for neutron reaction properties on prompt fission products.

REFERENCES

1. W. Hauser and H. Feshbach, Phys. Rev. 87, 366 (1952).

2. J. P. Delaroche, Ch. Lagrange, and J. Salvy, "Nuclear Theory in Neutron Nuclear Data Evaluation," IAEA-190, 251 (1976).

3. J. D. Ferrer, J. D. Carlson, and J. Rapaport, Nucl. Phys. A275, 325 (1977).

4. C. M. Newstead and J. P. Delaroche, in Nuclear Structure Study with Neutrons, edited by J. Ero and J. Szucs, Budapest (Plenum Press, NY, 1974) p. 142.

5. Ch. Lagrange, Second Advisory Group Meeting on Fission Product Nuclear Data, Petten (Sept. 1977).

6. D. Madland, Los Alamos Scientific Laboratory, personal communication (1979).

7. A. Gilbert and A. G. W. Cameron, Can. J. Phys. 43, 1446 (1965).

8. J. L. Cook, H. Ferguson, and A. R. de L. Musgrove, Aust. J. Phys. 20, 477 (1967).

9. C. Kalbach, Z. Phys. A287, 319 (1978).

10. C. L. Dunford, Atomics International Report AI-AE-12931 (1970).

11. P. G. Young and E. D. Arthur, Los Alamos Scientific Laboratory report LA-6947 (1977).

# NEANDC SPECIALISTS' MEETING ON NEUTRON CROSS SECTIONS OF FISSION PRODUCT NUCLEI

## Status of the Capture Cross Section for the Most Important FP Nuclei

### Report of Working Group 1


Schenter R.E., Chairman
Harker Y.D., Secretary
Coceva C.
Heijboer R.J.
Iijima S.
Janssen A.J.
Kaeppeler F.
Menapace E.
Patrick B.H.
Poenitz W.P.
Reffo G.
Vaccari M.
Voignier J.J.


## I. Introduction

Significant progress has been made to improve the quality and the understanding of data discrepancies for the capture cross sections of the important FP nuclei since the PETTEN meeting. Several new differential and integral measurements have been completed and analyzed. In addition, important studies have been made with evaluation efforts and nuclear model techniques. Essentially all these developments have been reported in the invited and contributed papers of this meeting. In this section we present a detailed discussion of these data and illustrate the general requirements. Finally, we present recommendations and courses of action to further improve and refine the capture cross section data with the goal of satisfying requesters' needs as indicated, for example, in WRENDA 78/80 and Section IV.5.1 of the PETTEN/FPND report.

## II. General Requirements

Since the PETTEN meeting, requirements in the fission product field have been issued in the U.S. request list (1), U.K. request list (2) and the Japanese request list (3). In addition, a World Request List (WRENDA) was published by IAEA (4). Moreover, the subgroup on Technical Activities of the NEANDC, at its 21st meeting in Geel, has worked out a list of requirements of highest priority in the OECD area (5).

From a general survey, it may be remarked that both evaluations and measurements (differential and integral) are necessary.

No new requirements for fission product cross sections were presented at the meeting, for either thermal or fast neutrons. Instead the general requirements stated at the PETTEN meeting (6,7) and some more recent French requirements (8) were assumed to hold (9). Briefly, the primary requirement for thermal reactors is for data on cross sections which determine the reactivity effects of fission products, i.e. thermal capture cross sections and capture resonance integrals.

Fos fast reactors, the needs are for cross sections which affect burn-up and reactivity. There is a requirement (6) to be able to calculate the reactivity effects of FP to an accuracy of $\pm 10\%$. Translated into cross section accuracies

of bulk fission products, this means ± 10% on the spectrum-averaged capture cross sections and ± 30% on inelastic scattering. Because of possible systematic effects, these accuracies also apply to the most important individual fission products. A long range goal of ± 7% was suggested at the PETTEN meeting [7] and uncertainties as low as ± 5% are required for French fast breeders [8,9].

It is suggested that some sensitivity calculations be carried out in order to provide specific requests for accuracies in different energy regions, as better guidance for experimenters and evaluators.

There is also a need for a knowledge of the shape of the cross sections so that the influence on Sodium void and Doppler effects can be determined. In order to define the most important cross sections, sensitivity studies are required. Some such studies have been carried out [9] as well as some measurements [10]. In view of the uncertainties in the work so far, further investigations are recommended.

The growing interest in alternative fuel cycles might lead to additional requirements for fission product cross section data. Likewise, high burn-up reactors could lead to requirements for more accurate fission product cross section data.

References

(1) BNL-NCS-51005; DOE/NDC-16/U

(2) J. Rowlands, U.K. request list 1979

(3) JAERI-M 7081; INDC(JAP)-36/G; NEANDC(J)-50/AL

(4) INDC(SEC)-73/URSF

(5) To be issued as a NEANDC document

(6) J.L. Rowlands, IAEA-213, p. 41

(7) IAEA-213, p. 803

(8) P. Hammer, Neutron Physics and Nuclear Data, Harwell, 1978, p. 551, OECD (1978)

(9) R.J. Heijboer and A.J. Janssen, this meeting

(10) K. Koyama, H. Mitani and H. Kuroi, IAEA Symp. on Fast Reactor Physics, Aix-en-Provence (1979) IAEA-SM-244/2

## III. Fast Cross Sections

### III.1 Differential Data

There is a large number of new data sets which are not yet utilized in the most recent evaluations. Many of these new data sets were reported at the present meeting. These data include measurements by Yamamuro and Asami [1] for isotopes of Nd and measurements by Poenitz [2] for elemental Nd.

The data by Yamamuro and Asami agree with recent measurements by Musgrove et al. [3]. Neodymium is of specific interest because it is often used as a burn-up monitor and the new data should help to improve the accuracy of the evaluated cross sections.

Uncertainties of recent data obtained with prompt detection techniques are ≈ 10%. Data on Rh and isotopes of Ru and Pd were reported by Macklin et al. [4] with uncertainties of 4-10%, data on Nb, I, Cs and isotopes of Nd, Sm and Eu by Yamamuro and Asami [1] with uncertainties larger than 5%, data on Rb, I, Nb, Cs, Ce and isotopes of Gd by Voignier et al. [5] with uncertainties of 8-16%, data on Rh, Pd, Nd and Sm by Poenitz with uncertainties of 10-15% and data on Xe and isotopes of Kr by Leugers and Kaeppeler [6] with 8-20%.

Most recent data spread over ranges of ±10-15% (for example Rh). There appears to be a substantial problem between experimental differential data and

integral data for the even isotopes of Palladium.

Other recent data were measured by Kononov et al.[7] for isotopes of Eu, Nd and Sm and by Musgrove et al.[6] for La, Pr and isotopes of Nd, Mo and Pd. The data by Kononov et al. differ substantially, specifically at lower energies, from the data by Musgrove et al., and by Yamamuro and Asami.

The usefulness of elemental data as a constraint for evaluated cross sections was emphasized. This specifically applies to the higher keV and MeV range where evaluations often differ by factors of 2-10.

Other Data

Though capture cross section data are of major concern it should be realized that for many FP nuclei, these cross sections will have to be calculated with nuclear models. The quality of such model calculations depend on optical model parameter sets which in turn must be determined with total and scattering cross section data. A general lack or lack of good data for total and scattering cross sections in the FP mass range was observed. Satisfactory optical model parameter sets will probably automatically fulfill the requirements for inelastic scattering data which affect reactivity by only 10-15% relative to capture.

References

(1) Yamamuro N., Asami A., this meeting

(2) Poenitz W.P., this meeting

(3) Musgrove A.R. de L., Harwell Conference on Neutron Physics, 1978

(4) Macklin R.L., Winters R.R. and Halperin J., this meeting

(5) Voignier J., Joly S., Grenier G., this meeting

(6) Leugers B. and Kaeppeler F., this meeting

(7) Kononov et al., Yadernaya Phyzica, vol. 27, p. 10 (1978)

III.2 Integral Data

III.2.1 Individual Nuclides

Fast integral data for individual fission product nuclides have been measured in STEK, FRO, MASURCA, ERMINE, CFRMF, RAPSODIE, PHENIX and EBR-II. Most of the integral data were available at the 1977 PETTEN meeting and since that time the irradiation experiments performed in PHENIX and EBR-II have been analyzed [1,2]. A new PHENIX irradiation experiment is in progress and the CFRMF activation data have been re-analyzed using updated decay information [3].

The integral data from these experiments have been used in the evaluations leading to fission product files in RCN-2A, ENDF/B-V, CARNAVAL-IV and JENDL-2.

At this meeting results of comparisons using these data files have been presented by Iijima [4], Gruppelaar [5] and Schenter [6]. For most nuclides, good consistency is achieved between different integral measurements; however, some discrepancies are noted and they are listed below:

1. $^{99}$Tc: The CFRMF integral value is approximately 25% lower than the STEK results [4].
2. $^{105}$Pd: Evaluations based on STEK data are lower similar data (CARNAVAL-IV) based on the French integral experiments [5].
3. $^{108}$Pd: STEK data are lower than the CFRMF value. The differential data do not agree with either [4].
4. $^{127}$I: The CFRMF value is approximately 25% lower than the STEK data [4].
5. $^{151}$Sm: STEK and French integral data have sample problems. A new irradiation experiment in PHENIX is in progress [5].

6. $^{147}Pm$: Data from STEK/CFRMF are not in agreement with data from ERMINE/FRO. More accurate integral (activation) data are needed [5].

7. $^{109}Ag$: STEK data approximately 13% lower than CFRMF. Improved integral data are needed [5].

8. $^{104}Ru$: The existing reactivity worths have high uncertainties and are not in agreement with the ERMINE activation value [5]. The new CFRMF value has an uncertainty of only 6.3% [3].

For the observations noted above, considerations should be given to new measurements and/or new analyses to resolve the problems. There is also concern that neutron self-shielding in the samples is not being properly accounted for. It is recommended that further study on this matter is needed and that the measurement laboratories as well as the evaluators consider what may be done to account for self-shielding. New measurements for certain nuclides using "thinner" samples would certainly be helpful.

References

(1) L. Martin-Deidier, Rapport CEA-R-5023 (1979)

(2) R.A. Anderl, Y.D. Harker, this meeting

(3) Y.D. Harker, R.A. Anderl, this meeting

(4) S. Iijima, T. Watanobi, T. Yoshida and Y. Kikuchi, this meeting

(5) H. Gruppelaar, P. Hammer, L. Martin-Deidier, this meeting

(6) R.E. Schenter and T.R. England, this meeting

III.2.2 Pseudo Sets

Evaluations: The good agreement between RCN-2, CNEN/CEA and JENDL-1 found in 1977 (differences in fast spectrum averaged $\bar{\sigma}_c$'s about 1%) has been reconfirmed at this meeting. The numbers of isotopes in the three evaluations have been extended (RCN-2: from 29 to 38; CNEN/CEA: from 50 to 63; JENDL-1: from 28 to 67). For ENDF/B-4 $\bar{\sigma}_c$ is 10% lower. At this meeting it became clear that this value will probably rise by at least 5% when the new evaluations and adjustments for ENDF/B-5 are incorporated.

Data sets adjusted to integral measurements of individual nuclides: For the RCN-2A set the average $\bar{\sigma}_c$ differs from the RCN-2 value by not more than 0.5%. The value based on the French CARNAVAL-IV set (which is not available) is 5% higher.

Accuracy of average $\bar{\sigma}_c$'s: For RCN-2A the accuracy is estimated to be 6-9% ($1\sigma$) and consists mainly of possible systematic errors in the interpretation of the STEK measurements. For CARNAVAL-IV the estimated accuracy is 4-5%.

Comparison with integral measurements of lumped fission products: The preliminary experimental data of the French (presented at the 1977 PETTEN meeting) have been published in 1978 [1]. On the average, (nine reactivity measurements) the E/C ratio (for CARNAVAL-IV) is 0.82 + 0.04 ($1\sigma$). This is in contradiction with the results obtained with the Dutch HFR-101 integral sample containing f.p. of thermal reactor fuel, where good agreement was found with RCN-2A in 1977. Part of the discrepancy may be due to uncertainties in yields (4%) and migration of gaseous f.p. (1.5%)[2]. Further measurements are planned by the French.

Required accuracy of pseudo f.p. reactivity effects: Presently required: 10%. Required for future reactors: 7% (according to the 1977 PETTEN meeting). Presently required by the French [2]: 5%. Required by the French in future: 3.5%. Improvements to be expected in the near future:

Average $\overline{\sigma}_c$ uncertainties: 4%

Yield uncertainties: 1.5% (most probably already reached)

References

(1) L. Martin-Deidier, et al., Proc. Int. Conf. on Neutron Physics and Nuclear Data for Reactors, Harwell, September 1978, page 1016. OECD (1978)

(2) Ph. Hammer, Proc. Int. Conf. on Neutron Physics and Nuclear Data for Reactors, Harwell, September 1978, page 551, OECD (1978).

## III.3 Evaluations

Since 1977, re-evaluations have been performed or are going on in the U.S.A., Netherlands (ECN), Italy/France (CNEN/CEA) and Japan, taking into account new differential capture and integral data.

CNEN-CEA have extended the library from 50 to 63 nuclides and have made new evaluations of Pd-105, Nd-143, Sm-149 and Sm-151, taking into account recent differential and integral data.

The U.S. performed complete new capture evaluations for about 70 nuclides (out of 196 total), which will appear in early 1980 (ENDF/B-V). For a number of these nuclides, simultaneous adjustments to integral data (CFRMF, EBR-II, STEK) and differential data were performed.

The Japanese library, JENDL-1 contains 67 nuclides (1977). A re-evaluation is planned to be finished by the end of 1980. Re-evaluation of Sm and Nd isotopes are going on. An extension to about 100 nuclides is planned (JENDL-2 library).

In the Netherlands the Nd isotopes and Pm-147 were evaluated, the library was extended from 29 to 38 fission product nuclides. The existing evaluation was improved by adding the (n,p) and (n,$\alpha$) cross sections. Further extension of the library is planned and also re-evaluation of important nuclides.

Intercomparison of evaluated capture cross sections shows that there exist large discrepancies of about a factor of 2 or more in the MeV region. As to the (elastic and) inelastic scattering cross sections, there seems to be still larger discrepancies among evaluated data. But, because of lack of experimental data, not much effort has been devoted to improve this situation.

## III.4 Nuclear Models

The nuclear models adopted for cross section calculations were not changed with respect to those described at the Kiev Conference and at the IAEA meeting at Petten in 1977. The largest effort has been devoted to the improvement of level density parameters and average radiative widths, through systematics and recent theoretical approaches. In connection with that, an effort was put to the determination of Dobs, neutron strength functions and average radiation widths from resolved resonance data. Concerning mean radiative widths, it has been shown that only gross trend systematics can be found.

Substantial improvement in the determination of mean radiative width with model calculation was obtained with the acquisition of Giant Resonance Parameter systematics.

After 1977, increasing efforts have been devoted to the application of the deformed optical model to the analysis of the experimental data and the cross section calculations mainly for even-A isotopes of Neodymium, Samarium and Gadolinium.

In the resolved resonance region, the use of multilevel B.W. formulas has been adopted for Nd and Sm isotopes, for which the mean level spacings are small.

For the unresolved region the "statistical strength function model" is mostly adopted. The correct junction of the capture cross section calculated from strength functions and those of H.F. calculations with optical model transmission coefficients generally requires to reproduce the strength function values as calculated from the optical model at low energies (except for those mass regions where intermediate structure might be present). It has been observed that width fluctuation effects in inelastic neutron scattering may be important up to 3-4 MeV, which is suggesting an extension of such a correction also to continuum region.

### III.5 Summary Table for Important Nuclides

Table 1 presents summary information on requirements ("Request"), differential and integral status ("Status"), and recommended actions ("Action") to improve the accuracy of the forty three "most important" FP nuclides for a fast breeder reactor system. The format follows that given in the PETTEN meeting report and in fact has the literal PETTEN remarks (above the dashed line). Conclusions by this working group are given (below the dashed line). Changes since the PETTEN meeting have been also indicated by drawing lines through the PETTEN information.

Table 1: Requests, Status and Action for Fast Capture Data [a)]

| Nuclide | Requests[b)] | Status[c)] Differential | Integral | Action |
|---|---|---|---|---|
| $^{93}Zr$ | 20% | only 1 resonance<br>no keV data<br>not met | only STEK oscill./13/<br>~~probably~~ met | further analysis of STEK data |
| | | | probably not met | |
| $^{95}Mo$ | 10% | many resonances<br>~~new~~ data of Musgrove ~~/1/ <90keV~~<br>status 15% | STEK oscill<br>PHENIX irrad./14/<br>FRO oscill./15/<br>(agreement)<br>met | ~~no action~~ |
| | | new data<br>20eV-100keV-RPI/19/<br>3-200 keV-AUA,<br>Musgrove /20/<br>not met | discrepancy between STEK & PHENIX<br>not met | measure differential data above 100 keV |
| $^{97}Mo$ | 10% | many resonances<br>new data of Musgrove<br>/1/ <90keV<br>status 15% | STEK oscill<br>PHENIX irrad.<br>FRO oscill.<br>(agreement)<br>met | ~~no action~~ |
| | | new data<br>3-200 keV-AUA,<br>Musgrove/20/ | | measure differential data above 100 keV |
| $^{98}Mo$ | 20% | many resonances<br>new data of Musgrove<br>/1/ <90keV<br>bad for E >90keV<br>status 15% | STEK oscill<br>CFRMF activ./3/<br>ERMINE activ.<br>(~~not very~~ good agreement between STEK/<br>/CFRMF) met | no action |
| | | new data<br>24 keV BNC<br>3-200 keV AUA,<br>Musgrove/20/ | good agreement between STEK,CFRMF and ERMINE | |
| $^{99}Mo$ | (ρ(t)) | Interpolation by<br>Musgrove/1/ | | reevaluation is recommended |

(continued)

Table 1: Requests, Status and Action for Fast Capture Data [a)]

| Nuclide | Request[b)] | Status[c)] Differential | Integral | Action |
|---|---|---|---|---|
| $^{100}$Mo | 20% | many resonances<br>new data of Musgrove /1/ <90keV<br>~~status 15%~~ | STEK oscill.<br>CFRMF activ.<br>(in same direction)<br>ERMINE activ.<br>met | ~~no action~~ |
| | | status 20%<br>new data<br>9eV-24keV ORNL(CINDA)<br>3-200keV AUA,Musgrove /20/ | discrepant data<br>probably not met | resolve discrepancies in differential and integral data. |
| $^{99}$Tc | 10% | only one set of data for E < 50keV/2/<br>very discrepant calculations for E >100keV<br>not met | STEK oscill.<br>French oscill./14/<br>CFRMF activ.<br>FRO oscill.<br>(discrepancies)<br>not met | ~~planned:resolved resonances experiments in Kiel~~<br>recommended:<br>measurements of average $\sigma$ for E=1 to 500 keV; $\langle\Gamma_\gamma\rangle$ measurement irradiation in EBR-2 |
| $^{101}$Ru | 10% | many resonances<br>unpublished RPI data /4/<br>not met | STEK oscill.<br>FRO oscill.<br>PHENIX irrad.<br>(good agreement)<br>probably met | analyze data of Hockenbury /4/ compare with integral data |
| | | new data<br>1-600 keV ORNL, Macklin /21/ | | |
| $^{102}$Ru | 20% | few resonances;<br>unpublished RPI data /4/<br>not met | French oscill.<br>FRO oscill.<br>STEK oscill.<br>CFRMF activ.<br>ERMINE activ.<br>(very good agreement)<br>met | (perhaps more resonances required) compare RPI data with integral data |
| | | new data<br>1-600 keV ORNL, Macklin /21/ | | |

Table 1: Requests, Status and Action for Fast Capture Data [a)]

| Nuclide | Request[b)] | Status[c)] Differential | Integral | Action |
|---|---|---|---|---|
| $^{103}Ru$ | 20% | no data at all<br>very large differences between evaluations<br>not met | no data | evaluation with new microscopic + integral data of 101, 102, $^{104}Ru$ |
| | | | | irradiation experiment desirable |
| $^{104}Ru$ | 20% | ~~see $^{102}Ru$~~ | ~~see $^{102}Ru$~~<br>~~(no French oscill.)~~ | ~~see $^{102}Ru$~~ |
| | | new data<br>1-600keV ORNL, Macklin /21/ | French activation measurements, also STEK & CFRMF<br>Probably in agreement. | |
| $^{103}Rh$ | 10% | many data<br>uncertain: 1-10keV<br>status: 10 to 15% | French oscill<br>FRO oscill.<br>STEK oscill<br>CFRMF activ.<br>(good agreement<br>met | no action |
| | | new data<br>.5-3.0 MeV BRC, Voignier /23/<br>.5-4.0 MeV ANL, Poenitz /22/<br>1-600 keV ORNL, Macklin /21/ | | |
| $^{105}Rh$ | | (for time dependence of reactivity) | | reevaluation recommended |
| $^{105}Pd$ | 10% | resonances to 160 eV<br>recent RPI /5/ and ORELA /6/ data in keV range; discr. near 100 keV<br>no data for 160 eV≤E≤ few keV | STEK oscill<br>French oscill.<br>PHENIX irrad.<br>(16% discrepancies between STEK and PHENIX; irradiations: difficult to obtain pure sample)<br>not met | resolved resonances in Geel<br>ongoing: resolved resonances in RPI<br>recommended: microscopic data for 160 eV ≤ E≤10keV; integral irradiation experiments |

Table 1: Requests, Status and Action for Fast Capture Data [a)]

| Nuclide | Request[b)] | Status[c)] Differential | Integral | Action |
|---|---|---|---|---|
| $^{105}$Pd (cont.) | | new data<br>3-200 keV, AUA, Musgrove /20/<br>1-600 keV, ORNL, Macklin /21/<br>.5-4.0 MeV, ANL, Poenitz /22/ | | Completed: resolved resonance measurements (Geel)<br>Geel plans capture measurements up to 100 keV |
| $^{107}$Pd | 10% | no data; ~~to be publ.~~<br>RPI data in resolved resonance range<br>not met | only STEK oscill. (not a very high accuracy)<br>not met | new evaluation RPI + STEK data |
| | | RPI data published /24/ | | irradiation experiment performed |
| $^{109}$Ag | 10% to 20% | many resonances discrepant series of data in keV region<br>data also available for $^{107}$Ag, natural Ag<br>not met | CFRMF activ.<br>STEK oscill.<br>French oscill.<br>~~(reasonably good agreement)~~<br>~~met~~ | evaluations can be improved with integral + micr. data of $^{107}$Ag, natural Ag. |
| | | | STEK 13% lower than CFRMF<br>not met | irradiation experiment performed |
| $^{127}$I | 10% (St) | new resonances (Geel /7/) many data; discrepancy between stat. model and keV data;<br>status 20% | STEK oscill.<br>CFRMF activ.<br>(in agreement with most keV data)<br>(status; ~~met~~ for reactor physics purposes) | more microscopic data in keV range to become a secondary standard |
| | 5% (St) | new data<br>24 keV Kyoto (CINDA)<br>3-80 keV Kyoto (CINDA)<br>.02-5 keV Geel (CINDA)<br>3-270 keV Yamamuro /25/ and Asami | STEK and CFRMF discrepant by 25%<br>not met | additional integral and differential measurements performed |

(continued)

Table 1: Requests, Status and Action for Fast Capture Data [a)]

| Nuclide | Request[b)] | Status[c)] Differential | Integral | Action |
|---|---|---|---|---|
| $^{129}I$ | 20% | few resonances, γ not known<br>no keV data<br>not met | STEK oscill.<br>CFRMF activ.<br>(good agreement)<br>met | no action |
| | | | | resolve differences between evaluations |
| $^{131}Xe$ | 20% | no data at all;<br>large discr.between evaluations<br>not met | only STEK oscill.<br>(FP mixture)<br>not yet analyzed | analyze STEK data |
| $^{132}Xe$ | 30% | no data<br>not met | STEK oscill.<br>(FP mixture)<br>CFRMF activ.<br>not yet analyzed | analyze STEK data |
| | | | | look into possibility of using elemental data |
| $^{133}Cs$ | 10%<br>(~~5 to 10% Fh~~) | many resonances;<br>discrepant series of keV data;<br>to be published RPI data /8/,<br>Japanese data /16/, /17/<br>not met | CFRMF activ.<br>STEK,French oscill.<br>PHENIX irrad.<br>(good agreement between STEK/French oscill.,CFRMF data lower;transm.and activ.data in agreement)<br>probably 10% met | recommended:<br>evaluate new data |
| | | new data<br>.002-100 keV RPI (CINDA)<br>55-150 keV Kyoto (CINDA)<br>3-80 keV Kyoto (CINDA)<br>3-270 keV Yamamuro and Asami /25/<br>.5 - 3MeV Voignier /23/<br>data are discrepant<br>not met | | |

(continued)

Table 1: Requests, Status and Action for Fast Capture Data [a)]

| Nuclide | Request[b)] | Status[c)] Differential | Integral | Action |
|---|---|---|---|---|
| $^{135}Cs$ | 10% | no data at all<br>planned:<br>Kiel /9/ mixed FP resolved res.<br>not met | only STEK oscill. (sample not very good)<br>not meet | recommended: integral activation measurements evaluation with Cs133,136 data |
| $^{139}La$ | 20% | many resonances<br>many keV data<br>~~nearly met ?~~ | STEK oscill.<br>CFRMF activ.<br>(good agreement)<br>met | no action |
| | | new data<br>3-200 keV AUA,Musgrove /20/<br>met | | |
| $^{141}Pr$ | 20% | many resonances<br>many keV data<br>Discr. at high E<br>~~not met~~ | STEK oscill.<br>CFRMF activ.<br>French oscill.<br>ERMINE activ.<br>(good agreement)<br>met | no action |
| | | new data<br>.002-100keV RPI(CINDA)<br>3-200keV AUA,Musgrove/20/<br>probably met | | |
| $^{143-150}Nd$ | 10% (BU) | resolved res.known recent data of Musgrove et al. E=1 to 19 keV/10/<br>status: ∿15% | STEK oscill.(~~not yet analyzed~~)<br>Nd145:PHENIX irrad. ~~in progress~~:stable Nd143-150<br>EBR-2 irrad.<br>planned:Nd143<br>~~PHENIX~~ irrad.<br>status:unknown | ~~evaluate Musgrove's data; analyze STEK data~~ |
| | | new data<br>many new measurements<br>RPI (CINDA)<br>AUA (CINDA)<br>JAEN (CINDA)<br>FEI (CINDA)<br>3-200 keV AUA, Musgrove /20/<br>3-270 keV Yamamuro and Asami /25/<br>.5-4.0 MeV Poenitz /22/ | | resolve inconsistencies between evaluations. Evaluate new differential data. |

Table 1: Requests, Status and Action for Fast Capture Data [a)]

| Nuclide | Request[b)] | Status[c)] Differential | Integral | Action |
|---|---|---|---|---|
| $^{147}Pm$ | 10% | many resonances<br>no keV data, evaluations in good agreement,<br>not met | STEK oscill.<br>~~(not analyzed)~~<br>CFRMF activ.<br>French oscill.<br>FRO oscill.<br>~~(good agreement)~~<br>not met | microscopic keV data required.<br>planned:<br>integral activ.ERMINE |
| | | | discrepancy between STEK/CFRMF and French and FRO data | |
| $^{148m}Pm$ | Dh | no data at all<br>probably met with ENDF/B-IV | no data | no action |
| $^{149}Pm$ | ($\rho$(t)) | no data | | reevaluation recommended |
| $^{149}Sm$ | 10% | many resonances;<br>Russian keV data/11/<br>to be published:<br>RPI keV data/4/<br>not met | FRO oscill.<br>STEK oscill.<br>PHENIX irrad.<br>EBR-2 irrad.~~(to be analyzed)discrepancy between STEK and recent keV data~~<br>not met | recommended:<br>evaluate new data |
| | | new data<br>5-300 keV FEI,Kononov (CINDA)<br>3-270 keV Yamamuro and Asami /25/<br>data are discrepant | discrepancies still exist between integral and recent keV data | resolve discrepancies for both integral and differential data.<br>Perform differential measurement at one point ~ 100 keV |
| $^{151}Sm$ | 10% | many resonances;<br>no keV data | STEK oscill.(not accurate)<br>PHENIX irrad.(perhaps new PHENIX irrad. in future)<br>not met | keV data required |
| | | | sample problems both in STEK and PHENIX measurements (large discrepancies) | PHENIX data made available.Use new average resonance parameter data for nucl.model calc. |

Table 1: Requests, Status and Action for Fast Capture Data [a)]

| Nuclide | Request[b)] | Status[c)] Differential | Integral | Action |
|---|---|---|---|---|
| $^{152}Sm$ | 20% | many resonances<br>few activation data<br>/12/<br>not met | STEK oscill.<br>CFRMF activ.<br>(good agreement)<br>probably met | |
| | | new data<br>5-300 keV FEI, Kononov (CINDA) | | resolve differences between evaluations |
| $^{153}Eu$ | 20% | resonances up to 100eV<br>discrepant keV data<br>~~to be~~ published:<br>JAERI data<br>~~probably met~~ with new data | STEK oscill.(not analyzed)<br>CFRMF activ.<br>FRENC oscill.<br>probably met | analyze STEK, ~~JAERI~~ data |
| | | new data<br>5-300 keV FEI, Kononov (CINDA)<br>3-270 keV Yamamuro and Asami /25/<br>discrepancies between recent differential data<br>not met | EBR-2 irradiations | |
| $^{151}Eu$<br>$^{152}Eu$<br>$^{153}Eu$<br>$^{154}Eu$<br>Eu nat | 5%<br>20%<br>5%<br>20%<br>? | required for control rod materials | for several isotopes there are data from STEK,CFRMF and EBR-2<br>(to be analyzed) | |
| | | new data<br>3-100 keV Yamamuro and Asami /25/<br>for $^{151}Eu$,$^{153}Eu$ and Nat Eu<br>$^{151}Eu$ 5% requirement not met | | Analyze STEK data and intercompare integral measurements |

Table 1: Requests, Status and Action for Fast Capture Data [a)]

| Nuclide | Request[b)] | Status[c)] Differential | Integral | Action |
|---|---|---|---|---|
| $^{155}Eu$ | 20% | no data at all<br>planned: data from Kiel /9/<br>not met | no data | |

a) Table 1 Contents:

This table gives the "request", "status" and "action" information from Table 12 of the Petten meeting (above the dashed line) and the same data as presently summarized by this working group (below the dashed line). Changes since the PETTEN meeting have been also indicated by drawing lines through the PETTEN information.

b) Source of Requests:

All requests are for reactivity calculations, except where stated otherwise:

- ρ(t) --- is a request for the time dependence of reactivity at begin of cycle.
- Fh --- Fuel handling (request made at Bologna Panel)
- BU --- burnup monitors
- Dh --- decay heat calculation
- St --- secondary standard

c) References:


/1/ A.R. Musgrove, Nucl. Phys. A270 (1976)108
/2/ Chou. J. of Nucl. Energy 27 (1973)811
/3/ Y.D. Harker, in "Progress in FPND", INDC(NDS)-86, p. 77-83 (1977)
/4/ Hockenbury; Bull. Am. Phys. Soc. 20(1976)560 (abstract, no data) see also EXFOR 10552
/5/ Hockenbury, NBS-Spec. Publ.-425 (1975 Washington Conf.) p. 904
/6/ see INDC(NDS)-86 ("Progress in FPND")p.72 (1977)
/7/ G. Rohr et al, Int. Conf. on Interactions of Neutrons with Nuclei, Lowell, Massachusetts, 6-9 July 1976; p. 1249
/8/ Hockenbury, Bull. Am. Phys. Soc. 21 (1976)537 (abstract no data)
/9/ see INDC(NDS)-86 ("Progress in FPND") p. 10 (1977)
/10/ A.R. Musgrove, to be published in Nucl. Phys. See also EXFOR 30360
/11/ Kononov et al., YK-22(1976)29
/12/ F. Bensch, H. Ledermann, INDC(AUS)-2/G, p.1 (1971)
/13/ J.J. Veenema, A.J. Janssen, "Small sample reactivity worths of FP isotopes and some other materials measured in STEK", ECN-10(1976)
/14/ Langlet and Martin-Deidier, contribution to RP 14 of this meeting. Published in INDC(NDS)-87 (1978). ("French oscill." means: ERMINE and MASURCA oscillation experiments)
/15/ T.L. Anderson, AE-428 (1971)
/16/ N. Yamamuro et al., Conf. on Nuclear Cross Sections and Technology Washington D.C. (1975), NBS-SP-425, p. 802
/17/ N. Yamamuro, private communication 1977
/18/ L. Koch, private communication 1977

/19/ RPI, see CINDA Mo-95
/20/ A.R. Musgrove et al., Harwell Conference, Sept. 1978
/21/ R.L. Macklin et al., this meeting
/22/ W.P. Poenitz, this meeting
/23/ J. Voignier et al., this meeting
/24/ RPI, Nucl. Sci. and Eng., 1979
/25/ N. Yamamuro and A. Asami, this meeting

## IV. Thermal Cross Sections

Thermal data needs and status were not directly addressed at this meeting, except as referred to in the ENDF/B-5 status paper (1), Appendix A. It is recommended that the work of Wilson and England (2) and the Petten report be referred to for guidance in this area.

### References

(1) R.E. Schenter and T.R. England, this meeting
(2) W.B. Wilson and T.R. England, in Symposium Proceedings: Nuclear Data Problems for Thermal Reactor Applications, EPRI NP-1098 (June 1979)

## V. Recommendations

1. New measurements of differential fast capture should be performed as indicated in Table 1.
2. New measurements of integral measurements of fast capture should be performed as indicated in Table 1.
3. Additional action items in Table 1 should be considered.
4. A more precise description of request uncertainties and energy ranges should be made.
5. Use of activation measurements in the fission spectrum neutron field should be investigated.
6. The measurement of data at some selected energies in the fast energy range is recommended. These singular points may be sufficient together with nuclear model calculations to fulfill many data requests. The most important energy point would be 30 keV. Other energy points would be 500 keV and 2 MeV.
7. The measurement of total and scattering cross section in the FP mass region is recommended in order to provide and improve the data base for a better definition of optical model parameters.
8. Evaluations of capture cross sections of FP nuclei should make use of elemental data constraints. This specifically applies to the higher keV and MeV range where isotopic data are unavailable and nuclear model calculations can differ by large factors.
9. Older experimental data should be renormalized with newer reference cross sections and decay data before they are used in evaluations.

NEANDC SPECIALISTS' MEETING ON NEUTRON CROSS SECTIONS
OF FISSION PRODUCT NUCLEI

# Status of Evaluation and Theory on $\langle D \rangle$, and the Neutron and $\gamma$-Ray Strength Functions; Intercomparison of Methods to Determine Average Resonance Parameters

## Report of Working Group 2


| | | |
|---|---|---|
| Gruppelaar H., | Chairman | |
| Stefanon M., | Secretary | Mughabghab S.F. |
| Delfini G. | | Osterhage W.W. |
| Fort E. | | Priesmeyer H.G. |
| Froehner F.H. | | Ribon P. |
| Lagrange Ch. | | Rohr G. |
| Lammer G. | | Staveloz P. |
| Moore M.S. | | Ventura A. |


## I. Requirements

Average resonance parameters of fission-product nuclides (FP) are required for model calculation of $\sigma_{n\gamma}$. The most important quantity is the ratio $\langle\Gamma_\gamma\rangle/\langle D\rangle$, which is related to $\sigma_{n\gamma}$ in the energy range of interest to fast power reactors. For the 20 most important nuclides (table I of Heijboer and Janssen's paper) the requirements for $\langle\sigma_{n\gamma}\rangle$ are about $\pm 10\%$. ($\langle\sigma_{n\gamma}\rangle$ = average capture cross section in a fast power reactor spectrum). This means that $\langle\Gamma_\gamma\rangle$ and D are required to within $\pm 7\%$. The s- and p-wave neutron strength functions $S_0$ and $S_1$ play a rôle at energies from a few keV to about 50 keV. The estimated requirements for the 20 most important FP are: $\pm 10\%$ in $S_0$ and $\pm 15\%$ in $S_1$ (for nuclides with A=80 to 90 the requirements for $S_1$ may be even more stringent).

It should be noted that model calculations based upon average resonance parameters are only one of the possible tools to obtain $\sigma_{n\gamma}$; mostly the evaluator will combine results from model calculations and capture data. However, this tool is very important to predict $\sigma_{n\gamma}$ of radioactive FP as listed in table II of Heijboer and Janssen's paper. In that case parameters from systematics obtained from neighbouring nuclides could be used to obtain $\sigma_{n\gamma}$.

The requirements for the less important FP isotopes (not mentioned in Table I of Heijboer and Janssen's paper) are less stringent. Again, the use of systematics of the average parameters can be quite helpful for these nuclides.

## II. Status of Average Parameters Derived from Experimental Data

From the papers presented at the meeting a complete view of the current status of the 20 most important FP cannot be obtained, since for many isotopes the new data now available have not been analysed as yet. Therefore, only some general comments are given in this section.

### II.1 Level Spacing D

For the 20 most important FP (table I of Heijboer and Janssen's paper) there is ±5% uncertainty only for 3 or 4 nuclides, and ±10% uncertainty for about 5 nuclides. The remainder have larger uncertainties. These conclusions are based upon data available in 1977. A clear discrepancy between evaluated data in the literature exists for $^{151}$Sm. This is largely due to the fact that the total cross section measurements were carried out on a thin $^{151}$Sm sample thus missing the weak resonances. It was noted that the error estimates on D are doubtful. The opinion of the participants at the Meeting was that an accuracy of ±7% in D can be reached when a set of high-quality resolved resonance parameters is used; see further sect. IV.

### II.2 Average Capture Widths

Mughabghab reports values for $\langle\Gamma_\gamma\rangle$ for only 6 of the 20 most important FP ; his report did not cover all of these 20 nuclides. It seems that for many FP nuclides there are still not enough resonance parameters with experimental values of $\Gamma_\gamma$. What is needed are values for $\ell=0$ and $\ell=1$ separately. It is noted that non-statistical effects in $\Gamma_\gamma$ may prevent calculating a meaningful average which can be used in model calculations.

### II.3 γ-Ray Strength Functions

Gardner and Gardner have proposed to extract γ-ray strength functions from average neutron or proton capture measurements, for use in model calculations. The status of these data was not discussed at this meeting, since the paper was not presented (see abstract).

### II.4 s- and p-Wave Neutron Strength Functions

From resolved resonance parameters of the 20 most important FP nuclides $S_0$ has been determined typically not much better than within 30%, with smaller uncertainties (±10%) in favourable cases, e.g. for $^{103}$Rh, $^{127}$I (see Delfini and Gruppelaar's paper). It should be noted that this conclusion is based upon data available in 1977. Another method to obtain $S_0$ is from analysis of average $\sigma_t$-data. Because of the difficulty in determining the $\ell$-values of many resonances, information on $S_1$ deduced from resolved resonance parameters is quite uncertain; hence, it is more reliable to use average $\sigma_t$-data. Unfortunately, many average $\sigma_t$-data in the range from a few keV to 100 keV are lacking. When D is small average capture data could also be used to determine $S_1$ .

## III. Status of Average Parameters Derived from Systematics or Theory

### III.1 D

From global systematics (see Reffo's paper) there is uncertainty up to a factor of 2 between values obtained from the systematics and experimental values. By using "local systematics", D can be deduced with an uncertainty of about 30% when measured data of neighbouring nuclides can be used for interpolation. From the BCS-model (see paper by Benzi et al.), values of D with uncertainties of ±30% can be obtained for most nuclides. The procedure suggested by Rohr et al. has been applied so far only to the actinides, with uncertainties in D of about 22%.

III.2 $\langle \Gamma_\gamma \rangle$

According to Reffo's paper, $\langle \Gamma_\gamma \rangle$ can be calculated to within about 30% when deformation parameters, giant-dipole resonance parameters and level-density parameters are reasonably well known. However, for most nuclides also level-scheme data of the low-lying levels are needed up to a few MeV. The parity distribution of low-lying states is particularly important to predict $\langle \Gamma_\gamma \rangle_{\ell=0}$ and $\langle \Gamma_\gamma \rangle_{\ell=1}$. To estimate non-statistical effects other models are needed. In Mughabghab's paper simple estimates for $\langle \Gamma_\gamma \rangle$ are quoted, which are accurate to within about a factor of 2.

III.3 Strength Functions

No information is given on systematics of $S_0$ and $S_1$ at this meeting. Probably the uncertainty in $S_0$, $S_1$ derived from systematics is not better than 30%.

IV. Conclusions and Recommendations Related to Experimental Data

Considerable progress has been made in resolved resonance measurements performed since the 1977 meeting at Petten (e.g. Pd-isotopes, Ru-isotopes). However, many recent data have still to be analysed with the methods proposed at this meeting. For this reason it is difficult to specify further requests exactly. The definition of these requests will be greatly facilitated after publication of the new edition of BNL-325 (first half of 1980).

Some global recommendations are:

a) Though some measurements have been carried out on FP nuclides, higher quality resolved resonance parameters over extended energy regions are, nevertheless, required. This applies particularly to the long-lived unstable nuclides, $^{99}$Tc, $^{107}$Pd, $^{151}$Sm, $^{147}$Pm, $^{135}$Cs and $^{103}$Ru. This may require further development of techniques to measure small samples of radioactive material.

b) Use of s- and p-wave discrimination methods as employed by Staveloz et al. for the Pd-isotopes is recommended. For this method the parities of the low-lying states of the final nuclide need to be known. M. Moore suggested exploring this method also in measurements of average cross sections.

c) For many nuclides $S_0$ and $S_1$ could be determined from average $\sigma_t$ (or $\sigma_c$) data. For this reason average total cross section measurements are required in the energy range 5 to 100 keV.

d) Gardner's suggestion to extract $\gamma$-ray strength functions from experimental capture cross sections should be further investigated by means of analysis of $(n,\gamma)$ or $(p,\gamma)$ data. This could be of relevance for unstable FP nuclides.

e) Further developments of theory and systematics are recommended, in particular with regard to D and $\langle \Gamma_\gamma \rangle$.

f) With regard to the method for estimating level densities and average reduced neutron widths from resolved resonance parameters, see sects. V and VI.

V. Methods of Estimating Level Densities and Average Reduced Neutron Widths from Resonance Parameters Data

General agreement was reached that an analysis based only upon the observed resonance energies, making use of statistical properties of pure sequences (Linear statistics, $\Delta_3$ statistics of Dyson etc...) is unreliable and is to be avoided. (Lowell, 1976, CONF-760715-P2, p. 1456; see also Fort's paper, this meeting). The estimating procedures currently used by most laboratories represented in the working group are based essentially on the Porter-Thomas distribution corrected for a threshold in the $g\Gamma_n$ values. Certain simplifying physical assumptions are also generally common, like the (2J+1)-dependence of the level density and

the independence of the strength function of the spin of the resonances.

The methods differ however in the following:

a) The possibility of dealing also with data composed of mixed unassigned p-wave and s-wave resonances.

b) The way to determine the lower threshold for $g\Gamma_n$, which is either automatically calculated or assumed as a variable input parameter.

c) The methods used to check for deviations of the data behaviour from the Porter-Thomas law (variation of number of resonances in prescribed $g\Gamma_n$ intervals or stability of the output for different thresholds).

d) There are large differences in the calculation of errors. It is pointed out that the only possible way to obtain reliable statistical errors is a statistically significant Monte Carlo simulation of experimental data.

This method has already been developed (Lowell, 1976, CONF-760715-P2, p. 1456; see also Rohr's and Stefanon's papers, this meeting) and is therefore recommended for all estimation procedures.

## VI. Intercomparison of Methods Used to Determine Average Spacing from Sets of Individual Resonance Parameters

It has been decided to promote an inter-laboratory exercise supported by NEANDC and organized by P. Ribon.

The exercise consists of generating a small number of sets of resonance parameters according to Ribon's proposal (Ribon: this meeting) and to submit the results to different laboratories for analysis.

There is majority agreement that this exercise is a useful test of methods and codes.

M. Stefanon and C. Coceva point out that such an exercise does not lead to any meaningful information on the variance of the estimates due to its low statistical significance and to biases due to guessing of input values like $S_0/S_1$.

The following approximate time schedule is given:

February : distribution of data;

July : dead line for submitting the results of the analysis;

October : presentation of the result of the intercomparison.

The following laboratories have already adhered to the exercise:

Bhabha Atomic Research Centre, Bombay, India

Inst.de Fiz.si.Ing.Nucleara, Bucharest, Rumania

KFK, Karlsruhe, Germany, F.R.

AERE, Harwell, UK

BCMN, Geel, Belgium

The NEA Data Bank, Saclay, will look after accepting applications to the exercise and collecting the results.

# LIST OF PARTICIPANTS

1 V BENZI, CNEN, Bologna, Italy
2 C COCEVA, CNEN, Bologna, Italy
3 G DELFINI, ECN, Petten, The Netherlands
4 F FABBRI, CNEN, Bologna, Italy
5 E FORT, CEA, Cadarache, France
6 F H FROEHNER, KFK, Karlsruhe, FRG
7 H GRUPPELAAR, ECN, Petten, The Netherlands
8 Y D HARKER, EG&G Idaho Inc , Idaho Falls, USA
9 R J HEIJBOER, ECN, Petten, The Netherlands
10 S IIJIMA, NAIG, Kawasaki, Japan
11 A J JANSSEN, ECN, Petten, The Netherlands
12 L JEKI, CRIP, Budapest, Hungary
13 F KAEPPELER, KFK, Karlsruhe, FRG
14 Ch LAGRANGE, CEA, Bruyères-le-Châtel, France
15 G LAMMER, IAEA, Vienna, Austria
16 G MAINO, CNEN, Bologna, Italy
17 E MENAPACE, CNEN, Bologna, Italy
18 M S MOORE, CEC, JRC, Geel, Belgium
19 M MOTTA, CNEN, Bologna, Italy
20 S F MUGHABGHAB, BNL, Upton, USA
21 W W OSTERHAGE, NEA, Paris, France
22 G C PANINI, CNEN, Bologna, Italy
23 B H PATRICK, AERE, Harwell, UK
24 W P POENITZ, ANL, Argonne, USA
25 H G. PRIESMEYER, Kiel University, Kiel, FRG
26 G REFFO, CNEN, Bologna, Italy
27 P RIBON, CEA, Saclay, France
28 G ROHR, CEC, JRC, Geel, Belgium
29 R E SCHENTER, HEDL, Richland, USA
30 P STAVELOZ, CEC, JRC, Geel, Belgium
31 M STEFANON, CNEN, Bologna, Italy
32 M VACCARI, CNEN, Bologna, Italy
33 A VENTURA, CNEN, Bologna, Italy
34 J J VOIGNER, CEA, Bruyères-le-Châtel, France

Riprodotto presso il laboratorio tecnografico
del Centro Studi e Ricerche " E. Clementel "

Operatori : G. Abelli - R. Abelli